Wolfgang A.G. Sauerwein · Andrea Wittig
Raymond Moss · Yoshinobu Nakagawa *Editors*

Neutron Capture Therapy

Principles and Applications

Springer

Neutron Capture Therapy

Wolfgang A.G. Sauerwein • Andrea Wittig
Raymond Moss • Yoshinobu Nakagawa
Editors

Neutron Capture Therapy

Principles and Applications

Springer

Editors
W.A.G. Sauerwein
NCTeam,
Department of Radiation Oncology
University Hospital Essen,
University Duisburg-Essen
D-45122, Essen
Germany

Andrea Wittig
Department of Radiotherapy
and Radiation Oncology
Philipps-University Marburg,
Marburg
Germany

Raymond Moss
Joint Research Centre, Institute for Engergy
European Commission
Petten
The Netherlands

Yoshinobu Nakagawa
Department of Neurosurgery
Kagawa National Children's Hospital
Zentsuji
Kagawa
Japan

ISBN 978-3-642-31333-2 ISBN 978-3-642-31334-9 (eBook)
DOI 10.1007/978-3-642-31334-9
Springer Heidelberg New York Dordrecht London

Library of Congress Control Number: 2012950993

Printed on acid-free paper

Springer is part of Springer Science+Business Media (www.springer.com)

Preface

Boron Neutron Capture Therapy (BNCT) is based on the ability of the non-radioactive isotope boron-10 to capture with a very high probability thermal neutrons. This nuclear reaction produces two high-LET particles (He-4 and Li-7) with ranges in tissue limited to the diameter of a single cell. This offers the possibility to target single tumor cells and to destroy them with high efficiency while sparing other tissues containing less boron-10. Such a radiotherapy on the cellular level can provide an extremely precise dose delivery allowing to efficiently treat tumors and to reduce side effects. It also has the potential to successfully treat types of cancer that are actually incurable.

In recent years major progress was made in conventional radiation oncology to improve precision. However, the radiation dose still has to be delivered to a volume that necessarily also includes normal tissues. Even more so, physicians have to define this volume, which depends from the imaging modalities available and which will vary from one physician to another. BNCT with its biological targeting of single cells has the potential to overcome these inherent problems of conventional radiotherapy.

However, the success of BNCT is not guaranteed. It depends on two conditions: the preferential uptake of boron-10 atoms into each cancer cell and the delivery of a high fluence of thermal neutrons into the target volume. To realize these technical and biological prerequisites, BNCT needs multi-disciplinary science relying on the collaboration of medicine and biology, nuclear and medical physics, chemistry and pharmacology, mathematics and information technologies.

This book has brought together a number of reputable clinicians and scientists in the field of BNCT, who have collaborated to write chapters covering the whole range of topics within BNCT. It has been designed as a guide to BNCT providing the reader with a definitive, authoritative, and comprehensive review of the topic. For the editors, it was a challenging task to coordinate this multi-disciplinary and multi-cultural approach. The reader may appreciate the resulting variety but he will also recognize the need of further development of standards in the reporting of BNCT.

After more than 50 years of research in BNCT, substantial progress is now within reach: Hospital-based accelerators delivering high intensity epithermal neutron beams will facilitate clinical trials and will allow for the inclusion of more patients into such trials. This creates a market attractive for the pharmaceutical industry, which is mandatory for any new drug development in BNCT. We therefore see

a great future for BNCT and we sincerely hope that all the efforts necessary to realize this book will help to advance all aspects of BNCT. We would like here to take the opportunity to express our gratitude to Mrs. Reiko Matsuoka, who supported and accompanied the development of BNCT from its beginning. She entered the topic as Prof. Hatanaka's secretary and after he passed away she promoted the International Society for Neutron Capture Therapy supporting congresses around the world and facilitating exchange between Japanese and non-Japanese scientists. Her continuous voluntary engagement behind the scenes has been a tremendous support for many colleagues working in the field.

The editors would like to thank all the authors, who accepted multiple corrections and rewriting. We are very grateful to Springer Verlag to publish this book. We especially appreciate the kind but determined support of our assistant editor Meike Stoeck who accompanied the sometimes laborious birth over a long time period. We also thank the project coordinator Wilma McHugh and the project manager Ms. Madona Samuel, who made from a simple manuscript this book now in your hands.

Essen, Germany — Wolfgang A.G. Sauerwein
Marburg, Germany — Andrea Wittig
Petten, The Netherlands — Raymond Moss
Kagawa, Japan — Yoshinobu Nakagawa

Contents

Principles and Roots of Neutron Capture Therapy

1

Wolfgang A.G. Sauerwein

Contents

1.1 Principles

Boron neutron capture therapy is a binary form of radiation therapy using the high propensity of the nonradioactive nuclide boron-10 to capture thermal neutrons resulting in the prompt nuclear reaction $^{10}B(n,\alpha)^{7}Li$. The products of this reaction have high linear energy transfer characteristics (α particle approximately 150 keVμm^{-1}, ^{7}Li-nucleus approximately 175 keVμm^{-1}). The path lengths of these particles in water or tissues are in the range of 4.5–10 μm: hence resulting an energy deposition limited to the diameter of a single cell. Theoretically, therefore, it is possible to selectively

W.A.G. Sauerwein
NCTeam, Department of Radiation Oncology,
University Hospital Essen, University Duisburg-Essen,
D-45122, Essen, Germany
e-mail: w.sauerwein@uni-due.de

W.A.G. Sauerwein et al. (eds.), *Neutron Capture Therapy*,
DOI 10.1007/978-3-642-31334-9_1, © Springer-Verlag Berlin Heidelberg 2012

irradiate those tumor cells that have taken up a sufficient amount of ^{10}B and simultaneously spare normal cells. The basic nuclear reaction is shown in more detail below:

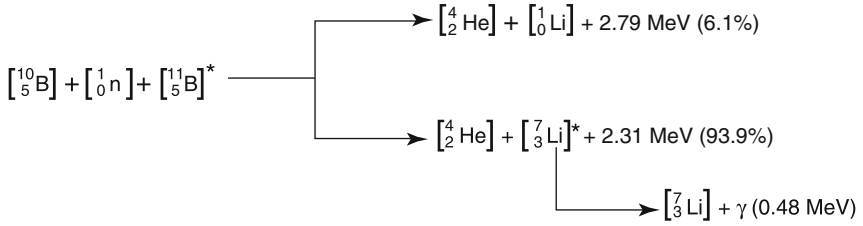

Shortly after the discovery of the neutron by Chadwick in 1932 [1] and the description of the $^{10}B(n,\alpha)^{7}Li$ reaction by Taylor and Goldhaber 1935 [2], the basic idea to use neutron capture reactions in cancer treatment was published by Locher in 1936 [3]: "In particular, there exist the possibility of introducing small quantities of a strong neutron absorber into the regions where it is desired to liberate ionization energy (a simple illustration would be the injection of a soluble, non-toxic compound of boron, lithium, gadolinium or gold into a superficial cancer, followed by bombardment with slow neutrons)."

A number of nuclides exist that have a high propensity for absorbing thermal neutrons (Table 1.1) that hypothetically might be used in neutron capture therapy (NCT). The probability of a nucleus to capture thermal neutrons, referred to as the neutron capture cross section (σ_{th}), is measured in barns (1 b = 10^{-28} m^2).

Most of the nuclides listed in Table 1.1 interact with thermal neutrons by the (n,γ)-reaction. The effect of the resulting photon irradiation is not restricted to the labeled "target cells"; therefore, the postulated selectivity of NCT will not be attained. On the other hand, such a γ–irradiation may lead to a more homogenous dose distribution in small volumes. Some authors were attracted by this option especially interested by the very high cross section of ^{157}Gd. In a first glance, this approach seems also attractive because of the use of Gd as paramagnetic agent for contrast-enhanced

Table 1.1 Isotopes with high values of thermal neutron capture cross sections [4–7]

Nuclide	Interaction	Cross section σ_{th} (b)
^{3}He	(n,p)	5,333
^{6}Li	(n,α)	940
^{10}B	(n,α)	3,835
^{113}Cd	(n,γ)	20,600
$^{135}Xe^{a}$	(n,γ)	2,720,000
^{149}Sm	(n,γ)	42,080
^{151}Eu	(n,γ)	9,200
^{155}Gd	(n,γ)	61,100
^{157}Gd	(n,γ)	259,000
^{147}Hf	(n,γ)	561
^{199}Hg	(n,γ)	2,150
$^{235}U^{a}$	(n,f)	681
$^{241}Pu^{a}$	(n,f)	1,380
$^{242}Am^{a}$	(n,f)	8,000

[a]Radioactive

NMR imaging. A number of preclinical investigations have been made, without showing a real benefit of this approach [8–18]. The suggestion to use Auger electrons that are produced during the (n,γ)-reaction with ^{157}Gd could not be realized in clinically relevant biological experiments [19, 20]. Another approach that however is not much investigated is the use of ^{6}Li and ^{235}U, whose reaction products might have larger biological effects as compared to ^{10}B [21–26]. In particular, the radioactivity of ^{235}U and its affinity for bone together with the wide energy range of its fission products make it difficult to handle. Its use as shielded seed implants together with an external irradiation has been proposed to overcome such problems but never has been tested. The fact that both isotopes are restricted, because of their military and strategic importance, has probably limited investigations and publications.

The essential experimental work and all clinical applications in neutron capture therapy are based on ^{10}B.

Kruger published the first experiments on BNCT in 1940 [27]. He treated tumor fragments in vitro with boric acid and neutron irradiation. After implantation in mice, these tumors showed a lower transplantation efficiency compared to controls, which have been treated only by boric acid or thermal neutrons, respectively. In the same year, Zahl et al. investigated the efficiency of NCT in vivo after injection of boric acid or boron in an oily suspension in a mouse sarcoma [28]. Quite soon, the treatment of brain tumors by NCT was proposed [29] suggesting a selective uptake of boron compounds in the tumor due to the missing blood–brain barrier there whereas the normal brain would be protected [30]. Higher boron concentrations in brain tumors than in normal brain were demonstrated in humans [31].

Ten years after the early biological experiments, first clinical applications in humans were performed. The history of clinical applications of BNCT can be divided in four sections:

- The early clinical applications in the USA from 1951 to 1961
- The pioneering work of Hatanaka and others in Japan from 1968 to end of the 1980s
- The period of prospective early clinical trials starting mid of the 1990s and still ongoing
- And finally the use of accelerator-based epithermal neutron facilities that will start nowadays

1.2 Early Clinical Applications in the USA

From February 1951 to January 1953, the first ten patients suffering from malignant glioma (probably glioblastoma multiforme) were treated at the Brookhaven Graphite Research Reactor [131–134]. Eight of these patients had previously undergone conventional radiation therapy for their brain tumor. Ninety-six percent ^{10}B-enriched borax was used as boron carrier. Immediately prior the irradiation, 100 ml of an aqueous solution containing 20 g borax was given as i.v. injection. No serious radiation-induced side effects were observed although the large amount of borax led to some toxicity [32, 33]. Irradiations were performed in one, two, or four fractions with intervals of 5–6 weeks. A short-time improvement of the clinical situation was observed in nine of the ten cases. All patients died of their progressive disease. The median survival of the patients in this first series was 97 days (43–185 days) and comparable to the results after treatment with photons.

The reactor was modified with the aim to optimize the facility prior starting a second series, which included nine patients suffering from highly malignant brain tumors. Now, sodium pentaborate was used, which showed less toxicity as compared to borax. The amount of ^{10}B administered was higher than in the first series. Now, serious side effects occurred such as untreatable radiodermatoses of the scalp, some with deep ulcerations [34]. The median survival was 147 days (93–337 days) [35].

In a third series of nine patients, immediately prior irradiation, sodium pentaborate was injected into the internal carotid artery of the tumor-bearing hemisphere with the intention to avoid high ^{10}B concentrations at the scalp. None of these patients developed severe skin reactions. The median survival was 96 days (29–158 days). This result was similar to the outcome after conventional radiotherapy at these days [36].

In a next step, it was intended to reduce the time of irradiation to a period where an optimal ^{10}B gradient between tumor and brain was expected. With the intention to increase the fluence rate, a compact high-flux reactor, the 5-MW water-moderated Brookhaven Medical Research Reactor (BMRR), was constructed. Between 1959 and 1961, 18 patients suffering from brain tumors were treated. Temporary skin flaps were reflected and protected by ^{6}Li shielding. Although this precaution avoided nonhealing ulcerations, it did not prevent radiation dermatitis altogether. Moreover, postoperative infections within the irradiation field occurred. Rises of intracranial pressure were treated by continuous drainage of the cerebrospinal fluid and by i.v. application of urea. Nevertheless, four out of 18 patients died within 2 weeks after irradiation because of cerebral edema and intractable shock. The median survival was 3 months (3–170 days) [35, 37].

At the same time period, another 17 patients (16 with glioblastoma, one with medulloblastoma) were irradiated at the reactor of the Massachusetts Institute of Technology after injection of ^{10}B-enriched 4-carboxlyphenyl boronic acid. Some of these patients received disodium decahydrodecarborate ($Na_2B_{10}H_{10}$) that is less toxic and contains much more boron [38]. The median survival in this cohort was 5.7 months [39]. This was similar to the survival time of patients treated by the same physicians at the Massachusetts General Hospital by conventional modalities. However, severe side effects such as acute brain edema and perivascular fibrosis but especially the appearance of brain necroses were observed within a few months [39, 40].

In 1961, these disappointing results lead to the cessation of BNCT in the USA for three decades. There are several explanations for these poor results: The boronated compounds available were not selectively accumulated in tumor tissue. Some of the observations only can be explained by high boron concentrations in blood, brain, and skin. A relevant part of the misadventure may be based on the poor depth-dose distribution of thermal neutrons, causing a low dose to the tumor and a high dose to the skin. Another important aspect however was the underestimation of the contribution to the applied dose from incident fast neutrons and photons as well as from the protons and gammas produced by nuclear reactions in the patient [36, 37, 41–43]. It also has to be reminded that in those days, corticosteroids to avoid brain edema after high-dose irradiation were not yet available.

1.3 The Pioneering Work in Japan

In 1968, Hiroshi Hatanaka started the renewal of BNCT introducing into clinical application the boron compound disodium mercaptoundecahydro-closo-dodecaborate $Na_2 B_{12}H_{11}SH$ (BSH), which was recently synthesized by Soloway et al. [44, 45]. The drug was intra-arterially injected. The treatment was performed after tumor excision as an intraoperative radiotherapy (Fig. 1.1) exposing directly the tumor bed and shielding of the skull [46–49]. Hatanaka reported exciting results, the 5-year survival rate being 58 % in a small group of highly selected patients suffering from malignant glioma grades 3 and 4 [48]. In 1989, I met him for the first time in Paris at the 17th International Congress of Radiology; he was very much concerned that nobody except me really appreciated his work and his results. This interaction resulted in a nice dinner together, and I obtained from him a print out of his results on computer paper, which I show here as Fig. 1.2. After some hesitations, these data stimulated worldwide new efforts to start new clinical trials outside of Japan.

The group around Hatanaka made a multitude of innovative approaches to BNCT that cannot be all mentioned here, such as the application of heavy water to the patient in order to obtain a better dose distribution [50, 51], BNCT for brain tumors in children [52], and pharmacokinetics of BSH [135].

Another pioneer from Japan has to be mentioned here, who introduced the second drug used in BNCT clinical trials: In 1987, Mishima started to treat superficial malignant melanoma using p-boronophenylalanine (BPA) [53–55]. It was supposed that the specific metabolic activities of malignant melanoma by producing melanin might facilitate the uptake of this analogon of a melanin precursor. Even if this hypothesis was not confirmed, BPA now is the drug mostly used in modern clinical trials for BNCT. The superficial localization of skin melanoma also allowed the treatment of these tumors with thermal neutron beams. This approach was an important step to apply BNCT for other tumors outside the central nervous system.

1.4 Epithermal Reactor-Based Neutron Sources and Prospective Clinical Trials

In the early 1990s, epithermal neutron sources were developed in the USA and Europe to treat deeper-seated tumors. These facilities created the conditions to start controlled prospective clinical trials at Brookhaven [56] and Cambridge (MA) [57] in 1994 and in Petten [58] in 1996. These were soon followed by the creation of similar facilities in Finland [59], Sweden [60], the Czech Republic [61], Japan [62–64], Argentina [65], and Taiwan [66] where patients were treated. The clinical indications for BNCT were extended to other diseases such as head and neck tumors [67–69], meningioma [70], pleural mesothelioma [71], and hepatocellular carcinoma [72]. All these clinical efforts cannot be described in detail in this chapter, but most of them are part of the content of the book you have in your hands.

Despite all these activities, BNCT has still to be considered as an experimental modality, and further research activities are mandatory to develop this promising

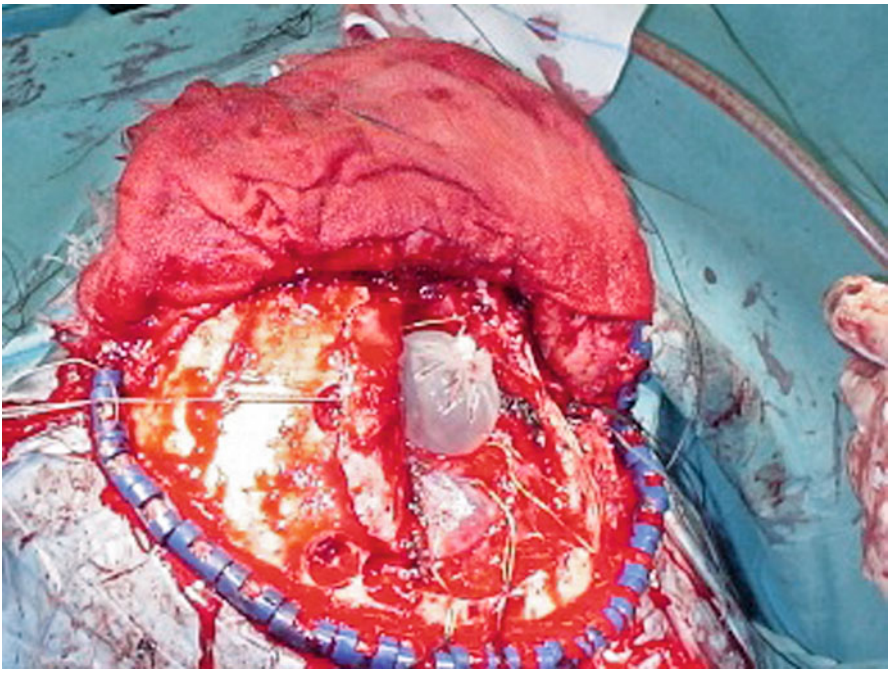

Fig. 1.1 Intraoperative BNCT performed by H. Hatanaka and Y. Nakagawa

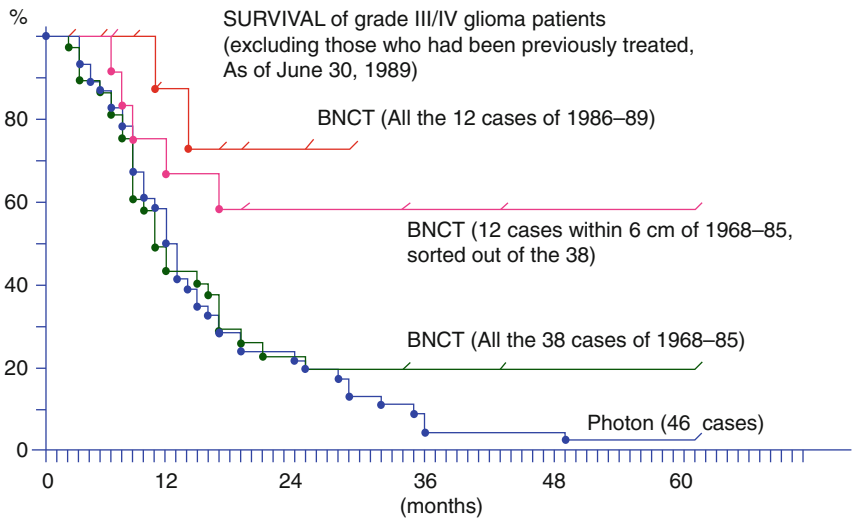

Fig. 1.2 Copy of H.Hatanaka's printed results shown 1989 at the 17th International Congress of Radiology in Paris

idea to a clinically available therapy. The real important progress in this period however was the realization that BNCT as a novel tumor therapy has to follow the normal procedures of evidence-based medicine. Preclinical efforts as well as clinical trials have to be designed to collect data that will permit regulatory authorities to approve this modality as therapy. The clinical trials themselves are highly complex, applying to a human patient "new," non-commercially available drugs and an irradiation beam not used in conventional radiotherapy.

One of the first groups, which was forced to follow this way, was created in the frame of several research projects supported by the European Commission around the HFR in Petten. The international approach that was demanded by EU Commission led to a situation where a German radiation oncologist had to irradiate a French or Austrian patient at a reactor owned by the EU Commission, the experimental drug being prepared and applied in a Dutch hospital. In this situation, regulatory authorities from different European countries were involved, and special efforts had to be made with respect to quality management on all levels concerning organizational aspects, medical physics and dose reporting, trial design and statistics, radiation protection, etc. [58, 73–85]. Special support given by the European Organisation for Research and Treatment of Cancer (EORTC) was a prerequisite to overcome such hurdles [58].

BNCT results in a highly complex dose distribution with different dose components having different biological effects. This challenging side of BNCT is addressed from the point of view of radiation biology and medical physics. International organizations started to recognize the need to develop standards. The IAEA published in 2001 a Technical Document on NCT [86]. In the frame of an EU research project, an international code of practice for dosimetry on BNCT was developed [87]. Radiobiologic and dosimetric intercomparison of epithermal beams at different facilities were started [88–91].

Instead of all these efforts and scientific progresses, an intrinsic problem leads to a severe backlash worldwide. Up to now, only nuclear reactors produce a (epi-)thermal neutron beam of an intensity high enough for BNCT. These facilities strongly depend from political support. For different reasons, most of the BNCT facilities that were constructed and opened in the 1990s had to interrupt patient treatments. These closures were due to political and economical reasons and not due to the clinical results. BNCT treatments actually are only possible at the Tsing Hua Open-pool Reactor (THOR) at National Tsing Hua University (Taiwan), and the RA-6 reactor at the Bariloche Atomic Center (Argentina).

1.5 Outside the Mainstream of BNCT

A far different approach was applied at Pavia where the thermal column at the TRIGA reactor was used to treat in two patients their explanted livers with multiple metastases from colorectal cancer followed by a retransplantation of the irradiated

Fig. 1.3 The isocentric gantry of the fast neutron therapy facility at the University Hosptial Essen (Germany)

organ [92–95]. One of the two patients survived for several years. This success stimulated other groups to evaluate further the possibility of an extracorporeal BNCT [96–102].

In the 1970s and 1980s of the last century, fast neutron therapy was perceived as an important contribution in the fight against cancer due to the high LET of these particles [103–106]. Unfortunately, a benefit of fast neutron therapy could only be demonstrated for some few indications in rare diseases [107–109]. Fast neutrons interacting with material are thermalized in tissues. It is possible to use this thermalized component to initiate neutron capture reactions and specifically enhance the radiation dose in tumor cells. Using the $^{10}B(n,\alpha)^{7}Li$ reaction to boost radiation effects in tumor cells would considerably enhance the therapeutic ratio of fast neutrons and avoid the problem of poor depth dose, poor collimation, and poor skin sparing. In multiple preclinical experiments, a neutron capture-enhanced fast neutron therapy has been developed [23, 110–128]. Despite of the promising results, a clinical trial has never been started. The thermalized component in a fast neutron beam will be larger in beams with relatively low primary energies. Two such fast neutron beams are still in use: the Essen Medical Cyclotron Facility installed in 1978 (Fig. 1.3), which produces d(14)+Be fast neutrons with a mean energy of approximately 5.8 MeV [23, 129], and the recently installed fast neutron therapy facility at FRM II in Munich [130]. BNCT-enhanced fast neutron radiotherapy may have a high therapeutic effectiveness in a wide variety of clinical situations and is without doubt an area of research that needs to be pursued.

1.6 Outlook on the Future

The key factor for success and failure in BNCT is first of all the collaboration between very different disciplines, ranging from nuclear physics to surgery, from chemistry to radiation oncology, and from mathematics to radiation biology. Such a diverse collection of intellect requires dedicated coordination structures to develop the synergies needed to move forward. A second important aspect is the availability of a reliable hospital-based neutron source. As long as this technical challenge cannot be realized, there will be no real progress in BNCT. The drug aspect, which in the past often has been perceived as the bottleneck of BNCT, is less important. The two drugs that have been used in clinical trials, namely, BSH and BPA, offer already a very good boron gradient between several tumors and surrounding normal tissues to design and continue clinical trials. Real progress in this area will only be possible when the pharmaceutical industry can be involved in a drug development program. A prerequisite for such expensive campaigns is the existence of a market for the drugs to be developed. Such a market can only be generated if accelerators for epithermal neutrons beams by become available in every large hospital.

References

1. Chadwick J (1932) The existence of a neutron. Proc R Soc London A 136:692–708
2. Taylor HJ, Goldhaber M (1935) Detection of nuclear disintegration in a photographic emulsion. Nature (London) 135:341–348
3. Locher GL (1936) Biological effects and therapeutic possibilities of neutrons. Am J Roentgenol Radium Ther 36(1):1–13
4. Garber DJ, Kinsey RR (1976) Neutron cross sections, 3rd edn. Brookhaven National Laboratory, New York
5. Mughabghab SF (1984) Neutron cross sections. Academic, Orlando
6. Kohlrausch F (1986) Praktische physik. B. G. Teubner, Stuttgart
7. Sears VF (1992) Neutron scattering lengths and cross sections. Neutron News 3(3):22–37
8. Brugger RM, Shih JA (1989) Evaluation of gadolinium-157 as a neutron capture therapy agent. Strahlenther Onkol 165(2–3):153–156
9. Akine Y, Tokita N, Matsumoto T, Oyama H, Egawa S, Aizawa O (1990) Radiation effect of gadolinium-neutron capture reactions on the survival of Chinese hamster cells. Strahlenther Onkol 166(12):831–833
10. Matsumoto T (1992) Transport calculations of depth-dose distributions for gadolinium neutron capture therapy. Phys Med Biol 37(1):155–162
11. Shih JA, Brugger RM (1992) Gadolinium as a neutron capture therapy agent. In: Allen BJ, Moore DE, Harrington BV (eds) Progress in neutron capture therapy for cancer. Plenum Press, New York/London, pp 183–186
12. Khokhlov VF, Yashkin PN, Silin DI, Djorova ES, Lawaczeck R (1995) Neutron capture therapy with gadopentetate dimeglumine: experiments on tumor-bearing rats. Acad Radiol 2(5): 392–398
13. Hofmann B, Fischer C-O, Lawaczeck R, Platzek J, Semmler W (1999) Gadolinium neutron capture therapy (GdNCT) of melanoma cells and solid tumors with the magnetic resonance imaging contrast agent gadobutrol. Invest Radiol 34(2):126–133
14. Tokuuye K, Tokita N, Akine Y, Nakayama H, Sakurai Y, Kobayashi T, Kanda K (2000) Comparison of radiation effects of gadolinium and boron neutron capture reactions. Strahlenther Onkol 176(2):81–83

15. Takahashi K, Nakamura H, Furumoto S, Yamamoto K, Fukuda H, Matsumura A, Yamamoto Y (2005) Synthesis and in vivo biodistribution of BPA-Gd-DTPA complex as a potential MRI contrast carrier for neutron capture therapy. Bioorg Med Chem 13(3):735–743
16. Salt C, De Stasio G, Schürch S, Casalbore P, Mercanti D, Weinreich R, Kaden TA (2002) Novel DNA-seeking contrast agents for gadolinium neutron capture therapy. In: Sauerwein W, Moss R, Wittig A (eds) Research and development in neutron capture therapy. Monduzzi Editore, Bologna, pp 803–806
17. Stalpers L, Stecher-Rasmussen F, Kok T, Boes J, van Vliet-Vroegindeweij C, Slotman B, Haveman J (2002) Radiobiology of gadolinium neutron capture therapy. In: Sauerwein W, Moss R, Wittig A (eds) Research and development in neutron capture therapy. Monduzzi Editore, Bologna, pp 825–830
18. Cerullo N, Bufalino D et al (2009) Progress in the use of gadolinium for NCT. Appl Radiat Isot 67(7–8 Suppl):S157–S160
19. Martin RF, D'Cunha G, Pardee M, Allen BJ (1988) Induction of double-strand breaks following neutron capture by DNA-bound Gd-157. Int J Radiat Biol 54(2):205–208
20. Martin RF, D'Cunha G, Pardee M, Allen BJ (1989) Induction of DNA double-strand breaks by 157-Gd neutron capture. Pigment Cell Res 2(4):330–332
21. Luessenhop AJ, Sweet WH, Robinson J (1956) Possible use of the neutron capturing isotope Lithium-6 in the radiation therapy of brain tumors. Am J Roentgenol 76:376–392
22. Sauerwein W, Heselmann I, Pöller F, Rassow J, Szypniewski H, Streffer C, Sack H (1992) Neutron capture reactions in a d(14)+Be fast neutron beam. In: Allen BJ, Moore DE, Harrington BV (eds) Progress in neutron capture therapy for cancer. Plenum Press, New York, London, pp 199–202
23. Sauerwein W (1993) Neutroneneinfangreaktionen zur Optimierung der Strahlentherapie mit schnellen Neutronen. Habiliationsschrift. Medizinische Fakultät der Universität GHS, Essen
24. Tobias CA, Weymouth PP, Wasserman LR, Stapleton GE (1948) Some biological effects due to nuclear fission. Science 107:115–118
25. Passalacqua F (1958) Untersuchungen über das Verhalten schwerer Elemente bei Tieren mit experimentellen Tumoren. Zur Speicherung von U-235-Nitrat in Ehrlich-Tumoren. Fortschr Röntgenstr 89(3):361–365
26. Liu HB, Brugger RM, Shih JL (1992) Neutron capture therapy with ^{235}U seeds. Med Phys 19(3):705–708
27. Kruger PG (1940) Some biological effects of nuclear disintegration products on neoplastic tissue. Proc Natl Acad Sci USA 26:181–192
28. Zahl PA, Cooper FS, Dunning JR (1940) Some in vivo effects of localized nuclear disintegration products on transplantable mouse sarcoma. Proc Natl Acad Sci USA 26(10):589–598
29. Zahl PA, Cooper FS (1941) Physical and biological considerations in the use of slow neutrons for cancer therapy. Radiology 37:673–682
30. Sweet WH (1951) The uses of nuclear disintegration in the diagnosis and treatment of brain tumor. N Engl J Med 245(23):875–878
31. Sweet WH, Javid M (1951) The possible use of slow neutrons plus boron-10 in the therapy of intracranial tumors. Trans Am Neurol Assoc 76:60–63
32. Conn HL, Antal BB, Farr LE (1955) The effect of large intravenous doses of sodium borate on the human myocardium as reflected in the electrocardiogram. Circulation 12:1043–1046
33. Locksley HB, Farr LE (1955) The tolerance of large doses of sodium borate intravenously by patients receiving neutron capture therapy. J Pharmacol Exp Ther 114:484–489
34. Archambeau JO (1970) The effect of increasing exposures of the $^{10}B(n,\alpha)^{7}Li$ reaction on the skin of man. Radiology 94:178–187
35. Slatkin DN (1991) A history of boron neutron capture therapy of brain tumours. Brain 114: 1609–1629
36. Slatkin DN, McChesny DD, Wallace DW (1986) A retrospective study of 457 neurosurgical patients with cerebral malignant glioma at the Massachusetts General Hospital 1952–1981: implications for sequential trials of postoperative therapy. In: Second international symposium on neutron capture therapy, Nishimura, Tokyo, pp 434–446

37. Sauerwein W (1993) Principles and history of neutron capture therapy. Strahlenther Onkol 169(1):1–6
38. Sweet WH, Soloway AH, Brownell GL (1963) Boron-slow neutron capture therapy of gliomas. Acta Radiol (Stockholm) 1:114–121
39. Asbury AK, Ojeman RG, Nielsen SL, Sweet WH (1972) Neuropathological study of fourteen cases of malignant brain tumor treated by boron-10 slow neutron capture radiation. J Neuropathol Exp Neurol 31(2):278–303
40. Farr LE, Calvo WG, Haymaker WE, Lippincott SW, Yamamoto YL, Stickley EE (1961) Effect of thermal neutrons on the central nervous system (apparent tolerance of central nervous system structures in man). Arch Neurol 4:246–257
41. Coderre JA, Glass JD, Micca P, Fairchild RG (1989) Neutron capture therapy for melanoma. Basic Life Sci 50(219):219–232
42. Goodman JH, Fairchild RG (1990) Boron neutron capture therapy for cerebral neoplasia. Perspect Neurol Surg 1(1):93–110
43. Farr LE (1991) Neutron capture therapy: years of experimentation – years of reflection. Report BNL-47087. Brookhaven National Laboratory, New York
44. Soloway AH, Hatanaka H, Davis MA (1967) Penetration of brain and brain tumor. VII. Tumor binding sulfhydryl boron compounds. J Med Chem 10:714–717
45. Hatanaka T (1969) Future possibility of neutron capture therapy of malignant tumors by use of low energy neutron from nuclear reactors and other sources. Gan No Rinsho 15(4): 367–369
46. Hatanaka H, Sano K (1972) A revised boron-neutron capture therapy for malignant brain tumors. In: Fusek I, Kunc Z (eds) Present limits in neurosurgery. Czechoslovak Medical Press, Prague, pp 83–85
47. Hatanaka H (1986) Boron-neutron capture therapy for tumors. Preface. In: Boron-neutron capture therapy for tumors. Nishimura Co. Ltd, Niigata
48. Hatanaka H (1990) Clinical results of boron neutron capture therapy. Basic Life Sci 54(15):15–21
49. Hatanaka H, Sweet WH, Sano K, Ellis F (1991) The present status of boron-neutron capture therapy for tumors. Pure Appl Chem 63(3):373–374
50. Takeuchi A, Kadosawa T, Hatanaka H (1988) Application of deuterium water to boron-neutron capture therapy of cerebral gliomas. In: 3rd international symposium on neutron capture therapy, Bremen, 1988, Abstract-book
51. Nakagawa Y, Hatanaka H, Moritani M, Kitamura K, Matsumoto K, Kobayashi M (1994) Partial deuteration and blood–brain barrier (BBB) permeability. Acta Neurochir Suppl Wien 60(410):410–412
52. Nakagawa Y, Pooh K, Kageji T, Kitamura K, Komatsu H, Tsuji F, Hatanaka H, Minobe T (1996) Boron neutron capture therapy for malignant brain tumors in children. Cancer neutron capture therapy. Mishima/Plenum Press, New York/London, pp 725–731
53. Mishima Y, Ichihashi M, Hatta S, Honda C, Sasase A, Yamamura K, Kanda K, Kobayashi T, Fukuda H (1989) Selective thermal neutron capture therapy and diagnosis of malignant melanoma: from basic studies to first clinical treatment. Basic Life Sci 50(251): 251–260
54. Mishima Y, Honda C, Ichihashi M, Obara H, Hiratsuka J, Fukuda H, Karashima H, Kobayashi T, Kanda K, Yoshino K (1989) Treatment of malignant melanoma by single thermal neutron capture therapy with melanoma-seeking 10B-compound [letter]. Lancet 2(8659):388–389
55. Mishima Y, Ichihashi M, Hatta S, Honda C, Yamamura K, Nakagawa T, Obara H, Shirakawa J, Hiratsuka J, Taniyama K, Tanaka C, Kanda K et al (1989) First human clinical trial of melanoma neutron capture. Diagnosis and therapy. Strahlenther Onkol 165(2–3):251–254
56. Chanana AD, Capala J, Chadha M, Coderre JA, Diaz AZ, Elowitz EH, Iwai J, Joel DD, Liu HB, Ma R, Pendzick N, Peress NS, Shady MS, Slatkin DN, Tyson GW, Wielopolski L (1999) Boron neutron capture therapy for glioblastoma multiforme: interim results from the phase I/II dose-escalation studies. Neurosurgery 44(6):1182–1193

57. Busse PM, Harling OK, Palmer MR, Kiger WS 3rd, Kaplan J, Kaplan I, Chuang CF, Goorley JT, Riley KJ, Newton TH, Santa Cruz GA, Lu XQ, Zamenhof RG (2003) A critical examination of the results from the Harvard-MIT NCT program phase I clinical trial of neutron capture therapy for intracranial disease. J Neurooncol 62(1–2):111–121
58. Sauerwein W, Zurlo A (2002) The EORTC boron neutron capture therapy (BNCT) group: achievements and future projects. Eur J Cancer 38(Suppl 4):S31–S34
59. Joensuu H, Kankaanranta L, Seppala T, Auterinen I, Kallio M, Kulvik M, Laakso J, Vahatalo J, Kortesniemi M, Kotiluoto P, Seren T, Karila J, Brander A, Jarviluoma E, Ryynanen P, Paetau A, Ruokonen I, Minn H, Tenhunen M, Jaaskelainen J, Farkkila M, Savolainen S (2003) Boron neutron capture therapy of brain tumors: clinical trials at the finnish facility using boronophenylalanine. J Neurooncol 62(1–2):123–134
60. Capala J, Stenstam BH, Skold K, Rosenschold PM, Giusti V, Persson C, Wallin E, Brun A, Franzen L, Carlsson J, Salford L, Ceberg C, Persson B, Pellettieri L, Henriksson R (2003) Boron neutron capture therapy for glioblastoma multiforme: clinical studies in Sweden. J Neurooncol 62(1–2):135–144
61. Dbaly V, Tovarys F, Honova H, Petruzelka L, Prokes K, Burian J, Marek M, Honzatko J, Tomandl I, Kriz O, Janku I, Mares V (2002) Contemporary state of neutron capture therapy in Czech Republic (part 2). Ces a slov Neurol Neurochir 66/99(1):60–63
62. Nakagawa Y, Pooh K, Kobayashi T, Kageji T, Uyama S, Matsumura A, Kumada H (2003) Clinical review of the Japanese experience with boron neutron capture therapy and a proposed strategy using epithermal neutron beams. J Neurooncol 62(1–2):87–99
63. Yamamoto T, Matsumura A, Nakai K, Shibata Y, Endo K, Sakurai F, Kishi T, Kumada H, Yamamoto K, Torii Y (2004) Current clinical results of the Tsukuba BNCT trial. Appl Radiat Isot 61(5):1089–1093
64. Ono K, Ueda S, Oda Y, Nakagawa Y, Miyatake S, Osawa M, Kobayashi T (1997) Boron neutron capture therapy for malignant glioma at Kyoto University reactor. In: Larsson B, Crawford J, Weinreich R (eds) Advances in neutron capture therapy, vol I. Elsevier Science, Amsterdam, pp 39–45
65. Gonzalez SJ, Bonomi MR, Santa Cruz GA, Blaumann HR, Calzetta Larrieu OA, Menendez P, Jimenez Rebagliati R, Longhino J, Feld DB, Dagrosa MA, Argerich C, Castiglia SG, Batistoni DA, Liberman SJ, Roth BM (2004) First BNCT treatment of a skin melanoma in Argentina: dosimetric analysis and clinical outcome. Appl Radiat Isot 61(5):1101–1105
66. Liu YW, Huang TT, Jiang SH, Liu HM (2004) Renovation of epithermal neutron beam for BNCT at THOR. Appl Radiat Isot 61(5):1039–1043
67. Kato I, Ono K, Sakurai Y, Ohmae M, Maruhashi A, Imahori Y, Kirihata M, Nakazawa M, Yura Y (2004) Effectiveness of BNCT for recurrent head and neck malignancies. Appl Radiat Isot 61(5):1069–1073
68. Aihara T, Hiratsuka J, Morita N, Uno M, Sakurai Y, Maruhashi A, Ono K, Harada T (2006) First clinical case of boron neutron capture therapy for head and neck malignancies using 18 F-BPA PET. Head Neck 28(9):850–855
69. Kankaanranta L, Seppala T, Koivunoro H, Saarilahti K, Atula T, Collan J, Salli E, Kortesniemi M, Uusi-Simola J, Makitie A, Seppanen M, Minn H, Kotiluoto P, Auterinen I, Savolainen S, Kouri M, Joensuu H (2007) Boron neutron capture therapy in the treatment of locally recurred head and neck cancer. Int J Radiat Oncol Biol Phys 69(2):475–482
70. Tamura Y, Miyatake S, Nonoguchi N, Miyata S, Yokoyama K, Doi A, Kuroiwa T, Asada M, Tanabe H, Ono K (2006) Boron neutron capture therapy for recurrent malignant meningioma. Case report. J Neurosurg 105(6):898–903
71. Suzuki M, Endo K, Satoh H, Sakurai Y, Kumada H, Kimura H, Masunaga S, Kinashi Y, Nagata K, Maruhashi A, Ono K (2008) A novel concept of treatment of diffuse or multiple pleural tumors by boron neutron capture therapy (BNCT). Radiother Oncol 88(2):192–195
72. Suzuki M, Sakurai Y, Hagiwara S, Masunaga S, Kinashi Y, Nagata K, Maruhashi A, Kudo M, Ono K (2007) First attempt of boron neutron capture therapy (BNCT) for hepatocellular carcinoma. Jpn J Clin Oncol 37(5):376–381

73. Gabel D, Sauerwein W (1994) Clinical implementation of boron neutron capture therapy in Europe. In: Amaldi U, Larsson B (eds) Hadrontherapy in oncology. Elsevier Science, Amsterdam, pp 509–517
74. Sauerwein W, Hideghéty K, Gabel D, Moss RL (1998) European clinical trials of boron neutron capture therapy for glioblastoma. Nuclear News 41(2):54–56
75. Hideghety K, Sauerwein W, Haselsberger K, Grochulla F, Fankhauser H, Moss R, Huiskamp R, Gabel D, de Vries M (1999) Postoperative treatment of glioblastoma with BNCT at the petten irradiation facility (EORTC protocol 11,961). Strahlenther Onkol 175(Suppl 2):111–114
76. Gahbauer R, Gupta N, Blue T, Sauerwein W, Wambersie A (2001) Reporting of BNCT irradiation: application of the ICRU recommendations to the specific situation in BNCT. In: Hawthorne MF, Shelly K, Wiersema RJ (eds) Frontiers in neutron capture therapy. Kluwer Academic/Plenum Publishers, New York, pp 565–569
77. Rassow J, Stecher-Rasmussen F, Voorbraak W, Moss R, Vroegindeweij C, Hideghéty K, Sauerwein W (2001) Comparison of quality assurance for performance and safety characteristics of the facility for boron neutron capture therapy in Petten/NL with medical electron accelerators. Radiother Oncol 59(1):99–108
78. Hüsing J, Sauerwein W, Hideghety K, Jöckel KH (2001) A scheme for a dose-escalation study when the event is lagged. Stat Med 20(22):3323–3334
79. Sauerwein W (2003) Therapeutic strategies for boron neutron capture therapy (boron imaging). Today's research for tomorrow's treatments – cell factory research projects with clinical relevance: 14–15. Publications Office of the EU Commission EUR20802 ISBN 92-894-5957-3
80. Verbakel WF, Sauerwein W, Hideghety K, Stecher-Rasmussen F (2003) Boron concentrations in brain during boron neutron capture therapy: in vivo measurements from the phase I trial EORTC 11961 using a gamma-ray telescope. Int J Radiat Oncol Biol Phys 55(3):743–756
81. Rassow J, Sauerwein W, Wittig A, Bourhis-Martin E, Hideghéty K, Moss R (2004) Advantage and limitations of weighting factors and weighted dose quantities and their units in boron neutron capture therapy. Med Phys 31(5):1128–1134
82. van Rij CM, Sinjewel A, van Loenen AC, Sauerwein WA, Wittig A, Kriz O, Wilhelm AJ (2005) Stability of 10B-L-boronophenylalanine-fructose injection. Am J Health Syst Pharm 62(24):2608–2610
83. Vos MJ, Turowski B, Zanella FE, Paquis P, Siefert A, Hideghety K, Haselsberger K, Grochulla F, Postma TJ, Wittig A, Heimans JJ, Slotman BJ, Vandertop WP, Sauerwein W (2005) Radiologic findings in patients treated with boron neutron capture therapy for glioblastoma multiforme within EORTC trial 11961. Int J Radiat Oncol Biol Phys 61(2):392–399
84. Wittig A, Moss RL, Stecher-Rasmussen F, Appelman K, Rassow J, Roca A, Sauerwein W (2005) Neutron activation of patients following boron neutron capture therapy of brain tumors at the high flux reactor (HFR) Petten (EORTC Trials 11961 and 11011). Strahlenther Onkol 181(12):774–782
85. Sauerwein W, Moss R (eds) 2009 Requirements for boron neutron capture therapy (BNCT) at a nuclear research reactor. EUR 2383 EN. Office for Official Publications of the European Commission, Luxembourg. EUR – Scientific and Technical Research series – ISSN 1018–5593. ISBN 978-92-79-12431-0. DOI 10.2790/11743
86. IAEA (2001) Current status of neutron capture therapy. IAEA-TECDOC-1223 Technical reports series. International Atomic Energy Agency, Vienna
87. Järvinnen H, Voorbraak WP, Auterinen I, Gonçalves IC, Grseen S, Kosunen A, Marek M, Mijnheer BJ, Moss RL, Rassow J, Sauerwein W, Savolainen, Serén T, Stecher-Rasmussen F, Uusi-Simola J, Zsolnay EM (2003) Recommendations for the dosimetry of boron neutron capture therapy (BNCT). NRG Report 21425/03.55339/C Petten (NL)
88. Gueulette J, Binns PJ, De Coster BM, Lu XQ, Roberts SA, Riley KJ (2005) RBE of the MIT epithermal neutron beam for crypt cell regeneration in mice. Radiat Res 164(6):805–809
89. Binns PJ, Riley KJ, Harling OK (2005) Epithermal neutron beams for clinical studies of boron neutron capture therapy: a dosimetric comparison of seven beams. Radiat Res 164(2): 212–220

90. Binns PJ, Riley KJ, Harling OK, Auterinen I, Marek M, Kiger WS 3rd (2004) Progress with the NCT international dosimetry exchange. Appl Radiat Isot 61(5):865–868
91. Binns PJ, Riley KJ, Harling OK, Kiger WS III, Munck af Rosenschöld PM, Giusti V, Capala J, Sköld K, Auterinen I, Serén T, Kotiluoto P, Uusi-Simola J, Marek M, Viererbl L, Spurny F (2005) An international dosimetry exchange for boron neutron capture therapy, part I: absorbed dose measurements. Med Phys 32(12):3729–3736
92. Zonta A, Prati U, Roveda L, Ferrari C, Valsecchi P, Trotta F, DeRoberto A, Rossella C, Bernardi G, Zonta C, Marchesi P, Pinelli T, Altieri S, Bruschi P, Fossati F, Barni S, Chiari P, Nano R (2000) La terapia per cattura neutronica (BNCT) dei tumori epatici. Boll Soc Med Chir 114(2):123–144
93. Nano R, Barni S, Chiari P, Pinelli T, Fossati F, Altieri S, Zonta C, Prati U, Roveda L, Zonta A (2004) Efficacy of boron neutron capture therapy on liver metastases of colon adenocarcinoma: optical and ultrastructural study in the rat. Oncol Rep 11(1):149–153
94. Roveda L, Zonta A, Staffieri F, Timurian D, DiVenere B, Bakeine GJ, Crovace A, Prati U (2009) Experimental modified orthotopic piggy-back liver autotransplantation. Appl Radiat Isot 67(7–8 Suppl):S306–S308
95. Zonta A, Pinelli T, Prati U, Roveda L, Ferrari C, Clerici AM, Zonta C, Mazzini G, Dionigi P, Altieri S, Bortolussi S, Bruschi P, Fossati F (2009) Extra-corporeal liver BNCT for the treatment of diffuse metastases: what was learned and what is still to be learned. Appl Radiat Isot 67(7–8 Suppl):S67–S75
96. Nievaart VA, Moss RL, Kloosterman JL, van der Hagen TH, van Dam H, Wittig A, Malago M, Sauerwein W (2006) Design of a rotating facility for extracorporal treatment of an explanted liver with disseminated metastases by boron neutron capture therapy with an epithermal neutron beam. Radiat Res 166(1):81–88
97. Wittig A, Malago M, Collette L, Huiskamp R, Buhrmann S, Nievaart V, Kaiser GM, Jockel KH, Schmid KW, Ortmann U, Sauerwein WA (2008) Uptake of two 10B-compounds in liver metastases of colorectal adenocarcinoma for extracorporeal irradiation with boron neutron capture therapy (EORTC Trial 11001). Int J Cancer 122(5):1164–1171
98. Wittig A, Moss R, Kaiser GM, Malago M, Nievaart V, Sauerwein WA (2009) Boron neutron capture therapy for an explanted organ: the logistical challenges. Appl Radiat Isot 67(7–8 Suppl):S302–S305
99. Hampel G, Wortmann B, Blaickner M, Knorr J, Kratz JV, Lizon Aguilar A, Minouchehr S, Nagels S, Otto G, Schmidberger H, Schutz C, Vogtlander L (2009) Irradiation facility at the TRIGA Mainz for treatment of liver metastases. Appl Radiat Isot 67(7–8 Suppl): S238–S241
100. Nagels S, Hampel G, Kratz JV, Aguilar AL, Minouchehr S, Otto G, Schmidberger H, Schutz C, Vogtlander L, Wortmann B (2009) Determination of the irradiation field at the research reactor TRIGA Mainz for BNCT. Appl Radiat Isot 67(7–8 Suppl):S242–S246
101. Cardoso J, Nievas S, Pereira M, Schwint A, Trivillin V, Pozzi E, Heber E, Monti Hughes A, Sanchez P, Bumaschny E, Itoiz M, Liberman S (2009) Boron biodistribution study in colorectal liver metastases patients in Argentina. Appl Radiat Isot 67(7–8 Suppl):S76–S79
102. Gadan M, Crawley V, Thorp S, Miller M (2009) Preliminary liver dose estimation in the new facility for biomedical applications at the RA-3 reactor. Appl Radiat Isot 67(7–8 Suppl):S206–S209
103. Catterall M, Rogers C, Thomlinson RH, Field SB (1971) An investigation into the clinical effects of fast neutrons. Methods and early observations. Br J Radiol 44(524):603–611
104. Catterall M, Bewley DK, Sutherland I (1977) Second report on results of a randomized clinical trial of fast neutrons compared with X or gamma rays in the treatment of advanced tumours of head and neck. Br Med J (London) 1:1642
105. Battermann JJ (1978) Clinical experience with fast neutrons in Amsterdam. Radiol Clin 47(6):464–472
106. Schmitt G, Sauerwein W, Scherer E (1981) Preliminary results of neutron irradiation of soft tissue sarcomas in Essen. J Eur Radiother 2:119–122
107. Laramore GE, Krall JM, Griffin TW, Duncan W, Richter MP, Saroja KR, Maor MH, Davis LW (1993) Neutron versus photon irradiation for unresectable salivary gland tumors: final report

of an RTOG-MRC randomized clinical trial. Radiation Therapy Oncology Group. Medical Research Council. Int J Radiat Oncol Biol Phys 27(2):235–240
108. Lindsley KL, Cho P, Stelzer KJ, Koh WJ, Austin-Seymour M, Russell KJ, Laramore GE, Griffin TW (1996) Clinical trials of neutron radiotherapy in the United States. Bull Cancer Radiother 83 Suppl(Suppl 1):78s–86s
109. Wambersie A, Menzel HG (1996) Present status, trends and needs in fast neutron therapy. Bull Cancer Radiother 83 Suppl((Suppl1)):68s–77s
110. Waterman FM, Kuchnir FT, Skaggs LS, Bewley DK, Page BC, Attix FH (1978) The use of B-10 to enhance the tumour dose in fast-neutron therapy. Phys Med Biol 23(4):592–602
111. Wakabayashi H, Yoshii K, Sasuga N, Yanagi H (1983) Mixed dose distributions of fast neutrons and boron neutron captures for the fast neutron beam from YAYOI. In: First international symposium on neutron capture therapy, Brookhaven, 1983, BNL 51730
112. Kadosawa T, Kawasaki T, Nishimura R, Ohashi F, Takeuchi A (1985) Possible use of fast neutrons in boron neutron capture therapy for expanded or deeply located tumor lesions. In: 2nd international symposium on neutron capture therapy, Nishimura, Tokyo (1986)
113. Sauerwein W, Ziegler W, Olthoff K, Streffer C, Rassow J, Sack H (1989) Neutron capture therapy using a fast neutron beam: clinical considerations and physical aspects. Strahlenther Onkol 165:208–210
114. Ziegler W, Sauerwein W, Streffer C (1989) Fast neutrons from the Essen Cyclotron can be used successfully for neutron capture experiments in vitro. Strahlenther Onkol 165:210–212
115. Wagner FM, Koester L (1989) Fast neutrons for BNCT. Strahlenther Onkol 165(2/3):115–117
116. Sauerwein W, Ziegler W, Szypniewski H, Streffer C (1990) Boron neutron capture therapy (BNCT) using fast neutrons: effects in two human tumor cell lines. Strahlenther Onkol 166:26–29
117. Pöller F, Sauerwein W, Rau D, Wagner FM, Olthoff K, Rassow J, Sack H (1990) Neutronenfluenzmessungen im d(14)+Be- Neutronenstrahlungsfeld des Zyklotrons in Essen. Strahlenther Onkol 166:426–429
118. Pöller F, Sauerwein W, Rassow J (1991) Dosimetry and fluence measurements with a new irradiation arrangement for neutron capture therapy of tumours in mice. Radiother Oncol 21:179–182
119. Pöller F, Sauerwein W, Rassow J (1993) Monte Carlo calculation of dose enhancement by neutron capture of 10B in fast neutron therapy. Phys Med Biol 38:397–410
120. Laramore GE, Wootton P, Livesey JC, Wilbur DS, Risler R, Phillips M, Jacky J, Buchholz TA, Griffin TW, Brossard S (1994) Boron neutron capture therapy: a mechanism for achieving a concomitant tumor boost in fast neutron radiotherapy. Int J Radiat Oncol Biol Phys 28(5):1135–1142
121. Pöller F, Sauerwein W (1995) Monte Carlo simulation of the biological effects of boron neutron capture irradiation with d(14)+Be neutrons in vitro. Radiat Res 142:98–106
122. Pöller F, Bauch T, Sauerwein W, Böcker W, Wittig A, Streffer C (1996) Comet assay study of DNA damage and repair of tumour cells following boron neutron capture irradiation with fast d(14)+Be neutrons. Int J Radiat Biol 70:593–602
123. Laramore GE, Risler R, Griffin TW, Wootton P, Wilbur DS (1996) Fast neutron radiotherapy and boron neutron capture therapy: application to a human melanoma test system. Bull Cancer Radiother 83 Suppl(Suppl 1):191s–197s
124. Ludemann L, Matzen T, Schmidt R, Scobel W (1996) BNCT as a boost for fast neutron therapy? Bull Cancer Radiother 83 Suppl(Suppl 1):198s–200s
125. Breteau N, Sauerwein W, Gabel D, Chauvel P (1997) Potentialisation par captures de neutrons pour les glioblasomes inextirpables. J Chim Phys 94:1872–1880
126. Pignol JP, Courdi A, Paquis P, Iborra-Brassart N, Fares G, Hachem A, Lonjon M, Breteau N, Sauerwein W, Gabel D, Chauvel P (1997) Potentialisation par Captures de Neutrons pour les glioblastomes inextirpables [Neutron capture enhancement of fast neutron irradiation for unremovable glioblastoma]. J Chim Phys Phys Chim Biol 94(10):1827–1830
127. Wittig A, Sauerwein W, Pöller F, Fuhrmann C, Hidghéty K, Streffer C (1998) Evaluation of boron neutron capture effects in cell culture using sulforhodamine-B assay and a colony assay. Int J Radiat Biol 73:679–690

128. Pöller F, Wittig A, Sauerwein W (1998) Calculation of boron neutron capture cell inactivation in vitro based on particle track structure and x-ray sensitivity. Radiat Environ Biophys 37:117–123
129. Rassow J (1979) Die Zyklotronanlage im Universitätsklinikum Essen CIRCE und PARCE. Biotechnische Umschau 3:36–46
130. Wagner F, Kneschaurek P, Kastenmüller A, Loeper-Kabasakal B, Kampfer S, Breitkreutz H, Waschkowski W, Molls M, Petry W (2008) The Munich fission neutron therapy facility MEDAPP at the research reactor FRM II. Strahlenther Onkol 184(12):643–646
131. Farr LE, Sweet WH, Locksley HB, Robertson JS (1954) Neutron capture therapy of gliomas using boron-10. Trans Am Neurol Assoc 79:110–113
132. Farr LE, Sweet WH, Robertson JS, Foster CG, Locksley HB, Sutherland DL, Mendelsohn ML, Stickley EE (1954) Neutron capture therapy with boron in the treatment of glioblastoma multiforme. Am J Roent Ther Nucl Med 71:279–293
133. Farr LE, Robertson JS, Stickley EE (1954) Physics and physiology of neutron capture therapy. Proc Natl Acad Sci USA 40:1087–1093
134. Godwin JT, Farr LE, Sweet WH, Robertson JS (1955) Pathological study of eight patients with glioblastoma multiforme treated by neutron capture therapy using boron 10. Cancer 8:601–615
135. Kageji T, Nakagawa Y, Kitamura K, Matsumoto K, Hatanaka H (1997) Pharmacokinetics and boron uptake of BSH (Na2B12H11SH) in patients with intracranial tumors. J Neurooncol 33(1–2):117–130

Part I

Neutron Sources

Fission Reactor-Based Irradiation Facilities for Neutron Capture Therapy

2

Otto K. Harling and Kent J. Riley

Contents

2.1 Introduction

The principal objective of beam design for neutron capture therapy is to create a uniform distribution of low-energy (thermal) neutrons in the targeted treatment volume which may include a margin around the enhancing tumor as well as regions with suspected infiltrating disease. Buildup and broadening in the thermal neutron distribution are usually evident that are created as incident, higher energy neutrons slow down via elastic scattering interactions while passing through hydrogenous

O.K. Harling
Nuclear Science and Engineering Department,
Massachusetts Institute of Technology, Cambridge, MA, USA
e-mail: oharling@mit.edu

K.J. Riley (✉)
Massachusetts General Hospital,
Boston, MA, USA
e-mail: kriley@rmdinc.com

W.A.G. Sauerwein et al. (eds.), *Neutron Capture Therapy*,
DOI 10.1007/978-3-642-31334-9_2, © Springer-Verlag Berlin Heidelberg 2012

tissue. Tumor dose conformity is attained by thermal neutron capture in boron that is selectively targeted to the tumor and retained during irradiation. This binary strategy mitigates the need for complex tailoring of the beam spatial profile. The treatment volume can therefore be considerably larger than in conventional radiotherapy as the dose absorbed in normal tissue from the neutron beam itself is smaller than neutron capture in tumors containing boron. Neutron beams do require collimation to help avoid irradiating organs or other normal tissues peripheral to the field that may be radiosensitive or retain some of the administered boron. The adventitious dose whether from neutrons interacting with the constituents of normal tissue or boron retained in normal tissue should also be limited for critical organs both inside and outside the treatment volume. Judicious selection of the neutron beam characteristics helps to fulfill many of these aims. However, in a clinical setting, treatment planning calculations are performed to optimize tumor doses within the constraints of normal tissue dose limits by simulating various beam placements, aperture sizes, and even beam filtration options. Clinical trials in BNCT have thus far comprised mainly investigations into the safety and feasibility of this experimental modality, and the available clinical data are insufficient to fully optimize therapeutic beam delivery. Consequently, although certain neutron beam characteristics are known to be desirable, irradiation *facilities* must be versatile and able to adapt by making tradeoffs in beam characteristics as clinical experience is gained.

2.1.1 Beam Characteristics

A number of computational studies provide useful guidance on desirable characteristics for neutron beams used in BNCT [6, 9, 13, 39, 47, 53, 57–59]. More general requirements for NCT facilities have been outlined elsewhere [38], and fission reactor sources for NCT have been reviewed critically [20].

The earliest trials of BNCT employed low-energy thermal neutrons because these beams are relatively easy to create with virtually negligible unwanted fast neutron and gamma-ray contamination using a fission reactor. Thermal neutrons do not possess enough energy to penetrate deeply into tissue, and the absorbed dose profiles for the inherent, nonselective beam components therefore have maxima near the surface. These beams are therapeutically useful for superficial and relatively shallow tumors at depths of less than approximately 4 cm in tissue, depending on selectivity of the tumor boron uptake. In the earliest human clinical trials at Brookhaven (1951–1961) and at the Massachusetts Institute of Technology (1959–1961) [50], thermal neutrons were used for treatment of brain cancer, glioblastoma multiforme (GBM). Intraoperative NCT irradiations were used by Dr. W Sweet in these trials [16] because slow neutrons could not adequately penetrate to the tumor site, and this approach was subsequently continued in Japan under the leadership of Dr. H. Hatanaka [24].

Recognizing the benefit of external beam radiotherapy where deep-seated tumors (e.g., near the brain midline, approximately 8 cm deep laterally) are treated without the need to surgically reflect tissue and bone, researchers began to consider more

energetic neutron beams that could achieve the desired buildup of thermal neutrons at depth in tissue. Intermediate energy or epithermal neutrons undergo moderation in tissue and produce improved thermal neutron distributions at significantly greater depths in tissue than is possible with slow neutrons. Optimizing the therapeutic parameters of beams for neutron capture therapy soon became a major subject of study in BNCT with particular emphasis on the neutron energy spectrum that is incident upon the patient.

Early studies on the effects of the incident neutron energy used Monte Carlo calculations to determine RBE-weighted depth-dose profiles along the central axis of a representative phantom and derive figures of merit collectively called advantage parameters that indicate relative performance in terms of tumor dose rate, therapeutic selectivity, and beam penetration [13]. These studies used geometrical phantoms of water or polyethylene to represent the clinical target volume and unidirectional as well as monoenergetic neutron beams or simplified energy spectra without contamination from unwanted neutrons or photons. Moreover, these optimizations were necessarily independent of other important parameters such as tumor size/location, boron uptake in tissue and tumor, beam/target size, collimation, and dose weighting factors. Indeed, increasing beam collimation as well as increasing aperture size relative to the target was found to significantly improve figures of merit by deepening penetration of the thermal neutron component [57]. Aperture size, collimation, and beam placement are also critical aspects for limiting dose to organs at risk in or near the treatment field and for minimizing patient whole-body exposure that can lead to secondary cancers or other radiation-induced injuries. As computational techniques advanced, more sophisticated multiparameter optimizations were undertaken to determine how factors such as tumor location or boron uptake influence the outcome of optimizations [6, 39]. These studies confirmed earlier results, indicating that a broad range of neutron energies from approximately 1 eV up to tens of keV are therapeutically advantageous for external beam NCT with the keV range appearing generally useful for a broad range of tumor depths and boron uptake. There does not appear to be a well-defined neutron energy range that is optimum for all therapeutic conditions envisioned. The optima are slowly varying and depend upon tumor location, size, normal tissue constraints, boron uptake, and other factors. Beams comprising a range of neutron energies are perhaps therefore most suitable for BNCT at this stage of development with flexibility incorporated into the beam delivery system to facilitate investigating new ideas derived from accrued clinical results.

As reactor-based NCT centers began to develop and implement resonance scattering filters that produce beams of epithermal neutrons, the necessary tradeoffs between beam intensity and purity from unwanted photons and neutrons rapidly became apparent. An epithermal beam intensity of 10^8 n cm^2 s^{-1} results in a peak absorbed dose rate in brain of approximately 0.025 Gy min^{-1}, and this was near the minimum feasible for beginning safety-related dose-escalation trials where peak brain doses of 8–10 Gy were specified. The kerma for epithermal neutrons in tissue is approximately 2×10^{-12} Gy cm^2 [18], and restricting total beam kerma from unwanted photons as well as fast and thermal neutrons to less than 10 % of this (2×10^{-13} Gy cm^2) is a desirable objective to avoid degrading therapeutic beam

performance. The filtration needed to achieve this, however, significantly reduces beam intensity, and many facility designers instead found it necessary or practical to accept higher levels of contamination, recognizing that boron retained in normal tissue will also contribute to the nonselective dose. A study of measurements in 7 different clinical epithermal neutron beams found that when boron retention in normal tissue is 18 μg g^{-1} (as with boronated phenylalanine, BPA), further deleterious effects in beam penetration and therapeutic ratio occur only at relatively high contamination levels greater than approximately 3×10^{-12} Gy cm^2. Significant degradation in the advantage parameters is, however, apparent for all but the lowest beam contamination levels when a very low amount of boron is retained in tissue, for example, less than 1 μg g^{-1} as with more advanced compounds currently under development [4].

2.1.2 Beam Monitoring and Control

Reliably and reproducibly administering the prescribed dose in external beam therapy requires a method for monitoring and integrating beam output while a radiation field is administered. In BNCT, most of the absorbed dose is derived from neutron interactions in tissue, and so a method is needed for monitoring neutrons transmitted by the beam. Uranium-lined fission counters are used in many systems [21, 41, 51] because they easily discriminate against the gamma rays inevitably contained in the beam and can be fabricated with the sensitivity necessary for sampling output in the epithermal energy range without significantly perturbing beam characteristics. Helium or boron gas-filled detectors are also a good choice for these reasons and have been used successfully at some clinical centers. These detectors are inherently sensitive to thermal neutrons, and it is therefore common practice to use a thermal neutron-absorbing shroud such as cadmium to reduce this response, which may arise from neutrons that backscatter toward the detector in either the collimator or patient. Gamma rays emitted by the beam itself sometimes comprise a nonnegligible portion of the absorbed dose in tissue, and beam monitoring systems may therefore contain either ionization chambers or Geiger-Müller detectors that are sensitive to gamma rays. In practice, since this dose component mostly derives from activation of beamline components, it is generally proportional to the neutron output of the beam, and the gamma-ray monitor is used only for informational purposes. The beam monitoring system is frequently equipped with a computer for displaying and archiving readings from the beam monitors throughout an irradiation.

The administered neutron fluence may also be monitored in situ by activation foils or wires usually comprised of gold that are inserted in the cavity remaining after surgical resection of the tumor [1, 27]. Activation foils are insensitive to gamma rays and for low neutron energies have an energy-dependent response very similar to that for neutron capture in boron. These measurements therefore accurately record the thermal neutron fluence in unresected tumor for individual patients, and this information can be used to determine absorbed dose. Since activation wires are

integrating passive dosimeters, irradiations are frequently paused to remove the wire (or in some cases, the wire is remotely removed) for counting (measurement of the activation) that enables a determination of the remaining irradiation time. These measurements may also be augmented with small thermoluminescent dosimeters (TLDs) to measure the gamma-ray dose in situ. Although wires and TLDs may be affixed to the skin for monitoring external beam irradiations, this approach is most practical for intraoperative BNCT where detectors may be implanted near the tumor. Relatively long irradiations are required for this technique to ensure that there is enough time to complete the necessary measurements and determine the appropriate stopping time.

The precision and accuracy required for timing control in patient irradiations are inversely proportional to beam intensity. Irradiations using higher intensity beams are invariably shorter, and small errors in starting or stopping the irradiation become a relatively larger proportion of the administered field. As fields become increasingly short, on the order of minutes, an automated control system with safety interlocks is needed to help avoid human errors inadvertently causing a significant deviation from the planned exposure.

Various methods are used to control NCT beams, but fields are invariably based on integral beam monitor readings since beam output, although normally constant during an irradiation, is dictated by reactor operating conditions which can vary from day to day, especially at multipurpose reactors. Some research reactors such as the FiR-1 in Finland have a short beamline without much space for beam control shutters. This reactor is dedicated to BNCT research and beam output is controlled by manipulating reactor power. Beam output is not constant during the early part of these irradiations as the reactor gradually approaches full power, but this effect is taken into account by the beam monitors. Irradiations may be terminated rapidly by lowering reactor power or inserting all control rods to scram the reactor.

At facilities such as Petten and MIT, the reactor operates continuously for long period of time to service a variety of experimental needs, and it is not feasible to alter reactor power except in the case of an emergency. These facilities therefore employ a series of beamline shutters to turn the beam on and off, enabling free access to the medical room even when the reactor is at full power. Normally there is at least one beamline shutter that controls the irradiation by acting quickly enough so that the irradiation has a well-defined start and stop time.

2.1.3 Irradiation Facility and Patient Support

The experimental hall of most existing research reactors is enclosed by a containment building that is not easily penetrated or expanded and therefore represents a fixed boundary constraining the available space for constructing medical facilities. The epithermal beams used in NCT research require approximately 1 m of concrete shielding to keep ambient radiation levels low while the facility is in use, and this combined with space required for other experiments supported

by the reactor often severely restricts the available options for NCT irradiation and patient support facilities. Design of the medical irradiation room is most important to mitigate constraints inherently imposed by the fixed beamline by providing enough space to accommodate staff and equipment as well as flexibility to orient the patient in any direction for fields on any part of the body. An area outside the therapy room to accommodate equipment for beam monitoring and control is also needed, and this space must be large enough for beam operators as well as responsible medical personnel to monitor the patient. Each of these components (including the shielding walls) must be carefully sized so as to avoid adversely impacting their functionality while meeting available space constraints. Other important facilities such as simulation setup areas or examination and observation rooms for pre- and postirradiation procedures although ideally located near the therapy room can be accommodated outside the containment building where space constraints are less severe.

Layout inside the therapy room is dictated by the fixed and usually horizontal beamline which ideally is centered in the room some distance from the entrance to avoid complications from entering and exiting traffic. A beamline about waist high above the floor is a comfortable working position for staff and is easiest for patients getting on and off the therapy table. Relatively short patient-to-aperture distances of a few cm or less are used in BNCT because these beams spread significantly in air, except at Petten where the beam is highly collimated and an air gap of 30 cm does not adversely affect beam characteristics. In the former cases, patient positioning is made easier by bringing the beam into the room through a cone-shaped collimator that affords space near the aperture to orient the patient at any angle to the beam. This is also convenient because the collimator is then readily accessible from inside the medical room so that differently sized or shaped apertures can be easily implemented. A photograph from the Harvard-MIT clinical trials is shown in Fig. 2.1 where the long protruding collimator is used to set up a lateral field irradiation with a small air gap of 3 cm.

Wall and ceiling mounted lasers to illuminate the beam central axis enable using field setup practices developed for conventional radiotherapy, and this improves patient comfort by making setup easier and more efficient. Axial back pointing and beam's eye view lasers as implemented in the MIT therapy room are also useful for confirming beam entry or exit that may be used as a reference in treatment plans. At the FiR-1 reactor in Finland, a mock-up of the beamline with a specially designed docking couch is used to pre-position the patient outside the therapy room where more space is available. Once the patient is in place, the couch may be moved into the therapy room and accurately positioned using a matching dock and coordinate settings on the couch [29].

Two-way audio communication between the control console and therapy room is important for both operational convenience and safety so that staff may easily communicate and monitor the patient during irradiations. Visual monitoring is similarly important, and this is often done via closed-circuit television. Some facilities are also equipped with a shielded window which is not susceptible to electric power failure and helps reassure the patient with a view to outside the room.

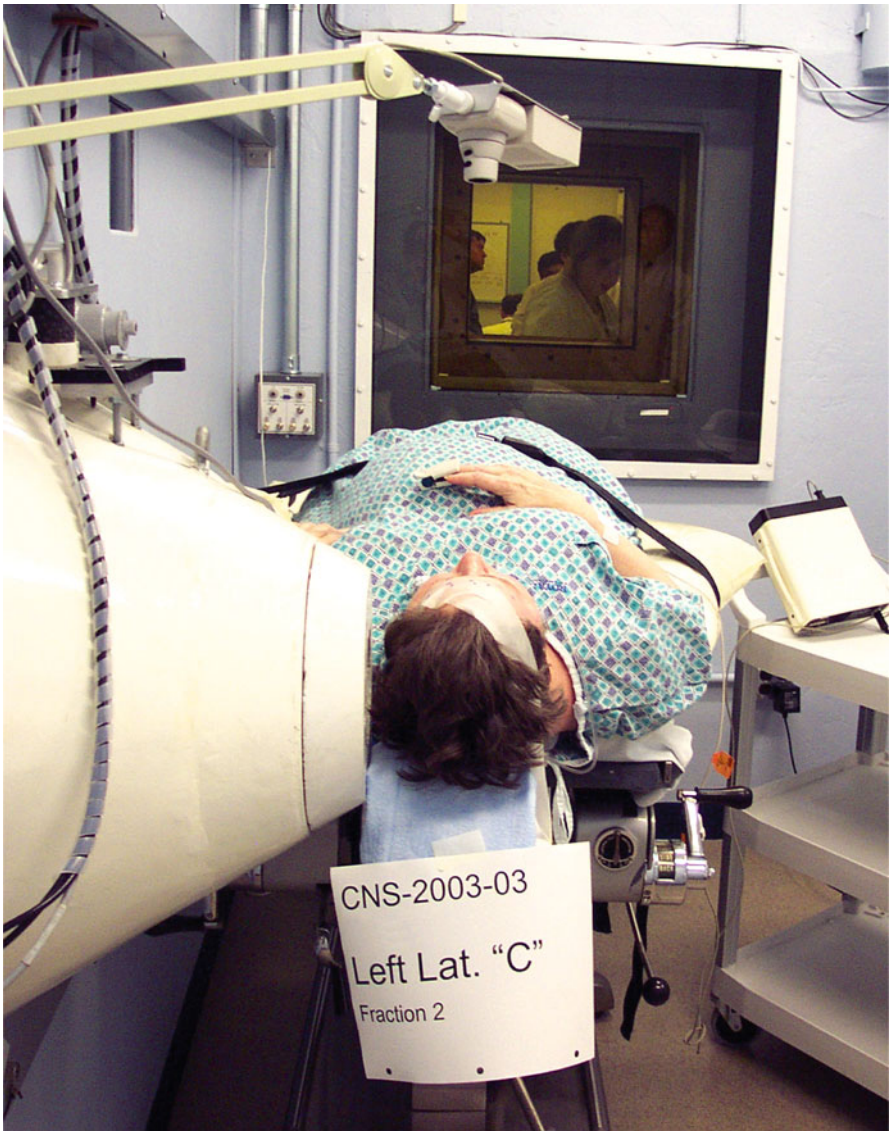

Fig. 2.1 A lateral field irradiation setup using the long protruding collimator in the MIT FCB and an air gap of 3 cm

2.1.4 Summary

This section described epithermal neutron irradiation facilities using fission reactor sources, which together with currently approved boron delivery drugs can attain useful therapeutic effect for tumors up to approximately 9-cm depth in soft tissue.

The following characteristics and capabilities are recommended for future NCT facilities to enable efficient and productive clinical studies as well as more routine clinical use where higher throughput may eventually be needed:

1. High intensity to facilitate delivering radiation fields in several minutes as is normally done with conventional photon therapy. Short irradiation times also enable better temporal targeting of the beam during the optimum boron pharmacokinetic window that may be relatively brief. Additional beam intensity is invaluable for improving other beam parameters such as collimation, purity, or energy filtration that may eventually prove advantageous and which will inevitably reduce beam output. Short irradiation times also significantly improve patient comfort and reduce the need for rigid restraint to keep the patient properly positioned.
2. The neutron beam purity and energy spectrum should achieve a therapeutic ratio greater than unity up to and beyond 9-cm depth using a boron delivery drug like BPA where tissue and tumor uptake is approximately 18 and 65 μg g^{-1}, respectively.
3. Well-collimated beams, with an accessible portion of the beamline near the patient, and a wide range of apertures is desirable. This will afford flexibility in treatment planning for a variety of treatment sites using multiple beam placements, in an effort to optimize tumor dose while restricting dose to sensitive organs in the field and keeping whole-body exposure acceptably low.
4. A large (approximately 9 m^2 or larger) shielded medical irradiation room with a long, protruding beam snout, or patient collimator, eases patient setup and enables comfortably placing beams for any envisioned tumor site. Figure 2.1 illustrates the use of a long patient collimator during a lateral brain irradiation at the MIT FCB.
5. The NCT irradiation facility should be able to operate reliably with high capacity factor and, if needed, 24 h/day and 7 days/week.
6. Systems for observing, monitoring, and communicating with the patient inside the medical therapy room are necessary.
7. An automated beam monitoring and control system which ensures accurate dose delivery by precisely monitoring beam output with interlocks to help assure safety of both patients and staff is essential.
8. A system for conveniently positioning the patient and aligning the planned irradiation fields is important.

Specific parameters based on these criteria for epithermal neutron irradiation facilities are summarized in Table 2.1. Reactor-based epithermal neutron facilities are able to meet or exceed these first-order requirements and thereby help advance clinical research in BNCT. A few facilities presently fulfill all of these criteria, and several others satisfy most except, for example, intensity or contamination. Regardless of the parameters, each facility used in clinical BNCT plays an important role by accruing valuable information that is needed to develop this modality. Clinical experience gained with the beams available today is needed to guide future designs or modifications and to help judge the relative importance of various beam

Table 2.1 Suggested performance characteristics of epithermal neutron irradiation facilities for BNCT of brain tumors (or comparable soft tissue) using the tumor-targeting agent BPA and associated weighting factors [14]

Characteristics	Desired facility performance for BPA
Neutron and photon beam contamination	$<2\times10^{-12}$ Gy cm^{2a}
Advantage depth (useful penetration)	>8 cm
Energy	~0.4 eV < E < ~10–20 keV
Collimation (calculated current to flux ratio)	$J/\varphi > 0.75$
Beam aperture	Adjustable size and shape, 0–16 cm diam. for brain
Intensity, epithermal neutron flux	$\geq 2\times10^{9}$ n cm^{-2} s^{-1b}
Treatment time	~10 min
Patient positioning	Beam placement on any part of the body facilitated by a long protruding collimator, large irradiation room, visual field alignment tools
Beam control	Fluence delivery to ± 1 % of prescription
	Safety interlocks to protect staff and patient
Patient support	Visual and audio communication for monitoring patient, rapid egress during emergencies

[a]Equivalent to 2.8 × 10–12 Gy cm^2 when applying weighting factors of 3.2 and 1.0 for photons and neutrons respectively

[b]Higher intensities are desirable for tumors with deeper target volumes or when using more advanced compounds with lower uptake in tissue (but with improved selectivity) to keep irradiation times as short as possible

parameters for sustaining or possibly improving clinical performance. Most BNCT irradiation facilities available today are suitable for this purpose, and the best are able to accommodate more advanced clinical implementations where significantly higher patient throughput is needed.

The following sections discuss two different approaches for using fission reactors as sources for epithermal neutron-based NCT. The performance of current reactor-based epithermal neutron facilities is described, illustrating how they satisfy the operational characteristics outlined above, followed by a section on a state-of-the-art epithermal irradiation facility as well as a concluding summary.

2.2 Approaches to Using Reactors for Epithermal Neutron NCT

In the past, neutron beam facilities for NCT have not generally been part of the original design specifications for research or test reactors. The two exceptions are the Massachusetts Institute of Technology Research Reactor (MITR) [52] and the now decommissioned Brookhaven Medical Research Reactor (BMRR) [17], both of which were commissioned in the 1950s when interest in testing the

concept of BNCT initially developed. The NCT facilities at these reactors were designed specifically for thermal neutron NCT and were used in the early clinical studies during the 1950s. During the 1990s, Brookhaven [32] and MIT [46] each constructed epithermal neutron beams at these reactors that were subsequently used in more recent trials of BNCT. More recently, a new, small (30 kW) reactor specifically designed for NCT has been constructed near a hospital site in Beijing, China [19]. This is the first reactor constructed specifically for BNCT since the 1950s and may become the first modern facility suitable for hospital siting.

Research interest in BNCT grew rapidly in the 1990s, and as the feasibility of external beam irradiations became clear, a significant number of research or test reactors were modified to incorporate epithermal neutron beams. The most common approach for retrofitting these reactors is to use the reactor core directly as the source for the epithermal neutron beam [2, 7, 11, 12, 33, 35, 40, 46, 49]. Reactors ranging in power from 100 kW to several MW have been successfully converted using this approach. Examples include the low-power (250 kW) Finnish reactor FiR-1 [2], the 1 MW Washington State University Reactor [40], and the high-power (45 MW) test reactor, HFR, at Petten [42]. Small, low-power ultrasafe reactors could also be built to obtain high-performance epithermal neutron beams using designs that are specifically optimized for BNCT. These reactors would require only 100–300 kW of fission power because core neutrons could be used directly as a source for the epithermal neutron beam. Several preliminary designs have been proposed for this type of special purpose reactor [30, 31]. These special purpose NCT reactors could be expected to meet the requirements for clinical investigations of BNCT as well as more routine clinical treatments.

Another approach to modifying existing reactors for epithermal NCT is to use a subcritical array of fuel called a fission converter originally proposed by Rief et al. [43] that is located outside the reactor core and driven by thermalized neutrons from the moderator. The first such facility, known as the fission converter beam (FCB), was constructed at the MITR [22, 23, 25]. A few other fission converter-based beams have been designed, one for the 3-MW BMRR [32] and another for the 2 MW McClellan Air Force Base Reactor [34]. A fission converter is particularly appropriate for higher power or multipurpose research reactors without a movable core that support a broad range of experiments. These reactors cannot accommodate frequent power changes or shutdowns that are used for beam control at some low-power facilities without integrated beamline shutters. Moreover, due to the large number of experimental stations at some reactors, it is often impractical or impossible to install a medical room near the reactor core to attain the necessary epithermal neutron flux. A fission converter could be incorporated into the initial design of a multipurpose research or test reactor to help accommodate the desired experimental facilities. Whether using a fission converter or the reactor core directly, careful consideration of the NCT facility during the initial reactor design should generally result in better and less expensive facilities than those made by retrofitting existing reactors.

2.3 Performance of Some Current Epithermal Neutron Irradiation Facilities

Table 2.2 summarizes parameters and figures of merit published for most epithermal neutron beams that have been used in NCT clinical trials together with pertinent details about the corresponding irradiation facilities. The figures of merit are described in detail elsewhere [14] and are good first-order indicators of beam performance. More sophisticated analyses, such as treatment plans for identical targets showing tumor isodose contours as well as dose to nearby normal tissue, are beyond the scope of this chapter. The data in Table 2.2 are taken from an experimental study comparing seven different clinical epithermal neutron beams [4] as well as published reports on the performance and features of the irradiation facilities [1, 49, 55]. Unless otherwise noted, the figures of merit (where available) are all derived using a common set of dose conversion parameters, boron concentrations, and weighting factors that are representative of brain irradiations using both BPA and an advanced compound.

The advantage depth (AD) or useful beam penetration should exceed a minimum of 8 cm if external beam brain irradiations are contemplated. An 8–10-mm-thick filter of pure ^{6}Li as in the case of the Studsvik and MIT beams hardens the neutron energy spectrum and provides a significant increase in AD, thereby improving dose coverage for the deepest tumors [5]. A lithium filter does, however, reduce therapeutic margin in shallow tumors and is associated with a roughly 50 % reduction in beam intensity that increases treatment time. ^{6}Li filtration is therefore best used as an option for deeper tumors in beams with the highest intensity where the reduced output does not lead to excessively long irradiations. All of the currently available epithermal neutron beams achieve an AD of at least 8 cm with BPA, increasing significantly when parameters for an advanced compound are applied, where the most penetrating beams have an AD exceeding 11 cm.

The advantage ratio (AR) is the total tumor-to-normal-tissue dose ratio averaged from the beam entrance to the advantage depth. This varies between five and six in most beams when using BPA which indicates an average tumor dose five to six times higher than in nearby normal tissue. The advantage ratio is generally higher in beams with lower contamination, but this figure of merit depends principally on the boron uptake parameters, increasing to nearly 12 for an advanced compound in the cleanest beams.

High beam intensity is important to minimize treatment times. Short irradiations are more comfortable for the patient and more efficient for clinical staff. Shorter fields also mitigate degradation in the therapeutic advantage that may occur as the compound is washed out of tissue and tumor following administration. However, patient throughput is at present limited by the clinical resources available to BNCT rather than the duration of irradiations or the capacity and availability of suitable neutron sources. High beam intensity is nevertheless desirable for the reasons described earlier and for future development to enable larger, more comprehensive studies that rigorously evaluate the efficacy of this modality. Table 2.2 lists the incident epithermal flux intensity together with the irradiation time to reach a

Table 2.2 Facility characteristics and beam performance figures of merit for various clinical NCT centers determined by in-air and in-phantom measurements using BPA and where available (in brackets) a hypothetical advanced boron compound

	MIT FCB								
	w/o filter	Li filter	Studsvik	FiR-1	BMRR	ReZ	HFR	KUR[a]	JRR-4
AD (cm)	9.3 (11.3)	9.9 (11.7)	9.7 (11.2)	9.0 (10.5)	9.3 (10.6)	8.6 (9.5)	9.7 (11.0)	8.0	–
AR	6.0 (11.8)	5.7 (10.7)	5.6 (10.1)	5.8 (10.9)	6.0 (11.9)	4.2 (6.2)	5.4 (9.3)	5.7	–
Time to reach 12.5 RBE Gy (min)	6.7 (14)	12.5 (25)	19 (31)	28 (52)	38 (77)	24 (31)	66 (104)	44	–
φ_{epi} (10^9 n cm^{-2} s^{-1})	6.4	3.0	1.4	1.2	1.1	0.60	0.33	0.46	2.2
Photon contamination (10^{-13} Gy cm^2)	3.6	4.6	12.6	0.9	1.5	10.8	3.8	2.8	2.6
Fast neutron contamination (10^{-13} Gy cm^2)	1.4	2.3	8.3	3.3	2.6	16.9	12.1	6.2	3.1
Beam diameter (cm)	12		14×10 (rectangular)	14	12	12	12	12	15
Protruding collimator	Y		Y	N	Y	N	N (high collim.)	N	N
Positioning angles (°)	180		180	<180	180	<180	180	<180	<180
Medical room area (m^2)	14			6.4	20	8.8	12.2	7.8	27

Boron concentrations of 18 and 65 μg g^{-1} are assumed in normal brain and tumor tissue, respectively, for BPA and 0.65 and 65 μg g^{-1} for the advanced compound. The applied RBEs are 1.0 for photons and 3.2 for neutrons. The cRBEs are 1.35 in brain and 3.8 in tumor for BPA and 3.8 in both tissue and tumor for the advanced compound

[a]Advantage parameters for the KUR epithermal neutron beam are reported for tumor and brain boron concentrations of 40 and 11.4 μg g^{-1}, respectively

peak brain dose of 12.5 Gy (w) using a single field that is representative of irradiations in the brain cancer trials performed to date. Irradiation time is inversely related to the incident epithermal neutron flux although the two quantities are not directly proportional. MIT and Studsvik with the highest beam intensities can reach tolerance doses in several minutes, and this duration is comparable to fields routinely administered with other forms of radiotherapy. Irradiations at other facilities last two to six times longer than those at MIT, and these are manageable for clinical investigations but would become a limiting factor with significant increases in clinical enrollment. Irradiation times could also become substantially longer in trials using better tumor-targeting agents where the normal tissue dose rate is lower due to much lower retention of boron in normal tissue.

Neutron beam characteristics are relatively straightforward to quantify, and based on the clinical experience to date, some of the most recently constructed facilities have reached a practical optimum in terms of intensity, beam purity, and therapeutic effectiveness. The operational characteristics of these irradiation facilities are, however, equally important for implementing clinical programs and eventually incorporating new ideas derived from translational and preclinical research. Reactor-based beamlines are fixed (usually horizontal), but many designs have incorporated flexibility in terms of beam delivery and patient positioning as summarized in the bottom four rows of Table 2.2. Brain irradiations in BNCT normally apply circular beam apertures with diameters ranging from 12 to 16 cm. Variable aperture sizes are used at several facilities, and these are helpful in minimizing collateral dose and improving tumor dose conformity while restricting doses to organs at risk.

A highly collimated neutron beam also helps to minimize normal tissue dose and is associated with increased beam penetration [4] that can improve coverage for deep-seated tumors. Good collimation eases patient positioning and minimizes uncertainties associated with dose falloff from the aperture of the beam. In the FCB facility at MIT, the epithermal neutron flux decreases at a rate of approximately 0.7 % mm^{-1}, and the routinely applied air gap of 3 cm modestly reduces intensity of the incident beam by approximately 20 % [45]. Positioning uncertainties of approximately 5 mm therefore result in up to a 3.5 % error in the administered dose which is comparable to other sources of uncertainty. An even larger air gap between the patient and beam aperture is feasible at the facility in Petten where the neutron beam has extraordinarily high collimation and intensity drops by less than 20 % over 30 cm from the beam aperture. The full width at half maxima (FWHM) of epithermal neutron profiles measured in air 30 cm from the collimator are only 10 % (or less) wider than the nominal beam aperture. Patients may therefore be positioned at this distance without adversely affecting beam targeting, and axial positioning uncertainties are negligible [42].

A beam collimator that protrudes into the medical room helps to comfortably position patients, especially in cranial irradiations where the shoulders of the patient may interfere. With the advent of relatively intense and pure epithermal neutron beams, greater consideration is now being given to operational characteristics,

for example, in Finland where the facility was recently modified to make patient positioning easier [3]. A long, protruding patient collimator accessible from inside the irradiation room that can be readily adapted to accommodate apertures of different sizes or shapes affords more beam placement options and greater flexibility in treatment planning and facilitates easier patient setups for a multitude of disease sites. A medical therapy room with an area of approximately 9 m^2 centered about the beam is large enough to accommodate the length of a patient for either side of a lateral brain irradiation. Some of the facilities listed in Table 2.2 are larger than this and have ample space for the patient and associated monitoring equipment. Field placement may however still be encumbered by room geometry that restricts angles relative to the beam centerline for positioning patients. An example is the medical room at JRR-4 which is spacious but long and narrowest near the beam aperture so patient positions are relatively restricted. Facilities with less than a full 180º arc for positioning patients about the beam centerline are noted in Table 2.2.

Some facilities have incorporated options to control the neutron energy spectrum by adding one or more tanks to the beamline that can be filled with heavy water to moderate neutrons with low parasitic absorption [12, 49, 55]. Other groups have augmented their beamline to accommodate cassettes containing solid lithium metal which hardens the neutron energy spectrum and may be added or removed as needed [5, 12]. Reactor-based beamlines can therefore extract neutrons spanning the entire energy range of interest in BNCT from thermal up to ~10 keV, and this may prove advantageous because no single neutron energy is optimum for tumors at all depths in tissue.

Clinical trials in BNCT have thus far been carried out exclusively with reactor-based neutron sources. This reflects the suitability and relative abundance of the aforementioned facilities that are located at research reactors around the world near large metropolitan areas with research hospitals. Several accelerator-based sources are being developed for BNCT, mainly in physics research laboratories. Research results from these programs indicate that intensities for these sources must increase by more than an order of magnitude over currently achievable levels to match the beam characteristics of existing reactor-based beams [8, 10, 15, 28, 56]. The limitations arise mainly from engineering challenges in beamline and target development, and if these problems are resolved, accelerator-based sources may become a competitive option for clinical research. Accelerator-based beamlines could be more readily transferred to a radiation oncology center than reactor-based sources.

2.4 A State-of-the-Art Epithermal Neutron Irradiation Facility

A state-of-the-art epithermal neutron irradiation facility was designed and constructed at MIT to meet all of the requirements for a clinical BNCT research facility with the capability for high patient throughput in support of larger clinical trials or more routine therapy. Constructed at the 6 MW MITR, the FCB provides

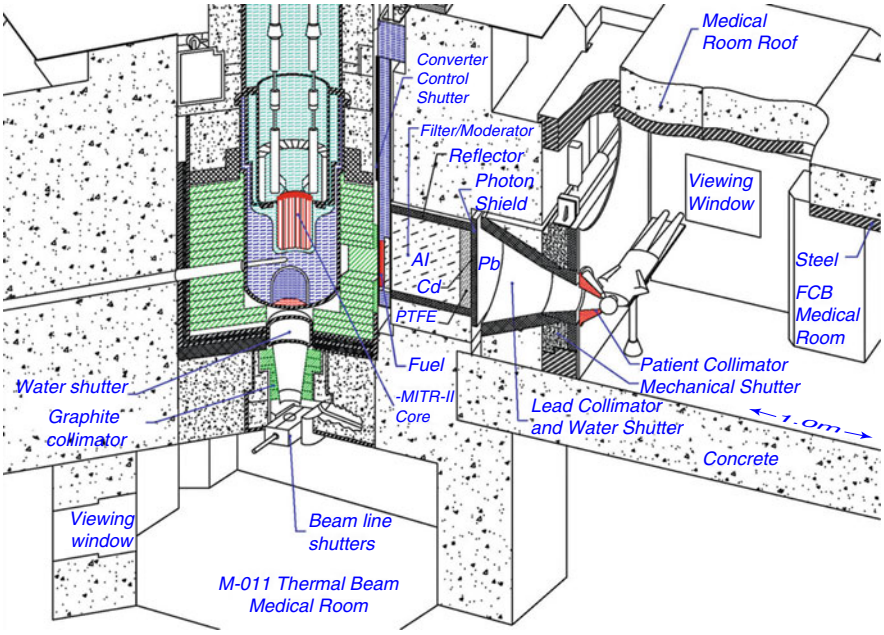

Fig. 2.2 Isometric drawing of the MITR-II depicting components of the vertical thermal neutron beam and (horizontal) fission converter-based epithermal neutron beam

a high-performance irradiation facility suitable for clinical studies and large animal experiments that is capable of administering irradiations to several patients a day in support of larger trials or more routine clinical implementation. A fission converter-based neutron source comprised of a subcritical array of fuel was chosen because the reactor core is fixed in the center of the surrounding reflector/moderator, making it difficult to access core neutrons directly. Figure 2.2 shows an isometric view of the FCB epithermal neutron irradiation facility [22, 23]. Also depicted in the lower left-hand corner of Fig. 2.2 are the vertical thermal neutron beamline and medical irradiation room that were included in the original design of the MITR and provide a high-quality thermal neutron beam for NCT research. The fission converter is presently configured to produce 120 kW by using 11 standard MITR-II fuel elements cooled with D_2O and was designed and licensed to operate up to 250 kW. Considerable increases in neutron source strength are therefore possible in the future, which can be achieved by using an optimized converter fuel rather than MITR fuel elements or by increasing the reactor power. Details on the characteristics and performance of the epithermal neutron beam are documented elsewhere [44].

A shielded horizontal beamline 2.5 m long directs neutrons from the converter to the treatment room as shown schematically in Fig. 2.2. The beamline consists of a series of Al (81 cm), Teflon® (13 cm), and Cd (0.5 mm) neutron filter/moderators; a

lead photon shield (8 cm); and a large conical collimator 1.1 m long with lead walls 15 cm thick that is followed by a final patient collimator. An experimental study of radiation damage effects has verified that the fluorine contained in Teflon® is chemically stable and the material retains adequate mechanical properties during the expected lifetime of the FCB [23]. The 0.42-m-long patient collimator is made from a mixture of lead and boron or lithium-loaded (95 % enriched in ^{6}Li) epoxy that extends the beamline into the shielded medical therapy room. The patient collimator has provisions for inserting a cassette into the beamline that contains an 8-mm-thick lithium metal disc (also 95 % enriched in ^{6}Li). This filter hardens the neutron beam by removing some of the lower energy neutrons and can increase the useful therapeutic beam penetration for deep-seated tumors.

The neutron beam is controlled by three in-line shutters acting independently that are installed along the length of the beamline. The first of these, starting near the reactor core, is the converter control shutter (CCS) that is a 0.5-mm layer of Cd followed by a 6.4-mm sheet of aluminum alloyed with boron of natural isotopic abundance. This shutter modulates the fission rate in the converter (and beam intensity) between 1 and 100 % by shielding the converter fuel against thermal neutrons incident from the MITR-II reflector region. Downstream from the converter fuel is a 68-cm-long tank that when filled with light water provides effective neutron attenuation. Following this is the mechanical shutter that effectively turns the beam on and off (reducing beam intensity by 2–3 orders of magnitude) within 3 s during therapy and comprises a large sliding slab to fill a section of the collimator with a 20-cm thickness of borated (100 mg cm^{-3} ^{10}B) high-density ($\rho = 4.0$ g cm^{-3}) concrete and 20 cm of lead. The room entrance is shielded from direct beam radiation by a short hallway as well as a 0.28-m-thick steel door driven by an air motor that opens the door in 10 s.

The medical room in Fig. 2.3 is built with 1.1 m-thick walls of high-density concrete with a roof of 15 cm-thick steel beneath 55 cm of high-density concrete. The wall of the medical room nearest the FCB control console includes a large window containing layers of quartz and lead glass as well as mineral oil as shown schematically in Fig. 2.3. Inner surfaces of the walls and ceiling are lined with 2.5 cm of borated polyethylene to absorb thermal neutrons and reduce activation of the steel-reinforced concrete walls and steel ceiling. A 1 cm thick boron loaded epoxy ground reduces activation of the concrete floor.

During operation at full beam intensity, dose equivalent rates outside the medical room are a maximum of 12 μSv h^{-1} measured behind the rear wall opposite the beam, with no significant neutron contribution. Since the observed values are only marginally higher than the nominal background of approximately 8 μSv h^{-1} in the reactor hall without the converter operating, no additional access control to the experimental hall is required when the FCB is in use. Inside the medical room with all shutters closed, a dose equivalent rate of 100 μSv h^{-1} is apparent at the patient position (somewhat higher immediately following an irradiation) that is due entirely to photons emanating from the beamline. General area dose rates of approximately 20 μSv h^{-1} are observed away from the patient collimator in the medical room with

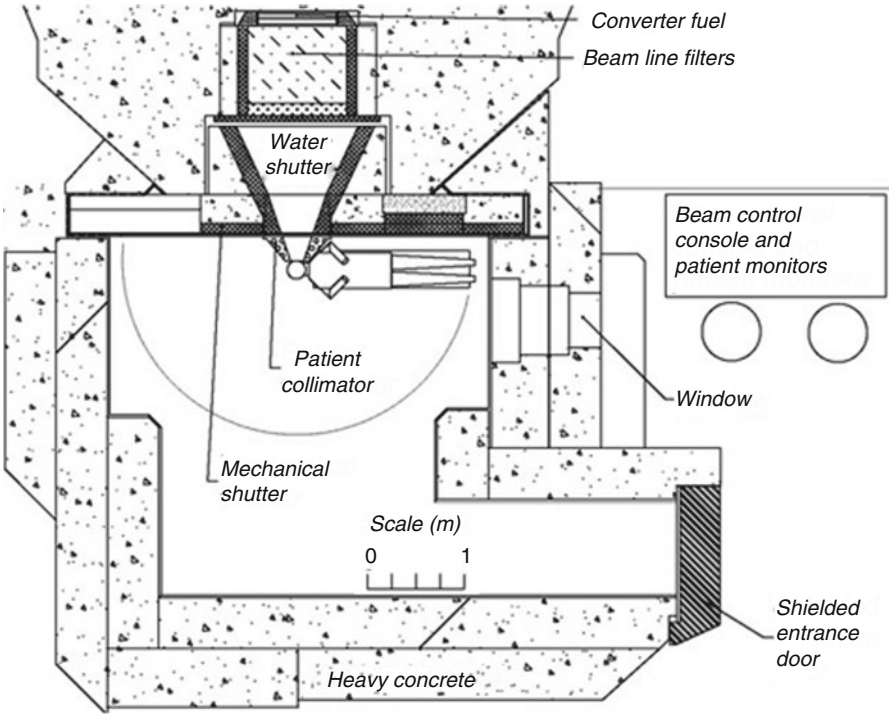

Fig. 2.3 Plan view of the medical irradiation facility for the MIT fission converter-based epithermal neutron beam

the reactor at full power, and staff can therefore freely enter the room without the need to lower reactor power.

The beam centerline in the medical room is 0.42 m above the floor, and the patient collimator can be readily configured to provide aperture diameters of 80, 100, 120, and 160 mm that conveniently extend up to 0.42 m beyond the wall of the medical room. The collimator diameter tapers from 0.67 m at its base to 0.3 m near the patient, and this, combined with ample (14 m^2) floor space in the medical room allows patients to be comfortably positioned for cranial irradiations in a full 180° arc around the beam centerline while lying supine on the treatment couch. A laser projection illuminates the central axis of the beam to help with patient positioning as well as optics that penetrate the wall of the collimator to provide a beam's eye view. Prior to commencing an irradiation, the laser and optics are withdrawn and replaced with a plug that has a composition identical to the patient collimator walls.

Four fission counters positioned in the periphery of the beam near the base of the patient collimator operate in pulse mode and serve as integral monitors of the neutron fluence as it is delivered to the patient. Fields are prescribed as an integral number of counts in these detectors based on a correlation with absorbed dose

measurements that are used to benchmark treatment plans [26]. Signals are fed to NIM electronics, and irradiations are administered with a redundant pair of programmable logic controlled (PLC) systems that automatically terminates the irradiation when the integrated counts on any of the four beam monitors reach the prescribed target. Data from instrumentation in the FCB cooling system and beamline shutters are also fed to the PLCs, which are programmed with automated interlocks to help ensure the safety of the patient and operational staff alike. The facility is operated from the control console that includes a dedicated computer for displaying progress of an irradiation and archiving data from the PLCs. During an irradiation, the patient and his or her vital signs are monitored through the shielded viewing window and closed-circuit cameras which contain an integrated audio system for two-way communication between the medical room and control console.

Prior to commencing an irradiation, a series of safety interlocks must be satisfied before the shutters can be opened to turn the beam on. The prescribed monitor units are entered using a numeric keypad on the console. The operator commences therapy with a single pushbutton, and the PLCs issue commands to open each shutter in sequence and initiate data acquisition. It takes 2 min for all shutters to open. Monitor counts accumulate continuously on the updated display. The PLCs repeatedly interrogate all safety interlocks, check that the accumulated monitor counts are below the preset targets, and store the data to the computer in programmed intervals of 10 s. Like conventional radiotherapy machines, no other actions are required from the operator unless they need to intervene, for which there is a manual override that terminates an irradiation by closing shutters or scramming the reactor. When the accumulated counts on any one of the four beam monitors first reach the set target, the PLCs signal all shutters to close. To defend against overexposures that might be caused by some mechanical or electrical failure during shutter closure, programmed safety interlocks automatically scram the reactor if any channel exceeds 102 % of the prescribed target value [21, 54].

Controls for opening shutters are deactivated when the shield door to the medical room is open to help prevent inadvertent beam exposure of staff inside the room. The entrance to the medical room is equipped with motion sensors that stop sideways movement of the pneumatically operated 11 t shielding door if anyone is in the vicinity and pressure-sensitive strips run along its leading edge to stop the door upon any contact.

Loss of building power would automatically scram the MITR-II, but if electrical power fails only to the medical area, uninterruptible power supplies keep the PLCs, computer, and other vital instrumentation running for at least 20 min to enable an irradiation field to be completed as planned. The mechanical shutter can be rapidly closed using a hand crank located on the outside of the room, while the water shutter and CCS close automatically under the force of gravity. The shielding door can also be opened by hand in an emergency to quickly gain access to the medical room.

The fission converter concept has proven suitable for obtaining a high-purity beam of epithermal neutrons for BNCT with intensities that result in irradiation times as short as a few minutes. The relatively low power (120 kW) generated in the converter illustrates the efficiency of the fission process for producing epithermal beams and the feasibility of small reactor-based sources for dedicated use in a hospital.

Since the MITR-II is not dedicated solely to BNCT research, the FCB operates independently of other experiments and does not affect regular reactor operation. The beamline is presently optimized for brain tumor studies although it can be easily reconfigured to treat other disease sites. The operational characteristics of the facility closely match those established for conventional radiotherapy, which together with nearly optimum beam characteristics ensure that the FCB is capable of determining whether the radiobiological promise of this cellular tumor-targeting therapy can be realized in routine practice.

2.5 Summary

This short chapter provides some guidance for those planning to design and construct reactor-based epithermal neutron irradiation facilities for neutron capture therapy. Important performance capabilities for these facilities are presented, and different approaches for using reactors as epithermal neutron irradiation facilities are described. Reactor-based facilities that are presently available generally meet the requirements for clinical studies with more recently constructed facilities making important advances in terms of patient comfort, flexibility, and ease of use. A few of the newer facilities can support larger clinical trials with high patient throughput that is typical of more routine clinical application. Patient throughput and development of BNCT are presently not restricted by the characteristics of existing reactor-based facilities but rather by the level of resources committed to BNCT that in some programs are by necessity centered at institutes hundreds of kilometers away instead of nearby hospitals. Epithermal neutron beams designed for BNCT have been optimized based upon established clinical programs and the trial experience gathered thus far. Additional optimization or customization may become desirable as more data are accrued and a clinical rationale is developed for exploring other tumors outside the brain. Although gains from these optimizations are likely to be small compared, for example, with those derived from improved boron targeting, new facilities should nevertheless seek to incorporate flexibility into beamline designs to be able to realize the full benefit of progress in clinical research. At present, a strong basis for widespread implementation of BNCT does not exist, and it is difficult to envision a major demand for new neutron sources. New reactor-based BNCT facilities could be constructed if needed by modifying more research reactors as described in this chapter or by using currently available and well-proven technology to construct low-power ultrasafe reactors.

References

1. Akutsu H, Yamamoto T, Matsumura A, Shibata Y, Nakai K, Yasuda S, Matsushita A, Nose T, Yamamoto K, Kumada H, Hori N, Torii Y (2000) In: 9th international symposium on neutron capture therapy. International Society for Neutron Capture Therapy, Osaka, 2000, pp 199–200
2. Auterinen I, Hiismäki P, Kotiluoto P, Rosenberg RJ, Salmenhara S, Seppälä T, Seren T, Tanner V, Aschan C, Kortesniemi M, Kosunen A, Lampinen J, Savolainen S, Toivonen M, Välimäki P

(2001) Metamorphosis of a 35 year-old TRIGA reactor into a modern BNCT facility. In: Hawthorne MF (ed) Frontiers in neutron capture therapy, vol I. Kluwer Academic/Plenum Publishers, New York, pp 267–275
3. Auterinen I, Kotiluoto P, Hippeläinen E, Kortesniemi M, Seppälä T, Serén T, Mannila V, Pöyry P, Kankaanranta L, Collan J, Kouri M, Joensuu H, Savolainen S (2004) Design and construction of shoulder recesses into the beam aperture shields for improved patient positioning at the FiR1 BNCT facility. Appl Radiat Isot 61:799–803
4. Binns PJ, Riley KJ, Harling OK (2005) Epithermal neutron beams for clinical studies of boron neutron capture therapy: a dosimetric comparison of seven beams. Radiat Res 164:212–220
5. Binns PJ, Riley KJ, Ostrovsky Y, Gao W, Albritton JR, Kiger WS III, Harling OK (2007) Improved dose targeting for a clinical epithermal neutron capture beam using optional ^{6}Li filtration. Int J Radiat Oncol Biol Phys 67:1484–1491
6. Bisceglie E, Colangelo P, Colonna N, Santorelli P, Variale V (2000) On the optimal energy of epithermal neutron beams for BNCT. Phys Med Biol 45:49–58
7. Blaumann HR, Calzetta-Larrieu O, Longhino JM, Albornoz AF (2001) NCT facility development and beam characterization at the RA-6 reactor. In: Hawthorne MF, Shelly K, Wiersema RJ (eds) Frontiers in neutron capture therapy, 1st edn. Kluwer Academic/Plenum Publishers, New York, pp 313–317
8. Bleuel DL, Donahue RJ, Ludewigt BA, Vujic J (1998) Designing accelerator-based epithermal neutron beams for boron neutron capture therapy. Med Phys 25:1725–1734
9. Brugger RM, Constantine G, Harling OK, Wheeler FJ (1990) Rapporteurs' report. In: Harling OK, Bernard JA, Zamenhof RG (eds) Neutron beam, design, development and performance for neutron capture therapy. Plenum Press, New York, p 54
10. Burlon AA, Kreiner AJ (2008) A comparison between a TESQ accelerator and a reactor as a neutron sources for BNCT. Nucl Instrum Methods Phys Res B 266:763–771
11. Burn KW, Casalini L, Martini S, Mazzini M, Nava E, Petrovich E, Rosi G, Sarotto M, Tinti R (2004) An epithermal facility for treating brain gliomas at the TAPIRO reactor. Appl Radiat Isot 61:987–991
12. Capala JA, Stenstam BH, Sköld K, Munck af Rosenschöld P, Giusti V, Persson C, Wallin E, Brun A, Franzen L, Carlsson J, Salford L, Ceberg C, Persson B, Pellettieri L, Henriksson R (2003) Boron neutron capture therapy for glioblastoma multiforme: clinical studies in Sweden. J Neurooncol 62:135–144
13. Clement SD, Choi JR, Zamenhof RG, Harling OK (1990) Monte Carlo methods of neutron beam design for neutron capture therapy at the MITR-II. In: Harling OK, Bernard JA, Zamenhof RG (eds) Neutron beam, design, development and performance for neutron capture therapy. Plenum Press, New York, pp 51–70
14. Coderre JA, Makar MS, Micca PL, Nawrocky MM, Liu HB, Joel DD, Slatkin DN, Amols HI (1993) Derivations of relative biological effectiveness for the high-LET radiations produced during boron neutron capture irradiations of the 9L rat gliosarcoma in vitro and in vivo. Radiat Res 27:1121–1129
15. Culbertson CN, Green S, Mason AJ, Picton D, Baugh G, Hugtenburg RP, Yin Z, Scott MC, Nelson JM (2004) In-phantom characterization studies at the Birmingham accelerator-generated epithermal neutron source (BAGINS) BNCT facility. Appl Radiat Isot 61: 734–738
16. Farr LE, Sweet WH, Robertson JS, Foster CG, Locksley HB, Sutherland DL, Mendelsohn ML, Stickley EE (1954) Neutron capture therapy with boron in the treatment of glioblastoma multiforme. Am J Roentgenol Radium Ther Nucl Med 71:279–293
17. Godel JB (1960) Description of facilities and mechanical components, medical research reactor (MRR) Brookhaven National laboratory, BNL-600, Brookhaven National Laboratory, Upton
18. Goorley JT, Kiger WS III, Zamenhof RG (2002) Reference dosimetry calculations for neutron capture therapy with comparison of analytical and voxel models. Med Phys 29:145–156
19. Guotu K, Ziyong, S, Feng, S (2009) The study of physics and thermal characteristics for in hospital neutron irradiator (IHNI). Appl Radiat Isot 67:S234-S7
20. Harling OK, Riley KJ (2003) Fission reactor neutron sources for neutron capture therapy – a critical review. J Neurooncol 62:7–17

21. Harling OK, Moulin SJ, Chabeuf JM, Solares GS (1995) On-line beam monitoring for neutron capture therapy at the MIT research reactor. Nucl Instrum Methods Phys Res B 101:464
22. Harling OK, Riley KJ, Newton TH, Wilson BA, Bernard JA, Hu LW, Fonteneau EJ, Menadier PT, Ali SJ, Sutharsan B, Kohse GE, Ostrovsky Y, Stahle PW, Binns PJ, Kiger WS III, Busse PM (2002) The fission converter based epithermal neutron irradiation facility at the Massachusetts Institute of Technology reactor. Nucl Sci Eng 140:223–240
23. Harling OK, Kohse GE, Riley KJ (2002) Irradiation performance of polytetrafluoroethylene (Teflon ®) in a mixed fast neutron and gamma radiation field. J Nucl Mater 304:83–85
24. Hatanaka H (1975) A revised boron-neutron capture therapy for malignant brain tumors. II. Interim clinical result with the patients excluding previous treatments. J Neurol 209:81–94
25. Kiger WS III, Sakamoto S, Harling OK (1999) Neutronic design of a fission converter-based epithermal neutron beam for neutron capture therapy. Nucl Sci Eng 131:1–22
26. Kiger WS III, Lu XQ, Harling OK, Riley KJ, Binns PJ, Kaplan J, Patel H, Zamenhof RG, Shibata Y, Kaplan ID, Busse PM, Palmer MR (2004) Preliminary treatment planning and dosimetry for a clinical trial of neutron capture therapy using a fission converter epithermal neutron beam. Appl Radiat Isot 61:1075–1081
27. Kobayashi T, Sakurai Y, Kanda K (2001) Characteristics of neutron irradiation facility and dose estimation method for neutron capture therapy at Kyoto University Research Reactor Institute. In: Current status of neutron capture therapy, IAEA Tecdoc 1223, IAEA, Vienna, 2001, pp 175–185
28. Kononov OE, Kononov VN, Bokhovko MV, Korobeynikov VV, Soloviev AN, Sysoev AS, Gulidov IA, Chu WT, Nigg DW (2004) Optimization of an accelerator-based epithermal neutron source for neutron capture therapy. Appl Radiat Isot 61:1009–1013
29. Kortesniemi M (2002) Solutions for clinical implementation of boron neutron capture therapy in Finland. Ph.D. thesis, University of Helsinki, Helsinki, ISBN 951-45-8955-6; http://ethesis.helsinki.fi, pp 54–68
30. Liu HB (1995) Design of neutron beams for neutron capture therapy using a 300 kw slab TRIGA reactor. Nucl Technol 109:314–326
31. Liu HB, Brugger RM (1994) Conceptual designs of epithermal neutron beams for boron neutron capture therapy from low-power reactors. Nucl Technol 108:151–156
32. Liu HB, Brugger RM, Rorer DC, Tichler PR, Hu JP (1994) Design of a high-flux epithermal neutron beam using 235U fission plates at the Brookhaven Medical Research Reactor. Med Phys 21:1627–1631
33. Liu HB, Greenberg DD, Capala J, Wheeler FJ (1996) An improved neutron collimator for brain tumor irradiations in clinical boron neutron capture therapy. Med Phys 23:2051–2060
34. Liu HB, Razvi J, Rucker R, Cerbone R, Merrill M, Whittemore W, Newell D, Autry S, Richards W, Boggan J (2001) TRIGA fuel based converter assembly design for a dual-mode neutron beam system at the McClellan Nuclear Radiation Center. In: Hawthorne MF, Shelly K, Wiersema RJ (eds) Frontiers in neutron capture therapy, 1st edn. Kluwer Academic/Plenum Publishers, New York, pp 295–300
35. Liu YWH, Huang TT, Jiang SH, Liu HM (2004) Renovation of epithermal neutron beam for BNCT at THOR. Appl Radiat Isot 61:1039–1043
36. Marek M, Burian J, Rataj J, Polák J, Spurny F (1997) Reactor based epithermal neutron beam enhancement at Rež. Radiat Prot Dosimetry 70:567–570
37. Moss RL, Aizawa O, Beynon D, Brugger R, Constantine G, Harling O, Liu HB, Watkins P (1997) The requirements and development of neutron beams for neutron capture therapy of brain cancer. J Neurooncol 33:27–40
38. Moss RL, Stecher-Rasmussen F, Ravensberg K, Constantine G, Watkins P (1992) Design, construction and installation of an epithermal neutron beam for BNCT at the high flux reactor Petten. In: Allen BJ et al. (eds) Progress in Neutron Capture Therapy for Cancer. Plenum Press, New York, pp 63–66
39. Nievaart VA, Moss RL, Kloosterman JL, van der Hagen THJJ, van Dam H (2004) A parameter study to determine the optimal source neutron energy in boron neutron capture therapy of brain tumors. Phys Med Biol 49:4277–4292

40. Nigg DW, Venhuizen JR, Wemple CA, Tripard GE, Sharp S, Fox K (2004) Flux and instrumentation upgrade for the epithermal neutron beam facility at Washington State University. Appl Radiat Isot 61:993–996
41. Raaijmakers CPJ, Nottelman EL, Konijnenberg MBJ (1995) Dose monitoring for boron neutron capture therapy using a reactor-based epithermal neutron beam. Phys Med Biol 41:2789–2797
42. Raaijmakers CPJ, Konijnenberg MW, Mijnheer BJ (1997) Clinical dosimetry of an epithermal neutron beam for neutron capture therapy: dose distributions under reference conditions. Int J Radiat Oncol Biol Phys 37:941–951
43. Rief H, Van Heusden R, Perlini G (1993) Generating epithermal neutron beams for neutron capture therapy in TRIGA reactors. In: Soloway AH, Barth RF, Carpenter DE (eds) Advances in neutron capture therapy. Plenum Press, New York, pp 85–88
44. Riley KJ, Binns PJ, Harling OK (2003) Performance characteristics of the MIT fission converter based epithermal neutron beam. Phys Med Biol 48:943–958
45. Riley KJ, Binns PJ, Harling OK (2004) The design, construction and performance of a variable collimator for epithermal neutron capture therapy beams. Phys Med Biol 49:2015–2028
46. Rogus RD, Harling OK, Yanch JC (1994) Mixed field dosimetry of epithermal neutron beams for boron neutron capture therapy at the MITR-II research reactor. Med Phys 21:1611–1625
47. Sakamoto S, Kiger WS III, Harling OK (1999) Sensitivity studies of beam directionality, beam size and neutron spectrum for a fission converter-based epithermal neutron beam for boron neutron capture therapy. Med Phys 26:979–988
48. Sakurai F, Torii Y, Kishi T, Kumada H, Yamamoto K, Yokoo K, Kaieda K (2001) Medical irradiation facility at JRR-4. In: IAEA - TECDOC-1223 Current Status of Neutron Capture Therapy. International Atomic Energy Agenct, Vienna, pp 142–146
49. Sakurai Y, Kobayashi T (2002) The medical-irradiation characteristics for neutron capture therapy at the heavy water neutron irradiation facility of Kyoto University Research Reactor. Med Phys 29:2328–2337
50. Slatkin DN (1991) A history of boron neutron capture therapy of brain tumors. Brain 114:1609–1629
51. Tanner V, Auterinen I, Helin J, Kosunen A, Savolainen S (1999) On-line beam monitoring of the Finnish BNCT facility. Nucl Instrum Methods Phys Res A 422:101–105
52. Thompson TJ, Benedict M, Cantwell T, Axford RA (1956) Final hazards summary report to the Advisory Committee on reactor safeguards on a research reactor for the Massachusetts Institute of Technology. Published Cambridge, MIT [1956] located in the Institute archives, non-circulating collection 2 TK9202.M36
53. Wallace SA, Mathur JN, Allen BJ (1994) Treatment planning figures of merit in thermal and epithermal boron neutron capture therapy of brain tumors. Phys Med Biol 39:897–906
54. Wilson BA, Riley KJ, Harling OK (2000) Automatic control and monitoring of the MIT fission converter beam. In: 9th international symposium on neutron capture therapy. International Society for Neutron Capture Therapy, Osaka, 2000, pp 237
55. Yamamoto T, Matsumura A, Shibata Y, Nose T, Yamamoto K, Kumada H, Hori N, Torii Y, Ono K, Kobayashi T, Sakurai Y (2000) Radiobiological characterization of epithermal and mixed thermal-epithermal beams at JRR-4. In: 9th international symposium on neutron capture therapy. International Society for Neutron Capture Therapy, Osaka, 2000, pp 205–206
56. Yanch JC, Blue TE (2003) Accelerator-based epithermal neutron sources for boron neutron capture therapy of brain tumors. J Neurooncol 62:19–31
57. Yanch JC, Harling OK (1993) Dosimetric effects of beam size and collimation of epithermal neutrons for boron neutron capture therapy. Radiat Res 135:131–145
58. Yanch JC, Zhou XL, Brownell GL (1991) A Monte Carlo investigation of the dosimetric properties of monoenergetic neutron beams for neutron capture therapy. Radiat Res 126:1–20
59. Zamenhof RG, Murray BW, Brownell GL, Wellum GR, Tolpin EI (1975) Boron neutron capture therapy for the treatment of cerebral gliomas. I: theoretical evaluation of the efficacy of various neutron beams. Med Phys 2:47–60

Accelerator-Based BNCT

3

Andres J. Kreiner

Dedicated to the memory of Alejandro A. Burlon

Contents

A.J. Kreiner
Physics Department, Gerencia de Investigación y Aplicaciones,
Centro Atomico Constituyentes,
Av. Gral Paz 1499, 1650 San Martin, Argentina

Escuela de Ciencia y Tecnología, Universidad de San Martín,
San Martín, Argentina

CONICET, Buenos Aires, Argentina
e-mail: kreiner@tandar.cnea.gov.ar

W.A.G. Sauerwein et al. (eds.), *Neutron Capture Therapy*,
DOI 10.1007/978-3-642-31334-9_3,

3.1 Introduction

Boron neutron capture therapy (BNCT), as testified by the present book and the lively biennial series of international conferences held uninterruptedly around the world since 1982, is considered by a significant international community as a promising option for the treatment of certain types of cancer [37, 53]. While a great deal of progress has been made and will continue to be made using nuclear reactors, we are convinced that the advancement of BNCT requires neutron sources suitable for installation in hospital environments. Low-energy particle accelerators are most appropriate for this purpose and can be constructed for modest cost, comparable to that of other conventional radiotherapy medical devices [7]. Furthermore, it is highly likely that the presence of these devices in specialized health-care institutions may be decisive for the future of BNCT in terms of a qualitative improvement in our ability to gather data and experience, patient recruitment, on-site resources, and institutional commitment. A major advantage of accelerator-based BNCT (AB-BNCT) over reactor-based neutron sources is the potential for siting within a hospital. Accelerators offer a number of advantages over reactor-based sources for clinical applications: (a) Accelerators can be easily turned off when the neutron field is no longer required while reactors have a large permanent inventory of radioactive material. This, and the fact that neutrons are not produced via a critical assembly of fissile material, means that licensing and regulations associated with installing and maintaining the neutron source are substantially simplified. (b) The capital expense of an AB-BNCT system is likewise substantially lower than that associated with the installation of a reactor system in or near a hospital. (c) Accelerators have been a prominent feature of radiotherapy departments in hospitals for years, and hence, clinicians have a long-standing experience with similar devices for patient irradiation. (d) Very importantly, the neutron energy spectrum from certain nuclear reactions is much "softer" (less energetic) than the one coming from fission, which makes it easier to generate the "ideal" epithermal neutron spectrum needed to treat a deep-seated tumor, and hence, the quality of the neutron field can be designed to significantly exceed the quality of the neutron field for reactor-based neutron sources.

In this chapter, a variety of possible charged-particle-induced nuclear reactions and the characteristics of the resulting neutron spectra will be discussed along with corresponding particle accelerators as neutron-producing sources. Different past and present efforts to develop such facilities worldwide will be described including an ongoing project to develop a tandem-electrostatic-quadrupole (TESQ) accelerator for accelerator-based (AB)-BNCT.

3.2 Different Neutron-Producing Reactions of Interest for Accelerator-based BNCT

There are basically two ways of producing neutrons. The first one is nuclear fission of ^{235}U induced by thermal neutrons, taking place in nuclear reactors, and it is the one which has been used so far for BNCT. The neutrons emitted from the fission

fragments are quite energetic. They can be well represented by the following distribution: $F(E) = 0.770\ \sqrt{E}\ \exp(-0.775E)$. This spectrum extends out to 10 MeV and has an average energy of about 2 MeV. These neutrons have to be moderated, either to thermal energies to treat superficial lesions (in the context of BNCT, these are neutrons of energies below 0.5 eV) or to epithermal energies (energies in the interval 0.5 eV–10 keV, ideally centered near the upper end of this range) for deep-seated tumors in order to spare the healthy tissue allowing for final moderation in the tissue located between the skin entrance point of the patient and the tumor site.

The other process is a nuclear reaction induced by charged particles. Namely, a certain projectile, accelerated to a sufficiently high energy to overcome the repulsive Coulomb barrier, impinges on an appropriate target nucleus leading to a "residual" or product nucleus and a neutron. There are two types of reactions, from the energetic point of view: Those called exothermic, which do not require a minimum kinetic energy of the projectile (except for the one to overcome the Coulomb repulsion). For these reactions, the Q value is positive (Q is equal to the energy associated with the rest mass $M_i c^2$ of the incoming particles minus $M_o c^2$ of the reaction products). A typical example is the d + d reaction (a deuteron impinging on another deuteron) to produce the residual nucleus ^{3}He and a neutron. The Q value is 3.270 MeV and the neutron energy at negligible projectile energy is 2.451 MeV, even larger than the average fission neutron energy. The other type of reaction is called endothermic and requires a minimum threshold energy to take place. Near this threshold, the neutron energy is very low, so that the use of these neutrons for BNCT is very efficient.

3.2.1 The Endothermic ^{7}Li(p,n)^{7}Be and ^{9}Be(p,n)^{9}B Reactions

The most popular endothermic reaction for AB-BNCT is ^{7}Li(p,n)^{7}Be (a notation equivalent to $^7\mathrm{Li} + \mathrm{p} \rightarrow {}^7\mathrm{Be} + \mathrm{n}$). The Q value is −1.644 MeV (the minus sign shows explicitly the endothermic character), and the threshold energy for the impinging proton is 1.880 MeV (the relation between Q value and threshold energy E_{th} is given by the center of mass, c.m., to lab transformation, $E_{th} = |Q|(M_p + M_t)/M_t$; p stands for projectile and t for target). At this bombarding energy, the neutron is emitted with zero energy in the c.m., it moves in forward direction following the c.m. and has about 30 keV kinetic energy in the lab frame. This energy is not very far from the epithermal regime. There are in fact proposals to work in this regime [29–31]. Below 1.92 MeV, the function is bi-valued reflecting the fact that the velocity of the isotropically emitted neutron in the c.m. frame is smaller than the c.m. velocity in the lab leading to its confinement to forward angles in the lab frame. At 1.91 MeV, the maximum and average neutron energies are 105 and 42 keV and the maximum and average emission angles are 60° and 28° [39, 40]. This angular confinement ("kinematic collimation") allows for a very efficient utilization of the neutrons (in terms of the ratio of utilized neutrons/produced neutrons). Even for energies well above the threshold, the emission pattern in the lab is mainly concentrated in the forward hemisphere, and neutron energies for angles larger than 90° are small.

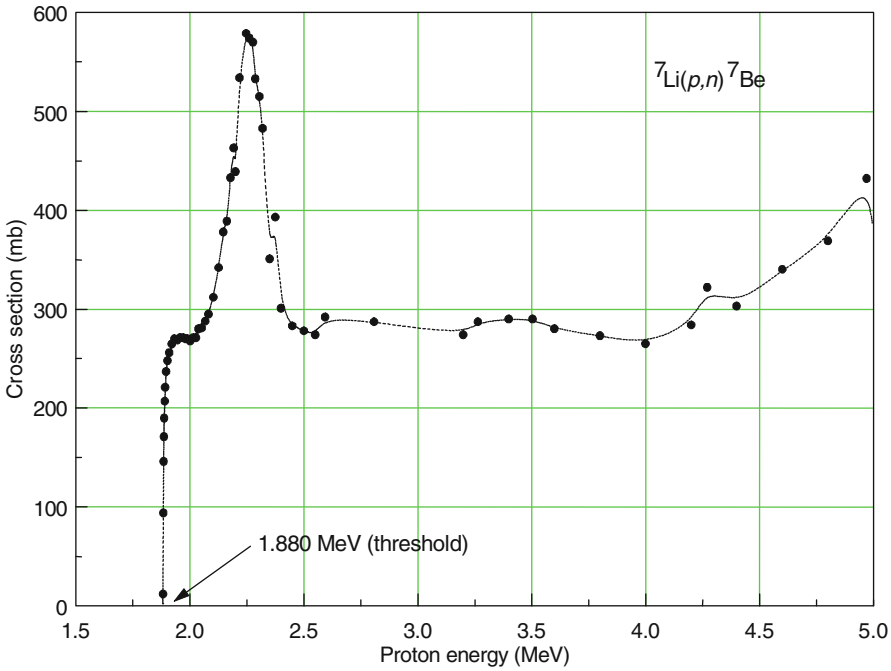

Fig. 3.1 Reaction cross section for ^{7}Li(p,n) for different proton bombarding energies. The pronounced resonance is at 2.25 MeV [42]

In addition to the kinematics of the reaction, it is important to examine the cross section as a function of the proton energy in the lab which will determine the actual neutron production. Figure 3.1 shows a very steep rise from the threshold on and a small plateau starting at about 1.93 MeV (reaching a value of 270 mb) before the pronounced resonance at 2.25 MeV (reaching 580 mb). This translates, as examples, into the following values for total thick target Li neutron yield: 6.3×10^9 n/(mA s) for 1.89 MeV and 5.8×10^{11} n/(mA s) for 2.3 MeV proton bombarding energy ([40, 41]; see also Table 3.1).

Working near threshold would require very little moderation (at 1.89 MeV, the maximum neutron energy is 67 keV) but at the same time, would impose a very stringent demand on the energy/voltage stability of the accelerator of 0.1 % [4] in order to maintain the production rate sufficiently constant. In our studies [10–12], we have concluded that 2.3 MeV incident proton energy is a very good compromise between an already significant value of the production cross section (taking advantage of the resonance) and still a sufficiently low maximum neutron energy of 573 keV (the exact value of the best energy may depend, though, on the tumor depth). The minimum neutron energy is 35 keV (at an angle of 180°), and the average energy is 233 keV for a thick target (a thick target is defined as one in which the projectile looses enough energy to cross below the reaction threshold). One sees that working with an endothermic reaction has the advantage of having a much softer neutron spectrum as compared to the fission one. Fast neutrons (defined, in the

Table 3.1 For different neutron-producing reactions, the table lists the threshold and bombarding energy, the total thick target neutron production for different bombarding energies, the percentage for which the maximum neutron energy is less than 1 MeV, and the maximum and minimum neutron energies [17, 22, 39, 40]

Reaction	E_{th} (MeV)	E_{in} (MeV)	Total production (n/mA s)	Fraction $E_n < 1$ MeV (%)	$E_{n,max}$ (keV)	$E_{n,min}$ (keV)
^{7}Li(p,n)^{7}Be	1.880	1.880	0	100	30	30
		1.890	6.3×10^{9}	100	67	0.2
		2.500	9.3×10^{11}[a]	100	787	60
		2.800	1.4×10^{12}[b]	92	1,100	395
^{9}Be(p,n)^{9}B	2.057	2.057	0	100	20	20
		2.500	3.9×10^{10}	100	574	193
^{9}Be(d,n)^{10}B	0	0	0	50	3,962	3,962
		1.500	3.3×10^{11}	50	4,279	3,874
^{13}C(d,n)^{14}N	0	0	0	75	4,974	4,964
		1.500	1.9×10^{11}	70	6,772	5,616
^{12}C(d,n)^{13}N	0.327	0.327	0	100	4	3
		1.500	6.0×10^{10}	80	1,188	707
d(d,n)^{3}He	0	0	0	0	2,451	2,451
		0.120	3.3×10^{8}[c]	0	2,898	2,123
		0.200	1.1×10^{9}	0	3,054	2,047
t(d,n)^{4}He	0	0	0	0	14,050	14,050
		0.150	4.5×10^{10}	0	14,961	13,305

[a]Average between the values reported in Colonna et al. [17] and Lee and Zhou [39, 40]
[b]Allen and Beynon [2]
[c]Ganda et al. [22]

context of BNCT, as having energies larger than 10 keV) are very radiotoxic and have no selectivity whatsoever (they are at the opposite end of the philosophy sought for in BNCT). These neutrons transfer their energy to recoil protons through elastic collisions, and these low-energy protons have a high linear energy transfer (LET) and hence a high ionization density leading to a large relative biological effectiveness (RBE) value. For reference, a 20 keV proton has a LET of 59 keV μm^{-1} in water [52]. (It is worth remembering that the maximum in the RBE vs. LET curve lies in the region 100–150 keV μm^{-1}.) They have to be avoided by all means in a therapeutic beam. Neutron filtering and moderation from a fission spectrum down to a pure epithermal spectrum is an inefficient and difficult undertaking (to put this into numbers, it is interesting to recall that a 0.1-MW reactor produces 10^{16} n/s vs. 10^{13} n/s for a 10 mA proton beam on a Li target at 2.3 MeV). The best option is to use a process which minimizes the production of fast neutrons in the first place.

To use the ^{7}Li + p reaction would hence demand an accelerator of 2.3 MV "effective" voltage if it is a single-ended machine (the term effective is to indicate that it is not necessarily an electrostatic voltage, e.g., if the accelerator is electrodynamic) or 1.15 MV if it is a tandem (we shall discuss the different accelerator options later on). In addition, the necessary therapeutic thermal neutron flux of the order of 10^{9} n cm^{-2} s^{-1} at the tumor position demands relatively high currents (order of tens

of mAs), and here is where the real challenge lies. The high-power density deposited in the target material, here metallic Li in the most efficient case, is very high (of the order of 1 kW cm^{-2}), and its cooling represents a challenging technological problem in itself, particularly in view of the rather low melting point (180.5 K) and thermal conductivity (85 $W\,m^{-1}\,K^{-1}$) of Li.

Finally, a brief comment about the other endothermic reaction induced by protons on Be. As shown in Table 3.1, the yield of the $^{9}Be(p,n)^{9}B$ reaction at 2.5 MeV is much lower than the one of protons on Li at the same energy. In order to get a comparable production, one has to go to energies of about 4 MeV. At these bombarding energies, the average neutron energy is significantly higher than for the p + Li case (between 1.1 and 2.1 MeV), and in addition, the effective voltage has to be 4 MV (or 2 MV for a tandem) which increases the cost of the accelerator significantly. Such a facility is actively pursued by the LNL-INFN Italian group [15] but to generate thermal neutrons and treat superficial lesions.

3.2.2 Exothermic-Deuteron-Induced Reactions

We shall now discuss several deuteron-induced nuclear reactions which have been mentioned in the literature in the context of AB-BNCT. The best option would be a reaction at low projectile energy (which means low voltage and hence a less expensive machine), low neutron energy (avoidance of fast radiotoxic neutrons, ease of moderation, and efficient use of the produced flux), and large production cross section (means less primary beam intensity). Table 3.1 gives some information on the energetics and thick target total yield of different neutron-producing reactions.

The so-called "fusion" reactions d + d and d + t have already significant yields at very low energies (e.g., 120 keV), but their high Q values (especially for d + t, this value is 17.59 MeV) lead to very high neutron energies and also to near-isotropic emission in the lab frame. The devices used to accelerate the deuterons or tritons, usually in the 100–200 keV energy range, go by the name of neutron generators. They are advantageous from the point of view of the required voltage. Quite sophisticated compact neutron generators are being developed [18], but extremely high currents are necessary to generate fluxes useful for BNCT due to limited yield in the appropriate energy range and inherent inefficiency associated with high-energy and isotropic neutron production. These sources can generate 10^{12} d-d n/s and 10^{14} d-t n/s, respectively. The d-t case is disfavored by its very high neutron energies (which demand large moderation and shielding volumes) and by the known difficulties associated with working with tritium, particularly in a hospital environment. In the first case, a 2 A deuteron current at 200 keV is designed to produce a source intensity of 2.3×10^{12} n/s, which is still, for the d-d reaction, a factor of about 30 too short of the intensity needed for treating a deep-seated tumor with BNCT. Already at these levels, the cost of electricity (400 kW) becomes excessive. The possibility has been envisaged [22] of coupling this d-d generator with a subcritical fission assembly as a neutron multiplier. Such a device is likely to become too complex and expensive to be installed in a hospital.

The d-d reaction has also been studied [13] at higher energies up to 1.3 MeV to explore its applicability to skin tumor treatment (i.e., as a source of thermal neutrons). A thick TiD_2 target and heavy water moderation (of 30 cm depth) would yield a useful thermal flux of 10^9 n cm^{-2} s^{-1} at the tumor position with a deuteron beam of about 100 mA. A single-session BNCT treatment would demand 170 min under these conditions. These numbers are still marginal. On the other hand, the use of the ^{9}Be(d,n)^{10}B leads to very acceptable results for the treatment of superficial lesions [13] which will be discussed in the following. This reaction has often been mentioned in the past as a possible source of neutrons for BNCT (e.g., [17]). Being an exothermic reaction, it has the advantage of no threshold and a significant neutron production cross section at relatively low energies. Its drawback is its high Q value which leads to significant fast neutron production (about 4 MeV for 1.5 MeV bombarding energy, see Table 3.1). There is however a very interesting feature of this reaction noted some time ago [25]. ^{10}B, the heavy product in the ^{7}Be(d,n) reaction, being a doubly odd nuclide, is already a relatively complex nucleus. It has a number of excited states, but in particular, it has three states at excitation energies between 5.1 and 5.2 MeV which are strongly populated as soon as they become energetically accessible. Hence, if the final state is one of that group, the reaction becomes effectively endothermic and the emitted neutrons have very small energies depending on the exact bombarding energy. The Q value is −0.802 MeV and the corresponding threshold is 0.981 MeV. At 1.2 MeV bombarding energy, the maximum neutron energy is only 297 keV (and the minimum is 68 keV). This fact opens the possibility for suppressing most of the fast neutrons produced in this reaction. If one takes a thin Be target (about 2 μm thick), so that a 1.2 MeV deuteron looses about 100 keV, the whole fast neutron production from 1.1 MeV downward is suppressed while the low-energy neutron production remains intact. Under these circumstances, a thin Be target and heavy water moderation (of 15 cm depth) with a 20 mA beam allow a single-session BNCT treatment in 48 min [13]. This means that for superficial lesions, a single-ended machine of 1.2 MV in the terminal would suffice, while a tandem would only require 600 kV. This kind of machine is envisaged as an intermediate step in a project under development [34, 36, 37]. In addition, the thermomechanical properties of Be are quite good as compared to Li: a melting point of 1,290 K and a thermal conductivity of 190 W m^{-1} K^{-1}. More recently, this reaction has been studied by our group in connection with epithermal deep-seated tumor treatment with encouraging results [14].

To complete the discussion of the reactions shown on Table 3.1, we have to consider carbon as a target, which has excellent thermomechanical properties: a melting point of 3,550 K and a thermal conductivity of 230 W m^{-1} K^{-1}. It is a very stable material, and the construction of a target is relatively simple. The ^{12}C(d,n)^{13}N reaction is not competitive due to its low neutron production, but ^{13}C(d,n)^{14}N at 1.5 MeV bombarding energy is characterized by a relatively large yield with interesting spectral features for AB-BNCT. This reaction has been studied both by [17] and by our group in collaboration with scientists from LABA-MIT [9], and there is some promise here in the case of low-energy machines.

3.3 Beam-Shaping Assemblies

As shown above, from the neutronics point of view, the ^{7}Li(p,n)^{7}Be reaction, in the 1.9–2.5 MeV range, is the best choice, in particular, for deep-seated tumors. The main advantages of this reaction are its high yield at the lowest bombarding energy and at the same time its low-energy neutron spectrum (average energy in the 34–326 keV range). The moderation volumes necessary to get rather pure epithermal neutron spectra out of the beam-shaping assemblies (BSAs) are modest and smaller than for other target materials. A small BSA implies fewer neutron losses due to capture reactions, with higher useful flux per unit accelerator current. The problem of an optimal BSA has been thoroughly studied in the last decade, including geometry, proton energy, and materials [6]. These authors proposed an optimal BSA in the 2.1–2.6 MeV proton energy range consisting of (a) a 22-cm-deep ^{7}LiF moderator for 2.3 MeV protons and (b) a 34-cm-deep Al/AlF3 moderator for 2.4 MeV protons, in both cases surrounded by an Al_2O_3 reflector. For a 20 mA beam, the treatment times were 40 and 54 min, respectively. The advantage depths (AD, depth where the tumor dose equals the limiting healthy skin tissue dose) of the ^{7}LiF and Al/AlF_3 moderated beams of 9.5 cm were found to be about 1 cm more than that of the Brookhaven Medical Research Reactor beam (the one in use at that time). These more penetrating beams lead to a significantly increased tumor dose at depth (50 % at 8 cm) and represent a clear clinical advantage. Hence, it became clear [50] that the spectral distribution of the neutrons and the associated depth-dose distribution are essential to determine the tumor control probability (TCP, see [46]). In our studies [8, 12], we have come up with an optimal BSA consisting of a 34-cm-thick Al/PTFE/LiF moderator and a Pb reflector. A 30 mA proton beam on Li leads to a TCP of 98 % at 6.4 cm inside the brain (keeping the maximum healthy tissue dose at 11.6 Gy-Eq, namely, below the limit at 12.5 Gy-Eq) in a 27-min treatment. The AD for that beam and BSA turns out to be 11.5 cm. Figure 3.2 shows the general layout of such a BSA. Further studies exploring systematically the geometry and the impinging proton energy have essentially confirmed these results [44].

3.4 Accelerators and Facilities

In spite of the long history of BNCT, there has not been to date a single accelerator-based facility with the necessary characteristics to carry out a BNCT clinical program in an optimized way. There are many different types of accelerators ranging from low-energy electrostatic machines to higher energy cyclotrons and to still much higher energy linacs or synchrotrons, which are being considered for neutron production and BNCT. However, these latter machines produce neutrons with energies far too high for BNCT purposes, and while “brute force” moderation can be applied (namely large enough moderation assemblies), high-energy neutron tails are likely to survive. In addition, these facilities may lend themselves for experimental programs but are unlikely to provide the optimal solution in terms of space

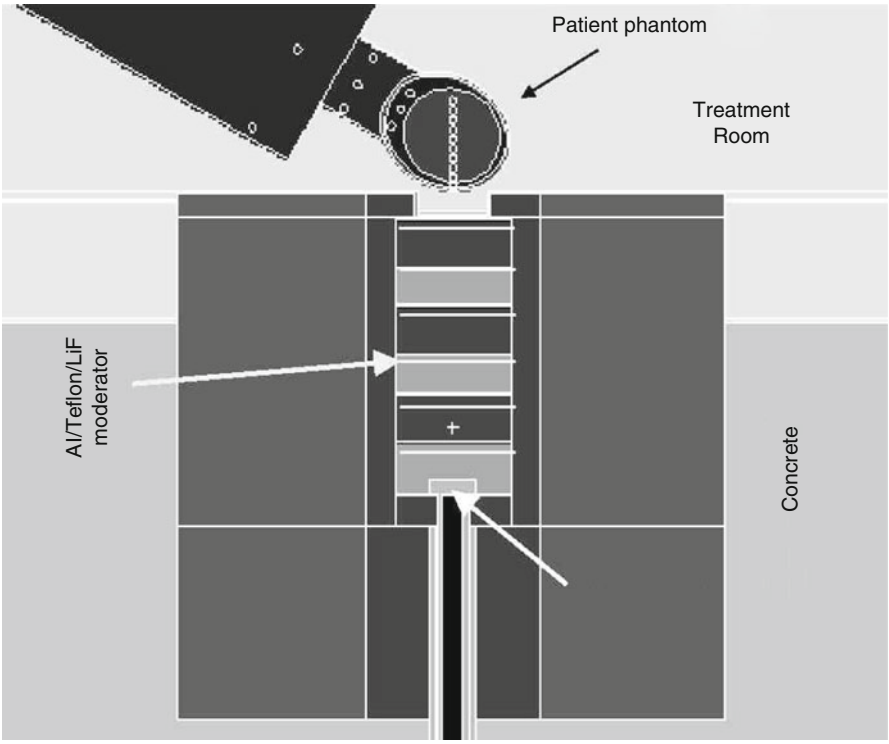

Fig. 3.2 Beam-shaping assembly for TESQ accelerator [8]

and cost for BNCT to become a widespread hospital-based modality. Hence, we shall here limit the discussion to past and ongoing attempts to build and develop high current (beyond the mA range) proton accelerators of a few MV (1–3 MV) to be used in connection with one of the best endothermic reactions discussed above (namely, protons on Li or Be). For the most part, these machines have been and still are electrostatic, and we shall start with them.

3.4.1 Electrostatic Accelerators

Work conducted during the 1990s in Lawrence Berkeley Lab (LBNL) was aimed at developing a 2.5 MeV, 100 mA proton single-ended electrostatic machine [3, 38]. The innovation consisted in considering electrostatic quadrupoles (ESQs) to provide sufficiently strong transverse focusing to counteract space charge effects of the intense beam. This machine never got built, and the major challenge was in developing the proper power supply system. A thin Li target on a Cu or Al backing with microchannels and convective water cooling was developed, demonstrating that for a 50-kW load, the target remained below the Li melting point [43].

Another very important milestone in the development of an AB-BNCT facility was the compact tandem promoted at the Laboratory for Accelerator Beam Applications at MIT [28, 51]. This machine operated up to voltages of 2 MV (4 MeV proton and deuteron beams) and currents of the order of 1 mA. An active research program, including animal studies aimed at developing BNC synovectomy, unfolded around that machine.

A currently active AB-BNCT program is based around a 3 MV Dynamitron accelerator in the School of Physics and Space Research at the University of Birmingham, UK [2, 24]. It is a single-ended machine enclosed in an SF6-filled pressurized vessel and, the high voltage is generated through rectified RF power [16]. At Birmingham, this machine operates regularly at 2.8 MV and 1–2 mA and is entirely and successfully devoted to multiple aspects of the AB-BNCT activity (e.g., [23]). It operates with a heavy water submerged jet-cooled solid Li target (Scott, private communication, 2008) and a Fluental-based beam-shaping assembly (BSA) with a beam port at 90° to the vertical beam direction. In order to conduct an optimal clinical program, this facility would need an upgrade in terms of beam current. This same machine, with an upgraded ion source, is proposed as the core of a BNCT facility which is intended to operate at 2.8 MeV and 20 mA on a thin solid Li target at about 0.5 kW cm^{-2} power density [20].

Another facility under development is based around a vacuum-insulated compact tandem at the Budker Institute of Nuclear Physics in Novosibirsk, Russia [4]. The goal for this facility is the production of near-threshold neutrons from the $p+{}^{7}Li$ reaction at about 1.9 MeV and currents up to 10 mA. First low current tests have been performed [5]. Progress has been made in the design and construction of a solid Li target which can be evaporated within the vacuum of the beam line [48]. To date, the maximum currents achieved are at about 2.7 mA [1].

There is also another installation under development around a high current cascade generator [33] at the IPPE, Obninsk, Russia, which has so far operated at 2.3 MeV and 3 mA.

Finally, a project to build a tandem-electrostatic-quadrupole (TESQ) accelerator facility is under development in Argentina [34–37] based on the ESQ concept developed at LBNL. The machine being designed and constructed is a folded TESQ with a terminal of up to 1.2 MV intended to work in air, to avoid the need for a pressure vessel and for an insulating gas installation. The project aims at developing a machine capable of delivering a proton beam of about 2.4 MeV and 30 mA to irradiate a Li metal (or a refractory Li compound) target in order to produce a high-quality therapeutic neutron beam (i.e., with the least possible fast neutron contamination) after appropriate beam shaping. The general geometric and mechanical layout, its associated electrostatic fields, and the acceleration tube have been simulated using a 3D finite element codes. The electromechanical structure including the high voltage column, the accelerator tubes, the generators, and the power supplies is under construction. Beam transport calculations through the accelerator have been performed [41, 49] using the self-consistent 3D code WARP [21] and other finite element codes. Likewise, work related to strippers and neutron production targets is in progress, and a prototype of an optimized beam-shaping assembly is completed [8, 44].

3.4.2 Electrodynamic Machines

There are presently two ongoing projects to develop AB-BNCT facilities based on radiofrequency machines. The first one to be commented on, currently in its final construction phase, is the AB-BNCT project at the *Laboratori Nazionali de Legnaro* (LNL) of the Italian INFN organization [45] based on a high-intensity radiofrequency quadrupole operating at 5 MeV proton energy and 30 mA and intended to be used, with the ^{9}Be(p,xn) reaction, for the development of a thermal neutron source for the treatment of skin melanoma [15, 19]. A high power (150 kW) and quite sophisticated solid Be target has already been developed and the corresponding BSA designed.

The second project is based on a superconducting linac, currently under construction at the Soreq research center, Israel. The high-intensity proton beam (of about 2 MeV and 2–4 mA) will be converted in a liquid Li target configured as a windowless forced flowing Li jet [26, 27].

These interesting projects are based on machines which are likely to be more expensive and complex than electrostatic ones for hospital-based facilities.

It should finally be mentioned that there is a 30 MeV proton cyclotron being currently installed at Kyoto University in combination with a Be target, to start clinical work in the near future [47].

3.5 Summary and Conclusions

The advancement of BNCT requires neutron sources suitable for installation in hospital environments. Low-energy particle accelerators are most appropriate for this purpose. Furthermore, it is highly likely that the presence of these devices in specialized health-care institutions may be decisive for the future of BNCT. Major advantages of accelerator-based BNCT (AB-BNCT) over reactor-based neutron sources are (a) the potential for siting within a hospital; (b) less radiation hazards; (c) larger simplicity in licensing, installation, and maintenance; (d) substantially lower capital expense than that associated with the installation of a reactor system in or near a hospital; and (e) very importantly, the neutron energy spectrum from certain nuclear reactions is much "softer" (less energetic) than the one coming from fission, which makes it easier to generate the "ideal" epithermal neutron spectrum needed to treat a deep-seated tumor, and hence, the quality of the neutron field can be designed to significantly exceed the quality of the neutron field for reactor-based neutron sources.

In this chapter, a variety of possible charged-particle-induced nuclear reactions and the characteristics of the resulting neutron spectra are discussed along with corresponding beam-shaping assemblies and particle accelerators as neutron-producing sources. The endothermic reaction ^{7}Li(p,n)^{7}Be at proton energies around 2.3 MeV and currents in the 20–30 mA range coupled to appropriate BSAs, with either solid or liquid Li targets provides the best solution for the production of epithermal neutron beams for treatment of deep-seated tumors. Possibly, near-threshold operation with this reaction is also likely to be a good option. Other reactions at lower energies,

like $^{9}Be(d,n)^{10}B$ at 1.2 MeV, may be possible for the treatment of both superficial and deep-seated lesions. Different past and present efforts to develop such facilities worldwide are described including an ongoing project to develop a tandem-electrostatic-quadrupole (TESQ) accelerator for accelerator-based (AB)-BNCT.

References

1. Aleynik V et al (2011) BINP accelerator based epithermal neutron source. Appl Radiat Isot 69:1635–1638
2. Allen DA, Beynon TD (1995) A design study for an accelerator-based epithermal neutron beam for BNCT. Phys Med Biol 40:807–821
3. Anderson OA, Alpen EL, Kwan JW et al (1994) ESQ-focused 2.5 MeV DC accelerator for BNCT. In: Proceedings of the 4th European particle accelerator conference. London, 1994, pp 2619–2621
4. Bayanov BF, Belov VP, Bender ED et al (1998) Accelerator-based neutron source for the neutron-capture and fast neutron therapy at hospital. Nucl Instrum Methods Phys Res A 413: 397–426
5. Bayanov B, Burdakov A, Chudaev et al (2008) First neutron generation in the BINP accelerator based neutron source. In: Proceedings of the 13th international congress on neutron capture therapy. ENEA, pp 514–517
6. Bleuel DL, Donahue RJ, Ludewigt BA et al (1998) Designing accelerator-based epithermal neutron beams for BNCT. Med Phys 25:1725–1734, and refs. therein
7. Blue T, Yanch J (2003) Accelerator-based epithermal neutron sources for boron neutron capture therapy of brain tumors. J Neurooncol 62(1):19–31, and refs. therein
8. Burlon AA, Kreiner AJ (2008) A comparison between a TESQ accelerator and a reactor as a neutron source for BNCT. Nucl Instrum Methods Phys Res B 266:763–771 and Proceedings of the 13th international congress on neutron capture therapy. ENEA, pp 458–461
9. Burlon AA, Kreiner AJ, White SM et al (2001) In-phantom dosimetry using the $^{13}C(d,n)^{14}N$ reaction for BNCT. Med Phys 28:796–803
10. Burlon AA, Kreiner AJ, Valda AA et al (2002) Optimization of a neutron production target and beam shaping assembly based on the $^{7}Li(p,n)^{7}Be$ reaction. In: Research and development in neutron capture therapy. Monduzzi Editore, Bologna, pp 229–234
11. Burlon AA, Kreiner AJ et al (2004) An optimized neutron-beam shaping assembly for accelerator-based BNCT. Appl Radiat Isot 61:811
12. Burlon AA, Kreiner AJ, Valda AA et al (2005) Optimization of a neutron production target and a beam shaping assembly based on the 7Li(p, n) reaction for BNCT. Nucl Instrum Methods Phys Res B 229:144–156
13. Burlon AA, del V Roldan T, Kreiner AJ et al (2008) Nuclear reactions induced by deuterons and their applicability to skin tumor treatment through BNCT. Nucl Instrum Methods Phys Res B 266:4903–4910
14. Capoulat ME, Minsky DM, Kreiner AJ (2011) Applicability of the 9Be(d,n)10B reaction to AB-BNCT skin and deep tumor treatment. Appl Radiat Isot 69:1684–1687
15. Ceballos C et al (2011) Towards the final BSA modeling for the accelerator-driven BNCT facility at INFN LNL. Appl Radiat Isot 69:1660–1663
16. Cleland MR (2006) Industrial applications of electron accelerators. CAS Proc. Yellow reports CERN 2006-012:383–416
17. Colonna N, Beaulieu L, Phair L et al (1999) Measurements of low-energy (d, n) reactions for BNCT. Med Phys 26(5):793–798
18. Custodero S, Leung K, Mattioda F (2008) Feasibility study for the upgrade of a compact neutron generator for NCT application. In: Proceedings of the 13th international congress on neutron capture therapy. ENEA, pp 450–453

19. Esposito J, Colautti P, Fabritsiev S et al (2008) Be target development for the accelerator-based SPES-BNCT facility at INFN Legnaro. In: Proceedings of the 13th international congress on neutron capture therapy. ENEA, pp 466–469
20. Forton E, Stichelbaut F, Cambriani A et al (2008) Overview of the IBA accelerator-based BNCT system. In: Proceedings of the 13th international congress on neutron capture therapy. ENEA, pp 530–534
21. Friedman A, Grote DP, Haber I (1992) Particle simulation of heavy ion fusion beams. Phys Fluids B 4:2203
22. Ganda F, Vujic J, Greenspan E et al (2008) Accelerator-driven sub-critical multiplier for BNCT. In: Proceedings of the 13th international congress on neutron capture therapy. ENEA, pp 526–529
23. Ghani Z, Green S, Wojnecki et al (2008) BNCT beam monitoring, characterization and dosimetry. In: Proceedings of the 13th international congress on neutron capture therapy. ENEA, pp 647–649 and refs. therein
24. Green S (1998) Developments in accelerator based BNCT. Radiat Phys Chem 51(4–6):561–569
25. Guzek J, Tapper U, McMurray W et al (1997) Characterization of the 9Be(d, n)10B reaction as a source of neutrons employing commercially available radiofrequency quadrupole (RFQ) linacs. In: Proceedings of SPIE, The International Society for Optical Engineering, 2867, pp 509–512
26. Halfon S, Paul M, Steinberg D et al (2008) High power accelerator-based BNC with a liquid Li target and new applications to treatment of infectious diseases. In: Proceedings of the 13th international congress on neutron capture therapy. ENEA, pp 470–473 and references therein
27. Halfon S et al (2011) High power liquid-lithium target prototype for accelerator-based boron neutron capture therapy. Appl Radiat Isot 69:1654–1656
28. Klinkowstein R, Shefer R, Yanch JC, et al (1997) Operation of a high current tandem electrostatic accelerator for boron neutron capture therapy. Advances in neutron capture therapy, Medicine and Physics, Elsevier Science B. V., Amsterdam, vol. 1, pp 522
29. Kobayashi T, Sakurai Y, Ono K (1998) Neutron irradiation systems for BNCT using accelerators and research reactors. Proc ECOMAP-98: 370–375
30. Kobayashi T, Bengua G, Tanaka K (2008) Neutrons for BNCT from the near threshold ^{7}Li(p,n)^{7}Be on a thick Li target. In: Proceedings of the 13th international congress on neutron capture therapy. ENEA, pp 478–481 and refs. therein
31. Kononov VN, Androsenko PA, Bohovko MV et al (1994) ^{7}Li(p, n)^{7}Be reaction near the threshold: the prospective neutron source for BNCT. In: Proceedings of the 1st international workshop on accelerator-based neutron sources for BNCT. vol 2, pp 477–483
32. Kononov et al (1996) Accelerator-based and intense directed neutron source for BNCT. In: Conference proceedings, 7th international symposium on neutron capture therapy. vol 1, pp 528–532
33. Kononov VN, Bohovko MV, Kononov OE, et al (2006) Neutron therapy facility based on high current proton accelerator KG-2,5. Proceedings of RuPAC, Novosibirsk, Russia, pp 118–119
34. Kreiner AJ, et al (eds) (2011a) Proceedings of the 14th international congress on neutron capture therapy. Appl Radiat Isot vol 69(12)
35. Kreiner AJ, Kwan JW, Burlon AA et al (2007) A tandem-electrostatic-quadrupole for accelerator-based BNCT. Nucl Instrum Methods B 261:751–754
36. Kreiner AJ, Thatar Vento V, Levinas P et al (2008) Development of a Tandem-electrostatic-quadrupole accelerator facility for BNCT. In: Proceedings of the 13th international congress on neutron capture therapy. ENEA, pp 482–485
37. Kreiner AJ et al (2011) Development of a tandem-electrostatic-quadrupole facility for accelerator-based boron neutron capture therapy. Appl Radiat Isot 69:1672–1675
38. Kwan JW, Ackerman GD, Chan CF et al (1995) Acceleration of 100 mA of H- in a single channel electrostatic quadrupole accelerator. Rev Sci Instrum 66(7):3864
39. Lee CL, Zhou XL (1999) Thick target neutron yields for the ^{7}Li(p, n)^{7}Be reaction near threshold. Nucl Instrum Methods Phys Res B 152:1–11

40. Lee CL and Zhou XL (1999b) An algorithm for computing thick target differential p-Li neutron yields near threshold. In: Duggan JL et al (eds) Proceedings of the 15th international conference on the applications of accelerators in research and industry, pp 227–230
41. Levinas P, Kreiner AJ, Henestroza E (2008) Transport of high-intensity proton and deuteron beams through a TESQ accelerator. In: Proceedings of the 13th international congress on neutron capture therapy. ENEA, pp 411–414 and refs. therein
42. Liskien H, Paulsen A (1975) Neutron production cross section and energies for the reactions 7Li(p, n)7Be and 7Li(p, n)7Be*. At Data Nucl Data Tables 15:57–84
43. Ludewigt BA, Chu WT, Donahue RJ et al (1997) An epithermal neutron source for BNCT based on an ESQ-accelerator. LBNL report 40642
44. Minsky DM, Kreiner AJ, Valda AA (2011) AB-BNCT BSA based on the 7Li(p,n)7Be reaction optimization. Appl Radiat Isot 69:1668–1671
45. Pisent A, Colautti P, Esposito J et al (2006) Progress on the accelerator based SPES-BNCT project at INFN Legnaro. J Phys Conf Ser 41:391–399. doi:10.1088/1742-6596/41/1/043, and references therein
46. Porter EH (1980) The statistics of dose/cure relationships for irradiated tumours. Part I. Br J Radiol 53:210
47. Tanaka H et al (2011) Experimental verification of beam characteristics for cyclotron-based epithermal neutron source (C-BENS). Appl Radiat Isot 69:1642–1645
48. Taskaev S, Bayanov B, Belov V et al (2006) Development of Li target for AB-BNCT. Advances in NCT. Neutrino, Osaka, pp 292–295
49. Vento VT et al (2011) Electrostatic design and beam transport for a folded tandem electrostatic quadrupole accelerator facility for accelerator-based boron neutron capture therapy. Appl Radiat Isot 69:1649–1653
50. Wheeler F, Nigg D, Capala J et al (1999) BNCT: implications of neutron beam and boron compound characteristics. Med Phys 26(7):1237–1244
51. Yanch JC, Zhou X-I, Shefer RE et al (1992) Accelerator-based epithermal neutron beam design for NCT. Med Phys 19:709–721, and references therein
52. Ziegler JF (2008) The stopping and range of ions in matter. www.srim.org/SRIM/SRIM2008.htm. Accessed 2009
53. Zonta A et al (eds) (2008) BNCT: a new option against cancer. Proceedings of the 13th international congress on neutron capture therapy, Appl Radiat Isot. Florence, Italy, 67(7–8): s1–s380

Compact Neutron Generator for BNCT

4

Ka-Ngo Leung

Contents

4.1 Introduction

Neutron sources are commonly used in research, industry, and clinical applications. Many of these are in sealed radiological sources used in petroleum engineering (e.g., well logging for oil exploration), in medicine (cancer treatment, pacemakers, and diagnostics), in homes (smoke detectors), and to make electricity (in radiothermal generators that generate power in remote areas ranging from lighthouses to outer space). For example, Cf-252 and Am-Be are used to provide multi-MeV neutrons for activation analysis and well logging. Radioactive sources can be portable or fixed, and most are quite small, ranging from tiny brachytherapy needles or seeds

K.-N. Leung
Department of Nuclear Engineering, University of California,
Berkeley, CA, USA

Lawrence Berkeley National Laboratory,
Berkeley, CA, USA
e-mail: knleung@lbl.gov

W.A.G. Sauerwein et al. (eds.), *Neutron Capture Therapy*,
DOI 10.1007/978-3-642-31334-9_4, © Springer-Verlag Berlin Heidelberg 2012

(implanted for localized cancer treatment) to thimble-sized plugs sealed within secure capsules for industrial gauges.

In recent years, substantial effort has been spent in the development of radio frequency (RF) plasma-based neutron generators that can provide high yields of neutrons for clinical applications such as boron neutron capture therapy (BNCT). By using the D-D fusion reaction, 2.4 MeV neutrons can be produced with a compact generator operating with ~100 keV of deuterium beam energy. Similarly, 14 MeV neutrons can be produced by the D-T fusion reaction. These RF plasma-based neutron sources are safe to operate and they can be turned on and off conveniently. A number of these D-D neutron generators have already been operating in universities, research institutions, and private industries around the world to replace the radioisotope neutron sources. In particular, a compact D-D neutron generator has been installed in Turin, Italy, for BNCT development.

BNCT brings together two components. The first component is the delivery of ^{10}B – a stable isotope of boron with a large cross section for thermal neutron absorption – preferentially to the tumor cells with the help of tumor-seeking compounds. The second component is a beam of low-energy neutrons. When a thermal neutron is captured by ^{10}B, the reaction $^{10}B(n,\alpha)^{7}Li$ occurs, releasing two high-energy ions. Because of the high linear energy transfer and relative biological effectiveness (RBE) of these ions, only cells in close proximity to the reaction are damaged, leaving adjacent cells unaffected. The enhanced uptake of the boron-labeled agent in tumor cells versus normal cells results in selective killing of tumor cells, due to the higher dose that can be delivered to them. So far, the neutrons used for BNCT are produced mostly in a fission reactor. In recent years, attempts have been made to generate the neutrons by using a compact neutron generator so that one can house the complete BNCT system inside a medical facility.

4.2 RF-Driven Plasma Source for Neutron Production

A compact neutron generator consists of three components: an ion source, an electrostatic accelerator, and a target electrode (Fig. 4.1). RF-driven plasma source is now commonly used for ion beam generation. A schematic of an RF-driven plasma source is shown in Fig. 4.2. This type of ion source is being used in all compact neutron generators developed by the Plasma and Ion Source Technology Group at Lawrence Berkeley National Laboratory (LBNL). Three deuterium ion species (D^+, D_2^+, and D_3^+) are present in a deuterium gas discharge plasma. The atomic D^+ ions are preferred for neutron production because they can provide full energy for the fusion reaction when they impinge on the target surface. The molecular deuterium D_2^+ and D_3^+ ions will disintegrate into two or three atoms at the target. Each of these atoms will carry only one-half or one-third of the beam energy. With lower interaction energy, the fusion neutron production rate will be reduced.

The ion source is operated with a 13.5 MHz power supply and an impedance matching network. The plasma is produced by RF induction discharge via a copper coil antenna covered with quartz tubing. By operating the source with pure deuterium

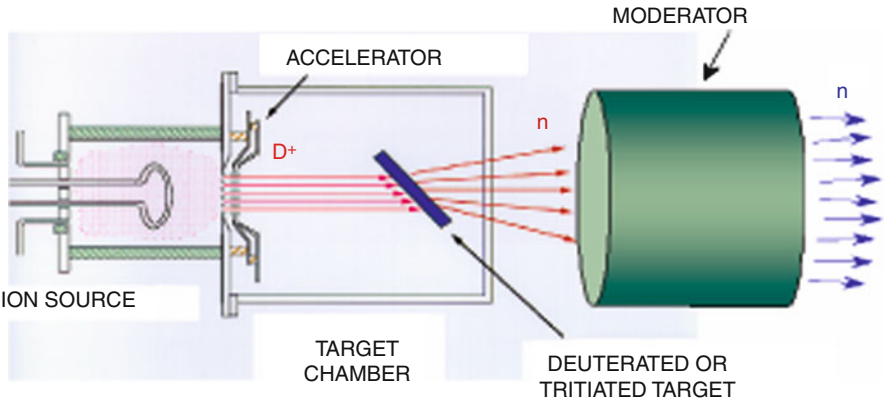

Fig. 4.1 An axial-type neutron generator

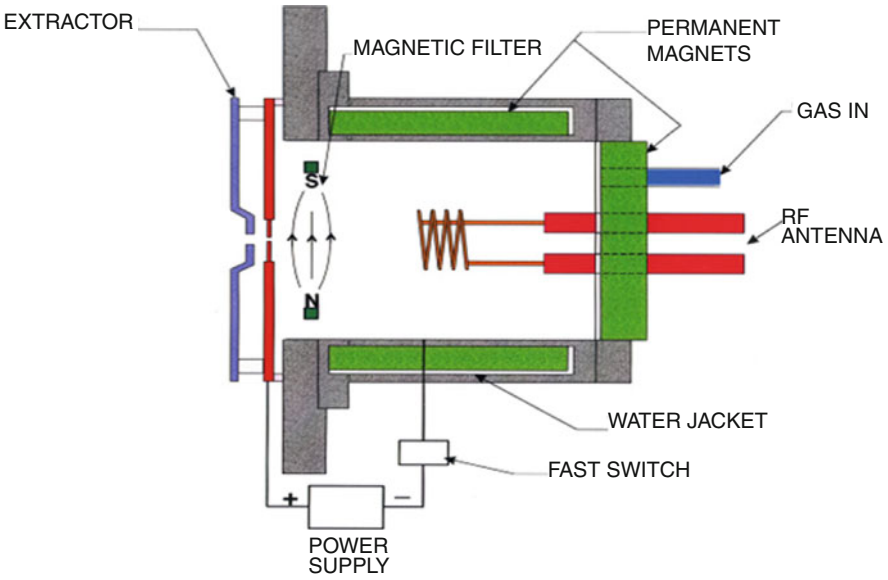

Fig. 4.2 An RF-driven multicusp ion source

gas (or a mixture of deuterium and tritium gas), D^+ ions (or D^+ and T^+ ions) will be extracted from the exit aperture of the source. A simple single gap extraction system is used to accelerate the ions to 100 keV or higher energy. An actively cooled Ti target electrode is used to catch the accelerated D^+ (or D^+ and T^+) ion beam. As a result, the target surface will continue to be loaded with deuterium (or deuterium and tritium). The incoming D^+ ions will react with the D atoms on the target surface forming the 2.45 MeV D-D neutrons (or the 14 MeV D-T neutrons). This type of *beam-loaded target* has been employed in all the neutron generators developed at LBNL. It provides a very long-life operation and can be designed in various

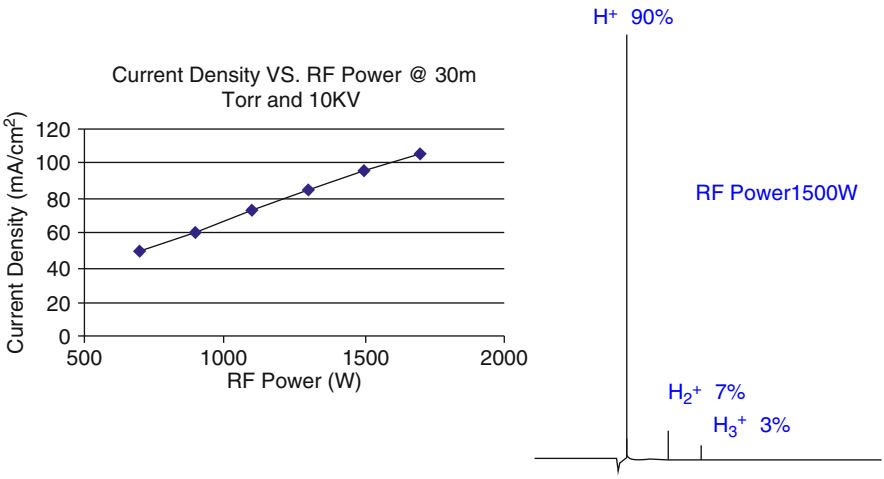

Fig. 4.3 Current density as function of RF input power and ion species distribution

configurations. With a 100 keV, 1 A D^+ ion beam, one should be able to achieve a D-D neutron yield $>10^{11}$ n/s (or D-T neutron yield $>10^{13}$ n/s).

Compared with other types of ion sources (such as the Penning discharge source used in most commercial neutron generators), the RF-driven ion source has two advantages. It can provide high atomic D^+ or T^+ ion percentage (>90 %), and it can easily generate deuterium (or tritium) ion current density higher than 100 mA/cm^2 with modest RF input power. Figure 4.3 shows the ion species distribution when a beam is extracted from a 10-cm-diam RF-driven hydrogen plasma source. It can be seen that the atomic ion concentration is higher than 90 % with 1.5 kW of RF input power. Similar results are obtained with a deuterium, tritium, or a mixed deuterium-tritium RF discharge.

Figure 4.3 shows the extractable ion current density from the RF-driven plasma source increases linearly with the RF input power. In principle, there is no limitation on the extractable ion current density as long as the RF power supply is capable of providing the required input power. However, for optimal neutron production, the beam power density on the target electrode of the neutron generator should not exceed 700 W/cm^2. If the beam energy is 100 keV, the current density should not exceed 7 mA/cm^2 on the target surface. In order to increase the neutron yield, one has to increase the fusion reaction rate by increasing the total beam current *and* at the same time maintaining the optimum beam power density on the target electrode. One can meet these two requirements by using multiple beamlet extraction, and at the same time, spreading the ion beamlets to a large target surface.

The external surface of the ion source chamber is normally surrounded with columns of permanent-magnets forming a series of magnetic line-cusp field for plasma confinement. This type of *multicusp* plasma source can provide large areas of very uniform plasma density (Fig. 4.4) that will enable multi-beamlet extraction and therefore high neutron output.

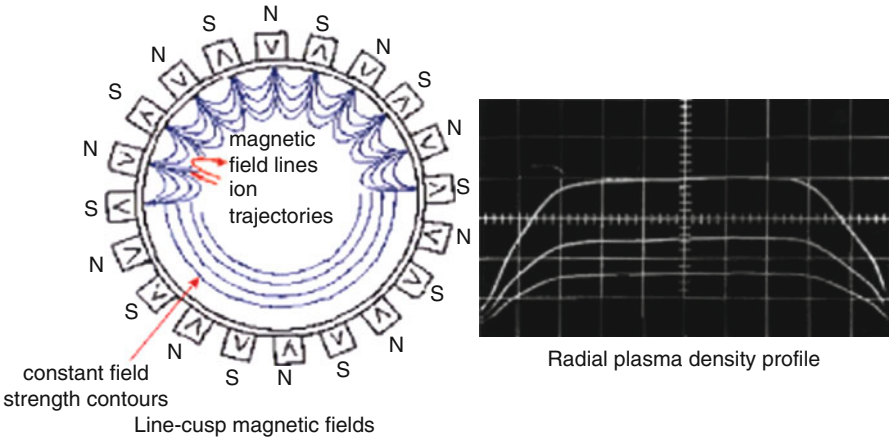

Fig. 4.4 Cross-sectional view of source chamber and radial plasma density profiles

4.3 Compact Neutron Generator for High Neutron Yield

Two neutron generator configurations have been used to provide high neutron yield. The first is the *axial-type* configuration shown schematically in Fig. 4.1. In this type of generator, the external surface of the ion source chamber is surrounded with columns of permanent-magnets for plasma confinement (a *multicusp* ion source). As a result, a large area of very uniform plasma density can be formed. Multiple ion beams can be extracted from the uniform plasma density region. Figure 4.4 shows the cross-sectional view of a 30-cm-diam *multicusp* ion source chamber and the radial plasma density profile for three different discharge power. The *multicusp* source configuration enables multi-beamlet extraction and therefore high total beam current.

Figure 4.5 shows a schematic diagram of a sealed axial-type D-T neutron generator [1]. In this system, the RF-driven ion source, the accelerator column, and the target electrode are all housed in a sealed metal container without external pumping. During operation, deuterium and tritium will be released from the reservoir element and the target. After operation, both gases will return to the reservoir element and target due to their lower temperatures. The ion beamlets are extracted from one side of the ion source. In order to reduce the beam power density, the beamlets are focused at the high-voltage electrode. They then spread out to a much larger area on the target electrode as illustrated in Fig. 4.5. With a 150 keV and 2 A mixed D^+ and T^+ beam hitting a well-cooled target, a neutron yield of 10^{14} n/s can be achieved over long periods of operation.

In order to treat deep brain tumor with BNCT, one has to deliver thermal neutrons to it. A previous study showed that one ideally needs to supply epithermal neutrons with an energy distribution peaking at ~10 keV [2]. The high hydrogen content of the brain slows down the incoming epithermal neutrons in such a way

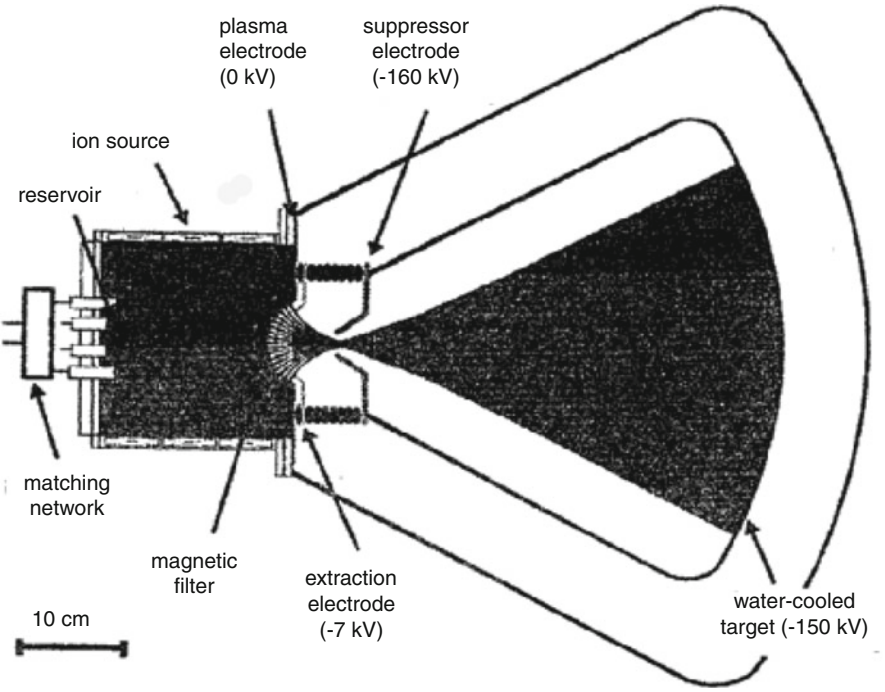

Fig. 4.5 Schematic diagram of the sealed axial-type D-T neutron generator

that they become thermalized when they reached the desired depth. Verbeke et al. [3] and Cerullo et al. [4] demonstrated that the 14 MeV D-T neutrons can be moderated to the desired energy range without reducing the neutron flux to a negligible level. With the optimal moderator and lead reflector configuration, a 1-A mixed D^+/T^+ beam with energy of 150 keV accelerated onto a titanium target leads to a treatment time of 1 h [3]. The dose near the center of the brain obtained with this neutron generator and moderator system is more than 65 % higher than the dose from a typical spectrum produced by the Brookhaven Medical Research Reactor and is comparable to the dose obtained by the other accelerator-produced neutron beams. Figures 4.6 and 4.7 show the beam-shaping assembly (BSA) design and the resulting neutron energy distribution as reported in Ref. [3].

The second configuration is the *coaxial type* of source (Fig. 4.8). In this arrangement, the ion source is cylindrical in shape and is located at the center of the generator. The target is a larger diameter aluminum cylinder with the inner surface coated with a layer of titanium. In normal operation, the ion source chamber is at ground potential while the target is biased at −120 kV. The plasma is produced by 13.5 MHz RF induction discharge. Positive deuterium ions are extracted from the apertures on the source chamber wall and they will be accelerated toward the target. When the deuterium ions impinge on the titanium target surface, neutrons will be generated by the D-D fusion reaction. If the ion source is operated with a mixture of deuterium

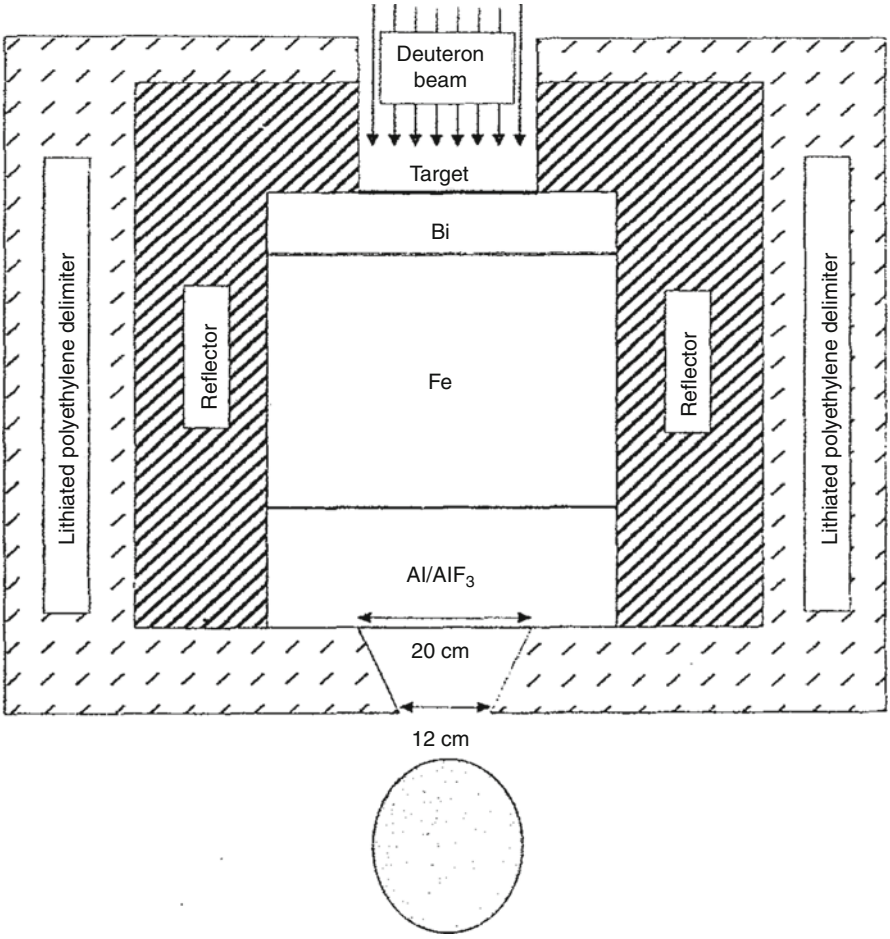

Fig. 4.6 A design of the beam-shaping assembly (BSA) based on a sealed D-T neutron generator

and tritium discharge, both D^+ and T^+ ions will be extracted and accelerated to the target cylinder. In this case, both D-T, D-D, and T-T neutrons will be produced. Since the D-T reaction has a much larger cross section, most of the neutrons produced will have energies of 14 MeV.

Columns of permanent-magnets are installed in the target chamber so as to suppress the secondary emission electrons generated by the ion beams. These electrons will constitute a large power supply drain current. They will also generate unwanted X-rays when they impinge on the ion source chamber. Since the diameter of the target chamber is larger than that of the ion source, the applied electric field will spread the ion beam to a larger surface area. As a result, the beam power density on the target electrode is reduced (at least by a factor of R_t/R_s where R_t and R_s are the

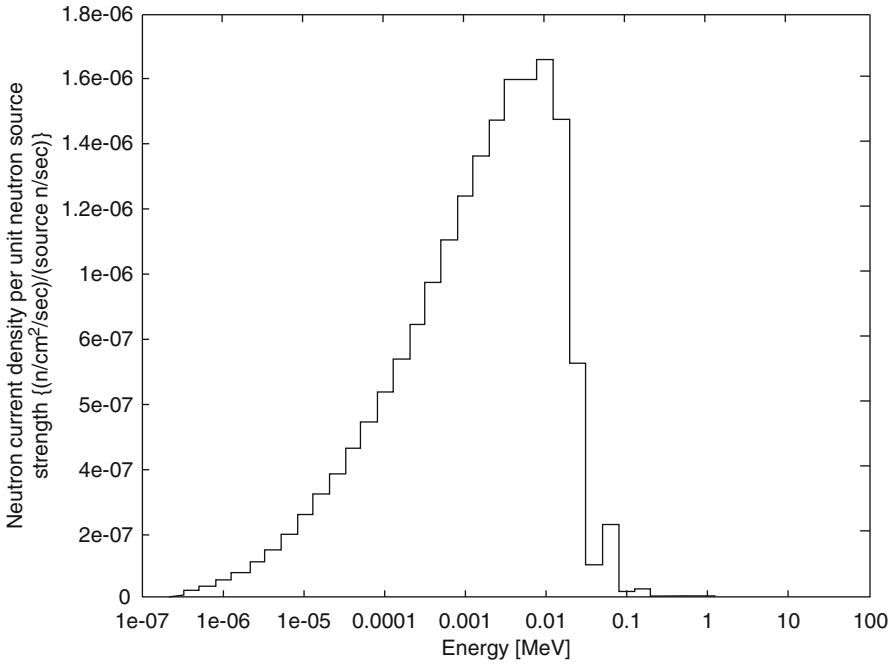

Fig. 4.7 Neutron energy distribution after moderation with an optimal BSA for D-T neutrons

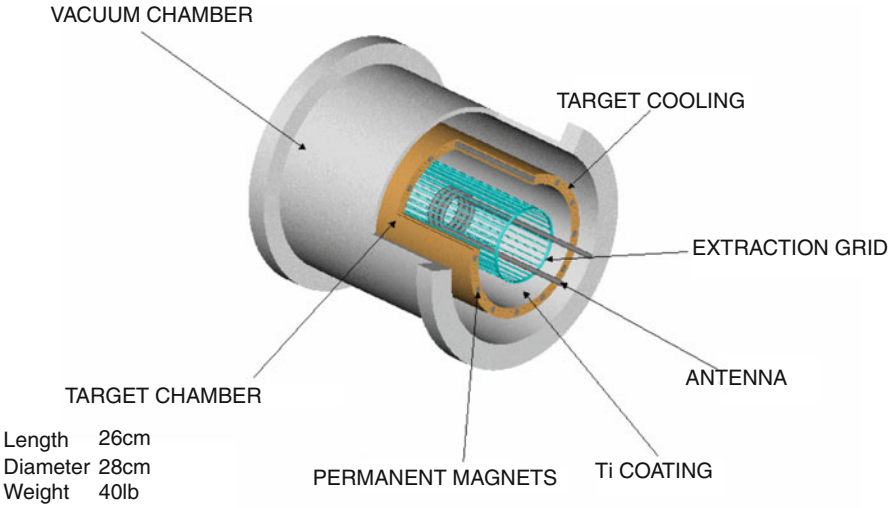

Fig. 4.8 A schematic drawing of the coaxial type neutron generator

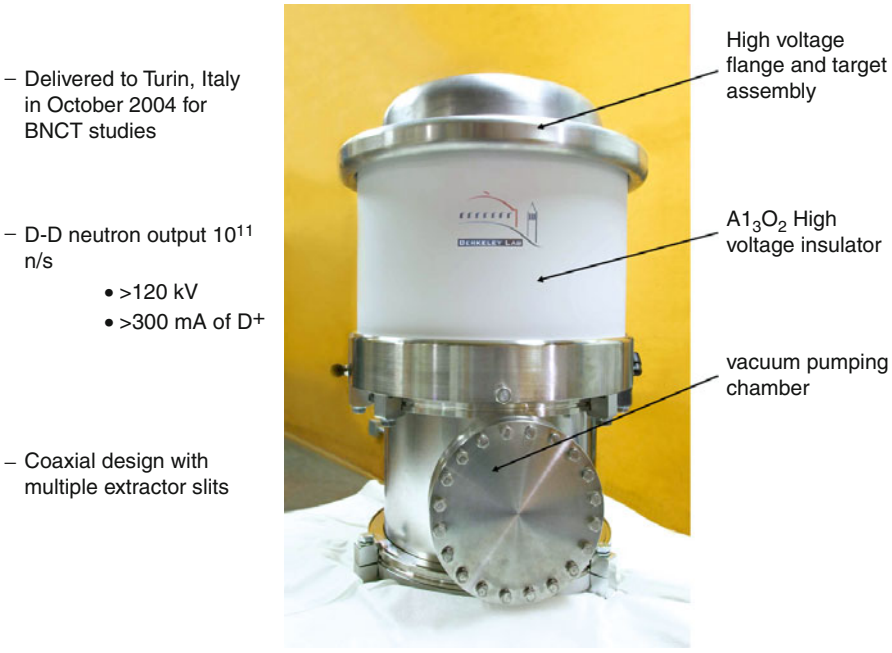

Fig. 4.9 The EUROSEA Coaxial-type D-D neutron generator

radius of the target chamber and the ion source chamber, respectively). Thus, one can produce high neutron flux without overheating the target surface.

A photograph of a coaxial type D-D neutron generator is displayed in Fig. 4.9. This generator was developed by LBNL for the EUROSEA Committee in Turin, Italy, for BNCT application. Both the ion source and the target electrode are designed to operate with a total beam power of 120 kV, 1 A so that a D-D neutron yield higher than 10^{11} n/s can be achieved. This coaxial neutron generator was delivered to Turin, Italy, at the end of 2004. The commissioning of this D-D neutron generator was performed in the University of Turin in March, 2005. In order to reduce the treatment time for liver tumor, MCNP computation shows that the neutron yield has to increase to about 2×10^{12} n/s. Different schemes for upgrading the EUROSEA generator yield to higher than 10^{12} D-D n/s have been investigated, and the results were reported in the 13th International Congress on Neutron Capture Therapy, November 2–7, 2008, Florence, Italy.

4.4 Moderator Design for the Coaxial Neutron Generator

D-D fusion neutrons have energies of 2.45 MeV, and D-T fusion neutrons have energies of 14 MeV. These neutrons need to be moderated to the optimal neutron energy spectrum for BNCT. MCNP computation code has been employed for the moderator design study. Preliminary results have been reported by H. Koivunoro

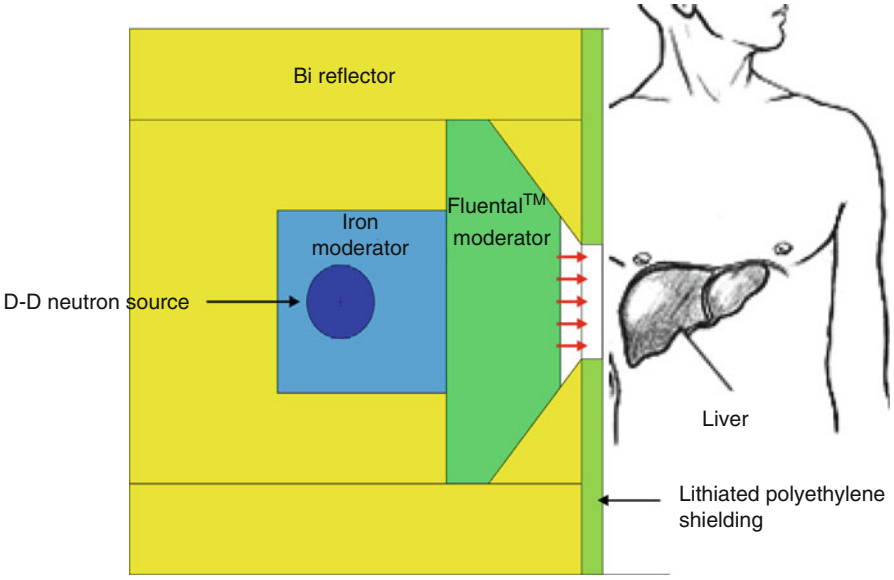

Fig. 4.10 A beam shaping assembly (BSA) for liver cancer treatment

et al. [5]. Figure 4.10 shows one of the moderator designs developed by the Plasma and Ion Source Technology Group at LBNL. With the use of a different material such as Fluental and iron, one can optimize the neutron energy spectrum for liver cancer treatment as illustrated in Fig. 4.11. In order to optimize the therapeutic ratio, various beam shaping assemblies (BSA) have been investigated by E. Durisi et al. [6] using different materials and geometrical shapes.

4.5 Use of a Subcritical Multiplier for BNCT

Even though the upgraded coaxial neutron generator can provide a D-D neutron source intensity of 2×10^{12} n/s, it is still an order of magnitude short of the intensity needed for BNCT of deep-seated brain tumors. The feasibility of using a small, safe, and inexpensive subcritical fission assembly (SCM) to multiply the D-D fusion neutrons from a compact neutron generator (CNS) has recently been investigated [7]. This will enable one to treat deep-seated brain tumors in approximately one hour. It was identified that the optimal design of a passively cooled SCM should be made of 20 %-enriched, aluminum clad metallic uranium fuel. The SCM geometry was designed so as to increase the solid angle by which the SCM "views" the CNS (Fig. 4.12); it was arranged as a "cup" shape that surrounds the CNG on three sides: k_{eff} is 0.98. The required 20 %-enriched uranium amount is 8.5 kg. The required SCM power level is estimated at 400 W when driven by a 1×10^{12} D-D n/s neutron source. This translates into consumption of only about 0.5 % of the initially loaded ^{235}U atoms during 50 years of continuous operation. It thus appears that the SCM

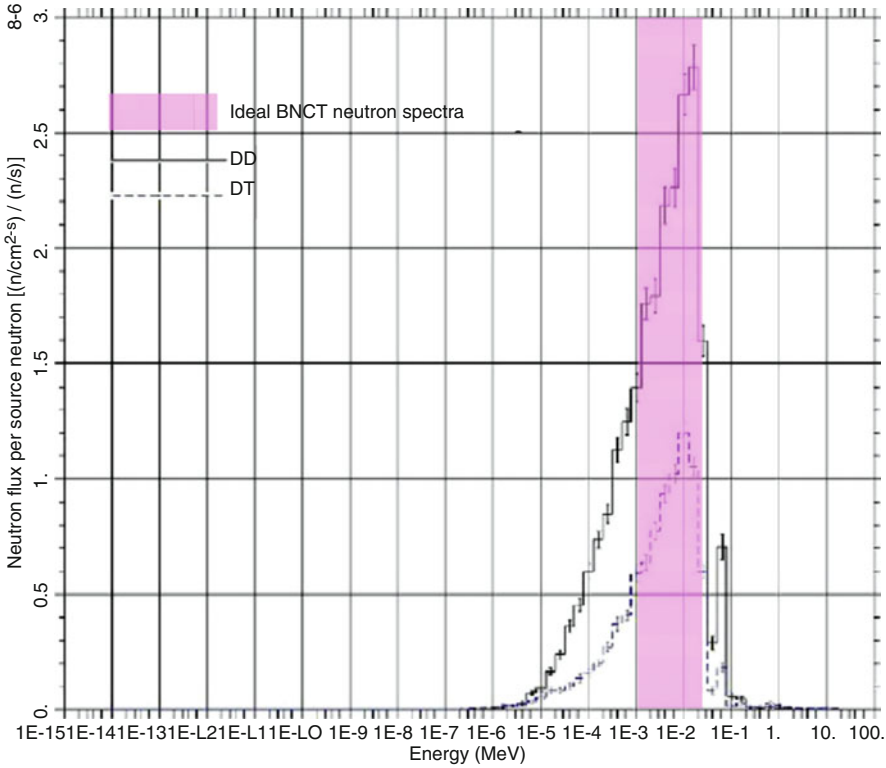

Fig. 4.11 Moderated neutron spectra for D-D and D-T neutrons

could operate continuously for the entire lifetime of the machine without refueling. Also as desired, cooling the SCM does not pose a challenge; it may be accomplished passively; i.e., without resorting to forced circulation.

Two optimal beam shaping assembly (BSA) designs were identified: one for maximizing the dose rate (illustrated in Fig. 4.13) and the other for maximizing the total dose that can be delivered to a deep-seated tumor. The maximum dose rate that can be delivered by the former is 10.1 Gy/h, and the maximum dose that can be delivered by the latter is 51.8 Gy. The former features a harder neutron spectrum and relatively high neutron dose component to the skin, while in the latter the neutron, gamma-ray, and boron-dose components in the skin are comparable. The corresponding maximum dose rates that can be delivered to the tumor are 10.1 Gy/h and 51.8 Gy.

The study concludes that the addition of a SCM makes it possible to increase the treatment beam intensity by a factor of 18 – from 0.56 to 10.1 Gy/h, with the CNS intensity of 1×10^{12} n/s. Therefore, a practical BNCT facility based on the optimal system identified in this study could deliver the desired tumor dose in less than an hour, if either one of the following approaches is adopted: (1) irradiating the patient in 3 to 4 one-hour sessions; (2) irradiating the patient using 3 or 4 beams simultaneously;

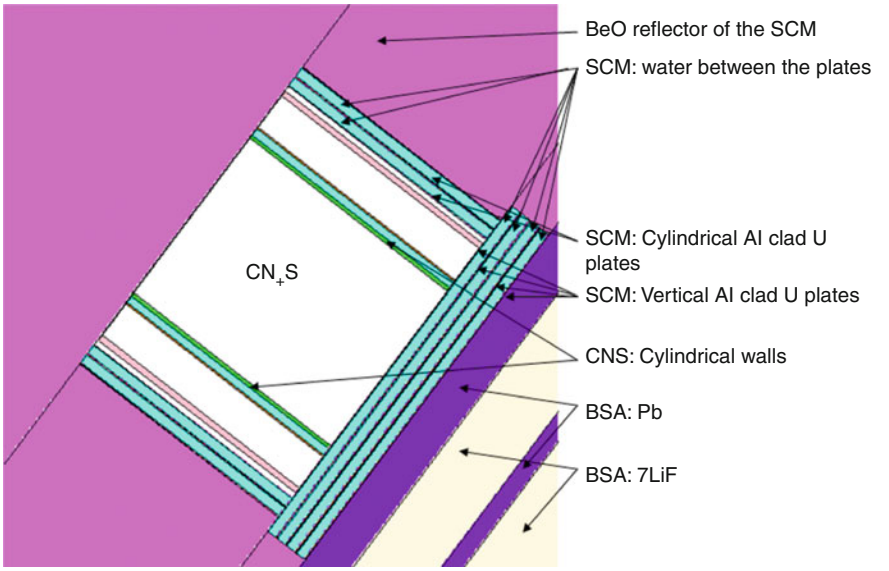

Fig. 4.12 Cross-sectional view of the "cup shape" SCM that surrounds the CNS

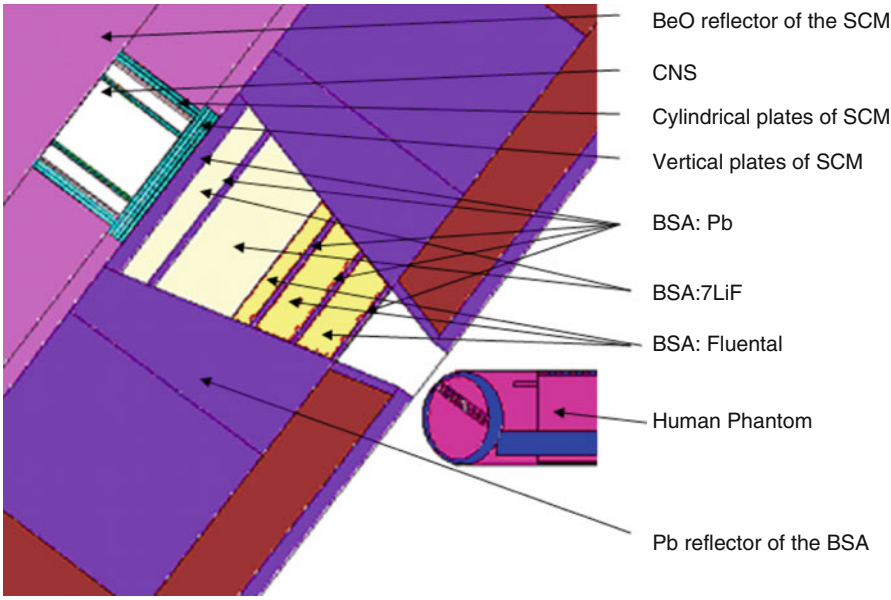

Fig. 4.13 Cross-sectional view of the BSA design that maximizes the dose rate

or (3) increasing the permissible SCM maximum k_{eff} to 0.995. However, if the CNS intensity of 2.3×10^{12} n/s could be achieved, the above mentioned remedies would not be needed.

4.6 Summary

In summary, compact neutron generators based on the D-D and D-T fusion reactions can provide the required neutron yield for boron neutron capture therapy. Two neutron generator configurations have been developed to meet the BNCT requirement. These compact neutron generators coupled with the proper moderator design and efficient boron-10 compound can provide a low cost and easy to operate BNCT facility well-suited for installation in the hospital environment.

Acknowledgment The author would like to thank members of the Plasma and Ion Source Technology Group at Lawrence Berkeley National Laboratory, the Nuclear Engineering Department at the University of California, Berkeley, and the EUROSEA Committee in Turin, Italy, for the material presented in this article.

References

1. Verbeke JM, Leung KN, Vujic J (2000) Development of a sealed-accelerator-tube neutron generator. Appl Radiat Isot 53:801–809
2. Yanch JC, Zhou XL, Brownell GL (1991) A Monte Carlo investigation of the dosimetric properties of monoenergetic neutron beams for neutron capture therapy. Radiation Res 126:1–20
3. Verbeke JM, Vujic J, Leung KN (2000) Neutron beam optimization for boron neutron capture therapy using the D-D and D-T high-energy neutron sources. Nucl Technol 129:257–278
4. Cerullo N, Esposito J, Leung K-N, Custodero S (2002) An irradiation facility for Boron Neutron Capture Therapy application based on a radio frequency driven D–T neutron source and a new beam shaping assembly. Rev Sci Instrum 73(10):3614
5. Koivunoro H, Bleuel DL, Nastasi U, Lou TP, Reijonen J, Leung KN (2004) BNCT dose distribution in liver with epithermal D-D and D-T fusion-based neutron beams. Appl Radiat Isot 61:853–859
6. Durisi E, Zanini A, Manfredotti C, Palamara F, Sarotto M, Visca L, Nastasi U (2007) Design of an epithermal column for BNCT based on D-D fusion neutron facility. Nucl Instrum Methods Phys Res A 574:363–369
7. Ganda F. Vujic J, Greenspan E, Leung K (2010) Compact D-D neutron source-driven subcritical multiplier and beam-shaping assembly for boron neutron capture therapy. Nucl Technol 172(3):302–324

Californium-252 as a Neutron Source for BNCT

5

Albert Miller

Contents

5.1 Physical Properties of Californium-252

In November 1952, the isotope Cf-252 was discovered in the debris from the MIKE thermonuclear test at Enewetak [1]. Early investigations of its properties indicated a half-life of between 2 and 3 years (actually 2.645 years) and significant branching fractions for decay by spontaneous fission (SF), making Cf-252 an especially good and compact source of neutrons. Due to its availability in macroscopic quantities, Cf-252 has been one of the most extensively studied transplutonium isotopes. Most of the effort has been directed at understanding the spontaneous fission properties, some of which are summarised in Table 5.1. These properties make Cf-252 one of the most useful neutron emitters out of all the ~3,000 known radionuclides. Though isotopes such as Cf-254 and Md-260 have higher rates of spontaneous fission, their half-lives are too short, i.e. weeks, to permit large-scale fabrication. The majority,

A. Miller
Department of Radiation Medical Physics,
Institute of Oncology, Vilnius University, Santariskiu-1, 06880 Vilnius, Lithuania
e-mail: albert.miller@varian.com

W.A.G. Sauerwein et al. (eds.), *Neutron Capture Therapy*,
DOI 10.1007/978-3-642-31334-9_5, © Springer-Verlag Berlin Heidelberg 2012

Table 5.1 Decay and spontaneous fission properties of Californium 252 [3–5]

Half-life	2.645 years
Specific activity	536.3 Ci/g
Decay mode	α (96.908 %), SF (3.092 %)
Neutron multiplicity	3.768 n/fission
Mean fission neutron spectrum energy	2.13–2.15 MeV
Prompt γ-ray multiplicity (mean)	~10/fission
Average prompt γ-ray energy	0.7–0.9 MeV

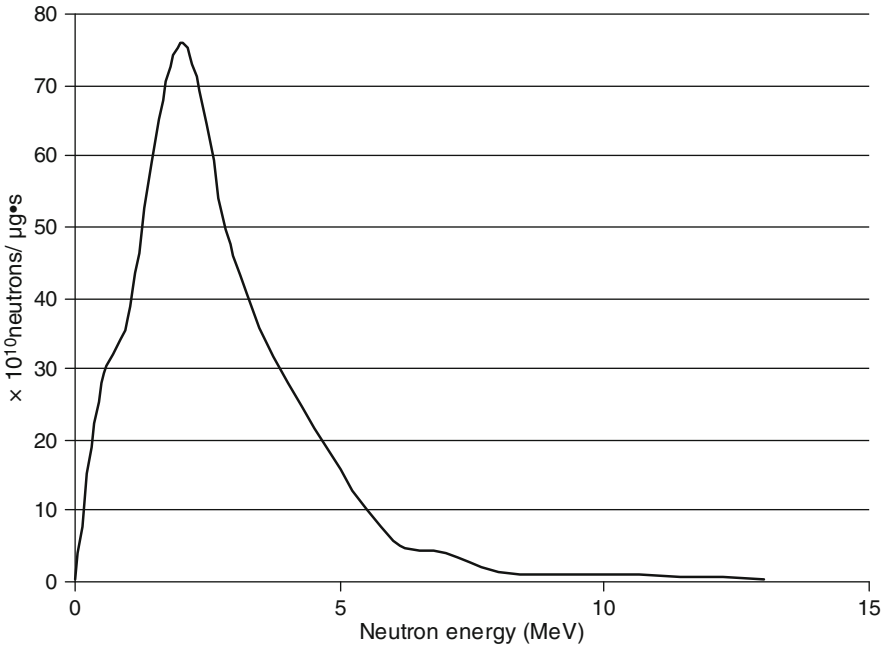

Fig. 5.1 Neutron energy spectrum from spontaneous fission of Cf-252 (total = 2.31×10^{12} neutrons/µg·s)

96.9 %, of Cf-252 decays are through alpha decay, but due to the nature of encapsulation, these He-4 nuclei do not escape the confines of the source. A small 3.092 % but significant proportion of Cf-252 decays via spontaneous fission which produces fission fragments, as well as a neutron yield of 3.768 n/fission (2.31434×10^{12} neutrons/s/g of Cf-252). The Cf-252 neutron energy spectrum is shown in Fig. 5.1. These neutrons have an energy spectrum which can be modelled as either a Maxwellian or a Watt fission spectrum. The National Bureau of Standards (NBS) evaluated this spectrum (Table 5.2) and made compensation for the deviations from an ideal Maxwellian spectrum with the use of energy-dependent adjustment functions. The relative uncertainty in the NBS neutron energy spectrum is small, with exceptions of the relative uncertainties in the 0–0.25 and 8–12 MeV groups. However, the number of neutrons emitted in these two energy groups is small,

Table 5.2 NBS evaluation of the Cf-252 neutron spectrum [5] $X_{Cf} = [0.6672(E)^{1/2}\exp(-E/1.42)]\cdot\mu(E)$, where E is in MeV

Energy interval (MeV)	$\mu(E)$	Relative uncertainty (1σ) (%)
0–0.25	$1+1.20E-0.237$	±13
0.25–0.8	$1-0.14E+0.098$	±1.1
0.8–1.5	$1+0.24E-0.0332$	±1.8
1.5–6.0	$1-0.00062E+0.0037$	±(1.0–2.1)
6.0–20	$1.0\exp[-0.03(E-6.0)]$	±8.5

compared with the total neutron emission. Other Cf-252 emissions include prompt gammas and also photons from the fission products [2]. The total gamma emission spectrum is shown in Fig. 5.2.

5.2 Californium-252 Medical Sources

Clinical brachytherapy (interstitial and intracavitary) can be performed with essentially three different types of source designs: seed, needle, and applicator tube. Seed sources are more often used in the form of a flexible assembly. The characteristics of these Cf-252 medical sources are summarised in Table 5.3.

The clinical application of needls and flexible Cf-252 sources are limited because of their low neutron activity. On the other hand, the maximum possible licensed activity cannot be more than 100 μg of Cf-252 because of the neutron dose incurred by medical personnel during manual loading into patients. Use of miniature high activity more than 1 mg of Cf-252 (2.5×10^9 n/s), remotely, afterloaded sources, significantly reduce treatment times, eliminate radiation hazard to the medical staff, and expedite treatment of brain and other tumours.

5.3 Dosimetric Properties of Cf-252 Sources

The dose deposition in tissue, in the vicinity of the Cf-252 source, is well known and basically has four components:

$D = D_n + D_\gamma + D_{n\,\gamma} + D_p$ (primary neutron dose, primary photon dose, secondary photon dose, and proton dose).

The primary neutron dose is produced by the emitted neutrons with properties described above. This main component of the total absorbed dose in the tissue decreases rapidly with increasing distance from the source. The primary photon dose is due to the photons emitted by source, either from the spontaneous fission or by decay by-products. Close to the source, the photon dose is about half of the neutron component (see Fig. 5.3), but due to the increased penetrating ability through the tissue of photons compared to the neutrons, its proportional contribution increases at larger distances. The secondary photon dose is due to radiation capture of slow neutrons by hydrogen. Contribution of this component depends on the

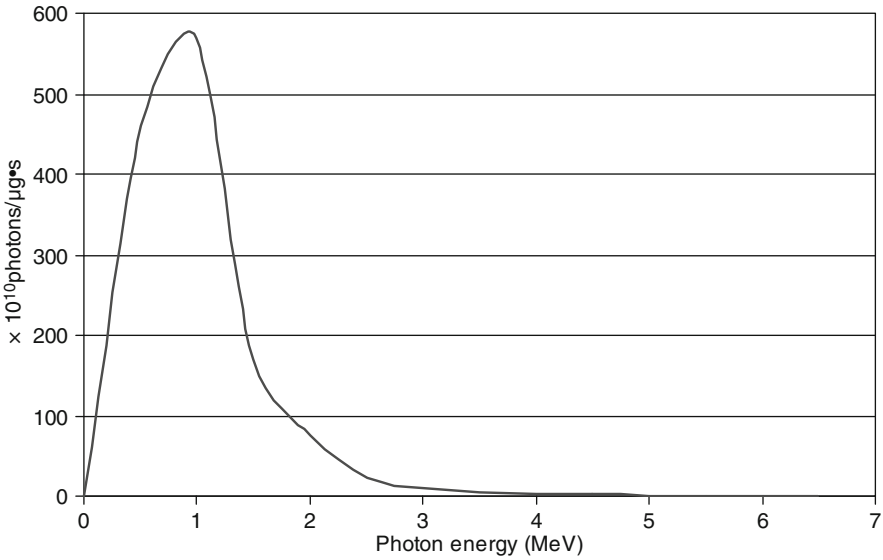

Fig. 5.2 Photons energy spectrum from spontaneous fission of Cf-252 (total = 1.322×10^{13} photons/µg·s)

Table 5.3 Properties of Cf-252 medical sources

Source type	Neutron fluence n/s	Source size (mm)		Encapsulation	Country of origin
		Diameter	Length		
Needle	2×10^6–1.5×10^7	1.2	15–35	1	Russia
	1.7×10^6–3.5×10^6	0.96	18–33	1	USA
	2.6×10^6–5×10^6	1.2	35	1	Germany
Flexible	5.5×10^6–1×10^7	1.1	40–60	1	Russia
	3.5×10^6–8×10^6	1.1	30–80	1	USA
	3.0×10^6–6×10^6	1.0	40–90	1	France
Applicator tube	2.3×10^7–3.7×10^9	3.0	15	2	Russia
	4.6×10^7–2.3×10^9	2.8	14–23	2	USA
	2.3×10^8	4.7	9.8	2	Japan

fluence of slow (thermalized) neutrons at the point of interest. It is negligibly small close to the source, but quite significant at distances up to 2–3 cm (see Fig. 5.4). The proton dose is a consequence of the $^{14}N(n,p)^{14}C$ capture reaction, and its contribution also depends on the thermal neutron fluence.

5.4 Clinical Applications of Cf-252 Sources

Needles and seeds of Cf-252 have been used clinically for interstitial soft tissue implants and surface applicators. These treatment techniques require manual loading of radioactive sources and are almost obsolete nowadays due to radiation

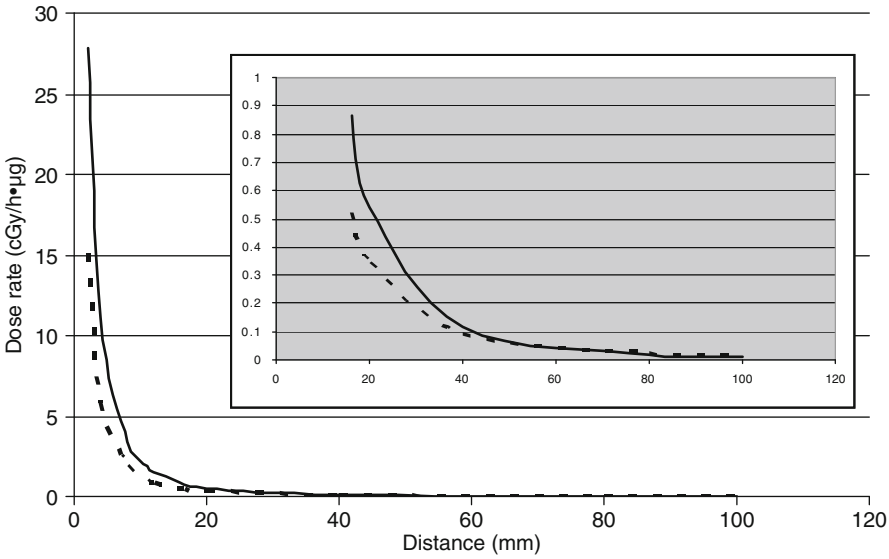

Fig. 5.3 Neutron and gamma absorbed dose rate (cGy/h·µg) in homogeneous tissue equivalent media from HDR afterloader source (active part diameter 1.5 mm, length 1 cm) [6]

protection concerns. Such sources are also of little interest to BNCT as the neutron fluence is far too low. The tube sources, on the other hand, with activities from more than 1 mg of Cf-252, produce considerably higher neutron fluences and may be of interest for BNCT.

Cf-252 remote afterloading devices with three sources (two "ovoids" and "tandem" with initial activities of 0.4 and 1.3 µg of californium, respectively) have been designed for gynaecological applications [7]. The physical size of the source also allows their application for the treatment of other cancer sites, such as rectum, esophageal, and brain tumours. Considering the sufficiently high fluence of thermal neutrons from this type of source and the increase in the relative fluence of slow neutrons with distance (see Fig. 5.4), some investigators have explored boron-10 enhancement Cf-252 brachytherapy [8]. Administration of a B-10 compound to the treatment site combined with the insertion of high activity Cf-252 into the tumour can improve significantly the dose distribution, especially in areas of micro-invasion. However, current boron drugs are still viewed as giving insufficient tumour-to-blood and tumour-to-tissue concentrations.

For the treatment of bulky brain tumours, it is essential that the dose distribution is conforming to the irregularly shaped, gross target volume and at the same time, delivers the necessary dose to the areas of clinically suspected disease. Due to the symmetrical nature of the dose distribution from a single Cf-252 source, these requirements are impossible to achieve in most cases. The use of small Gd-157 pellets (seeds or needles) as the NCT agent, in the case of bulky brain tumours, could provide the clinician with more flexibility to provide the desired dose distribution.

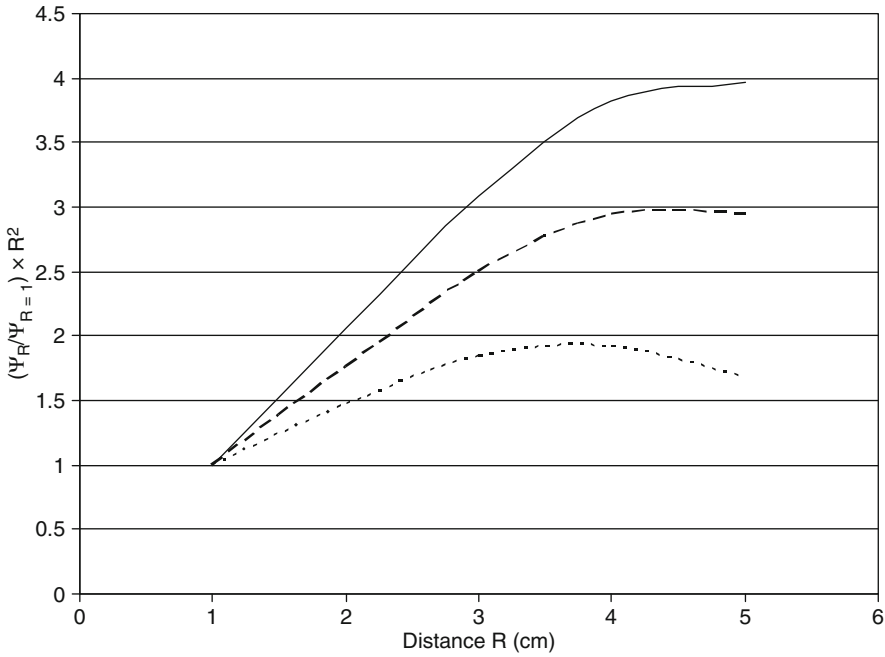

Fig. 5.4 The relative changes of thermal neutron fluence in tissue equivalent media. The fluence is normalised to 1 cm distance from the source and is corrected for inverse square law. *Solid line* – neutrons with energy $E = 1$ keV, *dashed line* – neutrons with energy $E = 10$ keV, *dotted line* – neutrons with energy $E = 100$ keV [7]

References

1. Fields PR et al (1956) Transplutonium elements in thermonuclear test debris. Phys Rev 102:180–182
2. Knauer JB, Alexander CW, Bigelow JE (1991) Cf-252 properties, production, source fabrication and procurement. Nucl Sci Appl 4:3–17
3. Browne E, Firestone RB, Shirley VS (eds) (1986) Table of radioactive isotopes. Wiley-Interscience, New York, pp 249–1 – 254–1
4. Axton NE (1987) Intercomparison of neutron source emission rates (1979–1984). Metrologia 23:129–144
5. Grundl J, Eisenhauer C (1975) Fission rate measurements for materials neutron dosimetry in reactor environments. In: Proceedings of the first ASTM-EURATOM symposium on reactor dosimetry, Petten, 1975, pp 425–454
6. Anderson LL (1986) Cf-252 physics and dosimetry. Nucl Sci Appl 2:273–282
7. Zyb A (ed) (1996) Effects of Cf-252 gamma-neutron irradiation. Energoatomizdat, Moscow
8. Maruyama Y (1984) Cf-252 neutron brachytherapy an advance for bulky localized cancer therapy. Nucl Sci Appl 1:677–748

Part II

Boron

Boron Chemistry

6

Luigi Panza and Davide Prosperi

Contents

L. Panza (✉)
Dipartimento di Scienze del Farmaco, Università del Piemonte Orientale "A. Avogadro", Largo Donegani, 2–28100, Novara, Italy
e-mail: panza@pharm.unipmn.it

D. Prosperi
Dipartimento di Biotecnologie e Bioscienze, Università di Milano-Bicocca, Piazza della Scienza 2, Edificio U3 – 20126, Milano, Italy
e-mail: davide.prosperi@unimib.it

W.A.G. Sauerwein et al. (eds.), *Neutron Capture Therapy*,
DOI 10.1007/978-3-642-31334-9_6, © Springer-Verlag Berlin Heidelberg 2012

6.1 Introduction

Boron is a peculiar and intriguing element, and, mainly because of its particular electronic configuration, can give rise to an eclectic and complex chemistry. In view of the context of the book in which this chapter is included, we will limit our discussion to some basic elements of boron chemistry, both from inorganic and organic chemistry viewpoints. During the past, and also in the present, its unique properties have stimulated not only the development of preparative and theoretical chemistry, but also industrial and technological applications [1].

Looking at the periodic table (Fig. 6.1), boron is located at the top of group 13, being the only non-metal in this group. Moreover, its chemical behavior has many similarities with the following element, carbon, and its diagonal neighbor, silicon. Then, like them, it has a strong tendency to form covalent bonds, but it differs clearly from them as it has four bonding orbitals, but only three external electrons, so it can be defined as electron deficient. This feature has a dramatic effect on its chemistry and is the main reason for the choice of boron in medicinal chemistry, together with its large cross-section for neutron capture, as it is possible to easily incorporate boron atoms in organic compounds.

Historically, boron has long been used for the production of borosilicate glasses. Boron was first isolated, although in impure form, by Davy, Gay-Lussac, and Thénard in 1808. Only in 1892 was a quite pure form obtained by Moissan, who prepared elemental boron by the reduction of B_2O_3 with Mg, while high-purity boron was obtained only in the past century. Among the methods available for elemental boron production, the most effective for obtaining high-purity material is the reduction of boron compounds (e.g., halides) with H_2 at high temperature on a heated tantalum filament; the crystallinity improves by increasing the temperatures, and the crystal structure is also temperature dependent. The name, introduced by Davy, derives from its main source (*bor*ax) and from its behavior, similar to that of carb*on*.

Boron is relatively scarce in the earth's crust (about 10 ppm), being found as borate minerals or borosilicates, with the main deposits being found in California and Turkey. Other isolated deposits have also been found in Argentina, Chile, Russia, China, and Peru.

Only silicates have more complex structures than boron compounds, and various allotropic forms of boron itself are known.

6.2 Elemental Boron

6.2.1 Structure

The many-sided properties of boron are reflected in the unique complexity of its allotropic modifications. The origin of such complexity is the tactics used by boron to try to solve the problem of having more atomic orbitals than electrons. Metal compounds, which have a similar situation, usually solve the problem by metallic

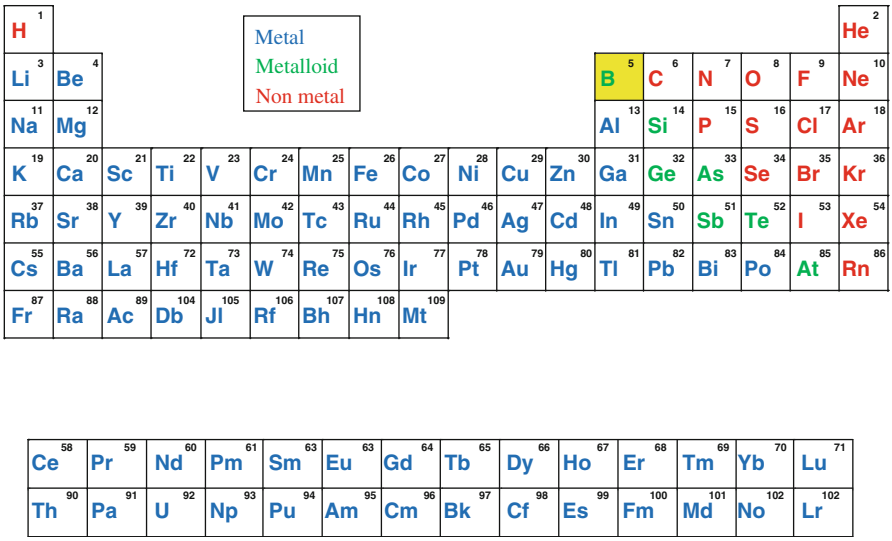

Fig. 6.1 Schematic representation of the periodic table

bonds, but boron's small size and high ionization energy lead to a much more pronounced tendency to form covalent bonds. The final result is that the most represented structural unit in various boron allotropes is the B-12 icosahedron, which also occurs in metal borides, boron hydrides, and boron-carbon hydrides.

As the B-12 icosahedral packing is not very efficient, leaving empty spaces even in the closely packed α-rhombohedral form, other allotropic modifications can accommodate extra atoms (boron or others) such as in α-tetragonal boron in which 2C or 2N atoms, each 50 B atoms, seem to be required to form this phase.

The crystal structures of more polymorphs have been elucidated, such as β-rhombohedral, while others, e.g., the β-tetragonal phase, are even more complex and elusive [2].

It is important to emphasize that the structural representation of boron and boron compounds (such as in Fig. 6.2) simply represents the geometry of the cluster of boron atoms, but does not describe the compounds in terms of localized bonds containing couples of electrons between pairs of atoms. Later, we will briefly describe the electronic behavior of the boron atoms involved in bond formation.

6.2.2 Physical Properties

Natural boron has two stable isotopes, namely ^{10}B and ^{11}B, with a natural abundance of about 20 and 80 %, respectively. Small variations in their concentration are observed. For instance, borates from California are more abundant in ^{11}B, whereas those from Turkey are more abundant in ^{10}B, thus preventing a precise determination of the atomic weight (Table 6.1). Both isotopes show a nuclear spin, allowing

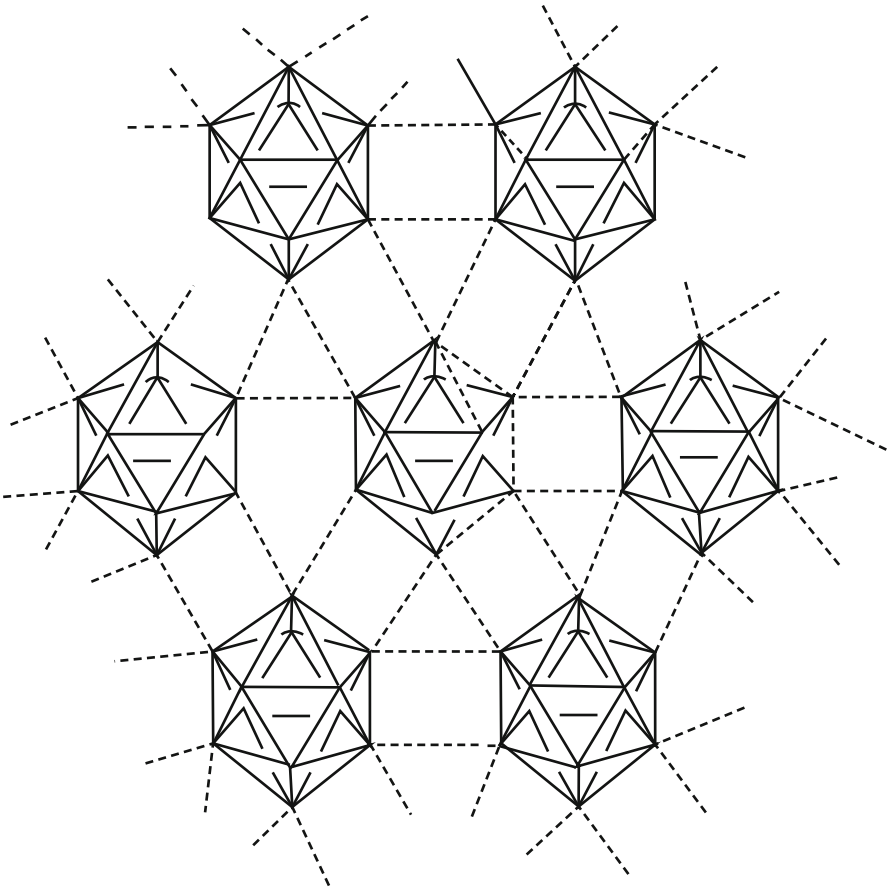

Fig. 6.2 Representation of the structure of the basal plane of α-rhombohedral boron in a quite densely packed arrangement of boron icosahedra

Table 6.1 Physical information

Atomic number	5
Relative atomic mass ($^{12}C = 12.000$)	10.811(7)
Melting point (β-rhombohedral)/K	2,352
Boiling/point/K	4,000
Density/kg m^3	2,340 (293 K)
Ground state electron configuration	$[He]2s^2 2p^1$

the use of NMR spectroscopy for the structural characterization of boron-containing compounds, with the ^{11}B isotope being generally preferred [3].

A relevant nuclear property of the ^{10}B isotope is the high cross section for neutron capture, which has opened the possibility of the therapeutic use of boron compounds for boron neutron capture therapy (BNCT) (Table 6.2).

Table 6.2 Boron isotopes

Nuclide	^{10}B	^{11}B
Relative mass	10.01294	11.00931
Natural abundance (%)	19.055–20.316	80.945–79.684
Half-life	Stable	Stable
Nuclear spin parity	3	3/2
Cross section for neutron capture (barns)1 barn 10^{-28} m^2	3,835	0.005

The ionization energies are 800.6, 2,427.1, and 3,659.7 kJ/mol, much larger than those of the other elements of the same group. The electronegativity is 2.0, close to that of H (2.1), but lower than that of C (2.5), which means that the polarity of the B–H bond is reversed with respect to that of the C–H bond, a factor that plays a role in the hydroboration reaction. The physical properties are difficult to determine precisely because of the polymorphisms and difficulty obtaining high purity. Elemental boron has low density, extreme hardness (close to that of diamonds), and very low conductivity, and appears as a dark powder.

6.2.3 Chemical Properties

The chemistry of boron is probably the most complex and varied of all the elements in the periodic table. The last 50 years have seen tremendous developments in boron chemistry, with many different structures being elucidated and the nature of bonding better understood.

The main features that influence the chemical behavior of boron are its small size, high ionization energy, and electronegativity that is close to that of C and H (and Si), leading to an unusual ability to form covalent bonds.

Similar to C and Si, it shows a marked propensity to form covalent molecular compounds, but it differs sharply from them in having one less valence electron with respect to the number of valence orbitals, being therefore electron deficient. Therefore, although the presence of three external electrons accounts for its propensity to form tervalent compounds, much of its chemistry derives from the tendency to act as an electron-pair acceptor and to give multicenter bonds. Finally, it has a high affinity for oxygen, which is the basis of the vast chemistry of oxygen derivatives.

Different classes of boron compounds can thus be recognized; we have tentatively divided boron compounds in the following classes:

1. Boron–oxygen compounds
2. Other boron-heteroatom compounds (we will focus on halides and B–N derivatives)
3. Metal borides
4. Boron hydrides (including boron clusters, carbaboranes, and metal derivatives thereof)
5. Organoboron compounds (molecular species containing localized B–C bonds)

6.3 Classes of Boron Compounds

6.3.1 Boron-Oxygen Compounds

Boron always occurs in nature as oxygen compounds, and it has never been found as an element or bound to other elements [4]. As for elemental boron, borides and boranes, boron–oxygen compounds show an enormous structural complexity and variety. Moreover, a large number of organic boron compound containing B–O bonds are known (namely BPA) and have found many application in synthesis.

The main oxide derivative of boron is boric oxide, B_2O_3, which can be prepared by cautious dehydration of boric acid. Its structure consists of a network of trigonal BO_3 units in which boron atoms are linked through oxygen atoms.

It is largely employed for the preparation of borosilicate glasses.

Hydrolysis of most inorganic boron compounds gives boric acid, $B(OH)_3$, which is mainly obtained by acid treatment of aqueous solutions of borax ($Na_2B_4O_7{\cdot}H_2O$). It forms white crystals in which the molecules are connected by a network of hydrogen bonds. Partial dehydration of $B(OH)_3$ above 100° yields metaboric acid HBO_2, whose structure is shown in Fig. 6.3.

Boric acid is a very weak acid having a pK_a of 9.25. Its acid behavior is not due to a proton donation, but to its reaction with water as a Lewis acid accepting an OH and releasing a proton, as shown in Fig 6.4:

Boric acid is highly reactive towards alcohols and easily forms esters. Moreover boric acid, as well as other boron–oxygen compounds (e.g., boronic acids), is able to form acetal-like derivatives with diols [5]. This elevated affinity for diols strongly influences the pK_a of boric acid; for example, the complexation with mannitol leads to a pK_a of 5.15 according to Fig. 6.5.

Also in borate salts a complex structural variability is observed, and they have been intensively studied for their industrial relevance, as they are found in many minerals. Some common features are recognized. Boron can link three or four oxygen atoms, forming trigonal or tetrahedric structures, polynuclear anions are formed by sharing a single vertex oxygen, and they can be hydrated, can contain boric acid units and form polymeric structures [6] (Fig. 6.6).

Examples of frequent units containing tri- or tetracoordinated boron are shown in the previous figure.

6.3.2 Other Boron–Heteroatom Compounds

6.3.2.1 Boron Halides

Boron halides can be found either as monomeric boron trihalides, which have been extensively studied, or polynuclear derivatives, including halogenated polyhedral compounds. We will limit our discussion to trihalides, which are the most important for industrial application. Indeed, this class of boron derivatives is involved in the preparation of elemental boron and used as catalysts for a variety of organic

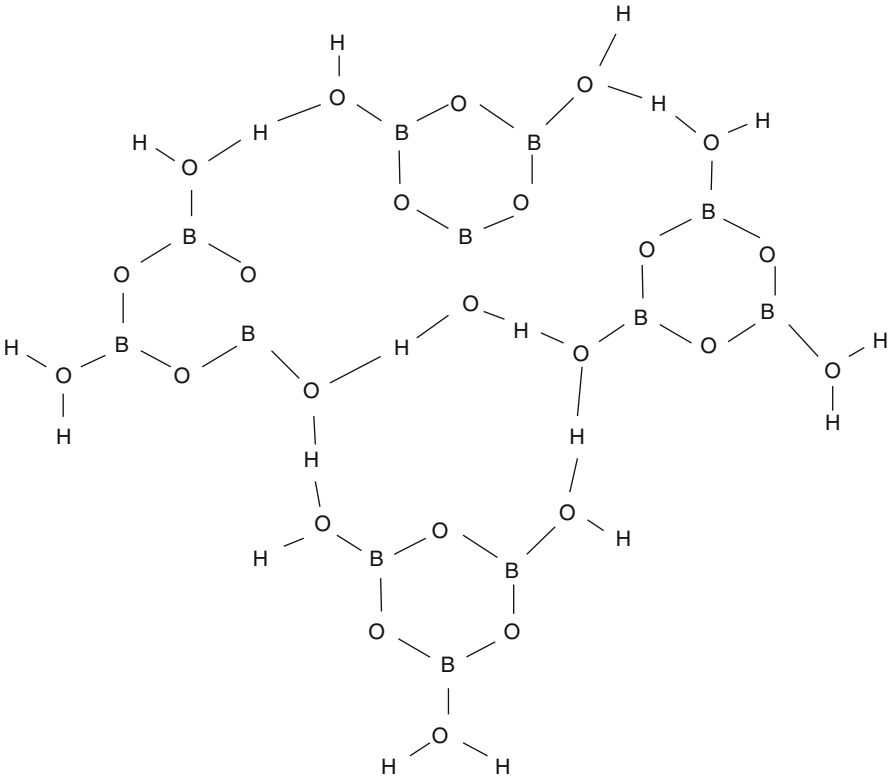

Fig. 6.3 Metaboric acid

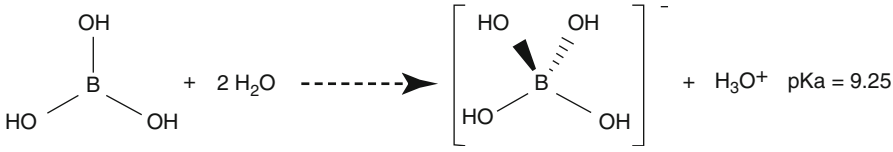

Fig. 6.4 Acidity properties of boric acid

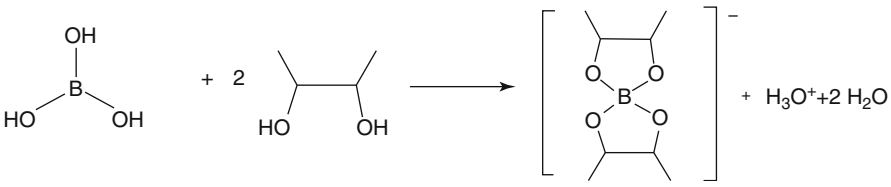

Fig. 6.5 Increased boric acid acidity by complexation

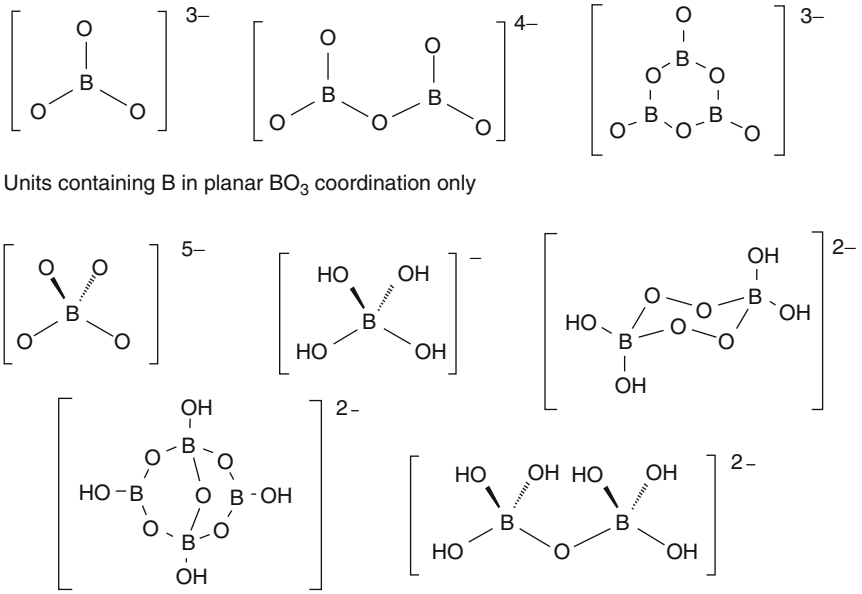

Fig. 6.6 Common units in boron oxo-compounds

reactions, such as the Friedel-Crafts reaction [7], olefin polymerization [8], cracking of hydrocarbons [9], and nitration and sulfonation of aromatic compounds.

Boron trihalides are very volatile and highly reactive compounds. Structurally they are planar trigonal molecules like organoboranes; they are very strong Lewis acids because of the combined effects of the empty p orbital and of the electronegativity of the bound halogens. The B–X bond energies are very high, and the bond distances are shorter than those expected for a single bond. This can be attributed to an overlap between the empty orbital on boron with halogen lone-pair containing orbitals [10].

When mixed, different boron trihalides give rise to a rapid halogen exchange, forming mixtures of mixed halides: $BX_3 + BY_3 \rightarrow BX_3 + BY_3 + BX_2Y + BXY_2$.

Boron trifluoride can be obtained by fluorination of borates with CaF_2 or HF in the presence of concentrated sulfuric acid. Boron trichloride and tribromide are obtained by treating boron oxide with elemental bromine or chlorine, respectively, in the presence of carbon, while boron triiodide is prepared by reacting elemental iodine with sodium or lithium borohydride.

Like the other Lewis acids, boron trihalides form stable complexes with Lewis bases such as ethers or amines (Fig. 6.7). The stability of the adducts follows the order $BF_3 < BCl_3 < BBr_3 < BI_3$, most likely because of the previously mentioned

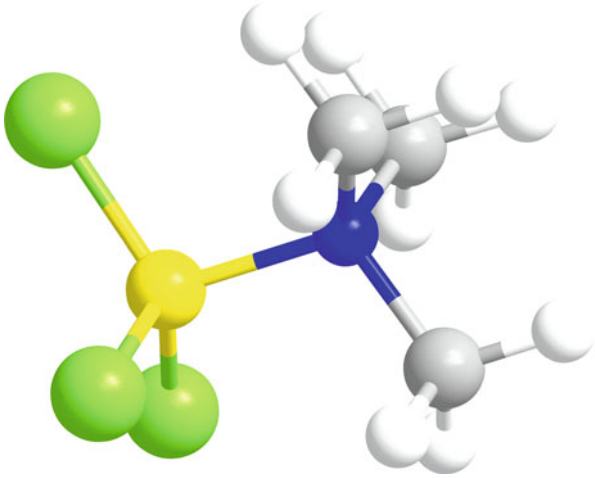

Fig. 6.7 BCl_3-trimethylamine complex

Table 6.3 Properties of B, C and N

Element	B	C	N
Valence electrons	3	4	5
Electronegativity	2.0	2.5	3.0
Radius (Å)	0.88	0.77	0.70

orbital interaction, geometry reorganization from trigonal to tetrahedral, and the electronegativity effect, with a complex interplay between these factors [11].

6.3.2.2 Boron–Nitrogen Compounds

Boron–nitrogen compounds have raised considerable interest for three main reasons: the electronegativities of the three elements, including carbon, are quite similar, with that of carbon being intermediate between nitrogen and boron; they have similar sizes, and, very importantly, the B–N unit is isoelectronic with a C–C bond (Table 6.3). The features of the B–N bond in amine–borane complexes have been discussed to a large extent. Usually such bonds are represented as follows: $R_3N \rightarrow BX_3$ or $R_3N^+ = {}^-BX_3$, which suggests that the origin of the bond is a donation of a pair of electrons from nitrogen to boron. However, it does not mean that nitrogen becomes positively charged and boron negatively, as the electron density distribution depends on the atoms' characteristics, mainly electronegativity.

Calculation indicates that there is a decrease of positive charge on boron and a decrease of electron density on nitrogen, but without reversal of charge.

A similar situation is found in compounds of the type shown in Fig. 6.8, from which the isoelectronic analogy with alkenes is evident.

From the electronic point of view, however, the previous consideration can be applied also to this type of compounds. The possibility of replacing a single or double carbon-carbon bond with a B–N or B═N unit has opened the possibility

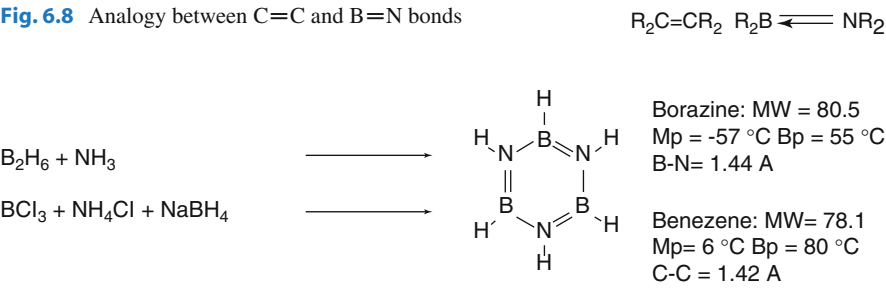

Fig. 6.8 Analogy between C=C and B=N bonds

Fig. 6.9 Borazine synthesis and properties

obtaining a large number of new classes of compounds, but the discussion is beyond the scope of this chapter.

However, a particular example deserves to be mentioned, namely borazine, shown in the following figure (Fig. 6.9):

Borazine is prepared by the reaction of diborane with ammonia or, more efficiently, by the reaction of BCl_3 and NH_4Cl, followed by reduction with $NaBH_4$.

Borazine can be considered as an analog of benzene and, actually looking at their physical properties, they appear quite similar. Moreover, borazine has a structural similarity to benzene, being a planar, regular hexagonal ring, and discussions on its aromaticity are still ongoing [12]. However, the analogies do not go further as borazine's chemical behavior shows few aromatic properties. In fact, borazine can easily yield addition reactions, usually initiated by nucleophiles reacting with boron atoms.

Apart from discrete molecules, boron–nitrogen compounds can also be found in boron nitrides, which are isoelectronic with graphite and have a similar hexagonal layer structure; other structures are known, but obtaining them requires harsh conditions. Differently from graphite, however, boron nitride has the layers superposed, having B on one layer located on N on the adjacent layer; moreover, boron nitrides have good electric conductibility and high chemical resistance. For these reasons, boron nitrides are mainly applied in ceramic materials and composites [13].

6.3.3 Metal Borides

6.3.3.1 Properties and Preparation

Boron is able to form metal-rich binary compounds showing, a surprising variability in stoichiometry and structural motifs, as well as some non-stoichiometric derivatives or ternary and more complex combinations. The boron-metal ratio can vary from rich metal compounds, e.g., M_5B, to very rich boron derivatives, such as MB_{66}; X-ray diffraction has been a powerful technique for their structural elucidation. Beyond academic attention, these compounds also stimulate a significant industrial interest because of their relevant physical and chemical properties.

Metal borides are, in fact, exceptionally hard, non-volatile, chemically inert, and refractory (ceramic) materials with melting points often exceeding 3,000 °C.

They are usually obtained as powders, but can be made up into the desired shape by standard metallurgical and ceramic techniques, and can be applied in heavy-duty apparatuses, such as turbine blades, rocket nozzles, and combustion chambers, as well as having nuclear applications because of the very high neutron capture cross section even with high-energy neutrons. Metal borides can be obtained with a variety of methods either for laboratory or industrial preparation. The main method for small-scale preparation is the direct combination of the elements at high temperature; all the other methods are based on the reduction of boron and/or metal oxides or halides exploiting boron or metal itself, or external reductants (e.g., C, other metals, and H_2), or by electrolysis of molten salts.

6.3.3.2 Structure of Borides

As already found for other classes of boron compounds, also in this case a structural variability is observed. Metal-rich borides can contain isolated boron atoms, or, alternatively, boron can form pairs, linear or branched chains, as well as planar networks. Increasing the percentage of boron results in a predominant occurrence of B–B bonds in which boron is present as icosahedral units, and the metal atoms are located in specific cavities or vacant sites. A compound that is strictly structurally related to rhombohedral elemental boron is boron carbide, for which the formula B_4C was originally proposed, but is not better written as $B_{13}C_2$, although the stoichiometry can slightly differ from that. It is interesting to remember that boron carbide was first prepared in 1899, and it is produced in large amounts, but still waits for a conclusive structural characterization [14].

Figure 6.10 shows a pictorial representation of boron carbide in which icosahedron units are clearly visible, joined by C–B–C units, besides B–B bonds.

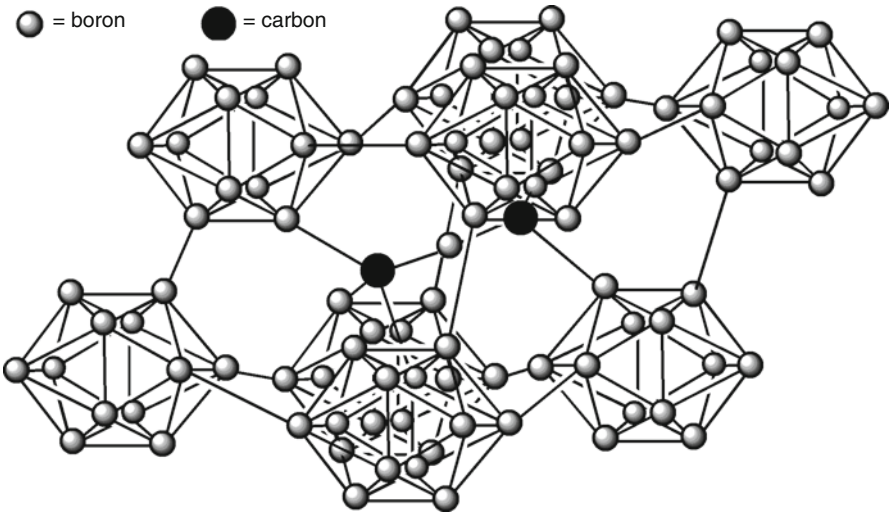

Fig. 6.10 Structure of boron carbide

Other metal borides with large electropositive metals such as lantanides have simpler structures. For example, MB_{12} has a structure similar to that of NaCl in which the 12 boron atoms form a cubic octahedral cluster that behaves like the Cl^- ion in NaCl crystals, and MB_6 compounds form CsCl-type structures in which Cl^- is replaced by an octahedral B_6. From the structural complexity and properties of borides, it is apparent that boron bonding (and more generally, in inorganic compounds) is inadequately described as ionic, covalent, or metallic. A more appropriate description requires the use of a molecular orbital approach. We will briefly discuss such problems in the borane section.

6.4 Boranes

6.4.1 General Features

Borane chemistry was initially explored at the beginning of the twentieth century thanks to investigations of Stock. Later, the inorganic chemistry of boranes and related carbaboranes attracted tremendous research interest for different reasons: the new principles involved in borane structures, the intriguing properties of bonds in boranes, which constituted a serious problem for Lewis electronic theory and forced the development of molecular orbital theory, and, finally, an extensive reactivity peculiar to this class of compounds. This part of the story ended with the 1976 Nobel Prize to Lipscomb for his "studies on boranes, which have illuminated problems of chemical bonding." Besides these investigations of the theoretical and inorganic aspects, Brown, a young chemist who joined the Schlesinger group as a Ph.D. student, started up the study of the reactivity of boranes with organic compounds. This was the beginning of a rapid development of new reagents and new reactions in organic chemistry, which culminated with a second Nobel Prize awarded to Brown in 1979 (shared with Wittig) for "their development of the use of boron- and phosphorus-containing compounds, respectively, into important reagents in organic synthesis."

Boron is the only element other than carbon that can make a complex and extended series of hydrides. Comparing the structures of boron hydrides with those of carbon hydrides (or, better hydrocarbons) shows that while carbon hydrides have a tendency to form chains and rings, boranes prefer to give rise to three-dimensional clusters (Fig. 6.11).

6.4.2 Chemical Bonding in Boranes

The understanding of the structure of boranes started with the determination of the structure of decaborane [15] by Harker, who showed the existence of an icosahedral structure together with four hydrogen atoms bridging couples of boron atoms. Later on, the structure of diborane was demonstrated, showing the presence of bridging H

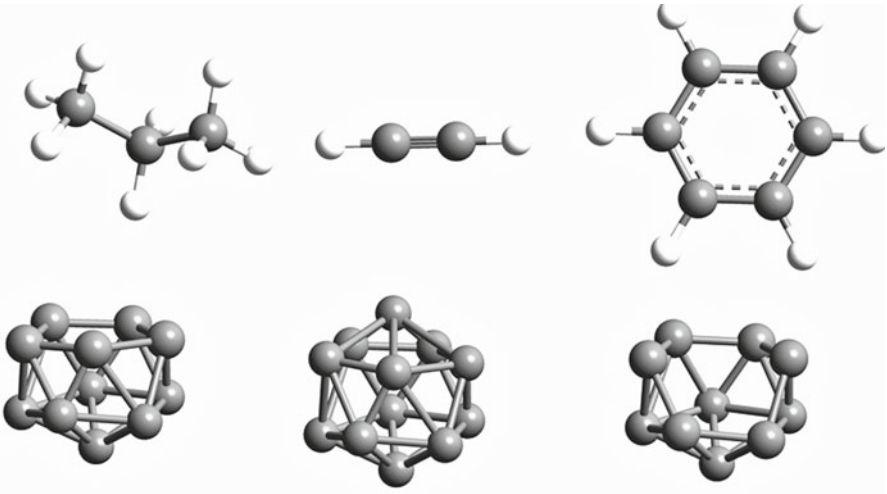

Fig. 6.11 Comparison between carbon and boron hydride structures

atoms. To explain such structures, the concept of a tricentric bond, namely three centers and two electrons, was initially introduced in 1949 by Longuett-Higgins [16]. The concept was then applied to higher boranes and developed by the Lipscomb group [17]. In bonding theory, atomic orbitals can be linearly combined to give molecular orbitals; in localized bonds, a pair of atomic orbitals is combined to give two molecular orbitals, one bonding and one antibonding. The pair of electrons occupies the lower energy bonding orbital. In a more general situation, linear combination of n atomic orbitals gives rise to n molecular orbitals, which can be bonding, antibonding, and non-bonding. As a consequence, not only two center, but also three or multicenter orbitals can be obtained by calculation.

When applied to the B–H–B bond in diborane, the molecular orbital theory gives rise to the orbitals shown in Fig. 6.12 in which only the bonding orbital is occupied, essentially meaning that the two electrons are used to keep three atoms together.

In a similar way, for more complex boron clusters, also three-center bonds can be described for boron atoms; in Fig. 6.12b, a pictorial representation of the three-center boron orbital overlap is shown.

More complex structures with clusters of boron atoms can also be obtained, for which this concept of multicenter bonds explains the stability of such polyhedral boranes.

Structure and bonding descriptions were attained through a topological theory by Lipscomb [17], and the relation between electron counting and cluster geometry resulted in Wade's rules in 1971 [18]. These aspects will not be described in detail as they are beyond the scope of this chapter.

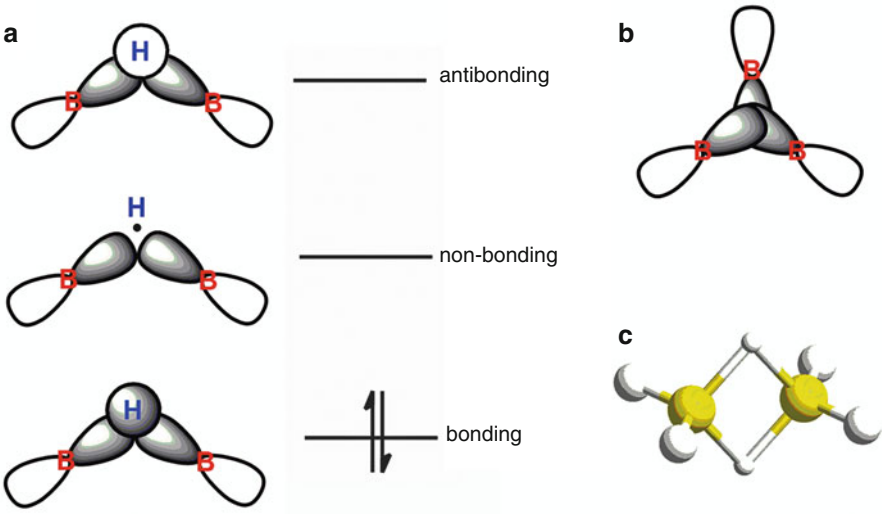

Fig. 6.12 Three-center bond in boranes: (**a**) B–H–B orbitals; (**b**) B_3 orbitals overlap; (**c**) diborane

6.4.3 Structure of Boranes

Three main structures of boranes can be envisaged together with two other minor classes:

- *Closo*-boranes with a polyhedral closed structure of the general formula $B_nH_n^{2-}$
- *Nido*-boranes having a non-closed structure and the formula B_nH_{n+4} or $B_nH_{n+3}^-$
- *Arachno*-boranes with an even more open structure and the formula B_nH_{n+6}

Besides these, two supplementary groups have been classified: *hypno*-boranes, for which adducts are known, and *conjuncto*-boranes, which are derived by linking together the above-mentioned structures (at least five different structures have been identified).

Boranes are usually named by indicating the number of B atoms with a Latin prefix with the number of H atoms in parentheses, e.g., B_5H_9 pentaborane(9); anion names end in "ate" and contain both the number of B and H atoms and the charge, e.g., $B_3H_8^-$ is octahydrotriborate(1-). Additional information on the structure (*closo*-, *nido*-, etc.) can be included (in italics).

Figure 6.13 shows few examples of the possible borane structures.

6.4.4 Preparation and Reactivity of Boranes

Low terms can be obtained thanks to the availability of anionic monoborane, e.g., BH_4^- or $B_3H_8^-$, which allows easy access to diborane or B_3H_7, respectively.

$$BX_3 + BH_4- \rightarrow HBX_3- + ½\ B_2H6$$

$$BX_3 + B_3H_8- \rightarrow HBX_3- + B_3H_7$$

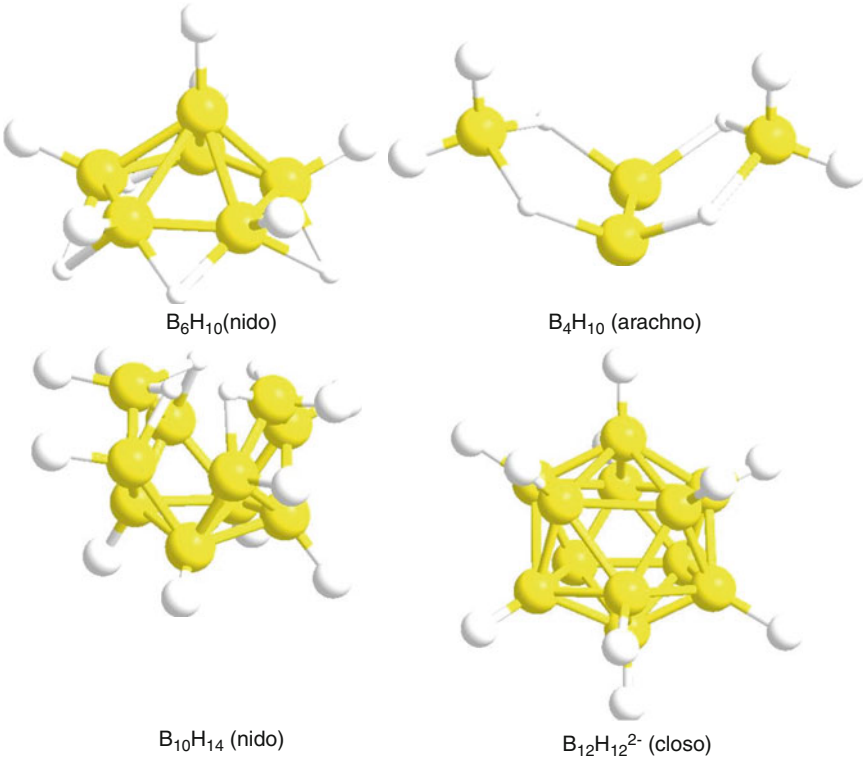

Fig. 6.13 Some borane structures

Diborane can be obtained on a small scale by the reaction of $NaBH_4$ and Et_2OBF_3 in diglyme and used directly without isolation:

$$3NaBH_4 + 4Et_2OBF_3 \rightarrow 3NaBF_4 + 2B_2H_6 + 4Et_2O$$

Higher terms are typically obtained by thermolysis of smaller boranes. The elucidation of the thermal behavior of boranes took a long time from its first observation by Stock because of the complexity of the system and the instability of intermediates, requiring reliable tools for product analysis and detailed mechanistic studies. Precise optimization of the reaction conditions can allow obtaining an acceptable yield of intermediate boranes.

Boranes are extremely reactive compounds, and many of them are pyrophoric and ignite spontaneously in air. This tendency and, more generally, the reactivity are very high in *arachno*-boranes and decrease in *nido*-derivatives; in general, reactivity decreases with increasing molecular weight. *Closo*-boranes are surprisingly stable, suggesting the concept of three-dimension aromaticity [19].

The chemistry of the lower terms of boranes, namely BH_4^- and B_2H_6, will be discussed, together with few information on boron clusters in the context of BNCT compounds.

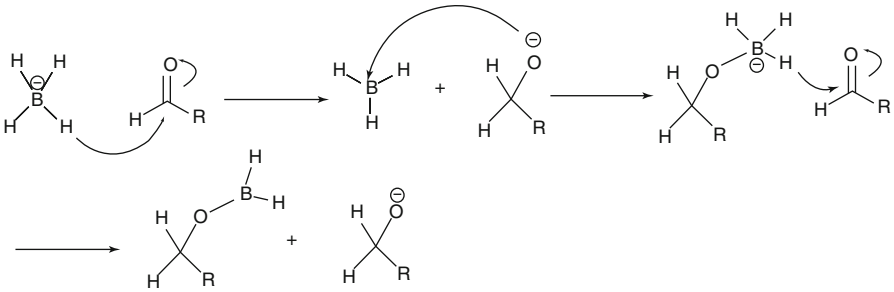

Fig. 6.14 Mechanism of $NaBH_4$ reduction of carbonyl compounds

Boron hydrides have been widely used in both the laboratory and industrial applications. One of the most commonly used hydrides is sodium borohydride, which is cheap, easy to handle, and can be used in protic solvents. Sodium borohydride allows for the reduction of electrophilic compounds including aldehydes, ketones, imines and related derivatives, and, to some extent, esters [20].

In carbonyl reduction, the hydrogen atom, together with the pair of electrons from the B–H bond, will be transferred to the carbon atom of the C═O group (Fig. 6.14).

Though no hydride ion, H^-, is actually involved in the reaction, the transfer of a hydrogen atom with an attached pair of electrons can be regarded as a 'hydride transfer. The oxyanion produced in the first step can help stabilize the electron-deficient BH_3 molecule by adding to its empty *p* orbital. Now a tetravalent boron anion is formed again and could transfer a second hydrogen atom (with its pair of electrons) to another molecule of carbonyl compound.

The alkoxyborane intermediate then reduces a second molecule of the carbonyl compound, and the reaction can continue until all hydrides are consumed, so that BH_4^- is able to reduce four molecules of carbonyl derivative. From the above mechanism, the interplay between tri- and tetracoordination on the boron atom can be easily noticed.

An alternative to BH_4^-, B_2H_6 is also able to reduce carbonyl compounds. As such, it is a gaseous substance, but it can be tamed by complexation with Et_2O or Me_2S. Although at first glance borane appears similar to borohydride, it is not an ion, which is the basis of the difference in its reactivity. Whereas borohydride prefers to react with the most electrophilic carbonyl groups, the reactivity of borane is dominated by its tendency to accept an electron pair into its empty p orbital, thus showing its soft Lewis acid properties. In the context of carbonyl group reductions, this means that it reduces electron-rich carbonyl groups fastest. As a consequence, apart from aldehydes and ketones, it is able to reduce amides to the corresponding amines efficiently, whereas the reduction of esters is very slow. On the other hand, borane is able to reduce carboxylic acids very efficiently as it initially forms a borate anhydride with the carboxylic group, making the carbonyl group much more electrophilic. In fact, in carboxylic derivatives, the carbonyl group is usually less electrophilic than in other carbonyl compounds, e.g., ketones, because of conjugation between the carbonyl group and the lone pair of the sp^3 hybridized oxygen atom, but, in these boron esters,

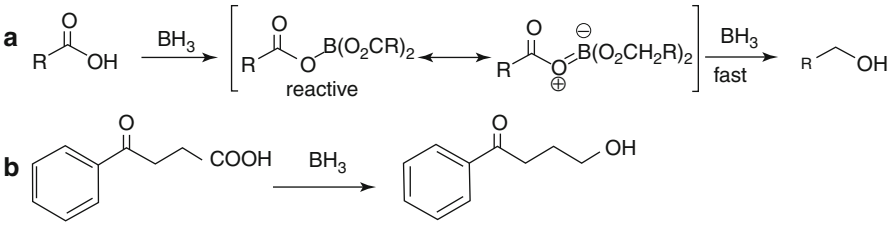

Fig. 6.15 Reduction of carboxylic acids with borane: (**a**) schematic mechanism; (**b**) example of selectivity

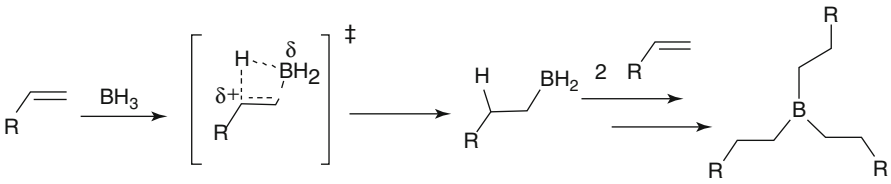

Fig. 6.16 Addition of borane to alkenes

the oxygen next to the boron has to share its lone pair between the carbony l group and the boron's empty *p* orbital, so they are considerably more reactive than normal esters (Fig. 6.15a). In this way, it is even possible to reduce a carboxylic acid in the presence of a ketone (Fig. 6.15b).

The most relevant reaction of borane, however, is the hydroboration of alkenes and alkynes, which was discovered and developed by Brown, who was awarded the 1979 Nobel Prize, as previously mentioned [21]. Hydroboration is an electrophilic addition reaction of borane to multiple bonds. It is a regioselective reaction as the boron shows a tendency to attack preferentially the less substituted carbon atom of the multiple bond in a so-called anti-Markovnikov approach. This behavior has an electronic justification, as the more electrophylic boron preferentially attacks the carbon atom, which leads to the formation of a better stabilized positive charge on the more substituted carbon atom in the transition state. Besides electronic reasons, steric factors also play a major role in the regioselectivity. Looking at the transition state, it is also apparent that the reaction is stereospecific, with the boron and the hydrogen atoms approaching the same face of the double bond (Fig. 6.16). The reaction can go further by adding two other alkene molecules.

Alkyl boranes are easily converted in other derivatives. Their oxidation with hydrogen peroxide in basic conditions leads to the corresponding alcohol; the hydroxyl group replaces boron with retention of the configuration. The mechanism, shown in Fig. 6.17, once more illustrates the ability of boron to go back and forth between planar neutral structures and anionic tetrahedral structures.

Superior boron clusters have also been explored [22], but the discussion will be limited here to some information on *nido*-decaborane $B_{10}H_{14}$ and to just an example of *closo*-dodecaborane $B_{12}H_{12}^{2-}$ in the context of BNCT.

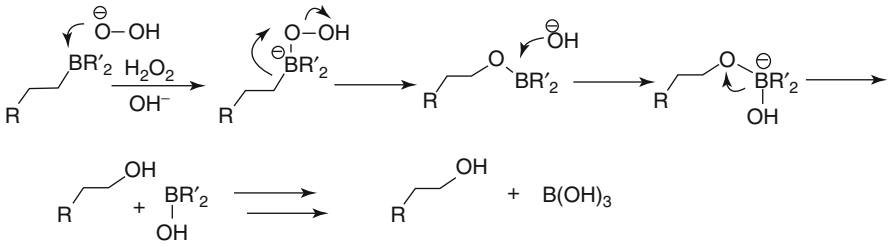

Fig. 6.17 Oxidation of organoboranes

Nido-$B_{10}H_{14}$ is probably the most studied among polyhedral boranes and has been produced in the past in large amounts for potential application in high-power fuels. It can be obtained on a small scale by pyrolysis of diborane at 100–200°C in the presence of weak Lewis bases. Decaborane is insoluble in water, but freely soluble in many organic solvents; however, its reactivity strongly limits the range of solvents that can be used. Decaborane behaves as a relatively strong protic acid and can be titrated in hydroalcoholic solutions showing a pK_a of 2.70. Deprotonation can also be observed using other strong bases such as MeO^-, NH_2^-, etc.

Treatment of decaborane with donor ligands gives rise to replacement of two hydrogen atoms:

$$B_{10}H_{14} + 2L \rightarrow B_{10}H_{12}L_2 + H_2$$

The ligand can be either inorganic or organic, neutral or anionic. Ligands can activate decaborane for several types of reactions, including degradation reactions in the presence of protic compounds, e.g., alcohols:

$$B_{10}H_{12}L_2 + 3ROH \rightarrow B_9H_{13}L + B(OR)_3 + L + H_2$$

Another example of reactions of activated decaborane will be considered later.

Decaborane can undergo reactions in which boron or other atoms are incorporated to give an expanded cluster. In this way, metallaboranes can be generated easily.

Closo-boranes, obtained by pyrolysis, are very stable. They are relatively reactive towards electrophiles, but much less so with nucleophiles. An important substituted derivative of this class is BSH, (sodium mercaptoundecahydrododecaborate, $Na_2B_{12}H_{11}SH$), which is currently being used for clinical trials in BNCT. It can be obtained from $B_{12}H_{12}^{2-}$ by a reaction with *N*-methylthiopyrrolidone [23], as shown in Fig. 6.18:

6.5 Carboranes

Carboranes [24] (or, better, carbaboranes) can be structurally seen as boron clusters in which one or more of the BH groups in boranes are substituted by a CH. The different number of external electrons introduced in the cluster by a formal B to C

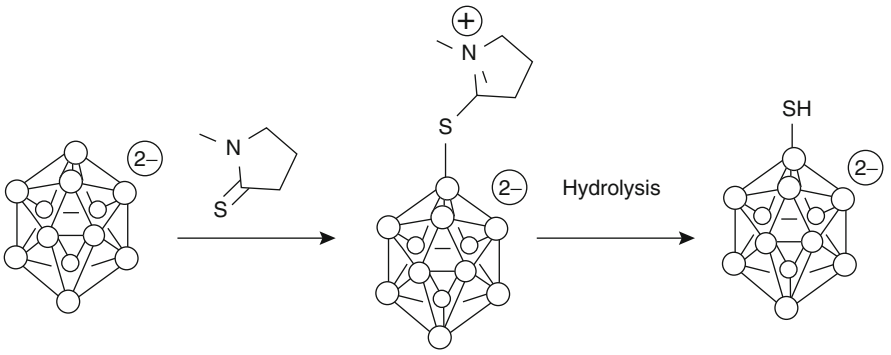

Fig. 6.18 A preparation of BSH

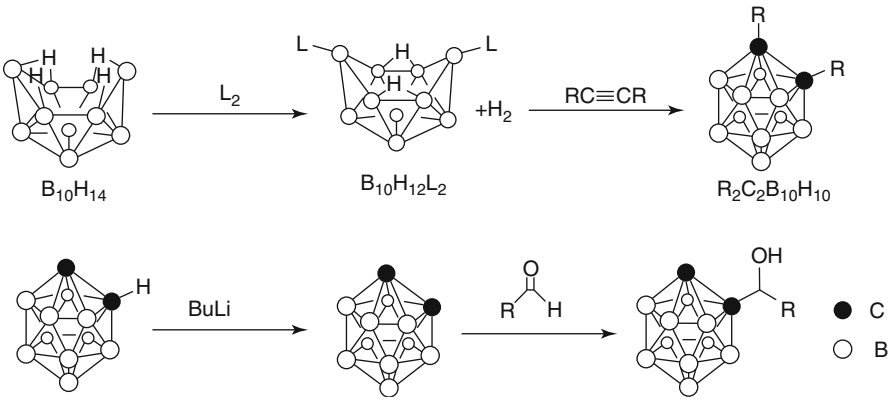

Fig. 6.19 Preparation of substituted carboranes

substitution is compensated by the elimination of an H atom involved in a three-center bond. The most represented carboranes have the stable *closo* structure and can be obtained by pyrolytic reaction between a borane and an alkyne. As for boranes, many substitution derivatives, including metallacarboranes, have been extensively studied and even today are still of great interest. Only the icosahedral carborane $C_2B_{10}H_{12}$ will be briefly considered in this context. The three isomeric $C_2B_{10}H_{12}$ (*ortho-*, *meta-* and *para-* according to the relative position of the carbon atoms) are by far the most studied because of their easy preparation and great stability.

Two main strategies for the preparation of substituted carboranes are usually exploited (Fig. 6.19):

- The addition of ligand-activated decaborane to alkynes
- The addition of deprotonated carboranes to electrophiles as carbon atoms in decaborane are quite acidic (pK_a around 23).

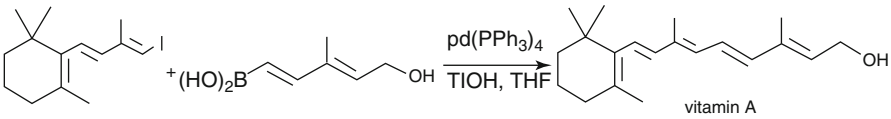

Fig. 6.20 Suzuki vitamin A synthesis

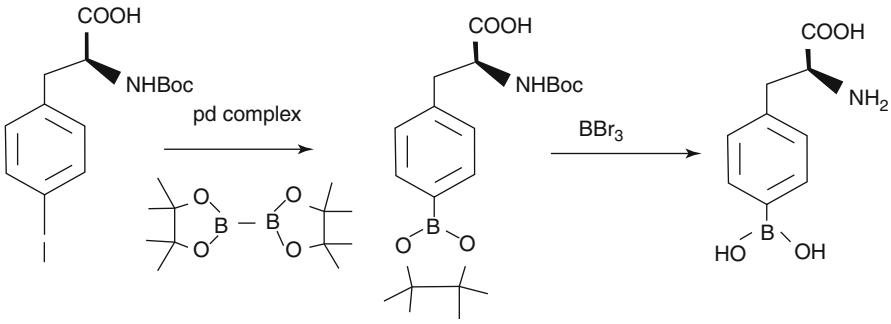

Fig. 6.21 Palladium-catalyzed synthesis of BPA

Although carboranes are usually stable, they are sensitive to bases such as HO^-, MeO^-, R_2NH, giving rise to the *nido*-derivative by extraction of a boron atom [25]. A large number of structures containing carboranes have been synthesized with the above and other strategies [26].

6.6 Organoboron Compounds

Besides reactivity concerns, boron chemistry has been extensively studied in a number of other aspects. The ability of boron to form stable bonds with carbon allows its easy incorporation in organic molecules. Many carbon-carbon bond-forming reactions exploiting organoborane are known [27]. Of particular interest are aryl and vinylboronic acids, which can be applied for carbon-carbon bond-forming reactions, such as Suzuki coupling [28].

Boronic acids can be obtained in a variety of ways, with the reaction of vinyl or aryl lithium or Grignard reagents with triethylborate followed by hydrolysis being the most common methods. Such a reaction has also been applied for the synthesis of 4-borono-L-phenylalanine, BPA, a compound approved for clinical use in BNCT together with BSH [29].

A large number of compounds have been synthesized exploiting Suzuki cross-coupling. The synthesis of vitamin A reported in Fig. 6.20 is just one example [30].

Boronic acids can also be obtained from palladium-catalyzed cross coupling, and this approach has been used for the synthesis of BPA. One example is reported in Fig. 6.21 starting from partially protected 4-iodophenylalanine and bis-pinacolato diboronate in the presence of a Pd catalyst [31].

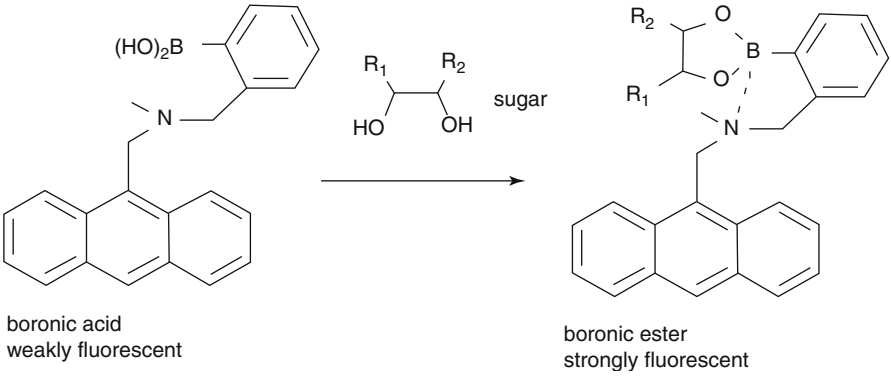

Fig. 6.22 Boronic acids as sugar sensors

Finally, boronic acid also has other applications apart from synthesis. As previously mentioned, it can provide stable boron acetals with diols and has been used as a protecting group to give better solubility in water, as in the case of the complex between BPA and fructose, or as an analytical tool for selective sugar recognition based on fluorescence variations (Fig. 6.22) [32].

References

1. Greenwood NN (1975) Boron. Pergamon Press, Oxford
2. Prasad DLVK, Balakrishnarajan MM, Jemmis ED (2005) Electronic structure and bonding of β-rhombohedral boron using cluster fragment approach. Phys Rev B 72:195102/1–195102/6
3. Heřmánek S (1992) ^{11}B NMR spectra of boranes, main-group heteroboranes, and substituted derivatives. Factors influencing chemical shifts of skeletal atoms. Chem Rev 92:325–362
4. Bowden GH (1980) Supplement to Mellor's comprehensive treatise on inorganic and theoretical chemistry, vol 5, Boron, Part A, Boron-oxygen compounds. Longman, London
5. van den Berg R, Peters JA, van Bekkum H (1994) The structure and (local) stability constants of borate esters of mono- and di-saccharides as studied by ^{11}B and ^{13}C NMR spectroscopy. Carbohydr Res 253:1–12
6. Yuan G, Xue D (2007) Crystal chemistry of borates: the classification and algebraic description by topological type of fundamental building blocks. Acta Crystallogr B 63:353–362
7. Olah GA (1973) Friedel-crafts chemistry. Wiley, New York
8. Kennedy JP, Huang SY, Feinberg SC (1977) Cationic polymerization with boron halides. III. BCl_3 coinitiator for olefin polymerization. J Polym Sci A 15:2801–2819
9. Nederlandse V, Raffinadery Van Petroleumproducten Sparndamseweg N (1971) Refining of hydrocarbon with boron trifluoride. US Patent 3617533 (Haarlem, NL)
10. Branchadell V, Oliva A (1991) The Lewis acidity scale of boron trihalides: an *ab initio* study. Theochem 236:75–84
11. Branchadell V, Oliva A (1991) Complexes between formaldehyde and boron trihalides. An ab initio study. J Am Chem Soc 113:4132–4136
12. Islas R, Chamorro E, Robles J, Heine T, Santos JC, Merino (2007) Borazine: to be or not to be aromatic. Struct Chem 18:833–839
13. Paine RT, Narula CK (1990) Synthetic routes to boron nitride. Chem Rev 90:73–91

14. Will G, Kossobutzki KH (1976) An X-ray diffraction analysis of boron carbide $B_{13}C_2$. J Less Common Metals 47:43–48
15. Kasper JS, Lucht CM, Harker D (1948) The structure of the decaborane molecule. J Am Chem Soc 70: 881. Kasper JS, Lucht CM, Harker D (1950) The crystal structure of the decaborane, B10H14. Acta Crystallogr 3: 436–455
16. Longuet-Higgins HC, de Roberts MV (1955) The electronic structure of an icosahedron of boron atoms. Proc R Soc Lond A Math Phys Sci 230:110–119
17. Lipscomb WN (1963) Boron hydrides. Benjamin, New York. Lipscomb WN (1976) Nobel lecture, http://nobelprize.org/nobel_prizes/chemistry/laureates/1976/lipscomb-lecture.pdf
18. Wade K (1976) Structural and bonding patterns in cluster chemistry. Adv Inorg Chem Radiochem 18:1–66
19. Greenwood NN (1989) Boron hydride clusters. In: Roesky M (ed) Rings, clusters and polymers of main group and transition elements. Elsevier, Amsterdam
20. Sayden-Penne J (1991) Reductions by the alumino- and borohydrides in organic synthesis. VCH, New York
21. Brown HC (1975) Organic synthesis via boranes. Wiley, New York. Brown HC (1979) Nobel lecture, http://nobelprize.org/nobel_prizes/chemistry/laureates/1979/brown-lecture.pdf
22. Greenwood NN (1992) Taking stock: the astonishing development of boron hydride cluster chemistry. Chem Soc Rev 20:49–57
23. Komura M, Aono K, Nagasawa K, Sumimoto S (1987) A convenient preparation of 10B-enriched B12H11SH2–, an agent for neutron capture therapy. Chem Express 2:173–176. Tolpin EI, Wellum GR, BerleyS A (1978) Synthesis and chemistry of mercaptoundecahydrocloso-dodecaborate2(−). Inorg Chem 17:2867–2873
24. Grimes RN (1970) Carboranes. Academic, New York
25. Taoda Y, Sawabe T, Endo Y, Yamaguchi K, Fujiid S, Kagechika H (2008) Identification of an intermediate in the deboronation of ortho-carborane: an adduct of ortho-carborane with two nucleophiles on one boron atom. Chem Commun 2049–2051
26. Valliant JF, Guenther KJ, King AS, Morel P, Schaffer P, Sogbein OO, Stephenson KA (2002) The medicinal chemistry of carboranes. Coord Chem Rev 232:173–230
27. Negishi E, Idacavage M (1985) Formation of carbon-carbon and carbon-heteroatom bonds via organoboranes and organoborates. Org React 33:1–246
28. Alonso F, Beletskaya IP, Yus M (2008) Non-conventional methodologies for transition-metal catalysed carbonecarbon coupling: a critical overview. Part 2: the Suzuki reaction. Tetrahedron 64:3047–3101
29. Park KC, Yoshino K, Tomiyasu H (1999) A high-yield synthesis of 4-borono-dl-phenylalanine. Synthesis 1999:2041–2044
30. Torrado A, Iglesias B, López S, de Lera AR (1995) The Suzuki reaction in stereocontrolled polyene synthesis: retinol (vitamin A), its 9- and/or 13-demethyl analogs, and related 9-demethyl-dihydroretinoids. Tetrahedron 51:2435–2454
31. Malan C, Morin C (1998) A concise preparation of 4-borono-L-phenylalanine (L-BPA) from L-phenylalanine. J Org Chem 63:8019–8020. See also Nakamura H, Fujiwara M, Yamamoto Y (2000) A practical method for the synthesis of enantiomerically pure 4-borono-L-phenylalanine. Bull Chem Soc Jpn. 73: 231–235
32. Samankumara Sandanayakea KRA, Jamesa TD, Shinkaia S (1996) Molecular design of sugar recognition systems by sugar-diboronic acid macrocyclization. Pure Appl Chem 68:1207–1212

Boron Compounds: New Candidates for Boron Carriers in BNCT

7

Hiroyuki Nakamura and Mitsunori Kirihata

Contents

7.1 New Candidates for Boron Carriers in BNCT

The cell-killing effect of BNCT is due to the nuclear reaction of two essentially non-toxic species, boron-10 (^{10}B) and thermal neutrons, whose destructive effect is well observed in boron-loaded tissues. Therefore, the high accumulation and selective delivery of ^{10}B into the tumor tissue are the most important requirements to achieve efficient neutron capture therapy for cancer [1, 2]. In order to fatally damage tumor cells with BNCT, three important parameters should be considered in the development of boron carriers: (1) the boron concentrations in the tumor should be in the range of 20–35 μg ^{10}B/g; (2) the tumor/normal tissue ratio should be greater than 3–5; and (3) the toxicity should be sufficiently low [3]. So far, two boron compounds, sodium mercaptoundecahydrododecaborate ($Na_2{}^{10}B_{12}H_{11}SH$; $Na_2{}^{10}BSH$) [4] and L-*p*-boronophenylalanine (L-^{10}BPA) [5], have been clinically utilized for the treatment of patients with malignant brain tumors [6] and malignant melanoma [7]. Recently, BNCT has been applied to various cancers, including head and neck cancer, lung

H. Nakamura (✉)
Department of Chemistry, Faculty of Science, Gakushuin University,
1-5-1, Mejiro, Toshima-ku, Tokyo, 171-8588, Japan
e-mail: hiroyuki.nakamura@gakushuin.ac.jp

M. Kirihata
Graduate School of Agriculture and Life Sciences, Osaka Prefecture University,
Osaka, Japan
e-mail: kirihata@biochem.osakafu-u.ac.jp

W.A.G. Sauerwein et al. (eds.), *Neutron Capture Therapy*,
DOI 10.1007/978-3-642-31334-9_7, © Springer-Verlag Berlin Heidelberg 2012

cancer, hepatoma, chest wall cancer, and mesothelioma [8–10]. Therefore, the development of new boron carriers is one of the most important issues that should be resolved to extend the application of BNCT to various cancers. As the novel review written by Soloway and coworkers covered boron carriers reported until 1998 in detail [1], we review herein new and promising candidates for boron carriers developed in the last 10 years.

In the last decade, boron carrier development has taken two directions: small boron molecules and boron-conjugated biological complexes. Unlike approaches using pharmaceuticals, boron carriers require high tumor selectivity and should be essentially nontoxic. Therefore, the latter approach has become one of the recent trends to accumulate a large amount of ^{10}B in tumor tissues.

7.1.1 Small Boron Molecules

A small boron molecule includes a ^{10}B moiety and a tumor-affinity function. Water solubility is also an important requirement for the boron molecule to act as a boron carrier. Boronic acid, carboranes, and various boron clusters [11, 12] have been chosen as ^{10}B moieties in the molecules. Boron molecules designed and synthesized in the last decade are divided into five classes: amino acid derivatives, nucleic acid derivatives, porphyrins and related derivatives, carbohydrates, and other biomimetics.

7.1.1.1 Amino Acid Derivatives

As L-^{10}BPA was found to be actively accumulated in malignant melanoma cells, much attention has been focused on the development of boron-containing amino acids and related peptides. Kabalka and coworkers synthesized various boron-containing cyclic amino acids [13]. Biodistribution studies in mice bearing melanoma tumors indicated that boronated amino acids were taken up by the tumors selectively [14]. Slepukhina and Gabel developed dodecaborate-containing amino acids. An assay for in vitro toxicity using V79 Chinese hamster cells revealed that the dodecaborate-containing amino acids (LD50 of 5.7 mM) displayed approximately the same toxicity as BSH (LD50 of 5.5 mM) [15]. Hattori and coworkers synthesized fluorinated BPA derivatives in an effort to devise practical tools for both magnetic resonance imaging (MRI) and BNCT agents [16] (Fig. 7.1).

7.1.1.2 Nucleic Acid Derivatives

Initial approaches focused on boron incorporation into nucleic acid bases, such as purines and pyrimidines [17, 18]. Another approach was the direct conjugation of a boron moiety to nucleic acids. Various boronic-acid- and carborane-conjugated nucleic acids were developed in the 1990s [1]. Recent advances in boron-containing nucleoside conjugates include carborane-containing thymidine analogs and metallacarborane derivatives. Al-Madhoun and coworkers found that thymidine analogs containing o-carboranylalkyl groups at the 3-position are potential substrates for human thymidine kinase 1 (TK1) [19]. Lesnikowski and coworkers developed metallacarborane derivatives of all four of the canonical nucleosides, thymidine (T),

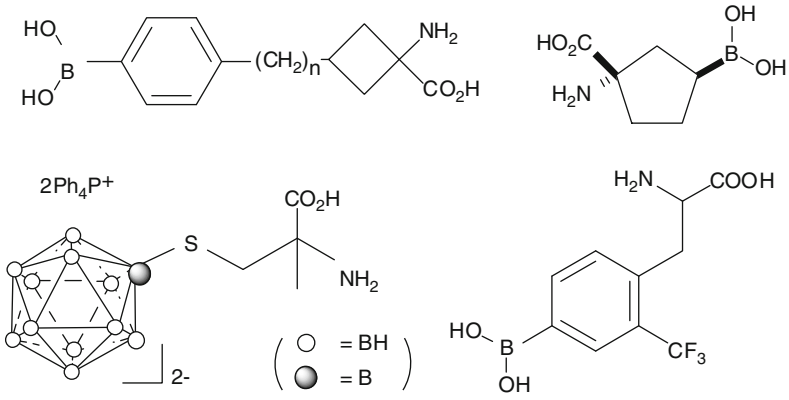

Fig. 7.1 Structures of boron-containing amino acids

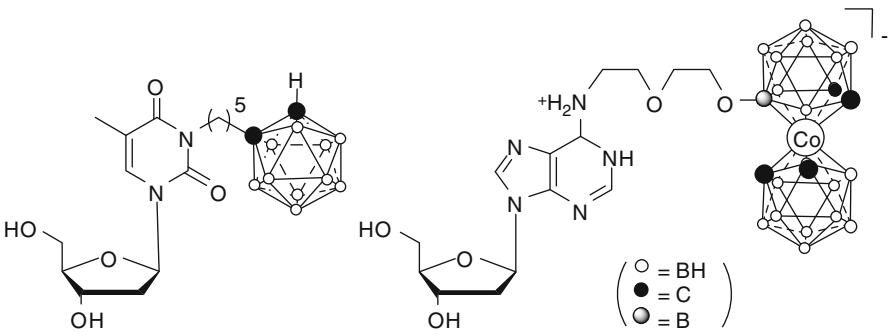

Fig. 7.2 Structures of boron-containing nucleic acids

2′-*O*-deoxycytidine (dC), 2′-*O*-deoxyadenosine (dA), and 2′-*O*-deoxyguanosine (dG). The availability of this methodology has made studies of a broad spectrum of nucleoside conjugates bearing metals and the incorporation of these metal centers into DNA oligomers at designated locations possible [20] (Fig. 7.2).

7.1.1.3 Porphyrins and Related Derivatives

Porphyrins and related macrocyclic nitrogen heterocycles are known to accumulate in a wide variety of solid tumors and are thus proposed for dual application as boron delivery agents and photosensitizers for photodynamic therapy (PDT). Studies of boronated porphyrins for BNCT were pioneered by Kahl, Morgan, Miura, Gabel, and their associates [21–25]. Among them, boronated protoporphyrin (BOPP) developed by Kahl and Koo [21] has been studied for possible use as a BNCT/PDT dual sensitizer. BOPP is selectively taken up by tumor cells in xenograft models of glioma and localizes predominantly in tumor cell mitochondria. Thus, phase I clinical study was carried out using BOPP. However, thrombocytopenia was observed in the patients due to the

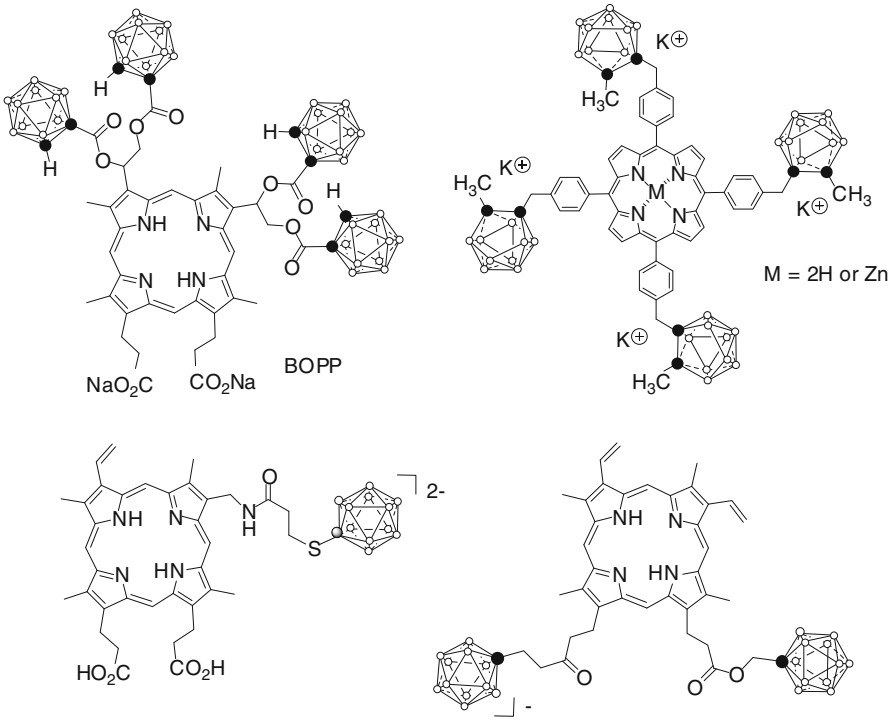

Fig. 7.3 Structures of porphyrin derivatives

direct toxic effect of BOPP or its metabolites on platelets [26]. In order to overcome this drawback, various boronated porphyrins and related macrocyclic nitrogen heterocycles were synthesized and evaluated by several research groups. Vicente and coworkers developed four *nido*-carborane cluster-linked porphyrins via aromatic linkage [27]. These amphiphilic porphyrins displayed very low cytotoxicity, were taken up by 9L and U-373MG cells in both time- and concentration-dependent manners, and localized preferentially in cell lysosomes. Matsumura, Gabel, and their coworkers introduced BSH into the protoporphyrin framework to improve solubility in water [28, 29]. As other boron sources, *closo*-monocarbon carborane [30], cobalt bis(dicarbollide) [31], and azanonaborane [32] have been investigated (Fig. 7.3).

7.1.1.4 Carbohydrates

An increased rate of glycolysis is often observed in many cancer cells, and therefore, boron-containing carbohydrates have recently sparked much interest. The sugar moiety is expected to not only confer water solubility to the otherwise hydrophobic boron cluster but also accumulate selectively in tumor tissues through the glucose transport system. Tjarks and coworkers reported that *o*-carboranylglucose significantly accumulated in F98 glioma cells [33]. Various water-soluble *o*-carborane-containing glycosides [34, 35], functionalized glycosylated carboranes [36, 37], mono- and bisglucuronylated

carboranes [38], and ribofuranosylaminobutylazanonaborates [39] have been synthesized, and their biological properties as boron carriers are being investigated.

7.1.1.5 Other Biomimetics

One of the recent remarkable advances in boron cluster chemistry is the possible use of carboranes as components of biologically active molecules in pharmaceutical science. Endo and coworkers focused on the exceptionally hydrophobic character and spherical geometry of carboranes and reported the first example of the design, synthesis, and biological evaluation of retinoids containing a carborane cage as a hydrophobic pharmacophore. They found that *p*-carboranylphenol derivatives exhibited at least ten-fold higher estrogen agonist activity than 17L-estradiol in the luciferase reporter gene assay, and their interaction with the estrogen receptor was demonstrated by computational docking simulation. The *p*-carboranylphenol derivatives also showed potent in vivo effects on the recovery of uterine weight and bone loss in ovariectomized mice [40, 41]. As alternative carborane pharmacophores, transthyretin amyloidosis inhibitors have been investigated by Hawthorne and coworkers [42]. Kang and coworkers reported the synthesis of *o*-carboranyl triazine derivatives and are currently investigating in detail the biological mode of action [43]. Carboranes are versatile cores that can be used not only as bioisosteres for aryl groups or other hydrophobic moieties but also as platforms for preparing radionuclide-conjugated molecular imaging agents [44].

7.1.2 Boron-Conjugated Biological Complexes

The effect of BNCT depends on the selective and relatively large amount of ^{10}B delivery to tumor cells while sparing adjacent normal cells. Recent promising approaches entail the use of boron-conjugated biological complexes, such as boron polymers, growth factors, and monoclonal antibodies (mAbs). As an alternative approach, drug delivery systems, including emulsion, virus envelope, and liposomes, have been utilized for selective boron delivery to tumor tissues in BNCT. These approaches involve ligands targeting certain receptors, the overexpression of which has been observed on the surface of many tumor cells.

7.1.2.1 Boron-Containing Polymers

A polyamidoamine dendrimer is arranged in a starburst pattern and thus has been the subject of recent attention as a spherical precision macromolecule. The first boronated polyamidoamine dendrimer was synthesized by Barth, Soloway, and their coworkers in 1993 [45]. Tjarks and coworkers investigated the possibility of targeting the folate receptor on cancer cells using folic acid conjugates of boronated poly(ethylene glycol) (PEG)-containing third-generation polyamidoamine dendrimers to obtain ^{10}B concentrations necessary for BNCT by reducing the uptake of these conjugates by the reticuloendothelial system (RES). Among the prepared combinations, a boronated dendrimer containing ~13 decaborate clusters, ~1 PEG2000 unit, and ~1 PEG800 unit with folic acid attached to the distal end exhibited the lowest hepatic uptake in C57BL/6 mice. Biodistribution studies of

this conjugate in C57BL/6 mice bearing folate receptor (+) murine 24JK-FBP sarcomas resulted in selective tumor uptake (6.0 % ID/g tumor), but also high hepatic (38.8 % ID/g) and renal (62.8 % ID/g) uptake, indicating that the attachment of a second PEG unit and/or folic acid may adversely affect the pharmacodynamics of this conjugate [46].

Hosmane and coworkers took advantage of the fact that functionalized single-wall carbon nanotubes (SWCNTs) were able to cross cell membranes and concentrate in a number of neoplastic cells without obvious toxic effects. The nido-carboranes were attached to the side walls of SWCNTs to produce water-soluble macromolecular boron carriers and injected into mice bearing an EMT6 mammary cancer tumor. It was found that the boron persisted in the tumor cell giving a 21.5 B/g tumor and a tumor-to-blood ratio of 3.12:1 [47, 48].

Srebnik, Rubinstein, and coworkers focused on the tissue uptake of ^{99m}Tc that was increased by cationic dextran in a charge-dependent manner in bladder carcinoma patients. They prepared boronated cationic copolymers composed of different ratios of acrylamide, *N*-acryloyl-3-aminophenylboronic acid, and *N*-acryloyldiaminoethane (the cationic moiety). Direct analysis of tissue boron levels showed that polymeric aminophenylboronic acid (APB) uptake was higher in colonic polyps than in surrounding normal tissues. Free APB, however, was found in similar quantities in both tissues. When tested in normal jejunum and colon of the rat, polymeric APB uptake was directly proportional to the molar content of the cationic monomer in the copolymers. The presence of magnesium ions, free boron cationic monomer, and mucin interfered with this uptake in a concentration-dependent manner. APB accumulation in colonic polyps was inversely proportional to the cationic monomer content in the copolymers, suggesting an increased amount of mucus around the polyps, which probably impeded the electrostatic attachment of the polymer to the malignant tissue [49].

7.1.2.2 Boron Peptides and Antibodies

The majority of high-grade gliomas express the amplified epidermal growth factor receptor (EGFR) gene, and increased numbers of EGFRs are found on the cell surface. Barth and coworkers developed the EGF-conjugated boronated starburst polyamidoamine dendrimer (EGF-BSD) that contains ~960 boron atoms per EGF molecule. As determined by electron spectroscopic imaging, EGF-BSD initially was bound to the cell surface membrane and then was endocytosed, which resulted in the accumulation of boron in lysosomes [50]. Either F98 wild-type ($F98_{WT}$) receptor (–) or EGFR gene-transfected $F98_{EGFR}$ cells were stereotactically implanted into the brains of Fischer rats. Biodistribution studies revealed that 33.2 % of the injected dose/g of EGF-BSD was retained by $F98_{EGFR}$ gliomas compared with 9.4 % of the injected dose/g in $F98_{WT}$ gliomas by 24 h after an intratumoral (i.t.) injection of ^{125}I-labeled EGF-BSD, and the corresponding boron concentrations were 21.1 and 9.2 μg/g, respectively. The rats that received an i.t. injection of EGF-BSD (~60 μg ^{10}B/~15 μg EGF) either alone or in combination with i.v. BPA (500 mg/kg) were irradiated at the Brookhaven Medical Research Reactor 24 h after the i.t. injection. Irradiated controls had a mean survival time (MST) of 31 ± 1 days, whereas animals

bearing $F98_{EGFR}$ gliomas, which had received i.t. EGF-BSD and BNCT, had an MST of 45 ± 5 days compared with 33 ± 2 days for animals bearing $F98_{WT}$ tumors, and rats that received i.t. EGF-BSD in combination with i.v. BPA had an MST of 57 ± 8 days compared with 39 ± 2 days for i.v. BPA alone [51].

The anti-EGF mAb cetuximab (IMC-C225) has been also utilized as a delivery agent for BNCT. BSD was chemically linked to cetuximab [52] and the bioconjugate (BD-C225) was specifically taken up by $F98_{EGFR}$ glioma cells in vitro compared with receptor-negative $F98_{WT}$ cells (41.8 vs. 9.1 μg/g). As regards the in vivo biodistribution of $F98_{WT}$ or $F98_{EGFR}$ glioma rats, BD-C225 was given intracerebrally by either convection-enhanced delivery (CED) or direct i.t. injection. The amount of boron retained by $F98_{EGFR}$ gliomas 24 h following CED and i.t. injection was 77.2 and 50.8 μg/g, respectively, with normal brain and blood boron values (<0.05 μg/g). When BNCT was carried out 24 h after CED of BD-C225, either alone or in combination with i.v. BPA, the corresponding MSTs were 54.5 and 70.9 days, respectively, with one long-term survivor (more than 180 days). In contrast, the MSTs of irradiated and untreated controls were 30.3 and 26.3 days, respectively. These data show the therapeutic efficacy of molecular targeting of EGFR using a boronated mAb either alone or in combination with BPA [53].

7.1.2.3 Emulsion

Lipiodol is an iodinated and esterified lipid of poppy seed oil and is coadministered with chemotherapeutic agents for transcatheter arterial chemoembolization. Suzuki and coworkers found that the intra-arterial administration of BSH/lipiodol emulsion provided selectively high ^{10}B concentrations (approximately 200 ppm 6 h after administration) in experimental liver tumors [54]. This high ^{10}B accumulation in the liver tumor can be attributed to the embolizing effect of lipiodol on tumor vessels. Furthermore, they also investigated degradable starch microspheres (DSMs) that cause transient and reversible embolization in small arteries and increase the retention of chemotherapeutic agents within a liver tumor, as the other embolizing agent. The biodistribution of ^{10}B after the intra-arterial administration of BSH/DSM emulsion was investigated using a rat liver tumor model. ^{10}B concentration in the tumor at 1 h after administration of BSH with DSM was 231 ppm. At 6 h, the ^{10}B concentration in the tumor in the BSH + DSM group was 81.5 ppm. On the other hand, the ^{10}B concentration in the liver at 1 h after administration of BSH with DSM was 184 ppm. At 6 h, the ^{10}B concentration in the liver in the BSH + DSM group was 78 ppm. The tumor/liver ^{10}B concentration ratios (T/L ratios) in the BSH + DSM group were significantly smaller than those in the BSH + lipiodol group at 1 h (1.4 vs. 3.6) and 6 h (1.1 vs. 14.9). Therefore, BSH/DSM-based BNCT was not suitable for the treatment of multiple liver tumors due to the low T/L ratio. However, the high ^{10}B accumulation in the liver tumors following intra-arterial administration of BSH/DSM emulsion suggests that BSH/DSM-based BNCT has the potential for application to malignant tumors in other sites [55].

The water-in-oil–water (WOW) emulsion has been used as the carrier of anticancer agents in arterial injections in clinical cancer treatment. Yanagie and coworkers prepared BSH-entrapped WOW emulsion for selective arterial injection for the

treatment of hepatocellular carcinoma. WOW emulsion was administered by arterial injections via the proper hepatic artery. The antitumor activity of the emulsion was compared with that of the BSH/lipiodol emulsion or BSH solutions, using VX-2 rabbit hepatic tumor models. The concentration of ^{10}B in VX-2 tumor on delivery of WOW emulsion was superior to that of conventional BSH/lipiodol emulsion. Electron microscopic images delineated the accumulation of fat droplets of WOW emulsion in the tumor site, but there was no accumulation of fat droplets in the BSH/lipiodol emulsion [56].

7.1.2.4 HVJ Envelope

The HVJ envelope (HVJ-E) vector system is a novel fusion-mediated gene delivery system that is based on inactivated hemagglutinating virus of Japan (HVJ; Sendai virus). The HVJ liposome, a liposome fused with HVJ-E [11], has higher boron trapping efficiency than HVJ-E alone. Nakai, Kaneda, and coworkers investigated boron delivery into cultured cells with HVJ-E and HVJ-liposome systems. The cellular ^{10}B concentration after 60-min incubation with HVJ-E containing BSH was 24.9 μg/g cell pellet for BHK-21 cells (baby hamster kidney cells) and 19.4 μg/g cell pellet for SCC VII cells (murine squamous cell carcinoma). These results indicate that HVJ-E fused with tumor cell membrane to rapidly deliver boron agents, and that the HVJ-E-mediated delivery system is applicable to BNCT [57, 58].

7.1.2.5 Boron-Encapsulated Liposomes

The first liposomal boron delivery system was reported by Yanagie and coworkers in 1991. They investigated a BSH-encapsulated liposome that conjugated with mAb specific for carcinoembryonic antigen (CEA). The liposome was prepared from egg yolk phosphatidylcholine, cholesterol, and dipalmitoylphosphatidylethanolamine (1/1/0.05), and BSH was encapsulated. The liposome was treated with dithiothreitol and suspended in the *N*-hydroxysuccinimidyl-3-(2-pyridyldithio)propionate-treated Ab solution for conjugation. This immunoliposome was shown to bind selectively to human pancreatic carcinoma cells (AsPC-1) bearing CEA on their surfaces, and to inhibit tumor cell growth on thermal neutron irradiation in vitro [59]. Furthermore, the cytotoxic effects of locally injected BSH-encapsulated immunoliposomes on AsPC-1 xenografts in nude mice were evaluated. After i.t. injection of the immunoliposomes, boron concentrations in tumor tissue and blood were 49.59 ± 6.59 and 0.30 ± 0.08 ppm, respectively. Tumor growth in mice that received an i.t. injection of BSH-encapsulated immunoliposomes was suppressed with thermal neutron irradiation in vivo. Histopathologically, hyalinization and necrosis were found in the immunoliposome-treated tumors [60].

In 1992, Hawthorne and coworkers prepared boron-encapsulated liposomes with mean diameters of 70 nm or less from distearoylphosphatidylcholine (DSPC) and cholesterol. Hydrolytically stable borane anions, $B_{10}H_{10}^{2-}$, $B_{12}H_{11}SH^{2-}$, $B_{20}H_{17}OH^{4-}$, and $B_{20}H_{19}^{3-}$, and the normal form and the photoisomer of $B_{20}H_{18}^{2-}$ were encapsulated in the liposomes as soluble sodium salts. Although the boron compounds used do not exhibit any affinity for tumors and are normally rapidly cleared from the body, the liposomes were observed to selectively deliver borane anions to tumors. The highest tumor concentrations reached the therapeutic range (>15 μg of boron per g of tumor)

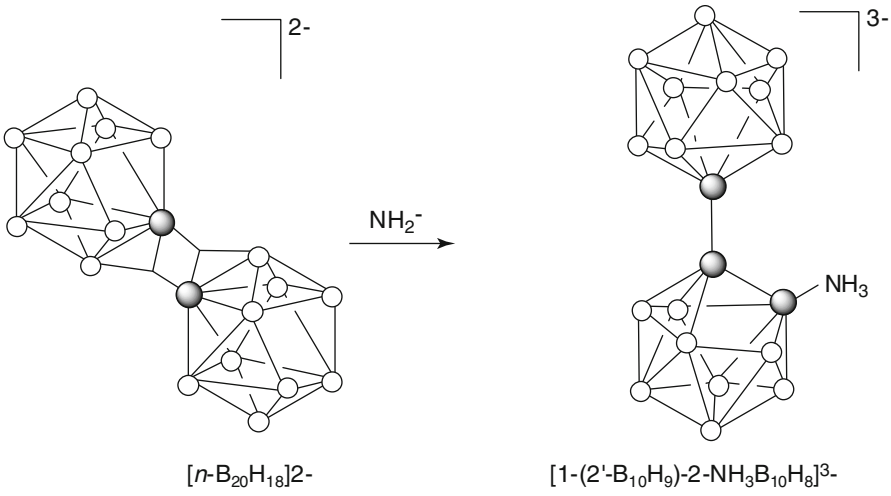

Fig. 7.4 Conversion of $[n\text{-}B_{20}H_{18}]^{2-}$ into $[1\text{-}(2'\text{-}B_{10}H_9)\text{-}2\text{-}NH_3B_{10}H_8]^{3-}$

while maintaining high tumor-boron/blood-boron ratios (>3). The most favorable results were obtained with the two isomers of $B_{20}H_{18}^{2-}$. These boron compounds have the ability to react with intracellular components after they have been deposited in tumor cells by liposomes, thereby preventing the release of the borane ion into blood [61]. Furthermore, an apical-equatorial (*ae*) isomer of the $B_{20}H_{17}NH_3^{3-}$ ion, $[1\text{-}(2'\text{-}B_{10}H_9)\text{-}2\text{-}NH_3B_{10}H_8]^{3-}$, which was produced by the reaction of the polyhedral borane ion $B_{20}H_{18}^{2-}$ with liquid ammonia, was encapsulated by liposomes prepared with 5 % PEG-200-distearoylphosphatidylethanolamine. The PEGylated liposomes exhibited long circulation lifetimes due to escape from the RES, resulting in the continued accumulation of boron in the tumor over the entire 48-h experimental period and reaching a maximum of 47 μg of boron per g of tumor [62] (Fig. 7.4).

Boron-containing folate receptor (FR) targeted liposomes were developed by Lee and coworkers. FR expression is frequently amplified in human tumors. Two highly ionized boron compounds, $Na_2[B_{12}H_{11}SH]$ and Na_3 ($B_{20}H_{17}NH_3$), were incorporated into liposomes by passive loading with encapsulation efficiencies of 6 and 15 %, respectively. In addition, five weakly basic boronated polyamines were investigated, as shown in Fig. 7.5. These were incorporated into liposomes by a pH-gradient-driven remote-loading method with varying loading efficiencies. High loading efficiencies were obtained with low molecular weight boron derivatives, using ammonium sulfate as the trapping agent, compared to those obtained with sodium citrate. The in vitro uptake of folate-derivatized, boronated liposomes was investigated using human KB squamous epithelial cancer cells that have amplified FR expression. Much higher cellular boron uptake was observed with FR-targeted liposomes (up to 1,584 μg/10^9 cells) than with nontargeted control liposomes (up to 154 μg/10^9 cells), irrespective of the chemical form of the boron and the method used for liposomal preparation [63].

Kullberg and coworkers investigated an EGF-conjugated PEGylated liposome-delivery vehicle containing water-soluble boronated phenanthridine, WSP1, or

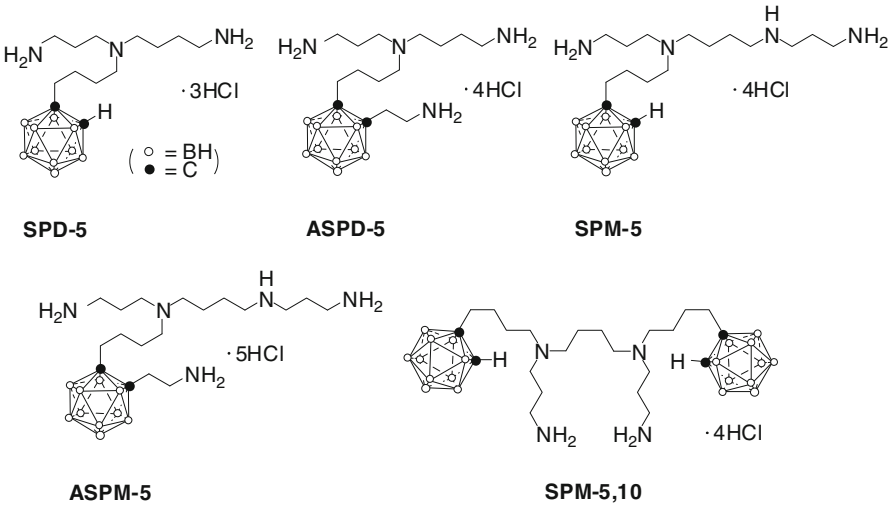

Fig. 7.5 Structures of boronated polyamine derivatives

water-soluble boronated acridine, WSA1, for EGFR targeting. In the case of WSA1, ligand-dependent boron uptake was achieved and the boron uptake was as good as that when free WSA1 was administered. No ligand-dependent boron uptake was seen for WSP1-containing liposomes. Thus, WSA1 is a candidate for further studies. Approximately 10^5 boron atoms were loaded into each liposome. Critical assessment indicated that after optimization, up to 10^6 boron atoms can be loaded. In vitro boron uptake by glioma cells (6.29 ± 1.07 μg/g cells) was observed with WSA1-encapsulated EGF-conjugated PEGylated liposomes [64] (Fig. 7.6).

Transferrin (TF)-receptor-mediated endocytosis is a normal physiological process by which TF delivers iron to cells, and a high concentration of TF receptor has been observed on most tumor cells in comparison with normal cells. Maruyama and coworkers developed BSH-encapsulating, TF-conjugated PEGylated liposomes (TF-PEG liposomes). When TF-PEG liposomes were injected at a dose of 35 mg ^{10}B/kg, prolonged residence time in the circulation and low uptake by RES were observed in colon 26 tumor-bearing mice, resulting in enhanced accumulation of ^{10}B in the solid tumor tissue (e.g., 35.5 μg of boron per g of tumor). TF-PEG liposomes maintained a high ^{10}B level in the tumor, with concentrations exceeding 30 μg of boron per g of tumor for at least 72 h after injection. On the other hand, plasma ^{10}B level decreased, resulting in a tumor/plasma ratio of 6.0 at 72 h after injection. The administration of BSH encapsulated in TF-PEG liposomes at a dose of 5 or 20 mg ^{10}B/kg and the irradiation with 2×10^{12} neutrons/cm^2 for 37 min suppressed tumor growth and improved long-term survival compared with PEG liposomes, bare liposomes, and free BSH [65, 66]. Masunaga and coworkers evaluated the biodistribution of BSH and $Na_2B_{10}H_{10}$-encapsulated TF-PEG liposomes in SCC VII tumor-bearing mice. The time courses of the change in ^{10}B concentration in the

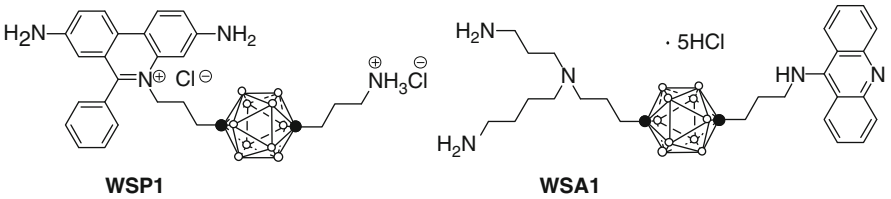

Fig. 7.6 Structures of water-soluble boronated phenanthridine (WSP1) and acridine (WSA1)

tumors loaded with both liposomes were similar except that ^{10}B concentrations were higher at 24 h after loading of $Na_2B_{10}H_{10}$ than BSH in TF-PEG liposomes, and ^{10}B concentration in the tumors was 35.6 μg of boron per g of tumor when $Na_2B_{10}H_{10}$-encapsulated TF-PEG liposomes (35 mg ^{10}B/kg) were injected [67].

Cetuximab-conjugated liposomes were also investigated as an alternative immunoliposome for targeting EGFR(+) glioma cells. Lee and coworkers developed cetuximab immunoliposomes via a cholesterol-based membrane anchor, maleimido-PEG-cholesterol (Mal-PEG-Chol), to incorporate cetuximab into the liposomes. BSH-encapsulated cetuximab immunoliposomes were evaluated for targeted delivery to human EGFR gene transfected $F98_{EGFR}$ glioma cells. Much greater (~8-fold) cellular boron uptake was achieved with cetuximab immunoliposomes in EGFR(+) $F98_{EGFR}$ than with nontargeted human IgG immunoliposomes [68].

7.1.2.6 Boron-Lipid Liposomes

The development of lipophilic boron compounds embedded within the liposome bilayer is an attractive means to increase the overall incorporation efficiency of boron-containing species, as well as to raise the gross boron content of the liposomes in the formulation. Selective boron delivery to tumors by lipophilic species incorporated in the membranes of unilamellar liposomes was first demonstrated by Hawthorne and coworkers. They synthesized nido-carborane amphiphile **1** (Fig. 7.7) and prepared boronated liposomes composed of DSPC, cholesterol, and **1** in the bilayer. After injecting liposomal suspensions into BALB/c mice-bearing EMT6 mammary adenocarcinomas, the time course of the biodistribution of boron was examined. At low injected doses normally used (5–10 mg ^{10}B/kg), peak tumor boron concentration of 35 μg of boron per g of tumor and tumor/blood boron ratio of −8 were achieved. These values are sufficiently high for the successful application to BNCT. The incorporation of both **1** and the hydrophilic species, $Na_3[1\text{-}(2'\text{-}B_{10}H_9)\text{-}2\text{-}NH_3B_{10}H_8]$, within the same liposomes significantly enhanced biodistribution characteristics as exemplified by the maximum tumor boron concentration of 50 μg of boron per g of tumor and the tumor/blood boron ratio of 6 [69].

In 2004, Nakamura and coworkers developed nido-carborane lipid **2**, which consists of the nido-carborane moiety as the hydrophilic functionality conjugated with two long alkyl chains as the lipophilic functionality. Analysis under a transmission electron microscope by negative staining with uranyl acetate showed stable vesicle formation of nido-carborane lipid **2**. Compound **2** was incorporated into

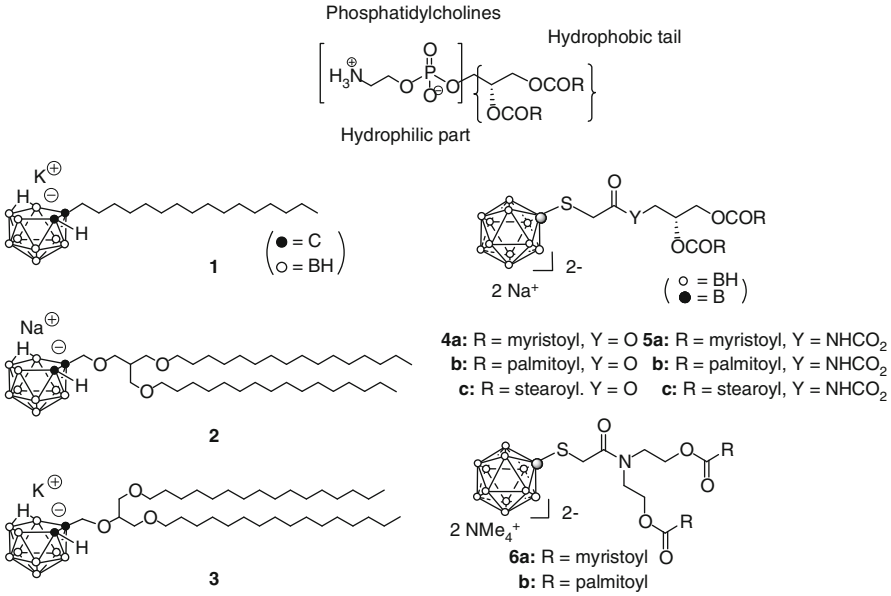

Fig. 7.7 Structures of boron lipids

DSPC liposomes in a concentration-dependent manner [70]. Furthermore, TF could be introduced to the surface of nido-carborane lipid liposomes (Tf(+)-PEG-CL liposomes) by coupling TF to the PEG-CO_2H moieties of Tf(−)-PEG-CL liposomes. The biodistribution of Tf(+)-PEG-CL liposomes injected intravenously into colon 26 tumor-bearing BALB/c mice revealed that Tf(+)-PEG-CL liposomes accumulated in tumor tissues and stayed there for a sufficiently long time to increase tumor/blood boron ratio, although Tf(−)-PEG-CL liposomes were gradually released from tumor tissues with time. A boron concentration of 22 μg of boron per g of tumor was achieved by injecting Tf(+)-PEG-CL liposomes (7.2 mg ^{10}B/kg) into tumor-bearing mice. As described before, BSH-encapsulated Tf(+)-PEG liposomes accumulated in tumors at 35.5 μg of boron per g of tissue 72 h after administration of 35 mg ^{10}B/kg. Therefore,^{10}B delivery to tumor tissues by Tf(+)-PEG-CL liposomes would be more efficient than that by BSH-encapsulated Tf(+)-PEG liposomes. However, significant acute toxicity was observed in 50 % of the mice when Tf(+)-PEG-CL liposomes were injected at a dose of 14 mg ^{10}B/kg. Injection of Tf(+)-PEG-CL liposomes at a dose of 7.2 mg ^{10}B/kg and irradiation with 2×10^{12} neutrons/cm^2 for 37 min at the KUR atomic reactor suppressed tumor growth, and the average survival rate of mice not treated with Tf(+)-PEG-CL liposomes was 21 days, whereas that of treated mice was 31 days [71]. Hawthorne and coworkers also synthesized nido-carborane lipid **3** and investigated the formation of boron-rich, DSPC-free liposomes from **3** and cholesterol. DSPC-free liposomes exhibited a size distribution pattern of 40–60 nm, which was in the range normally associated with selective tumor uptake. Animal studies showed that nido-carborane

lipid **3** liposomes were too toxic for use in BNCT [72]. However, liposomes prepared from lipids **2** and/or **3** contain a new type of bilayer constituent having high boron content.

In order to solve the problem of the significant toxicity of liposomes prepared from nido-carborane lipids **2** and **3**, closo-dodecaborate has been focused on as an alternative hydrophilic function of boron lipids. Nakamura and coworkers succeeded in the synthesis of double-tailed closo-dodecaborate lipids **4a**-**c** and **5a**-**c**, which have a $B_{12}H_{11}S$ moiety as the hydrophilic function, by S-alkylation of BSH with bromoacetyl and chloroacetocarbamate derivatives of diacylglycerols. Calcein encapsulation experiments revealed that the liposomes, prepared from boron cluster lipids **4**, DMPC, PEG-DSPE, and cholesterol, are stable at 37 °C in FBS solution for 24 h [73, 74]. The time-dependent biodistribution experiment of boronated liposomes prepared from closo-dodecaborate lipid **4c** and injected intravenously into colon 26 tumor-bearing BALB/c mice (20 mg ^{10}B/kg) showed high ^{10}B accumulation in the tumor tissue (22 μg of boron per g of tumor) 24 h after injection [75]. Besides the determination of ^{10}B concentration in various organs, the mice were anesthetized 24 h after administration of the boron liposomes and placed in an acrylic mouse holder where their whole bodies, except their tumor-implanted leg, were shielded with acrylic resin. Neutron irradiation was carried out in the JAEA atomic reactor (JRR-4). Tumor growth rate in mice-administered boron liposomes was significantly suppressed, although the administration of saline did not reduce tumor growth after neutron irradiation. Gabel and coworkers also developed closo-dodecaborate lipids **6a** and **6b**. Differential scanning calorimetry showed that **6a** and **6b** bilayers have main phase transition temperatures of 18.8 and 37.9 °C, respectively. When incorporated into liposomal formulations with equimolar amounts of DSPC and cholesterol, stable liposomes were obtained. ξ-Potential measurements indicated that both **6a-** and **6b-**containing vesicles are negatively charged, with the most negative potential described of any liposome so far. Liposomes prepared from **6a** were slightly less toxic to V79 Chinese hamster cells (IC_{50} = 5.6 mM) than unformulated BSH (IC_{50} = 3.9 mM), while liposomes prepared from **6b** were not toxic even at 30 mM [76].

Meanwhile, cholesterol is also indispensable for the stable formation of liposomes. Therefore, the development of boronated cholesterol derivatives is considered to be an alternative approach to boron embedment in the liposome bilayer. The first boronated cholesterol derivatives were reported by Feakes and coworkers [77]. Although they synthesized nido-carborane conjugated cholesterols **7a**-**b** (Fig. 7.8), the evaluation of their liposomes has not been reported yet. Nakamura, Gabel, and coworkers developed closo-dodecaborate-conjugated cholesterols **8a**-**c**.

The closo-dodecaborate-conjugated cholesterol **8a** liposome, which was prepared from dimyristoylphosphatidylcholine, cholesterol, **8a**, and PEG-conjugated distearoylphosphatidylethanolamine (1:0.5:0.5:0.1), exhibited higher cytotoxicity than BSH at the same boron concentration and the IC_{50} values of **8a** liposome and BSH toward colon 26 cells were estimated to be 25 and 78 ppm of boron concentration, respectively [78]. Tjarks and coworkers developed carboranyl cholesterol analog **9** as a lipid bilayer component for the construction of nontargeted and receptor-targeted

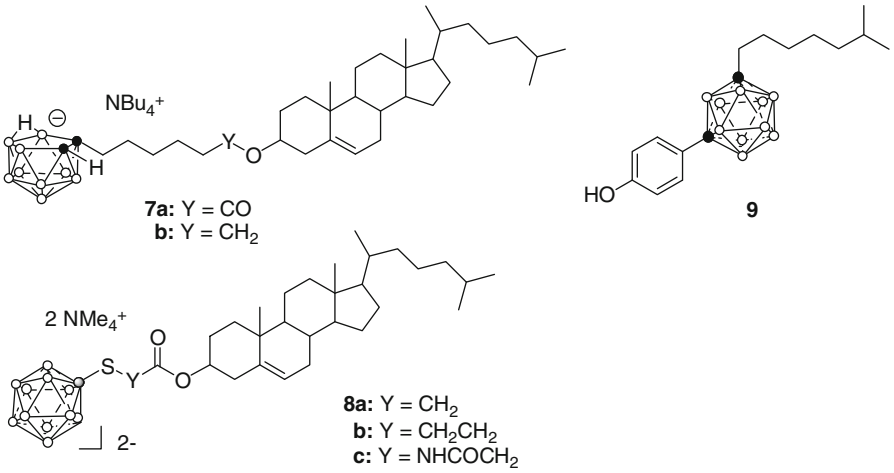

Fig. 7.8 Structures of boron cholesterols

boronated liposomes. The major structural feature of these boronated cholesterol mimics is the physicochemical similarity between cholesterol and carborane frameworks [40]. Cholesterol analog **9** was stably incorporated into non-, FR-, and vascular endothelial growth factor receptor-2 (VEGFR-2)-targeted liposomes. No major differences in appearance, size distribution, and lamellarity were found among conventional DPPC/cholesterol liposomes, nontargeted, and FR-targeted liposomal formulations of this carboranyl cholesterol derivative. FR-targeted boronated liposomes were taken up extensively by FR-overexpressing KB cells in vitro, and the uptake was effectively blocked in the presence of free folate. There was no apparent in vitro cytotoxicity in FR-overexpressing KB cells and VEGFR-2-overexpressing 293/KDR cells when these were incubated with boronated FR- and (VEGFR-2)-targeted liposomes, respectively, although the former accumulated extensively in KB cells and the latter effectively interacted with VEGFR-2 by causing autophosphorylation and protecting 293/KDR cells from SLT (Shiga-like toxin)-VEGF cytotoxicity [79].

References

1. Soloway AH, Tjarks W, Barnum BA et al (1998) The chemistry of neutron capture therapy. Chem Rev 98:1515–1562
2. Hawthorne MF (1993) The role of chemistry in the development of boron neutron capture therapy of cancer. Angew Chem Int Ed Engl 32:950–984
3. Barth RF, Soloway AH, Fairchild RG et al (1992) Boron neutron capture therapy for cancer, realities and prospects. Cancer 70:2995–3007
4. Soloway AH, Hatanaka H, Davis MA (1967) Penetration of brain and brain tumor. VII. Tumor-binding sulfhydryl boron compounds. J Med Chem 10:714–717
5. Snyder HR, Reedy AJ, Lennarz WJ (1958) Synthesis of aromatic boronic acids. Aldehydo boronic acids and a boronic acid analog of tyrosine. J Am Chem Soc 80:835

6. Nakagawa Y, Hatanaka H (1997) Boron neutron capture therapy. Clinical brain tumor studies. J Neurooncol 33:105–115
7. Mishima Y, Ichihashi M, Hatta S et al (1989) New thermal neutron capture therapy for malignant melanoma: melanogenesis-seeking 10B molecule-melanoma cell interaction from in vitro to first clinical trial, pigment. Cell Res 2:226–234
8. Kato I, Ono K, Sakurai Y et al (2004) Effectiveness of BNCT for recurrent head and neck malignancies. Appl Radiat Isot 61:1069–1073
9. Aihara T, Hiratsuka J, Morita N et al (2006) First clinical case of boron neutron capture therapy for head and neck malignancies using ^{18}F-BPA PET. Head Neck 28:850–855
10. Suzuki M, Sakurai Y, Hagiwara S et al (2007) First attempt of boron neutron capture therapy (BNCT) for hepatocellular carcinoma. Jpn J Clin Oncol 37:376–381
11. Adams L, Hosmane SN, Eklund JE et al (2002) A new synthetic route to boron-10 enriched pentaborane(9) from boric acid and its conversion to anti-$^{10}B_{18}H_{22}$. J Am Chem Soc 124:7292–7293
12. El-Zaria ME, Dorfler U, Gabel D (2002) Synthesis of (aminoalkylamine)-N-aminoalkyl) azanonaborane(11) derivatives for boron neutron capture therapy. J Med Chem 45:5817–5819
13. Srivastava RR, Singhaus RR, Kabalka GW (1999) 4-Dihydroxyborylphenyl analogues of 1-aminocyclobutanecarboxylic acids: potential boron neutron capture therapy agents. J Org Chem 64:8495–8500
14. Kabalka GW, Wu ZZ, Yao M-L et al (2004) The syntheses and in vivo biodistribution of novel boronated unnatural amino acids. Appl Radiat Isot 61:1111–1115
15. Slepukhina I, Gabel D, (2006) Synthesis and in vitro toxicity of new dodecaborate-containing amino acids. In: Nakagawa Y, Kobayashi T, Fukuda H. (eds.) Proceedings of ICNCT-12:247–250
16. Hattori Y, Kurihara K, Niki Y et al (2006) Synthesis and evaluation of the compounds containing ^{10}B and ^{19}F atoms as boron carrier and imaging agent. Peptide Sci 2005:337–340
17. Dewar MJS, Maitlis PM (1959) A boron-containing purine analog. J Am Chem Soc 81: 6329–6330
18. Matteson DS, Cheng T-C (1968) Displacement reactions of dibutyl iodomethaneboronate and the synthesis of boron-substituted pyrimidines. J Org Chem 33:3055–3060
19. Al-Madhoun AS, Johnsamuel J, Barth RF et al (2004) Evaluation of human thymidine kinase 1 substrates as new candidates for boron neutron capture therapy. Cancer Res 64:6280–6286
20. Olejniczak AB, Plesek J, Lesnikowski ZJ (2006) Nucleoside-metallacarborane conjugates for base-specific metal labeling of DNA. Chem Eur J 13:311–318
21. Kahl SB, Koo MS (1990) Synthesis of tetrakis-carborane-carboxylate esters of 2,4-bis-(α,β-dihydroxyethyl)-deuteroporphyrin IX. Chem Commun 1769–1771
22. Hill JS, Kahl SB, Kaye AH et al (1992) Selective tumor uptake of a boronated porphyrin in an animal model of cerebral glioma. Proc Natl Acad Sci USA 89:1785–1789
23. Miura M, Gabel D, Oenbrink G et al (1990) Preparation of carboranyl porphyrins for boron neutron capture therapy. Tetrahedron Lett 31:2247–2250
24. Phadke AS, Morgan AR (1993) Synthesis of carboranyl porphyrins: potential drugs for boron neutron capture therapy. Tetrahedron Lett 34:1725–1728
25. Oenbrink G, Jurgenlimke P, Gabel D (1988) Accumulation of porphyrins in cells influence of hydrophobicity aggregation and protein binding. Photochem Photobiol 48:451–456
26. Rosenthal MA, Kavar B, Hill JS et al (2001) Phase I and pharmacokinetic study of photodynamic therapy for high-grade gliomas using a novel boronated porphyrin. J Clin Oncol 19:519–524
27. Vicente MGH, Edwards BF, Shetty SJ et al (2002) Syntheses and preliminary biological studies of four *meso*-tetra[(*nido*-carboranylmethyl) phenyl] porphyrins. Bioorg Med Chem 10:481–492
28. Matsumura A, Shibata Y, Yamamoto T et al (1999) A new boronated porphyrin (STA-BX909) for neutron capture therapy: an in vitro survival assay and in vivo tissue uptake study. Cancer Lett 141:203–209
29. Ratajski M, Osterloh J, Gabel D (2006) Boron-containing chlorins and tetraazaporphyrins: synthesis and cell uptake of boronated pyropheophorbide A derivatives. Anti-Cancer Agents Med Chem 6:159–166
30. Ol'shevskaya VA, Evstigneeva RP, Luzgina VN et al (2001) Synthesis of closo-monocarbon carborane-substituted natural porphyrins. Mendeleev Commun 11:14–15

31. Hao E, Sibrian-Vazquez M, Serem W, Garno JC (2007) Synthesis, aggregation and cellular investigations of porphyrin–cobaltacarborane conjugates. Chem Eur J 13:9035–9042
32. Bauer C, Gabel D, Dörfler U (2002) Azanonaboranes [(RNH2)B8H11NHR] as possible new compounds for use in boron neutron capture therapy. Eur J Med Chem 37:649–657
33. Tjarks W, Anisuzzaman AKM, Liu L et al (1992) Synthesis and in vitro evaluation of boronated uridine and glucose derivatives for boron neutron capture therapy. J Med Chem 35:1628–1633
34. Tietze LF, Bothe U (1998) Ortho-carboranyl glycosides of glucose, mannose, maltose and lactose for cancer treatment by boron neutron-capture therapy. Chem Eur J 4:1179–1183
35. Tietze LF, Bothe U, Griesbach U et al (2001) *ortho*-Carboranyl glycosides for the treatment of cancer by boron neutron capture therapy. Bioorg Med Chem 9:1747–1752
36. Giovenzana GB, Lay L, Monti D et al (1999) Synthesis of carboranyl derivatives of alkynyl glycosides as potential BNCT agents. Tetrahedron 55:14123–14136
37. Stadlbauer S, Welzel P, Hey-Hawkins E (2009) Access to carbaboranyl glycophosphonates: an Odyssey. Inorg Chem 48:55005–55010
38. Ronchi S, Prosperi D, Thimon C et al (2005) Synthesis of mono- and bisglucuronylated carboranes. Tetrahedron Asymmet 16:39–44
39. El-Zaria ME, Genady AR, Gabel D (2006) The first synthesis of azanonaborane-containing sugars, possible boron carriers for neutron capture therapy. New J Chem 30:597–602
40. Endo Y, Iijima T, Yamakoshi Y et al (1999) Potent estrogenic agonists bearing dicarba-closo-dodecaborane as a hydrophobic pharmacophore. J Med Chem 42:1501–1504
41. Endo Y, Iijima T, Yamakoshi Y et al (2001) Potent estrogen agonists based on carborane as a hydrophobic skeletal structure. A new medicinal application of boron clusters. Chem Biol 8:341–355
42. Julius RL, Farha OK, Chiang J et al (2007) Synthesis and evaluation of transthyretin amyloidosis inhibitors containing carborane pharmacophores. Proc Natl Acad Sci USA 104:4808–4813
43. Lee C-H, Jin GF, Yoon JH et al (2008) Synthesis and characterization of polar functional group substituted mono- and bis-(o-carboranyl)-1,3,5-triazine derivatives. Tetrahedron Lett 49:159–164
44. Armstrong AF, Valliant JF (2007) The bioinorganic and medicinal chemistry of carboranes: from new drug discovery to molecular imaging and therapy. Dalton Trans 4240–4251
45. Barth RF, Adams DM, Soloway AH et al (1994) Boronated starburst dendrimer-monoclonal antibody immunoconjugates. Evaluation as a potential delivery system for neutron capture therapy. Bioconjug Chem 5:58–66
46. Shukla S, Wu G, Chatterjee M et al (2003) Synthesis and biological evaluation of folate receptor-targeted boronated pamam dendrimers as potential agents for neutron capture therapy. Bioconjug Chem 14:158–167
47. Yinghuai Z, Peng A, Carpenter K et al (2005) Substituted carborane-appended water-soluble single-wall carbon nanotubes: new approach to boron neutron capture therapy drug delivery. J Am Chem Soc 127:9875–9880
48. Hosmane NS, Yinghuai Z, Maguire JA et al (2009) Nano and dendritic structured carboranes and metallacarboranes: from materials to cancer therapy. J Organomet Chem 694:1690–1697
49. Azab A-K, Srebnik M, Doviner V, Rubinstein A (2005) Targeting normal and neoplastic tissues in the rat jejunum and colon with boronated, cationic acrylamide copolymers. J Control Release 106:14–25
50. Capala J, Barth RF, Bendayan M (1996) Boronated epidermal growth factor as a potential targeting agent for boron neutron capture therapy of brain tumors. Bioconjug Chem 7:7–15
51. Barth RF, Yang W, Adams DM et al (2002) Molecular targeting of the epidermal growth factor receptor for neutron capture therapy of gliomas. Cancer Res 62:3159–3166
52. Wu G, Barth RF, Yang W et al (2004) Site-specific conjugation of boron-containing dendrimers to anti-EGF receptor monoclonal antibody cetuximab (IMC-C225) and its evaluation as a potential delivery agent for neutron capture therapy. Bioconjug Chem 15:185–194
53. Wu G, Yang W, Barth RF et al (2007) Molecular targeting and treatment of an epidermal growth factor receptor positive glioma using boronated cetuximab. Clin Cancer Res 13:1260–1268
54. Suzuki M, Sakurai Y, Masunaga S et al (2003) Study of boron neutron capture therapy with borocaptate sodium (BSH)/lipiodol emulsion (BSH/lipiodol-BNCT) for treatment of multiple liver tumors. Int J Radiat Oncol Biol Phys 58:892–896

55. Suzuki M, Nagata K, Masunaga S et al (2004) Biodistribution of ^{10}B in a rat liver tumor model following intra-arterial administration of sodium borocaptate (BSH)/degradable starch microspheres (DSM) emulsion. Appl Radiat Isot 61:933–937
56. Yanagie H, Higashi S, Ikushima I et al. (2006) Selective enhancement of boron accumulation with boron-entrapped water-in-oil–water emulsion in VX-2 rabbit hepatic cancer model for BNCT. In: Nakagawa Y, Kobayashi T, Fukuda H. (eds.) Proceedings of ICNCT-12:211–214
57. Kaneda Y, Yamamoto S, Hiraoka K (2003) The hemagglutinating virus of Japan-liposome method for gene delivery. Methods Enzymol 373:482–493
58. Nakai K, Yamamoto T, Matsumura A (2006) Application of HVJ envelop system to boron neutron capture therapy. In: Nakagawa Y, Kobayashi T, Fukuda H. (eds.) Proceedings of ICNCT-12:207–210
59. Yanagie H, Tomita T, Kobayashi H et al (1991) Application of boronated anti-cea immunoliposome to tumour cell growth inhibition in in vitro boron neutron capture therapy model. Br J Cancer 63:522–526
60. Yanagie H, Tomita T, Kobayashi H et al (1997) Inhibition of human pancreatic cancer growth in nude mice by boron neutron capture therapy. Br J Cancer 75:660–665
61. Sherry K, Feakes DA, Hawthorne MF et al (1992) Model studies directed toward the boron neutron-capture therapy of cancer: Boron delivery to murine tumors with liposomes. Proc Natl Acad Sci USA 89:9039–9043
62. Feakes DA, Shelly K, Knobler DB et al (1994) Na3[B20H17NH3]: synthesis and liposomal delivery to murine tumors. Proc Natl Acad Sci USA 91:3029–3033
63. Pan XQ, Wang H, Shukla S et al (2002) Boron-containing folate receptor-targeted liposomes as potential delivery agents for neutron capture therapy. Bioconjug Chem 13: 435–442
64. Kullberg EB, Carlsson J, Edwards K et al (2003) Introductory experiments on ligand liposomes as delivery agents for boron neutron capture therapy. Int J Oncol 23:461–467
65. Maruyama K, Ishida O, Kasaoka S et al (2004) Intracellular targeting of sodium mercaptoundecahydrododecaborate (BSH) to solid tumors by transferrin-PEG liposomes, for boron neutron-capture therapy (BNCT). J Control Release 98:195–207
66. Yanagie H, Ogura K, Takaagi K et al (2004) Accumulation of boron compounds to tumor with polyethylene-glycol binding liposome by using neutron capture autoradiography. Appl Radiat Isot 61:639–646
67. Masunaga S, Kasaoka S, Maruyama K et al (2006) The potential of transferrin-pendant-type polyethyleneglycol liposomes encapsulating decahydrodecaborate-^{10}B (GB-10) as ^{10}B-carriers for boron neutron capture therapy. Int J Radiat Oncol Biol Phys 66:1515–1522
68. Pan X, Wu G, Yang W et al (2007) Synthesis of cetuximab-immunoliposomes via a cholesterol-based membrane anchor for targeting of EGFR. Bioconjug Chem 18:101–108
69. Feakes DA, Shelly K, Hawthornet MF (1995) Selective boron delivery to murine tumors by lipophilic species incorporated in the membranes of unilamellar liposomes. Proc Natl Acad Sci USA 92:1367–1370
70. Nakamura H, Miyajima Y, Takei T et al. (2004) Synthesis and vesicle formation of a nido-carborane cluster lipid for boron neutron capture therapy. Chem Commun 1910–1911
71. Miyajima Y, Nakamura H, Kuwata Y et al (2006) Transferrin-loaded nido-Carborane liposomes: tumor-targeting boron delivery system for neutron capture therapy. Bioconjug Chem 17:1314–1320
72. Li T, Hamdi J, Hawthrone MF (2006) Unilamellar liposomes with enhanced boron content. Bioconjug Chem 17:15–20
73. Lee J-D, Ueno M, Miyajima Y, Nakamura H (2007) Synthesis of boron cluster lipids: closo-Dodecaborate as an alternative hydrophilic function of boronated liposomes for neutron capture therapy. Org Lett 9:323–326
74. Nakamura H, Lee J-D, Ueno M, Miyajima Y, Ban HS (2008) Synthesis of *closo*-dodecaboryl lipids and their liposomal formation for boron neutron capture therapy. NanoBiotechnology 3:135–145
75. Nakamura H, Ueno M, Ban HS et al (2009) Development of boron nano capsules for neutron capture therapy. Appl Radiat Isot 67:S84–S87

76. Justus E, Awad D, Hohnholt M et al (2007) Synthesis, liposomal preparation, and in vitro toxicity of two novel dodecaborate cluster lipids for boron neutron capture therapy. Bioconjug Chem 18:1287–1293
77. Feakes DA, Spinler JK, Harris FR (1999) Synthesis of boron-containing cholesterol derivatives for incorporation into unilamellar liposomes and evaluation as potential agents for BNCT. Tetrahedron 55:11177–11186
78. Nakamura H, Ueno M, Lee JD et al (2007) Synthesis of dodecaborate-conjugated cholesterols for efficient boron delivery in neutron capture therapy. Tetrahedron Lett 48:3151–3154
79. Thirumamagal BTS, Zhao XB, Bandyopadhyaya AK et al (2006) Receptor-targeted liposomal delivery of boron-containing cholesterol mimics for boron neutron capture therapy. Bioconjug Chem 17:1141–1150

Drugs for BNCT: BSH and BPA

8

Wolfgang A.G. Sauerwein, Pierre M. Bet,
and Andrea Wittig

Contents

W.A.G. Sauerwein (✉)
NCTeam, Department of Radiation Oncology, University Hospital Essen,
University Duisburg-Essen,
D-45122, Essen, Germany
e-mail: w.sauerwein@uni-due.de

P.M. Bet
Department of Clinical Pharmacology and Pharmacy, Vrije Universiteit Medical Center,
Amsterdam, The Netherlands
e-mail: pm.bet@vumc.nl

A. Wittig
Department of Radiotherapy and Radiation Oncology, Philipps-University Marburg,
Marburg, Germany
e-mail: andrea.wittig@med.uni-marburg.de

W.A.G. Sauerwein et al. (eds.), *Neutron Capture Therapy*,
DOI 10.1007/978-3-642-31334-9_8, © Springer-Verlag Berlin Heidelberg 2012

8.1 Introduction

Boron neutron capture therapy (BNCT) is a binary therapy based on the interaction of thermal neutrons with ^{10}B that needs to be transported by dedicated molecules at a higher concentration into tumor cells as compared to surrounding normal tissues. Despite the decades of effort from chemists, only two compounds showing some tumor specificity are actually available for clinical use: the boron cluster sodium borocaptate (BSH) and the amino acid analogue boronophenylalanine (BPA). Even for these compounds, quite few data exist, which were collected in a controlled and reliable way. This situation is mainly due to the fact that all major research activities in the field were made by academic institutions to answer a scientific question but not by pharmaceutical industries with the goal to collect data for regulatory authorities for licensing a new drug.

Starting 1995, the European Organisation for Research and Treatment of Cancer (EORTC) made a first approach to design clinical trials with the goal to follow the principles of classical trial design for drug development intended to collect clinical data for regulatory authorities [1–18].

In this chapter, published data are summarized concerning physical, chemical, and pharmaceutical aspects, preclinical and clinical trials with information to toxicity, pharmacokinetics, and tissue distribution of the two drugs BSH and BPA.

Missing information with respect to the quality control of the drugs used for animal experiments but also in some pioneering clinical trials are a major concern by interpreting some of the observations reported in the past. We therefore will give a detailed description of the quality control procedures used for both drugs in the frame of the EORTC trials 11001 and 11011. The chapter is based on a shortened version of the investigators brochures from the EORTC clinical trials 11001 and 11011 concerning the boron compounds Sodium Borocaptate (BSH) and Boronophenylalanine (BPA). It summarizes essential information that might be asked by regulatory authorities. The intention of this chapter is to support and to facilitate the preparation of new clinical trials based on these compounds. However this compilation cannot offer a complete and final description of all aspects concerning these two compounds necessary to file for drug approval.

8.2 Sodium Borocaptate (BSH)

8.2.1 Introduction

Sodium mercaptoundecahydro-closo-dodecaborate (BSH, $Na_2{}^{10}B_{12}H_{11}SH$) synthesized by Soloway[19], is a polyhedral mercaptoboron molecule. Designed for the treatment of tumors of the central nervous system it was applied to patients first by Hatanaka [20] and investigated in a phase I trial for glioblastoma multiforme (EORTC 11961) [2, 11]. After infusion of BSH, ^{10}B is found in tumor lesions localized in the brain at concentrations similar to the blood concentration, but it is almost not present in healthy cells of the central nervous system [12] leading to tumor-to-healthy-tissue concentration ratios suitable for therapy. The majority of the studies on pharmacokinetics, toxicity and tissue uptake were performed on patients suffering from brain tumors [21–25]. Substantial data have been collected on the biodistribution of BSH in brain tumors and surrounding normal tissues (i.e. brain, skin, muscle and dura).

Table 8.1 Atomic weight of the atoms composing BSH

	Atom weight
Sodium (Na)	22.9898
Hydrogen (H)	1.0079
Sulfur (S)	32.0600
Boron (B)	
^{10}B	10.0129
^{11}B	11.0093

Little attention has been paid to investigate the tissue uptake of boron compounds in other tumor types [17, 18, 26–28]. Instead of the use of BSH for BNCT in clinical trials since many years, there are still important information on pharmacokinetics and metabolism missing. This chapter tries to summarize the actual knowledge. It is based on the pharmacy brochures for BSH of the EORTC trials 11001 and 11011, which received relevant information from the compilation of clinical and pre-clinical data collected by the European Collaboration on Boron Neutron Capture Therapy and published by Peters and Gabel 1997 [29].

8.2.2 Physical, Chemical, and Pharmaceutical Data

8.2.2.1 Physicochemical Properties

Names

Chemical names

- Dodecaborate(2-)-$^{10}B_{12}$, 1,2,3,4,5,6,7,8,9,10,11-undecahydro-12-mercapto-, disodium
- Sodium Mercaptoundecahydro-closo-Dodecaborate ^{10}B
- Disodium Mercaptoundecahydro-closo-Dodecaborate ^{10}B
- Disodium (1+) 1-Mercapto-2,3,4,5,6,7,8,9,10,11,12-Undecahydro-closo-Dodecaborate ^{10}B (2-)

Synonyms

- Sodium borocaptate ^{10}B
- BSH [^{10}B]
- Na2BSH [^{10}B]
- Sodium BSH [^{10}B]
- Hydrogen sulfide (H2S), boron-10 complex;
- Borocaptate sodium ^{10}B
- Borolife
- Sodium borocaptate (^{10}B)
- Sodium mercaptoundecahydrododecaborate-^{10}B ($Na_2{}^{10}B_{12}H_{11}SH$)

CAS registration number: 12448-24-7

Structural Formula

Molecular formula: $Na_2B_{12}H_{11}SH$

Molecular weight: Precise molecular weight is dependent upon the boron isotopic composition of the material.

A series of typical molecular weights is listed below for varying isotopic compositions (Table 8.1).

Table 8.2 Molecular weight of BSH according to its content of ^{10}B

	^{10}B content (%)	^{11}B content (%)	Atomic wt.	BSH MW
Natural boron	20	80	10.8100	219.8544
	90	10	10.1125	211.4844
	95	5	10.0220	210.4092

Fig. 8.1 The BSH molecule

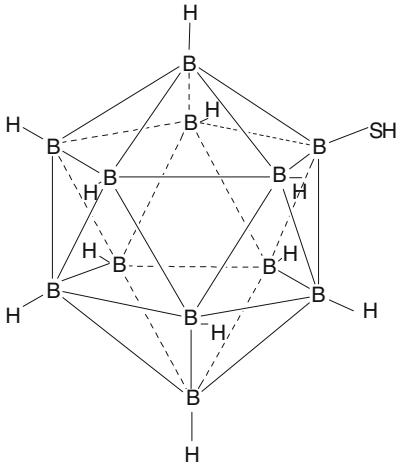

Therefore, BSH has the following molecular weight according to the varying ^{10}B and ^{11}B contents as shown (Table 8.2 and Fig. 8.1)

Physical and Chemical Characteristics
Solid state form: White hygroscopic crystalline powder
Solubility: Approximately 67 % w/v in water at 20 °C
Solution pH: 6.3 for a 1 % w/v solution
Specific rotation: Not applicable
Refraction index: Not known

8.2.2.2 Production, Purification, and Methods of Preparation

The manufacturing of BPA including production, purification, and control tests will depend on the procedures used by the chemical and/or pharmaceutical company producing the compound. Because of the ^{10}B-enrichment necessary for the use of BSH for BNCT, the production of the enriched compound, which normally is not done by pharmaceutical industry, is of major concern and might be an important source for unwanted impurities. The entire procedure has to follow the principles of good manufacturing practice including a strong quality control of the starting material. The solution of the BSH powder to produce the solution for injection to the patient is part of the production line; it has to be done by and under the control of approved pharmacists and needs special licensing if performed at the treating hospital.

8.2.2.3 Stability

Sodium borocaptate, ^{10}B enriched BSH, prior to be dissolved for the infusion solution is white or creamy white powder. The powder is hygroscopic and attracts

water on standing on air. It is suggested to store it in glass vials sealed with a septum and aluminum cap and well protected from humidity air, and light. The containers have to be labeled with the content, the batch number, and the weight of the contained material. Under such circumstances, the product can be stored for years. It is recommended to control the product on a yearly base using the appropriate quality control procedures as described later.

The stability of the infusion solution has not been published in detail. The experiences from the EORTC trials show that the infusion solution is stable toward degradation and especially oxidation for at least 1 day. Oxidation products (i.e., BSSH) are the major impurities appearing. Within this 24-h period, the conversion of BSH to BSSB is not significant, provided that the compound is carefully handled. This rate of conversion may change dramatically if large quantities of dissolved oxygen (or some yet unknown factor) are present. More precise experimentations are still missing to determine the reaction kinetics in more details.

8.2.3 Quality Control

For the EORTC trials 11001 and 11011, the quality control of the material was tested according to the following procedure. This procedure was written down in a SOP. The authors might be asked for more details.

8.2.3.1 Description of the Study Medication

BSH, ^{10}B-enriched ($Na_2{}^{10}B_{12}H_{11}SH$), is used as a white or creamy white lyophilized powder in glass vials sealed with a septum.

The containers are labeled with the content, the batch number, and the weight of the contained material.

The powder is hygroscopic and attracts water on standing on air.

8.2.3.2 Identification of BSH

Sodium

Test solution a: dissolve 10 mg in 0.1 ml 1 M hydrochloric acid. Heat a platinum wire in a colorless flame until no coloration is seen. Moist the platinum wire with test solution a and heat in the colorless flame. A yellow color is seen.

BSH, ^{10}B-enriched

Examine by infrared absorption spectrophotometry (see *European Pharmacopoeia*, 3rd edition 1997, section 2.2.24) using the golden gate method. The principal peaks appear at wave numbers 2,500, 880, 1,090, 1,015, and 750 cm^{-1}.

8.2.3.3 Purity of BSH

Oxidized Degradation Products

Examine by high-pressure liquid chromatography.

Mobile phase: methanol/water 60/40 (vol/vol), 10 mm tetrabutylammonium hydrogen sulfate, adjusted to pH 7.0 with tetrabutylammonium hydroxide. The mobile phase must be degassed before use.

Column: Merck Superspher RP-18 endcapped, 4 μm, 125 × 4 mm in diameter. The system must be equilibrated over night before injecting the test solution.

Flow: the flow rate of the mobile phase is set at 0.5 ml/min. Detection: the eluent is monitored at 220 nm.

Test solution b: to 50 mg add 10 ml 0.9 % sodium chloride solution. Dilute 10 μl to 1.0 ml with mobile phase. This solution must be freshly prepared and injected within 15 min. after preparation.

Inject 30 μl of test solution b on the column. BSH elutes at 6.5 min and the degradation product at 12.3 min. The material conforms to the demands if the integral for BSH is 98 % or more of the total integral, excluding the injection peak.

Pyrogens

Examine by Limulus amebocyte lysate test.

Test solution c: with a pyrogen-free spatula, 40.0 mg is weighed and dissolved in 4.0 ml pyrogen-free 0.9 % sodium chloride solution and dissolved. 33 μl of this solution is diluted to 1.0 ml with pyrogen-free water.

Carry the Limulus amebocyte lysate test out according to SOP "endotoxin assay." The material conforms to the demands if it contains less than 0.025 ie pyrogens/mg BSH.

8.2.3.4 Control of the BSH Content and the ^{10}B Enrichment

BSH Content

One vial of BSH is dissolved in water. Of this solution, an aliquot is diluted to 50–100 ppm boron. Three individual samples are analyzed for total boron content with mass spectrometry. The average of the three samples avg (total) and their relative standard deviation sd(total) is calculated. The total content of the vial is calculated from the indicated net weight and the indicated degree of enrichment. The theoretical molecular weight is calculated from the formula $Na_2B_{12}H_{11}SH$ with the atomic masses Na = 22.990, H = 1.008, S = 32.066, ^{11}B = 11.009, ^{10}B = 10.013. The material conforms to the specification if content of the vial is within 95–105 % of the amount given on the label.

Degree of Enrichment

In order to verify the actual degree of ^{10}B enrichment, an aliquot of the infusion solution is analyzed for ^{10}B by prompt gamma ray spectroscopy (PGRS) [30]. Three individual 1-ml samples of this solution are analyzed for ^{10}B contents with prompt gamma spectroscopy, with a counting time long enough to reach a counting statistics of better than 1 %. The average of the three samples avg(^{10}B) and their relative standard deviation sd(^{10}B) is calculated. The degree of enrichment avg(enrich) is the ratio of avg(^{10}B)/avg(total). The relative standard error is given by sd(enrich) = (sd(^{10}B + sd(total))). The material conforms with the demands if avg(enrich) (1 + 2sd(enrich)) is 0.95 or larger.

8.2.4 Studies in Animals

This part refers exclusively to animal experiments. The following animals were investigated: mice, rats, rabbits, and dogs. Reports on investigations in monkeys

were found, but cannot be referenced, as the company in question, Shionogi, has not permitted the use of their internal report.

Several of the studies were performed in the late 1960s. They were not performed according to good laboratory practice, as these guidelines did not exist at this time. Some of the information required by GLP is not obtainable because of the long time since the performance of the investigations. The newer studies were generally performed according to GLP.

It has to be stressed that some of the experiments were performed using ^{10}B enriched BSH and some others used non-enriched BSH which may influence pharmacodynamics and pharmacokinetics. Furthermore, most of the publication does not specify the quality control procedures used to control the compound tested. This is of major concern for the interpretation of toxicity.

8.2.4.1 Pharmacodynamics

Actions Relevant to the Use of BSH for Treating High-Grade Glioma

BNCT relies solely on the ability of compounds to selectively accumulate in or be selectively retained in tumor cells in comparison to surrounding normal cells. Accumulation or retention of the compound in organs outside the treatment volume reached by thermal neutrons is of no consequence for the selectivity, safety, and efficacy of the therapeutic action. Thus, compounds do not possess any chemical or physiological activity of their own at the dosages used, with exception of the selective accumulation and retention.

BSH has been investigated in brain malignancies, especially with the goal to treat high grade malignant glioma, that is, glioblastoma multiforme. It was suggested that its transport from the blood to the tumor cells occurs through an alteration in the blood–brain barrier (BBB). Following this hypothesis, once in contact with the tumor cells, it is taken up into the cells and was even being found in the cytoplasm and the nucleus of glioma cells [31, 32]. More recent observation [18, 27, 28] cast doubts on this hypothesis but does not show a more convincing explanation. In summary, no final assessment can be made as to the mechanism by which BSH is taken up by glioma cells or how different concentration of BSH is reached in different tissues. The most promising approach to investigate further the behavior of this small molecule probably is perfusion imaging of the interested tissues. The knowledge of these mechanisms is certainly desirable but not absolutely necessary for assessing the therapeutic potential of BSH (or other boron compounds) for BNCT.

Several publications using BSH on glioma models are published in mice [33–35] and rats [36, 37].

Other Actions Investigated

Very few data applying BSH to other tumor models than glioma are available in mice [27, 38].

Interactions

There is no information available on the interaction of cellular BSH uptake with other molecules also taken up by cells.

8.2.4.2 Toxicity

Very few animal experiments were performed to systematically investigate the toxicity of BSH. Compared to other drugs, very high amounts of boron compounds are needed for BNCT in order to reach a relevant tissue concentration of ^{10}B. Such amounts already have been applied to humans without fateful consequences; it therefore might be concluded that the acute toxicity of BSH is very low (as compared to other drugs for medical use). Under such circumstances, the preparation of the infusion solution, its amount, and its infusion rate may have a major impact on toxicity. This aspect too is not very well investigated.

Single Intravenous Injection

Mice

The initial studies of toxicity in mice were carried out with intraperitoneal injection. A value for LD50 was determined to be 73 mg/kg. From subsequent publications, it can be deduced that the original compound contained greater amounts of oxidation products than the ones used in later studies [39]. Further studies reported by the same authors [39] using intravenous administration showed a greatly reduced toxicity. The problem of impurities may be amenable to measurement with newer chromatographic methods for determining purity [40].

For intravenous infusion of BSH, Hatanaka et al. [39] found a strong dependence of LD50 on the speed of infusion. Whereas LD50 for slow infusion (33 mg/kg/min) was >1,000 mg/kg, the values for 200 and 1,200 mg/kg/min were 300 and 215 mg/kg, respectively. Details on the cause of death are not given in the publication. Elsewhere [39] in the same monography, convulsion and instant spasm of the blood vessels with resulting thrombosis or hemorrhagic infarction were found in rabbits.

Rats

LaHann reports on infusion of BSH intravenously into rats [41]. Lethal events are described of single doses of 375 mg BSH/kg. Different batches of BSH were used; they appear to be of no good chemical purity, as judged by the presence of odor and color (Centronic), and occasional odor (Boron Biologicals Inc.). Thus, some or much of the toxicity reported could also be caused by contaminants of the product used. No distinction is made in the report on which batches were used for which experiment.

An effect of the volume rate of administration on the toxicity of BSH was found, as already described for mice (see above). With a dose of 550 mg/kg, the ratio of dead/injected animals was 7/8 at 0.283 ml/min/kg, 3/3 at 0.213, and 1/4 at 0.142 ml/min/kg. No indication is available as to the concentrations of the infusion solutions.

With administration of BSH at a rate of 1.8 mg/min/kg, a dose of 550 mg/kg was not lethal in three animals, whereas the same dose resulted in death of 6/7 animals when administered at a rate of 28.3 mg/min/kg. Administration of BSH at a rate of 28.3 mg/kg/min and at dose of 375 mg/kg resulted in death of 4/13 animals. Conscious rats showed better tolerance to BSH infusion as rats under general anesthesia and noninstrumented rats better than instrumented rats.

With doses of 500 mg/kg (no infusion speed given, but given elsewhere in the report as between 7.1 and 200 mg/mg/kg/min), death usually occurred within 6 h of the infusion. Pulmonary parameters (rate, flow, and tidal volume) were little affected by BSH until just prior to death. Respiratory depression did not appear to be a primary cause of BSH-induced death, since artificial respiration was not an effective antidote. Cardiovascular parameters were rapidly and substantially altered by BSH administration. The following effects on the heart were seen: initial positive inotropic effect; over time, decrease in cardiac contractility; massive increase in total peripheral resistance; initially increased arterial blood pressure and variable effects on heart rate; and EKG changes indicative of cardiac rhythm (disturbances; reduction in cardiac output). Thus, death is concluded to be secondary to cardiovascular collapse.

Administrations of 375–500 mg/kg were often associated with delayed death, the animals often did not succumbing until 1–4 days post-infusion. The delayed time to death associated with these doses of BSH would make cardiovascular failure or respiratory arrest unlikely causes of death. Observations indicated that beginning within a few hours of BSH infusion, animals were edematous, had low urine output, and at autopsy, displayed enlarged kidneys.

Morris reported that 200 mg/kg BSH, infused intravenously over 10 min, killed the rats. No fatalities were observed with 100 mg/kg. The material used was from Callery Chemical Co. No cause of death was given [42].

Changes of glomerular filtration rate (GFR) measured as ^{14}C-inulin clearance and urine flow rate (UFR) after a slow intravenous injection of BSH (25 and 50 mg/kg body weight, respectively) were investigated in rats under pentobarbital anesthesia [43]. The effect of BSH has been compared with that of its disulfide (BSSB), which is spontaneously generated by oxidation of BSH during storage. It was found that BSH decreases GFR in relation to dose and, in the same way, causes a temporary increase of UFR. On the other hand, BSSB (50 mg/kg) induced a large reversible decrease of GFR as well as a decrease of urine excretion. It was supposed that kidney function changes after BSH or BSSB administration might be related to a high retention of BSH or BSSB in the kidneys.

Dogs

Large animal studies have been utilized to define tolerance of normal brain to irradiation and verify treatment planning programs with epithermal neutron beams [44]. Some information can also be deduced from treatment of spontaneous brain tumors in dogs by BNCT [45]. However, these studies do not give a major contribution to the toxicity evaluation of the drug BSH.

Hatanaka reported the application of 34.8 mg/kg boron (= 60.6 mg/kg BSH) into the common carotid artery of a single dog autopsied on the fifth postinjection day [39]. No toxicological effect was observed.

Gavin et al. gave an overview of animal studies and dog treatments performed at Washington State University and JRC Petten [46]. BSH was applied up to a concentration of 131 mg/kg body weight through slow intravenous infusion. The studies focused on defining the proton RBE for the contaminant fast neutrons and from

nitrogen capture of thermal neutrons and boron capture reaction biologic effect. These studies on healthy tissue tolerance were performed with subsequent neutron irradiation. For this reason, the dogs received dexamethasone. No fatality was observed and no late toxicity due to the drug was apparent. Observation period was up to 1 year, depending on the development of neurological symptoms following radiotherapy.

Toxicity with Repeated Administration of BSH

Mice

BSH and BSSB were infused through intraperitoneal pumps. Administration was for 9 days. Doses administered were from 160 to 680 mg/kg. No fatalities were observed. Neither of the two substances influenced leukocyte numbers or hemoglobin concentrations in the blood, but each was hepatotoxic, BSSB more so than the monomer. There was histopathological evidence of liver regeneration at similar rates 5 days after infusion of BSH and BSSB [39].

Rabbits

Male and female New Zealand white rabbits were injected with 40 mg/kg boron (= 71 mg/kg BSH) for 5 consecutive days. The animals were observed for 30 days following the last injection [19]. Rapid injection of a solution with 13.5 mg/ml boron was hazardous, being capable of provoking thrombosis, vasospasm, or exerting some type of phlebotoxic effect. Autopsied animals showed evidence of pulmonary infarction, cerebral arterial thrombosis, multiple hemorrhagic infarction of the brain stem, and scar-like foci in the lungs, kidneys, liver, and intestinal tract. With a slow intravenous injection of a more dilute solution (6–7 mg/ml boron), no apparent alteration in normal function was observed. Following sacrifice at 30 days, a complete histopathological examination of the organs revealed no atrophy or other abnormal pathology.

One rabbit was given an intravenous dose of 60 mg/kg boron (= 71 mg/kg BSH) daily for 5 consecutive days [39: pp. 60, 64, 65]. No change in blood chemistry or blood count was seen.

Janku et al. have reported on toxic effects on rabbits following multiple BSH injections [47]. The animals were male Chinchilla rabbits fed on laboratory diet. BSH was administered into the ear vein for 7 days, each dose (bolus injection) containing 50 or 25 mg/kg BSH. Animals were sacrificed 17 h after the last dose. Samples of brain, lung, heat, liver, spleen, kidneys, and adrenals were excised for histopathological examination. Red and white blood cell counts were performed before and after the dosage of BSH, as were serum levels of glucose, cholesterol, bilirubin, urea, and creatinine, as well as activities of aminotransferases. Lethal effects were observed after the fifth daily dose in two of five animals receiving 25 mg/kg BSH and in one of seven animals receiving 50 mg/kg. The major toxic effect was on kidney function, with a rise of blood urea at 50 mg/kg (164 ± 85 % of control). In histopathological examination of tissue, non-dose-dependent alterations of kidney and brain were found. A sample of BSH from the same supplier (Léciva Pharmaceuticals) was later analyzed in Gabel in Bremen (personal communication)

by HPLC for the stability investigation. Multiple peaks were observed, with a major component (44 % of the integrated UV absorbance) being caused by a single, highly hydrophobic compound of unknown nature. Thus, it is highly probable that the toxic and lethal effects might not be caused by BSH but by some impurities, which obviously were present in the preparation used.

Dogs

Preparing the EORTC trial 11961, four dogs received four doses of BSH (44 mg/kg) intravenously on 4 consecutive days. The dogs received also dexamethasone, in order to reduce edema of the brain after radiation. Blood was sampled repeatedly during the 4 days, in order to determine the boron concentration in the blood. Blood count was performed up to 40 days after the irradiation. Except for the known effects of dexamethasone on white blood count and differential count and the effect of the repeated blood sampling on red blood count and hematocrit, no effect was seen. The dogs were sacrificed after 1 year, with no apparent effect on organs.

Chronic Toxicity Trials

Toxicity trials with the goal to observe long-term toxicity (3 months and more) are not published. A long-term observation period is only available from the canine trial performed in Petten: A total of 39 dogs received up to 100 mg/kg BSH as part of a study for healthy tissue tolerance to BNCT. No drug-related late effects were seen during the observation period, which was a minimum of 4.5 months (when the first animals had to be sacrificed for radiation-induced neurological damage) and 1 year (when all remaining animals were sacrificed).

Fetal Toxicity and Fertility Studies

No studies for fetal toxicity and fertility studies have been carried out.

Mutagenic Potential

To investigate the mutagenic effect in boron neutron capture therapy, Chine hamster ovary cells were incubated with ^{10}B-enriched BSH for 2 and 20 h. After removal of the BSH, the cells were irradiated with thermal neutrons. The biological end point of cell survival was measured by colony formation assay. The mutagenicity was calculated from the mutation frequency at the hypoxanthine-guanine phosphoribosyltransferase (HPRT) locus. The mutagenicity of BSH was similar to that of ^{10}B boric acid when the cells were irradiated with neutrons at an isosurvival dose after 2 h preincubation. Preincubation with BSH for 20 h, compared with preincubation for just 2 h, had no effect on either cytotoxicity or mutagenicity [48].

Carcinogenic Potential

No studies for carcinogenic potential have been carried out.

Conclusions

As already mentioned for many of the studies quoted below, the quality of the compound used was not well established. Reports of odor and color of the compounds,

found occasionally in the literature, indicate the presence of high concentrations of unwanted material. Thus, especially the presence of toxic signs might not be attributable solely to BSH but also to other compounds present. Even within one study, it is not clear that the material used was of constant quality. The LD50 value of the oxidation products of BSH are much higher than for BSH, being quoted as 62 mg/kg for the disulfide BSSB and 53 mg/kg for the sulfoxide product [39: p. 15], as compared to over 800 mg/kg for BSH. Thus, even the presence of only a few percent of BSSB could influence greatly the observed toxicity of the preparation.

Single intravenous injection and especially single intravenous infusion of BSH is tolerated well in animals. Also, multiple infusions are tolerated without major side effects. The toxicity levels for pure BSH preparations appear to be high. Toxic effects were described on the cardiovascular system, on the renal system, and on liver. Once the initial phase of toxic reaction of a few days has passed, the values normalize.

8.2.4.3 Pharmacokinetics and Tissue Distribution in Animals

Animal experiments (mice, rats, rabbits, and dogs) that gives some information on pharmacokinetic and tissue uptake are summarized below. Most of the trials were not designed for pharmacokinetic studies in the proper sense of the term. In most trials, boron and not BSH was measured. Sometimes, it is not mentioned if ^{10}B-enriched or non-enriched BSH has been applied.

Half-Lives in Plasma

The half-life of boron in blood after application of BSH was investigated following intravenous infusion and intraperitoneal injection. A two-compartment model could be used for evaluation provided that data were available for sufficient time periods after infusion. The half-lives are summarized in Table 8.3.

Pharmacokinetic Scaling

The total clearance and steady state volume of distribution in humans and in laboratory animals were analyzed as a function of species body weight using an allometric equation for the interspecies scaling. Linear relationships were obtained

Table 8.3 Half-life of boron after application of BSH in different species

Animal	Route	Amount (mg/kg)	Infusion time (min)	$T½\alpha$ (h)	$T½\beta$ (h)	Author
Rat	i.p	87	Bolus	1.3	29.1	[49]
Rat	i.v	87–261	Bolus	12.1	n.a.1	[49]
Rat	i.v	50	Bolus	0.62	6.17	[32]
Rat	i.v	100	10	2.78	18.1	[50]
Mouse	i.p	61	Bolus	2.58	145	[33]
Dog	i.v	96	55	14.5	n.a.[a]	[51]
Rat	i.v.	30	Bolus	0.2	1.7	[52]
Rat	i.v.	100	Bolus	1.2	17	[52]
Rat	i.v.	300	Bolus	0.2	19	[52]
Rat	i.v	100	Cont. Inf	0.9	13.5	[52]

[a]Data suffice only for an one-compartment analysis

between the logarithms of Cl (L/h) and weight (kg) as well as de logarithms of Vdss (L) and weight (kg). BSH clearance in various species was shown to be a constant fraction (0.26) of creatinine clearance, the relationship being independent of body weight. The results indicate that the BSH data obtained in laboratory animals could be used to generate preliminary estimates of the pharmacokinetic parameters in humans [53].

Plasma Protein Binding

The interaction between BSH and serum albumin is of interest because it is related to the pharmacokinetics of BSH. Early research suggested that covalent disulfide bridges might be involved in the interaction [54]. Subsequent studies, using ^{11}B-nuclear magnetic resonance spectroscopy have not supported this hypothesis [18, 55–57].

Another investigation reported that there is no covalent binding and no formation of disulfide bridges between BSH and the three types of albumin investigated (human, bovine, and canine) [58]. Furthermore, a fast exchange of bound and unbound BSH was demonstrated. The number of binding sites for BSH on albumin is about 3–5. At a serum albumin concentration of 5 % and a temperature of 37 °C, between 68 and 98 % of the total BSH (200 μg/ml) were bound to the protein.

Distribution and Excretion

Yamaguchi et al. studied the distribution and excretion of boron after intravenous administration of BSH to rats [52]. AUC (32, 219, and 4030 μg·h/ml) increased with the dose, but there was no proportionality among the values. Total clearance decreased drastically from 233 ml/h/kg (100 mg/kg) to 38 ml/h/kg (300 mg/kg). As boron was excreted mainly into the urine, these results suggest that renal function failure might occur with dosing of 300 mg/kg. In case of continuous infusion of 100 mg/kg of BSH for 30 min, the pharmacokinetic parameters were similar to those of rapid injection of 100 mg/kg. The highest boron concentrations were observed in the kidney and the lowest in the brain. After multiple dosing of BSH at 100 mg/kg/day × 14 days, the boron concentrations in blood, liver, lung and kidney at 24 h after the last dosing were higher than those after single dosing and were similar to those of simulated values calculated from single dosing parameters. The results clearly indicate that boron does not accumulate unexpectedly in any tissue with multiple dosing of 100 mg/kg of BSH for 2 weeks.

Metabolism

No information is available on the metabolism of BSH and the form in which it is excreted.

Tissue Distribution

Normal Brain

Only very small boron concentration was detected in normal brain tissues [27, 32, 33, 51]. The amount of boron found in normal brain corresponds slightly to the content of blood in average brain tissues and is close to 4 %.

Wittig et al. published in 2009 an extensive study in male athymic nude mice (HsdCpb:NMRI-nu/nu) [27]. Animals received twice the dose of BSH per kg body weight that was given to patients in the EORTC 11961; the compound was injected intraperitoneally in a 1-ml volume: 200 mg/kg (113.2 mg ^{10}B/kg). The compound was purchased from Katchem Ltd. Rez, Czech Republic. The ^{10}B enrichment was 99 %. The quality control and the preparation of the injection solutions were performed according to standard operating procedures established for the EORTC clinical trials. 2.5 h after BSH injection, a blood concentration of ^{10}B was measured with 16 ± 8 μg/g. The ^{10}B concentration was high in kidneys (26 ± 20 μg/g) and liver (20 ± 12 μg/g); medium in lung (11 ± 5 μg/g), skin (8.4 ±6.6 μg/g), spleen (8.5 ± 7.3 μg/g), bone (5.3 ±2.7 μg/g), testes (5.3 ± 2,7 μg/g), and heart (4.7 ± 2.3 μg/g); but was low in fat (2.1 ± 2.4), muscle (1.9 ± 1.2 μg/g), and brain (1.0 ± 0.8 μg/g).

In large animals (dogs), Kraft et al. have intensively investigated tissue concentrations of boron after BSH application [51]. At time intervals of 2, 6, and 12 h after BSH infusion, the concentration of boron in bone (scalp) and oral mucosa was lower than that in blood (around 70 % of the blood concentration). Concentrations in pituitary gland and tongue were around 50 % of the blood concentration. Concentration in muscle was about 250 % of that in blood. Over the observed time period, the concentration ratios tissue/blood was approximately constant. Uptake in 30 spontaneous tumors occurring in dog heads has been studied. The histology of the tumors was astrocytoma (protoplastic, fibrillary, and diffuse astrocytoma included) (6 cases), meningioma (7 cases), pituitary adenocarcinoma (7 cases), choroid plexus papilloma (5 cases), nasal adenocarcinoma (3 cases), and other histologies (2 cases). Uptake was determined to 35.6 ± 4.6 μg/g tissue at 2 h (n = 15), 22.5 ± 6.0 μg/g at 6 h (n = –9), and 7.0 ± 1.1 μg/g at 12 h (n = 6). At all time points, the boron concentration in tumor was around 50 % of that of blood.

8.2.5 Clinical Studies

Few data are published for BSH with respect to results on pharmacodynamics, pharmacokinetics, toxicity, and side effects as well as tissue uptake in humans. The data of one of the few controlled prospective phase I trials (EORTC 11961) are still not yet fully available in the accessible literature. After the pioneering work initiated by Hatanaka and Nakagawa [39], BSH [19] was used in modern clinical trials for treatments of glioblastoma [11, 59] and in combination with L-*para*-boronophenylalanine ($C_9H_{12}{}^{10}BNO_4$, BPA) for the treatment of glioblastoma [60] and of squamous cell carcinoma of head and neck [61].

8.2.5.1 Pharmacodynamics

Pharmacological Actions

The substance itself is not toxic and does not inhibit cell growth or proliferation in the concentrations of clinical relevance. The use of BSH for BNCT is solely dependent on the differential accumulation of ^{10}B in tumor cells as compared to surrounding normal tissues. The molecule has to be perceived as a carrier

transporting ^{10}B to target cells without any known secondary pharmaceutical capacity. There is a controversial discussion how and why BSH leads to a differential boron concentration in different tissues. The most plausible explanation might be the diffusion of the small molecule following the perfusion of the different organs including the effect of some physiological barriers such as the blood–brain barrier. Some authors discuss the oxidation/reduction of BSH in tissues or suggest some specific binding.

Intracellular Distribution of Boron after BSH Application

Because of the short range of the highly energetic particles ^{4}He and ^{7}Li resulting from the $^{10}B(n,\alpha)^{7}Li$ reaction, the efficacy of BNCT not only depends from the boron concentration measured in macroscopic volumes but is strongly dependent on localization of ^{10}B inside a cell [62].

An early study published by Amano in 1985 [63] suggests some intracellular and also intranuclear localization of boron in tumor tissue. The author points out the tentative nature of the results. Otersen et al. investigated the binding of boron present in surgically removed tumor tissue from patients infused with BSH [64]. Freeze-dried sections retained boron independent of the fixation method (formalin vapor, formalin solution, and glutaraldehyde solution). In addition, boron could not be removed with reducing agents or acids. Kageji et al., using differential centrifugation after tissue homogenization, found the highest amount of boron in the fraction containing cytoplasm (and extracellular fluid) [65]. In a similar study by Ceberg et al., tumor material from patients infused with BSH and operated around 18 h following infusion showed that about 60 % of the total boron of the tissue was present in cytoplasm and extracellular fluid. Twenty-one percent was present in the nuclear fraction and 18 % in the mitochondrial fraction [66]. With LAMMA as analytical technique, Haselsberger et al. [67] detected boron only in patients whose tumor accumulated larger amounts of boron. When found, boron could be detected only in the nuclei of tumor cells. The detection of boron with this method is rather insensitive.

Such analyses are extremely depending on the correct sample preparation, which never is easy [68, 69]. For example, with electron energy-loss spectroscopy (EELS) it could be shown that early boron locating studies had reported artifacts [70, 71]. In addition, the use of such highly elaborated techniques is time demanding and expensive and needs well-trained personal. To obtain a reliable result in biological systems, a lot of samples have to be analyzed in order to reach a statistically significant result. Up to now, such an expensive effort could not be realized.

Boron Concentration in Tissues after Application of BSH

During the 1990s, in Europe, a research project funded by the European Commission called “European Collaboration on Boron Neutron Capture Therapy” made major efforts to further evaluate BSH [22], resulting a first BSH pharmacy brochure that was the starting point of the later EORTC investigators brochure [29]. The total number of patients included in this pharmacokinetic and tumor uptake studies as well as the amount of BSH applied are shown in Table 8.4.

Table 8.4 Clincial trials on BSH of the European Collaboration on Boron Neutron Capture Therapy. The following hospitals participated: (1) Zentralkrankenhaus Bremen, Germany; (2) Neurochirurgische Klinik Graz, Austria; (3) Neurosurgical Clinic Lausanne, Switzerland; (4) Neurosurgical Clinic Lund, Sweden. Abbreviations: male (m), female (f), years (y)

Hospital	Patients included	Patients receiving multiple BSH applications	sex (range of age)	histology	BSH mg/kg (range)	publications
1	41	7	23 m; 18 f (31-72 y)	Astrocytoma WHO grade III-IV	11.2-58.1	[71-71]
2	19	7	13 m; 6 f (52-67 y)	Astrocytoma WHO grade IV	75.0	[74,75]
3	39	2	19 m; 20 f (30-82 y)	different tumor entities	8.6-86.0	[76-80]
4	8	0	2 m; 6 f (31-61 y)	astrocytoma WHO grade II- IV	42.9-69	[64]

The mean tumor-to-blood ratios (± SD) found by the different investigators for samples taken at different time points investigating different brain malignancies were the following: Bremen 2.0 (± 1.1), Graz 1.3 (± 0.3), Lausanne 1.9 (± 4.4), and Lund 1.6 (±1.8). Using ICP-OES, it was found that boron from BSH would be taken up into tumor tissue with a time constant of some hours, peaking at around 12 h after the infusion of BSH. There was a drop of boron concentration in the tumor with time thereafter, roughly parallel with the boron concentration in blood. Thus, after around 12 h, concentration ratios between the average concentration in tumor and in blood were around 1–2 (with considerable interpatient variations) [29].

Horn reports the tissue distribution after infusion of 25 mg/kg borocaptate sodium in 10 patients with malignant brain tumors investigated by atomic emission spectrometry. Differences in boron content were found not only in relation to the type of tissue but also with respect to the time interval which elapsed from termination of the BSH infusion. Average uptake in tumor was 12.1, 12.4, 16.5, and 10.4 μg/g after 3, 6, 12, and 18 h, respectively. Tumor-to-blood ratios higher than 1.5 can only be obtained after at least 12 h [82].

The uptake of BSH in tumor and normal tissues was investigated in the frame of the EORTC phase I trial “Postoperative treatment of glioblastoma with BNCT at the Petten Irradiation Facility (EORTC trial 11961)”. The boron concentration in blood, tumor, normal brain, dura, muscle, skin, and bone was detected using inductively coupled plasma-atomic emission spectroscopy in 13 evaluable patients. In a first group of 10 patients, 100 mg BSH/kg body weight (BW) were administered; a second group of 3 patients received 22.9 mg BSH/kg BW. The toxicity due to BSH was evaluated. The average boron concentration in the tumor was 19.9 ± 9.1 ppm (1 standard deviation (SD)) in the high-dose group and 9.8 ± 3.3 ppm in the low-dose group; the tumor/blood ratios were 0.6 ± 0.2 and 0.9 ± 0.2, respectively. The highest boron uptake has been detected in the dura; very low uptake was found in the bone,

the cerebrospinal fluid, and especially in the brain (brain/blood ratio 0.2 ± 0.02 and 0.4 ± 0.2). The study underlines the importance of a further investigation of BSH uptake in order to obtain enough data for significant statistical analysis. The boron concentration in blood seems to be a quite reliable parameter to predict the boron concentration in other tissues [25, 83].

8.2.5.2 Pharmacokinetics of BSH

Although BSH has been used clinically for many years, its pharmacokinetics and metabolism are still not fully understood. Pharmacokinetic studies that used various study designs but all included a limited number of patients investigated single-dose applications of BSH [24, 29, 81, 82, 84, 85]. A first report on pharmacokinetic investigations for multiple doses of BSH was incomplete [86].

Of note, all pharmacokinetic parameters that were reported characterize the boron or ^{10}B disposition after BSH infusion but not the disposition of the molecule BSH. The reason is that assays to quantify BSH on a routine basis still do not exist [87, 88]. Instead, the assays used (PGRA, ICP-AES, direct current plasma-atomic emission spectroscopy (DCP-AES)) cannot distinguish between whether ^{10}B is bound within the parent drug (BSH), to any boronated metabolites, and/or to oxidation products. As BNCT efficacy relies on the preferential accumulation of ^{10}B in the target cells and not on the chemical form of ^{10}B, assays used for pharmacokinetic profiling of ^{10}B are sufficient to optimize delivery.

Most authors report that ^{10}B disposition after i.v. infusion of BSH follows a classical three-compartment open model with zero-order input and first-order elimination. Horn et al. [82] administered a 1-h infusion of 25 mg BSH/kg to 10 patients with malignant glioma. They reported a mean boron-blood clearance of 19.8 ml/min and a terminal half-life of 44.0–92.8 h. Goodman et al. [24] and Gibson et al. [84] describe the results from a group of 19 patients with malignant glioma, who were infused with BSH at doses of 26.5–88.2 mg BSH/kg b.w. over a 1-h period at the Ohio State University and the Beijing Neurosurgical Institute. They found a boron-blood clearance of 18.3 ± 4.5 ml/min and a terminal half-life of 79.6 ± 32.8 h. Kageji et al. [85] reported the results of a retrospective pharmacokinetic and biodistribution analysis in 123 patients who received a one-hour i.v. infusion of 12–100 mg BSH/kg. In most patients, blood samples were taken over a 36-h time interval only; in some patients, they were taken for up to 6 days. The patient concentration-time data were fitted to a two-compartment model. With this, the mean blood boron clearance was 60 ml/min, which was far greater than the blood clearance values determined by the former authors. The harmonic mean terminal half-life was 77.2 ± 54.1 h. Finally, Stragliotto et al. [81] studied a group of 61 patients with intracranial tumors, who received one infusion of 10–100 mg BSH/kg b.w. In only 7 patients, who received 10–20 mg BSH/kg b.w., blood samples were taken over a period of 7 days. In all other patients, samples were taken over a period of 24–48 h only. Resulting data were best described by a 3-exponential model. The clearance of ^{10}B from blood was 0.21 ± 0.1 ml/min/kg; the mean residence time was 29.9 ± 18.6 h.

Unpublished results of the EORTC trials are in reasonable agreement with these earlier reports. Thirty patients were included in trial EORTC 11961 (21 males, 9 females, mean age: 60.8 years), of whom 26 patients were included in the BNCT-treatment study (17 males, 9 females, mean age: 60.0 years) receiving repeated BSH infusions. Fourteen patients (12 males and 2 females, mean age: 61.2 years) participated in the biodistribution substudy. Between June 2003 and December 2007, 10 other patients were enrolled in EORTC trial 11001, who received BSH. The mean age was 54.1 years with 5 males and 5 females. The mean ^{10}B-clearance from the blood was 11 ± 8 ml/min. The half-life for boron disposition was 94 ± 70 h (22–288 h) after a single dose of BSH. Multiple doses of BSH can also best be described with a three-compartment model. It could be shown that systemic clearance as well as the volume of distribution of ^{10}B both increase with increasing BSH dose. Higher doses of BSH do not increase the blood boron concentration and possibly do not lead to increased tumor boron concentrations. BSH doses below 100 mg BSH/kg b.w. seem sufficient to reach the therapeutic effect and should be considered to avoid drug-related side effects.

In all studies, the intra- and interpatient variability in blood boron concentrations was remarkably high. This observation is common to all BSH biodistribution reports. This variability underlines the necessity for individual measurements of the blood ^{10}B concentration at least during irradiation in each patient. Missing individual measurements would create a large uncertainty in the calculations based on boron concentration, especially calculations of the irradiation dose.

8.2.5.3 Toxicology of BSH

BSH administration was always followed by surgery and/or irradiation for BNCT with concomitant medication. Therefore, possible toxic effects of BSH cannot be easily differentiated from those of general anesthesia, surgery, and other medication.

The most reliable toxicity data have been collected in the EORTC study protocol 11961 (clinicaltrials.gov registration number NCT00004015), a phase I dose finding trial aiming to determine the safety and toxicity of a BSH-mediated BNCT in patients with glioblastoma multiforme. The patients received BNCT in 4 fractions on 4 consecutive days. BSH was given prior each fraction. The trial investigated dose limiting toxicity and maximum tolerated radiation dose of BNCT as a postoperative treatment. A secondary end point was the systemic toxicity of BSH and the antitumor effect. Cohorts of patients suffering from glioblastoma were irradiated with four fractions of BNCT after complete resection of the tumor. Thirty patients have been entered into the study, 21 males and 9 females. Mean age of the patients on study registration was 60 years (50–74). The performance status at inclusion was very good with a median Karnofski index of 90 (70–100). In the first cohort, three patients with a remaining tumor volume larger than 30 % of the initial tumor size had to be excluded from the procedure of BNCT. One patient could not undergo

BNCT because of an intercurrent infection and prolonged recovery after the surgery. All of the 16 patients entered for treatment in the cohorts 2–4 where treated with BNCT. Four cohorts of patients (26 patients) were treated with BNCT in the trial. BNCT was performed in 4 fractions on 4 consecutive days, except one case, in which the third and fourth fractions of irradiation were delivered subsequently on the same day. On the day prior to the first irradiation, 100 mg/kg BSH was administered i.v. at a dose rate of 1 mg/kg/min. On the following days, both the amount (range 9.5–107.1 mg/kg) and the time point of BSH administration (range 8–14 h prior to the radiation) were modified to achieve an average boron concentration of 30 ppm ^{10}B in blood over the four fractions. The amount, start of the infusion, and duration were adapted each day after obtaining the actual pharmacokinetic data (from the regularly taken blood samples) by prompt gamma ray spectroscopy. In the 26 patients treated, the mean blood boron concentration over the four fractions of BNCT was 30.2 ppm (range 27.3–32.3 ppm). No drug-related toxicity was detected in the EORTC trial 11001.

Only one event of serious toxicity was reported and described as possibly related to the drug BSH: the first irradiated patient developed a WHO grade 4 granulocytopenia during the week of BNCT. The granulocytopenia was treated by GSF and resolved within 36 h. Some grade 1–2 toxicity regarding hematological changes, erythema and urticaria, erythema, flash-like sensation during infusion, nausea and vomiting, hypokalemia, and hyponatremia were detected and interpreted as possibly related to BSH. Grade 1, 2, and 3 fever possibly related to the study medication occurred in three patients. In summary, no dose-limiting toxicity has been observed [89].

No BSH related toxicity was detected in the EORTC trial 11001.

The intensive biodistribution studies performed by Fankhauser and Stragliotto [77–81] were not designed to detect toxicity. A retrospective analysis of the patient files to investigate unexpected hematological and metabolic toxicity (including liver and renal function) following BSH infusion was undertaken. A follow-up for 40 of 61 patients is available. No specific drug-related toxicity was observed.

A safety evaluation of patients following single and multiple BSH infusions without and with concomitant hyaluronidase application performed by Haselsberger in Graz [75, 90] can be summarized as follows: Seven patients having received multiple doses of BSH (each dose 75 mg/kg body weight), spaced 24 h apart, were evaluated together with three patients of the group having received a single dose of BSH (75 mg/kg). Follow-up was usually available only for the immediate postoperative period. Common side effects in 7 of 10 patients (without concomitant hyaluronidase treatment) of the Austrian investigation were facial flushing during the BSH infusion that did not require treatment and resolved spontaneously upon completion of treatment (WHO-grade l). One of the patients (with concomitant hyaluronidase treatment) experienced a slight allergic skin reaction following BSH infusion (WHO-grade 3 because of therapy with Ca^{++}).

From patients treated by Haritz in Bremen [72–74], following toxicity data are available: For the 22 patients who received BSH in a dose up to 41 mg/kg and 2 patients who received BSH 2 times subsequently, the blood and laboratory values were evaluated statistically by using the Wilcoxon test with a 95 % level of significance and revealed no differences between the BSH group and the control group of 10 patients [91]. During the BSH infusion and over the observation period, cardiovascular function remained unchanged (with exception of patients, who had disturbances of cardiovascular function in their medical history). Furthermore, no allergic skin reactions were observed; moreover, the patients did not complain of any subjective disorders like nausea and vomiting. A transient skin reddening (flush) was observed twice when BSH was infused with high concentration and over shorter time periods. There was no indication that BSH (in the administered doses) had myelosuppressive effects on the bone marrow. Because of the large number of concomitant treatments, it was difficult to distinguish any definite toxic influence of BSH on liver function. There is no correlation of BSH dose dependency and disturbance of liver function. Abnormal values were either preexisting or could be attributed to other reasons (i.e., concomitant application of phenytoin). In these series, there was no registration of a potential toxic BSH effect on renal function.

In summary: Flush-like symptoms and nausea during BSH infusions might be related to infusion of the drug at a higher rate than 1 mg/kg/min. It is important not to apply the drug at higher speed.

BSH proved to be safe for clinical application at a dose of 100 mg BSH/kg infused and at a dose rate of 1 mg/kg/min.

8.3 Boronophenylalanine (BPA)

8.3.1 Introduction

Boronophenylalanine (BPA) is a derivative of the neutral amino acid phenylalanine, its synthesis was published in 1958 [92]. The molecular structure of BPA resembles tyrosine. It was thought to act as a substrate for tyrosinase in melanoma cells, leading eventually to macromolecular incorporation via the melanin metabolic pathway. However, the mechanism seems to be more complex; BPA accumulates in both melanotic and amelanotic tumors [93] as well as in a number of other malignant cell types [93–97]. Cellular uptake is selective for the L-stereoisomer, indicating a physiological transport mechanism rather than passive diffusion which was found to be the neutral amino acid transport mechanism, namely, the L-amino acid transport system [98]. An increased rate of cell division and catabolism alone do not account for the increased accumulation in tumor cells, leading to speculation that the neutral amino acid pathway is less selective in tumors, that is, melanoma than in normal tissue [99]. For reasons of solubility, BPA is often complexed with fructose to produce an infusion solution.

8.3.2 Physical, Chemical, and Pharmaceutical Data

8.3.2.1 Physicochemical Properties

Names

Chemical names

L-Phenylalanine, 4-(borono-^{10}B)

Synonyms

- (^{10}B)-4-Borono-L-phenylalanine
- 4-(Borono-^{10}B)-L-phenylalanine
- L-(p-[^{10}B]Boronophenyl)alanine
- L-para-Boronophenylalanine
- L-4-[^{10}B]Boronophenylalanine
- p-[^{10}B]Borono-L-phenylalanine
- BPA [^{10}B]

CAS registration number: 80994-59-8

Structural Formula

Molecular formula: $C_9H_{12}{}^{10}BNO_4$

Molecular weight: Precise molecular weight is dependent upon the boron isotopic composition of the material (Fig. 8.2).

A series of typical molecular weights is listed below for varying isotopic compositions.

Carbon	12,011
Hydrogen	1,0079
Boron	
Isotope 10	10,0129
Isotope 11	11,0093
Nitrogen	14,0067
Oxygen	15,9994

Therefore, BPA has the following molecular weight according to the varying boron 10 and 11 contents as shown in Table 8.5.

Physical and Chemical Characteristics

Solid state form: White crystals without smell

Solubility: Insoluble in water, soluble in acids and alkalis.

Optical rotation: $[\acute{a}]_D^{25}$ -10.1 (c = 0.25, 0.1 N HCl)

Melting point: 283–293 °C, decomposes

Density: 0.89 g/cm^3

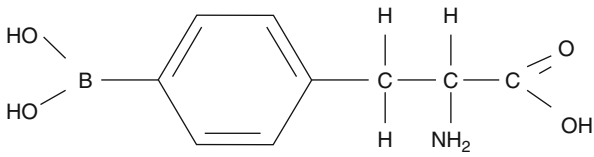

Fig. 8.2 The BPA molecule

Table 8.5 Molecular weight of BPA according to varying ^{10}B content

	Boron 10 content (%)	Boron 11 content (%)	Atomic wt.	BPA MW
Natural boron	20	80	10.81002	209.0008
	90	10	10.11254	208.3106
	95	5	10.06272	208.2608

8.3.2.2 Production, Purification, and Methods of Preparation

The manufacturing of BPA including production, purification, and control tests will depend on the procedures used by the chemical and/or pharmaceutical company producing the product. Its synthesis is less demanding as compared to BSH; therefore, several producers are offering the chemical compound in a ^{10}B-enriched and non-enriched version. The whole procedure has to follow the principles of good manufacturing practice including a strong quality control of the starting material. Up to now, the pharmaceutical industry does not provide the drug ready for infusion. Producing a complex with fructose is mostly used for the preparation of a solution for injection to the patient (BPA-F). This step is part of the pharmaceutical production line; it has to be done by and under the control of approved pharmacists and needs special licensing if performed at the treating hospital.

Preparation of the BPA-Fructose Solution

Here, the definition is given on the detailed procedure of preparation of the BPA-fructose (boronophenylalanine-fructose) infusion solution used for study protocol EORTC 11001 "^{10}B-uptake in different tumors using the boron compounds BSH and BPA" [100].

- Clean, wrap, and autoclave all glassware and utensils and store in sterile environment until use.
- The following instructions for dosing refer exclusively to protocol EORTC 11001. BPA is administered at a concentration of 100 mg/kg body weight. Vials contain exactly 1,000 mg of BPA each.
  First day of preparation
- Calculate the correct amount of BPA and fructose (1:1.1 molar ratio) for the patient (e.g., patient weight 65 kg, 6,500 mg BPA, and 6,180 mg fructose).
- Clean bench area and equipment with sterile 70 % alcohol for disinfection and then place all other equipment in the hood.
- Disinfect hands with ethanol 70 % for hand disinfection; then wear gloves. Spray the gloves with sterile 70 % ethanol before working in the hood.
- Calibrate the pH meter with pH 7 and pH 10 buffer. Rinse the electrode with sterile water several times.
- Prepare 10 g fresh 10 N solution of NaOH from sodium hydroxide and water for injection (10 N = 40 %; 4 g sodium hydroxide in 10 ml NaOH solution).

- Weigh out the correct amount of BPA in a 500-ml sterile beaker with a stir magnet, and add 50 % or less of the total volume using sterile water for injection.
- Stir for 5 min with a magnetic stirrer.
- The BPA–water mixture should look very cloudy. Measure the initial pH, which should be 4.5–6. Rinse electrode directly into solution using sterile water.
- Add 10 N NaOH until the pH reaches 9. At a pH of 9, add 10 N NaOH drop by drop so that you can stop when the solution becomes clear, with a pH of 10.5. The BPA solutes at this pH and further on the BPA-F complex will be formed at this pH so that the pH should not rise higher than 12.
- Stir the solution for 20 min and check that the solution is clear.
- Weigh out the correct amount of fructose in a 100-ml beaker and add it to the clear BPA solution.
- Stir for 10 min with a magnetic stirrer.
- Record the pH.
- Slowly add concentrated HCl to bring the pH down to 8 but be careful to avoid precipitate formation.
- Add 1 N HCl to reduce the pH to above or equal to 7.4.
- Stir for 10 min with a magnetic stirrer.
- Filter the clear BPA-F solution into a sterile receiver with a stir magnet using a combined 5-μm/0.45-μm filter unit (first 5-μm filter, then 0.45-μm filter).
- Add sterile water to adjust the volume of the solution to the desired volume.
- Stir for a few minutes and recheck the pH.
- Cap the sterile receiver with a sterile cap and refrigerate overnight.
  Second day of preparation
- Keep the BPA-F solution out of the refrigerator and wait for it to return to room temperature.
- Recheck the pH of 7.4.
- Filter the BPA-F solution into a sterile infusion bag or several sterile 50-ml syringes using a 0.22-μm filter unit.
- Ensure that no air gets into the bag or syringe.
- Protect the bag from light.
- Can be stored in refrigerator (2–8 °C) and protected from light for no more than 12 days.

8.3.2.3 Stability

Stability of the Substance

Yearly retesting of the BPA material revealed that the BPA in substance is stable at room temperature for years.

Stability of the ^{10}B-L-Boronophenylalanine-Fructose Injection

The stability of ^{10}B-L-BPA-F injection solution containing 30 mg ^{10}BPA/mL was investigated. The 30 mg/ml BPA (as BPA-fructose) infusion was aseptically prepared at the Department of Pharmacology of the Vrije Universiteit Amsterdam [101]. Two batches of 40 ^{10}B-L-BPA-F infusions were prepared (for details cf.

chapter "preparation of the ^{10}B-L-boronophenylalanine-fructose injection solution"), stored at room temperature (15–20 °C), and protected from light. Three bottles from each batch were analyzed in duplicate at the time of preparation and on days 2, 3, 6, 10, 13, 15, and 21 (batch A) or on days 1, 2, 5, 9, 12, 14, and 20 (batch B). Furthermore, three samples of each batch were stored at 2–8 °C to determine whether decomposition was affected by temperature.

A decrease of the BPA-F concentration in time was observed, indicating a limited shelf life of the product. With 95 % reliability (with a lower limit of 90 % of the nominal ^{10}B-BPA concentration), a maximum shelf life of 11.9 and 12 days was found for batches A and B, respectively. No degradation products exceeded 1 % of the parent compound in any of the chromatograms. These results match the shelf life of 12 days established by the Food and Drug Administration [102].

In conclusion, a ^{10}B-L-BPA-F solution containing 30 mg ^{10}B-L-BPA/ml was stable for 12 days when stored at room temperature and protected from light. Shelf life did not improve significantly when the solution was stored at 2–8 °C [101].

8.3.3 Quality Control

For the EORTC trials 11001 and 11011, the quality control of the material was tested according to the following procedure. This procedure was written down in a SOP.

8.3.3.1 Description of the Active Ingredient

BPA, ^{10}B-enriched is used as white or creamy white lyophilized powder in glass vials sealed with a septum.

The containers are labeled with the content, the batch number, and the weight of the contained material.

The powder is hygroscopic and attracts water on standing on air.

8.3.3.2 Identification of BPA

Appearance

White crystals without smell packed to 1-, 10-, or 20-ml vials sealed with rubber septum and aluminum cap

Melting point

283–293 °C, decomposes

Infrared spectrum

Examine by Fourier transform infrared (FTIR) absorption spectroscopy (see *European Pharmacopoeia*, 3rd edition 1997, section 2.2.24). The principal peaks appear at 3582, 1333, 1595, 1504, 652, 955, 746, 713, 826 cm^{-1}

8.3.3.3 Purity of BPA

HPLC Analysis

Column: Nucleosil 120RP18, 5 micron, LiChroCART. Stabilized more than 12 h before analysis. Detection: uv 254 nm. Flow: 1.0 ml/min.

Mobile phase: Phosphate 12.5 mM + acetonitrile (5 + 95)

50 mg BPA is solved in 10.0 ml 0.1 M sodium hydroxide. 10.0 µl is diluted with mobile phase to 1.00 ml. 30 µl is injected on the column. The solution should be freshly prepared and analyzed within 15 min. Purity is accepted if the surface of the principal peak (Rt 5.5 min) is more than 98 % of the integrated surface.

Pyrogens

Examination by the Limulus amebocyte lysate test.

Test solution c: with a pyrogen-free spatula, 20.0 mg is weighed and dissolved in 2.0 ml pyrogen-free 0.9 % sodium chloride solution and dissolved. 50 µl of this solution is diluted with 1.45 ml pyrogen-free water.

Carry the Limulus amebocyte lysate test out according to SOP "endotoxin assay." The material conforms with the demands if it contains less than 0.050 i.e., pyrogens/mg BPA.

8.3.3.4 Control of the ^{10}B Enrichment

A test solution of BPA is diluted to a ^{10}B-concentration in the range of 50–75 ppm. The volume of this solution should be at least 10 ml. With this solution, the following tests are performed.

Determination of ^{10}B Content

The PGRA officer prepares three individual vials of 1 ml each with the test solution. Prompt gamma ray analysis is performed and the concentrations of ^{10}B are detected.

Determination of the Total Boron Content (^{10}B + ^{11}B)

After completion of the prompt gamma ray analysis, the three samples mentioned above are transferred to ICP preparation and analyzed for total boron content (^{10}B + ^{11}B) and total boron concentration.

Control of Degree of Enrichment

The degree of enrichment (with standard deviation) is calculated as the ratio between the ^{10}B concentration (from prompt gamma ray analysis) and the total boron concentration (from ICP). The degree of enrichment is accepted if it equals 0.995 within two standard deviations.

8.3.4 Pre-clinical Studies

8.3.4.1 In Vitro Trials

Pharmacodynamics

BNCT relies solely on the ability of compounds to selectively accumulate in or be selectively retained in tumor cells in comparison to surrounding normal cells. Accumulation or retention of the compound in organs outside the treatment volume reached by thermal neutrons is of no consequence for the selectivity, safety, and efficacy of the therapeutic action. Thus, compounds are not required to carry any

chemical or physiological activity of their own, with exception of the selective accumulation resp. retention.

Uptake of BPA in Cells

The transport of L-BPA·HCl and its metabolic fate have been studied in human uveal melanoma cell line isolated from a primary enucleated tumor. The results of this trial suggest that BPA is actively transported into melanoma cells, but not metabolized [103].

The mechanism of transport of BPA through the cell membrane was investigated in vitro using rat gliosarcoma cells. The results of this study support the hypothesis that ^{10}B-BPA is actively transported by the L system, which can be further stimulated by amino acids preaccumulated in the cell by either L or A amino acid transport systems [98].

Papaspyrou et al. studied the effects of preloading mouse melanoma cells with L-tyrosine. They found that this preloading increased the intracellular boron concentration by a factor of 3. They concluded that ^{10}B-D,L-p-BPA is transported by L and presumably ASC (alanine, serine, cysteine) systems and that boron uptake can be stimulated by L-tyrosine preloading [104].

Mutagenic Potential of BPA in Cells

Kinashi et al. investigated the mutagenic effects of BPA and BSH in Chinese hamster ovary cells. They incubated the cells with ^{10}B-enriched BPA or BSH and exposed them to thermal neutrons. Mutagenicity was measured by the occurrence of mutations at the hypoxanthine-guanine phosphoribosyltransferase locus. They concluded that, after 20 h of incubation, BPA was less mutagenic than BSH. The mutagenic study of BPA or BSH revealed a reduced mutagenicity. The authors state that these results suggest that the retention of BPA and BSH in the cell causes a more accurate assault on the cell and lessens the chance of a misrepair after neutron irradiation [48].

8.3.4.2 In Vivo Trials

This part refers exclusively to animal experiments. The following animals were investigated: mice, rats, and dogs. The studies were generally performed in the spirit of GLP.

Pharmacodynamics and Pharmacokinetics

According to Matalka et al., the finding that the L-isomer of BPA-F was taken up 1.8 × higher in tumor cells than the D,L racemic mixture indicates that ^{10}B-BPA accumulates in tumors through a metabolic pathway rather than through diffusion [105].

Biodistribution

Tumor Accumulation of BPA

Gregoire et al., who were among the first to recognize the tumor specificity of L-BPA-F, investigated mice with murine tumors [106]. In a second trial, they found

a tumor-plasma ratio of L-BPA-F of 3.2 in melanoma-bearing mice. Their pharmacokinetic parameters are subject to large errors according to the authors and are therefore not included here [107].

Pignol et al. have studied the selective delivery of ^{10}B-L-BPA.HCl to soft tissue sarcoma in 24 rats. They used intraperitoneal doses of BPA (300, 600, and 1,200 mg/kg). The neutron capture radiology analysis showed that the tumor-to-muscle ratio was 13 ± 4 and the tumor-to-blood ratio 15 ± 3, 6 h after an intraperitoneal dose of 600 mg/kg. The amount of ^{10}B incorporated into the tumor was 36 ± 4 μg/g [108].

Matalka et al. used a rat brain tumor model to study the pharmacokinetics and tissue distribution of BPA using intracerebrally implanted human melanoma cells. They injected 120 mg of ^{10}B enriched L-BPA-F intraperitoneally into the rats. Six hours after infusion, they obtained ^{10}B rates of 23.7 (tumor), 9.4 (blood), and 8.4 μg/g (normal brain) [105].

Morris et al. evaluated the biodistribution of ^{10}B-BPA-F (4.9% ^{10}B) using a rat spinal cord model. Different doses of the compound (700, 1,000, and 1,600 mg/kg) were used to establish the biodistribution of ^{10}B in blood, spinal cord, and brain after intraperitoneal administration. These doses matched ^{10}B blood concentrations of approximately 12, 42, and 93 μg/g. At the two highest doses, BPA exhibited a biphasic clearance profile, with blood concentrations highest at 1 h after infusion. The ^{10}B blood-to-CNS ratio increased with higher doses, reaching a value of 10 at the 1,000 and 1,600 mg/kg dose (t = 1 h after infusion). After 3 h, this ratio was decreased to 3 [109].

A high boron uptake and a heterogenous subcellular microdistribution of ^{10}B after BPA was demonstrated in a murine sarcoma by Wittig et al. [38].

Distribution of BPA to Normal Tissues

The biodistribution of L-p-BPA was investigated in a mouse model by Wittig et al. [27]. Samples were taken 1.5 h after i.p. injection of ^{10}BPA as a fructose complex at a dose of 700 mg/kg (33.4 mg ^{10}B/kg). The following mean ^{10}B concentration were reached (in μg/g ± SD): blood 11.3 ± 6.1, brain 5.4 ± 2.6,muscle 10.1 ± 5.3,fat 2.4 ± 1.3, heart 11.5 ± 5.1, testes 10.2 ± 4.3, bone 8.3 ± 3.5, skin 12.3 ± 8.5, spleen 16.7 ± 8.1, lung 12.5 ± 9.8, liver 12.1 ± 6.3, and kidney 37.8 ± 24.8.

Factors Influencing Biodistribution

Joel et al. investigated the effect of dose, infusion time, and route of infusion on the delivery of ^{10}B-L-BPA-F in rats bearing gliosarcoma. They increased the dose from 250 to 1,000 mg/kg, which resulted in an increase of tumor boron concentration (from 30 to 70 μg ^{10}B/g) with a constant tumor-to-blood-ratio of 3.7, 1 h after the end of the infusion. Extension of the infusion time from 2 to 6 h (dose 125 mg/kg) had the same effects. Only intracarotid infusion of BPA (1 h, 125 mg BPA/kg) changed the tumor-to-blood ratio to 5.0 with a boron concentration of 38 μg/g [110].

Metabolism

Kiger et al. state that the excretion of BPA mainly involves the renal pathway [111].

Table 8.6 Summary of the toxicity study published by Taniyama et al. [114]

Route	pH	LD50
i.p.	1	640 mg/kg (male)
		710 mg/kg (female)
s.c.	1	>1,000 mg/kg (male and female)
i.p.	7	>3,000 mg/kg (male and female)
s.c.	7	>3,000 mg/kg (male and female)

There is no conclusive information available on the metabolism of BPA and the form in which it is excreted. Svantesson et al. have found evidence that BPA is indeed metabolized, but further research is necessary to determine the identity of the possible metabolite(s) [112].

For the intended pharmacological action, the chemical form of boron is not of relevance. Only if the metabolites represent toxic substances, the nature of these molecules would be of importance in order to possibly counteract their toxic action.

Plasma Half-Life

Coderre et al. investigated in a canine model the pharmacokinetics and biodistribution of ^{10}B-BPA-F. They found that the blood boron concentration decreases in a bi-exponential way after infusion, indicating that at least two compartments can be distinguished. The investigators suspect that the first phase consists of redistribution of the blood boron into the water compartment ($T½ = 10$ min) and that the second phase consists of renal clearance of the BPA ($T½ = 3$ h) [113].

Toxicology

Toxicology of BPA

Taniyama et al. investigated acute and subacute toxicity of ^{10}B-BPA.HCl in rats injected i.p. and s.c. They used doses ranging from 300 to 3,000 mg/kg. Acute toxicity decreased dramatically by adjusting the pH of the solution to neutral value (Table 8.6).

The subacute toxicity was determined by injecting rats subcutaneously daily for 28 days at doses of 300, 700, and 1,500 mg/kg. All rats survived. All rats showed an increase in urine ketone level. No further differences were observed between control rats and rats with low doses of ^{10}B-BPA.HCl. At the highest dose level, hematologic changes were observed including a decrease in hemoglobin and leukocyte count and an increase in reticulocyte count and neutrophil-lymphocyte ratio. The authors suggest that these findings could be caused by hemolysis and local reactions at the injection site [114].

Kulvik et al. conducted a study on the toxicity of L-BPA-F in male albino Sprague Dawley rats. Eight of the rats were infused with 2.8 g L-BPA/kg as BPA-F. The control group consisted of five rats who received fructose solution only. The following laboratory results were collected: hemoglobin, leukocytes, C, aspartate aminotransferase, alkaline phosphatase, glucose, cholesterol, triglyceride, albumin, and á-, â-, and ã-globulin. No statistically significant differences were detected between control and L-BPA-F rats [115].

There are no more data available investigating the toxicity of BPA in animals.

Toxicology of BNCT using BPA

Unfortunately, the reporting of the applied dose is for most of the animal trials not done following the suggestions of the IAEA as proposed in IAEA TECDOC-1223 [116]. The reported results are therefore difficult to interpret and their comparison is highly problematical.

Setiawan et al. investigated the effect of ^{10}B-L-BPA-F and BNCT on mouse brain dopaminergic neurons. The mice received a dose of 12 mg ^{10}B-BPA intraperitoneally and a radiation dose to the brain of 4.4 Gy ("boron dose") plus 4.0 ("nonboron dose"). They measured damaging effect to dopaminergic tracts as tyrosine hydroxylase immunohistochemical activity. Their findings state that no permanent damage on dopaminergic tracts was observed at 120 h postradiation [117].

Coderre et al. evaluated the effects of BNCT on oral mucosa using a rat model. All rats received 700 mg/kg ^{10}B-L-BPA-F i.p. and irradiation doses of 13.4, 4.2, or 3.0 Gy. Ulceration of the tongue was evident at all doses approximately 7 days after irradiation; healing speed was dose-dependent [118].

Coderre et al. investigated the tolerance of the normal canine brain to epithermal neutron irradiation in the presence of BPA. They used twelve dogs, which were intravenously infused with 950 mg/kg ^{10}B-BPA-F. The dogs were irradiated at the left hemisphere. Peak doses (delivered to 1 cm^3 of brain at the depth of maximum thermal neutron flux) ranged from 7.6 to 11.6 Gy, while the average dose was 6.6 to 10.0 Gy to the left hemisphere. The whole brain received an irradiation dose of 3.0 to 8.1 Gy. They found a significant drop in lymphocyte and platelet count following BNCT. At 6–8 days after irradiation, lymphocyte count had dropped from 8,000–11,000/μl to 4,000/μl. Platelet count was lowest after 11–17 days and decreased from 200–350,000 to 50–150,000. Lymphocyte count returned to normal 3–4 weeks after irradiation; platelet count returned to normal after 30–40 days. The investigators found dose-related effects on skin, resulting in hair loss at the irradiation field together with hyperpigmentation of the skin and loss of hair pigment. Effects on muscle were minor and were only seen at high doses (Peak dose in brain (PDB) 9.0 Gy). Above a certain threshold, all dogs developed dose-dependent MRI changes, neurological deficits, and focal brain necrosis. This threshold was 9.5 Gy for the peak dose, 8.2 Gy for the left hemisphere, and 6.7 Gy for the whole brain. These neurological changes were severe and generally responded to steroid treatment for only a short period [113].

Morris et al. evaluated the central nervous system tolerance to BNCT with ^{10}B-BPA-F using a rat spinal cord model. Different doses of ^{10}B-BPA-F (700, 1,000, and 1,600 mg/kg, 4.9 % ^{10}B) were used intraperitoneally. The follow-up period was 32 weeks after irradiation. No rats were lost during this period of time. They observed the ED50 values (i.e., radiation value at which 50 % of rats developed radiation myelopathy). At 1,000 mg/kg, the ED50 was 17.5 ± 0.7 Gy, and at 1,600 mg/kg, the ED50 was 25.0 ± 0.6 Gy [109].

Fetal Toxicity and Fertility Studies

No studies for fetal toxicity and fertility studies have been carried out.

Table 8.7 Results on survival of neutron irradiation after injection of BPA [105]

Treatment	Radiation dose (Gy)	Tumor dose (Gy)	Survival (days)
Untreated	0		44
Irradiation	2.7		76
Irradiation	3.6		93
120 mg BPA	1.8	5	170
120 mg BPA	2.7	7.5	182
120 mg BPA	3.6	10.1	262

Mutagenic Potential

No in vivo studies for mutagenic potential have been carried out.

Carcinogenic Potential

No studies for carcinogenic potential have been carried out.

Conclusions

BPA in neutral solution is tolerated well, p.o., i.p., i.v., and i.c. (intracarotidly). Toxic effects were found almost only after irradiation.

Effectiveness

Effectiveness of BNCT Using BPA

Coderre et al. studied the effect of irradiation using ^{10}B-BPA in mice carrying melanoma s.c. on the thigh. ^{10}B concentrations in the tumor ranged from 15 to 40 ppm. They have found that p.o. delivery of BPA results in significantly higher amounts of ^{10}B in tumor than via intraperitoneal injections. They concluded that long-term tumor growth control after neutron irradiation was higher after BPA administration (11 of 19) than without BPA administration (4 of 22) [119].

Tamaoki et al. investigated the use of nude mice carrying melanoma allografts in ^{10}B-BPA BNCT. Each mouse received 10 mg ^{10}B-BPA.HCl (400 mg/kg) 4 h prior to irradiation. Thirty mice were divided into three groups of ten. The first group only received neutron irradiation, the second group received both BPA and irradiation, and the third group did not get any treatment. The tumor growth was significantly suppressed for 4 weeks after BPA and irradiation [120].

Matalka et al. used a rat brain tumor model to study the pharmacokinetics and tissue distribution of BPA using intracerebrally implanted human melanoma cells. They injected 120 mg of ^{10}B-enriched BPA-F i.p. The reported results are summarized in Table 8.7. The authors conclude that BNCT using BPA is effective against intracranial melanoma in a rodent model [105].

Effectiveness of BNCT Using Simultaneously BPA and BSH

Ono et al. tried to increase the effect of BPA BNCT by adding BSH (sodium borocaptate) to the therapy. They studied mice bearing mouse squamous cell carcinoma. They administered ^{10}B-D,L-BPA.HCl intragastrically and ^{10}B-BSH-Na intravenously. They found that the combination of these compounds was more effective in tumor cure than using the single compounds [121].

Table 8.8 Survival of rats and ratios tissue/blood after BPA injection ± blood–brain barrier disruption ± neutron irradiation

Administration	BBB-D, yes/no	BPA	Neutron irradiation, yes/no	Survival (days)	^{10}B-ratio tumor/blood ± SD	^{10}B-ratio tumor/brain
i.c.	Y	500 mg/kg	Y	69	10.9 ± 6.3	7.5 ± 4.3
i.c.	N	500 mg/kg	Y	48	8.5 ± 3.5	5.9 ± 2.0
i.v.	N	500 mg/kg	Y	37	3.2 ± 2.7	5.0 ± 2.1
None	N	0	Y	29	NA	NA
None	N	0	N	24	NA	NA

Enhanced Delivery of BPA in Brain Tumors

Barth et al. investigated the difference between i.v. and i.c. injection of ^{10}B-BPA-F and the effect of blood–brain barrier disruption (BBB-D). BBB-D was achieved by infusing a 25 % solution of mannitol via the internal carotid artery to rats bearing F-98 glioma. Approximately, 10 % of animals died within 6–12 h following BBB-D due to cerebral edema. The results observed are summarized in Table 8.8. The ^{10}B concentrations were measured with DCP-AES (direct current plasma-atomic emission spectrometry):

These results indicate that i.c. administration and BBB-D enhance ^{10}B concentration in the tumor, resulting a higher radiation dose to the tumor and improving survival [122].

In another study, Barth et al. investigated whether ^{10}B-BPA-F delivery to the tumor could be enhanced by adding Cereport, a bradykinin analogon, which produces a transient, pharmacologically mediated opening of the blood–brain barrier. They used F98 glioma-bearing rats. The rats were injected intravenously or intracarotidly with 300 mg/kg BPA-F and 1.5–7.5 μg/kg Cereport. Cereport i.c. significantly increased tumor boron uptake [123]. In a later trial, it could be shown that Cereport can not only increase tumor uptake of ^{10}B-BPA-F but also enhances the efficacy of BNCT [124].

8.3.5 Clinical Trials with BPA

In order to treat cancers with BNCT, it is necessary to accumulate ^{10}B in the tumor prior to irradiation and to ensure at the same time that healthy tissue unavoidably present in the neutron beam contains a minimal amount of boron. Because of the short range of the high-LET particles ^{4}He and ^{7}Li resulting from the ^{10}B(n,α)^{7}Li reaction, the efficacy of BNCT is strongly dependent on ^{10}B distribution in tissues. Several boron carriers have been subject of trials, among which BPA is one of the most promising.

The concentration of boron in the tissues exposed to the neutron beam is of utmost importance for the predication of healthy tissue damage and cancer control. Several clincal trials to determine the pharmacokinetics and biodistribution

of BPA have therefore been performed. This chapter is dedicated to data on human pharmacology.

8.3.5.1 Pharmacodynamics

Pharmacological Actions

The substance itself, an amino acid analogue, is not toxic and does not inhibit cell growth or proliferation in the concentrations of clinical relevance (see Sect. 8.3.4.2.2).

Its use in BNCT is solely dependent on its selective accumulation resp. retention in tumor tissue and its own contents of boron.

Pharmacodynamic Mechanisms Underlying the Therapeutic Effects: Uptake of Boron in Tumor Tissue

In 1994, Mallesch et al. investigated the uptake of BPA for glioma and brain metastases of melanoma. The results for the metastatic melanoma patients were encouraging with an average tumor/blood boron concentration ratio and standard deviation of about 4.4 ± 3.2 and a maximum value of 10 for the cerebral metastasis. The glioma patients involved high-grade glioma for which the tumor/blood ratio was 2.2 ± 1. The authors pointed out that the uptake of boron in tumor tissue is based upon its amino acid properties. D,L-BPA-F was postulated to be taken up by active metabolic pathways in cells. It was suggested that due to elevated metabolism of tumor cells, the molecule will be accumulated in these tissues [125]. Wittig et al. [98] showed in vitro that BPA is mainly transported through the membrane by the L-amino acid transport system. In a clinical trial (EORTC 11001), no correlation between BPA uptake and the LAT1 and Ki67 expressions in tumor samples was found [126].

The uptake of BPA into glioma and melanoma was measured by tissue sampling in several trials [127–130]. After the extracorporal irradiation of an explanted liver to treat metastases of colorectal cancer [131], different groups investigated the uptake of BPA in colorectal liver metastases sampled during surgery [26, 132, 133], all demonstrating a higher uptake of ^{10}B in the metastases as compared to normal liver tissue. Only one trial investigated the uptake of BPA in squamous cell carcinoma of the head and neck by tissue sampling showing a promising ^{10}B concentration and demonstrating for the first time the change of boron concentration over time in the tumor [17]. The hypothetic approach to treat thyroid cancer by BNCT [134] could not be supported by data from the EORTC trial 11001 showing no boron uptake in tissues from several thyroid cancers [135].

8.3.5.2 Pharmacokinetics of BPA

Absorption, Including Bioavailability

Some of the older melanoma trials have been performed using oral administration of L-BPA. The reason for oral administration was the limited aqueous solubility of BPA at physiological pH. Coderre concluded that the fraction of the oral ^{10}B-L-BPA dose that is actually absorbed from the gastrointestinal tract is 42.1 ± 17.8 % (n = 13). In these patients, a slurry of a crystalline-free, slightly soluble amino acid analogue was used [136].

In later trials with patients suffering from glioblastoma multiforme (GBM), malignant melanoma, and cancers of the head and neck, as well as for EORTC 11001, BPA was infused through a central venous catheter. BPA was complexed with fructose to solve the solubility difficulties (^{10}B-L-BPA-F). This significantly raised blood boron concentrations from 6 μg/g (oral) to 32 μg/g (intravenous) [111]. One trial actually investigates the potential of BPA complexed with mannitol [137].

Protein Binding

The action of BPA might be dependent on the protein binding of the drug. There are no studies known about this parameter.

Plasma Half-Life

Several authors have published data on plasma concentrations as a function of time. Generally, these data are considered to consist of biphasic kinetics, with a redistribution and an elimination phase. Exact data are given in the next paragraph

Pharmacokinetics

Almost all trials were aimed at composing a model with which the blood and/or tumor level of BPA could be estimated out of limited data. These models were two, three, and four compartmental. The results of different pharmacokinetic trials will be summarized below.

Elowitz et al. concluded that ^{10}B-L-BPA-F exhibits biphasic clearance kinetics. During the first phase, blood boron concentrations decreased with a half-time of approximately 1.2 h (redistribution). The second phase (elimination) had a half-time of 8.2 h [96].

Ryynänen et al. combined two models (an open two-compartment model and a biexponential function) to describe the clearance of ^{10}B from blood after 290 mg/kg BPA (^{10}B-BPA-F) infusion. The combined model is created for predicting the ^{10}B blood concentration. The pharmacokinetic parameters used in these models are described in Table 8.9 [138].

Fukuda et al. took another approach and studied the pharmacokinetics of ^{10}B-D,L-BPA-F in skin and blood of melanoma patients. Their results are summarized in Table 8.10 [129].

Mallesch et al. [125] studied the pharmacokinetics of D,L-BPA-F in patients with metastatic melanoma and glioma. BPA-F was administered as an intravenous bolus (12.06 ± 3.2 mg/kg). Tissue and blood samples were measured. They concluded that tumor-selective uptake of BPA in patients with brain metastases of malignant melanoma is higher than in patients with glioma. They also normalized all results to a nominal dose of 20 mg/kg, average weight 75 kg, and obtained the pharmacokinetic parameters stated in the Table 8.11.

Kiger et al. designed a pharmacokinetic two compartment model for the concentration of ^{10}B in blood following the administration of (^{10}B-L-BPA-F). They included 24 patients, 21 with GBM, 2 with metastatic melanoma, and 1 with subcutaneous melanoma. They found a biphasic exponential clearance profile. The pharmacokinetic parameters are presented in Table 8.12. The validity of this

Table 8.9 Pharmacokinetic parameters for BPA-F of the combined model from Ryynänen [138]

No. of patients	Histology	BPA mg/kg	K 12 (min^{-1})	K 21 (min^{-1})	K el (min^{-1})	T1/2 redistribution	T1/2 elimination
7 m, 3 f	GBM	290	0.325 (± 0.207)	0.06 (± 0.033)	0.031 (± 0.005)	16 (± 5) min	6.6 (± 2.0) h
40–81 years							

Table 8.10 Compilation of the pharmacokinetic data published by Fukuda and all [129]

No. of patients	Histology	BPA i.v. (mg/kg)	Additional BPA (mg/kg)	*T½* redistribution	*T½* elimination	Ratio, skin/blood	Ratio, tumor/blood
9	Melanoma	170–210		2.8 h	9.2 h	1.31 ± 0.22 Constant during 6 h post infusion	3.40 ± 0.83 Constant during 6 h post infusion
7	Melanoma	85		2.2 h	9.2 h	7	Melanoma
7	Melanoma	170–190	30 s.c.	3.3 h	9.0 h		
2	Melanoma		50 i.m. × 5				

Table 8.11 Pharmacokinetic parameters for BPA-F published by Mallesch et al. [125]

Dose BPA (mg/kg)	Weight (kg)	Dose ^{10}B (mg)	Initial conc. (μg/ml)	K el (h^{-1})	Half-life	AUC (μg/h/ml)	Vd (l)
20	75	71.46	1.02	0.05	5.05	23.76	59.6

Table 8.12 Pharmacokinetic parameters following Kiger et al. [111]

No. of patients	BPA dose (mg/kg)	*T½* redistribution	*T½* elimination	K 12 (min^{-1})	K 21 (min^{-1})	K el (min^{-1})	Vd (kg/kg)
11 male, 13 female	250 (12)	0.34 ± 0.12 h	9.0 ± 2.7 h	0.0227 ± 0.0064	0.0099 ± 0.0027	0.0052 ± 0.0016	0.235 ± 0.042
24–82 years	300 (2)						
	350 (10)						

model was demonstrated by successfully predicting the average pharmacokinetic response for a cohort of 32 patients [111]. This model was also reliable predicting the ^{10}B concentration in patients suffering from melanoma brain metastases and irradiated in the frame of EORTC 11011 [139].

Elimination

The metabolization path of BPA is unknown. The excretion is mainly made via the kidneys. BPA can be found nonmetabolized in the urine of patients [140].

BPA Distribution

Analysis of boron has been carried out through prompt gamma ray spectroscopy (PGRS) and direct current plasma-atomic emission spectrometry (DCP-AES). The

former provides an accurate assessment of boron in larger quantities of tissue (around 1,000 mg); the latter is more sensitive and allows accurate measurement of ^{10}B and ^{11}B in 10- to 20-mg samples.

Using these methods, Elowitz et al. concluded that tumor-to-blood ratios were highly variable. Seventeen GBM patients received different intravenous amounts of ^{10}B-enriched L-BPA-F: 130 mg BPA/kg ($n=5$), 170 mg/kg ($n=6$), 210 mg/kg ($n=3$), and 250 mg/kg ($n=3$).The blood boron concentration reached a maximum at the end of the 2-h BPA infusion and was proportional to the administered dose. The maximum boron concentration did not increase when infusion time was decreased to 1 h. Considerable variation in the measured boron concentration of resected tumor specimens was seen from patient to patient and among multiple samples from individual patients. The average tumor-to-blood-boron ratio was 1.6 (± 0.8). The concentration of boron in normal brain is generally equal to or less than that in blood. An initial qualitative analysis relating tumor histopathology and boron concentrations indicated that samples from more cellular areas exhibited a higher boron uptake than samples containing a high degree of necrosis [96].

Coderre et al. also concluded that boron concentrations correlate with tumor cellularity. They measured 107 surgical samples from 15 patients with glioblastoma multiforme receiving 98–290 mg 95 % ^{10}B-enriched BPA per kg. The blood boron concentration reached a maximum at the end of the 2-h ^{10}B-enriched BPA-F infusion and was proportional to the administered dose of BPA. Boron concentration (normalized to a BPA dose of 250 mg/kg) between patients and between samples from individual patients varied significantly. However, they found that the boron concentration in tumor samples correlated to the cellularity of the sample ($r=0.84$) calculated using the formula: $B=9.1+61.9$*CI, in which $B=$concentration ^{10}B in tissue (μg/g) and CI = cellularity index. They concluded that the accumulation of boron in tumor cells is a linear function of the administered dose of BPA and that the variation observed in boron analysis of multiple samples from individual patients was due to the inclusion of nontumor tissue (i.e., necrotic tissue or normal brain). The results of the cellularity analysis and the correlation with measured boron concentrations (normalized to a BPA dose of 250 mg/kg) indicated that the intracellular boron concentration in GBM was approximately 50 μg ^{10}B/g. They found an average blood boron concentration of 12.2 ± 1.6 μg ^{10}B/g, resulting in an average tumor-to-blood boron ratio of approximately 4, measured between 30 and 90 min after an infusion over 2 h [97]. It was also found in this trial that there is no difference in clearance kinetics between anesthetized and conscious patients.

A special aspect of BPA distribution in metastases of colorectal adenocarcinoma due to the high amount of noncellular materials in these tissues was discussed by Wittig et al. [26].

Several researchers have used positron-emission tomography (PET) for determining pharmacokinetic parameters of BPA. They all used a derivative of BPA, that is, ^{18}F-^{10}B-BPA-F. Because of this modification of the original structure of BPA-F, it is uncertain whether these data are to be extrapolated to BPA-F. Therefore, these results are not included here.

8.3.5.3 Toxicology of BPA

Toxicity of the Drug

Kulvik et al. administered 100 mg L-BPA/kg as BPA-F to 5 schwannoma and 3 meningioma patients and 450 mg L-BPA/kg as L-BPA-F to 1 glioblastoma patient. Monitored parameters were blood leukocytes, blood erythrocytes, hemoglobin, thrombocytes, C-reactive protein, creatinine, alanine aminotransferase and ã-glutamyltransferase. No clinically significant adverse events attributable to L-BPA-F infusions were observed [115].

In the EORTC trial 1101, patients suffering from melanoma brain metastases were irradiated in 2 fractions on 2 consecutive days. Prior to each fraction of irradiation, each patient received a dose of 14.0 g BPA/m^2 body surface, which is equivalent to 350 mg/kg body weight for a person of 80 kg and with a body surface of 2 m^2. BPA will be administered as ^{10}B-BPA-fructose complex. The infusion was applied intravenously via central venous catheter over 90 min. In the four treated patients, no drug-related toxicity was observed. However in the urine of the patients, crystals were observed. The crystallization occurred outside the patient and was therefore not seen as a toxic event. This effect may cause troubles if patients are treated with long irradiation times and obtain an urine catheter.

Patients treated in the frame of the biodistribution trial 11001 received only 100 mg/kg BPA dissolved in a volume of 30 mg BPA-F/ml solution that was infused over 1 h. No drug-related side effects were observed. Single BPA crystals in the urine could be detected after carefully searching under the microscope.

Toxicity of BPA-Mediated BNCT

A high uptake of BPA in skin and mucosa has been described in animal experiments and clinical trials [17, 26, 27, 129, 141–143]. Skin reactions and mucositis are expected as well as observed side effects of BPA-mediated BNCT.

References

1. Gabel D, Sauerwein W (1995) Approaching clinical trials of boron neutron capture therapy in Europe. In: Kogelnik HD (ed) Progress in radio-oncology V. Monduzzi Editore, Bologna, pp 315–319
2. Sauerwein W, Hideghéty K, Gabel D, Moss R (1998) European clinical trials of boron neutron capture therapy for glioblastoma. Nuclear News 41:54–56
3. Sauerwein W, Moss R, Rassow J, Stecher-Rasmussen F, Hideghéty K, Wolbers JG, Sack H (1999) Organisation and management of the first clinical trial of BNCT in Europe (EORTC Protocol 11961). Strahlenther Onkol 175:108–111
4. Hideghéty K, Sauerwein W, Haselsberger K, Grochulla F, Fankhauser H, Moss R, Huiskamp R, Gabel D, de Vries M (1999) Postoperative treatment of glioblastoma with BNCT at the Petten Irradiation facility (EORTC Protocol 11961). Strahlenther Onkol 175:111–114
5. Pignol JP, Paquis P, Breteau N, Chauvel P, Sauerwein W, EORTC BNCT Study Group (1999) Boron neutron capture enhancement of fast neutron for nonremoved glioblastomas: rationale of a clinical trial. Front Radiat Ther Oncol 33:43–50
6. Hideghéty K, Moss R, Sauerwein W, EORTC BNCT Study Group (2000) Controversies in establishment of dose limiting qualitative and quantitative toxicity for radiation modality. Radiother Oncol 57:S7–S9

7. Hüsing J, Sauerwein W, Hideghéty K, Jöckel K-H (2001) A scheme for a dose-escalation study when the event is lagged. Stat Med 20:3323–3334
8. Sauerwein W, Hideghéty K, Rassow J, Moss RL, Stecher-Rasmussen F, Heimans J, Gabel D, de Vries MJ, Touw DJ, the EORTC BNCT Study Group (2001) Boron neutron capture therapy: an interdisciplinary cooperation. In: IAEA-TECDOC-1223 "Current status of neutron capture therapy", International Atomic Energy Agency, Vienna, 2001, pp 96–107
9. Sauerwein W, Hideghéty K, Rassow J, de Vries MJ, Götz C, Paquis P, Grochulla F, Wolbers JG, Haselsberger K, Turowski B, Moss RL, Stecher-Rasmussen F, Touw D, Wiestler OD, Fankhauser H, Gabel D, the EORTC BNCT Study Group (2001) First clinical results from the EORTC phase I trial "Postoperative treatment of glioblastoma with BNCT at the Petten irradiation facility". In: IAEA-TECDOC-1223 "Current status of neutron capture therapy", International Atomic Energy Agency, Vienna, 2001, pp 250–256
10. Michel J, Sauerwein W, Wittig A, Balossier G, Zierold K (2002) Boron localisation in cells by electron energy loss spectroscopy. In: Sauerwein W, Moss R, Wittig A (eds) Research and development in neutron capture therapy. Monduzzi Editore, Bologna, pp 925–928
11. Sauerwein W, Zurlo A, on behalf of the EORTC Boron Neutron Capture Therapy Group (2002) The EORTC Boron Neutron Capture Therapy (BNCT) Group: achievements and future projects. EJC 38:S31–S34
12. Hideghéty K, Sauerwein W, Wittig A, Götz C, Paquis P, Grochulla F, Haselsberger K, Wolbers J, Moss R, Huiskamp R, Fankhauser H, de Vries M, Gabel D (2003) Tissue uptake of BSH in patients with glioblastoma in the EORTC 11961 phase I BNCT trial. J Neurooncol 62:145–156
13. van Rij CM, Wilhelm AJ, Sauerwein WAG, van Loenen AC (2005) Boron neutron capture therapy for glioblastoma multiforme. Pharm World Sci 27:92–95
14. Mauri PL, Basilico F, Wittig A, Heimans J, Huiskamp R, Sauerwein W (2006) Pharmacokinetics and metabolites of ^{10}B-containing compounds in biological fluids. In: Nakagawa Y, Kobayashi T, Fukuda H (eds) Advances in neutron capture therapy 2006. International Society for Neutron Capture Therapy and Neutrino OSAKA Inc, Osaka, pp 271–273. ISBN 4-990342-0-X
15. Wittig A, Malago M, Collette L, Huiskamp R, Bührmann S, Nievaart V, Kaiser GM, Jöckel KH, Schmid KW, Ortmann U, Sauerwein W (2008) Uptake of two ^{10}B-compounds in liver metastases of colorectal adenocarcinoma for extracorporeal irradiation with boron neutron capture therapy (EORTC trial 11001). Int J Cancer 122:1164–1171
16. Wittig A, Collette L, Moss R, Sauerwein WA (2009) Early clinical trial concept for boron neutron capture therapy: a critical assessment of the EORTC trial 11001. Appl Radiat Isot 67:S59–S62
17. Wittig A, Collette L, Appelman K, Bührmann S, Jäckel MC, Jöckel KH, Schmid KW, Ortmann U, Moss R, Sauerwein WA (2009) EORTC trial 11001: distribution of two (10)B-compounds in patients with squamous cell carcinoma of head and neck, a translational research/phase 1 trial. J Cell Mol Med 13:1653–1665
18. Bendel P, Wittig A, Basilico F, Mauri P, Sauerwein W (2010) Metabolism of Borono-phenylalanine-fructose complex (BPA-fr) and Borocaptate Sodium (BSH) in cancer patients – results from EORTC trial 11001. J Pharm Biomed Anal 51:284–287
19. Soloway AH, Hatanaka H, Davis M (1967) Penetration of brain and brain tumor. VII. Tumor binding sulfhydryl compounds. J Med Chem 10:714–717
20. Hatanaka H (1975) A revised boron-neutron capture therapy for malignant brain tumors. II. Interim clinical result with the patients excluding previous treatments. J Neurol 209:81–94
21. Gabel D, Sauerwein W (1994) Clinical implementation of boron neutron capture therapy in Europe. In: Amaldi U, Larsson B (eds) Hadrontherapy in oncology. Elsevier Science, Amsterdam, pp 509–517
22. Gabel D, Preusse D, Haritz D, Grochulla F, Haselsberger K, Fankhauser H, Ceberg C, Peters HD, Klotz U (1997) Pharmacokinetics of $Na_2B_{12}H_{11}$ SH (BSH) in patients with malignant brain tumours as a prerequisite for a phase I clinical trial of boron neutron capture. Acta Neurochir (Wien) 139:606–612
23. Gibson CR, Staubus AE, Barth RF, Yang W, Ferketich AK, Moeschberger MM (2003) Pharmacokinetics of sodium borocaptate: a critical assessment of dosing paradigms for boron neutron capture therapy. J Neurooncol 62(1–2):157–169

24. Goodman JH, Yang W, Barth RF et al (2000) Boron neutron capture therapy of brain tumors: biodistribution, pharmacokinetics, and radiation dosimetry sodium borocaptate in patients with gliomas. Neurosurgery 47:608–621
25. Hideghety K, Sauerwein W, Wittig A, Götz C, Paquis P, Grochulla F, Haselsberger K, Wolbers J, Moss R, Huiskamp R, Fankhauser H, De Vries M, Gabel D (2003) Tissue uptake of BSH in patients with glioblastoma in the EORTC 11961 phase I BNCT trial. J Neurooncol 62:145–156
26. Wittig A, Malago M, Collette L, Huiskamp R, Bührmann S, Nievaart V, Kaiser GM, Jöckel K, Kw S, Ortmann U, Sauerwein W (2008) Uptake of two ^{10}B-compounds in liver metastases of colorectal adenocarcinoma for extracorporeal irradiation with boron neutron capture therapy (EORTC trial 11001). Int J Cancer 122:1164–1171
27. Wittig A, Huiskamp R, Moss RL, Bet P, Kriegeskotte C, Scherag A, Hilken G, Sauerwein WAG (2009) Biodistribution of ^{10}B for Boron Neutron Capture Therapy (BNCT) in a Mouse Model after Injection of Sodium Mercaptoundecahydro-closo-dodecaborate and L-para-Boronophenylalanine. Radiat Res 172:493–499
28. Wittig A, Stecher-Rasmussen F, Hilger RA, Rassow J, Mauri P, Sauerwein W (2011) Sodium mercaptoundecahydro-closo-dodecaborate (BSH), a boron carrier that merits more attention. Appl Radiat Isot. doi:10.1016/j.apradiso.2011.02.046
29. Peters HD, Gabel D (1997) Treatment of glioma with boron neutron capture therapy with $Na_2B_{12}H_{11}SH$ – compilation of literature data on toxicity and pharmacokinetics in animals. Summary of the European phase I toxicity and pharmacokinetics study. European Collaboration on Boron Neutron Capture Therapy: 1–47
30. Wittig A, Michel J, Moss RL, Stecher-Rasmussen F, Arlinghaus HF, Bendel P, Mauri P, Altieri S, Hilger R, Salvadori PA, Menichetti L, Zamenhof R, Sauerwein WAG (2008) Boron analysis and boron imaging in biological materials for Boron Neutron Capture Therapy (BNCT). Crit Rev Oncol Hematol 68:66–90
31. Haselsberger K, Radner H et al (1994) Subcellular boron-10 localization in glioblastoma for boron neutron capture therapy with Na2B12H11SH. J Neurosurg 81:741–744
32. Clendenon NR, Barth RF, Gordon WA et al (1990) Boron neutron capture therapy of a rat glioma. Neurosurgery 26:47–55
33. Gabel D, Holstein H, Larsson B et al (1987) Quantitative neutron capture radiography for studying the biodistribution of tumor-seeking boron-containing compounds. Cancer Res 47:5451–5454
34. Joel DD, Slatkin DN, Micca PL, Nawrocky MMD, Velez C (1989) Uptake of boron into human gliomas of athymic mice and into syngeneic cerebral gliomas of rats after intra carotid infusion of sulfhydryl boranes. In: Fairchild RG, Bond VP, Woodhead AD (eds) Clinical aspects of neutron capture therapy. Plenum Press, New York, pp 325–332
35. Joel DD, Slatkin DN, Micca PL, Nawrocky MM, Dubois T, Velez C (1989) Uptake of boron into human gliomas of athymic mice and into syngeneic cerebral gliomas of rats after intracarotid infusion of sulfhydryl boranes. Basic Life Sci 50:325–332
36. Joel D, Slatkin D, Fairchild R, Micca P, Nawrocky M (1989) Pharmacokinetics and tissue distribution of the TI – sulfhydryl boranes (monomer and dimer) in glioma-bearing rats. Strahlenther Onkol 165:167–170
37. Joel D, Slatkin D, Coderre J (1993) Uptake of 1OB in gliosarcoma :following the injection of glutathione monoethyl ester and sulfhydryl borane. In: Soloway AH, Barth RF, Carpenter DE (eds) Advances in neutron capture therapy. Plenum Press, New York, pp 501–504
38. Wittig A, Arlinghaus H, Kriegeskotte C, Moss R, Appelman K, Schmid K, Sauerwein W (2008) Laser postionization secondary neutral mass spectrometry in tissue: a powerful tool for elemental and molecular imaging in the development of targeted drugs. Mol Cancer Ther 7:1763–1771
39. Hatanaka H (1997) Boron neutron capture therapy for tumors. Nishimura, Niigata
40. Harfst S, Moller D, Ketz H, Roesler J (1994) Reversed-phase separation of ionic organoborate clusters by high-performance liquid chromatography. J Chromatogr A 678:41

41. LaHann TR, Daniell G (1997) Death following single dose administration of borocaptate sodium. In: Larsson B, Crawford I, Weinreich R (eds) Chemistry and biology, vol II. Elsevier Science, Amsterdam, pp 175–180
42. Morris GM, Constantine G, Ross G, Yeung TK, Hopewell JW (1993) Boron neutron capture therapy long term effects on the skin and spinal cord of the rat. Radiat Res 135:330–386
43. Horn V, Buchar E, Janku I (1997) Kidney function changes in rats after single-dose administration of borocaptate sodium. Physiol Res 46:279–283
44. Gavin PR, DeHaan CE, Kraft SL, Moore MP, Wendling LR, Dorn RV (1994) Large animal normal tissue tolerance with boron neutron capture. Int J Radiat Oncol Biol Phys 28(5): 1099–1106
45. Gavin PR, Kraft SL, Wendling LR, Miller DL (1989) Canine spontaneous brain tumors – a large animal model for BNCT. Strahlenther Onkol 165(2/3):225–228
46. Gavin PR, Kraft SL, Huiskamp R, Coderre JA (1997) A review: CNS effects and normal tissue tolerance in dogs. J Neurooncol 33(1–2):71–80
47. Janku I, Buchar E, Jiricka Z (1993) Nephrotoxicity of borocaptate after short-term administration in rabbits. Toxicology 79:99–108
48. Kinashi Y, Masunaga S-I, Ono K (2002) Mutagenic effect of borocaptate sodium and borophenylalanine in neutron capture therapy. Int J Radiat Oncol Biol Phys 54:562–567
49. Sweet WH, Messer JR, Hatanaka H (1986) Supplementary pharmacological study between 1972 and 1977 on purified mercaptoundecahydrododecaborate. In: Hatanaka H (ed) Boron neutron capture therapy for tumors. Nishimura, Niigata, pp 59–76
50. Morris GM, Coderre JA, Hopewell JW, Micca PL, Rezvani M (1994) Response of rat skin to boron neutron capture therapy with p-boronophenylalanine or borocaptate sodium. Radiother Oncol 32:144–153
51. Kraft SL, Gavin PR, Leathers CW, DeHaan CE, Bauer WF, Miller DL, Dorn RV, Griebenow ML (1994) Biodistribution of boron in dogs with spontaneous intracranial tumors following borocaptate sodium administration. Cancer Res 54(5):1259–1263
52. Yamaguchi T, Nakajima Y, Miyamoto H, Mizobuchi M, Kanazu T, Kadono K, Nakamoto K, Ikeuchi I (1998) Distribution and excretion of boron after intravenous administration of disodium mercaptoundecahydro-closo-dodecaborate to rats. J Toxicol Sci 23:577–585
53. Mehta SC, Lu DR (1995) Interspecies pharmacokinetic scaling of BSH in mice, rats, rabbits, and humans. Biopharm Drug Dispos 16:735–744
54. Nakagawa T, Nagai T (1976) Interaction between albumin and mercaptoundecahydrododecaborate ion (an agent for boron neutron capture therapy of brain tumour). Chem Pharm Bull 24:2934–2954
55. Bauer WF, Bradshaw KM, Richards TL (1992) Interaction between boron containing compounds and serum albumin observed by nuclear magnetic resonance. In: Allen BJ, Moore DE, Harrington BV (eds) Progress in neutron capture therapy for cancer. Plenum Press, New York, pp 339–344
56. Samsel EG, Miller DL (1989) High resolution ^{10}B and ^{11}B nuclear magnetic resonance (NMR) spectroscopy of $Na_2B_{12}H_{11}SH$ impurities and metabolites. Strahlenther Onkol 165:140
57. Bradshaw KM, Schweizer M, Glover G, Hadley J (1993) Pharmacokinetics of borocaptate sodium in canine head determined by ^{11}B. In: Soloway AH, Barth RF, Carpenter DE (eds) Advances in neutron capture therapy. Plenum Press, New York, pp 579–583
58. Tang PP, Schweizer MP, Bradshaw KM, Bauer WF (1995) ^{11}B nuclear magnetic resonance studies of the interaction of borocaptate sodium with serum albumin. Biochem Pharmacol 49:625–632
59. Kawabata S, Miyatake S, Nonoguchi N, Hiramatsu R, Iida K, Miyata S, Yokoyama K, Doi A, Kuroda Y, Kuroiwa T, Michiue H, Kumada H, Kirihata M, Imahori Y, Maruhashi A, Sakurai Y, Suzuki M, Masunaga S, Ono K (2009) Survival benefit from boron neutron capture therapy for the newly diagnosed glioblastoma patients. Appl Radiat Isot 67:15–18
60. Matsuda M, Yamamoto T, Kumada H, Nakai K, Shirakawa M, Tsurubuchi T, Matsumura A (2009) Dose distribution and clinical response of glioblastoma treated with boron neutron capture therapy. Appl Radiat Isot 67:S19–S21

61. Kato I, Ono K, Sakurai Y, Ohmae M, Maruhashi A, Imahori Y, Kirihata M, Nakazawa M, Yura Y (2004) Effectiveness of BNCT for recurrent head and neck malignancies. Appl Radiat Isot 61:1069–1073
62. Pöller F, Wittig A, Sauerwein W (1998) Calculation of boron neutron capture cell inactivation in vitro based on particle track structure and x-ray sensitivity. Radiat Environ Biophys 37:117–123
63. Amano K (1986) Boron-10-mercaptoundecahydrododecaborate distribution in human brain tumors as studied by neutron-induced alpha-autoradiography. In: Hatanaka H (ed) Boron neutron capture therapy for tumors. Nishimura, Niigata, pp 112–115
64. Otersen B, Haritz D, Grochulla F, Bergrnann M, Sierralta W, Gabel D (1996) Binding and immunohistochemical localization of Na2B12HI11SH to tumor tissue of gliorna patients in boron neutron capture therapy. In: Mishima Y (ed) Neutron capture therapy for human cancers. Plenum Press, New York, pp 627–633
65. Kageji T, Nakagawa Y, Kitamura K, Matsumoto K, Hatanaka H (1997) Pharmacokinetics and boron uptake of BSH ($Na_2B_{12}H_{11}SH$) in patients with intracranial tumors. J Neurooncol 33:117–130
66. Ceberg CP, Persson A, Brun A et al (1995) Performance of BSH in patients with astrocytoma grades III-IV – a basis for boron neutron capture therapy. J Neurosurg 83:79–85
67. Haselsberger K, Radner H, Gössler W, Schlagenhaufen C, Pendl G (1994) Subcellular boron-10 localization in glioblastoma for boron neutron capture therapy with Na2B12H11SH. J Neurosurg 81:741–744
68. Thellier M, Chevallier A, His I, Jarvis MC, Lovell MA, Ripoll C, Robertson D, Sauerwein W, Verdus MC (2001) Methodological developments for application to the study of physiological boron and to boron neutron capture therapy. J Trace Microprobe Tech 19:623–657
69. Wittig A, Wiemann M, Fartmann M, Kriegeskotte C, Arlinghaus HF, Zierold K, Sauerwein W (2005) Preparation of cells cultured on silicon wafers for mass spectrometry analysis. Microsc Res Tech 66:248–258
70. Michel J, Balossier G, Wittig A, Sauerwein W, Zierold K (2005) EELS spectrum-imaging for boron detection in biological cryofixed tissues. Instrum Sci Technol 33:631–644
71. Michel J, Sauerwein W, Wittig A, Balossier G, Zierold K (2003) Subcellular localization of sodium borocaptate in cultured melanoma cells by electron energy-loss spectroscopy of freeze-dried cryosections. J Microsc 210:25–34
72. Haritz D, Gabel D, Klein H, Huiskamp R, Pettersson OK (1992) BSH in patients with malignant glioma: distribution in tissues, comparison between BSH concentration and histology. In: Gabel D, Moss RL (eds) Boron neutron capture therapy, toward clinical trials of glioma treatment. Plenum Press, New York, pp 103–174
73. Haritz D, Gabel D, Klein H, Piscol K (1992) Clinical investigations boron neutron capture therapy (BNCT). Pharmacokinetics, biodistribution, and toxicity of $Na_2B_{12}H_{11}$ SH (BSH) in patients with malignant glioma. Adv Neurosurg 21:247–252
74. Haritz D, Gabel D, Huiskamp R (1994) Clinical phase-I-study of $Na_2B_{12}H_{11}SH$ (BSH) in patients with malignant glioma as precondition for boron neutron capture therapy (BNCT). Int J Radiat Oncol Biol Phys 28:1175–1181
75. Haselsberger K, Radner H, Pendl G (1994) Boron neutron capture therapy: boron biodistribution and pharmacokinetics of Na-2B-12H-11SH in patients with glioblastoma. Cancer Res 54:6318–6320
76. Haselsberger K, Radner H, Gössler W, Schagenhaufen C, Pendl G (1994) Subcellular boron-10 localization in glioblastoma for boron neutron capture therapy with Na2B12H11SH. J Neurosurg 81:741–744
77. Fankhauser H, Stragliotto G, Zbinden P (1992) Borocaptate sodium (BSH) pharmacokinetic in glioma patients. In: Gabel D, Moss RL (eds) Boron neutron capture therapy toward clinical trials of glioma treatment. Plenum Press, New York, pp 155–1644
78. Stragliotto O, Schüpbach D, Gavin P, Fankhauser H (1993) Update on biodistribution of borocaptate sodium (BSH) in patients with intracranial tumors. In: Soloway AH, Barth RF, Carpenter DE (eds) Advances in neutron capture therapy. Plenum Press, New York, pp 719–726

79. Stragliotto G, Fankhauser H (1992) Biodistribution of boron sulfhydryl (BSH) in patients with intracranial tumors. In: Allen BJ, Moore DE, Harrington BV (eds) Progress in neutron capture therapy for cancer. Plenum Press, New York, pp 551–556
80. Stragliotto G, Fankhauser H, Gavin P, Meuli R (1993) Correlation of BSH uptake with CT scan contrast enhancement in patients with intracranial tumors. In: Soloway AH, Barth RF, Carpenter DE (eds) Advances in neutron capture therapy. Plenum Press, New York, pp 715–717
81. Stragliotto G, Fankhauser H (1995) Biodistribution and pharmacokinetics of boron-sulfhydryl for boron neutron capture therapy in patients with intracranial tumors. Neurosurgery 36:285–293
82. Horn V, Slansky J, Janku I, Strouf O, Sourek K, Tovarys F (1998) Disposition and tissue distribution of boron after infusion of borocaptate sodium in patients with malignant brain tumors. Int J Radiat Oncol Biol Phys 41:631–638
83. Paquis P, Hideghety K, Wittig A et al (2002) Tissue uptake if BSH in patients with glioblastomas in the EORTC 11961 phase I trial. In: Sauerwein W, Moss RL, Wittig A (eds) Research and development in neutron capture therapy. Monduzii Editore S.p.A, Bologna, pp 1017–1022
84. Gibson CR, Staubus AE, Barth RF et al. Pharmacokinetics of sodium borocaptate, based on boron concentrations, after intravenous administration to glioma patients and simulations to optimize dosing for neutron capture therapy. J Pharmacokin Biopharm 2000
85. Kageji T, Nagahiro S, Kitamura K, Nakagawa Y, Hatanaka H, Haritz D, Grochulla F, Haselsberger K, Gabel D (2001) Optimal timing of neutron irradiation for boron neutron capture therapy after intravenous infusion of sodium borocaptate in patients with glioblastoma. Int J Radiat Oncol Biol Phys 51:120–130
86. Sauerwein W, Hilger RA, Appelman K, Moss R, Heimans J, Bet P, Wittig A (2008) Pharmacokinetics of BSH – results from EORTC trials. In: Zonta A, Altieri S, Roveda L, Barth R (eds) Neutron capture therapy: a new option against cancer. ENEA (Italian National Agency for New Technologies, Energy and the Environment), Florence, pp 58–61. ISBN 8-8286-176-8
87. Mauri PL, Basilico F, Pietta PG, Pasini E, Monti D, Sauerwein W (2003) New approach for the analysis of BSH and its metabolites using capillary electrophoresis and ESI-MS. J Chromatogr 788:9–16
88. Basilico F, Sauerwein W, Pozzi F, Wittig A, Moss R, Mauri PL (2005) Analysis of ^{10}B antitumoral compounds by means of flow-injection into ESI-MS/MS. J Mass Spectrom 40: 1546–1549
89. Wittig A, Hideghety K, Paquis P et al (2002) Current clinical results of the EORTC-study 11961. In: Sauerwein W, Moss RL, Wittig A (eds) Research and development in neuron capture therapy, Essen (Germany). Monduzzi Editore S.p.A, Bologna, pp 1117–1121
90. Haselsberger K, Radner H et al (1998) Boron neutron capture therapy for glioblastoma: improvement of boron biodistribution by hyaluronidase. Cancer Lett 131(1):109–111
91. Haritz D, Gabel D, Klein H, Huiskamp R (1993) Results of continued clinical investigations of BSH in patients with malignant glioma. In: Soloway AH, Barth RF, Carpenter DE (eds) Advances in neutron capture therapy. Plenum Press, New York, pp 727–730
92. Snyder HR, Reedy AJ, Lennarj WJ (1958) Synthesis of aromatic boronic acids. Aldehyde boronic acids and a boronic acid analog of tyrosine. J Am Chem Soc 80:835–838
93. Coderre JA, Glass JD, Packer S, Micca P, Greenberg D (1990) Experimental boron neutron capture therapy for melanoma: systemic delivery of boron to melanotic and amelanotic melanoma. Pigment Cell Res 3:310–318
94. Coderre JA, Chanana AD, Joel DD, Elowitz EH, Micca PL, Nawrocky MM, Chadha M, Gebbers JO (1998) Biodistribution of boronophenylalanine in patients with glioblastoma multiforme: boron concentration correlates with tumor cellularity. Radiat Res 149:163–170
95. Coderre JA, Glass JD, Fairchild RG, Micca PL, Fand I, Joel DD (1990) Selective delivery of boron by the melanin precursor analogue p-boronophenylalanine to tumors other than melanoma. Cancer Res 50:138–141
96. Elowitz EH, Bergland RM, Coderre JA, Joel DD, Chadha M, Chanana AD (1998) Biodistribution of p-boronophenylalanine (BPA) in patients with glioblastoma multiforme for use in boron neutron capture therapy. Neurosurgery 42:463–469

97. Solares G, Zamenhof R, Saris S, Wazer D, Kerley S, Joyce M, Madoc-Jones H, Adelman L, Harling O (1992) Biodistribution and pharmacokinetics of p boronophenylalanine in C57BL/6 mice with GL261 intracerebral tumors, and survival following neutron capture therapy. In: Allen BJ, Harrington BV, Moore DE (eds) Progress in neutron capture therapy for cancer. Plenum Press, New York and London, pp 475–478. ISBN 0·306·44104·7
98. Wittig A, Sauerwein WA, Coderre JA (2000) Mechanisms of transport of *p* boronophenylalanine through the cell membrane *in vitro*. Radiat Res 153:173–180
99. Dagrosa MA, Viaggi M, Kreimann E, Farias S, Garavaglia R, Agote M, Cabrini RL, Dadino JL, Juvenal GJ, Pisarev MA (2002) Selective uptake of p-boronophenylalanine by undifferentiated thyroid carcinoma for boron neutron capture therapy. Thyroid 12:7–12
100. Sauerwein W (2005) ^{10}B-uptake in different tumors using the boron compounds BSH and BP. EORTC protocol 11001 Version 2.0. EORTC boron neutron capture therapy group. European Organization for Research and Treatment of Cancer, Bruxelles, 2005
101. Van Rij CM, Sinjewel A, Van Loenen AC, Sauerwein WAG, Wittig A, Kriz O, Wilhelm AJ (2005) Stability of ^{10}B-L-boronophenylalanine-fructose injection. Am J Health Syst Pharm 62:2608–2610
102. Chanana AD (1998) Request for extension of shelf-life for BPA-fructose solutions for patient infusions. FDA report # 43,317. 15-6-1998
103. Belkhou R, Abbe J-C, Pham P, Jasner N, Sahel J, Dreyfus H, Moutaouakkil M, Massarelli R (1995) Uptake and metabolism of boronophenylalanine in human uveal melanoma cells in culture. Relevance to boron neutron capture therapy of cancer cells. Amino Acids (Vienna) 8:217–229
104. Papaspyrou M, Feinendegen LE, Muller-Gartner HW (1994) Preloading with L-tyrosine increases the uptake of boronophenylalanine in mouse melanoma cells. Cancer Res 54: 6311–6314
105. Matalka KZ, Bailey MQ, Barth RF et al (1993) Boron neutron capture therapy of intracerebral melanoma using boronophenylalanine as a capture agent. Cancer Res 53:3308–3313
106. Gregoire V, Huiskamp R, Verrijk R, Begg AC (1992) Comparative pharmacokinetics and distribution studies of boric acid, L-BPA and BSH in two murine tumour models. In: Allen BJ, Moore DE, Harrington BV (eds) Progress in neutron capture therapy for cancer, vol S. Plenum Press, New York and London, pp 443–445. ISBN 0·306·44104·7
107. Gregoire V, Begg AC, Huiskamp R, Verrijk R, Bartelink H (1993) Selectivity of boron carriers for boron neutron capture therapy: pharmacological studies with borocaptate sodium, L-boronophenylalanine and boric acid in murine tumors. Radiother Oncol 27:46–54
108. Pignol JP, Oudart H, Chauvel P, Sauerwein W, Gabel D, Prevot G (1998) Selective delivery of ^{10}B to soft tissue sarcoma using ^{10}B-L-borophenylalanine for boron neutron capture therapy. Br J Radiol 71:320–323
109. Morris GM, Coderre JA, Micca PL, Fisher CD, Capala J, Hopewell JW (1997) Central nervous system tolerance to boron neutron capture therapy with p-boronophenylalanine. Br J Cancer 76:1623–1629
110. Joel DD, Coderre JA, Micca PL, Nawrocky MM (1999) Effect of dose and infusion time on the delivery of p-boronophenylalanine for neutron capture therapy. J Neurooncol 41: 213–221
111. Kiger WS, Palmer MR, Riley KJ, Zamenhof RG, Busse PM (2001) A pharmacokinetic model for the concentration of ^{10}B in blood after boronophenylalanine-fructose administration in humans. Radiat Res 155:611–618
112. Svantesson E, Capala J, Markides KE, Pettersson J (2002) Determination of boron-containing compounds in urine and blood plasma from boron neutron capture therapy patients. The importance of using coupled techniques. Anal Chem 74:5358–5363
113. Coderre JA, Gavin PR, Capala J, Ma R, Morris GM, Button TM, Aziz T, Peress NS (2000) Tolerance of the normal canine brain to epithermal neutron irradiation in the presence of p-boronophenylalanine. J Neurooncol 48:27–40
114. Taniyama K, Fujiwara H, Kuno T et al (1989) Acute and subacute toxicity of ^{10}B-paraboronophenylalanine. Pigment Cell Res 2:291–296

115. Kulvik M, Vahatalo J, Buchar E et al (2003) Clinical implementation of 4-dihydroxyborylphenylalanine synthesised by an asymmetric pathway. Eur J Pharm Sci 8:155–163
116. Wambersie A, Gahbauer RA, Whitmore G, Levin CV Dose and volume specification for reporting NCT: an ICRU-IAEA initiative. Current status of neutron capture therapy (International Atomic Energy Agency Report No. IAEA-TECDOC-1223, 2001), pp 9–10
117. Setiawan Y, Halliday GM, Harding AJ, Moore DE, Allen BJ (1995) Effect of L-^{10}B-p-boronophenylalaninefructose and the boron neutron capture reaction on mouse brain dopaminergic neurons. Cancer Res 55:874–877
118. Coderre JA, Morris GM, Kalef-Ezra J et al (1999) The effects of boron neutron capture irradiation on oral mucosa: evaluation using a rat tongue model. Radiat Res 152:113–118
119. Coderre JA, Kalef-Ezra JA, Fairchild RG, Micca PL, Reinstein LE, Glass JD (1988) Boron neutron capture therapy of a murine melanoma. Cancer Res 48:6313–6316
120. Tamaoki N, Ueda M, Tamauchi S, Yamamoto K, Mishima Y (1989) Use of nude mice in experimental neutron capture therapy with ^{10}B-BPA. Pigment Cell Res 2:343–344
121. Ono K, Masunaga S, Suzuki M, Kinashi Y, Takagaki M, Akaboshi M (1999) The combined effect of boronophenylalanine and borocaptate in boron neutron capture therapy for SCCVII tumors in mice. Int J Radiat Oncol Biol Phys 43:431
122. Barth RF, Yang W, Rotaru JH et al (1997) Boron neutron capture therapy of brain tumors: enhanced survival following intracarotid injection of either sodium borocaptate or boronophenylalanine with or without blood–brain barrier disruption. Cancer Res 57:1129–1136
123. Barth RF, Yang W, Bartus RT, Moeschberger ML, Goodman JH (1999) Enhanced delivery of boronophenylalanine for neutron capture therapy of brain tumors using the bradykinin analog cereport (receptor-mediated permeabilizer-7). Neurosurgery (Baltimore) 44:351–359
124. Yang W, Barth RF, Bartus RT et al (2000) Improved survival after boron neutron capture therapy of brain tumors by cereport-mediated blood–brain barrier modulation to enhance delivery of boronophenylalanine [in process citation]. Neurosurgery 47:189–197
125. Mallesch JL, Moore DE, Allen BJ, McCarthy WH, Jones R, Stening WA (1994) The pharmacokinetics of p-boronophenylalanine fructose in human patients with glioma and metastatic melanoma. Int J Radiat Oncol Biol Phys 28:1183–1188
126. Wittig A, Sheu-Grabellus S-Y, Collette L, Moss R, Brualla L, Sauerwein W (2011) BPA uptake does not correlate with LAT1 and Ki67 expressions in tumor samples (results of EORTC trial 11001). Appl Radiat Isot 69:1807–1812
127. Bergenheim AT, Capala J, Roslin M, Henriksson R (2005) Distribution of BPA and metabolic assessment in glioblastoma patients during BNCT treatment: a microdialysis study. J Neurooncol 71(3):287–293
128. Liberman SJ, Dagrosa A, Jimenez Rebagliati RA, Bonomi MR, Roth BM, Turjanski L, Castiglia SI, Gonzalez SJ, Menendez PR, Cabrini R, Roberti MJ, Batistoni DA (2004) Biodistribution studies of boronophenylalanine-fructose in melanoma and brain tumor patients in Argentina. Appl Radiat Isot 61(5):1095–1100
129. Fukuda H, Honda C, Wadabayashi N, Kobayashi T, Yoshino K, Hiratsuka J, Takahashi J, Akaizawa T, Abe Y, Ichihashi M, Mishima Y (1999) Pharmacokinetics of ^{10}B-p-boronophenylalanine in tumours, skin and blood of melanoma patients: a study of boron neutron capture therapy for malignant melanoma. Melanoma Res 9(1):75–83
130. Chadha M, Capala J, Coderre JA, Elowitz EH, Iwai J, Joel DD, Liu HB, Wielopolski L, Chanana AD (1998) Boron neutron-capture therapy (BNCT) for glioblastoma multiforme (GBM) using the epithermal neutron beam at the Brookhaven National Laboratory. Int J Radiat Oncol Biol Phys 40(4):829–834
131. Zonta A, Prati U, Roveda L, Ferrari C, Valsecchi P, Trotta F, DeRoberto A, Rossella C, Bernardi G, Zonta C, Marchesi P, Pinelli T, Altieri S, Bruschi P, Fossati F, Barni S, Chiari P, Nano R (2000) La terapia per cattura neutronica (BNCT) dei tumori epatici. Boll Soc Med Chir 114(2):123–144
132. Altieri S, Bortolussi S, Bruschi P, Chiari P, Fossati F, Stella S, Prati U, Roveda L, Zonta A, Zonta C, Ferrari C, Clerici A, Nano R, Pinelli T (2008) Neutron autoradiography imaging of selective boron uptake in human metastatic tumours. Appl Radiat Isot 66(12):1850–1855

133. Cardoso J, Nievas S, Pereira M, Schwint A, Trivillin V, Pozzi E, Heber E, Monti Hughes A, Sanchez P, Bumaschny E, Itoiz M, Liberman S (2009) Boron biodistribution study in colorectal liver metastases patients in Argentina. Appl Radiat Isot 67(7–8 Suppl):S76–S79
134. Pisarev MA, Dagrosa MA, Juvenal GJ (2005) Application of boron neutron capture therapy to the treatment of anaplastic thyroid carcinoma: current status and future perspectives. Curr Opin Endocrinol Diabetes 12(5):352–355
135. Wittig A, Sheu S-Y, Kaiser GM, Lang S, Jöckel K-H, Moss R, Stecher-Rasmussen F, Rassow J, Collette L, Sauerwein W (2008) New indications for BNCT? Results from the EORTC trial 11001. In: Zonta A, Altieri S, Roveda L, Barth R (eds) Neutron capture therapy: a new option against cancer. ENEA (Italian National Agency for New Technologies, Energy and the Environment), Florence, pp 39–42. ISBN 88-8286-167-8
136. Coderre JA (1992) A phase 1 biodistribution study of p-boronophenylalanine. In: Gabel D, Moss R (eds) Boron neutron capture therapy: towards clinical trials of glioma treatment. Plenum Press, New York, pp 111–121
137. Cruickshank GS, Ngoga D et al (2009) A cancer research UK pharmacokinetic study of BPA-mannitol in patients with high grade glioma to optimise uptake parameters for clinical trials of BNCT. Appl Radiat Isot 67(7–8 Suppl):S31–S33
138. Ryynanen PM, Kortesniemi M, Coderre JA, Diaz AZ, Hiismaki P, Savolainen SE (2000) Models for estimation of the (10)B concentration after BPA-fructose complex infusion in patients during epithermal neutron irradiation in BNCT. Int J Radiat Oncol Biol Phys 48:1145–1154
139. Wittig A, Sauerwein W, Moss R, Stecher-Rasmussen F, Nivaart V, Grabbe S, Heimans J, Collette L, van Loenen A, Buehrmann S, Roca A, Hoving A, Rassow J (2006) Early phase II study on BNCT in metastatic malignant melanoma using the boron carrier BPA (EORTC protocol 11011). In: Nakagawa Y, Kobayashi T, Fukuda HE (eds) Advances in neutron capture therapy 2006. Proceedings of ICNCT-12 Y. International Society for Neutron Capture Therapy, Kagawa, 2006, pp 284–287
140. Mauri P, Basilico F, Wittig A, Heimans J, Huiskamp R, Sauerwein W (2006) Pharmacokinetics and metabolites of ^{10}B-containing compounds in biological fluids. In: Nakagawa Y, Kobayashi T, Fukuda HE (eds) Advances in neutron capture therapy 2006. Proceedings of ICNCT-12. International Society for Neutron Capture Therapy, Kagawa, 2006, pp 271–273
141. Coderre JA, Morris GM, Kalef-Ezra J, Micca PL, Ma R, Youngs K, Gordon CR (1999) The effects of boron neutron capture irradiation on oral mucosa: evaluation using a rat tongue model. Radiat Res 152(2):113–118
142. Kiger WS 3rd, Micca PL, Morris GM, Coderre JA (2002) Boron microquantification in oral mucosa and skin following administration of a neutron capture therapy agent. Radiat Prot Dosimetry 99(1–4):409–412
143. Morris GM, Smith DR, Patel H, Chandra S, Morrison GH, Hopewell JW, Rezvani M, Micca PL, Coderre JA (2000) Boron microlocalization in oral mucosal tissue: implications for boron neutron capture therapy. Br J Cancer 82(11):1764–1771

Part III

Analysis and Imaging

Boron Analysis and Boron Imaging in BNCT

9

Andrea Wittig and Wolfgang A.G. Sauerwein

Contents

A. Wittig (✉)
Department of Radiotherapy and Radiation Oncology, Philipps-University Marburg, Marburg, Germany
e-mail: andrea.wittig@uni-due.de

W.A.G. Sauerwein
NCTeam, Department of Radiation Oncology, University Hospital Essen, University Duisburg-Essen, D-45122, Essen, Germany
e-mail: w.sauerwein@uni-due.de

W.A.G. Sauerwein et al. (eds.), *Neutron Capture Therapy*,
DOI 10.1007/978-3-642-31334-9_9, © Springer-Verlag Berlin Heidelberg 2012

9.1 Introduction

Boron has two stable naturally occurring isotopes, ^{10}B and ^{11}B, with natural abundance of approximately 19 and 81 %, respectively. In biology, boron is an essential trace element for the growth of higher plants. Even in organisms in which boron is present but has not been established as essential (e.g., animals and humans), this element has been recognized to be beneficial.

Boron neutron capture therapy (BNCT) exploits the ability of the isotope ^{10}B to capture thermal neutrons with a very high probability, leading to the nuclear reaction $^{10}B(n,\alpha,\gamma)^{7}Li$. This reaction produces 478 keV gamma rays, He-4 particles, and Li-7 recoil ions, the latter two having high linear energy transfer (LET) properties and a high relative biological effectiveness (RBE) relative to photon irradiation. The range of these particles in tissue is limited to 8 and 4 μm, respectively, which restricts their effects to one cell diameter. Therefore, if the ^{10}B can be selectively delivered to tumor cells, the short range of the high LET-charged particles offers the potential for a targeted irradiation of individual tumor cells [1, 2].

The energy released in matter by the α and ^{7}Li particles is inhomogeneous. As the range of these particles is so small, the clinical efficacy of the therapy is only guaranteed if the boron is located inside a tumor cell and ideally close to the cell nucleus.

It is therefore a crucially important requirement to investigate the physiological and pharmacological behavior of the ^{10}B in the patient. The methods used should be suitable for accurately measuring the bulk ^{10}B concentration in tissue and fluids such as blood and urine as well as its microscopic spatial distribution at the cellular or subcellular level. Ideally, these methods should be noninvasive, allowing for in vivo measurements in the patient, and results should be obtained within a time period allowing for clinical decisions based on such results.

The following sections describe methods for measuring the quantitative distribution of boron and boron compounds on a microscopic and macroscopic level. All methods have been used in BNCT applications both in preclinical and clinical investigations and have partly been adapted for this special purpose. This chapter aims at describing and comparing these methods with emphasis on a short technical background, the specific endpoint, application possibilities complexity, and pitfalls. This chapter condenses a more detailed description especially of technical aspects as published in 2008 [2], which might be additionally consulted by the interested reader.

9.2 Description of Methods

9.2.1 Prompt Gamma-Ray Spectroscopy

Prompt gamma-ray analysis (PGRA) is a fast method for measuring the average ^{10}B content in macroscopic samples [3–5], which has been used in BNCT studies since many years [6–10].

The principle of PGRA is based on gamma-ray spectroscopy following neutron capture in ^{10}B. The recoiling ^{7}Li nuclei from the $^{10}B(n, \alpha)^{7}Li$ reaction decays to the ground state of ^{7}Li by the emission of 478 keV photons. The emission rate of the photons is proportional to the reaction rate of the neutron capture reaction and therefore carries information of the ^{10}B concentration. Among other possibilities, nuclear reactors provide the most usual sources of neutrons. Often, filtering systems are needed to produce a beam of neutrons with the appropriate quality. Other elements present in the sample also emit photons after neutron capture, the most relevant being the 2.2 MeV photon from the $^{1}H(n, \gamma)$ reaction. The count rate of this hydrogen line can be used as a neutron fluence monitor [11].

Of note, exclusively the ^{10}B isotope can be quantified with this method. PGRA is not applicable for ^{11}B and only indirectly applicable for the naturally occurring B isotope if the ^{10}B to ^{11}B ratio is precisely known.

The content of the ^{10}B line in PGRA for an unknown sample must be calibrated against ^{10}B reference samples with known ^{10}B concentrations. Intercalibration between PGRA and other methods for ^{10}B quantitation, is mandatory for the detection of possible systematic errors.

Sample changing and ^{10}B analysis can be fully automatized. Facilities operating 24 h a day are therefore suited to process a large number of samples. Sample preparation is quite simple. For liquid samples (e.g., blood, urine), a fixed volume is injected into a standard vial and then weighted. Tissue samples are just weighted. The vials are positioned in a sample changer, which allows for automatic measurements.

Present PGRA facilities provide fast (about 5 min/sample), accurate (standard deviation about 0.5 ppm), and nondestructive measurements of ^{10}B concentrations down to 1 ppm, suited for macroscopic samples (0.4–1.0 ml) of tissue, blood, and urine.

The major limitation of this method, the relatively large sample size, can be further reduced by improvement of the shielding and the geometry of the facility to decrease the background in the gamma-ray spectra. PGRA measures the integral ^{10}B concentration within a sample; therefore, it cannot show any inhomogeneities of the ^{10}B concentration within a possibly inhomogeneous sample. Such inhomogeneities can however be relevant in BNCT as the tissue volume, which can be measured with PGRA, is far bigger than the volume irradiated with a boron neutron capture reaction.

The PGRA has been applied to quality control of the compounds BSH and BPA, boron uptake studies, pharmacokinetic studies, and blood-boron concentration measurements during BNCT of patients [2, 5]. The latter is an important tool for the patient treatment planning adjustment and dosimetry during BNCT: the measured ^{10}B concentration in the blood of a patient can be used to adjust the calculated pharmacokinetic curve to the actual situation of an individual patient. This allows readjustment of the calculated beam exposure time during a BNCT treatment to reach the intended total absorbed dose. To make such adjustment during a BNCT treatment, a very quick analytical method is mandatory, as is the case for PGRA. As of today, PGRA is the only available tool for such purpose; therefore, the method plays an essential role for clinical BNCT [2].

Further application of PGRA for BNCT includes the possibility of in vivo gamma-ray spectroscopy of the patient during treatment [12, 13]. The gamma-ray telescope can provide in vivo dosimetry and measurement of ^{10}B concentrations, averaged over

a volume of several cm^3 and over a time interval of about 2 min. This method, however, needs further improvement for implementation in a clinical routine [2].

9.2.2 Inductively Coupled Plasma Spectroscopy

Inductively coupled plasma atomic emission spectroscopy (ICP-AES), also referred to as inductively coupled plasma optical emission spectrometry (ICP-OES), is an emission spectrophotometric technique, exploiting the fact that excited electrons emit energy at a given wavelength as they return to ground state. The fundamental characteristic of this process is that each element emits energy at specific wavelengths peculiar to its chemical character. Thus, by determining which wavelengths are emitted by a sample and by determining their intensities, the elemental composition of the given sample relative to a reference standard can be quantified [2].

ICP-MS (inductively coupled plasma mass spectrometry) is a type of mass spectrometry that is highly sensitive and capable of the determination of a range of metals and several nonmetals at concentrations below one part in $10 \times E^{12}$. It is based on coupling an inductively coupled plasma as a method of ionization with a mass spectrometer as a method of separating and detecting the ions. ICP-MS is also capable of monitoring isotopic speciation for the ions of choice such as the individual isotopes of boron with the atomic masses of 10 and 11. Hence, ICP-MS can quantify each isotope individually.

ICP-MS methods are applicable to quantify boron at ppb levels in serum, plasma, urine, saline, water, and tissue. Boron isotopes are determinable with better than 2 % relative standard deviation (RSD), which means very accurate data can be obtained using isotope dilution. While the sensitivity of ICP-MS for boron and other elements is excellent, their backgrounds, their tendency to adsorb onto glass, and their chemistry all have to be controlled for successful quantitative analysis in complex matrices such as biological fluids or tissues [2]. Therefore, a rugged, validated analytical procedure for sample preparation and analysis using ICP-MS is to be demanded for boron determination.

The principal concerns when using ICP-MS for isotopic determinations of boron are memory effects and mass discrimination. Special washing agents help preventing the memory effect [2]. Mass discrimination between ^{11}B and ^{10}B is accentuated due to the 10 % isotopic mass difference and arises during ion transport caused by instrumental adjustments or by the sample matrix [14]. The instrumental effect is corrected by analyzing a reference standard with a certified $^{11}B/^{10}B$ ratio [15]. The sample matrix effect on mass discrimination can be corrected using internal standards [16, 17].

The ICP-MS is often the method of choice over ICP-OES and spectrophotometric methods for analysis of boron [18]. The advantages of ICP-MS over other methods are higher sensitivity, lower detection limits, and simultaneous measurement of ^{10}B to ^{11}B isotopic ratio and total B concentration in a sample. The ability of ICP-MS to measure B isotope ratios renders this instrument especially suitable for biological B tracer studies [19].

The detection limits are at the ppb level, e.g., 1 ppb [20] to 3 ppb [18] in biological materials, 0.15 ppb in saline waters [16], and 0.5 ppb in human serum [21]. The uniqueness of ICP-MS is also due to its capability to carry out B determination by the isotope dilution method which is considered the most precise for quantitative determination. Laakso et al. [22] compared both the ICP-MS as well as the ICP-AES (ICP-OES) method and found a strong correlation between results of the ICP-AES and ICP-MS ($r = 0.994$). They concluded, that their established ICP-AES method is also feasible, accurate, and one of the fastest for boron determination during BNCT. ICP-AES has been applied to quality control of the compounds and boron uptake studies as well as boron concentration measurements in blood of patients [23].

ICP-MS is a reliable technique for the determination of the mean concentration of total boron and mean isotopic ratios of boron in biological samples. It is possible to quantify boron in liquids and – after suitable disintegration – in tissue samples. In contrast to PGRA which measures the mean ^{10}B concentration in a sample, an irradiation with neutrons is not necessary, and therefore the method is independent of a nuclear reactor site. ICP-MS however is destructive. It is not appropriate for imaging the distribution of boron in histological preparations [2].

9.2.3 High-Resolution Alpha Autoradiography, Alpha Spectroscopy, and Neutron Capture Radiography

9.2.3.1 High-Resolution Alpha Autoradiography

The first experiments in which a neutron-induced nuclear reaction was utilized to image a stable nuclide in a sample was reported by Ficq [24] and reported in the context of BNCT first by Edwards [25]. Subsequently, variants of Edwards' approach that provide cellular level spatial resolution have been reported by Solares et al. [26, 27] and Yam et al. [28]. These approaches are based on the transient activation of the stable isotope ^{10}B using thermal neutron activation to convert ^{10}B to the unstable isotope ^{11}B. ^{11}B disintegrates into alpha and ^{7}Li particles sharing 2.3–2.4 MeV of kinetic energy between them. These charged particles have corresponding ranges in tissue of 8 and 4 μm, respectively, making the mapping of these particles a useful surrogate measurement of the ^{10}B distribution itself.

The high-resolution alpha-track autoradiography (HRAR) is possible in small tissue samples, which are surgically removed after ^{10}B compound administration and immediately frozen. One to two μm thick histological frozen tissue sections are cut and mounted on top of submicrometer thick Ixan and Lexan films on top of a quartz glass slide. The quartz slide/tissue/Ixan/Lexan units are packed with dry ice and irradiated with thermal neutrons. Upon completion of irradiation, the tissue sections are histologically stained. The quartz glass slide is then remounted in contact with the tissue section on the opposing side of the unit thereby exposing the Lexan film. During neutron irradiation, the interaction of the alpha- and ^{7}Li-charged particles with the Lexan film from the ^{10}B neutron capture reactions in the frozen tissue causes molecular weakening of the Lexan along the paths of these particles.

Chemically etching the exposed surface of the Lexan film yields optically visible 1–2-μm diameter tracks. The Ixan film located between the frozen tissue section and the Lexan film act as a chemical barrier ensuring that the corrosive etchant fluid seeping through the etched tracks does not damage the stained tissue. Finally, digital microphotographs are taken of the superimposed tracks and stained tissue sections. Correlation of the distribution of tracks with the anatomical features of the stained tissue provides maps of ^{10}B distribution in the tissue. A calibration curve of track density in standard tissues vs. known concentration of boron provides the ability to relate the observed track densities in the experimental tissue samples to absolute boron concentrations. The HRAR calibration curve is highly linear over the entire range of boron concentrations of interest. Saturation effects at the high end of the calibration curve can be corrected by irradiation with lower thermal neutron fluence. This approach of track counting as opposed to film darkening, as utilized in boron neutron capture radiography, provides a more quantitative analysis of the boron distribution in tissue but does not provide the useful macroscopic visual depiction of boron distribution that is extremely useful for many applications in BNCT [2].

The method has been used to study the boron concentration in normal tissues and tumors BNCT animal models, e.g., rat tongue and brain [29, 30].

Another level of analysis using HRAR at the initial stage first described by Solares et al. [31] and Kiger et al. [30] uses a Monte Carlo code to simulate the trajectories of the alpha- and ^{7}Li-charged particles within the tissue using the measured track locations from the HRAR images to determine the number of nuclear "hits" and other important microdosimetric quantities. This approach investigates the more realistic domain of the expected responses of normal and tumor tissues to BNCT [2].

9.2.3.2 Neutron Capture Radiography

Neutron capture radiography (NCR) can be combined with particle spectroscopy and histological analysis of neighboring tissue sections to measure the ^{10}B concentration and its spatial distribution in relation to the histological information [32–36]. Unlike the HRAR technique, NCR provides intuitive visualization of the boron distribution, which may also be quantified on a macroscopic scale by densitometric analysis [37]. The ^{10}B concentration is measured using the spectroscopy of charged particles [38] emitted in the boron neutron capture reaction and is then spatially correlated with stained tissue sections. Tissue sample of a few millimeter thickness and an area of approximately 0.5 cm^2 is needed for the NCR technique. The tissue is cryofixed by immersion of the sample into liquid nitrogen to statically "freeze" the physiological distribution of the ^{10}B-containing molecule. For each measurement, a minimum of three neighboring slices are cut from the tissue block using a cryostat operating at a temperature of −20 °C.

1. The first section cut is deposited on a Mylar disk for charged particle spectroscopy.
2. The second section is deposited on a glass slice for histological analysis by hematoxylin-eosin staining using a light microscope coupled with software for

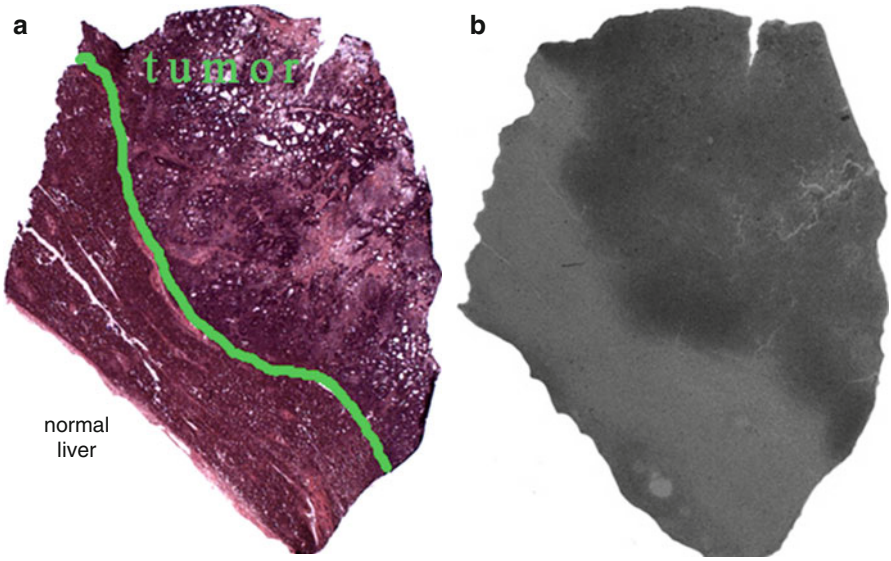

Fig. 9.1 Comparison between (**a**) histology and (**b**) neutron capture radiography of a liver sample from a patient with liver metastases of colorectal adenocarcinoma after infusion of BPA. The tumor zone is above the *green line* while normal liver is below it. In the neutron capture radiography image the *darker zone* (higher boron concentration) corresponds to the tumor while the *lighter one* (lower boron concentration) corresponds to normal liver. The boron concentration ratio between tumor and liver is about 3×. The tissue sample is 7 mm × 10 mm × 10 μm thick (S. Altieri, Department of Nuclear and Theoretical Physics, University of Pavia, and National Institute of Nuclear Physics (INFN) – Pavia Section, Pavia, Italy) (Reprinted from Wittig et al. [2])

image analysis. It is optimized to gain information on the biological composition of the sample, especially to evaluate the percentage of tumor cells, healthy parenchyma, necrosis, fibrosis, mucus, blood vessels, and other tissues in a specific sample.

3. The third slice is deposited on a solid state nuclear track detector for imaging of the macroscopic boron distribution by neutron capture radiography (NCR).

The third tissue slice is positioned on a nuclear detection film and exposed to thermal neutrons. At the locations in the tissue sample where a ^{10}B atom is present, an α particle and a ^{7}Li ion are emitted and cause damage to the nuclear detection film. After irradiation, the tissue sample is removed from the film, and the image of the ^{10}B distribution is obtained by chemical etching in a dilute NaOH solution [39]. The distribution of the tracks in the detector is representative of the macroscopic distribution of the ^{10}B atoms in the sample. Using the NCR technique, it is possible to digitally superimpose and compare the histological image with a map of the spatial ^{10}B distribution and relative ^{10}B concentration [2]. One example of such correlation between the macroscopic boron distribution and tissue histology is depicted in Fig. 9.1.

To determine the absolute ^{10}B concentration using particle spectroscopy, section 1 is used. If exclusively normal tissue is present in the sample, the absolute ^{10}B concentration can be directly determined by spectrometric analysis. If the sample

contains both, normal and tumor tissue, the regional tumor tissue ^{10}B concentration can be calculated by subtracting the amount of the boron contained in normal tissue (determined in a tumor-free location based on morphological appearance) from the total ^{10}B content.

The first tissue sample section on Mylar disk is placed in front of a silicone solid state detector (Si detector) in a vacuum container and exposed to thermal neutron irradiation. Alpha particles and ^{7}Li ions induced in the boron by the neutrons are detected in the Si detector and their energy distribution spectra are recorded by a multichannel analyzer.

The experimental error of this method is in the order of ±10 %. The lower limit of detection is approximately 0.5 ppm and is limited by the naturally occurring boron background concentration in tissue. The accuracy of the method depends on the number of counts, the irradiation time, and the number of boron atoms in the sample.

The main advantage of the charged particle spectrometry is the ability to measure the ^{10}B concentration as well as the ^{10}B distribution in a two-dimensional slice of tissue and to directly correlate the spatial information at the macroscopic level to the histology of the specimen analyzed. The lateral resolution of the method is limited to approximately 100 μm.

The necessity to irradiate tissue samples with thermal neutrons limits this method as the other two techniques described in this section to very few specialized nuclear research centers. Moreover, it is not possible to directly measure liquid samples using charged particle spectroscopy as samples have to be measured under vacuum. To obtain absolute results, it is necessary to know the mass stopping power for each material to be analyzed or to use a set of reference standards with known boron concentrations representing typical biological tissue types [2].

9.2.4 Laser Post-ionization Secondary Neutral Mass Spectrometry

The range of the alpha particles from the boron capture reaction is approximately 10 μm. If the irradiated volume is to be investigated, then methods are necessary that have a similar resolution. Determination of boron distributions at the subcellular level is crucial to understanding the behavior of boron compounds in tissues and cells and its impact on radiation response.

Laser post-ionization secondary neutral mass spectrometry (laser-SNMS) and secondary ion mass spectrometry (SIMS) are alternative techniques for element- and molecule-specific imaging. SIMS analysis utilizes a technique in which the sample is bombarded with a focused, energetic ion beam that sputters atoms and molecules off the surface. A fraction of these particles are ejected as ions which are extracted and mass analyzed. Combining SIMS with a time-of-flight mass spectrometer (ToF-SIMS), all masses can be detected simultaneously on each primary ion pulse, and charge compensation for insulator analysis is then possible using pulsed low-energy electrons, which are introduced during the time interval between ion pulses. If a liquid metal ion gun is used, the ion beam can be focused from a few μm down to <200 nm in diameter, enabling analysis with nanometer-scale spatial

resolution. Imaging is carried out either by scanning the ion beam over the sample (500 μm × 500 μm or smaller) or by moving the sample under a fixed ion beam position (up to 10 cm × 10 cm). By combining the imaging technique with an additional sputtering ion beam to remove successive atomic/molecular layers, a three-dimensional image of the chemical composition of the surface can be obtained [2].

Although SIMS has many advantages and has often been used in the dynamic SIMS mode for imaging boronated compounds in cell cultures and tissues [40–45], its application for boron imaging is often limited because of a lack of sensitivity and quantitation. Detection limit, efficiency, and quantitation, however, can be significantly improved by the use of laser-SNMS [46–48]. This technique, with the same technical features as ToF-SIMS, decouples the sputtering and ionization processes by applying laser beams to ionize the majority of neutral particles sputtered from the sample surface. The neutral particles yield is less affected by the chemical composition of the surface than the much smaller yield of secondary ions used for SIMS analysis, resulting in much greater sensitivity and accuracy of laser-SNMS than SIMS. Furthermore, laser-SNMS images are significantly less influenced by topographical effects than SIMS images.

Laser-SNMS has been used for examining the subcellular distribution of intrinsic elements and molecules as well as the potential of BSH and BPA to deliver ^{10}B to tumor cells in vitro and in vivo to cells of experimental tumors and of normal tissues. The analysis of the samples is carried out with a combined gridless reflectron-based laser-SNMS/ToF-SIMS instrument. Ion-induced electron images (IIEI) can be obtained from all samples to select regions of interest for further analysis [2].

In order to be able to analyze the samples in the vacuum system, cryofixation, freeze-fracturing, and freeze-drying of the living cell while preserving its structural and chemical integrity must be carried out [49–51]. A dedicated cryofixation method with very high cooling rate must therefore be used.

Laser-SNMS was used in vitro and in animal experiments employing the described preparation technique to analyze normal tissues and different experimental tumors after treatment of mice with the compounds BPA and BSH. Laser-SNMS simultaneously delivers maps of the distribution of elements and molecules such as K, Na, Ca, CN, and C_3H_8N as well as a distinct boron distribution. Proof of a Na and K concentration and distribution as known from living cells serve to ascertain successful preparation of the tissue.

A challenging task is however correlation of elemental/molecular maps with histological information [2]. Such correlation is possible through analysis of distinct molecular fragments: earlier studies on L-α-dipalmitoylphosphatidylcholine (DPPC) membrane model systems have shown that C_3H_8N is a typical fragment of the choline headgroup of the DPPC [52, 53]. The CN signal contribution originates mainly from DNA (purine and pyrimidine) and proteins. In particular, the subcellular distribution of the membrane-characteristic C_3H_8N signal shows a distinct pattern. The signal almost disappears in the center of some cells. It may be presumed that, in these areas, the nucleic membrane was removed by the fracturing process, leaving behind an open nucleus. In the CN pattern, however, no decreases are observed at the positions where the C_3H_8N signal almost disappears. This can be explained by the fact that CN originates not only from fragments of membrane constituents and

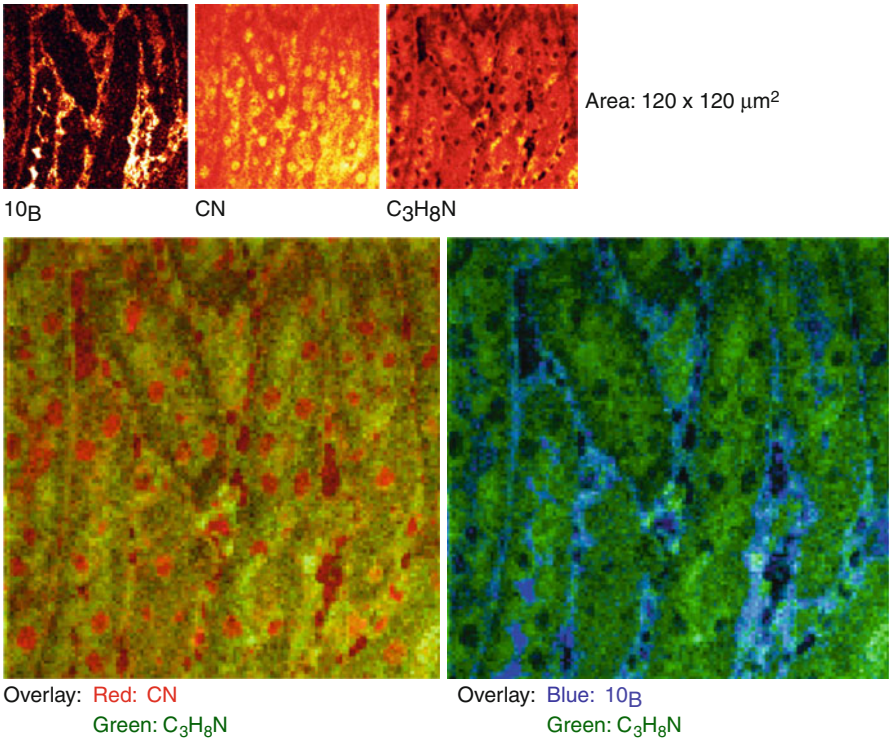

Fig. 9.2 Laser-SNMS images of a kidney sample from a NMRI nude mouse treated with a combination of BPA and BSH (H.F. Arlinghaus, Physikalisches Institut, Westfälische Wilhelms-Universität Münster, Münster, Germany) (Reprinted from Arlinghaus et al. [49])

proteins but also from fragments of DNA constituents such as purine and pyrimidine rings. Therefore, at the site of the nucleus, the CN signal should not disappear.

By overlaying images of the distribution of different molecules with distinct distribution [2], e.g., CN and C_3H_8N, it is possible to denote cell nuclei and cell membranes and to relate the boron signal to such regions. With this method, it is possible to investigate the boron concentration and distribution within single cells. The laser-SNMS has proven ^{10}B as delivered with BSH and BPA within tumor cells and even within the cell nucleus [2].

Figure 9.2 shows an example of laser-SNMS images of a kidney sample from a nude mouse treated with a combination of BPA and BSH. Intensive signals from several elements and molecules such as ^{10}B, CN, and C_3H_8N were observed in the laser-SNMS images (top row). The ^{10}B image (top left) shows a distinct boron distribution. The molecules (top middle and right) represent mainly lipids, proteins, and nucleic acids and also exhibit distinct features. The bottom images show overlay images, where the CN image is overlaid with the C_3H_8N image (bottom left) and ^{10}B with the C_3H_8N image (bottom right). Here, the CN signal, corresponding to nucleus

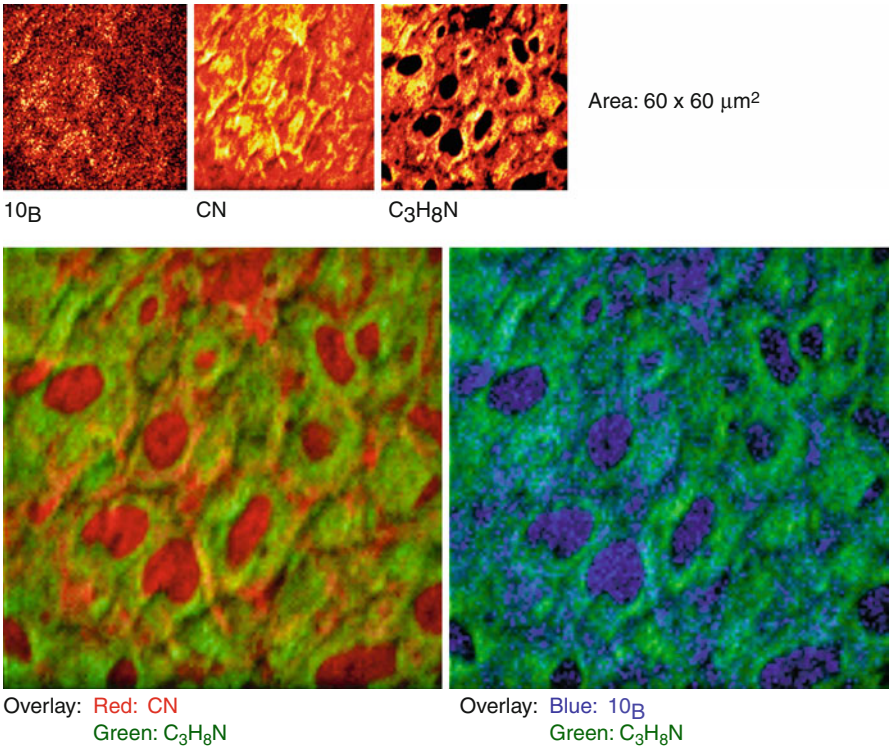

Fig. 9.3 Laser-SNMS images of a murine sarcoma tumor sample from a NMRI nude mouse treated with the compound BPA (H.F. Arlinghaus, Physikalisches Institut, Westfälische Wilhelms-Universität Münster, Münster, Germany) (Reprinted from Arlinghaus et al. [49])

sites, is presented as red, the C_3H_8N as green, and ^{10}B signal as blue in color. Individual kidney tubules and lumen can be identified in the overlay image (tubules surrounded by single cells). The high concentrations of boron are observed especially in the lumen of the tubule, which was cut along its longitudinal axis (bottom left part of the image), and in the basal membrane surrounding the tubules.

Figure 9.3 shows an image of a murine sarcoma grown in a mouse treated with BPA [2]. The top row shows the ^{10}B, CN, and C_3H_8N images again showing distinct distributions. The bottom row demonstrates images where CN is overlaid with C_3H_8N (bottom left) and ^{10}B is overlaid with C_3H_8N (bottom right). Here, the highest ^{10}B signal is presented as blue and the highest CN signal, which again denotes the nuclei, as red.

In summary, the cryopreparation techniques described preserve the structural and chemical integrity of cell cultures and tissues and make cellular structures directly accessible for laser-SNMS analysis. In particular, where molecular images are available, different functional areas of the cells can be identified. Laser-SNMS is particularly well suited for identifying specific cell structures and for imaging ultratrace ^{10}B concentrations in tissues with nanometer-scale lateral resolution and a detection limit in the upper ppb renage. These possibilities make laser-SNMS a very

valuable tool in directly imaging and quantifying ^{10}B and (simultaneously) other elements. Due to the necessity of the demanding preparation of cells or tissues and the challenging measurements, the method is reserved to special questions but not suitable as a routine method for direct clinical decisions [2].

9.2.5 Electron Energy Loss Spectroscopy

Regarding boron imaging, the best spatial resolution is obtained using methods based on electron microscopy. Two such methods exist: immunohistochemistry [54] and electron energy loss spectroscopy (EELS) [55, 56]. Immunochemistry is a very sensitive method, but it has its drawbacks: indirect detection leading to the possibility of artifacts (e.g., redistribution during the fixation process) and the need to prepare a specific antibody for each potential boron carrier molecule. EELS is based on the inelastic scattering of incoming electrons after interaction with the sample electrons. Inelastic scatter results in a characteristic energy loss depending on the atomic or molecular energy level involved. It has been well established that EELS is the most sensitive nanoanalytical method for detecting light elements such as carbon, boron, or even phosphorus and particularly in a biological tissue [57, 58].

Two experimentally different spectroscopic approaches have been derived from this theoretical basis: EELS and electron spectroscopic imaging (ESI), which is an imaging technique coupled with energy-filtering transmission electron microscopy (EFTEM). Furthermore, EELS is an analytical technique generally coupled with transmission or scanning transmission electron microscopy (TEM/STEM). It is important to keep in mind that despite significant experimental differences, these two approaches (EELS and ESI) are based on the same physical signal and that knowledge of the EELS spectrum is required in order to understand and to safely use the EFTEM images. An electron energy loss spectrum corresponds to the counting of the electrons passing through a defined area of the sample.

A critical point in the study of elemental distributions in tissues and cells is sample preparation. A cryopreparation method, avoiding any chemical treatments, has to be used in order to immobilize also small molecules and ions close to their positions in the natural state. It implies successive cryofixation, cryosectioning, and cryo-observation. A specific step in EELS is the need for ultrathin cryosections (100 nm or less), which are freeze-dried inside the microscope by raising the temperature to 193 K and finally investigated at a temperature below 110 K.

The boron signal in the EELS spectrum is very weak and superimposed over a strong noncharacteristic background, which requires a dedicated method based on digital filtering to extract the signal [59]. Moreover, the boron K edge located at 188 eV can be confused with the phosphorus L1 signal. Consequently, the experimental filtered spectrum has to be modeled as a sum of a boron-filtered reference and a phosphorus-filtered reference spectrum [56]. Neglecting the phosphorus signal can lead to erroneous images, where boron is systematically detected in phosphorus-rich regions. This problem has also to be resolved using ESI. The detection limits can be estimated to be around a few tens of ppm in, for a sample area of 0.1 μm^2 (see Ref. [56] for details of the method for boron detection and quantification).

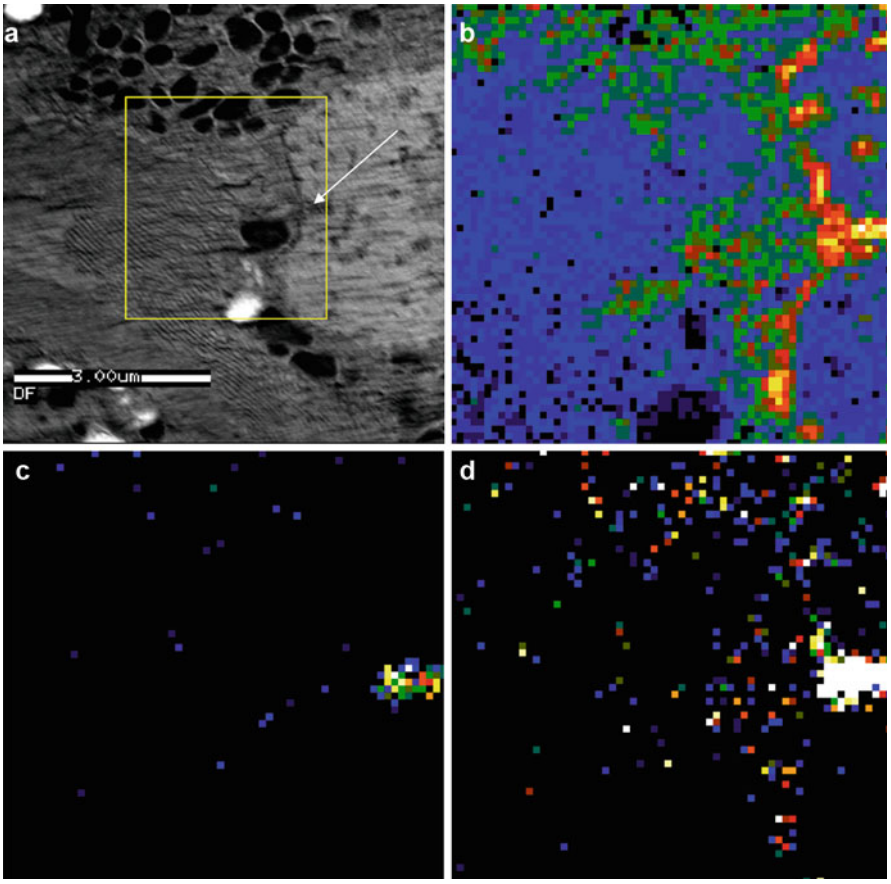

Fig. 9.4 (**a**) Dark-field STEM image (inverted contrast) of a freeze-dried cryosection of mouse kidney tissue. (**b**) Phosphorus map, (**c**) corrected boron map, (**d**) uncorrected boron map (J. Michel, Laboratoire de Microscopie Electronique Analytique, INSERM ERM 0203, Université de Reims Champagne-Ardenne, Reims, France) (Reprinted from Michel et al. [90])

Boron imaging is performed using the spectrum-imaging acquisition mode in which a spectrum is collected from each pixel in a defined STEM image area. In order to reveal the boron signal, each spectrum is processed (digital filtering, multiple least-squares fitting). Measured signals can then be presented as elemental maps to be correlated with the STEM image (Fig. 9.4) [2].

Measurements using EELS, thanks to their high spatial resolution, are most complementary to sensitive measurements obtained by other methods, such as SIMS or a nuclear microprobe technique. In this way, EELS can be a very specific tool to detect small accumulation areas of boron or boron compounds and to localize them at the subcellular level. Furthermore, a lack of boron in the EELS measurement in samples where boron is detected by other methods on a larger scale implies a homogeneous distribution of boron at the subcellular level in the limits of the EELS detection sensitivity. Boron detection by is independent of the isotopic form of

the element. The isotope ^{10}B cannot be discerned from ^{11}B in the measurements. ^{10}B contents have to be deduced from the previously known relative abundance of the different isotopes which can increase uncertainties in the final quantitative values. Similar to SIMS, EELS is an important data source for BNCT; the complexity of sample preparation, measurement, and data processing however prevents using EELS as a routine method [2].

9.2.6 Ion Trap Mass Spectrometry and Proteomic Technologies

The analytical methods described in the previous sections are usually applied to detect the isotope ^{10}B only, but cannot be used to analyze and characterize the specific molecule of the relevant ^{10}B-containing compound under investigation, which is highly desirable in in vivo and in clinical investigations.

This is however possible with ion trap mass spectrometry and proteomic technologies. For this technique, a liquid sample is injected into the mass spectrometer by means of electrospray interface (ESI). Thereafter, fragmentation of each specific molecule is performed using the ion trap mass spectrometer (tandem mass spectrometry) that allows isolation and fragmentation in the same space [60]. Ion trap mass spectrometry monitors the entire MS/MS spectrum with the same sensitivity. Mauri [61] proposed an analytical method using flow injection coupled with tandem mass spectrometry (FI/ESI-MS/MS) in order to obtain quantitative data of the boron carrier molecules. For such analysis, a sample is flow injected (FI) through an HPLC injector (injected volume approximately 1 μl) into the ESI-MS/MS system [2].

BSH is detected in a negative mode, and the main ion is *m/z* 187.4, corresponding to $[(^{10}B_{12}H_{11}SH)Na]^-$, while the product of its MS/MS fragmentation is an ion with an *m/z* of 131.5, due to the loss of the [SNa] residue. The dimer (BSSB) of BSH has a molecular weight of *m/z* 395.7, and its fragment ion is *m/z* 391.9 [61]. The detection of BPA has been performed in a positive mode, and its molecular and fragment ions are *m/z* 209.1 and *m/z* 163.1, respectively.

The FI/ESI-MS/MS methodology results in typical fingerprinting mass spectra of boron derivatives and allows for their quantitative determination [62]. When extracting the specific fragment ions, a linear relationship between the peak area and the concentration of the ^{10}B-containing compound is found in the range of 10–10,000 ng/ml.

The high sensitivity of the FI/ESI-MS/MS method allows for dilution of biological samples, which reduces the matrix effect occurring due to the high salt concentrations in urine and plasma. High salt concentration produces an overloaded response on the mass spectrometer and reduce the signal (ion suppression) related to the metabolites of interest. ^{10}B-containing compounds could be detected by FI/ESI-MS/MS in biological samples (urine and plasma, diluted 10,000- and 1,000-fold, respectively) when injecting a small volume (1 μl) of the diluted samples [62].

In conclusion, the FI/ESI-MS/MS is a rapid and quantitative method for the analysis of ^{10}B-containing compounds in pharmaceutical preparations and biological samples. The method is particularly suited for analyzing liquid samples. The assay of ^{10}B compounds in tissue samples requires extraction by 50 % methanol [2].

9.2.6.1 Ion Trap and Proteomics

Ion trap mass spectrometry coupled to two-dimensional chromatography (2DC-MS/MS) has been applied to develop a shotgun approach for proteomic studies [63]. It permits the simultaneous characterization of each of many proteins without limits concerning molecular weight or isoelectric point. Quantitative analysis is also possible [64]. This approach, also known as MudPIT (multidimensional protein identification technology), is very useful in clinical proteomics for biomarker discovery and to identify molecular targets for new drugs. This translational research aspect can also be applied for BNCT [65]. The MudPIT proteomic approach can be used for characterizing protein profiles of biological samples (urine and tissues) after ^{10}B application, investigating the accumulation of boron in cancer cells and combining proteomic with pharmacokinetic data. The use of the above methodologies means that transport, metabolism, and uptake of the different drugs used in BNCT can be investigated in great detail [2].

9.2.7 Nuclear Magnetic Resonance and Magnetic Resonance Imaging

Both the ^{10}B and ^{11}B nuclei are amenable for detection by nuclear magnetic resonance (NMR), and therefore their spatial distribution can be mapped using magnetic resonance imaging (MRI). MRI is a special type of the NMR method where the frequencies of the nuclear spins are encoded according to their locations in space. Moreover, NMR can distinguish between nuclei of the same type in different molecular species (typically through an interaction called "chemical shift") [2].

The sample is placed in the magnetic field of the NMR spectrometer or MRI scanner. Signal excitation and detection is achieved through a properly tuned radio-frequency (RF) coil, which (depending on its geometry) either encompasses the sample or is placed adjacent to it. Energy is delivered by short pulses (10^{-3}–10^{-6} s) and can be absorbed by the nuclear spins if it matches the gaps in energy levels corresponding to different spin states. The frequencies of these transitions are proportional to the strength of the magnetic field and are typically in the order of 10^6–10^8 Hz. The RF pulses perturb the Boltzmann equilibrium of the nuclear spin populations, which decay back to equilibrium after the pulses are turned off. During this return to equilibrium, the nuclei emit signals at their characteristic resonance frequencies, which are detected, digitized, and interpreted to create spectra or images. Immediately after the pulse, the signals from individual spins have the same phase and are therefore summed coherently, which is what makes the total signal detectable. The return to equilibrium proceeds exponentially at a rate characterized by a time constant T_1, which is rather short for ^{10}B and ^{11}B in the molecules used for BNCT. The short T_1 is an advantage for NMR detection because it permits to repeat successive signal excitations at a high rate, which is necessary to gain enough independent input for creating images, and achieving a sufficiently high signal-to-noise (S/N) ratio. The return to equilibrium also results in an irreversible, exponential loss of coherence, characterized by a time constant T_2, which is often significantly shorter than T_1. The short T_2 for ^{10}B and ^{11}B, especially in biological tissue, can be

problematic. The reason is that, for mainly technical reasons, a finite delay between signal excitation and detection is inevitable, and unless this delay is much shorter than T_2 (which is often not the case), a significant part of the signal is lost, which not only decreases the *S*/*N* ratio and sensitivity, but also introduces uncertainties in the quantitation of the boron presence in the sample [2].

NMR is quantitative as the signal is proportional to the total amount of the detected nucleus within the sample volume. For MRI, the image intensity is proportional to the amount of the detected nucleus in a voxel. Therefore, quantitation through comparison with the signal from calibration or reference samples should be straightforward. However, the accuracy of boron quantitation by NMR or MRI can be compromised by several factors, mainly due to the dependence of T_2 on molecular mobility. In practice, only boron in relatively mobile molecules in liquid or liquid-like environments can be properly detected. If the boron atoms themselves, or the molecules containing boron, are tightly bound or attached to entities with high molecular weight (e.g., membranes, proteins, nucleic acids), their NMR signal can either be completely missed or severely underestimated. This problem is usually worse for MRI and in vivo experiments than for "test-tube" spectroscopy, because in the latter case shorter detection "dead times" can be achieved. The quantification accuracy can be improved to some extent by measuring the T_2 decay rates and extrapolating the measured signal intensities to zero decay time [2].

Sensitivity and spatial resolution are inherently connected for MRI of boron compounds. The sensitivity, defined as the "minimum detectable concentration," is inversely proportional to the volume of the image voxel.

One of the aspired applications of boron imaging for BNCT is the real-time monitoring of ^{10}B-enriched compounds administered to patients, in and around the tumor, prior to irradiation with neutrons. This goal has not yet been achieved [66, 67], but due to the high potential, this method strongly deserved further development. Recently, Porcari et al. used (19)F MR Imaging ((19)F MRI) and spectroscopy ((19)F MRS) to evaluate the boron biodistribution and pharmacokinetics of 4-borono-2-fluorophenylalanine ((19)F-BPA) in vivo [68].

One of the most significant advantages of NMR or MRI is that there are relatively few restrictions on sample preparation. The analysis is noninvasive and nondestructive, and can be performed on homogeneous liquid samples but also on intact chunks of tissue, cells, etc. and most important on laboratory animals and human patients. Therefore, NMR has considerable potential to fulfill the desired function of noninvasive mapping of the spatial distribution of the administered ^{10}B carrier in the course of the treatment. Another advantage is its ability to distinguish between different molecular species, thereby providing an opportunity for assessing metabolism for the investigated compound. The main disadvantage is the rather low sensitivity of the method, particularly for imaging (Fig. 9.5) [2].

9.2.8 Positron Emission Tomography

Positron emission tomography (PET) is a key imaging tool in clinical practice and biomedical research to quantify and study biochemical processes in vivo. PET is a

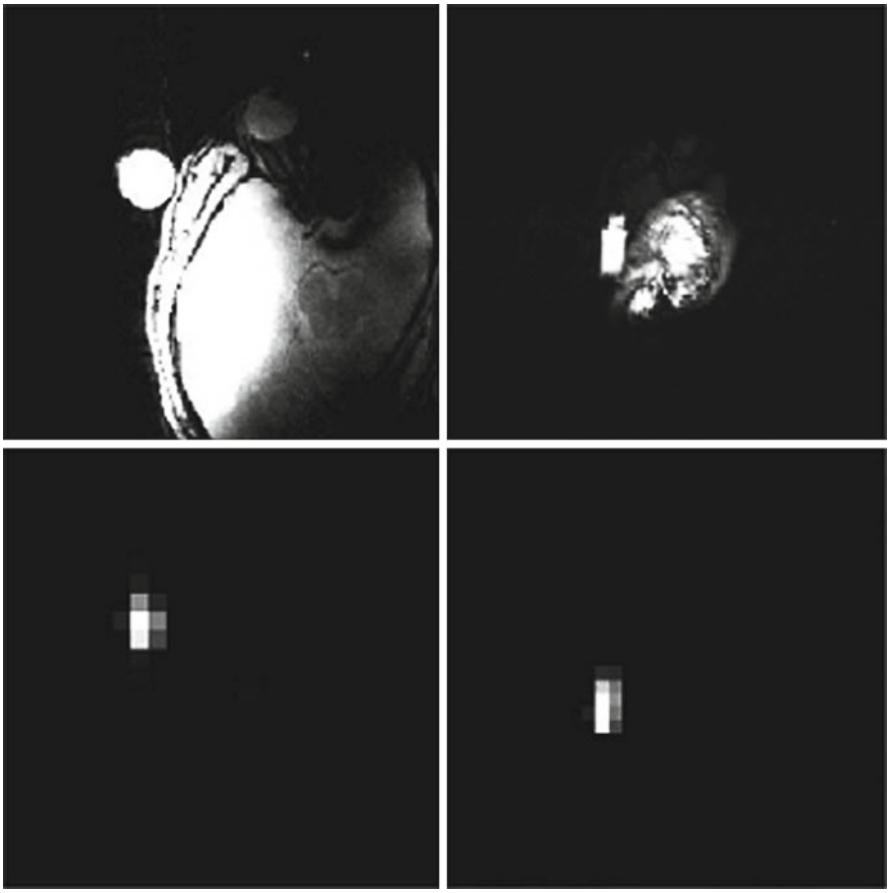

Fig. 9.5 The *upper* ^{1}H *images* show axial (*left*) and sagital (*right*) views through the head of a volunteer, with a cylindrical vial attached close to the ear and the temple. The *lower images* are the ^{10}B images at the corresponding orientations and geometric scale. The vial contained a solution of 28 mM BSH. The ^{10}B images have a voxel size of 1.7 cc (1.2 × 1.2 × 1.2 cm) and are slices through a 3D matrix acquired in under 3 min (P. Bendel, Chemical Research Support Department, The Weizmann Institute of Science, Rehovot, Israel) (Reprinted from Bendel et al. [91])

tracer technique based on the use of labeled molecules carrying a short-lived positron-emitting radionuclide [69]. PET can yield quantitative measurements of the distribution of radioactivity that is present in the scanned field of view (FOV) after correction for physical parameters, such as subject self-attenuation, spurious events (scattered, random), and scanner efficiency calibration. PET data are conveniently displayed in the form of 2D and volumetric 3D images (Bq/voxel). PET images are analyzed by defining regions of interest (ROI) in correspondence with relevant organs or organ substructures to assess activity concentration in the form of peak or average values. PET imaging can also be dynamic, to detect activity changes over an observation period. In this case, time-activity curves (TAC) can be extracted for the selected region. Pharmacokinetic modeling may be applied to such values during

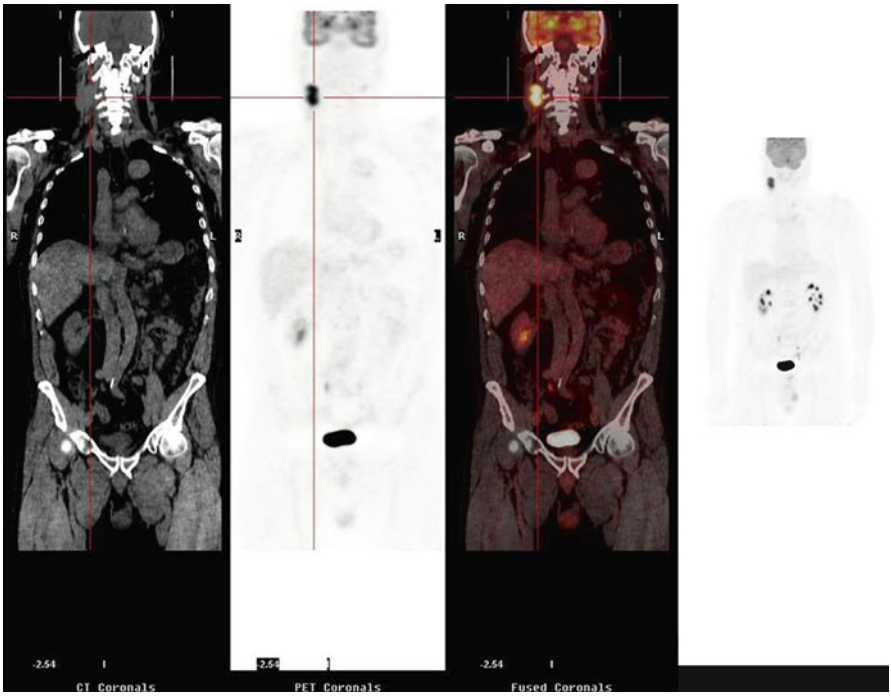

Fig. 9.6 Head and neck tumor, 66 years old patient, ^{18}F-FDG study performed with PET/CT model *GE Discovery RX* (L. Menichetti, C.N.R. Institute of Clinical Physiology, Pisa, Italy) (Reprinted from Wittig et al. [2])

image postprocessing to noninvasively assess the tracer kinetics in vivo. Arterial concentration of the tracer and PET tissue measurements are then used to calculate radiotracer regional kinetic parameters. Blood sampling may be necessary to calculate derived biochemical parameters and/or apply corrections for metabolites [2]. PET molecular imaging is thus a powerful pharmacological tool.

Labeling of biologically active molecules to assess their body distribution and regional concentrations has emerged as an outstanding application of PET imaging. The recent physical integration of PET and computed tomography (CT) in hybrid PET/CT scanners allows combining anatomical and functional imaging [70]. The high-resolution images produced by CT can be overlaid on to PET images, thus yielding anatomical reference to biochemical and metabolic measurements and reducing the lack in spatial resolution that has affected PET imaging (spatial resolution: 4–6 mm at best). This development has also prompted the use of PET/CT for treatment planning in radiotherapy, adding the metabolic information coming from PET imaging to the assessment of tumor volumes made by CT for the optimization of treatment on areas [2, 71, 72] (Fig. 9.6).

The in vivo pharmacokinetics of a boron carrier for BNCT and the quantification of ^{10}B in living tissue were already performed by PET in the late

1990s by W. Kabalka in the USA [73] and Y. Imahori in Japan [74, 75]. PET and PET/CT have been used to address the issue of pharmacokinetics, metabolism, and accumulation of BPA in target tissue. Imahori et al. [74] reported a method for the quantitative measurement of boronated drug uptake in patients with high-grade gliomas, based on the use of *L*-[^{18}F]-BPA. A three-compartment model was used to analyze PET data and to assess the tumor pharmacokinetics. The concentration of boron in the tumor calculated by the model was found to be close to that measured in surgical specimens. The similarity in pharmacokinetics between *L*-BPA and the labeled analogue was confirmed using a segmental convolution method. The estimated values of the ^{10}B concentration of BPA can be calculated from a four rate constants model applied to a dynamic study by PET using ^{18}F-BPA as a tracer. With this approach, the ^{10}B concentration was assessed during neutron irradiation of patients to be treated with BNCT after *L*-BPA administration. Following a similar approach, ^{18}F-BPA has been used to measure its uptake in recurrent cancer of the oral cavity and cervical lymph node metastases [76]; malignant glioma [77]; low-grade brain tumors, such as schwannoma and meningioma [78]; head and neck malignancies [79]; and metastatic malignant melanomas [73]. These early clinical findings with ^{18}F-BPA/PET led to study the transport and the net influx and accumulation of BPA and to show the capability of PET to screen the different types and different grades of tumor lesions as candidates for BNCT [2, 80].

The added value of the use of *L*-^{18}F-BPA and PET/CT in BNCT is to provide key data on the tumor uptake of ^{10}BPA and normal tissue and to predict the efficacy of the treatment of individual patients. Based on the assumption that the biochemical fate of the BPA is due to the molecular similarity to tyrosine [81–83], the PET of aromatic amino acid analogues might help in proving the pharmacokinetic rate constants (k_1, k_2, k_3, k_4) for the tumor and the input function for plasma *L*-BPA concentration (as previously demonstrated for L-BPA and *L*-^{18}F-BPA).

One key role of PET/CT in BNCT is further to test the *L*-^{18}F-BPA uptake in the tumor relative to surrounding normal tissues in individual patients and to use this information as a predictor for BNCT effectivity. Such data can be used as inclusion/exclusion criterion in clinical trials and might enormously help in patient selection to avoid treatment failures due to insufficient ^{10}B uptake in tumors of individual patients [76, 79].

Feasibility studies are moreover conducted to use single-photon emission computed tomography (SPECT) during BNCT treatments to compute online boron dose maps without the large current uncertainties in the assessment of the boron concentration in different tissues [84, 85].

One main challenge using PET for BNCT however is the need to prepare a radioactively labeled molecule for each potential boron carrier molecule, which has imaging qualities. To date, this was exclusively successful for the compound BPA. For BSH, the second compound used clinically, and even for newly designed compounds, such radioactively labeled compound is not available. New compounds, which come to the state of clinical testing, must undergo all legal testing requirements applicable for new drugs which will be a very cost and time-intensive process [2].

Conclusions

One crucially important requirement at every stage in the development of BNCT has been the ability to measure the concentration and image the spatial distribution of boron in biological samples. Without such capabilities, new boron compounds cannot be designed or evaluated and prospective controlled clinical trials cannot be developed. Furthermore, radiation dosimetry remains unacceptably basic, while the radiobiology of the ^{10}B neutron capture reaction leaves many open questions. Boron analysis and boron imaging is therefore one of the scientific pillars upon which the success or failure of this modality rests.

Boron analysis and boron imaging is a very complex task. After decades of research, presently, numerous methods are available with distinct endpoints and advantages/disadvantages. Therefore, it is of importance to carefully choose the appropriate technique which can correctly answer the clinical or experimental question addressed:

PGRA, ICP-AES, and ICP-MS are rapid, reliable methods for quantitation of the ^{10}B concentration in macroscopy. PGRA is suited for "online" measurements of the ^{10}B concentration in blood of patients during a BNCT treatment. However, it is of the utmost importance to realize that the ^{10}B compounds are inhomogeneously distributed on the microscopic level. However, measurements from PGRA, ICP-AES, and ICP-MS integrate the ^{10}B concentration over a volume, which is always larger than the volume irradiated by the BNC reaction. Hence, such measurements cannot be used to directly predict the radiation effect. Some research groups have proposed methods to overcome this shortcoming by analyzing the inhomogeneities of the sample, e.g., percentage of tumor cells, normal tissue, and necrosis in the analyzed volume and correcting the measured data by a factor derived from the analysis [86, 87]. Such factors can complicate the comparison of data measured by different groups especially if methodology and factors induced are not reported in detail [2].

Techniques that might help to solve this problem and are able to image the ^{10}B distribution in tissue with a lateral resolution similar that to histomorphological images are high-resolution alpha-track autoradiography and neutron capture radiography. Quantitative evaluations can be included to be able to consider the inhomogeneous ^{10}B distribution in tissues [88].

Laser microprobe mass analysis (LMMA) was the first technique to reach a subcellular resolution in BNCT [89]. Further developments using TOF-SIMS and especially laser-SNMS have the capability to quantitatively map the spatial boron distribution in biological matrices with a detection limit in the sub-ppm range, extremely high selectivity, and high spatial resolution. Methods based on electron microscopy (i.e., EELS) are less sensitive but have a much higher spatial resolution that readily satisfies the needs of BNCT for calculating radiation response. However, laser-SNMS and EELS are so time-, labor-, and cost-intensive that the small amount of information available until now does not yet satisfy the statistics necessary to evaluate biological phenomena [2].

Another important aspect that has been investigated to a little extent only is the metabolism of the compounds BPA and BSH that are actually used in clinical trials for BNCT. Ion trap mass spectrometry in combination with proteomic tech-

nologies offers a possibility to investigate metabolites and transport of target molecules. Such information is mandatory to optimize the application of these drugs on a scientifically solid basis.

For clinical purposes, noninvasive in vivo techniques to follow the pharmacological and chemical behavior of the boron carrier are needed. The labeling of BPA with ^{18}F and the use of PET to assess the molecule in a patient and the detection of boron compounds by MRI are feasible but not yet available for routine clinical use. PET with ^{18}F-labeled BPA is already used for patient selection in the recent clinical trials in Japan [78]. The expensive procedure to introduce a new radiopharmaceutical in clinical practice has limited this approach in Europe and the USA. In Europe, ^{18}F-BPA is available to patients in Finland only.

Available methods offer powerful tools to the clinical scientist to further investigate BNCT. However, none of these methods satisfies all needs at any time in each situation. Often, a complementary use of different techniques will become necessary. The complementary use of different methods, which are not accessible everywhere and which need special knowledge and trained personnel, is only feasible in the framework of a well-organized and structured network. Important tasks for such collaboration will be not only to establish a standardized system for reporting the ^{10}B concentration, especially in the clinical situation, but also to be able to provide answers to questions in basic science. Moreover, the design of standardized samples with known boron concentration and distribution should be developed, such that cross calibration and comparison of different analytical approaches can be made [2].

References

1. Sauerwein W (1993) Principles and history of neutron capture therapy. Strahlenther Onkol 169(1):1–6
2. Wittig A, Michel J, Moss RL, Stecher-Rasmussen F, Arlinghaus HF, Bendel P et al (2008) Boron analysis and boron imaging in biological materials for boron neutron capture therapy (BNCT). Crit Rev Oncol Hematol 68(1):66–90
3. Kobayashi T, Kanda K (1983) Microanalysis system of ppm order B-10 concentrations in tissue for neutron capture therapy by prompt gamma-ray spectrometry. Nucl Instrum Methods Phys Res 204:525–531
4. Konijnenberg MW, Raaijmakers CPJ, Constantine G, Dewit LGH, Mijnheer BJ, Moss RL et al (1993) Prompt gamma-ray analysis to determine ^{10}B-concentrations. In: Soloway AH (ed) Advances in neutron capture therapy. Plenum Press, New York, pp 419–422
5. Raaijmakers CPJ, Konijnenberg MW, Dewit L, Haritz D, Huiskamp R, Philipp K et al (1995) Monitoring of blood-^{10}B concentration for boron neutron capture therapy using prompt gamma-ray analysis. Acta Oncol 34(4):517–523
6. Fairchild RG, Gabel D, Laster BH, Greenberg D, Kiszenick W, Micca PL (1986) Microanalytical techniques for boron analysis using the ^{10}B(n, alpha)^{7}Li reaction. Med Phys 13(1):50–56
7. Matsumoto T, Aoki M, Aizawa O (1991) Phantom experiment and calculation for in vivo ^{10}boron analysis by prompt gamma ray spectroscopy. Phys Med Biol 36(3):329–338
8. Mukai K, Nakagawa Y, Matsumoto K (1995) Prompt gamma ray spectrometry for in vivo measurement of boron-10 concentration in rabbit brain tissue. Neurol Med Chir (Tokyo) 35:855–860

9. Wittig A, Huiskamp R, Moss RL, Bet P, Kriegeskotte C, Scherag A et al (2009) Biodistribution of ^{10}B for boron neutron capture therapy (BNCT) in a mouse model after injection of sodium mercaptoundecahydro-closo-dodecaborate and l-para-boronophenylalanine. Radiat Res 172(4): 493–499
10. Kashino G, Fukutani S, Suzuki M, Liu Y, Nagata K, Masunaga S et al (2009) A simple and rapid method for measurement of ^{10}B-para-boronophenylalanine in the blood for boron neutron capture therapy using fluorescence spectrophotometry. J Radiat Res 50(4): 377–382
11. Vega-Carrillo HR, Manzanares-Acuna E, Hernandez-Davila VM, Chacon-Ruiz A, Gallego E, Lorente A (2007) Neutron fluence rate measurement using prompt gamma rays. Radiat Prot Dosimetry 126(1–4):265–268
12. Munck af Rosenschold PM, Verbakel WF, Ceberg CP, Stecher-Rasmussen F, Persson BR (2001) Toward clinical application of prompt gamma spectroscopy for in vivo monitoring of boron uptake in boron neutron capture therapy. Med Phys 28(5):787–795
13. Verbakel WF, Sauerwein W, Hideghety K, Stecher-Rasmussen F (2003) Boron concentrations in brain during boron neutron capture therapy: in vivo measurements from the phase I trial EORTC 11961 using a gamma-ray telescope. Int J Radiat Oncol Biol Phys 55(3):743–756
14. Evans EH, Giglio JJ (1993) Interferences in inductively coupled plasma mass spectrometry – a review. J Anal Atomic Spectrom 8:1–18
15. Gregoire DC (1987) Determination of boron isotope ratios in geological materials by inductively coupled plasma mass spectrometry. Anal Chem 59:2479–2484
16. Gregoire DC (1990) Determination of boron in fresh and saline waters by inductively coupled plasma mass spectrometry. J Anal Atomic Spectrom 5:623–626
17. Al-Ammar A, Reitznerová E, Barnes RM (2000) Improving boron isotope ratio measurement precision with quadrupole inductively coupled plasma-mass spectrometry. Spectrochim Acta Part B 55:1861–1867
18. Evans S, Krahenbuhl U (1994) Boron analysis in biological material: microwave digestion procedure and determination by different methods. Fresenius Z Anal Chem 349:454–459
19. Brown PH, Hu H (1996) Phloem mobility of boron is species dependent: evidence for phloem mobility in sorbitol-rich species. Ann Bot 77:497–505
20. Smith F, Wiederin DR, Houk RS, Egan CB, Serfass RE (1991) Measurement of boron concentration and isotope ratios in biological samples by inductively coupled plasma mass spectrometry with direct injection nebulisation. Anal Chim Acta 248:229–234
21. Vanhoe H, Dams R, Vandecasteele C, Versieck J (1993) Determination of boron in human serum by inductively coupled plasma mass spectrometry after a simple dilution of the sample. Anal Chim Acta 281:401–411
22. Laakso J, Kulvik M, Ruokonen I, Vahatalo J, Zilliacus R, Farkkila M et al (2001) Atomic emission method for total boron in blood during neutron-capture therapy. Clin Chem 47(10): 1796–1803
23. Heber EM, Kueffer PJ, Lee MW Jr, Hawthorne MF, Garabalino MA, Molinari AJ et al (2012) Boron delivery with liposomes for boron neutron capture therapy (BNCT): biodistribution studies in an experimental model of oral cancer demonstrating therapeutic potential. Radiat Environ Biophys 51(2):195–204
24. Ficq A (1951) Autoradiographie par neutrons: dosage du lithium dans les embryons d'amphibiens. C R Acad Sci 233:1684–1685
25. Edwards LC (1956) Autoradiography by neutron activation: the cellular distribution of 10B in the transplanted mouse brain tumor. Int J Appl Radiat Isot 1:184–190
26. Solares G, Zamenhof R, Saris S, Walzer D, Kerley S, Joyce M et al (1992) Biodistribution and Pharmacokinetics of p-Borono-phenylalanine in C57BL/6 Mice with GL261 Intracerebral Tumours, and Survival Following Neutron Capture Therapy for Cancer. In: Allen BJ, Harrington BV, Moore DE (eds) Progress in neutron capture therapy for cancer. Plenum Press, New York, London, pp 475–478
27. Solares GR, Zamenhof RG (1995) A novel approach to the microdosimetry of neutron capture therapy. Part I. High-resolution quantitative autoradiography applied to microdosimetry in neutron capture therapy. Radiat Res 144:50–58

28. Yam CS, Solares GR, Zamenhof RG (1994) Validation of the HR microdosimetry. Trans Am Nucl Soc 71:142–144
29. Goodarzi S, Pazirandeh A, Jameie SB, Baghban Khojasteh N (2012) Differentiation in boron distribution in adult male and female rats' normal brain: a BNCT approach. Appl Radiat Isot 70(6):952–956
30. Kiger WS 3rd, Micca PL, Morris GM, Coderre JA (2002) Boron microquantification in oral muscosa and skin following administration of a neutron capture therapy agent. Radiat Prot Dosimetry 99(1–4):409–412
31. Solares GR, Zamenhof RG, Cano G (eds) (1993) Microdosimetry and compound factors for neutron capture therapy. Plenum Press, New York
32. Alfassi ZB, Probst TU (1999) On the calibration curve for determination of boron in tissue by quantitative neutron capture radiography. NIM A 428:502–507
33. Pugliesi R, Pereira MAS (2002) Study of the neutron radiography characteristics for the solid state nuclear track detector makrofol-de. NIM A 484:613–618
34. Roveda L, Prati U, Bakeine J, Trotta F, Marotta P, Valsecchi P (2004) How to study boron biodistribution in liver metastases from colorectal cancer. J Chemother 16(Suppl 5):5–8
35. Altieri S, Bortolussi S, Bruschi P, Chiari P, Fossati F, Stella S et al (2008) Neutron autoradiography imaging of selective boron uptake in human metastatic tumours. Appl Radiat Isot 66(12): 1850–1855
36. Schutz C, Brochhausen C, Altieri S, Bartholomew K, Bortolussi S, Enzmann F et al (2011) Boron determination in liver tissue by combining quantitative neutron capture radiography (QNCR) and histological analysis for BNCT treatment planning at the TRIGA Mainz. Radiat Res 176(3):388–396
37. Nano R, Barni S, Chiari P, Pinelli T, Fossati F, Altieri S et al (2004) Efficacy of boron neutron capture therapy on liver metastases of colon adenocarcinoma: optical and ultrastructural study in the rat. Oncol Rep 11(1):149–153
38. Chiaraviglio D, De Grazia F, Zonta A, Altieri S, Braghieri A, Fossati F et al (1989) Evaluation of selective boron absorption in liver tumors. Strahlenther Onkol 1989(2/3):170–172
39. Enge W, Grabisch K, Beaujean R, Bartholoma KP (1974) Etching behaviour of cellulose nitrate plastic detector under various etching conditions. NIM 115:263–270
40. Bennett BD, Zha X, Gay I, Morrison GH (1992) Intracellular boron localization and uptake in cell cultures using imaging secondary ion mass spectrometry (ion microscopy) for neutron capture therapy for cancer. Biol Cell 74(1):105–108
41. Chandra S, Morrison GM (1992) Sample preparation of animal tissues and cell cultures for secondary ion mass spectrometry (SIMS) microscopy. Biol Cell 74:31–42
42. Chandra S, Smith DR, Morrison GH (2000) Subcellular imaging by dynamic SIMS ion microscopy. Anal Chem 72(3):104A–114A
43. Chandra S, Lorey ID, Smith DR (2002) Quantitative subcellular secondary ion mass spectrometry (SIMS) imaging of boron-10 and boron-11 isotopes in the same cell delivered by two combined BNCT drugs: in vitro studies on human glioblastoma T98G cells. Radiat Res 157(6): 700–710
44. Smith DR, Chandra S, Barth RF, Yang W, Joel DD, Coderre JA (2001) Quantitative imaging and microlocalization of boron-10 in brain tumors and infiltrating tumor cells by SIMS ion microscopy: relevance to neutron capture therapy. Cancer Res 61(22): 8179–8187
45. Yokoyama K, Miyatake S, Kajimoto Y, Kawabata S, Doi A et al (2007) Analysis of boron distribution in vivo for boron neutron capture therapy using two different boron compounds by secondary ion mass spectrometry. Radiat Res 67(1):102–109
46. Arlinghaus HF, Spaar MT, Switzer RC, Kabalka GW (1997) Imaging of boron in tissue at the cellular level for boron neutron capture therapy. Anal Chem 69(16):3169–3176
47. Fartmann M, Kriegeskotte C, Dambach S, Wittig A, Sauerwein W, Arlinghaus HF (2004) Quantitative imaging of atomic and molecular species in cancer cultures with TOF-SIMS and Laser-SNMS. Appl Surf Sci 231(2(SI)):428–431
48. Arlinghaus HF (ed) (2002) Laser Secondary Neutral Mass Spectrometry (Laser-SNMS). Wiley-VCH Verlag GmbH & Co. KGaA, Weinheim

49. Arlinghaus HF, Kriegeskotte C, Fartmann M, Wittig A, Sauerwein W, Lipinsky D (2006) Mass spectrometric characterization of elements and molecules in cell cultures and tissues. Appl Surf Sci 252:6941–6948
50. Fartmann M, Dambach S, Kriegeskotte C, Lipinsky D, Wiesmann HP, Wittig A et al (2003) Subcellular imaging of freeze-fractured cell cultures by TOF-SIMS and Laser SNMS. Appl Surf Sci 203–204:726–729
51. Wittig A, Wiemann M, Fartmann M, Kriegeskotte C, Arlinghaus HF, Zierold K et al (2005) Preparation of cells cultured on silicon wafers for mass spectrometry analysis. Microsc Res Tech 66(5):248–258
52. Arlinghaus HF, Fartmann M, Kriegeskotte C, Dambach S, Wittig A, Sauerwein W et al (2004) Subcellular imaging of cell cultures and tissue for boron localization with laser-SNMS. Surf Interface Anal 36(8):698–701
53. Bourdos N, Kollmer F, Benninghoven A, Sieber M, Galla HJ (2000) Imaging of domain structures in a one-component lipid monolayer by time-of-flight secondary ion mass spectrometry. Langmuir 16(4):1481–1484
54. Neumann M, Kunz U, Lehmann H, Gabel D (2002) Determination of the subcellular distribution of mercaptoundecahydro-closo-dodecaborate (BSH) in human glioblastoma multiforme by electron microscopy. J Neurooncol 57(2):97–104
55. Zhu Y, Egerton RF, Malac M (2001) Concentration limits for the measurement of boron by electron energy loss spectroscopy and electron-spectroscopic imaging. Ultramicroscopy 87:135–145
56. Michel J, Sauerwein W, Wittig A, Balossier G, Zierold K (2003) Subcellular localization of boron in cultured melanoma cells by electron energy-loss spectroscopy of freeze-dried cryosections. J Microsc 210(Pt 1):25–34
57. Isaacson I, Johnson D (1975) The microanalysis of light elements using transmitted energy-loss electrons. Ultramicroscopy 1:33–52
58. Leapman RD, Kocsis E, Zhang G, Talbot TL, Laquerriere P (2004) Three dimensional distribution of elements in biological samples by energy filtered electron tomography. Ultramicroscopy 100:115–125
59. Michel J, Bonnet N (2001) Optimization of digital filters for the detection of trace elements in electron energy loss spectroscopy. Gaussian, homomorphic and adaptive filters. Ultramicroscopy 88:231–242
60. March RE (1997) An introduction to quadrupole ion trap mass spectrometry. J Mass Spectrom 32:351–369
61. Mauri PL, Basilico F, Pietta PG, Pasini E, Monti D, Sauerwein W (2003) New approach for the detection of BSH and its metabolites using capillary electrophoresis and electrospray ionization mass spectrometry. J Chromatogr B Analyt Technol Biomed Life Sci 788(1):9–16
62. Basilico F, Sauerwein W, Pozzi F, Wittig A, Moss R, Mauri PL (2005) Analysis of ^{10}B antitumoral compounds by means of flow-injection into ESI-MS/MS. J Mass Spectrom 40(12):1546–1549
63. Washburn MP, Wolters D, Yates JRI (2001) Large-scale analysis of the yeast proteome by multidimensional protein identification technology. Nat Biotechnol 19:242–247
64. Mauri P, Scarpa A, Nascimbeni AC, Benazzi L, Parmagnani E, Mafficini A (2005) Identification of proteins released by pancreatic cancer cells by multidimensional protein identification technology: A strategy for identification of novel cancer markers. FASEB J 19:1125–1127
65. Beretta L (2007) Proteomics from the clinical perspective: many hopes and much debate. Nat Methods 4:787–796
66. Bendel P (2005) Biomedical applications of ^{10}B and ^{11}B NMR. NMR Biomed 18(2):74–82
67. Bendel P, Koudinova N, Salomon Y (2001) In vivo imaging of the neutron capture therapy agent BSH in mice using ^{10}B MRI. Magn Reson Med 46:13–17
68. Porcari P, Capuani S, D'Amore E, Lecce M, La Bella A, Fasano F et al (2009) In vivo ^{19}F MR imaging and spectroscopy for the BNCT optimization. Appl Radiat Isot 67(7–8 Suppl):S365–S368

69. Martínez MJ, Ziegler SI, Beyer T (2008) PET and PET/CT: basic principles and instrumentation. Recent Results Cancer Res 170:1–23
70. Schöder H, Erdi YE, Larson SM, Yeung HW (2003) PET/CT: a new imaging technology in nuclear medicine. Eur J Nucl Med Mol Imaging 30:1419–1437
71. Lecchi M, Fossati P, Elisei F, Orecchia R, Lucignani G (2008) Current concepts on imaging in radiotherapy. Eur J Nucl Med Mol Imaging 35(4):821–837
72. Grosu AL, Piert M, Weber WA, Jeremic B, Picchio M, Schratzenstaller U et al (2005) Positron emission tomography for radiation treatment planning. Strahlenther Onkol 181(8): 483–499
73. Kabalka GW, Nichols TL, Smith GT, Miller LF, Khan MK, Busse PM (2003) The use of positron emission tomography to develop boron neutron capture therapy treatment plans for metastatic malignant melanoma. J Neurooncol 62(1–2):187–195
74. Imahori Y, Ueda S, Ohmori Y, Kusuki T, Ono K, Fujii R et al (1998) Fluorine-18-labeled fluoroboronophenylalanine PET in patients with glioma. J Nucl Med 39(2):325–333
75. Imahori Y, Ueda S, Ohmori Y, Sakae K, Kusuki T, Kobayashi T et al (1998) Positron emission tomography-based boron neutron capture therapy using boronophenylalanine for high-grade gliomas: part II. Clin Cancer Res 4(8):1833–1841
76. Ariyoshi Y, Miyatake S, Kimura Y, Shimahara T, Kawabata S, Nagata K et al (2007) Boron neuron capture therapy using epithermal neutrons for recurrent cancer in the oral cavity and cervical lymph node metastasis. Oncol Rep 18(4):861–866
77. Nariai T, Ishiwata K, Kimura Y, Inaji M, Momose T, Yamamoto T et al (2009) PET pharmacokinetic analysis to estimate boron concentration in tumor and brain as a guide to plan BNCT for malignant cerebral glioma. Appl Radiat Isot 67(7–8 Suppl):S348–S350
78. Havu-Auren K, Kiiski J, Lehtio K, Eskola O, Kulvik M, Vuorinen V et al (2007) Uptake of 4-borono-2-[18F]fluoro-L-phenylalanine in sporadic and neurofibromatosis 2-related schwannoma and meningioma studied with PET. Eur J Nucl Med Mol Imaging 34(1):87–94
79. Aihara T, Hiratsuka J, Morita N, Uno M, Sakurai Y, Maruhashi A et al (2006) First clinical case of boron neutron capture therapy for head and neck malignancies using 18F-BPA PET. Head Neck 28(9):850–855
80. Takahashi Y, Imahori Y, Mineura K (2003) Prognostic and therapeutic indicator of fluoroboronophenylalanine positron emission tomography in patients with gliomas. Clin Cancer Res 9(16 Pt 1):5888–5895
81. Wyss MT, Hofer S, Hefti M, Bartschi E, Uhlmann C, Treyer V et al (2007) Spatial heterogeneity of low-grade gliomas at the capillary level: a PET study on tumor blood flow and amino acid uptake. J Nucl Med 48(7):1047–1052
82. Wang HE, Wu SY, Chang CW, Liu RS, Hwang LC, Lee TW et al (2005) Evaluation of F-18-labeled amino acid derivatives and [18F]FDG as PET probes in a brain tumor-bearing animal model. Nucl Med Biol 32(4):367–375
83. Ishiwata K, Kawamura K, Wang WF, Furumoto S, Kubota K, Pascali C et al (2004) Evaluation of O-[11C]methyl-L-tyrosine and O-[^{18}F]fluoromethyl-L-tyrosine as tumor imaging tracers by PET. Nucl Med Biol 31(2):191–198
84. Minsky DM, Valda AA, Kreiner AJ, Green S, Wojnecki C, Ghani Z (2011) First tomographic image of neutron capture rate in a BNCT facility. Appl Radiat Isot 69(12):1858–1861
85. Murata I, Mukai T, Nakamura S, Miyamaru H, Kato I (2011) Development of a thick CdTe detector for BNCT-SPECT. Appl Radiat Isot 69(12):1706–1709
86. Wittig A, Malago M, Collette L, Huiskamp R, Buhrmann S, Nievaart V et al (2008) Uptake of two ^{10}B-compounds in liver metastases of colorectal adenocarcinoma for extracorporeal irradiation with boron neutron capture therapy (EORTC Trial 11001). Int J Cancer 122(5):1164–1171
87. Coderre JA, Chanana AD, Joel DD, Elowitz EH, Micca PL, Nawrocky MM et al (1998) Biodistribution of boronophenylalanine in patients with glioblastoma multiforme: boron concentration correlates with tumor cellularity. Radiat Res 149(2):163–170

88. Thellier M, Hennequin E, Heurteaux C, Martini F, Pettersson M, Fernandez T et al (1988) Quantitative estimations in neutron capture radiography. Nucl Instrum Methods Phys Res B 30:567–579
89. Haselsberger K, Radner H, Gössler W, Schagenhaufen C, Pendl G (1994) Subcellular boron-10 localization in glioblastoma for boron neutron capture therapy with Na2B12H11SH. J Neurosurg 81:741–744
90. Michel J, Balossier G, Wittig A, Sauerwein W, Zierold K (2005) EELS Sprctrum-Imaging for boron detection in biological cryofixed tissues. Instrumentation Sciences and Technology 33:632–644
91. Bendel P, Koudinova N, Salomon Y, Hideghéty K, Sauerwein W (2002) Imaging of BSH by ^{10}B MRI. In: Sauerwein W, Moss R, Wittig A, editors. Research and Development in Neutron Capture Therapy, Bologna: Monduzzi Editore, Bologna 877–880

Proteomic Investigations for Boron Neutron Capture Therapy

10

Pier Luigi Mauri and Fabrizio Basilico

Contents

Abbreviations

BSH	Sodium mercaptoundecahydro-*closo*-dodecaborate
BPA	L-*para*-boronophenylalanine
PVDF	Polyvinylidene fluoride transfer membranes
MudPIT	Multidimensional protein identification technology
LC-MS/MS	Liquid tandem mass spectrometry
IPG	Immobilized pH gradient
SDS-PAGE	Sodium dodecyl sulfate-polyacrylamide gel electrophoresis

P.L. Mauri (✉) • F. Basilico
Proteomics and Metabolomics Unit, Institute for Biomedical Technologies (ITB-CNR),
Via Fratelli Cervi, 93, 20090 Segrate Milan, Italy
e-mail: pierluigi.mauri@itb.cnr.it

W.A.G. Sauerwein et al. (eds.), *Neutron Capture Therapy*,
DOI 10.1007/978-3-642-31334-9_10,

10.1 Introduction

The term proteome, coined in the 1990s as an equivalent to the concept of genome [1], is used to describe the complete set of proteins that is expressed and modified following expression by the entire genome in the lifetime of a cell. It is also used in a less universal sense to describe the complement of proteins expressed by a cell at any given timepoint [2].

While a genome is relatively static and remains unchanged over time, the proteome is dynamic. The genome is organism specific, whereas the proteome is tissue and cell specific. For example, our liver and lung cells have the same genome, but they perform very different functions as a result of their different proteomes. Further, a cell's proteome expression changes in response to intracellular actions and/or because of environmental events. The changes may also be brought about by growth, differentiation, senescence, changes in the environment, genetic manipulation, or other reasons.

Investigation of the proteome of an organism, tissue, or cell requires the simultaneous identification and relative quantities of the various proteins expressed in the sample of interest. This protein "profiling" can be compared among different conditions, such as physiological versus pathological states, to discover the biomarkers related to a specific situation.

Clinical proteomic investigation has been recently introduced as part of proteomics, and could allow a novel and important approach for the diagnosis and follow-up of different diseases. In this context, the proteomes of a wide range of biological materials have been studied, such as body fluids, serum and urine, and tissues.

The protein profile is obtained with the aid of high-resolution techniques, such as two-dimensional electrophoresis (2DE). 2DE separates proteins based on two independent characteristics: charge and size. As a result, up to 10,000 proteins and peptides can be resolved from a complex mixture, and the resulting protein pattern is characteristic of a particular biological system in a particular state. Bioinformatic tools are used to compare different proteome fingerprints and identify changes of interest. These changes can be characterized using tandem mass spectrometry, providing amino acid sequence information that can be used to search protein and expressed sequence tag databases. Traditionally, characterization of the proteome is performed by means of 2DE methodology; however, the 2DE system is tedious and time-consuming, and analysis of hydrophobic proteins is not simple. In addition, proteins with extreme molecular weight (<10 and >200 kDa) or an isoelectric point (pI<4 or >10) are very difficult to detect [3]. For these reasons, in recent years, other approaches have been proposed, such as capillary electrophoresis [4], surface enhanced laser desorption ionization (SELDI) [5], and two-dimensional chromatography coupled to tandem mass spectrometry (2 DC-MS/MS, also called multidimensional protein identification technology, MudPIT) [6].

Today, proteomic methodologies are of primary importance for discovery-driven biomarker studies. Theoretically, the ideal approach for biomarker discovery could be its detection in a tumor's biofluids of specific structural and secreted proteins [7]. This approach is interesting and used by many researchers, but obtaining technically

well-reproducible results is not easy; in fact, the concentration of potential biomarkers may be high close to the tumor, but diluted in the circulatory system, which is also a complex matrix [8].

In this chapter, the classic, based on gel electrophoresis, and innovative, based on liquid chromatography, proteomic methodologies are described. In particular, more details are given for the MudPIT approach and its applications in clinical proteomics, specifically for BNCT studies.

10.2 Overview of the Main Proteomic Methodologies

The most popular method for characterizing protein profiles is surely two-dimensional gel electrophoresis (2DE). It is involves two separation systems for the protein mixture, such as an extract from body fluids or tissues: firstly, proteins are separated according their isoelectric point (pI) in the range 4–10 pH, and the second dimension of separation is related to the molecular weight of proteins in the typical range 10–200 kDa. Separated proteins are detected by means of silver or Coomassie staining, and the resulting images are compared for selecting differentially expressed spots to be identified one-to-one by means of tryptic digestion and mass spectrometry analysis (see Fig. 10.1). This approach is also called gel-based; in fact, the most important step is the gel separation of proteins. On the contrary, in the MudPIT proteomic strategy, the complex mixture of proteins has been digested previously, and the resulting peptides are separated by means of two-dimensional nano-chromatography (2 DC or LC/LC): firstly, peptides are separated on an ion-exchange column (first dimension) by means of increasing the concentration of salt (0–1,000 mM of ammonium chloride, acetate, or formate) and then on a reversed-phased column (C_{18} stationary phase, second dimension). The LC/LC system is directly coupled to tandem mass spectrometry (MS/MS), usually an ion trap mass spectrometer, for detecting molecular weight and fragments of eluted peptides. The identification of peptide sequences is obtained through an automated database search with appropriate software, such as the SEQUEST algorithm for data handling of mass spectra [9–11]. The experimental mass spectra (full MS and MS/MS) are correlated to tryptic peptide sequences by comparison with the theoretical mass spectra deduced from public protein or fully translated genomic databases [12]. The sequenced peptides permit identifying the correlated proteins present in the original sample. Because thousands of spectra are collected (20–50 thousand) for MudPIT analysis, it is better to use a Parallel Virtual Machine (CPU cluster) for data handling. Figure 10.1 summarizes the main steps involved in the 2DE (Fig. 10.1a) and MudPIT (Fig. 10.1b) approaches. In particular, 2DE presents some advantages, such as the high resolution and requiring little investment. However, 2DE has some disadvantages, such as limited pI and MW ranges, and being time consuming.

In contrast, the MudPIT approach provides a significant improvement over gel-based analysis, as it represents a fully automated technology that simultaneously allows separation of digested peptides, their sequencing, and the identification of the corresponding proteins. In this way, quantitative characterization [13, 14] of the

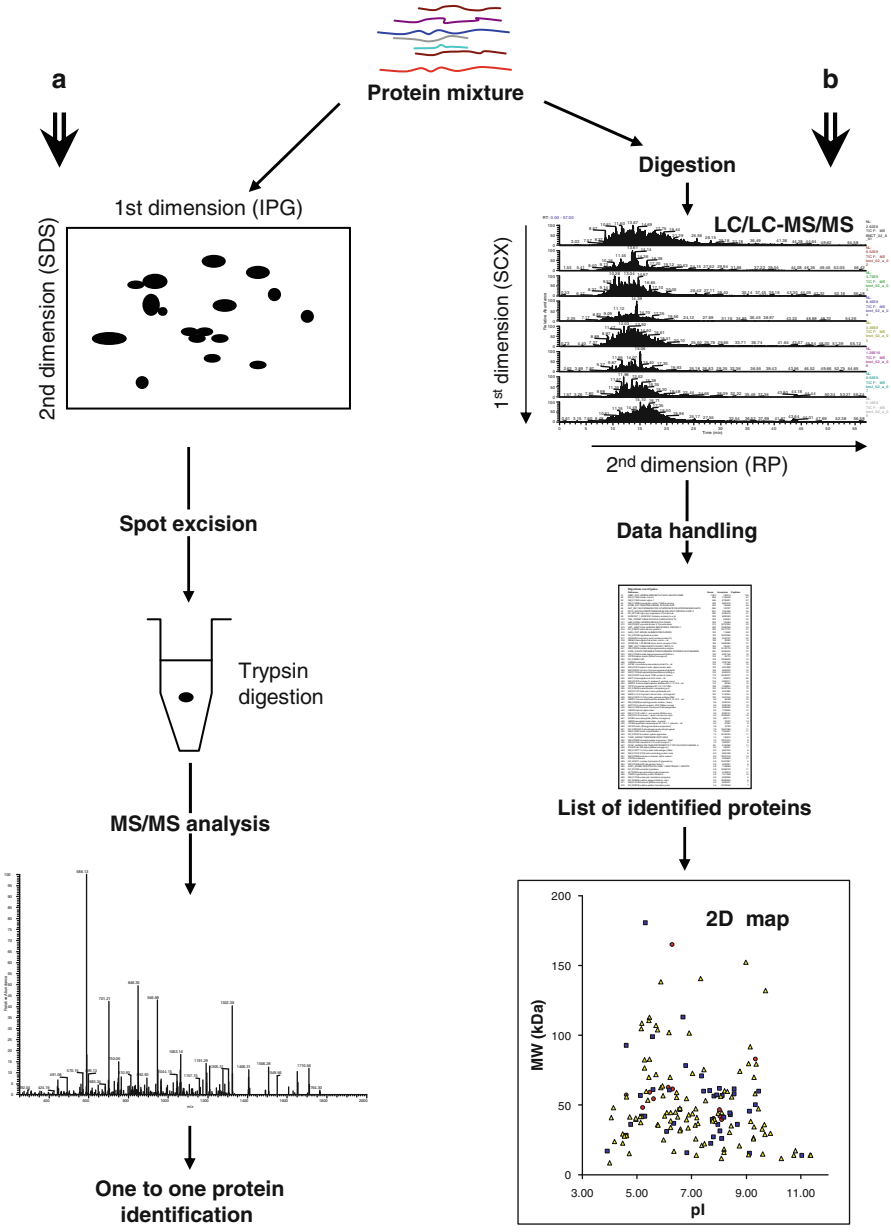

Fig. 10.1 Main steps used in (**a**) traditional 2DE and (**b**) MudPIT proteomic approach. 2DE methodology involves firstly the protein separation by means of *IPG* (first dimension) and *SDS*-PAGE (second dimension). The differential expressed protein spots are cut and in-gel digested. The resulting peptides are identified by means of mass spectrometry (usually tandem mass spectrometry, *MS/MS*, for obtaining peptide sequence). Digestion and *MS/MS* analysis require repetition for each spot of interest. On the contrary, MudPIT methodology involves the preliminary digestion of the complex protein mixture and separation of the resulting peptides by two-dimensional liquid chromatography (2DC or *LC/LC*) combined with mass spectrometry for identifying the eluted peptides. This gives the possibility to plot a list of proteins on a virtual 2D map using theoretical pI and MW of identified proteins

protein mixtures is possible in wide pI and MW ranges, and the membrane proteins are also identified. Concerning MudPIT analysis, it is confirmed to be "nascent methods for free-gel analysis of complex mixtures hold great promise" [15]. This technology is a part of so-called mass spectrometry-based proteomics.

Recently, a number of cancer investigations have been performed by means of MudPIT methodology for identifying biomarkers [16]. For example, the released proteins from pancreatic cancer cells were studied, and differentially expressed proteins correlated to extracellular matrix degradation and metastasis were identified [17]. Other authors obtained similar results by studying pancreatic cancer tissue directly [18]. Also, MudPIT analyses of ovarian cancer cells were performed, and it was possible to group the cell lines in relation to their motile and invasive capacity [19].

10.3 Results Related to BNCT

Up to now, few proteomic investigations have been performed in relation to BNCT. Mainly, these works have been oriented to the following aspects: (1) investigating the possibility of detecting proteins modified with ^{10}B-containing compounds and (2) characterizing tumor biomarkers and targets for ^{10}boron drugs.

Some experiments have been performed to verify possible chemical interaction between proteins and boron compounds; for example, phospholipid hydroperoxide glutathione peroxidase (PHGPx, about 2 μg) has been treated with BSH (about 0.05 mM), and the resulting products were separated by SDS gel electrophoresis (SDS-PAGE) and blotted on PVDF (polyvinylidene fluoride) transfer membrane. Using chemical staining of proteins, for example, using Ponceau red [20], two bands of around 22 and 14 kDa were detected, both with and without BSH reactions (see Fig. 10.2). On the contrary, using the physical method, based on the specific detection of ^{10}B obtained by neutron autoradiography [21], a protein band was detected in BSH-treated samples [22]. In particular, protein of around 14 kDa did not react with BSH, while the 22-kDa protein band contained ^{10}boron.

To confirm these results, the neutron-positive 22-kDa band was excited and digested with trypsin, and the resulting peptide mixture analyzed by liquid chromatography coupled to tandem mass spectrometry (LC-MS/MS). In this way, many peptides were sequenced, and it was also possible to identify one peptide containing a BSH residue (Fig. 10.3). In particular, the modified peptide corresponds to $T_{172\text{-}178}$, and BSH is linked to protein by a disulfur bridge with Cys_{175}. Of note, it was possible to observe the characteristic fragment (*m/z* 131) in the MS/MS spectrum of peptide (Fig. 10.3d) because of tandem mass spectrometry analysis of BSH [23].

The described results indicate that it is possible to detect post-translational modification due to the eventual interaction between protein and ^{10}B-compounds using the proteomic approach based on LC-MS/MS. Moreover, recently new antibodies have been developed that are specific for detecting BSH or BPA [24] in free form or linked to proteins by means of Western blot staining. These methodologies are of primary importance for investigating the targets of drugs applied for BNCT.

For investigating the mechanism of accumulation for boron drugs in tumor cells and grouping those presenting a higher reactivity, it is important to characterize

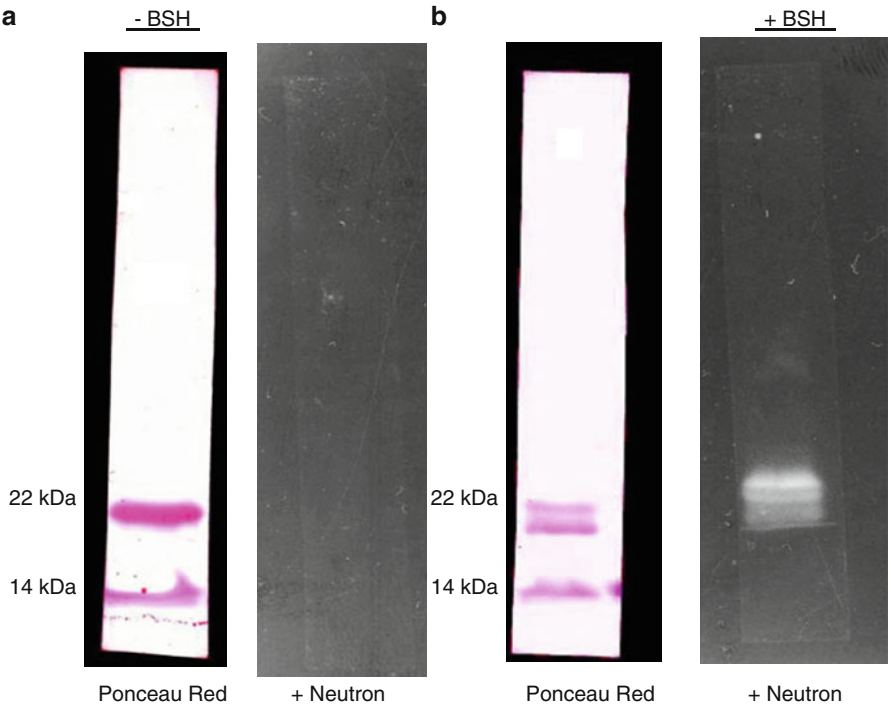

Fig. 10.2 Gel electrophoresis separation blotted on PVDF membrane of PHGP × untreated (**a**) and treated (**b**) with *BSH*, and stained with *Ponceau red* and neutron autoradiography

their proteome. To perform protein profile studies in relation of BNCT, the shotgun MudPIT approach has been used. As described above, this methodology permits the identification of many proteins for each analyzed sample and also allows obtaining quantitative results. Typically, normal and tumor tissues are analyzed in parallel for increasing the confidence of comparison.

Tissue is homogenized in 100 mM ammonium bicarbonate, pH 8, at 4 °C, and ultra-centrifuged for separating hydrophilic (supernatant) and hydrophobic (pellet) protein fractions. Each fraction is digested (4–16 h) by means of modified trypsin, in order to avoid protease autodigestion, at 37 °C. The substrate/enzyme ratio is around 50:1 (w/w) in 30–50 μl final volume; the reaction is stopped by the addition of formic acid so as to obtain a pH of equal or less than 2. For detecting cysteines, it is necessary to perform reduction and alkylation before digestion [25], but this procedure eliminates the eventual bonds between proteins and BSH. Sample desalting of tryptic digests permits increasing chromatography resolution and mass spectrometry sensitivity [26]. Five to ten microliters of trypsin-digested tissue sample is analyzed by MudPIT methodology: firstly, peptides are separated by strong ion

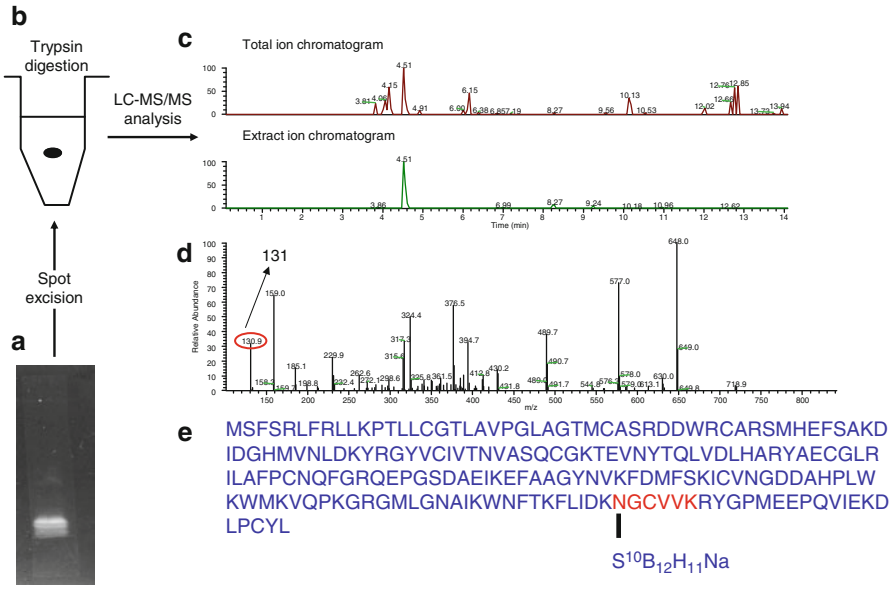

Fig. 10.3 *LC-MS/MS* analysis of protein detected by neutron autoradiography (see Fig. 10.1). (**a**) A 22-kDa protein was (**b**) digested by trypsin and analyzed by *LC-MS/MS*. This allowed (**c**) separation of obtained peptides, (**d**) their sequencing, and (**e**) identification of BSH modified peptide

exchange chromatography (SCX column, usually 0.30 i.d. ×100 mm) by applying a nine-step ammonium chloride concentration gradient (0, 20, 40, 80, 120, 200, 400, 700 mM) at a flow rate of around of 1–2 μl/min. The second dimension is obtained by loading, using a ten-port valve, each salt step elute directly into a reversed-phase column (C_{18}, 0.180 i.d. ×100 mm) and separating them with an acetonitrile gradient at a 1 μl/min.

Each peptide eluted from the C_{18} column is directly detected with a mass spectrometer for collecting full MS and MS/MS spectra in positive mode. The typical acquisition range is 400–1,700 *m/z*, and a data-dependent scan and dynamic exclusion are used [27].

The identification of the proteins is then obtained through an automated database search with appropriate software, such as the SEQUEST algorithm [28], for data handling the mass spectra. The experimental mass spectra produced are correlated to peptide sequences obtained by comparison with the theoretical mass spectra in the human protein database downloaded from the NCBI (www.ncbi.nlm.nih.gov). As an example, MudPIT analysis of the hydrophobic fraction of homogenized tumor liver permitted the characterization of more than 120 proteins for each sample. Table 10.1 reports a typical list of proteins identified by at least two different peptides.

To visualize the protein list output data in a user-friendly format, MAProMA (multidimensional algorithm protein map) software was developed, which automatically plots MW vs. pI for each identified protein [17]. A color-code/shape is automatically assigned according to a range of score values or different peptides identified

Table 10.1 Typical list of proteins identified by at least two different peptides from MudPIT analysis of hydrophobic fraction of homogenized tumor liver

Reference	Accession	Hits	Score
FINC_HUMAN fibronectin precursor (FN) (cold-insoluble globulin) (CIG)	2506872	16	160
Chaperonin	31542947	7	76
CO6A3_HUMAN collagen alpha-3(VI) chain precursor	5921193	7	70
Tenascin C (hexabrachion)	4504549	7	70
Keratin 8	4504919	6	60
I38369 beta-tubulin – human (fragment)	2119276	5	50
Ig heavy chain V region precursor	2146957	2	42
Glyceraldehyde-3-phosphate dehydrogenase	7669492	4	40
Keratin 18	4557888	4	40
Vimentin	62414289	4	40
POSTN_HUMAN periostin precursor (PN) (osteoblast-specific factor 2)	93138709	4	40
FLNA_HUMAN filamin-A (alpha-filamin) (Filamin-1)	116241365	3	36
Tyrosine 3/tryptophan 5 -monooxygenase activation protein	4507953	3	30
Myosin, heavy polypeptide 9, non-muscle	12667788	3	30
Enolase 1	4503571	3	30
Chain human serum albumin	4389275	3	30
Tubulin alpha 6	14389309	3	30
Prolyl 4-hydroxylase, beta subunit precursor	20070125	3	304
B chain B, T-To-T(high) quaternary transitions	61679604	3	30
B chain B, crystal structure of recombinant human fibrinogen fragment D	24987624	3	30
Serine (or cysteine) proteinase inhibitor, clade A	50363217	3	30
Fibrinogen, alpha polypeptide isoform alpha-E preproprotein	4503689	3	30
Heat shock 27-kDa protein 1	4504517	2	28
Glutathione transferase	4504183	2	20
Pyruvate kinase 3 isoform 1	33286418	2	20
Alpha 2 globin	4504345	2	20
Vinculin isoform meta-VCL	7669550	2	20
Heat shock 70-kDa protein 5	16507237	2	20
C chain C, crystal structure of fibrinogen fragment D	2781209	2	20

(continued)

Table 10.1 (continued)

Reference	Accession	Hits	Score
Eukaryotic translation elongation factor 1 alpha 1	4503471	2	20
Transforming growth factor, beta-induced, 68 kDa	4507467	2	20
A chain A, human platelet profilin complexed with the L-Pro10 peptide	3891601	2	20
CO1A2_HUMAN collagen alpha-2(I) chain precursor	82654930	2	20
Phosphoglycerate kinase 1	4505763	2	20
ATP synthase, H + transporting, mitochondrial F1 complex, beta subunit	32189394	2	20
Electron transfer flavoprotein, alpha polypeptide	4503607	2	20
H4 histone family, member A	4504301	2	20

by SEQUEST data analysis. This provides a 2D map overview of the obtained protein list (Fig. 10.4a) and allows a rapid evaluation of the identification confidence: higher score or peptide number correspond to higher confidence of protein identification. In addition, Fig. 10.4b reports the 2D map obtained from the hydrophobic fraction of homogenized normal liver. Comparing the two maps, it is possible to observe some differences. It is interesting that the traditional proteomic approach, based on 2D gel electrophoresis (2DE), is limited in the pI and MW ranges (typically 4–10 pH and 10–200 kDa for the isoelectric point and molecular weight, respectively) [29]. On the contrary, MudPIT analysis permits the identification of proteins in a wide range of pI (>10) and MW (>200 kDa).

10.4 Perspectives

A brief overview has been reported above for describing the main proteomic approaches available, gel based (2DE) and mass spectrometry based (MudPIT). Other technologies are available, for example, surface-enhanced laser desorption ionization coupled to time-of-flight mass spectrometry (SELDI-TOF) permits rapid screening from a small amount of sample; it allows protein peak profiles, but the sequence identification and post-translational modifications of proteins are not provided [30].

Proteomic technologies aim to provide clinicians with new tools for developing innovative research on biomarker and target discovery of diseases, such as cancer.

In particular, MudPIT methodology is an innovative and high-throughput proteomic approach that allows the identification of 100–1,000 proteins for each sample without pI or MW limits. In addition, a wide range of samples can be analyzed, such as cell, tissue (fresh, frozen, or formalin fixed, paraffin embedded [31]), and body fluid [32] samples. Concerning the BNCT investigations, in the future, it will be possible and important to apply proteomic approaches for characterizing protein

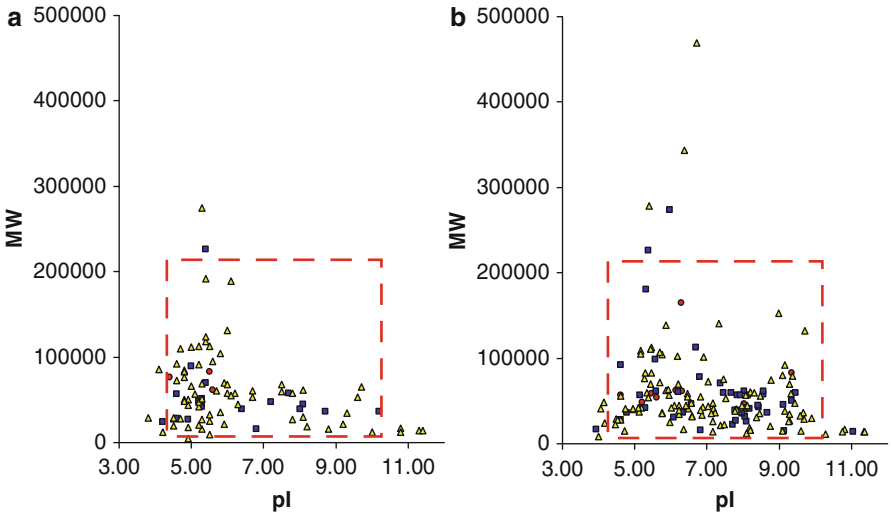

Fig. 10.4 Virtual 2D map (theoretical *pI* vs. *MW*) obtained by MAPROMA software for the list of proteins identified in the hydrophobic fraction of homogenized (**a**) tumor and (**b**) normal liver. A color/shape code is assigned to each virtual protein spot according the number of different peptides identified for each protein: *yellow/triangles*, 1, *blue/squares*, from ≥2 to <4, and *red/diamonds*, ≥4 peptides. *Red box* indicates the typical *pI* and *MW* ranges for the 2D electrophoresis method

profiles of untreated and treated patients, and to combine these studies with pharmacokinetic results. Specifically, correlation between ^{10}boron levels (qualitative and quantitative in tissues and body fluids) and differentially expressed proteins will be of primary importance for determining molecular mechanisms related to transport, metabolism, and uptake for the different ^{10}boron-containing compounds used in BNCT. The recent availability of antibodies against BPA and BSH will permit the validation of findings concerning protein-^{10}boron drug interactions (see Chap. 7). Finally, recent BNCT studies concerning the genetic incorporation of unnatural amino acids, such as modified phenylalanine, into proteins of mammalians cells are of great interest [33]. In our opinion, this may be an interesting approach to the biosynthesis of therapeutic proteins (such as antibodies or polypeptides for known tumor targets) containing BPA as an unnatural amino acid and will permit increasing the ^{10}boron concentration in tumors.

Acknowledgements The authors are grateful to Dr. A. Roveri and Dr. S. Altieri for the PHGPx reaction with BSH and neutron autoradiography, respectively.

References

1. Wilkins MR, Pasquali C, Appel RD, Ou K, Golaz O, Sanchez JC, Yan JX, Gooley AA, Hughes G, Humphrey-Smith I (1996) From proteins to proteomes – large-scale protein identification by 2-dimensional electrophoresis and amino acid analysis. Biotechnology 14:61–65

2. Wasinger VC, Cordwell SJ, Cerpa-Poljak A, Yan JX, Gooley AA, Wilkins MR, Duncan MW, Harris R, Williams KL, Humphery-Smith I (1995) Progress with gene-product mapping of the Mollicutes: mycoplasma genitalium. Electrophoresis 7:1090–1094
3. Mauri PL, Petretto A, Cuccabita D, Basilico F, Di Silvestre D, Levreri I, Melioli G (2008) Fractionation techniques improve the proteomic analysis of human serum. Curr Pharm Anal 4:69–77
4. Kaiser T, Kamal H, Rank A, Kolb HJ, Holler E, Ganser A, Hertenstein B, Mischak H, Weissinger EM (2004) Proteomics applied to the clinical follow-up of patients after allogeneic hematopoietic stem cell transplantation. Blood 104:340–349
5. Li J, Zhang Z, Rosenzweig J, Wang YY, Chan DW (2002) Proteomics and bioinformatics approaches for identification of serum biomarkers to detect breast cancer. Clin Chem 48:1296–1304
6. Florens L, Washburn MP (2006) Proteomic analysis by multidimensional protein identification technology. Methods Mol Biol 328:159–175
7. Sorio C, Mauri PL, Pederzoli P, Scarpa A (2006) Non-invasive cancer detection: strategies for the identification of novel cancer markers. IUBMB Life 58(4):193–198
8. Anderson NL, Anderson NG (2002) The human plasma proteome – history, character, and diagnostic prospects. Mol Cell Proteomics 1(11):845–867
9. Wolters DA, Washburn MP, Yates JR 3rd (2001) An automated multidimensional protein identification technology for shotgun proteomics. Anal Chem 73:5683–5690
10. Washburn MP, Wolters D, Yates JR 3rd (2001) Large-scale analysis of the yeast proteome by multidimensional protein identification technology. Nat Biotechnol 19:242–247
11. Wu CC, Yates JR 3rd (2003) The application of mass spectrometry to membrane proteomics. Nat Biotechnol 21:262–267
12. Lim H, Eng J, Yates JR 3rd, Tollaksen SL, Giometti CS, Holden JF, Adams MW, Reich CI, Olsen GJ, Hays LG (2003) Identification of 2D-gel proteins: a comparison of MALDI/TOF peptide mass mapping to mu LC-ESI tandem mass spectrometry. J Am Soc Mass Spectrom 14(9):957–970
13. Liu H, Sadygov RG, Yates JR 3rd (2004) A model for random sampling and estimation of relative protein abundance in shotgun proteomics. Anal Chem 76:4193–4201
14. Mauri PL, Dehò G (2008) A proteomic approach to the analysis of RNA degradosome composition in *Escherichia coli*. Methods Enzymol 447:99–117
15. Tyers M, Mann M (2003) From genomics to proteomics. Nature 422(6928):193–197
16. Maurya P, Meleady P, Dowling P, Clynes M (2007) Proteomic approaches for serum biomarker discovery in cancer. Anticancer Res 27(3A):1247–1255
17. Mauri P, Scarpa A, Nascimbeni AC, Benazzi L, Parmagnani E, Mafficini A, Della Peruta M, Bassi C, Miyazaki K, Sorio C (2005) Identification of proteins released by pancreatic cancer cells by multidimensional protein identification technology: a strategy for identification of novel cancer markers. FASEB J 19(9):1125–1127
18. Chen R, Yi EC, Donohoe S, Pan S, Eng J, Cooke K, Crispin DA, Lane Z, Goodlett DR, Bronner MP, Aebersold R, Brentnall TA (2005) Pancreatic cancer proteome: the proteins that underlie invasion, metastasis, and immunologic escape. Gastroenterology 129(4):1187–1197
19. Sodek KL, Evangelou AI, Ignatchenko A, Agochiya M, Brown TJ, Ringuette MJ, Jurisica I, Kislinger T (2008) Identification of pathways associated with invasive behavior by ovarian cancer cells using multidimensional protein identification technology (MudPIT). Mol Biosyst 4(7):762–773
20. Salinovich O, Montelaro RC (1986) Reversible staining and peptide mapping of proteins transferred to nitrocellulose after separation by sodium dodecylsulfate-polyacrylamide gel electrophoresis. Anal Biochem 156:341–347
21. Altieri S, Bortolussi S, Bruschi P, Chiari P, Fossati F, Stella S, Prati U, Roveda L, Zonta A, Zonta C, Ferrari C, Clerici A, Nano R, Pinelli T (2008) Neutron autoradiography imaging of selective boron uptake in human metastatic tumours. Appl Radiat Isot 66(12):1850–1855
22. Mauri PL, Basilico F, Wittig A, Heimans J, Sauerwein W (2006). Pharmacokinetics and metabolites of ^{10}B-contaning compounds in biological fluids. In: Oral presentation. 12th ICNCT, Kagawa, 9 Oct 2006

23. Mauri PL, Basilico F, Pietta PG, Pasini E, Monti D, Sauerwein W (2003) New approach for the detection of BSH and its metabolites using capillary electrophoresis and electrospray ionization mass spectrometry. J Chromatogr B 788(1):9–16
24. Doi A, Kawabata S, Iida K, Yokoyama K, Kajimoto Y, Kuroiwa T, Shirakawa T, Kirihata M, Kasaoka S, Maruyama K, Kumada H, Sakurai Y, Masunaga S, Ono K, Miyatake S (2008) Tumor-specific targeting of sodium borocaptate (BSH) to malignant glioma by transferrin-PEG liposomes: a modality for boron neutron capture therapy. J Neurooncol 87(3):287–294
25. Hale JE, Butler JP, Gelfanova V, You JS, Knierman MD (2004) A simplified procedure for the reduction and alkylation of cysteine residues in proteins prior to proteolytic digestion and mass spectral analysis. Anal Biochem 333(1):174–181
26. Winston RL, Fitzgerald MC (1998) Concentration and desalting of protein samples for mass spectrometry analysis. Anal Biochem 262(1):83–85
27. Regonesi ME, Del Favero M, Basilico F, Briani F, Benazzi L, Tortora P, Mauri P, Dehò G (2006) Analysis of the *Escherichia coli* RNA degradosome composition by a proteomic approach. Biochimie 88(2):151–161
28. Link AJ, Eng J, Schieltz DM, Carmack E, Mize GJ, Morris DR, Garvik BM, Yates JR 3rd (1999) Direct analysis of protein complexes using mass spectrometry. Nat Biotechnol 17(7):676–682
29. Righetti PG, Boschetti E (2007) Sherlock Holmes and the proteome – a detective story. FEBS J 274(4):897–905
30. Wulfkuhle JD, Paweletz CP, Steeg PS, Petricoin EF 3rd, Liotta L (2003) Proteomic approaches to the diagnosis, treatment, and monitoring of cancer. Adv Exp Med Biol 532:59–68
31. Ahram M, Flaig MJ, Gillespie JW, Duray PH, Linehan WM, Ornstein DK, Niu S, Zhao Y, Petricoin EF 3rd, Emmert-Buck MR (2003) Evaluation of ethanol-fixed, paraffin-embedded tissues for proteomic applications. Proteomics 3(4):413–421
32. Veenstra TD, Conrads TP, Hood BL, Avellino AM, Ellenbogen RG, Morrison RS (2005) Biomarkers: mining the biofluid proteome. Mol Cell Proteomics 4(4):409–418
33. Liu W, Brock A, Chen S, Chen S, Schultz PG (2007) Genetic incorporation of unnatural amino acids into proteins in mammalian cells. Nat Methods 4(3):239–244

Analysis and Imaging: PET

11

Tadashi Nariai and Kiichi Ishiwata

Contents

T. Nariai (✉)
Department of Neurosurgery, Tokyo Medical and Dental University,
1-5-45 Yushima, Bunkyo-ku, Tokyo 113-8519, Japan
e-mail: nariai.nsrg@tmd.ac.jp

K. Ishiwata
Positron Medical Center, Tokyo Metropolitan Institute of Gerontology,
1-1, Nakacho, Itabashi-ku, Tokyo 173-0011, Japan
e-mail: ishiwata@pet.tmig.or.jp

W.A.G. Sauerwein et al. (eds.), *Neutron Capture Therapy*,
DOI 10.1007/978-3-642-31334-9_11,

Abbreviations

BNCT	Boron neutron capture therapy
BPA	4-boronophenylalanine
[^{18}F]FBPA	4-borono-2-[^{18}F]fluorophenylalanine
FDG	2-deoxy-2-[^{18}F]fluoro-D-glucose
ICP-AES	Inductively coupled plasma-atomic emission spectroscopy
MET	L-[methyl-^{11}C]methionine
PET	Positron emission tomography
T/N	Tumor-to-normal-tissue ratio

11.1 Introduction

Positron emission tomography (PET) is a useful medical imaging modality for monitoring biological events inside the human body. PET can quantitate the distribution of positron-labeled molecules in living tissue by coincidence detection of gamma rays and attenuation correction with an external positron-emitting source [32]. Thus, the tomographic image obtained by PET serves well as an in vivo analogue of an autoradiograph [31, 33].

Another important advantage of PET is the existence of the positron-emitting isotopes ^{11}C and ^{15}O, two major constituents of organic molecules, and ^{18}F, a useful analogue of hydrogen. These isotopes have been used for the development of diagnostic probes for both clinical and experimental use, as their rates of uptake express various biological processes of the living body.

With these diagnostic probes, PET has served as one of the most powerful tools for investigating human brain function noninvasively [5]. Recently, however, the applications of PET have spread beyond mainly research settings into clinical settings with practical targets. Two of the major practical uses for PET are in the fields of oncology and pharmacology. In the former, the whole-body PET scan with 2-deoxy-2-[^{18}F]fluoro-D-glucose (FDG) is now accepted as a modality for routine use. Oncologists, meanwhile, await newer probes for the imaging of tumors, as FDG imaging lacks sufficient sensitivity in the organs in which FDG accumulates under normal conditions, such as the brain. Pharmacologists use PET as a tool to monitor pharmacokinetics in drug development [3, 35]. By injecting a small amount of a positron-labeled drug, researchers can noninvasively monitor the dynamics of the drug or the occupancy of the drug at target sites in human. The application of PET for boron neutron capture therapy (BNCT) amply demonstrates the benefits of PET in both oncology (i.e., tumor imaging with PET) and pharmacology (i.e., monitoring the pharmacokinetics of treatment substances).

In contrast to the other types of radiotherapy, BNCT confers a tumoricidal effect that is heavily influenced not by the type of irradiation but by the biological distribution of boronated substrate injected into the body. Thus, oncologists await the establishment of an imaging method capable of quantifying boron uptake into tumors and

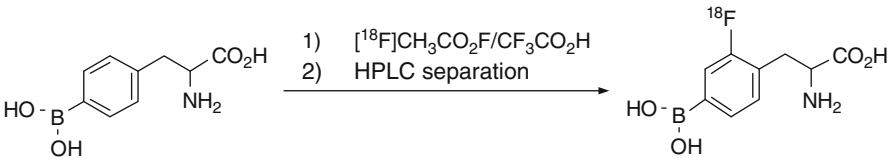

Fig. 11.1 Radiosynthesis of 4-borono-2-[^{18}F]fluorophenylalanine

surrounding normal tissue [38]. PET will serve as just such a tool, provided that an appropriate positron-labeled tracer is developed.

4-Borono-2-[^{18}F]fluorophenylalanine ([^{18}F]FBPA) is a positron label of 4-boronophenylalanine (BPA), a boron carrier for BNCT. Since its synthesis in the early nineties by one of the authors (KI) [13–16], [^{18}F]FBPA has been the only PET tracer capable of monitoring boron concentrations in vivo in human. The clinical protocol of [^{18}F]FBPA PET for BNCT was validated by two groups [10–12, 19] in the late nineties. Today, [^{18}F]FBPA PET is considered an inevitable screening tool for candidates for BNCT in Japanese clinical trials [1, 25, 39].

This chapter will define PET imaging with [^{18}F]FBPA and describe its radiopharmaceutical synthesis, experimental use, clinical use as a tumor-imaging agent, and use for BNCT.

11.2 Radiosynthesis of [^{18}F]FBPA

[^{18}F]FBPA is synthesized by direct fluorination of BPA with [^{18}F]acetyl hypofluorite ([^{18}F]AcOF) or [^{18}F]F_2, as shown in Fig. 11.1 [14, 19, 36, 37]. The radiolabeled [^{18}F]F_2 used is produced by deuteron irradiation of a high-pressure Ne gas containing a low-percentage (0.05–0.2 %) F_2, via the ^{20}Ne(d,α)^{18}F reaction. By passing a target Ne gas containing [^{18}F]F_2 through a column filled with potassium/sodium acetate, the [^{18}F]F_2 is converted to [^{18}F]AcOF. The effluent containing [^{18}F]AcOF is then bubbled into BPA in trifluoroacetic acid, and the [^{18}F]FBPA product is purified by high-performance liquid chromatography. Ishiwata et al. first prepared [^{18}F]FBPA using a mixture of D- and L-isomer of 4-boronophenylalanine as a precursor [14]. Later, they and other groups prepared [^{18}F]FBPA using a pure L-isomer, 4-[^{10}B]borono-L-phenylalanine. Ishiwata et al. used [^{18}F]FBPA for animal studies. The other groups decided to further composite [^{18}F]FBPA with fructose to produce [^{18}F]FBPA-fructose ([^{18}F]FBPA-Fr), as BPA conjugated with fructose has been proven to increase the solubility of the boron carrier [19, 37].

Because the [^{18}F]F_2 produced in pure Ne is very active and chemically adsorbed to the target holder, the presence of carrier F_2 is essential to recover [^{18}F]F_2. Thus, the radiosynthesis using carrier-added [^{18}F]F_2 via the ^{20}Ne(d,α)^{18}F reaction provides [^{18}F]FBPA with low specific activity (35–60 GBq/mmol [14] and 130 GBq/mmol [10]). Välhätalo et al., on the other hand, have produced [^{18}F]F_2 by an alternative procedure [36]. By applying the ^{18}O(p,n)^{18}F reaction, they produced a high specific activity [^{18}F]F^- and then

carried out a post-target conversion of [^{18}F]F^- to [^{18}F]F_2 via [^{18}F]CH_3F. Though only a small amount of carrier F_2 (1.2 μmol) was used in the conversion, [^{18}F]FBPA with relatively high specific activity was produced (850–1,500 GBq/mmol). With higher levels of initial activity for clinical studies, it becomes possible to increase the specific activity of [^{18}F]FBPA up to 3,700 GBq/mmol.

11.3 Experimental Studies of [^{18}F]FBPA in Animal Models

11.3.1 Tumor Accumulation

The potential of [^{18}F]FBPA for tumor imaging has been investigated in the following tumor models: FM3A mammary carcinoma in mice [13, 23], B16 melanoma in mice [15, 16, 23] or melanotic Greene's melanoma no. 179 and amelanotic Greene's melanoma no. 178 in hamsters [15, 16], and F98 glioma in rats [4, 37]. All of the reports demonstrate that [^{18}F]FBPA accumulates in tumors for the first 1–2 h, while decreasing in all other tissues. These results, particularly those in hamsters with Greene's melanomas [16], clearly confirm the potential of [^{18}F]FBPA as a PET tracer for tumor imaging.

Intriguingly, tumors with melanogenic capability have an enhanced uptake of [^{18}F]FBPA. In hamster models, Greene's melanoma no. 179, a melanotic cell line, showed an [^{18}F]FBPA uptake at 1.7 times higher than that in amelanotic Greene's melanoma no. 178 [15, 16]. Yet the same two melanomas exhibited similar metabolic activities in a tracer uptake study using L-[^{14}C]methionine, 2-deoxy-D-[^{14}C]glucose, and [^{3}H]thymidine, markers of mainly protein synthesis, glucose metabolism, and DNA synthesis, respectively [15, 16]. In a mouse model, the uptake of [^{18}F]FBPA was higher in a B16-F1 melanoma than in a B16-F10 melanoma, a tumor which grew faster and had a more highly metastatic potential (confirmed by uptake of FDG) but whose melanin content was lower. These findings stand to reason, as [^{18}F]FBPA is partially incorporated into the melanogenic cells [15, 16]. The studies by Ishiwata et al. on the topic were animal studies using a mixture of D- and L-isomer of [^{18}F]FBPA. Later, Ishiwata's group demonstrated that the tumor uptake of the L-isomer is higher than that of D-isomer and that both isomers are incorporated into the melanogenic cells to a similar extent [16].

11.3.2 Cellular Distribution

Kubota et al. investigated the cellular distribution of [^{18}F]FBPA in murine B16 melanoma sublines and FM3A mammary carcinoma by double-tracer microautoradiography in vivo [23]. According to their results, the greatest amount of [^{18}F]FBPA was found in S phase melanocytes and the lowest amount was found in non-S phase nonmelanocytes. The [^{18}F]FBPA accumulation is primarily related to the activity of DNA synthesis and secondarily related to the degree of pigmentation in melanocytes. The therapeutic efficacy of BNCT

with BPA may be greater in melanomas with higher DNA synthesis activity and higher melanin content.

11.3.3 Metabolism

The artificial amino acid [^{18}F]FBPA is generally thought to be taken up by tumors and other tissues via the amino acid transport system, without being incorporated into proteins. In mice with FM3A mammary carcinoma, [^{18}F]FBPA was found to be stable for metabolic alteration [13]. In an experiment with FM3A mammary carcinoma tissues, most radioactivity (>94 %) was detected as [^{18}F]FBPA over a 6-h postinjection, and the acid-insoluble fraction was present at levels of less than 2 %. In an experiment with B16 melanoma tissue, considerable amounts of the radioactivity were detected in the acid-insoluble fraction (27 % by 6 h). This suggests that [^{18}F]FBPA is involved in melanogenesis [15], as described above. On the other hand, the percentages of the acid-insoluble fraction in plasma were found to increase with time after injection of [^{18}F]FBPA (10 % by 2 h) [13]. This implies that a deboronation of the [^{18}F]FBPA takes place in vivo. Liver phenylalanine 4-monooxygenase may convert [^{18}F]FBPA to 2-[^{18}F]fluoro-L-tyrosine, a molecule used in the synthesis of plasma proteins recirculated into the bloodstream. If 2-[^{18}F]fluoro-L-tyrosine is recirculated into the bloodstream, it may contribute slightly to the total radioactivity of the tumor tissues. These findings suggest that there may be some discrepancy between the concentrations of ^{18}F radioactivity and ^{10}B in vivo.

11.3.4 Relationship Between Concentrations of ^{18}F Radioactivity and ^{10}B

Ishiwata et al. evaluated whether the concentration of ^{10}B can be measured by PET signals [16]. After injecting a mixture of [^{18}F]FBPA and an excess amount of BPA in B16 melanoma-bearing mice and Greene's melanoma-bearing hamsters, they estimated the concentrations of ^{10}B from the levels of radioactive uptake and specific activity of the [^{18}F]FBPA, then directly measured the concentrations of ^{10}B by inductively coupled plasma-atomic emission spectroscopy (ICP-AES) in the same tissues and blood from the test animals. In the B16-bearing mice, the ratios of the estimated concentration by the ^{18}F signal to the measured concentration by ICP-AES (^{18}F/ICP-AES ratios) were small in blood (0.24) and muscle (0.21) but relatively large in B16 (3.7) at 6 h after the injection. In the hamsters, the ^{18}F/ICP-AES ratios were 0.92 in blood, 0.70 in muscle, 1.00 in Greene's melanoma no. 179, and 0.96 in Greene's melanoma no. 178 at 6 h after the injection. Thus, the ^{18}F/ICP-AES ratios differed between the two animal species and also between the tissues. Wang et al. injected [^{18}F]FBPA-Fr and BPA separately into F98 glioma-bearing rats and then used ICP-AES to measure the concentrations of ^{10}B in normal brain hemispheres and in the brain hemispheres implanted with the glioma [36]. According to their findings, the uptake characteristics of [^{18}F]FBPA-Fr and BPA were similar [37].

11.3.5 Kinetic Analysis

Chen et al. performed a kinetic analysis of [^{18}F]FBPA-Fr in glioma-bearing rats by dynamic scanning with a high-resolution PET scanner for tracer kinetic modeling in trying to examine if such model analysis is applicable for a clinical use [4]. According to an estimation of the rate constants of BPA using a three-compartment model, the optimal irradiation time for BNCT was 4 h after the BPA-Fr injection.

11.4 Clinical Use of [^{18}F]FBPA

11.4.1 Clinical PET Imaging of Malignant Tumors with [^{18}F]FBPA

Tumor imaging with FDG, a glucose analogue, is an established clinical imaging tool. Whole-body imaging with FDG-PET is routinely used to diagnose cancer [6, 7]. As the sensitivity of PET tumor diagnosis depends on the uptake contrast of tracer into the tumor versus that into the surrounding normal tissue (*T*/*N*), FDG-PET can only be used to good effect in organs in which FDG do not accumulate in abundant levels under normal conditions. Thus, the method is not suitable for application for the brain and genitourinary system, and therefore, PET tracers based on principles other than FDG have also been clinically used, including amino acid probes such as L-[methyl-^{11}C]methionine (MET) for brain tumor [28, 29] and [^{11}C]choline for prostate cancer [8, 9].

BPA and its positron-labeled substance, [^{18}F]FBPA, are analogues of the amino acid phenylalanine and are taken up into tumor cells through a large neural amino acid transporter located at the luminal membranes of microvessels and cell membranes [24, 34]. Given that MET and all of the other positron-labeled amino acid probes are taken up into the tumor cells through the same transporter system, the [^{18}F]FBPA method can be regarded as an imaging method which uses amino acid PET tracers. Our comparison between [^{18}F]FBPA PET and MET-PET for malignant tumors of the brain and skull indicates that the two probes provide almost identical tumor images (Fig. 11.2) [30]. In another comparative study between MET-PET and the amino acid analogue O-[^{11}C]methyl-L-tyrosine, the PET tumor images using the two probes were also identical [17, 18]. It thus seems that the PET tumor images obtained by different amino acid probes, including [^{18}F]FBPA, are quite similar.

Artificial amino acid probes such as [^{18}F]FBPA or *O*-[^{11}C]methyl-L-tyrosine differ from nutritional amino acids such as MET in their uptake into normal tissue. As the former play no part in protein synthesis, they accumulate into tumor tissue selectively, as well as in excretion sites such as the kidney and bladder (Fig. 11.3). The latter, meanwhile, take part in protein synthesis and thus accumulate extensively in the liver and glandular organs such as the pancreas and salivary glands [22]. On this basis, [^{18}F]FBPA seems to have better potential as an imaging tool for malignant tumors in most parts of the body other than the urinary system. And by extension,

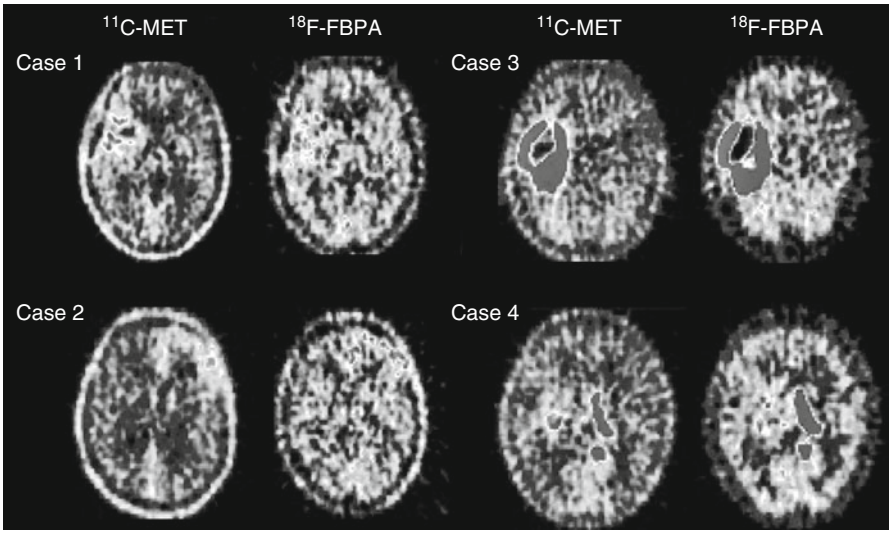

Fig. 11.2 PET images of four patients with glioblastoma. The [^{11}C]methionine (MET) images and [^{18}F]fluoroboronophenylalanine (FBPA) images are almost identical (Cited from [30])

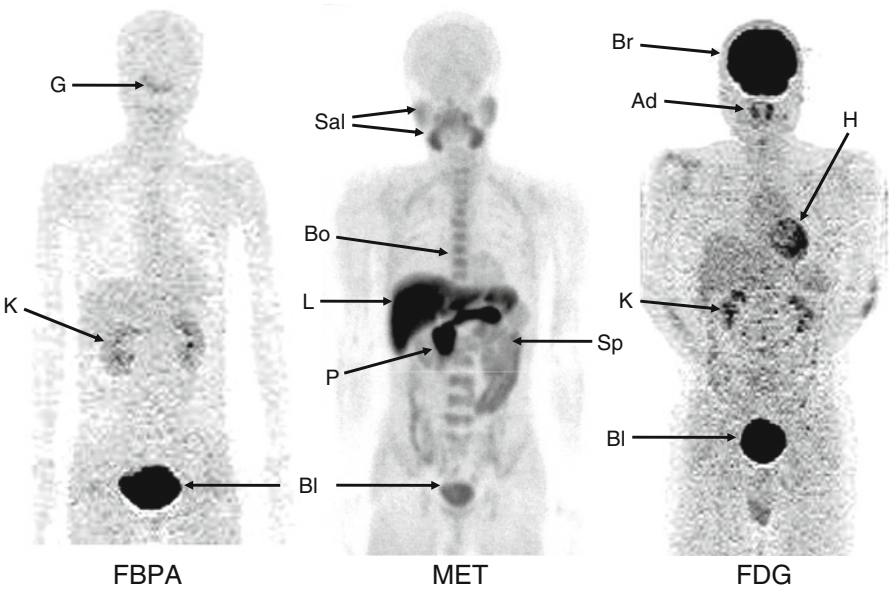

Fig. 11.3 Comparison of whole-body PET images obtained with [^{18}F]FBPA (a patient with low-grade cerebellar tumor), MET (a normal control), and FDG (a normal control with adenoids). Note the difference in the accumulation of these tracers into normal tissue. The image of MET was provided by Dr. Kazuo Kubota from the Division of Nuclear Medicine in the Department of Radiology at the International Medical Center of Japan. *Ad* adenoids, *Bl* bladder, *Bo* bone marrow, *Br* brain, *G* glioma, *H* heart, *K* kidney, *L* liver, *P* pancreas, *Sal* salivary glands, *Sp* spleen

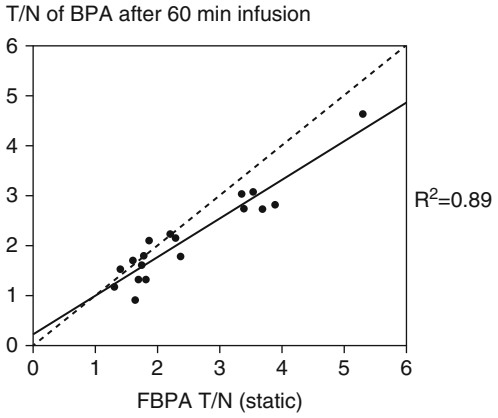

Fig. 11.4 A graph to indicate the relationship between the *T*/*N* ratio of [^{18}F]FBPA on a static PET scan (*x*-axis) and the *T*/*N* ratio of the tissue boron concentration after a 1-h constant infusion of BPA estimated by a pharmacokinetic analysis of a dynamic [^{18}F]FBPA PET scan (*y*-axis) (Cited from [30])

we can assess BPA as a superior pharmaceutical for sending boron into tumors wherever the contrast with surrounding tissue is high.

11.4.2 PET Imaging with [^{18}F]FBPA for BNCT

Imahori et al. [12] and Kabalka et al. [19] established and validated an [^{18}F]FBPA method to estimate the boron concentrations of malignant brain tumors in patients who received BNCT. First, they used dynamic PET scans to examine patients with glioblastoma multiforme before BNCT. Next, they constructed a three-compartment model to estimate the tumor concentration of boron administered via an i.v. injection of BPA. Finally, they measured the boron concentrations after the BPA injections directly from surgical specimens (from seven patients in the former study and from two patients in the latter). Both groups concluded that the estimation achieved by PET examination was close enough for practical use.

In practice, it is sufficient to determine the ratio of the boron concentration in the tumor to that in the surrounding normal tissue. To do so, it may be sufficient to compare a static scan of the activity of the tumor [^{18}F]FBPA with a static scan of the activity of the normal tissue (*T*/*N* of [^{18}F]FBPA). A recent analysis by our group has indicated that the estimated *T*/*N* of the boron concentration after a slow infusion of BPA had a significant linear correlation with the *T*/*N* of radioactivity after a bolus injection of [^{18}F]FBPA (Fig. 11.4) [30].

Researchers in Japan have conducted several BNCT series by setting certain thresholds on the *T*/*N* of [^{18}F]FBPA obtained by PET studies for patient selection. Three categories of tumor have been covered in these series: malignant glioma [25], malignant meningioma [26], and head and neck malignancies [1, 2, 21]. Kabalka et al. have reported a case of metastatic malignant melanoma in brain in whom [^{18}F]FBPA was useful to make decision to perform BNCT[20]. The dearth of comparative studies has made it difficult to verify the superiority of PET-based BNCT over non-PET-based BNCT or other radiotherapies. Findings have suggested, however,

that PET-based BNCT for glioblastoma is achieving progressively better results than the former protocol [39].

11.4.3 Practical Use of PET for BNCT

As long as BNCT is based on the transfer of the boron molecule to the tumor tissue, PET boron imaging will continue to play a key role in successful treatment. Of the various in vivo measurement methods, PET sensitivity is maximum with high-powered irradiation from a minimal quantity of molecular probe. To extend the use of BNCT on a practical basis, parallel efforts must be made to extend the use of PET clinically. As this chapter has described, [^{18}F]FBPA PET is categorizable as one of PET methods using amino acid tracers. Thus, PET studies with other amino acid tracers can be applied for the screening of tumor types or of individual patients who may benefit from BNCT, as long as BPA is used as the boron carrier agent. MET-PET may be suitable for this type of screening, in light of the ease with which it can be synthesized and the many years it has been used at PET institutes around the world.

The clinical application of PET for the posttreatment evaluation of patients who have received BNCT is also inevitable. PET should be useful to differentiate tumor regrowth from pseudoexpansion by radiation injury [27]. Without PET, the treatment effects of BNCT cannot be precisely evaluated. FDG-PET is also suited for evaluating the treatment effects of patients with whole-body malignancies, while amino acid PET is the better choice for patients with brain tumors. We are convinced that the routine use of PET tumor imaging with amino acid tracers, MET, [^{18}F]FBPA, and the like will support the widespread and beneficial use of BNCT.

11.5 Summary

An important step in the planning for optimal BNCT for malignant tumor is to estimate the *T*/*N* of the boron concentration. Investigators have developed the PET imaging probe [^{18}F]FBPA and have confirmed its efficacy in estimating boron concentrations in animal experiments. Others have established a clinical PET application using [^{18}F]FBPA and have started to use it for the selection of candidates for BNCT in clinical protocols in Japan. Comparative clinical imaging studies have revealed that [^{18}F]FBPA PET images are almost identical to the images obtained with another amino acid probe, MET. Static images of FBPA or MET-PET can be used for the planning of BNCT. PET imaging with amino acid probes may contribute significantly to the establishment of an appropriate BNCT application for patients with malignant tumors.

Acknowledgement We thank Dr. Kazuo Kubota from the Division of Nuclear Medicine in the Department of Radiology at the International Medical Center of Japan for kindly offering us whole-body PET images of MET uptake.

References

1. Aihara T, Hiratsuka J, Morita N, Uno M, Sakurai Y, Maruhashi A, Ono K, Harada T (2006) First clinical case of boron neutron capture therapy for head and neck malignancies using 18F-BPA PET. Head Neck 28:850–855
2. Ariyoshi Y, Miyatake S, Kimura Y, Shimahara T, Kawabata S, Nagata K, Suzuki M, Maruhashi A, Ono K, Shimahara M (2007) Boron neuron capture therapy using epithermal neutrons for recurrent cancer in the oral cavity and cervical lymph node metastasis. Oncol Rep 18:861–866
3. Bauer M, Wagner CC, Langer O (2008) Microdosing studies in humans: the role of positron emission tomography. Drugs R&D 9:73–81
4. Chen JC, Chang SM, Hsu FY, Wang HE, Liu RS (2004) MicroPET-based pharmacokinetic analysis of the radiolabeled boron compound [18F]FBPA-F in rats with F98 glioma. Appl Radiat Isot 61:887–891
5. Cherry S, Phelps M (1996) Imaging brain function with positron emission tomography. In: Toga A, Mazziotta J (eds) Brain mapping: the methods. Academic, San Diego, pp 191–221
6. Coleman RE (2002) Value of FDG-PET scanning in management of lung cancer. Lancet 359:1361–1362
7. Gould MK, Maclean CC, Kuschner WG, Rydzak CE, Owens DK (2001) Accuracy of positron emission tomography for diagnosis of pulmonary nodules and mass lesions: a meta-analysis. JAMA 285:914–924
8. Groves AM, Win T, Haim SB, Ell PJ (2007) Non-[18F]FDG PET in clinical oncology. Lancet Oncol 8:822–830
9. Hara T, Kosaka N, Kishi H (1998) PET imaging of prostate cancer using carbon-11-choline. J Nucl Med 39:990–995
10. Imahori Y, Ueda S, Ohmori Y, Kusuki T, Ono K, Fujii R, Ido T (1998) Fluorine-18-labeled fluoroboronophenylalanine PET in patients with glioma. J Nucl Med 39:325–333
11. Imahori Y, Ueda S, Ohmori Y, Sakae K, Kusuki T, Kobayashi T, Takagaki M, Ono K, Ido T, Fujii R (1998) Positron emission tomography-based boron neutron capture therapy using boronophenylalanine for high-grade gliomas: part I. Clin Cancer Res 4:1825–1832
12. Imahori Y, Ueda S, Ohmori Y, Sakae K, Kusuki T, Kobayashi T, Takagaki M, Ono K, Ido T, Fujii R (1998) Positron emission tomography-based boron neutron capture therapy using boronophenylalanine for high-grade gliomas: part II. Clin Cancer Res 4:1833–1841
13. Ishiwata K, Ido T, Kawamura M, Kubota K, Ichihashi M, Mishima Y (1991) 4-Borono-2-[18F]fluoro-D, L-phenylalanine as a target compound for boron neutron capture therapy: tumor imaging potential with positron emission tomography. Int J Rad Appl Instrum B 18:745–751
14. Ishiwata K, Ido T, Mejia AA, Ichihashi M, Mishima Y (1991) Synthesis and radiation dosimetry of 4-borono-2-[18F]fluoro-D, L-phenylalanine: a target compound for PET and boron neutron capture therapy. Int J Rad Appl Instrum A 42:325–328
15. Ishiwata K, Ido T, Honda C, Kawamura M, Ichihashi M, Mishima Y (1992) 4-Borono-2-[18F]fluoro-D, L-phenylalanine: a possible tracer for melanoma diagnosis with PET. Int J Rad Appl Instrum B 19:311–318
16. Ishiwata K, Shiono M, Kubota K, Yoshino K, Hatazawa J, Ido T, Honda C, Ichihashi M, Mishima Y (1992) A unique in vivo assessment of 4-[10B]borono-L-phenylalanine in tumour tissues for boron neutron capture therapy of malignant melanomas using positron emission tomography and 4-borono-2-[18F]fluoro-L-phenylalanine. Melanoma Res 2:171–179
17. Ishiwata K, Tsukada H, Kubota K, Nariai T, Harada N, Kawamura K, Kimura Y, Oda K, Iwata R, Ishii K (2005) Preclinical and clinical evaluation of O-[11C]methyl-L-tyrosine for tumor imaging by positron emission tomography. Nucl Med Biol 32:253–262
18. Ishiwata K, Kubota K, Nariai T, Iwata R (2008) Whole-body tumor imaging: [O-11C]methyl-L-tyrosine/positron emission tomography. In: Hayat M (ed) Cancer imaging: instrument and application, vol 2. Elsevier, Amsterdam, pp 175–179
19. Kabalka GW, Smith GT, Dyke JP, Reid WS, Longford CP, Roberts TG, Reddy NK, Buonocore E, Hubner KF (1997) Evaluation of fluorine-18-BPA-fructose for boron neutron capture treatment planning. J Nucl Med 38:1762–1767

20. Kabalka GW, Nichols TL, Smith GT, Miller LF, Khan MK, Busse PM (2003) The use of positron emission tomography to develop boron neutron capture therapy treatment plans for metastatic malignant melanoma. J Neurooncol 62:187–195
21. Kato I, Ono K, Sakurai Y, Ohmae M, Maruhashi A, Imahori Y, Kirihata M, Nakazawa M, Yura Y (2004) Effectiveness of BNCT for recurrent head and neck malignancies. Appl Radiat Isot 61:1069–1073
22. Kubota K (2001) From tumor biology to clinical PET: a review of positron emission tomography (PET) in oncology. Ann Nucl Med 15:471–486
23. Kubota R, Yamada S, Ishiwata K, Tada M, Ido T, Kubota K (1993) Cellular accumulation of 18F-labelled boronophenylalanine depending on DNA synthesis and melanin incorporation: a double-tracer microautoradiographic study of B16 melanomas in vivo. Br J Cancer 67:701–705
24. Langen KJ, Muhlensiepen H, Holschbach M, Hautzel H, Jansen P, Coenen HH (2000) Transport mechanisms of 3-[123I]iodo-alpha-methyl-L-tyrosine in a human glioma cell line: comparison with [3H]methyl]-L-methionine. J Nucl Med 41:1250–1255
25. Miyatake S, Kawabata S, Kajimoto Y, Aoki A, Yokoyama K, Yamada M, Kuroiwa T, Tsuji M, Imahori Y, Kirihata M, Sakurai Y, Masunaga S, Nagata K, Maruhashi A, Ono K (2005) Modified boron neutron capture therapy for malignant gliomas performed using epithermal neutron and two boron compounds with different accumulation mechanisms: an efficacy study based on findings on neuroimages. J Neurosurg 103:1000–1009
26. Miyatake S, Tamura Y, Kawabata S, Iida K, Kuroiwa T, Ono K (2007) Boron neutron capture therapy for malignant tumors related to meningiomas. Neurosurgery 61:82–90; discussion 90–81
27. Miyatake SI, Kawabata S, Nonoguchi N, Yokoyama K, Kuroiwa T, Ono K (2009) Pseudoprogression in boron neutron capture therapy for malignant gliomas and meningiomas. Neuro Oncol 11(4):430–436
28. Nariai T, Senda M, Ishii K, Maehara T, Wakabayashi S, Toyama H, Ishiwata K, Hirakawa K (1997) Three-dimensional imaging of cortical structure, function and glioma for tumor resection. J Nucl Med 38:1563–1568
29. Nariai T, Tanaka Y, Wakimoto H, Aoyagi M, Tamaki M, Ishiwata K, Senda M, Ishii K, Hirakawa K, Ohno K (2005) Usefulness of L-[methyl-11C] methionine-positron emission tomography as a biological monitoring tool in the treatment of glioma. J Neurosurg 103:498–507
30. Nariai T, Ishiwata K, Kimura Y, Inaji M, Momose T, Yamamoto T, Matsumura A, Ishii K, Ohno K (2009) PET pharmacokinetic analysis to estimate boron concentration in tumor and brain as a guide to plan BNCT for malignant cerebral glioma. Appl Radiat Isot 67:S348–S350
31. Phelps ME, Mazziotta JC (1985) Positron emission tomography: human brain function and biochemistry. Science 228:799–809
32. Phelps ME, Hoffman EJ, Mullani NA, Ter-Pogossian MM (1975) Application of annihilation coincidence detection to transaxial reconstruction tomography. J Nucl Med 16:210–224
33. Raichle ME (1983) Positron emission tomography. Annu Rev Neurosci 6:249–267
34. Sanchez del Pino MM, Peterson DR, Hawkins RA (1995) Neutral amino acid transport characterization of isolated luminal and abluminal membranes of the blood–brain barrier. J Biol Chem 270:14913–14918
35. Suhara T, Takano A, Sudo Y, Ichimiya T, Inoue M, Yasuno F, Ikoma Y, Okubo Y (2003) High levels of serotonin transporter occupancy with low-dose clomipramine in comparative occupancy study with fluvoxamine using positron emission tomography. Arch Gen Psychiatry 60:386–391
36. Vahatalo JK, Eskola O, Bergman J, Forsback S, Lehikoinen P, Jaaskelainen J, Solin O (2002) Synthesis of 4-dihydroxyboryl-2-[F-18] fluorophenylalanine with relatively high-specific activity. J Label Compd Radiopharm 45:697–704
37. Wang HE, Liao AH, Deng WP, Chang PF, Chen JC, Chen FD, Liu RS, Lee JS, Hwang JJ (2004) Evaluation of 4-borono-2-18F-fluoro-L-phenylalanine-fructose as a probe for boron neutron capture therapy in a glioma-bearing rat model. J Nucl Med 45:302–308

38. Wittig A, Michel J, Moss RL, Stecher-Rasmussen F, Arlinghaus HF, Bendel P, Mauri PL, Altieri S, Hilger R, Salvadori PA, Menichetti L, Zamenhof R, Sauerwein WA (2008) Boron analysis and boron imaging in biological materials for boron neutron capture therapy (BNCT). Crit Rev Oncol Hematol 68:66–90
39. Yamamoto T, Nakai K, Kageji T, Kumada H, Endo K, Matsuda M, Shibata Y, Matsumura A (2009) Boron neutron capture therapy for newly diagnosed glioblastoma. Radiother Oncol 91:80–84

Boron Imaging: Localized Quantitative Detection and Imaging of Boron by Magnetic Resonance

12

Peter Bendel

Contents

12.1 Introduction

Nuclear magnetic resonance (NMR) is a popular method for spectroscopy (magnetic resonance spectroscopy – MRS) or imaging (MRI) [11]. Many of the stable isotopes possess a magnetic moment and are therefore amenable for detection by NMR. Among these isotopes are ^{1}H, the prevalent detected nucleus for medical diagnostic MRI (due to its abundance in water molecules), as well as ^{10}B, ^{11}B, ^{19}F, ^{13}C, ^{31}P, and others.

Since about two decades ago, there has been a continuous effort to apply NMR in its different forms to various stages of BNCT-related research and clinical

P. Bendel
Department of Chemical Research Support, MR Center,
The Weizmann Institute of Science, Shoham 60850, Israel
e-mail: pbendel@aspectimaging.com

W.A.G. Sauerwein et al. (eds.), *Neutron Capture Therapy*,
DOI 10.1007/978-3-642-31334-9_12,

implementation. These studies can be divided into the following categories: (1) NMR as a research tool for studying and screening BNCT agents in the test tube, in vitro cell cultures, and in vivo animal models, (2) NMR and MRI targeted to the detection of BNCT compounds, applied to patients after administration of the agent and before neutron irradiation, and (3) NMR and MRI targeted to the detection of chemically or isotopically modified BNCT compounds, applied to patients in pretreatment "rehearsal" studies, similar to the use of positron emission tomography (PET) for this purpose [17, 20]. At this point, it should be mentioned that, although the title of this chapter is "Boron imaging," we include in this chapter the *molecular* detection of the boron-containing compounds used in BNCT, even if the detection is through any nucleus (possibly other than ^{10}B), located in the same molecule, or even through the interaction between the BNCT agents and surrounding water molecules. A previous review focused on the applications of ^{10}B and ^{11}B NMR [1].

12.2 Background

The main advantages of NMR, in the context of its implementation as auxiliary tool for preclinical research related to and clinical application of BNCT, are that it is utterly noninvasive and nondestructive and that it is (at least potentially) quantitative. Another advantage is that it is versatile and able to provide various levels of information beyond quantification, such as metabolism, pharmacokinetics, etc. Its main disadvantages are low sensitivity and, for the imaging of BNCT agents, relatively low spatial resolution and slow performance time.

MRS and MRI refer to different approaches for gaining information from NMR experiments, although they sometimes differ merely in the way in which the data are presented. MRS achieves "spectral resolution" of different chemical environments for the detected nuclear isotope. In traditional NMR spectroscopy, this spectral information is obtained from an entire homogeneous sample, and therefore, "spatial resolution" or imaging of this sample is not achieved and would be superfluous for a homogeneous distribution in space. For in vivo applications, however, where the "sample" is heterogeneous, both spectral and spatial features will affect the results. At the simplest level, one can apply what is known as "localized MRS," where the NMR spectrum is collected from a confined region in space, either by virtue of the geometry of the detection hardware (surface coils) or by appropriate experimental design and data manipulation, or both. In its simplest implementation, the information is gathered from a single location or volume element (single-voxel MRS). In more advanced implementations, the spectra are obtained from several or many volume elements. In this case, one can choose to present the results either in the form of localized spectra (the NMR spectrum from each of the locations) or in the form of "metabolite images" in which a separate image is presented for each of the signals identified in the spectra, a method known as "spectroscopic imaging," or MRSI. In this sense, traditional MRI can be considered a special case of MRSI, where the detected nucleus is ^{1}H and the imaged molecules are water and fat, simply because these molecules contain the

highest abundance of ^{1}H nuclei in human and laboratory animal tissue and overwhelm the signals from other molecules by orders of magnitude.

All molecules used for BNCT contain boron, present at natural abundance predominantly (80 %) as ^{11}B and for treatment >95 % enriched in ^{10}B. Both boron isotopes are NMR detectable, but so are other nuclei in these molecules, such as ^{1}H, which are, in principle, also candidates for imaging BNCT compounds. The choice of which nucleus to use for detection is complex, depending mostly on considerations about sensitivity (see below) but also on other factors. For example, the absence of an endogenous background signal weighs in favor of ^{10}B or ^{11}B NMR, but ^{1}H NMR is more straightforward to implement on clinical scanners which are commonly equipped for ^{1}H detection.

12.2.1 Sensitivity and Spatial Resolution

The basic and most important question to address when discussing the use of MRI for the imaging of BNCT compounds concerns sensitivity and spatial resolution. What are the limits of imaging performance in terms of (1) the smallest concentration or amount of the BNCT compound, (2) the spatial resolution, and (3) the time required for this imaging process? The answers to the above questions 1–3 are not independent but tightly coupled. For experiments targeted at the detection of BNCT compounds, spatial resolution and performance time are limited by the signal-to-noise ratio (*SNR*). The signal is detected by a receiver coil which is tuned to the resonance frequency of a specific isotope, and the *SNR* is proportional to the total number of nuclear spins (of the detected type). Moreover, in the *SNR*-limited regime, the *SNR* will be, to a good approximation, proportional to the square root of the total scan time. This can be cast into the following equation:

$$SNR \propto Vc\sqrt{t} \tag{12.1}$$

where V is the effective sample volume, c is the concentration of the relevant nuclear species, and t is the total scan time. The precise definition of V depends upon the type of experiment being conducted. For spatially nonselective experiments (MRS in its simplest form), V is the entire part of the sample within the sensitive volume of the receiver coil, while for MRI experiments, V is the volume of a single voxel in the image. In this case, V can be expressed in terms of a length unit, a, which, for a cubic voxel, will lead to:

$$SNR \propto a^{3}c\sqrt{t} \tag{12.2}$$

a is the measure of spatial resolution. The smaller the value of a, the better the spatial resolution, and the best achievable resolution is the size of the volume element for which the *SNR* is acceptable or sufficient. Let us denote by $c_{\min}$ the minimal concentration of BNCT agent that can be detected by MRI. To quantify this parameter, we need to specify the *SNR* value which is sufficient for the desired

detection. This will inevitably be a somewhat vague definition, depending on the desired accuracy and precision. In any case, regardless of the precise *SNR* value that we define for this purpose, it can be shown that:

$$c_{\min} \propto t^{-\frac{1}{2}} \tag{12.3}$$

and

$$c_{\min} \propto a^{-\frac{1}{3}} \tag{12.4}$$

Similarly, for any concentration or *SNR* value, the achievable linear resolution depends only weakly on the total scan time, since:

$$a \propto t^{-\frac{1}{6}} \tag{12.5}$$

12.2.2 Factors Which Affect the Signal-to-Noise Ratio

12.2.2.1 Coil Size, Nuclear Spin, Field Strength

After identifying the *SNR* as the key parameter that limits the performance for detecting or imaging BNCT agents by NMR, let us review the dependence of *SNR* on basic physical and experimental factors, besides those already included in Eq. 12.1 [15, 16]. First, it can be shown that the signal, *S*, is proportional to:

$$S \propto V_c^{-1} I(I+1)\gamma^2 B_o \omega_o \tag{12.6}$$

where V_c is the effective volume covered by the receiver coil, I and γ are the spin quantum number and gyromagnetic ratio of the detected nuclear species, B_o is the scalar magnitude of the magnetic field along its principal direction, and ω_o is the detection frequency, which is also the resonance frequency of the detected nuclei ("Larmor" frequency), defined by:

$$\omega_o = \gamma B_o \tag{12.7}$$

On the other hand, the noise (*N*) induced in the receiver coil also depends on the detection frequency, to an extent which may be described by:

$$N \propto \omega_o^{\beta} \tag{12.8}$$

β can assume values between 0.25 and 1, depending on how heavily the coil is loaded by the sample. The value will be close to the lower limit for small and nonconducting samples (e.g., organic solvents) and close to the upper limit for

large and conducting samples, such as biological tissue. The proportionality in Eq. 12.8 cannot be applied over an arbitrarily large frequency range, because β also depends to some extent upon ω_o, tending to the lower limit for low frequencies and increasing for high frequencies. The dependencies in Eqs. 12.6, 12.7, and 12.8 can be combined to:

$$SNR \propto V_c^{-1} I(I+1)\gamma^{(3-\beta)} B_o^{(2-\beta)} \tag{12.9}$$

Equation 12.9 shows that *SNR* can be increased by using small coils (which will of course also limit tissue or organ coverage) and by using the highest possible field strength. There will also be significant differences between nuclear species, depending on their characteristic values of I and γ. ^{1}H is the most sensitive nucleus for NMR detection. Comparing the relative NMR sensitivities for different nuclei at the same field strength and assuming to be in the regime where $\beta = 1$ (a reasonable approximation for human "samples" at high magnetic fields), one arrives at sensitivities of 0.8 for ^{19}F, 0.5 for ^{11}B, and 0.19 for ^{10}B, relative to an assumed value of 1.0 for ^{1}H. This comparison ignores, however, other factors that may be important for experiments under realistic conditions (in particular MRI), namely, relaxation times, which will be summarized in the following section.

12.2.2.2 Relaxation Times

Relaxation times (or their reciprocal measures, relaxation rates) are intrinsic properties of ensembles of nuclear spins in a nonequilibrium state, measuring their return to equilibrium, which, for most cases, can be approximated by an exponential time dependence. They depend not only on the nuclear species but also on the molecular environment, both the immediate neighbors of the nucleus in the molecule and the microscopic environment of the molecule, particularly the rates of its molecular motions. The rate at which a perturbed nuclear spin system returns to thermal equilibrium (Boltzmann distribution) is characterized by a time T_1, and the rate at which it loses phase coherence by a time T_2. These relaxation processes affect the SNR values of MRS and MRI experiments for the following reasons: First, in order to obtain sufficient information and accumulate sufficient *SNR*, each image or spectrum must be based on repeated excitations or perturbations of the spin system, which are separated by a time TR. These repeated excitations increase *SNR* by signal averaging, which was taken into account in Eq. 12.1. However, if TR is of the order of, or even shorter than, T_1, the spin population (or "magnetization") will not be able to recover to its full equilibrium value between successive perturbations, and this will decrease *SNR*. Second, for various technical reasons, it is not possible to detect the signal at its most coherent state, which is immediately at the end of the excitation. The inevitable delay between excitation and detection is denoted by a time *TE*, and the loss of coherence during this delay also diminishes *SNR*. The effect of these mechanisms on SNR can be approximated by:

$$SNR = (SNR)_o T_1^{-\frac{1}{2}} \exp\left(-\frac{TE}{T_{2,\text{eff}}}\right) \tag{12.10}$$

where SNR_o contains all contributions other than T_1 and T_2. The parameter $T_{2,eff}$ was introduced to indicate that, depending on the type of imaging or spectroscopy experiment, it may (or may not) include contributions from local inhomogeneities in the magnetic field. Equation 12.10 indicates that short T_1 and long T_2 will be advantageous for NMR detection. Usually, nuclear spins with long T_1 will also have long T_2 (and vice versa), and the optimal choice of nucleus for detecting a certain molecule will depend upon molecular structure and its degree of motional freedom in the in vivo environment. For example, while ^{10}B NMR is possible and may be even advantageous for imaging of BSH, it may not be practical for the imaging of BPA, where its T_2 is prohibitively short.

12.3 Applications

At the time of writing of this chapter, no applications of MRI to the detection of BNCT agents in patients directly before treatment were reported. NMR and MRI were applied for basic research about molecular and pharmacological properties of compounds used for BNCT, including rehearsal studies in patients as well as in studies aimed at validating and optimizing possible methods for direct detection in patients, conducted in phantoms and laboratory animals. These will be summarized in the following sections, classified according to the detected nuclear species. In some published studies, several nuclear species were utilized for detection, either for a direct comparison between different approaches [2, 12] or for gathering complementary information on metabolic mechanisms and processes [21]. Imaging studies are usually performed by obtaining a conventional MRI at high spatial resolution for anatomic registration and overlay of the image of the boron distribution.

12.3.1 ^{11}B

^{11}B NMR was traditionally the natural choice for detecting and studying BNCT compounds by NMR, since it has 80 % natural abundance and is inherently more NMR sensitive than ^{10}B. Although it is clearly not suitable for direct pretreatment detection in patients (where the molecules are >95 % enriched with ^{10}B), it can be applied for studying uptake properties in preliminary studies as well as for in vitro and in vivo investigations in animal models [5, 18]. ^{11}B has relatively high NMR sensitivity (about 50 % the *SNR* of protons, see Sect. 2.2.1), which is further enhanced by a short T_1, but the very rapid transverse relaxation (short T_2) makes the implementation of ^{11}B MRI either difficult (for BSH) or outright impossible (for BPA). One of the earlier studies employing ^{11}B MRI in a human patient [10] still remains, to this day, the only viable demonstration of MRI of a BNCT compound in a patient.

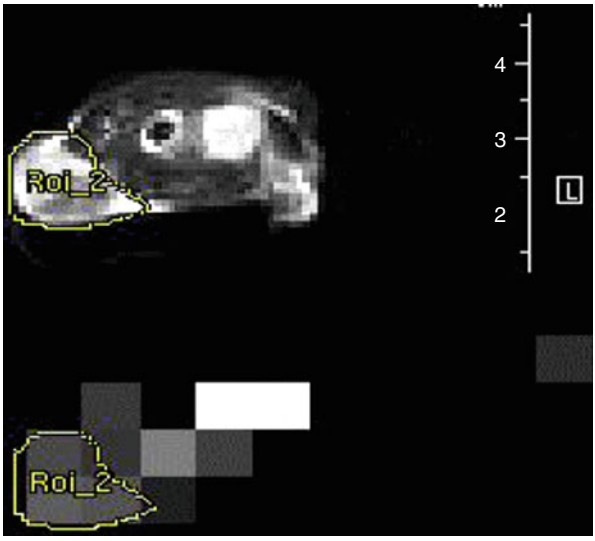

Fig. 12.1 The upper part is a conventional MRI showing a cross-sectional view through the lower abdominal region of a mouse. The lower part is a ^{10}B image shown on the same scale. The ^{10}B image is part of a 3D scan, obtained in 16 min with $(6\ \text{mm})^3$ isotropic resolution, 2 h after injection of BSH into the mouse's tail vein. The ^{10}B distribution shows the highest accumulation in the bladder (upper right side of the anatomy). The average concentration in an implanted M2R mouse melanoma tumor (lower left part of the anatomy) corresponds to 27 ppm (Reproduced with permission from Bendel et al. [6])

12.3.2 ^{10}B

Imaging or localized spectroscopy by ^{10}B NMR appears to be the natural choice for direct clinical implementation, since ^{10}B uniquely labels the administered BNCT agents. Although ^{10}B is a less-sensitive NMR nucleus than ^{11}B, its T_2 in biological environments is longer than that of ^{11}B at the same molecular location [2]. The implementation for detection in patients could be feasible for BSH but probably not for BPA where it has very short T_2, particularly in tissue environment. ^{10}B MRI of BSH was accomplished in mice [6], but only preliminary experiments were conducted to establish its feasibility for clinical implementation [7]. Figure 12.1 shows an example of BSH distribution in a mouse, imaged by ^{10}B MRI.

12.3.3 ^{19}F

^{19}F has almost the same sensitivity as ^{1}H for NMR detection and virtually no endogenous background signal in tissue and is therefore an attractive candidate for MRI or MRSI, since its chemical shift range also permits assignments to different molecules or molecular sites. It is also the 100 % natural abundant isotope of fluorine. An obvious method for labeling BNCT compounds is to substitute one of the

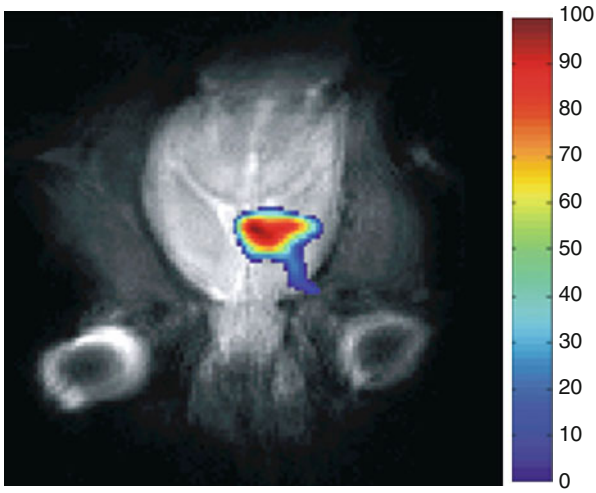

Fig. 12.2 Color overlay of a ^{19}F image superimposed upon a conventional MRI, obtained 2.5 h after administration of ^{19}F-BPA-fructose complex by ICA infusion. The high ^{19}F signal intensity coincides with the location of an implanted C6 rat glioma brain tumor. The ^{19}F image acquisition lasted for 77 min and has a spatial resolution of 1.85 × 1.85 × 40 mm (Reproduced with permission from Porcari et al. [22])

hydrogen atoms on the aromatic ring in BPA by fluorine, similar to the ^{18}F substitution used for PET. In contrast to PET, the fluorine-labeled BPA could also, in principle, be used for the neutron irradiation so that imaging and treatment would be achieved with the same molecule, although such a modified molecule would require separate approval for clinical use. The first demonstration for in vivo detection in a mouse tumor was reported over a decade ago using simple MRS localized by a surface coil [4], and recently, imaging of ^{19}F-labeled BPA was achieved in a rat brain tumor [22]. Figure 12.2 shows a representative image from this study.

12.3.4 ^{1}H

The use of proton detection is attractive, not only due to the inherent high sensitivity, but also because it can be implemented directly on commercial clinical MRI scanners. The drawback is that ^{1}H signals in vivo originate from an immense variety of molecules, and the task of separating and isolating the signals of the BNCT agents is not simple. Three categories of MRI and MRSI of BNCT compounds using ^{1}H NMR were reported:

The first obvious approach is the application of standard ^{1}H MRS or MRSI and identification of the signals from the administered boronated molecules. BSH has a prominent proton signal, but it is rather broad and overlaps with many other signals in the same chemical shift range. The situation is somewhat more favorable for BPA, where the aromatic-ring protons were identified as possible candidates for detection [24]. MRS and MRSI experiments using this approach were demonstrated in mice [8, 9], with a representative image shown in Fig. 12.3.

The second approach attempts to isolate the signal from the protons on the boronated molecules using their interaction (scalar coupling) with ^{10}B and thereby overcoming the problem of overlapping signals from other molecules [13]. In vivo, in vitro, and ex vivo results using this approach were reported [3, 12]. Practically,

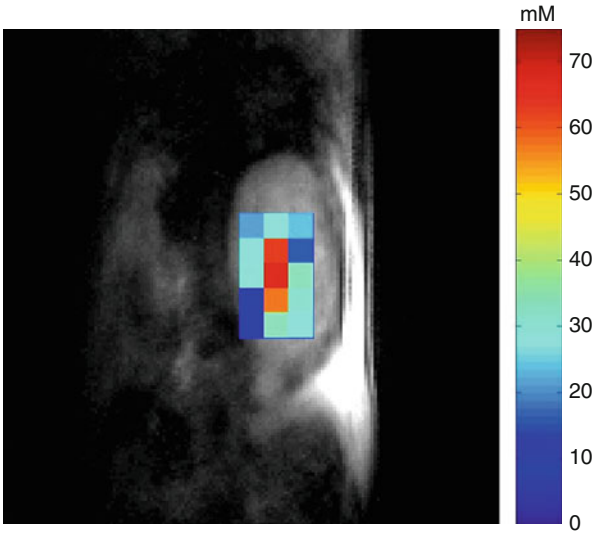

Fig. 12.3 The image shows a color overlay of the signal intensity from the aromatic-ring BPA protons, superimposed on a conventional MRI, focused on a mouse kidney. The *color bar* indicates the local concentration of total BPA (present as both free BPA and BPA-fructose complex). The MRSI data for the BPA image were acquired with a spatial resolution of 1.4×1.4×4.5 mm in 17 min. Image acquisition was started 18 min after the end of a 55-min long infusion of BPA-fructose into the tail vein (Reproduced with permission from Bendel et al. [8])

this approach is suitable only for BSH, although it was also argued that in this case (i.e., for BSH), the direct detection by ^{10}B NMR may provide comparable sensitivity [2]. Moreover, the implementation of this method is not straightforward on standard medical scanners, since it requires hardware suitable for the low ^{10}B frequency.

The third approach is different because it attempts to detect the BNCT agents not directly but rather through their influence on the relaxation properties of the water molecules in its vicinity, i.e., the boronated molecules act as conventional contrast agents. Therefore, the imaging is achieved with standard MRI, thereby providing a potentially tremendous improvement in sensitivity and spatial resolution. In order to achieve this goal, the boronated molecules have to be conjugated with paramagnetic or superparamagnetic moieties, which again raises problems concerning the degree of similarity between the uptake and washout properties between these modified compounds and the original molecules used for therapy, or the clinical approval of the contrast agents for NCT [19, 23]. Another possible variant for this approach would be applicable for GdNCT, since Gd-containing molecules are also MRI contrast agents [14].

12.4 Summary

There is no doubt that the clinical efficacy of BNCT would greatly benefit from an imaging method, which can provide noninvasive quantitative monitoring of the biodistribution of the administered BNCT agents, in real time. MRI (or localized

MRS) is potentially capable of this task but has so far not fulfilled this potential. There are several approaches and NMR techniques which could be applied, each with advantages and disadvantages, depending on the specific molecule that needs to be imaged. Direct ^{10}B MRI appears to be feasible for BSH, while the preferred approach for BPA is probably ^{1}H MRSI. Other approaches, such as ^{19}F MRI (for modified BPA) or contrast-enhanced ^{1}H MRI (for yet-to-be-developed combined BNCT-contrast agents) are also promising, but they work on molecules which are still not approved for the treatment itself. Whatever the method of choice, the sensitivity and spatial resolution of MRI will not be spectacular, reaching at best an imaging capability of ~10^0 ppm of Boron with linear spatial resolution of ~5 mm (in patients). The "indirect" detection of combined BNCT-contrast agents could achieve better performance. However, even at these modest levels of spatial resolution, the clinical benefit could be substantial.

References

1. Bendel P (2005) Biomedical applications of ^{10}B and ^{11}B NMR. NMR Biomed 18:74–82
2. Bendel P, Sauerwein W (2001) Optimal detection of the neutron capture therapy agent borocaptate sodium (BSH): a comparison between ^{1}H and ^{10}B NMR. Med Phys 28:178–183
3. Bendel P, Zilberstein J, Salomon Y (1994) In vivo detection of a boron neutron capture therapy agent in melanoma by proton observed ^{1}H-^{10}B double resonance. Magn Reson Med 32:170–174
4. Bendel P, Zilberstein J, Salomon Y, Frantz A, Reddy NK, Kabalka GW (1997) Quantitative in vivo NMR detection of BSH and ^{19}F-BPA in a mouse melanoma model. In: Larsson B, Crawford J, Weinreich R (eds) Advances in neutron capture therapy, vol II, Chemistry and biology. Elsevier, Amsterdam
5. Bendel P, Frantz A, Zilberstein J, Kabalka GW, Salomon Y (1998) Boron-11 NMR of borocaptate: relaxation and in vivo detection in melanoma-bearing mice. Magn Reson Med 39: 439–447
6. Bendel P, Koudinova N, Salomon Y (2001) In vivo imaging of the neutron capture therapy agent BSH in mice using ^{10}B MRI. Magn Reson Med 46:13–17
7. Bendel P, Koudinova N, Salomon Y, Hideghéty K, Sauerwein W (2002) Imaging of BSH by ^{10}B MRI. In: Sauerwein W, Moss R, Wittig A (eds) Research and development in neutron capture therapy. Monduzzi, Bologna
8. Bendel P, Margalit R, Koudinova N, Salomon Y (2005) Noninvasive quantitative in vivo mapping and metabolism of boronophenylalanine (BPA) by nuclear magnetic resonance (NMR) spectroscopy and imaging. Rad Res 164:680–687
9. Bendel P, Margalit R, Salomon Y (2005) Optimized ^{1}H MRS and MRSI methods for the in vivo detection of boronophenylalanine. Magn Reson Med 53:1166–1171
10. Bradshaw KM, Schweizer MP, Glover GH, Hadley JR, Tippets R, Tang PP, Davis WL, Heilbrun MP, Johnson S, Ghanem T (1995) BSH distributions in the canine head and a human patient using ^{11}B MRI. Magn Reson Med 34:48–56
11. Callaghan PT (1993) Principles of nuclear magnetic resonance microscopy. Clarendon, Oxford
12. Capuani S, Porcari P, Fasano F, Campanella R, Maraviglia B (2008) ^{10}B-editing ^{1}H-detection and ^{19}F MRI strategies to optimize boron neutron capture therapy. Mag Res Imag 26:987–993
13. De Luca F, Campanella R, Bifone A, Maraviglia B (1991) Boron-10 double resonance spatial NMR detection. Chem Phys Lett 186:303–306
14. Hofmann B, Fischer CO, Lawaczeck R, Platzek J, Semmler W (1999) Gadolinium neutron capture therapy (GdNCT) of melanoma cells and solid tumors with the magnetic resonance imaging contrast agent Gadobutrol. Invest Radiol 34:126–133

15. Hoult DI, Lauterbur PC (1979) The sensitivity of the zeugmatographic experiment involving human samples. J Magn Reson 34:425–433
16. Hoult DI, Richards RE (1976) The signal-to-noise ratio of the nuclear magnetic resonance experiment. J Magn Reson 24:71–85
17. Imahori Y, Ueda S, Ohmori Y, Kusuki T, Ono K, Fujii R, Ido T (1998) Fluorine-18 labeled fluoroboronophenylalanine PET in patients with glioma. J Nucl Med 39:325–333
18. Kabalka GW, Davis M, Bendel P (1988) Boron-11 MRI and MRS of intact animals infused with a boron neutron capture therapy agent. Magn Reson Med 8:231–237
19. Nakamura H, Fukuda H, Girald F, Kobayashi T, Hiratsuka J, Akaizawa T, Nemoto H, Cai J, Yoshida K, Yamamoto Y (2000) In vivo evaluation of carborane gadolinium-DPTA complex as an MR imaging boron carrier. Chem Pharm Bull 48:1034–1038
20. Nichols TL, Kabalka GW, Miller LF, Khan MK, Smith GT (2002) Improved treatment planning for boron neutron capture therapy for glioblastoma multiforme using fluorine-18 labeled boronophenylalanine and positron emission tomography. Med Phys 29:2351–2358
21. Panov V, Salomon Y, Kabalka GW, Bendel P (2000) Uptake and washout of borocaptate sodium and borono-phenylalanine in cultured melanoma cells: a multi-nuclear NMR study. Rad Res 154:104–112
22. Porcari P, Capuani S, D'Amore E, Lecce M, La Bella A, Fasano F, Campanella R, Migneco LM, Pastore FS, Maraviglia B (2008) In vivo ^{19}F MRI and ^{19}F MRS of ^{19}F-labelled boronophenylalanine–fructose complex on a C6 rat glioma model to optimize boron neutron capture therapy (BNCT). Phys Med Biol 53:6979–6989
23. Tatham AT, Nakamura H, Wiener EC, Yamamoto Y (1999) Relaxation properties of a dual-labeled probe for MRI and neutron capture therapy. Magn Reson Med 42:32–36
24. Zuo CS, Prasad PV, Busse P, Tang L, Zamenhof RG (1999) Proton nuclear magnetic resonance measurement of p-boronophenylalanine (BPA): a therapeutic agent for boron neutron capture therapy. Med Phys 26:1230–1236

Part IV

Physics

Physical Dosimetry and Spectral Characterization of Neutron Sources for Neutron Capture Therapy

13

David W. Nigg

Contents

D.W. Nigg
Nuclear Science and Engineering Division, Idaho National Laboratory,
MS 3860, P.O. Box 1625, Idaho Falls, ID 83415-3860, USA
e-mail: david.nigg@inl.gov

W.A.G. Sauerwein et al. (eds.), *Neutron Capture Therapy*,
DOI 10.1007/978-3-642-31334-9_13,

13.1 Introduction

In this chapter, we consider the experimental macroscopic physical dosimetry of neutron beams useful for boron neutron capture therapy (BNCT). Such neutron beams may be produced by small nuclear reactors or by particle accelerators and may be of the following types, categorized by their dominant ranges of neutron energy (E_n):

- Thermal beams ($E_n < 0.414$ eV) for cell and small-animal research.
- Hyperthermal ($E_n \sim 1$ eV) and epithermal ($0.414\ \text{eV} < E_n < 10$ keV) beams for small- and large-animal research and for human clinical applications.
- Fast-neutron ($E_n > 10$ MeV) beams for NCT-augmented fast-neutron therapy (NCT-FNT).

With minor variations, the techniques of macroscopic dosimetry covered in this chapter are applicable to all four beam types listed above. A detailed quantification of the spectral quality and physical dosimetric characteristics of the neutron source to be used is a key prerequisite for the practical application of BNCT. These characteristics include the following:

- The free-field neutron flux spectrum and intensity.
- Neutron-induced dose rates in standard phantoms and tissue resulting from neutron interactions that produce high linear energy transfer (LET) charged particles. Such particles include recoil protons from elastic scattering by hydrogen, 600 keV protons resulting from thermal neutron capture in nitrogen, and of course the alpha particles and lithium ions produced by neutron capture in boron, where boron is present.
- The dose rate of the incident photon component in the beam as well as the induced photon dose component, largely due to capture of thermal neutrons by hydrogen in tissue.
- Additional minor dose components due to neutron interactions with other tissue constituents, for example, neutron capture by chlorine and, at high energies, heaver ions resulting from elastic scatter by elements other than hydrogen. The latter interactions are ordinarily of significance only for NCT-FNT.

This information is required for confirmation that the neutron beam is in fact performing as intended, for use as input data in detailed radiation transport models of the patient anatomy used in treatment planning and clinical dosimetry, and for use as an aid in interpreting the results of preclinical and clinical studies. In recognition of this, the international BNCT research community has made significant efforts to identify and standardize certain key techniques and protocols that have been found useful. It is the intent of this article to offer a summary description of these, along with key supporting references, as a starting point and guide to further study for the practitioner entering this field of radiation oncology.

The scope of the discussion will be focused on the experimental quantification of the macroscopic *physical* performance characteristics of neutron beams for BNCT and their small, but inevitable, photon components incident to the neutron source production and the spectral tailoring process. Brief descriptions of advanced

radiation transport computational techniques and models useful as aids for experiment planning and beam performance data interpretation are also included.

The discussion is organized according to the various radiation measurement techniques that are commonly employed for physical dosimetry. It is assumed that the reader has some background and experience with radiation measurements at roughly the level of the classic texts by Knoll [33] and Attix [6]. A relatively detailed description of neutron activation spectrometry, generally viewed as the most robust (and the most reproducible and accurate) approach to the determination of the intensity and energy dependence of neutron sources used for BNCT will be presented first. Applications of gas-filled radiation detectors, both to provide additional neutron information and to separately quantify the incident photon component of the neutron source and the induced photon component in tissue, will then be covered. Finally, some specialized techniques that are useful in many situations are briefly summarized. Some recommended additional survey references for many of these subjects include Harker et al. [26], Rogus et al. [53], Järvinen and Voorbraak [31], Munck af Rosenschöld et al. [41], Auterinen et al. [7], Blaumann et al. [12], and Moss et al. [40].

It is important to note that the closely related field of treatment planning for BNCT is covered in a separate chapter. Discussions are also provided elsewhere for microdosimetry, the study of the basic physical and chemical mechanisms of radiation dose delivery on the cellular and subcellular levels of spatial resolution [55, 60, 61, 65]. This is also the case for biological dosimetry, the in vitro and in vivo study of the observable radiobiological effects that are induced in living organisms by neutron beams acting alone and in conjunction with the BNCT process [17, 46, 64]). The latter two fields are of crucial importance for the understanding of the biological effects of a given neutron beam (and of the BNCT process itself) and are dependent in turn on the physical characteristics of the neutron beam of interest, as is the treatment planning process.

Finally, it is important to recognize the importance of accurate and reproducible physical beam dosimetry as an essential tool for combination and intercomparisons of preclinical and clinical results from different centers. To this end, an international BNCT dosimetry exchange was conducted recently by the clinical BNCT research centers in Europe and in the Americas. This exchange has also served as a mechanism for further refinement and standardization of the most widely used experimental methods described here. Further details of this important effort are provided by Binns et al. [10, 11] and Riley et al. [50, 51].

13.2 Neutron Activation Spectrometry

Neutron activation spectrometry is based on the fact that different elements (and different isotopes of the same element) placed in a neutron beam will capture and scatter neutrons selectively with respect to the incident neutron energy. Some elements are primarily sensitive to capture of thermal neutrons; others have strong capture resonances in the epithermal energy range, while others exhibit interaction

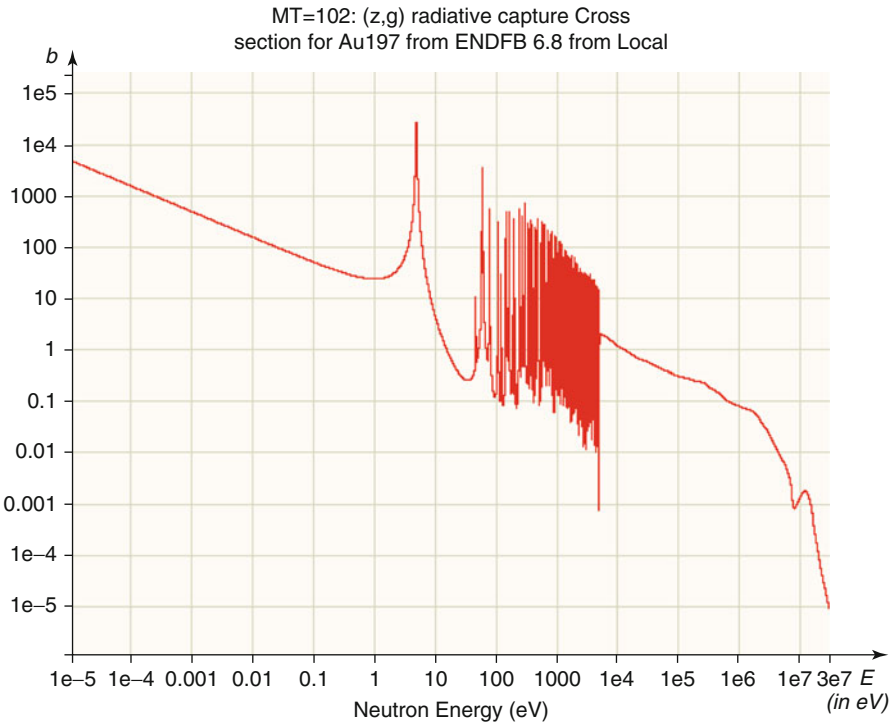

Fig. 13.1 Capture cross section (barns) of ^{198}Au (*Source*: OECD Janis 2.1)

energy thresholds for inelastic scatter, secondary neutron and charged particle emission, and fission, below which essentially no interactions occur. If the neutron interaction product for a particular nuclide is radioactive, then the induced radioactivity of a sample of that nuclide placed in a neutron beam will be largely proportional to the neutron flux at energies where interactions are most likely to occur in the sample. If different materials having different sensitivities to neutrons as functions of energy are activated in the same beam, it is ultimately possible to reconstruct a measured neutron spectrum from the induced activities. The level of spectral detail that can be reliably obtained generally corresponds to the number of different materials, and different interactions in the same materials, that are available.

13.2.1 Physical and Mathematical Basis

As an example to illustrate the underlying physics of activation spectrometry, Fig. 13.1 shows the capture cross section for ^{197}Au, which has a relatively high thermal neutron capture component as well as a prominent capture resonance at about 5 electron volts (eV). Capture of neutrons in a small sample (typically a foil or wire) of ^{197}Au produces ^{198}Au, which undergoes beta decay with emission of a

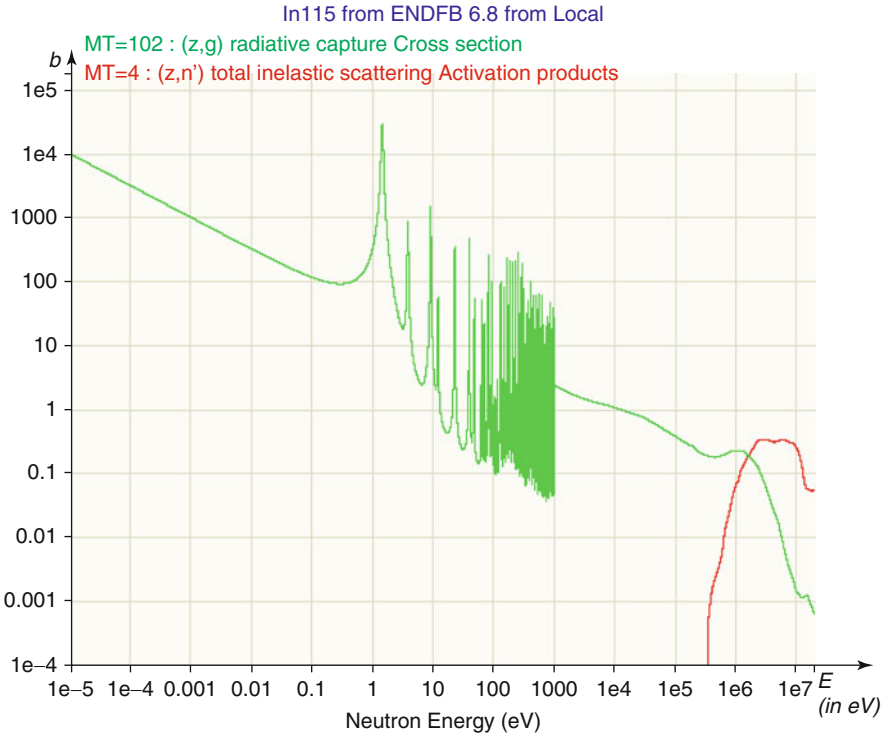

Fig. 13.2 Capture (*green*) and inelastic scatter (*red*) cross sections (barns) of ^{115}In (*Source*: OECD Janis 2.1)

prominent 0.411 keV gamma ray. The strength of this gamma ray is proportional to the neutron capture rate, which is for the most part proportional to the flux of neutrons at thermal energies and at 5 eV. If the sample is placed inside a cover made of cadmium, which absorbs essentially all incident thermal neutrons, then the interaction rate of the gold sample will be proportional to the neutron flux above thermal energies, primarily at 5 eV where the resonance occurs. The thermal and above-thermal neutron fluxes can then be separated by converting the measured induced activities to saturation activities (i.e., activation rates per atom), subtracting the activation rate of the cadmium-covered sample from that of the bare sample and computing the corresponding thermal neutron and total neutron fluxes. This is the classic cadmium difference method, and in effect it yields a two-energy group (thermal and above-thermal) spectrum. Elemental gold also exhibits several very useful and convenient threshold interactions for secondary neutron emission. These include (n,2n) up through (n,6n), covering the entire neutron energy range of interest for NCT as well as FNT, extending up to about 60 MeV [43].

As another example, cross-section data for ^{115}In are shown in Fig. 13.2. This nuclide (96 % abundance in natural indium) captures thermal neutrons, and it also has a strong neutron capture resonance at about 1 eV. In both cases, neutron capture

produces radioactive ^{116}In, which emits three prominent gamma rays with energies of 416, 1,097, and 1,293 keV. In addition, it will form an isomer by inelastic scatter of neutrons above about 400 keV. This yields ^{115m}In, which decays back to the ground state by emission of a 336 keV gamma ray. Hence, the inelastic scatter rate (and thus the neutron flux above the 400 keV threshold) is proportional to the measured activity of the 336 keV gamma ray, while the activities of the other three gamma rays, which also incidentally have a different half-life since they are associated with a different radionuclide (^{116}In), are largely proportional to the neutron flux at thermal energies and at 1 eV. If an indium foil is covered with cadmium, the thermal neutron capture rate is suppressed as described previously for gold. As a result, this single nuclide can be used to obtain information in three different energy ranges of the neutron spectrum of interest.

In the general case, a number of different activation responses (typically 8–12) are typically measured using a variety of different nuclides having different sensitivities to neutrons in the thermal, resonance, and fast-energy ranges. This permits the reconstruction of additional spectral detail in the unfolding process. Materials found useful for BNCT applications include gold and indium as described above, as well as copper, manganese, cobalt, dysprosium, uranium, copper, scandium, nickel, aluminum, and lanthanum.

We now consider some essential mathematical details of neutron activation spectrometry. In general, the volume-average activation rate per atom for a foil or wire dosimeter placed in a neutron flux field may be calculated as:

$$R = \int_0^\infty \sigma_d(E)\Psi_d(E)\mathrm{d}E \tag{13.1}$$

where $\sigma_d(E)$ is the microscopic activation cross section of interest for the dosimeter material, as a function of neutron energy, and $\psi_d(E)$ is the volume-average scalar neutron flux existing within the active dosimeter, again as a function of energy, and accounting for self-shielding effects, if any. Equation 13.1 can also be expressed as:

$$R = \int_0^\infty \sigma_d(E)\left(\frac{\Psi_d(E)}{\Psi(E)}\right)\Psi(E)\mathrm{d}E = \int_0^\infty \sigma_d(E)P_d(E)\Psi(E)\mathrm{d}E \tag{13.2}$$

where $\psi(E)$ is the unperturbed neutron flux that would exist at the measurement location in the absence of the flux perturbations caused by the dosimeter itself and any surrounding spectral modification devices and other structures placed in the beam (Cd covers, foil and wire positioning devices, etc.).

It may be noted here that, as a practical matter, the function $P_d(E)$ in Eq. 13.2 can be determined independently from $\Psi(E)$ if desired since it is simply a flux ratio. In this case, $\Psi(E)$ on the far right-hand side of Eq. 13.2 can be any appropriate a priori free-beam unperturbed flux estimate that is then modified by the self-shielding function $P_d(E)$.

Equation 13.2 may be written as a summation rather than as an integral by partitioning the range of the energy variable into a number of discrete contiguous energy groups:

$$R = \sum_{j=1}^{\mathrm{NG}} a_j \phi_j \tag{13.3}$$

where NG is the total number of energy groups,

$$a_j = \frac{\int_{\mathrm{EL}_j}^{\mathrm{EH}_j} \sigma_{\mathrm{d}}(E) P_{\mathrm{d}}(E) \Psi(E) \mathrm{d}E}{\int_{\mathrm{EL}_j}^{\mathrm{EH}_j} \Psi(E) \mathrm{d}E} \tag{13.4}$$

and

$$\phi_j = \int_{\mathrm{EL}_j}^{\mathrm{EH}_j} \Psi(E) \mathrm{d}E. \tag{13.5}$$

where EL_j and EH_j are the lower and upper energy limits of energy group j.

If additional dosimeter materials are placed in the beam, or if a particular material exhibits more than one independent activation response (e.g., gold or indium as noted earlier), then Eq. 13.3 may be written as a system of equations:

$$R_i = \sum_{j=1}^{\mathrm{NG}} a_{ij} \phi_j \tag{13.6}$$

where R_i is the total activation rate for interaction i and a_{ij} is the activation constant from Eq. 13.4 for reaction i due to neutrons in energy group j. There will be a total of NF equations, where NF is the total number of activation responses available.

Effective shielded cross sections $\sigma_{\mathrm{d}}(E)$ and the corresponding shielded and unshielded a priori neutron fluxes suitable for computing the function $P_{\mathrm{d}}(E)$ in the above equations may be obtained by any of several well-established neutron transport modeling techniques and nuclear data libraries. A typical approach involves computation of application-specific cross sections and a priori fluxes for each dosimeter in the beam using Monte Carlo techniques, for example, MCNP [14]. This is crucial if self-shielding or mutual shielding (as in a stack of foils) is significant. The Monte Carlo calculations for dosimeter packages generally include only the dosimeters and surrounding support structure with a representation for the incoming space-, angle-, and energy-dependent incident neutron source that has been precomputed using a Monte Carlo or deterministic computational model of the entire neutron beamline upstream from the irradiation location. The beamline computations may also be done with MCNP, or with a standard multidimensional discrete-ordinates

code such as DORT [49, 63]. It is also possible to use highly dilute foils [7] to avoid the need for a self-shielding correction, facilitating the direct application of standard dosimetry cross-section libraries. The dosimeter packages can usually also be designed to avoid mutual shielding, depending on the desired application.

The system of activation equations, Eq. 13.6, may be written out in matrix form as:

$$\begin{bmatrix} a_{11} & a_{12} & a_{12} & \cdots & a_{1\mathrm{NG}} \\ a_{21} & a_{22} & a_{23} & \cdots & a_{2\mathrm{NG}} \\ a_{31} & a_{32} & a_{33} & \cdots & a_{3\mathrm{NG}} \\ \vdots & \vdots & \vdots & & \vdots \\ \vdots & \vdots & \vdots & & \vdots \\ a_{\mathrm{NF1}} & a_{\mathrm{NF2}} & a_{\mathrm{NF3}} & & a_{\mathrm{NF\,NG}} \end{bmatrix} \begin{bmatrix} \phi_1 \\ \phi_2 \\ \phi_3 \\ \vdots \\ \phi_{\mathrm{NG}} \end{bmatrix} = \begin{bmatrix} R_1 \\ R_2 \\ R_3 \\ \vdots \\ \vdots \\ R_{\mathrm{NF}} \end{bmatrix} \tag{13.7}$$

or, more compactly:

$$[A][\Phi] = [R] \tag{13.8}$$

Equation 13.7 is exact, provided that the reaction rates R_i, the activation constants a_{ij}, and the group fluxes φ_j, are all self-consistent. If experimentally *measured* reaction rates (as opposed to the a priori reaction rates) for each interaction R_i are substituted into Eq. 13.7, a solution of the resulting new system of equations for "measured" fluxes corresponding to the measured reaction rates may also be obtained under certain conditions.

If NF = NG in Eq. 13.7, then the matrix [A] is square, its inverse will ordinarily exist, and the unknown flux vector may be obtained by any standard solution method that converges, provided that the rows of [A] are linearly independent to a sufficient degree and the measured reaction rates are sufficiently precise. In physical terms, the former requirement implies that the response functions (cross sections) for the activation interactions used in the measurement must be selected such that they have sufficiently different shapes as functions of energy. Spectral modification devices (e.g., cadmium covers) can also be used to force linear independence. It may be noted that positive fluxes are not guaranteed to result from this procedure, but if the elements of [A] are computed in a sufficiently valid, physically realistic manner for the specific measurement configuration and if the measured reaction rates are accurately determined, a positive solution will generally be obtained. In practice, this situation (NF = NG) is exemplified by the previously noted cadmium difference method, which can readily be shown to be a special case of Eq. 13.7, with only two rows in the matrix, one for the bare foil and one for the covered foil. It also typically occurs when measuring pointwise fluxes at resonance energies [26] using stacks of foils and when measuring simple spectra in phantoms using flux wires composed of alloys of two materials with different spectral responses, such as copper and gold, or manganese and gold.

There are two possibilities for the situation where NF, the number of available activation response functions, is not equal to NG, the number of energy groups for which it is desired to obtain unfolded fluxes. If NF < NG, the problem is underdetermined and additional information must be introduced in some manner to permit a solution, as is done in the various types of "adjustment" techniques for spectrum estimation from activation data. These methods involve the numerical modification of an input a priori spectrum to produce calculated responses that give the best overall match to the measured responses in a least-squares sense. If NF > NG, the problem is overdetermined and the "extra" information that is thereby available can be incorporated into the determination of a unique solution for the group fluxes and their propagated uncertainties by a linear least-squares procedure [43]. This "direct" unfolding method has an advantage in that it converges to a single unique solution.

The "adjustment" methods for spectral unfolding allow the estimation of a spectrum having more energy detail than the number of linearly independent activation responses, but with one exception, these do not produce a unique solution – many solutions are possible from the same input data. A unique solution can be obtained only by the generalized least-squares method, which requires covariance information for all of the input parameters, including the input spectrum as well as the activation cross sections and the measured responses. This covariance information in effect constrains the solution to a single physically realistic optimum in a least-squares sense. Several adjustment codes based on this approach have been developed. A popular example is the LSL code [57].

If the covariance information required for least-squares adjustment procedures is not available, other somewhat more empirical adjustment techniques are widely used, one popular example being the method described by Draper [20], implemented as an option in the SAND-II code [38]. Effective use of such methods requires good physical insight and intuition, as the form of the input a priori spectrum and its assumed uncertainty, as well as the iteration strategy used to produce a solution, can have a significant influence on the results. A more complete review of the various spectral unfolding and adjustment methods is provided by Järvinen and Voorbraak [31] or in any of several other comprehensive sources widely available in the neutron physics literature.

Neutron activation spectrometry can be applied to any neutron field for which suitable activation responses can be measured, either in air, in a phantom, or in vivo. It is used worldwide as a primary recommended method for characterization of epithermal neutron beams [10, 11, 31]. It has also been successfully applied to thermal neutron beams (e.g., [15]) and to accelerator-driven fast-neutron beams intended for use in BNCT-augmented fast-neutron therapy (e.g., [43]). It is capable of high precision (<5 %) if experimental uncertainties are carefully managed throughout every step of the process. Precautions to be taken include the following:

- Use of high-purity, accurately assayed activation materials
- Careful weighing, preparation, and handling of the foil packages to ensure accurate knowledge of the foil masses and to avoid contaminants
- Careful recording of the activation and post-irradiation decay times of the foils
- Irradiation at constant flux if at all possible

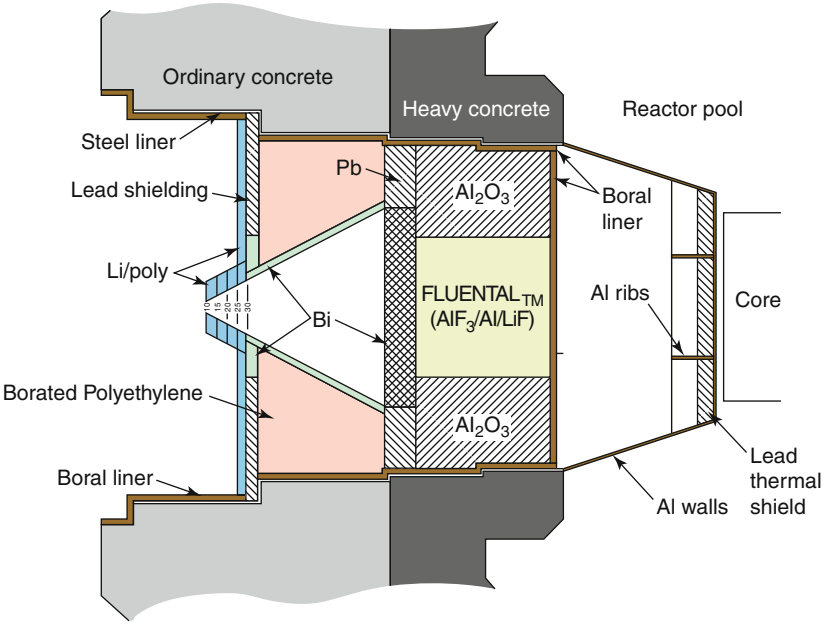

Fig. 13.3 WSU epithermal neutron beamline components. The reactor core is on the right

- Accurate, reproducible calibration of gamma spectrometers used for measurement of the foil activities, using certified, traceable standards
- Use of good techniques for the foil activity measurements in order to minimize uncertainties due to coincidence summing, counting geometry, etc.
- Thoughtful selection and application of unfolding techniques
- Use of multiple unfolding techniques to verify consistency

It is also important to recognize that in vivo activation measurements, especially in the case of thermal neutron beams, must be interpreted very carefully due to large flux gradients that depend on the specific target geometry, which can change in time and from one animal to the next because of respiration, motion, and other effects. As a result, reproducibility can be an issue and direct comparison with corresponding phantom measurements can be problematic.

13.2.2 Practical Application

Some recent measurements performed for the epithermal neutron beam constructed for preclinical BNCT research at Washington State University [44] provide a basic but illustrative example of an application of activation spectrometry for BNCT. Figure 13.3 shows a schematic diagram of the WSU epithermal neutron beam facility. The 1 MW WSU TRIGA™ reactor core is suspended from a movable bridge spanning an open pool. It can be positioned directly adjacent to a truncated

Fig. 13.4 Beam collimator installation at WSU showing the collimator with square exit port collar and lower borated polyethylene shielding

aluminum cone that extends horizontally into the reactor pool from the tank wall. This cone and the adjacent thermal column region penetrating the reactor shield monolith were originally filled with graphite. The epithermal neutron beam extraction components are located in this region.

A key distinguishing feature of the WSU facility is the incorporation of the high-efficiency neutron moderating and filtering material Fluenthal™, developed by the Technical Research Centre of Finland, into the design. A block of this material, which is composed of aluminum, aluminum fluoride, and lithium fluoride, is surrounded by aluminum oxide to produce the neutron filtering and moderating region shown in the figure. MCNP [14] and DORT [49] radiation transport design calculations using the BUGLE [54] cross-section library indicated that a free-beam epithermal neutron flux of approximately 10^9 n/cm^2-s would be produced at the irradiation position with the reactor core optimally loaded and operated at the design power of 1 MW. The background neutron kerma rate per unit useful epithermal neutron flux (a measure of the fast-neutron contamination) for the beam was calculated to be approximately 3.0×10^{-11} cGy/n-cm^2.

Figure 13.4 shows the bismuth collimator installation. The downstream end of the collimator is fitted with a bismuth collar designed to provide a transition from the circular shape of the cone to the square shape required to match with the lead shielding bricks comprising the final shield wall. The collar accommodates borated or lithiated polyethylene inserts to provide various beam aperture sizes and field shapes.

Neutron spectrum measurements for an imaginary transverse "source plane" passing through the base of the square flange on the downstream side of the bismuth collimator collar are summarized here. The source plane is a mathematical construct used for specifying the neutron source boundary conditions for the various dosimetry and treatment planning computations required to support each experimental irradiation. By definition, the physical beamline components upstream of the source plane do not change from one irradiation to the next. Components downstream of

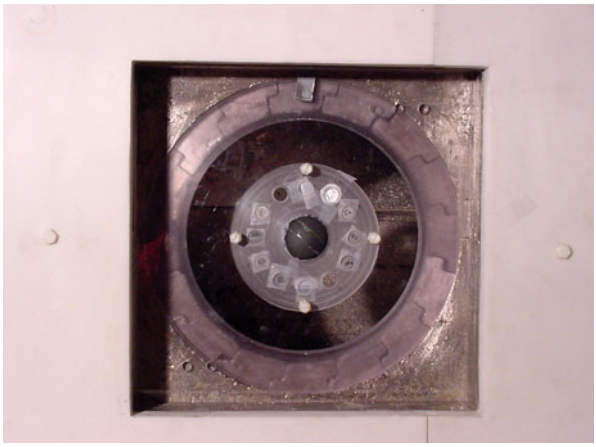

Fig. 13.5 Activation foil plate positioned in the WSU epithermal neutron beam source plane

Table 13.1 Activation interactions and foils used for the WSU epithermal neutron beam measurement example

Neutron interaction	Spectral modification	Energy range of primary response	Activation gamma energy of interest (keV)
^{197}Au (n, γ)	None	Thermal	411
^{115}In (n, γ)	Cadmium cover	1 eV resonance	1,293, 1,097, and 416
^{197}Au (n, γ)	Cadmium cover	5 eV resonance	411
^{186}W(n, γ)	Cadmium cover	18 eV resonance	686
^{55}Mn(n, γ)	Cadmium cover	340 eV resonance	847
^{63}Cu (n, γ)	Cadmium cover	1 keV resonance	511 (positron)
^{45}Sc(n, γ)	Cadmium cover	4.5 keV resonance	1,120, 889
^{115}In (n,n′)	Boron-10 shield	430 keV threshold	336

this plane, such as the field-shaping plates, can change for each irradiation and are therefore explicitly modeled in dosimetry and treatment planning computations. Time-consuming beam modeling computations are thus done only once for each beamline configuration upstream of the source plane, and the results are coupled to the patient dosimetry computations for each irradiation via a computed boundary condition specified for the source plane and validated by appropriate measurements such as described in this example.

Standard 12.7-mm (0.5") diameter In, Au, W, Mn, Cu, and Sc foils were used with a lexan foil positioning plate shown in Fig. 13.5. The neutron activation interactions and resulting gamma emissions of interest are listed in Table 13.1. These provide good coverage of the energy range of interest, but many other resonance and threshold interactions are available and are widely used [7, 31]. Cadmium covers are placed around some foils as indicated to suppress the thermal neutron response. Thus, each foil responds largely to neutrons having energies at or near the energy of the respective primary resonance of the foil material, as shown in the first six lines of Table 13.1. The covered foils were placed in outer foil positioning plate

positions. An uncovered gold foil was also placed in an outer position of the foil plate to measure the thermal flux. The foils had nominal thicknesses in the range of 0.0254 mm (0.001") to 0.127 mm (0.005"), depending on the material type.

An additional foil package is used to provide key spectral information in the energy range above epithermal ($E > 10$ keV). A heavy (~5 g) 25.4-mm diameter indium foil was placed in a small hollow boron sphere (inside diameter 2.8 cm, outside diameter 4.75 cm) located in the center of the foil positioning plate as can be seen in Fig. 13.5. The composition of the sphere is approximately 93 % ^{10}B and 7 % ^{11}B by weight, with a total boron density of 2.6 g/cm^3. This arrangement provides essentially total suppression of thermal *and* epithermal neutrons within the inner cavity of the boron sphere. Thus, an artificial threshold above the resonance neutron capture energy range for indium is imposed on the foil within the sphere. Since the activation gamma emissions that arise from neutron capture in indium are thereby suppressed, the relatively weak 336-keV gamma line from inelastic scatter in indium, which is of crucial interest in these measurements, is also much more prominent in the spectrum of the activated indium foil.

The irradiated foils used for this example were assayed at WSU using a standard high-purity germanium (HPGe) gamma spectrometry system (Canberra/Genie™). The induced activities in the foils were computed from the photopeak areas and system efficiencies based on calibration of the spectrometer using a National Institute of Standards and Technology (NIST)-traceable mixed europium-antimony calibration source. The measured activity of the heavy indium foil in the boron sphere was corrected for gamma self-shielding using an escape fraction at 336 keV calculated using a combination of MCNP computations and handbook data for the specific source-detector geometry that was used for the assay. This factor was 0.90 ± 0.01. The saturation activities of the various foils were then used to estimate the neutron spectrum by way of the overdetermined least-squares matrix unfolding procedure [43] discussed previously, with the required shielded foil cross sections computed using an MCNP model of the foil plate, the foils, and their surrounding spectral modification covers.

Figure 13.6 shows an unfolded 6-group free-field unperturbed neutron spectrum in the source plane, projected by the unfolding process (via the self-shielding factors) to the center of the foil positioning plate. The a priori 47-group neutron spectrum is also shown for comparison. The broad-group structure used for calculating the unfolded 6-group spectrum from the data for the eight activation interactions considered was selected to provide a well-conditioned unfolding matrix and to permit an accurate integration of the measured spectrum in the epithermal energy range to determine the total epithermal neutron flux. Integrating the measured curve over the epithermal energy range (0.5 eV–10 keV) produces a total epithermal neutron flux in the source plane of 1.66×10^9 n/cm^2-s at 1 MW with a propagated uncertainty of approximately 5 % (1σ).

A simple, but widely used, metric for the biophysical quality of reactor-based epithermal neutron beams is based on dividing the free-field neutron kerma rate of the beam (integrated over all energies above thermal) due to proton recoil by the useful epithermal neutron flux, again measured in the free field. This parameter is

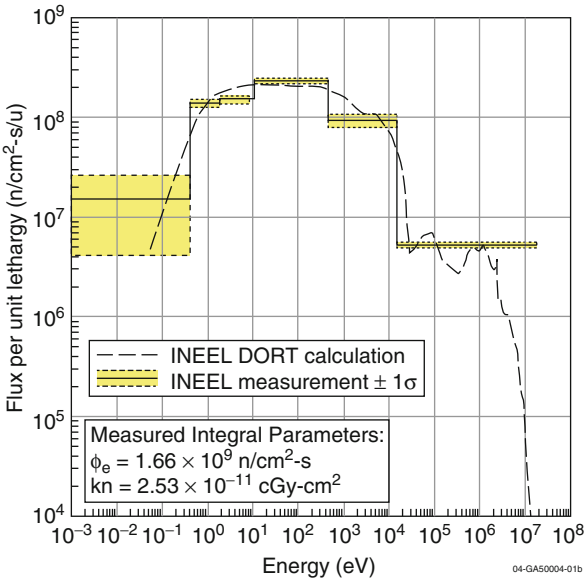

Fig. 13.6 Unfolded free-beam neutron spectrum in the source plane obtained by direct least-squares deconvolution for the WSU epithermal neutron beam facility. The reactor power is 1 MW

an indicator of the nonselective neutron background dose that will be produced in tissue by the above-thermal spectral component of the beam itself, in the absence of any neutron capture agent that may be administered to the patient. It is computed here for WSU using the measured flux spectrum in conjunction with broad-group kerma factors based on data for the components of standard tissue available on File 27 of the BUGLE [54] cross-section library. Fine-group neutron kerma factors are averaged over the broad unfolding group structure using the a priori spectrum as a weighting function to produce the necessary information. This procedure yields a measured free-beam spectral-average neutron kerma factor of 2.53×10^{-11} cGy total neutron kerma from all components per unit useful epithermal neutron flux, with an estimated uncertainty of about 7 %. This is in excellent agreement with the computed value of 2.75×10^{-11} cGy-cm^2.

Approximately 91 % of the direct background neutron dose from the WSU beam results from proton recoil. Additional background dose in tissue is of course produced by other nonselective, thermal-neutron-induced components, primarily neutron capture in nitrogen and hydrogen as noted earlier. These components are not directly indicative of the intrinsic biophysical quality of the incident beam. They must be taken into account in treatment planning, however, and are computed by folding the appropriate kerma factors with the measured spectrum in the same manner. The incident gamma component in the beam could also theoretically be measured by activation techniques (photoactivation of the ^{115}In isomer, e.g.), but this is not ordinarily done in BNCT practice for a number of reasons beyond the scope of this discussion.

Activation measurements are also widely used to characterize the neutron flux in various types of phantoms. Figure 13.7 shows a small polymethylmethacrylate (PMMA) phantom adjacent to a 10.16-cm beam aperture at WSU. Small segments

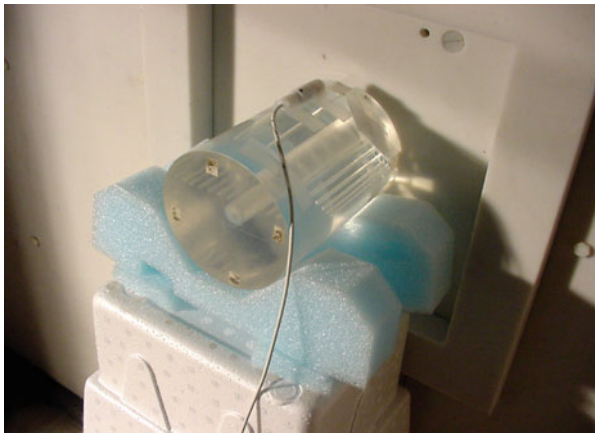

Fig. 13.7 Cylindrical PMMA phantom in the epithermal neutron beam at WSU. The diameter of the phantom is 12.5 cm and the length is 18.1 cm

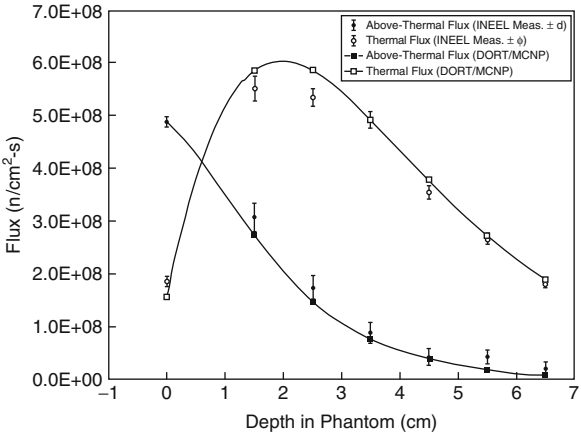

Fig. 13.8 Unfolded thermal and above-thermal flux along the central axis of a small PMMA phantom in the epithermal neutron beam at WSU. The horizontal axis corresponds to the distance downstream from the beam aperture plane

of copper wire containing 1.55 % gold by weight as placed on the axis of this phantom at various distances downstream from the aperture plane. Although copper has a weak resonance at about 1 keV, it is primarily sensitive to thermal neutrons, while gold is sensitive to both thermal and resonance neutrons, the latter primarily at about 5 eV. The gold and copper activation is measured simultaneously in each wire, and a two-group (thermal and above-thermal) spectrum can be unfolded from the data at each spatial location.

Figure 13.8 shows the results of the two-group spectral unfolding process for the phantom. Calculated and measured flux data are shown for comparison. Once the measured flux profiles are available, most of the significant BNCT dose components may be estimated as functions of depth in the phantom by application of appropriate spectrally averaged kerma factors as multipliers on the flux. The background hydrogen-recoil dose is essentially proportional to the above-thermal flux, while the nitrogen (n,p) dose and the boron neutron capture dose are proportional to the thermal

neutron flux. Neutron capture by hydrogen, which leads to emission of a 2.2 MeV gamma ray, is also proportional to the thermal flux, but the resulting photon source distribution is ordinarily used as input to a separate calculation of the photon dose that accounts for the fact that the source photons travel away from their initial locations prior to depositing significant radiation dose by the usual three mechanisms (photoelectric effect, Compton scattering, and pair production). The photon dose (both induced and incident) may also be measured directly by methods to be described in the following sections.

13.3 Gas-Filled Detectors

Various types of gas-filled radiation detectors have been successfully applied for measurement of the macrodosimetric properties of neutron sources for BNCT as well as for online beam intensity monitoring. The most important detector types that have been found useful for these applications are summarized in this section. These include ionization chambers, proton-recoil proportional counters, BF_3 and ^3He proportional counters, and fission chambers. Tissue-equivalent proportional counters, used primarily for microdosimetry, are not included here.

13.3.1 Ion Chambers

Paired ion chambers, one relatively more sensitive to neutrons and the other more sensitive to gammas, offer the most widely used method for online dosimetry of neutron sources used in BNCT. This approach provides additional information that complements what can be obtained from activation spectrometry and is in fact specifically recommended for separation of the incident gamma and neutron dose components in the "free" beam (i.e., the beam as it exits from the reactor or accelerator-based system used for neutron production and beam tailoring) as well as for measurements of the background neutron and gamma (incident and neutron-induced) dose components in standard water and tissue-equivalent plastic phantoms.

In general, ion chambers used for BNCT dosimetry should offer several design features that are important to this particular application [31]. The chamber size should be as small as possible, in order to minimize flux gradients across the active volume. The compositions of the wall and gas materials in the tissue-equivalent chamber should be the same as possible, and care should be taken so that the hydrogen and nitrogen contents are as close as possible to that of the tissue of interest. For example, A-150 plastic for the wall material is recommended as a good match to brain tissue. Minimum wall thickness for the tissue-equivalent chamber should be sufficient to provide charged-particle equilibrium for the most energetic recoil protons expected. The neutron-insensitive chamber should of course be constructed of materials with a minimum sensitivity to neutrons, especially in the thermal energy range. When used for in-phantom measurements, the wall thickness of

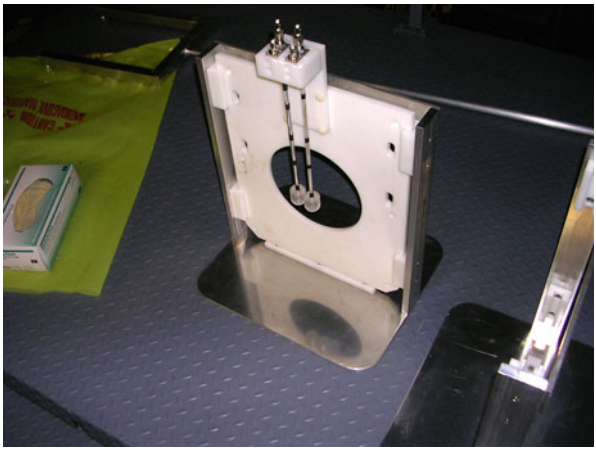

Fig. 13.9 Typical paired ion chambers used for BNCT dosimetry, with buildup caps in place for free-beam dosimetry

Fig. 13.10 Water phantom at WSU (*left*), with detail of paired ion chamber arrangement (*right*)

the neutron-insensitive chamber should be as thin as possible to minimize perturbation of the secondary electron fluence generated in the phantom.

Figure 13.9 shows a typical set of paired ion chambers, mounted on a lithiated polyethylene beam-shaping aperture plate that is used in the thermal neutron beam at the University of Missouri Research Reactor [15]. The active region of the gamma-sensitive chamber (FarWest™ IC-18) has a graphite wall with CO_2 gas. The neutron-sensitive chamber (FarWest™ IC-18 G) uses a tissue-equivalent gas (64.4 % CH_4, 32.5 % CO_2, and 3.1 % N_2 by volume) and a wall of tissue-equivalent plastic (e.g., A-150). The active volume of each of these chambers is 0.1 ml. Magnesium chambers with argon gas can also be used for the gamma measurement. Figure 13.10 shows the same chambers positioned in a standard water phantom at Washington State University [44].

These chambers feature several sophisticated details in their construction and operation. There is, for example, a grounded guard ring to bleed off leakage current between the actual active chamber region (a sphere at the tip of the long cylindrical stem) and the collection electrode. The chambers are connected to standard

electrometers and produce currents in the range of a few picoamperes in mixed neutron-gamma fields typical of BNCT applications. They typically operate with a bias voltage of 250 VDC, which for practical purposes is sufficient to achieve saturation. Low-noise cables should be used, and care should be taken to keep the cable out of the radiation field as much as possible to minimize spurious radiation-induced currents originating from locations other than in the chamber itself.

Ion chambers are initially calibrated by the manufacturer in a standard gamma field. For example, the IC-18G shown in the figures has a calibration of 1.64×10^{10} R/Coloumb. The corresponding tissue-equivalent chamber (IC-18) has a calibration of 2.25×10^{10} R/C. The chambers are calibrated for a standard gas flow rate, typically 5 ml/min at a specified gas pressure and temperature, typically 22 °C and 760 mm. Appropriate adjustments to the calibration are required if the gas conditions are not as stated in the calibration data. Use of buildup caps for measurements of the beam in air is generally recommended.

The responses of paired ion chambers may be characterized by the following two equations, which are solved simultaneously to determine the neutron and gamma doses:

$$N_u Q_u = h_u D_g + k_u D_n - t_u \varphi_{th} \tag{13.9}$$

$$N_t Q_t = h_t D_g + k_t D_n - -t_t \varphi_{th} \tag{13.10}$$

where:

D_g and D_n are the gamma- and neutron-absorbed doses in the reference material corresponding to the calibration (typically air or water).

N_u and N_t are the calibration factors (R/C) for the chambers for the neutron-insensitive and the tissue-equivalent chambers, respectively. Calibration data are generally provided by the manufacturer and may be used directly for beam design confirmation and preclinical dosimetry. *However, it is important to recognize that these factors must be independently confirmed against traceable standards in the case of clinical applications, as described elsewhere.*

Q_u and Q_t are the charges collected by the chambers, corrected for charge recombination (usually negligible) and for local temperature and air pressure as specified by the manufacturer.

h_u and h_t are the sensitivities of the chambers to the gamma radiation of interest relative to the sensitivities to the gamma field used for calibration and may be determined by any standard method that includes the effect of gamma spectral differences and, ideally, the local gamma field spatial perturbation by the chambers.

k_u and k_t are the sensitivities of the chambers to the neutron field of interest relative to the sensitivities to the gamma field used for calibration.

t_u and t_t are the sensitivities of the chambers per unit thermal neutron fluence.

ϕ_{th} is the thermal neutron fluence at the measurement location.

Determination of the sensitivities of the chambers to the neutron field of interest relative to the sensitivities to the gamma field used for calibration can be somewhat

complicated and application dependent. Useful information can be found in ICRU-26 [28] and ICRU-45 [29]. Typical values of relative neutron sensitivity for neutron-insensitive chambers range from zero to approximately 0.15, depending on details of the chamber construction and the specific application. Typical values for the tissue-equivalent chamber range from 0.9 to 1.4, depending again on the details of the chamber and on the application, as well as on the details of the correction for nitrogen (n,p) interactions. A complete discussion of these factors and their specific determination is beyond the scope of this chapter. Additional practical details on this subject, as well as on other key aspects of the paired ion chamber technique, are available in Rogus et al. [53], Raaijmakers et al. [47, 48], Kosunen et al. [35], and Roca et al. [52].

Paired ion chamber readings must be corrected to reflect dose in the reference tissue of interest relative to the response of the medium (e.g., a water phantom) used for beam characterization. In the case of the neutron-insensitive chamber, this is typically done using the ratio of the mass attenuation coefficients of the reference tissue relative to that of the phantom material, averaged over the gamma spectrum obtained from a calculation or perhaps from an actual spectral measurement. In the case of the tissue-equivalent chamber, the correction may be calculated using ratios of the neutron kerma factors for the two materials, averaged over the neutron spectrum.

Finally, the third terms on the right-hand side of Eqs. 13.9 and 13.10 are required to correct for thermal-neutron-induced dose to the chambers that is not characteristic of the tissue of interest. This is especially important in the case of the tissue-equivalent chamber since a significant component of its response results from the nitrogen (n,p) interaction, and the nitrogen content of the chamber wall and fill gas is not necessarily equivalent to that of the tissue of interest, which varies considerably (as much as a factor of 2) from one tissue type to another. The thermal neutron response of the chambers is typically computed using the thermal neutron flux determined by activation spectrometry as described previously, folded with the appropriate kerma factors for the chamber materials. Online measurement (e.g., [8]) can also be used to determine the chamber response of interest. In the case of of Eqs. 13.9 and 13.10, this response is subtracted from the chamber readings. The background dose to the tissue due to thermal-neutron-induced high-LET interactions such as (n,p) is then computed for the appropriate tissue composition and reported separately. Other, equivalent, mathematical formulations for the thermal neutron correction are also possible.

13.3.2 BF_3 and ^3He Detectors

The utility of these detectors is based on the fact that ^{10}B and ^3He have large cross sections for low-energy neutron capture with subsequent emission of energetic charged particles whose energy appears as collected charge in a suitable gas-filled tube [6, 33]. In the case of boron trifluoride, the emitted particles are lithium and helium ions, just as with the BNCT interaction in tissue. In the case of

^{3}He, energetic protons and tritons are released. These detectors are generally operated as proportional counters in pulse mode, allowing for discrimination against gamma radiation, but they do not generally provide any significant information about the energy of the incident neutrons. This type of detector, especially with boron trifluoride as the fill gas, has been found useful for online neutron beam monitoring and for thermal neutron measurements in various phantom and in vivo applications (see, e.g., [1, 58]).

13.3.3 Proton-Recoil Spectrometers

Recoil detectors for neutrons employ tubes filled with low molecular weight gasses (typically hydrogen or helium) at pressures up to a few atmospheres. Gas atoms that are elastically scattered by incident neutrons in the energy range where this type of detector is useful will be stripped of their electrons and will have sufficient energy to create many ion pairs in the surrounding gas as they slow down. The collected charge associated with each neutron scattering event will be proportional to the initial energy of the scattered ion. In the case of hydrogen-filled detectors, which have been the most popular for BNCT applications and therefore will be the primary subject of discussion here, the recoil proton spectrum bears a particularly simple relationship to the energy of the incident neutron. This is because (1) neutrons and protons have essentially the same mass and (2) elastic scattering of neutrons by hydrogen may be assumed to be isotropic in the center of mass system for neutrons having energies of interest in BNCT applications. As a result, it can be shown that the energy spectrum of the recoiling protons is constant with respect to energy, over the range from essentially zero up to the energy of the incident neutron. Furthermore, the elastic scattering cross section of hydrogen for neutrons in the energy range of interest for BNCT is also constant with respect to energy, facilitating the spectral unfolding process as described below.

Proton-recoil tubes are operated as proportional counters, in pulse mode. This typically requires that the neutron source of interest be operated at a much lower flux level for this type of measurement than is the case with actual clinical application. The measurements must thus be scaled to the full operating flux level, with any nonlinearity in the scaling factor properly accounted for. Each neutron scattering event in the detector gas produces a recoil proton. The ionization energy deposited in the gas by this proton appears as collected charge per pulse, and the signal is stored in the appropriate bin of a suitable multichannel analyzer. A proton-recoil spectrum is thus constructed, and the incident neutron spectrum may be unfolded from this spectrum using mathematical techniques based on the previously described relationship between the incident neutron energy and the recoil-proton energy spectrum. Basically, the magnitude of the proton-recoil spectrum at a given energy is proportional to the integral of all neutron scattering events that have occurred at this energy and above, and the incident neutron spectrum can in principal be obtained by simple differentiation of the recoil-proton spectrum. Energy calibration of the detector may be facilitated by the addition of a trace quantity of

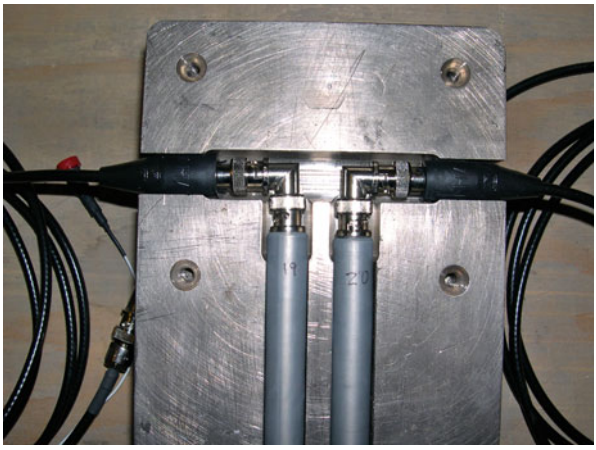

Fig. 13.11 Fission chambers used for beam monitoring at the Washington State University epithermal neutron beam facility (Reuter-Stokes Model P6-0402-101)

a suitable gas (e.g., nitrogen or ^{3}He) that exhibits a neutron capture reaction with emission of a proton or other charged particle with a known energy.

Although proton-recoil chamber counters can theoretically be used to detect neutrons of any energy, there are complications that limit their practical utility to the range of approximately 10 keV to typically a few MeV, and various corrections to the data are required. In the lower part of the useful energy range (10 keV up to approximately 100 keV for most devices), significant corrections must be made to separate the inevitable incident gamma content of essentially all neutron sources that are used for BNCT. These corrections can be made to some extent by direct subtraction if the absolute magnitude of the gamma contamination is known, and suitable gamma sources with spectra that are similar to that of the gamma content of the beam are available. Pulse-shape discrimination can also be used in the lowest part of the energy range to separate the gamma component, at the expense of somewhat more complicated electronics. In the higher parts of the energy range, corrections must be made for the fact that recoil protons may travel all of the way to the wall of the chamber without depositing all of their energy in the gas (the so-called wall effect). The correction for this effect is dependent on the pressure of the fill gas. As with all proportional counters, great care must be taken to avoid contamination of the fill gas with air, which would interfere with the charge multiplication process. A number of other considerations and precautions that must be observed in connection with the use of proton-recoil chambers, in general and specific to BNCT, are discussed in the literature [26, 33, 45].

13.3.4 Fission Chambers

Fission chambers used for BNCT applications generally take the form of small cylindrical tubes (Fig. 13.11) with a deposit of a fissionable nuclide on the inner surface. The fissionable material can be selected to permit detection of

fast neutrons, thermal neutrons, or both. They are used primarily as online beam intensity monitors, operated in current mode, but can also be operated in pulse mode, allowing discrimination of gamma radiation. A typical fission chamber used for BNCT has a small deposit (few milligrams) of ^{235}U on its inner surface and is therefore sensitive to low-energy neutrons. Typical fill gasses include argon or methane. Incident neutrons induce fissions in the uranium deposit, and the resulting fission fragments that travel into the gas cause ionization, and the resulting charge is collected and measured. The uranium deposit on the inner surface of the chamber may also include an appropriate quantity of ^{234}U as well to compensate for depletion of the ^{235}U during operation, especially if the chamber is to be used continuously.

Although the manufacturers of fission chambers generally provide calibration data, it is essential that fission chambers used for BNCT be calibrated for their specific application and their location in the neutron beamline relative to the source plane and the irradiation location. Calibration is typically accomplished via neutron activation spectrometry. Unlike self-powered neutron detectors (see Sect. 4.6), fission chambers conveniently provide an essentially immediate indication of any change in neutron beam intensity caused, for example, by the intentional closing of a beam shutter or by an unexpected change in reactor power or accelerator operating parameters.

13.4 Additional Techniques

Activation spectrometry and various gas-filled detectors have been the primary workhorses for neutron beam dosimetry and monitoring in BNCT. However, several additional radiation detection technologies, especially thermoluminescent dosimeters, have also been adapted for BNCT purposes and are used by various institutions and researchers for both beam characterization and some aspects of clinical dosimetry. The most prominent of these are described briefly in the following sections.

13.4.1 Scintillators

In the simplest sense, scintillation detectors are based on the emission of fluorescent light due to the excitation of atomic and molecular energy levels in the detector medium by ionizing radiation [33]. Scintillators may be in liquid or solid form and can be designed for measurement of neutrons or gammas. Inorganic crystals such as NaI and LaBr are widely used for radiation detection and spectrometry but have not seen significant use for direct beam characterization and dosimetry in BNCT. However, solid organic scintillators have been found useful. These may be in the form of pure organic crystals (e.g., anthracene, stilbene), or polymerized plastics (e.g., styrene, polyvinyl toluene, polymethylmethacrylate). Materials that feature a strong proton-recoil response are used for fast-neutron detection and spectrometry in BNCT, with the gamma response suppressed by pulse-shape discrimination.

Fig. 13.12 Thermoluminescent dosimeters arranged on a hamster phantom used for preclinical BNCT radiobiological studies [46]

Unfolding of the neutron flux from the recoil proton spectrum can in principal be accomplished by the same basic techniques as are used for gas-tube proton-recoil spectrometry although additional complications exist [31]. A boron compound can also be included in the scintillator, and the resulting signal is then largely proportional to the boron interaction rate at the measurement location. Applications of scintillators to BNCT are further described by Crawford et al. [18] and Ishikawa et al. [30]. Applications of scintillation in optical fibers have also been explored by Bliss et al. [13].

13.4.2 Thermoluminescent Dosimeters

In contrast to the types of scintillators described above, which emit a pulse of light essentially immediately after the deposition of radiation from a charged particle, thermoluminescent dosimeters (TLD) are designed to store the energy of the radiation in their solid crystal lattice until a later time, when the integrated energy, which is proportional to the radiation dose, is released by heating the dosimeter to a prescribed temperature. This design feature is accomplished by addition of so-called activator impurities that act as electron and hole trapping centers. The trapped charged carriers then recombine and produce optical photons when they are released by the heating process. Detailed descriptions of TLD physics are available in standard texts [6, 33].

Typical TLD materials include $CaSO_4$ with Mn added as an activator ($CaSO_4$:Mn), as well as CaF_2:Mn and LiF:Mn,Ti). LiF-based TLDs have seen the most use for BNCT applications. They are nearly tissue-equivalent and relatively inexpensive so that many measurements can be made at different locations in a phantom or in vivo subject (e.g., as in Fig. 13.12). Also, it is in principle possible to separate the neutron and gamma components of a mixed radiation field using lithium-based TLDs because they can be made sensitive primarily to neutrons through the use of enriched ^{6}Li (TLD-600), or

relatively insensitive to neutrons by use of ^{7}Li (TLD-700), although in the latter case, the neutron sensitivity cannot be completely eliminated and must be carefully accounted for in the analysis. Natural lithium LiF TLDs (TLD-100) are also available. Another type of lithium-based TLD that has been investigated for BNCT applications features a combination of Mg, Cu, and P as the activator and may offer somewhat improved capabilities for clean separation of neutron and gamma dose components.

A lengthy description of TLD applications and techniques in BNCT is beyond the scope of this chapter. The handling, calibration, and readout processes are complicated, but useful results can generally be produced with careful attention to detail. Excellent sources of additional information on BNCT-specific TLD applications include Järvinen and Voorbrack [31], Aschan et al. [3–5], Bilski et al. [9], Burn et al. [16], Croft and Perks [19], Kessler et al. [32], Konijnenberg et al. [34], Raaijmakers et al. [47, 48], Seppälä et al. [56], and Toivonen et al. [59].

13.4.3 Gel Detectors

Applications of Fricke dosimetry in tissue-equivalent gels have been explored as a possible means of two- and three-dimensional dosimetry in BNCT. In Fricke dosimetry, ferrous ions (Fe^{2+}) in a suitable medium (solution or gel) are converted to ferric (Fe^{3+}) ions through a complex series of chemical interactions that are induced by ionizing radiation. In the case of BNCT, gel detectors offer the possibility of three-dimensional dosimetry via, for example, irradiation of gel-based phantoms and subsequent imaging of the iron ion distribution using magnetic resonance imaging, whereby ferric and ferrous ions produce different perturbations of the proton relaxation rates in the medium [22]. Optical absorption imaging of the irradiated gel to quantify the dose distribution is also possible [23, 24].

13.4.4 Superheated Nucleation Detectors

The neutron activation approach for beam spectrometry is relatively simple and capable of very high accuracy in the energy ranges where many materials with linearly independent activation responses are available. However, it has a significant disadvantage when additional detail is desired for neutrons in the biologically important energy range of 10 keV to about 400 keV. Convenient materials with suitable characteristic activation responses (either resonance or threshold) are not readily available for detailed measurements in this radiobiologically important range of the neutron spectrum, just above the upper epithermal cutoff energy range. Other methods are available as noted elsewhere, but for the most part these also have their characteristic disadvantages. However, one promising low-cost alternate technique for this energy range is based on counting of radiation-induced nucleation sites in specialized superheated materials [2, 42].

An example of the implementation of this technique is provided by the RemSpec™ superheated drop detector (SDD) spectrometer. SDD dosimeter materials that are

Fig. 13.13 RemSpec superheated nucleation spectrometer unit positioned in the source plane at WSU

totally photon insensitive can be used with this device. These materials have thresholds for neutron detection between 50 keV and 1 MeV in the case of one medium and 500 keV to 10 MeV in the case of a second medium. In each case, the threshold energy can be fine-tuned by varying the temperature of the medium, and the response function of the medium above the threshold can be quantified. The RemSpec incorporates an SDD-containing vial, a temperature control system, and an acoustic sensor that records the formation of each nucleation site in real time, along with appropriate control and data acquisition software. Since the threshold and the response function of the SDD media are known at each temperature, it is possible to unfold the bubble formation data to produce a measured neutron spectrum within the energy range over which the medium is sensitive.

Figure 13.13 shows a RemSpec detector assembly positioned in the source plane of the previously described WSU beam. The actual detector material is enclosed in a tube that is incorporated into an insulated heating unit to vary the temperature as discussed above. An ion chamber is also suspended in the beam to provide an indication of the gamma dose rate in the free beam. The reactor power for the irradiation described here is on the order of a few tens of watts, in order to maintain a count rate within the specifications of the instrument.

Figure 13.14 shows some results from the RemSpec measurements. In this case, the fluxes are plotted on an expanded scale to show detail above about 30 keV, the lower threshold of the energy range that is detectable by this particular instrument. To obtain the results shown in this figure, the RemSpec detector response curves provided by the manufacturer were digitized to an 84-group equal-lethargy structure covering the energy range from 30 keV to 10 MeV. The a priori flux from the baseline beam design computations was likewise remapped into this same group structure. The spectrum implied by the RemSpec responses was estimated using a variation of the Sand-II empirical adjustment method [38] as described by Draper [20]. The measured results are normalized to a reactor power of approximately 300 kW in this particular case. The adjustment procedure produces a somewhat harder measured

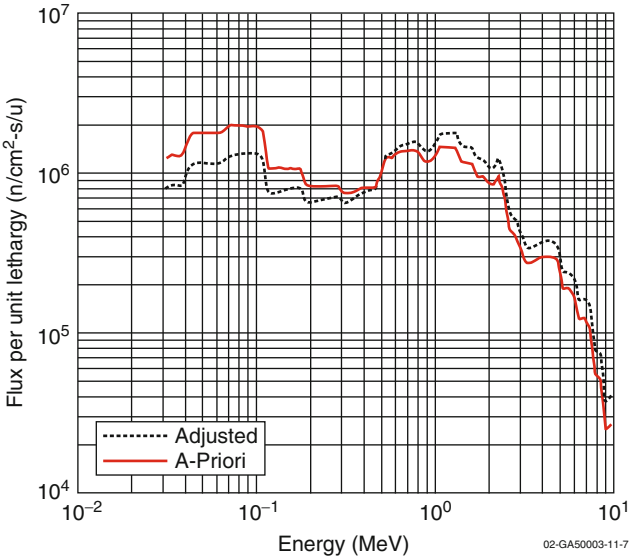

Fig. 13.14 Results of the RemSpec superheated nucleation detector measurements for the WSU epithermal neutron beam

spectrum compared to the a priori curve as seen in Fig. 13.14. Neutrons are shifted to the energy range above about 500 keV in order to produce the best fit to the observed detector responses.

13.4.5 Semiconductor Detectors

Semiconductors, which operate on the principle of electron–hole creation by radiation deposition, followed by pulse mode collection of the resulting current from each interaction, offer several advantages as radiation detectors and spectrometers. Their solid physical form provides significantly greater efficiency than gas-filled detectors, and the relatively low energy that is required to produce an electron–hole pair results in improved energy resolution compared to plastic or organic crystal scintillators. Germanium semiconductor detectors are of course very widely used for general high-resolution gamma spectrometry. These have been successfully applied for in-phantom monitoring of the 480 keV gamma that is produced by the boron-neutron interaction and the 2.2 MeV hydrogen capture gamma, yielding a viable method for monitoring of these dose components of BNCT therapy in vivo as well [62]. Silicon detectors alone, or with ^{10}B, ^{6}Li, or ^{235}U coatings that absorb neutrons to produce charged particles that subsequently create the detector signal, have also been used for neutron beam characterization [37] and as thermal neutron flux monitors in BNCT [25, 27, 36].

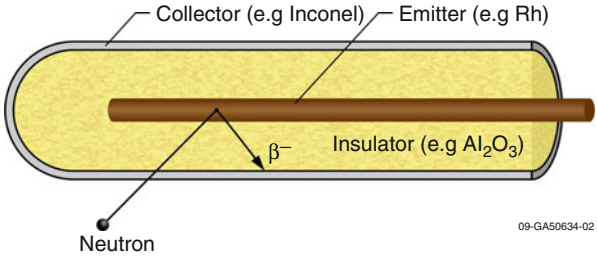

Fig. 13.15 Basic self-powered neutron detector design and operation

13.4.6 Self-Powered Neutron Detectors

Self-powered neutron detectors (SPND), or Hilborn detectors, offer a simple and robust method for online monitoring of neutron flux during BNCT irradiations. The basic principle of operation is illustrated in Fig. 13.15. A central electrode composed of a suitable metal with a relatively high neutron capture cross section is positioned within a surrounding cylindrical electrode, separated by an insulating material. In the most commonly employed mode of SPND operation, neutrons are captured in the central electrode, or emitter. Subsequent beta decay of the activation product produces energetic electrons that travel through the insulator to the outer electrode, producing a current in an external circuit. At equilibrium, this current is proportional to the neutron capture rate, and hence the neutron flux, at the location of the emitter.

Other interactions can also occur in an SPND and must be properly accounted for in the calibration process. These include prompt gamma production in the emitter and other structural materials, with subsequent Compton scatter of electrons that contribute to the detector current as well as production of electron currents via direct gamma interactions in the detector materials in the case of mixed neutron-gamma fields. Neutron and gamma interactions in the connection cable can also be significant and must be properly accounted for or canceled by suitable design of the external circuit.

Typical SPND emitter materials include vanadium and rhodium (Knoll 1999). Vanadium offers a lower sensitivity and is more suitable for measurements in high-flux fields typical of nuclear power reactors, whereas rhodium has a higher neutron cross section and corresponding higher sensitivity for neutron fluxes typical of BNCT (in the range of 10^9–10^{10} n/cm^2-s). Rhodium also has a shorter half-life for its most prominent beta decay mode, allowing equilibrium to be reached more quickly.

Miller et al. [39] have developed an implantable rhodium-zircaloy SPND that has proven useful for beam monitoring [15] as well as for in vivo neutron dosimetry [21]. This detector has an active length of 10 mm with an unusually small outer collector diameter of 2 mm to facilitate in vivo applications. Neutron calibration is typically accomplished by comparison with foil or wire neutron activation measurements.

Acknowledgments Preparation of this article was supported in part via a faculty-staff exchange grant administered by the Idaho National Engineering Laboratory under Battelle Energy Alliance, LLC contract no. DE-AC07-05ID14517 with the US Department of Energy. The author would also like to acknowledge Mr. Stuart Slattery, University of Wisconsin, for his assistance in compilation of the extensive bibliography that is presented here.

References

1. Alburger DE, Raparia D, Zucher MS (1999) Phantoms with $^{10}BF_3$ detectors for boron neutron capture therapy applications. Med Phys 25:1735–1738
2. Apfel RE, Lo Y-C (1979) Practical neutron dosimetry with superheated drops. Health Phys 56:79–83
3. Aschan C, Toivonen M, Savolainen S, Seppälä T, Auterinen I (1999) Epithermal neutron beam Dosimetry with thermoluminescence dosimeters for boron neutron capture therapy. Radiat Prot Dosimetry 81:47–56
4. Aschan C, Toivonen M, Savolainen S, Stecher-Rasmussen F (1999) Experimental correction for thermal neutron sensitivity of gamma ray TL dosimeters irradiated at BNCT beams. Radiat Prot Dosimetry 82:65–69
5. Aschan C, Lampinen JS, Savolainen S, Toivonen M (1999) Monte Carlo simulation of the influence of adjacent TL dosimeters on TL readings in simultaneous measurements in BNCT beams. Radiat Prot Dosimetry 85:349–352
6. Attix FH (1986) Introduction to radiological physics and radiation dosimetry. Wiley, New York
7. Auterinen I, Serén T, Uusi-Simola J, Kosunen A, Savolainen S (2004) A toolkit for epithermal neutron beam characterization in BNCT. Radiat Prot Dosimetry 110:587–593
8. Becker J, Brunckhorst E, Roca A, Stecher-Rasmussen F, Moss R, Böttger R, Schmidt R (2007) Setup and calibration of a triple ionization chamber system for dosimetry in mixed neutron/photon fields. Phys Med Biol 52:3715–3727
9. Bilski P, Budzanowski M, Ochab E, Olko P, Czopyk L (2004) Dosimetry of BNCT beams with novel thermoluminescent detectors. Radiat Prot Dosimetry 110:623–626
10. Binns PJ, Riley KJ, Harling OK, Kiger WS III, Munck af Rosenschöld PM, Giusti V, Capala J, Sköld K, Auterinen I, Serén T, Kotiluoto P, Uusi-Simola J, Marek M, Viererbl L, Spurny F (2005a) An international dosimetry exchange for boron neutron capture therapy, part 1: absorbed dose measurements. Med Phys 32:3729–3736
11. Binns PJ, Riley KJ, Harling OK (2005b) Epithermal neutron beams for clinical studies of boron neutron capture therapy: a dosimetric comparison of seven beams. Radiat Res 64:212–220
12. Blaumann HR, Gonzalez SJ, Longhino J, Santa Cruz GA, Calzetta Larrieu OA, Bonomi MR, Roth BMC (2004) Boron neutron capture therapy of skin melanomas at the RA-6 reactor: a procedural approach to beam setup and performance evaluation for upcoming clinical trials. Med Phys 31:70–80
13. Bliss M, Craig RA, Sunberg DS, Harker YD, Hartwell JK, Venhuizen JR (1997) Progress towards development of real-time dosimetry for BNCT. In: Larsson B, Crawford J, Weinrich R (eds) Advances in neutron capture therapy, vol I, Medicine and physics. Elsevier Science BV, Amsterdam
14. Breismeister JF (1993) MCNP – a general Monte Carlo N-particle transport code, Version 4A, LA-12625-M. Los Alamos National Laboratory, Los Alamos
15. Brockman J, Nigg DW, Hawthorne MF, McKibben C (2009) Spectral performance of a composite single-crystal filtered thermal neutron beam for BNCT research at the University of Missouri. Appl Radiat Isot 67:S222–S225
16. Burn KW, Colli V, Curzio G, d'Errico F, Gambarini G, Rosi G, Scolari L (2004) Characterization of the tapiro BNCT epithermal facility. Radiat Prot Dosimetry 110:645–649
17. Coderre JA, Morris GM (1999) The radiation biology of boron neutron capture therapy. Radiat Res 151:1–18

18. Crawford JF, Teichmann S, Stecher-Rasmussen F (1996) A direct comparison of neutron energy spectra at high and low powers in the HB11 beam at HFR Petten. In: Mishima Y (ed) Cancer neutron capture therapy. Plenum Press, New York
19. Croft S, Perks CA (1990) Corrections to gamma ray dosimetry measurements made in Harwell's two high-intensity filters neutron beams using ^{7}LiF thermoluminescent dosimeters owing to their neutron sensitivity. Radiat Prot Dosimetry 33:351–354
20. Draper EL Jr (1971) Integral reaction rate determinations – part I: tailored reactor spectrum preparation and measurement. Nucl Sci Eng 48:22–30
21. Gadan M, Crawley V, Thorp S, Miller M (2009) Preliminary liver dose estimation in the new facility for biomedical applications at the RA-3 reactor. Appl Radiat Isot 67:5206–5209
22. Gambarini G, Birattari C, Colombi C, Pirola L, Rosi G (2002) Fricke gel dosimetry in boron neutron capture therapy. Radiat Prot Dosimetry 101:419–422
23. Gambarini G, Colli V, Gay S, Petrovich C, Pirola L, Rosi G (2004) In-phantom imaging of all dose components in boron neutron capture therapy by means of gel dosimeters. Appl Radiat Isot 61:759–763
24. Gambarini G, Daquino GG, Moss RL, Carrara M, Nievaart VA, Vanossi E (2007) Gel dosimetry in the BNCT facility for extra-corporeal treatment of liver cancer at the HFR Petten. Radiat Prot Dosimetry 126:604–609
25. Harasawa S, Nakamoto A, Hayakawa Y, Egawa J, Aizawa O, Nozaki T, Minobe T, Hatanaka H (1981) Improved monitoring system of neutron flux during boron neutron capture therapy. Radiat Res 88:187–193
26. Harker YD, Anderl RA, Becker GK, Miller LG (1992) Spectral characterization of the epithermal neutron beam at the Brookhaven medical research reactor. Nucl Sci Eng 110:355–368
27. Hayakawa Y, Harasawa S, Nakamoto A, Amano K, Hatanaka H, Egawa J (1978) Simultaneous monitoring system of thermal neutron flux for boron neutron capture therapy. Radiat Res 75: 243–251
28. ICRU Report 26 (1977) Neutron dosimetry for biology and medicine. International Commission on Radiation Units and Measurement, Bethesda
29. ICRU Report 45 (1989) Clinical neutron dosimetry part 1: determination of absorbed dose in a patient treated by external beams of fast neutrons. International Commission on Radiation Units and Measurement, Bethesda
30. Ishikawa M, Ono K, Sakurai Y, Unesaki H, Uritani A, Bengua G, Kobayashi T, Tanaka K, Kosako T (2004) Development of real-time thermal neutron monitor using boron-loaded plastic scintillator with optical fiber for boron neutron capture therapy. Appl Radiat Isot 61:775–779
31. Järvinen H, Voorbraak WP (2003) Recommendations for the dosimetry of boron neutron capture therapy, Report 21425/03 55339/C, NRG Petten
32. Kessler C, Stecher-Rasmussen F, Rassow J, Garbe S, Sauerwein W (2001) Application of thermoluminescent dosimeters to mixed neutron-gamma dosimetry for BNCT. In: Hawthorne MF et al (eds) Frontiers in neutron capture therapy, vol 2. Kluwer Academic/Plenum Publishers, New York, pp 1165–1173
33. Knoll GF (2000) Radiation detection and measurement, 3rd edn. Wiley, New York
34. Konijnenberg MW, Raaijmakers CPJ, Dewitt L, Mijnheer BJ, Moss RL, Stecher-Rasmussen F, Watkins PRD (1992) Treatment planning of boron neutron capture therapy: measurements and calculations. Radiat Prot Dosimetry 44:443–446
35. Kosunen A, Kortesniemi M, Ylä-Mella H, Seppälä T, Lampinen J, Serén T, Auterinen I (1999) Twin ionization chambers for dose determinations in phantom in an epithermal neutron beam. Radiat Prot Dosimetry 81:187–194
36. Litovchenko PG, Moss R, Stecher-Rasmussen F, Appelman K, Barabash LI, Kibkalo TI, Lastovetsky VF, Litovchenko AP, Pinkovska MB (1999) Semiconductor sensors for dosimetry of epithermal neutrons, semiconductor physics. Quantum Opt Optoelectronics 2:90–91
37. Marek M, Viererbl L, Burian J, Jansky B (2001) Determination of the geometric and spectral characteristics of BNCT beam (neutron and gamma ray). In: Hawthorne F, Shelly K, Wiersema R (eds) Frontiers in neutron capture therapy. Kluwer Academic/Plenum Publishers, New York

38. McElroy WN, Berg S (1967) SAND-II neutron flux spectra determination by multiple foil activation iterative method. AWRL-TR-67-41, vol 1–4
39. Miller M, Mariani LE, Sztejnberg Gonçalves-Carralves ML, Skumanic M, Thorp S (2004) Implantable self-powered detector for online determination of neutron flux in patients during NCT treatment. Appl Radiat Isot 61:1033–1037
40. Moss RL, Stecher-Rasmussen F, Rassow J, Morrissey J, Voorbraak W, Verbakel W, Appelman K, Daquino GG, Muzi L, Wittig A, Bourhis-Martin E, Sauerwein W (2004) Procedural and practical applications of radiation measurements for BNCT at HFR Petten. Nucl Instrum Methods Phys Res B 213:633–636
41. Munck af Rosenschöld PM, Giusti V, Ceberg CP, Capala J, Sköld K, Persson BRR (2003) Reference dosimetry at the neutron capture therapy facility at Studsvik. Med Phys 30: 1569–1579
42. Nath R, Meigooni C, King C, Smolen S, d'Errico F (1993) Superheated drop detector for determination of neutron dose equivalent to patients undergoing high-energy X-ray and electron radiotherapy. Med Phys 20:78
43. Nigg DW, Wemple CA, Risler R, Hartwell JK, Harker YD, Laramore GE (2000) Modification of the University of Washington neutron radiography facility for optimization of neutron capture enhanced fast-neutron therapy. Med Phys 27:359–367
44. Nigg DW, Venhuizen JR, Wemple CA, Tripard GE, Sharp S, Fox K (2004) Flux and instrumentation upgrade for the epithermal neutron beam facility at Washington State University. Appl Radiat Isot 61:993–998
45. Perks CA, Gibson AB (1992) Neutron spectrometry and dosimetry for boron neutron capture therapy. Radiat Prot Dosimetry 44:425–428
46. Pozzi E, Nigg DW, Miller M, Thorp SI, Heber EM, Zarza L, Estryk G, Monti Hughes A, Molinari AJ, Garabalino M, Itoiz ME, Aromando RF, Quintana J, Trivillin VA, Schwint AE (2009) Dosimetry and radiobiology at the new RA-3 reactor boron neutron capture therapy (BNCT) facility: application to the treatment of experimental oral cancer. Appl Radiat Isot 67:S309–S312
47. Raaijmakers CPJ, Konijnenberg MW, Verhagen HW, Mijnheer BJ (1995) Determination of dose components in phantoms irradiated with an epithermal neutron beam for boron neutron capture therapy. Med Phys 22:321–329
48. Raaijmakers CPJ, Watkins PRD, Nottelman EL, Verhagen HW, Jansen JTM, Zoetelief J J, Mijnheer BJ (1996) The neutron sensitivity of dosimeters applied to boron neutron capture therapy. Med Phys 23:1581–1589
49. Rhoades WA, Childs RL (1988) The DORT two-dimensional discrete-ordinates transport code. Nucl Sci Eng 99:88–89
50. Riley KJ, Binns PJ, Harling OK, Kiger WS III, Gonzalez SJ, Casal M, Longhino J, Calzetta Larrieu OA, Blaumann HR (2008) Unifying dose specification between clinical BNCT centers in the Americas. Med Phys 35:1295–1298
51. Riley KJ, Binns PJ, Harling OK, Albritton JR, Kiger WS III, Rezaei A, Sköld K, Seppälä T, Savolainen S, Auterinen I, Marek M, Viererbl L, Nievaart VA, Moss RL (2008) An international dosimetry exchange for BNCT part II: computational dosimetry normalizations. Med Phys 35:5419–5425
52. Roca A, Nievaart VA, Moss RL, Stecher-Rasmussen F, Zamfir NV (2007) Validating a MCNPX model of Mg(Ar) and TE(TE) ionization chambers exposed to ^{60}Co gamma rays. Radiat Prot Dosimetry 129:365–371
53. Rogus RD, Harling OK, Yanch JC (1994) Mixed field dosimetry of epithermal neutron beams for boron neutron capture therapy at the MITR-II research reactor. Med Phys 21:1611–1625
54. Roussin RW (1980) BUGLE-80 coupled 47-neutron, 20 gamma-ray P3 cross section library, DLC-75. Radiation Shielding Information Center, Oak Ridge National Laboratory, Oak Ridge
55. Santa Cruz GA, Zamenhof RG (2004) The microdosimetry of the ^{10}B reaction in boron neutron capture therapy: a new generalized theory. Radiat Res 162:702–710

56. Seppälä T, Auterinen I, Aschan C, Serén T, Bevcizik J, Snellmn M, Huiskamp R, Abo Ramadan U, Kankaanranta L, Joensuu H, Savolainen S (2002) Dose planning with comparison to in-vivo dosimetry for epithermal neutron irradiation of the dog brain. Med Phys 29:2629–2640
57. Stallman FW (1986) LSL-M2: a computer program for least squares logarithmic adjustment of neutron spectra, NUREG/CR-4349, ORNL/TM-9933. Oak Ridge National Laboratory, Oak Ridge
58. Tattam DA, Allen DA, Beynon TD, Constantine G, Green S, Scott MC, Weaver DR (1998) In-phantom neutron fluence measurements in the orthogonal Birmingham boron neutron capture therapy beam. Med Phys 25:1964–1966
59. Toivonen M, Chernov V, Jungner H, Auterinen I, Toivonen A (1999) Response characteristics of LiF:Mg, Cu, P TL detectors in boron neutron capture therapy dosimetry. Radiat Prot Dosimetry 85:373–375
60. Van Vliet-Vroegendeweij C, Wheeler F, Stecher-Rasmussen F, Moss R, Huiskamp R (2001) Microdosimetry model for boron neutron capture therapy: I. Determination of microscopic quantities of heavy particles on a cellular scale. Radiat Res 155:490–497
61. Van Vliet-Vroegendeweij C, Wheeler F, Stecher-Rasmussen F, Huiskamp R (2001) Microdosimetry model for boron neutron capture therapy: II. Theoretical estimation of the effectiveness function and surviving fractions. Radiat Res 155:498–502
62. Verbakel WFAR (2001) Validation of the scanning γ-ray telescope for in-vivo dosimetry and boron measurements during BNCT. Phys Med Biol 46:1–17
63. Wheeler FJ, Parsons DK, Rushton BL, Nigg DW (1990) Epithermal neutron beam design for neutron capture therapy at the PBF and BMRR reactor facilities. Nucl Technol 92:106–118
64. Yamamoto T, Matsumura A, Yamamoto K, Kumada H, Hori N, Torii Y, Shibata Y, Nose T (2003) Characterization of neutron beams for boron neutron capture therapy: in-air radiobiological dosimetry. Radiat Res 160:70–76
65. Zamenhof RG (1997) Microdosimetry for neutron capture therapy: a review. J Neurooncol 33:81–92

The Clinical Commissioning of Beams for Neutron Capture Therapy

14

Per Munck af Rosenschöld

Contents

14.1 Introduction

The optimal energy for a neutron beam intended for BNCT for brain tumours is often referred to as epithermal, i.e. above thermal neutron energy (i.e. above 0.025 eV) [11, 46]. Depending on neutron production and on the design of the filter and the collimators, a neutron beam will exhibit different characteristics with respect to photon and fast neutron contamination [20]. Unique beam filter design has emerged through the computer optimisation process performed at each facility (e.g. [8, 16, 27]), which calls for individual characterisation of each neutron beam. Careful investigation and

P. Munck af Rosenschöld, M.Sc., Ph.D.
Department of Radiation Oncology – 3994, Radiation Medicine Research Center, Rigshospitalet, Blegdamsvej 9, Copenhagen, DK-2100, Denmark

Niels Bohr Institute, University of Copenhagen, Copenhagen, Denmark

Department of Medical Physics, Memorial Sloan-Kettering Cancer Center 10021, New York, USA
e-mail: per.munck@rh.regionh.dk

W.A.G. Sauerwein et al. (eds.), *Neutron Capture Therapy*,
DOI 10.1007/978-3-642-31334-9_14, © Springer-Verlag Berlin Heidelberg 2012

reporting of the properties of the radiation source, as well as the treatment details of clinical trials performed, are equally important in all radiotherapy modalities. The radiation absorbed dose delivered is traditionally one of the principal parameters in radiotherapy, as it is correlated to tissue response [18]. Thus, the uncertainty in the delivered absorbed dose is a treatment parameter that must be kept as low as possible. A few studies have discussed the acceptable level of total uncertainty in the dosimetry of a radiotherapy regime. The ICRU (Report 24 [21]) recommended that radiotherapy dosimetry should aim for an overall uncertainty of no more than 5 %, which has been interpreted as referring to an interval of 2 standard deviations (2 SD) [4]. Other authors suggested [12] that the uncertainty of the dose delivery in external photon and electron therapy should be no more than 3 % (1 SD) for curative treatments. Based on radiobiological considerations, Mijnheer et al. [41] found that the uncertainty of the dose delivery should be no more than 7.0 % (2 SD) in both photon and fast neutron therapy. Until information specifically relevant for NCT is made available, it is reasonable to assume the evaluation provided by Mijnheer et al. [41] applies also to NCT. The uncertainty associated with each individual step in the treatment procedure must thus introduce substantially lower dosimetric uncertainty in order to keep the overall uncertainty within these limits (Ahnesjö et al. [1]).

In the characterisation of mixed neutron-photon beams, it is necessary to quantify each dose component individually as the absorbed dose distributions and the relative radiobiological effect of the components in tissue are different (e.g. [14, 43–45]). We will now limit the discussion to the case of BNCT, but the formulation in this chapter can fairly easily be adapted to for instance gadolinium NCT. In BNCT, the irradiated tissue is subjected to (primarily) four biologically relevant absorbed dose components:

1. The photon absorbed dose
2. The fast neutron absorbed dose
3. The nitrogen absorbed dose
4. The boron absorbed dose

It is here suggested that the following definition is used: the photon absorbed dose is delivered by electrons produced in photon interactions. The boron absorbed doses and the nitrogen absorbed dose are delivered by the charged particles produced by neutron capture in boron and nitrogen, respectively. The fast neutron absorbed dose is the absorbed dose delivered by neutron scatter in hydrogen (producing recoiling protons). Please note that by this definition the "fast neutron absorbed dose" is delivered by neutrons with rather low kinetic energy down to some conveniently selected cut-off energy such as 0.5 eV. Other neutron interaction processes occur that give rise to absorbed dose in tissue, although these are of smaller relevance in BNCT and can often be considered negligible in comparison to the listed. A rigorous dose calculation in neutron beams would thus require a full simulation of neutron, photon and charged particle interactions, and a Monte Carlo-based approach is suitable and could be adopted for the purpose. In clinical BNCT, simplifications are often made in order to make the treatment planning process faster ([52, 53], see Chap. 16 for full details).

The topic of the following sections is the many measures needed to be taken before a radiotherapy treatment can be started.

14.2 Clinical Acceptance

The purpose of the clinical acceptance tests is to ensure that the equipment are safe to use in the clinic. The clinical acceptance procedure encompasses all tests needed to verify that the delivered equipment is meeting the specifications stipulated in the contract. The tests included are agreed upon as part of the purchase. The level of details of the specifications can vary and may even be non-existing such as in the case of a home-grown system. The acceptance procedure then involves the point-wise check of all delivered systems using previously agreed upon customer acceptance procedures. The tests are performed by representative/s of the manufacturer and the clinic. From the clinic's side, the person in charge of such a process is a certified medical physicist expert (EU Directive 97/43). In the case of a non-existing set of customer acceptance procedures, it is worthwhile to formulate a set of tests required to be fulfilled in order to ensure that the systems are safe for clinical use; there are many sources of information that could be drawn upon to this end (e.g. IAEA TRS-430, [5]).

All important parts of a facility must be subjected to an acceptance procedure, e.g. the beam and gantry (if applicable), the patient couch, the imaging system/s, the interlocks, radiation protection and safety, etc. In this chapter, however, we will limit the discussion to the beam. The acceptance and commissioning of the treatment planning system is detailed in Chap. 16. The main topics in interest related to the beam are the beam monitoring system and the beam properties (i.e. beam quality) and the reproducibility. Obviously, a beam intended for BNCT should not be heavily contaminated with photons and fast neutrons, or has a poor reproducibility in terms of beam quality or intensity, as that would compromise patient safety. Such serious problems would need to be corrected before a commissioning phase is started.

The performance of the beam monitors needs to be investigated during the acceptance procedure [9]. In particular, the accuracy, reproducibility and linearity of the beam monitors with neutron and photon fluence and fluence rate need to be carefully investigated as part of the acceptance. As an example, Fig. 14.1 shows one of the initial tests of the four beam monitors installed at the BNCT facility at Studsvik, Sweden. In the simple test shown in Fig. 14.1, the reactor power was stepwise increased, and the beam monitor count rate was recorded. As can be seen, the count rate was occasionally erroneously elevated in a few points. The problem was subsequently identified as a programming error in the control software and was corrected.

During the clinical acceptance phase, it is advisable to study parameters previously suggested by Zamenhof et al. [74]: advantage depth, advantage depth dose rate and advantage ratio. The parameters give an indication whether the neutron beam is well suited for BNCT, such an analysis was provided for instance by Kiger et al. [27] and Giusti et al. [16]. The advantage depth and advantage ratio parameters give an indication of the contamination of photons and fast neutrons. It must be pointed out that it is not sufficient to rely on a computer model for the generation of such data as impurities of the construction materials might significantly alter the beam properties; for instance, small impurities in materials at crucial positions in the beam line might impact the resultant photon component of the

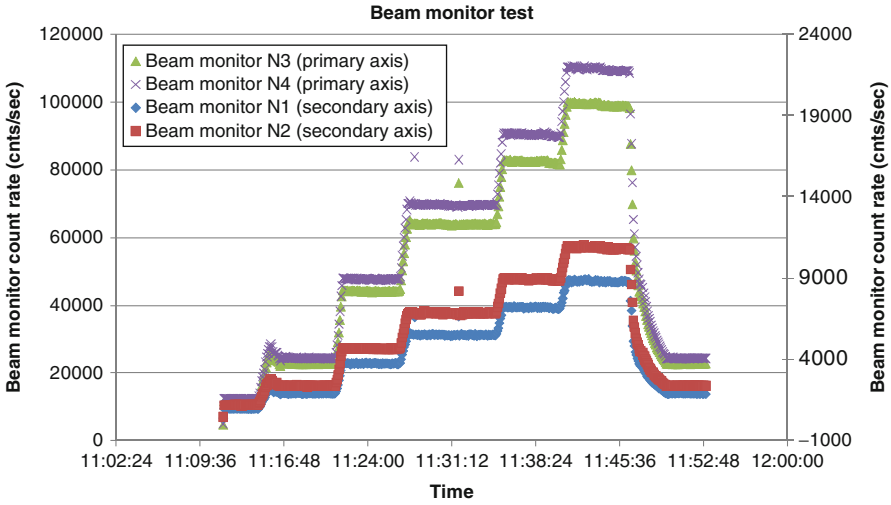

Fig. 14.1 Initial tests of the four beam monitors installed at the Studsvik facility, Sweden. The reactor power was stepwise increased, and the count rate of the beam monitors was recorded. As can be seen, the count rate was occasionally erroneously elevated in a few points. A programming error of the control system was detected and subsequently corrected.

beam. A computer model must be verified against measured data before it is used for calculation of advantage depth, advantage depth dose rate and advantage ratio.

Measurements free in air (or in a mini-phantom) (see for instance, [10]) have some interest for the validation of the computer model, but the clinical relevance of such data is less than in phantom data. In the end, the primary focus is to be able to get convergence of measured and calculated data using the treatment planning system in a tissue-equivalent phantom. The thermal neutron fluence and dose distribution in phantom are not overly sensitive to the photon and neutron spectra [17, 25]. For instance, for pure photon beams, it has been shown that it is adequate to know the average and spread of the energy in order to calculate a depth dose curve in water with high accuracy [25]. In-air measurements are therefore largely left out of the present treatise, and we limit the scope of the discussion to some brief comments. It should be noted that in-air data is useful for the purpose of comparison with existing and decommissioned neutron beams used for therapy such as that compiled by Harling et al. [20]. A beam with larger contamination of photons and fast neutrons than the previously used for BNCT is not advisable to accept for therapeutic purposes. One should be careful, however, to make sure that the same parameters are compared. Specifically, the kerma (kinetic energy released in matter) in air without the presence of the detector needs to be reported (refer to [50], for a full discussion). One should also be aware that significant deviations in calculated and measured in-air data have been observed, even for very elaborate computer models (for instance, [16]).

14.3 Commissioning

The steps that have been taken in the commissioning of facilities to date include characterisation of the beam in air, validation of the computer model usually constructed using a Monte Carlo-based model (e.g. MCNP, Briesmeister et al. [13]), dosimetry under reference conditions and finally clinical commissioning of the beam. These steps differ from those generally taken in commissioning of conventional radiotherapy equipment. However, dosimetric calculations in pure (or nearly so) photon beams are somewhat simpler and do not generally require a Monte Carlo-generated source file for dosimetric calculations of high accuracy, which is generally considered the case for BNCT – though some authors have experimented with a more simplistic approach for epithermal beams [58]. A comprehensive discussion regarding treatment planning systems in BNCT is provided in Chap. 16, and an overview of dosimetric detectors and methods for use in epithermal neutron beams is provided in Chap. 13.

As the beam has been deemed safe in the acceptance procedure, the aim of the commission process is thus to gather all data required for the clinical use. It is generally a quite extensive set of measurement data needed as input for or as verification data for the treatment planning system. The data set will then serve as reference for subsequent quality assurance procedures in which a subset of the commissioning parameters is checked. The procedure is commonly referred to as dosimetry under non-reference conditions. In addition to that, measurements need to be performed where the data is acquired in terms of absorbed dose per beam monitor unit (MU) for a reference point in a phantom, which is generally referred to as dosimetry under reference conditions [2, 4, 71].

14.3.1 Dosimetry Under Reference Conditions

Traditionally, BNCT dosimetry is loosely based on ICRU Report 26 [22] describing neutron dosimetry in biology and medicine and ICRU Report 45 [23] describing clinical dosimetry in fast neutron therapy. ICRU Report 45 was not intended for BNCT, which was also explicitly stated in the report, and it does not address a number of key issues for adequate BNCT dosimetry. The report serves however as a good source of information for neutron dosimetry in general. A report on BNCT dosimetry was recently stipulated by an international work group [71]; the following discussion follows largely the recommendations of that unique work.

14.3.1.1 Choice of Dosimeters

Two types of ionisation chambers are generally used for the determination of photon and fast neutron absorbed dose, while the thermal neutron fluence is best determined using activation detectors [34, 39, 49, 50, 54, 62, 63]. The detectors can be calibrated with a low uncertainty (about 1 %, 2 SD) at standards laboratories [50]. Two ionisation chambers of identical geometrical design but with different material choice is referentially used, which commonly referred to as the “twin” or

"paired ionisation chambers". A common choice is to make use of one chamber with a wall and central electrode of tissue-equivalent plastic (A-150 plastic) and flushed with tissue-equivalent gas ("TE/TE chamber") and one with a wall of magnesium and flushed with argon gas (a "Mg/Ar chamber"). The latter is often referred to as a "neutron-insensitive chamber", which is a fairly reasonable assumption looking at the neutron cross section of the materials, but in reality, oxidation of the magnesium causes a significant neutron response [50, 56]. An alternative ionisation chamber construction is to make use of graphite for wall and central electrode and flushing the chamber with carbon dioxide gas [63]. Graphite is a detector material in widespread use for photon dosimetry in the conventional field [4].

A significant amount of work has been performed using various kinds of dosimeters in epithermal neutron beams, including for instance thermoluminescence dosimeters [6, 7], dosimetry gels [67, 69], diodes [60], prompt gamma methods ([31]; Verbakel et al. [48, 70]), scintillator materials [33], proportional counters [42], activation detectors [10] and bubble detectors [15]. An overview of dosimeters in epithermal beams is presented in Chap. 13. For dosimetry under reference conditions in epithermal beams (often referred to as "absolute dosimetry"), it must be considered that ionisation chambers and activation (primarily) gold foils are currently the standard. Even so, somewhat surprisingly, the data appearing in open literature regarding correction factors to apply in clinical beams in the typical format found for other radiotherapy disciplines, i.e. reports AAPM TG51 [2] and IAEA TRS 398 [4], are scarce.

The use and corrections applicable to ionisation chamber measurements were provided in detail in the IAEA TRS-398 protocol [4], and the discussion provided in this reference is relevant also for measurements in neutron beams. Briefly, ionisation chamber signal collected needs to be corrected for temperature and pressure, polarisation, recombination effects and the electrometer charge collection correction. In addition, there is possibly also an unwanted signal arising from activation of parts of the detector materials when placing an ionisation chamber in the neutron beam. The signal caused by activation could be difficult to account for in practice considering that the irradiation history might not be known in sufficient detail. At the very least, the error introduced needs to be estimated and included in the uncertainty analysis.

14.3.1.2 Choice of Phantom

The ICRU Report 45 promotes the determination of absorbed dose to tissue inside a tissue-equivalent phantom, for instance in a water phantom. In fast neutron beams, the choice is reasonable given that the absorbed doses to water and tissue are comparable, and hence, the corrections required to account for the differences in the neutron/photon interaction properties are rather close to unity. This has then become the tradition within the neutron therapy community.

The situation is different in an epithermal neutron beam, however, where the total neutron absorbed dose during BNCT differs quite substantially in tissue and water. This dosimetric difference is due to the contributions of boron and nitrogen

neutron capture, causing the corrections related to the interaction properties to deviate quite strongly from unity. In addition, the geometry of the irradiated object affects the absorbed dose rate considerably in an epithermal neutron beam [51, 59]. Therefore, reporting absorbed doses resulting from boron and nitrogen capture, photons and fast neutrons to tissue inside a water phantom are not of high clinical relevance. By determining and reporting absorbed doses to the materials in which the measurements were performed, the problem is avoided in the sense that the clinical relevance of the values is not implied. This concept was introduced in Munck af Rosenschöld et al. [49]. More importantly, the suggested methodology allows adaptation of the mathematical formalism and dosimetric procedures concerning ionisation chambers to that formulated in the IAEA TRS-398 protocol [4]. The procedures in the IAEA report form the basis for radiotherapy dosimetry in general, and the exception is then only the fast neutron therapy field.

The effect of phantom material composition and size has been studied previously in epithermal neutron beams [32, 59, 65, 73]. In a previous work, an artificial "liquid brain" mixture was found to serve as an appropriate phantom material for dosimetry in epithermal neutron beams [65]. In other works, the authors used an ellipsoidal phantom for dosimetry under reference conditions to have a better representation of a human head [19, 63]. The material and geometric corrections from PMMA to brain tissue containing boron applicable in the Studsvik beam were presented in Munck af Rosenschöld [51], and strongly indicate their importance in BNCT dosimetry.

The international report on dosimetry of BNCT suggests the use of a water phantom for dosimetric measurements [71], the reference serves as an excellent and comprehensive guide for BNCT dosimetry, and this chapter largely adheres notation and methods described in that publication.

Though the geometry and material composition of a phantom have a large impact on the mixed neutron and photon radiation field of a beam optimised for BNCT, for dosimetry under reference conditions, a water phantom of a simple geometrical shape appears the best choice. Water is readily available, is cheap and practical to use and is also the choice for all other radiotherapy disciplines. Further, having a simple phantom geometry and composition to use for dosimetry under reference conditions simplifies future standardisation of measurement methodology and the collection and tabulation of correction factors for recommended dosimeters. However, in the subsequent step of commissioning the treatment planning system, it is useful to investigate the accuracy of the system to handle the effects of various geometrical shapes and composition in order to match the treatment situation more closely.

14.3.1.3 General Formalism

The commonly accepted formalism used in all disciplines of radiotherapy is here adopted and extended to cover neutron therapy [4], similar to what was previously suggested and presented [49], [50]. When a detector is calibrated in terms of absorbed dose to water is used at the reference depth in a water phantom for a

reference beam quality (Q_0) and in the absence of the detector, the absorbed dose is given by [2, 4]

$$D_{w,Q_0} = M_{Q_0} \cdot N_{D,w,Q_0} \tag{14.1}$$

In this work, it is assumed that the detector response could be separated into a signal arising from photons (index γ), fast neutrons (index *fn*) and thermal neutrons (index *tn*), giving

$$M_Q = M_Q^{\gamma} + M_Q^{fn} + M_Q^{tn} \tag{14.2}$$

Here, M_Q is the total detector response corrected for quantities affecting the measurement. The detector reading includes a response caused by interactions in the detector structures in the active medium in the detector. The corrected detector reading can be related to the absorbed dose to water (D_w) at the point of measurement in beam quality (Q) through the following equations:

$$D_{w,Q}^{\gamma} = M_Q^{\gamma} \cdot N_{D,w,Q}^{\gamma} \tag{14.3}$$

$$D_{w,Q}^{tn} = M_Q^{tn} \cdot N_{D,w,Q}^{tn} \tag{14.4}$$

$$D_{w,Q}^{fn} = M_Q^{fn} \cdot N_{D,w,Q}^{fn} \tag{14.5}$$

Three detectors with a different response to photons, thermal and fast neutrons are used in order to resolve the equation system arising from Eqs. 14.2, 14.3, 14.4, and 14.5. Instead of the dose to water from thermal neutrons (Eq. 14.4), it might be more convenient to refer to the thermal neutron fluence.

14.3.1.4 Photons

The calibration factor, $N_{D,w,Q}^{\gamma}$, needs to be known in order to derive the photon absorbed dose in the absence of the detector in the mixed beam. In a mixed radiation field, the calibration factor needs to be corrected by a beam quality correction factor that accounts for differences in perturbation effects and sensitivity (energy response) of the chamber compared to the calibration field. This yields a chamber calibration factor that can be used in the mixed radiation field Q, i.e.

$$N_{D,w,Q}^{\gamma} = N_{D,w,Q_0} \cdot k_Q^{\gamma} \tag{14.6}$$

where N_{D,w,Q_0} is the chamber calibration factor provided by a standards laboratory, herein assumed to be the quality of ^{60}Co gamma-rays, and k_Q^{γ} is the beam quality

correction factor applicable to the mixed radiation field for photons. This factor is therefore equivalent to the k_Q [2] and k_{Q,Q_0} factors [4] given by the recent dosimetry protocols based on absorbed dose to water standards. The k_Q factor is equal to unity for the reference beam quality by definition. The k_Q^γ factor for a mixed beam needs to be calculated. To my knowledge, presently, only data is available for a magnesium-walled and argon-flushed and an A-150-walled ionisation chamber for a decommissioned epithermal neutron beam in open literature [49]. In that reference, it was also shown that the beam quality of the epithermal neutron beam was similar to ^{60}Co gamma-rays which therefore is a reasonable reference beam quality. Equations 14.1 and 14.3 give

$$k_Q^\gamma = \frac{D_{w,Q}^\gamma / M_Q^\gamma}{D_{w,Q_0} / M_{Q_0}} \tag{14.7}$$

Preferably, the k_Q^γ factor is known through measurements in a number of beams. This is however not realistic in epithermal neutron beams given the dosimetric complexities involved of mixed beams and the lack of methods for absolute dosimetry methods. Instead, one has to rely on a calibration in a pure photon beam and calculations for the determination of a suitable correction of stopping power ratios and perturbation effects. Assuming that the detector signal per unit absorbed dose to the gas inside the ionisation chamber is the same regardless of the beam quality, one has

$$k_Q^\gamma = \frac{D_{w,Q}^\gamma / D_{\text{gas},Q}^\gamma}{D_{w,Q_0} / D_{\text{gas},Q_0}} \tag{14.8}$$

where D_{gas} is the absorbed dose to the detector gas originating from photons in the mixed beam (Q) and in the calibration (Q_0) beam. The assumption made in Eq. 14.8 is in fact the same as used in conventional photon and electron beam dosimetry, i.e. the average energy required for producing an ion pair in the detector gas is constant for the two beam qualities Q and Q_0 (c.f. IAEA TRS 277, Eqs. (5a) and (5b), [3]). All the factors in Eq. 14.8 can be calculated using a Monte Carlo computer program with a model of the detector and the two radiation beams and thus giving the k_Q^γ factor [49]. In lack of calculated data for the beam of interest, it might be necessary to assume that the k_Q^γ factor is equal to unity and assign an appropriate uncertainty.

14.3.1.5 Thermal Neutrons

The absorbed dose to water at point of interest can be derived as (assuming charge particle equilibrium)

$$D_{w,Q}^{tn} = f_{w,Q}^{tn} \cdot \Phi_{w,Q}^{tn} \tag{14.9}$$

where $f_{w,Q}^{tn}$ is the fluence-to-kerma conversion factor (i.e. "kerma factor") for water at the reference point in water in beam quality Q applicable for the thermal

neutron group fluence $\phi_{w,Q}^{tn}$. High-purity gold foils are recommendable for the determination of $\phi_{w,Q}^{tn}$, which is given by the following relation:

$$\dot{\phi}_{w,Q}^{tn} = A_{\mathrm{sat},Q} \cdot \left(\frac{\dot{\phi}_{w,Q}^{tn}}{A_{\mathrm{sat},Q}} \right)_{\mathrm{MC}} \tag{14.10}$$

Here, $\dot{\phi}_{w,Q}^{tn}$ is equal to the neutron fluence rate of the thermal group at the reference point without the presence of the foil, $\left(\dot{\phi}_{w,Q}^{tn}\right)_{\mathrm{MC}}$ is the corresponding thermal group fluence rate per source particle calculated by means of the Monte Carlo method for beam quality Q, $A_{\mathrm{sat},Q}$ is the measured saturated activity of the gold foil in Bq per gram of the sample and $\left(A_{\mathrm{sat},Q}\right)_{\mathrm{MC}}$ is the corresponding calculated saturated activity of the gold foil in Bq per gram of the sample and per source particle using the Monte Carlo method. The factors $\left(\dot{\phi}_{w,Q}^{tn}\right)_{\mathrm{MC}}$ are calculated in the position of the foil without the presence of the foil, and $\left(A_{\mathrm{sat},Q}\right)_{\mathrm{MC}}$ is calculated with the gold foil included in the computer model, preferably using Monte Carlo method. Thus, the ratio intrinsically includes the appropriate correction for the perturbation caused by the foil itself on the neutron field in the phantom at the reference position, within the limits of the accuracy of the Monte Carlo model.

The user could perform a comparative measurement using for instance a high-purity germanium crystal detector set-up with fixed settings of the analysis program (see for instance, Knoll [29] for information on such systems). Thus, allowing for a conversion between a signal measured (M_Q^{tn}) and the saturated activity reported by the standards laboratory for a fixed set of experimental conditions.

14.3.1.6 Fast Neutrons

The beam quality correction factor for fast neutrons is given by (cf Eq. 14.8)

$$k_Q^{fn} = \frac{D_{w,Q}^{fn} / M_Q^{fn}}{D_{w,Q_0} / M_{Q_0}} \tag{14.11}$$

where the factors were defined previously. Assuming that the detector reading can be written as the product of the absorbed dose delivered to the detector gas, $D_{\mathrm{gas},Q}$, the inverse of the average energy required to produce an ion pair in the detector gas for the actual charged particle spectra for beam quality Q, $\left(e/W\right)_Q^{\mathrm{eff}}$, and the mass of the detector gas, m_{gas}, gives

$$M_Q = D_{\mathrm{gas},Q} \cdot \left(e/W\right)_Q^{\mathrm{eff}} \cdot m_{\mathrm{gas}} \tag{14.12}$$

Inserting Eq. 14.11 in Eq. 14.12 gives

$$k_Q^{fn} = \frac{D_{w,Q}^{fn} \cdot W_Q^{fn,\mathrm{eff}} / D_{\mathrm{gas},Q}^{fn}}{D_{w,Q_0} \cdot W_{Q_0}^{\mathrm{eff}} / D_{\mathrm{gas},Q_0}} \tag{14.13}$$

Multiplication of dividend and divisor by $\left(f_m / f_t\right)_Q^{fn}$, i.e. the kerma factor ratio for the detector wall material, which is A-150 plastic (index = m), and muscle tissue (index = t) weighted by the actual neutron spectra at the point of interest gives

$$k_Q^{fn} = \frac{1}{k_t} \cdot \frac{D_{w,Q}^{fn} / D_{\mathrm{gas},Q}^{fn}}{D_{w,Q_0} / D_{\mathrm{gas},Q_0}} \cdot \left(f_m / f_t\right)_Q^{fn} \tag{14.14}$$

In Eq. 14.14, $k_t = \frac{\left(f_m / f_t\right)_Q^{fn} \cdot W_{Q_0}^{\mathrm{eff}}}{W_Q^{fn,\mathrm{eff}}}$, which is a simplified form of the neutron sensitivity factor for a tissue-equivalent detector for muscle tissue, k_t, that was calculated by Jansen et al. [24] as a function of neutron energy; it was given in its complete form in the ICRU Report No. 45. Calculation of the factors in Eq. 14.14 is possible by means of the Monte Carlo method.

14.3.2 Dosimetry Under Non-Reference Conditions

For clinical use, central-axis percentage depth dose (PDD) curves beam profiles (typically at several depths), and beam components as a function of distance from the aperture need to be measured. It might be practical and beneficial to use other dosimeters for the determination of the relative distributions as compared to the preceding chapter. For instance, using dosimeters with less need for MC derived corrections with high signal to noise appear attractive for use as long as the relative sensitivity to the beam dose components of the dosimeters can be established accurately.

The usefulness of varying the field size is probably less for NCT than for conventional photon therapy, so the number of useful field size combinations are likely to be less. The magnitude of the beam dose components and the relative distribution of the components does vary for as a function of aperture size for epithermal neutron beams (Raaijmakers et al. [57]). Therefore, if different field sizes or beam apertures are available, the dosimetry procedures need to be repeated for each beam.

14.4 Clinical Dosimetry

Once the dosimetric properties of the beam have been determined with sufficient accuracy and reproducibility, the following step involves the implementation of the accumulated data into the treatment planning system (TPS). If the implementation is done accurately, the TPS is then able to simulate a treatment set-up and derive the

resulting dose distribution, allowing for a certain amount of optimisation. Commissioning and use of a TPS are presented in Chap. 16. We here limited the discussion to a few comments regarding the actual implementation of beam data.

In the commissioning of the TPS, one needs to compare the calculated data in phantom vs. the measured data. At that point, it might be necessary to adjust the relative magnitude of the dose components in the computer source description in order to improve the agreement towards the measurements. In this comparison, it is of great importance to make sure that the same dosimetric data is used in all steps of the process, i.e. the same kerma factors and/or stopping power data are used in the TPS as are used in the derivation of absorbed dose in the preceding step. In the author's opinion, it is reasonable to normalise the TPS calculations towards the thermal neutron group fluence per beam monitor unit at the reference point in a water phantom. This might be advisable considering that the kerma factor for the thermal neutron absorbed dose in water is low (and the transition from fluence to absorbed dose does not improve the accuracy of the procedure). Then, adjust the photon intensity coming from the beam to match the measured photon absorbed dose per beam monitor unit at the reference point. The measurement of the fast neutron absorbed dose is generally very uncertain using the paired ionisation chamber technique (see [56], and others); therefore, in a similar fashion, adjusting the relative intensity of the fast neutron component of the beam based solely on ionisation chamber measurements for a well-optimised epithermal neutron beam is questionable.

The geometry and the material content of the irradiated volume in an epithermal neutron beam have great impact on the dose distribution ([19]; Wojnecki et al. [73]; [51]). The TPS ability to account for such effects correctly should be independently verified using calculations or phantom experiments (or both). The absorbed dose of a single treatment field to a patient (D_{pat}) of the dose component i to be delivered is given by the simple relation:

$$D_{\mathrm{pat},i} = \left(\frac{D_{\mathrm{pat},i}}{D_{\mathrm{ref},i}} \right)_{\mathrm{TPS}} \cdot \left(\frac{D_{\mathrm{ref},i}}{M} \right)_{\mathrm{Measured}} \cdot M \tag{14.15}$$

Here, M is the total number of beam monitor unit counts, $D_{\mathrm{ref},i}/M$ is the measured absorbed dose of component i per beam monitor count under reference conditions and the $D_{\mathrm{pat},i}/D_{\mathrm{ref},i}$ ratio is calculated using the TPS. Note that for $i = boron$ and $i = nitrogen$, $D_{\mathrm{ref},i}$ is replaced by $\phi_{\mathrm{ref},i}$ (i.e. the thermal neutron fluence determined under reference conditions).

14.5 Quality Assurance

In order to ensure safe radiotherapy, continuous quality assurance (QA) of equipment and procedures is of paramount importance. The subject of QA in radiotherapy has been discussed extensively in the literature (see, e.g. [35, 36]) and specifically

for a BNCT facility [9]. Rassow et al. [60] has compared the QA of medical accelerators and an epithermal neutron beam, which constitutes a good starting point for a QA programme. QA of beam output, photon contamination and neutron quality, as well as the stability of dosimeters, is of importance for a safe clinical practice. Raaijmakers et al. [56] investigated the long-term stability of these parameters for the epithermal neutron beam in Petten facility.

The same procedures as for conventional radiotherapy apply to the QA of epithermal neutron beams; therefore, the recent report by the American Association of Physicists in Medicine (AAPM) task group report 142 [28] provides a guideline and provides tolerances that could arguably be used also for epithermal neutron beams.

In addition to the standard tests of the neutron beam and the dosimeters, quality assurance procedures need to be established for the boron concentration measurement of tissue samples (Kobayashi et al. [26]; [30, 37, 38, 47, 55, 64, 68]), the measurement system for activation measurements [9] and in vivo dosimetry [51, 66, 72].

References

1. Ahnesjö A, Aspradakis MM (1999) Dose calculations for external photon beams in radiotherapy. Phys Med Biol 44(11):99–155
2. Almond PR, Biggs PJ, Coursey BM, Hanson WF, Huq MS, Nath R, Rogers DWO (1999) AAPM Task Group 51: protocol for clinical reference dosimetry of high-energy photon and electron beams. Med Phys 26:1847–1870
3. Andreo P, Cunningham J C, Hohlfeld K, Svensson H (1987) Absorbed dose determination in photon and electron beams: an international code of practice. IAEA Technical Report Series No. 277. IAEA, Vienna
4. Andreo P, Burns DT, Hohlfeld K, Huq MS, Kanai T, Laitano F, Smyth VG, Vynckier S (2000a) Absorbed dose determination in external beam radiotherapy: an international Code of Practice for dosimetry based on standards of absorbed dose to water. IAEA Technical Report Series No. 398. IAEA, Vienna
5. Andreo P, Izewska J, Shortt K and Vynckier S (2000b) Commissioning and quality assurance of computerized planning systems for radiation treatment of cancer. IAEA Technical Report Series No. 430. IAEA, Vienna
6. Aschan C, Toivonen M, Savolainen S, Seppälä T, Auterinen I (1999) Epithermal neutron beam dosimetry with thermoluminescence dosimeters for boron neutron capture therapy. Radiat Prot Dosim 81(1):47–56
7. Aschan C, Toivonen M, Savolainen S, Stecher-Rasmussen F (1999) Experimental correction for thermal neutron sensitivity of gamma ray TL dosimeters irradiated a BNCT beams. Radiat Prot Dosim 82:65–69
8. Auterinen I, Hiismäki P, Kotilouto P, Rosenberg RJ, Salmenhaara S, Seppälä T, Séren T, Tanner V, Aschan C, Kortesniemi M, Kosunen A, Lampinen J, Savolainen S, Toivonen M, Välimäki P (2001) Metamorphosis of a 35 year-old TRIGA reactor into a modern BNCT facility. In: Hawthorne MF, Shelly K, Weirsema RJ (eds) Frontiers in neutron capture therapy. Kluwer Academic/Plenum Publishers, New York, pp 267–275
9. Auterinen I, Serén T, Kotiluoto P, Uusi-Simola J, Savolainen S (2004) Quality assurance procedures for the neutron beam monitors at the FiR 1 BNCT facility. Appl Radiat Isot 61(5): 1015–1019
10. Auterinen I, Serén T, Anttila K, Kosunen A, Savolainen S (2004) Measurement of free beam neutron spectra at eight BNCT facilities worldwide. Appl Radiat Isot 61(5):1021–1026

11. Bisceglie E, Colangelo P, Colonna N, Santorelli P, Variale V (2000) On the optimal energy of epithermal neutron beams for BNCT. Phys Med Biol 45:49–58
12. Brahme A et al (1988) Accuracy requirements and quality assurance of external beam therapy with photons and electrons. Acta Oncol. (Suppl 1)
13. Briesmeister JF (2000) MCNP – a general Monte Carlo N-particle transport code, Version 4C, LA-12625-M, Los Alamos National Laboratory (LANL, NM)
14. Coderre JA, Morris GM (1999) The radiation biology of boron neutron capture therapy. Radiat Res 151:1–18
15. d'Errico F, Giusti V, Nava E, Reginatto M, Curzio G, Capala J (2002) Fast neutron spectrometry of BNCT beams. In: Sauerwein W, Moss R, Wittig A (eds) Research and development in neutron capture therapy. Monduzzi Editore, Bologna, pp 1139–1144
16. Giusti V, Munck af Rosenschöld PM, Sköld K, Montagnini B, Capala J (2003) Monte Carlo model of the Studsvik BNCT clinical beam: description and validation. Med Phys 30(12):3107–3117
17. Goorley JT, Kiger WS III, Zamenhof RG (2000) Reference dosimetry calculations for neutron capture therapy with comparison of analytical and voxel models. Med Phys 29(22):145–156
18. Hall EJ (1994) Radiobiology for the radiologist, 4th edn. J.B. Lippincott Company, Philadelphia
19. Harling OK, Roberts RA, Moulin DJ, Rogus RD (1995) Head phantoms for boron neutron capture therapy. Med Phys 22(5):579–583
20. Harling OK, Riley KJ, Binns PJ, Kiger WS III, Capala J, Giusti V, Munck af Rosenschöld PM, Sköld K, Auterinen I, Seren T, Kotiluoto P, Uusi-Simola J, Seppälä T, Marek M, Vierbl L, Spurny F, Stecher-Rasmussen F, Voorbrak WP, Morrissey J, Moss RL, Calzetta Larrieu O, Blaumann H, Longhino J (2002) International dosimetry exchange: a status report. In: Sauerwein W, Moss R, Wittig A (eds) Research and development in neutron capture therapy. Monduzzi Editore, Bologna, pp 333–340
21. International Commission on Radiation Units and Measurements (ICRU) (1976) Determination of absorbed dose in a patient irradiated by beams of X or gamma rays in radiotherapy procedures. ICRU Report No. 24. ICRU Publications, Bethesda
22. International Commission on Radiation Units and Measurements (ICRU) (1977) Neutron dosimetry for medicine and biology. ICRU Report No. 26. ICRU Publications, Bethesda
23. International Commission on Radiation Units and Measurements (ICRU) (1989) Clinical neutron dosimetry part I: determination of absorbed dose in a patient treated by external beams of fast neutrons. ICRU Report No. 45. ICRU Publications, Bethesda
24. Jansen JTM, Raaijmakers CPJ, Mijnheer BJ, Zeotelief J (1997) Relative neutron sensitivity of tissue-equivalent ionization chambers in an epithermal neutron beam for boron neutron capture therapy. Radiat Prot Dosim 70:27–32
25. Johnsson SA, Ceberg CP, Knöös T, Nilsson P (2000) On beam quality and stopping power ratios for high-energy x-rays. Phys Med Biol 45(10):2733–2745
26. Kashino G, Fukutani S, Suzuki M, Liu Y, Nagata K, Masunaga S, Maruhashi A, Tanaka H, Sakurai Y, Kinashi Y, Fujii N, Ono K (2009) A simple and rapid method for measurement of (10)B-para-boronophenylalanine in the blood for boron neutron capture therapy using fluorescence spectrophotometry. J Radiat Res (Tokyo) 50(4):377–382
27. Kiger WS III, Sakamoto S, Harling OK (1999) Neutronic design of a fission converter-based neutron beam for neutron capture therapy. Nucl Sci Eng 131:1–22
28. Klein EE, Hanley J, Bayouth J, Yin FF, Simon W, Dresser S, Serago C, Aguirre F, Ma L, Arjomandy B, Liu C, Sandin C, Holmes T (2009) Task Group 142 report: quality assurance of medical accelerators. American Association of Physicists in Medicine. Med Phys 36(9): 4197–4212
29. Knoll GF (2000) Radiation detection and measurement. Wiley, New York
30. Kobayashi T, Kanda K (1983) Microanalysis system of ppm-order 10B concentration in tissue for neutron capture therapy by prompt gamma spectrometry. Nucl Instr Meth 204:525–531

31. Kobayashi T, Sakurai Y, Ishikawa M (2000) A noninvasive dose estimation system for clinical BNCT based on PG-SPECT – conceptual study and fundamental experiments using HPGe and CdTe semiconductor detectors. Med Phys 27(9):2124–2132
32. Koivunoro H, Auterinen I, Kosunen A, Kotiluoto P, Seppälä T, Savolainen S (2003) Computational study of the required dimensions for standard sized phantoms in boron neutron capture therapy dosimetry. Phys Med Biol 48(21):N291–N300
33. Komeda M, Kumada H, Ishikawa M, Nakamura T, Yamamoto K, Matsumura A (2009) Performance measurement of the scintillator with optical fiber detector for boron neutron capture therapy. Appl Radiat Isot 67(7–8 Suppl):S254–7
34. Kosunen A, Kortesniemi M, Ylä-Mella H, Seppälä T, Lampinen J, Serén T, Auterinen I, Järvinen H, Savolainen S (1999) Twin ionization chambers for dose determinations in phantom in an epithermal neutron beam. Radiat Prot Dosim 81:187–194
35. Kouloulias VE (2003) Quality assurance in radiotherapy. Eur J Cancer 39(4):415–422
36. Kutcher GJ, Coia L, Gillin M, Hanson WF, Leibel S, Morton RJ, Palta JR, Purdy JA, Reinstein LE, Svensson GK, Weller M, Wingfield L (1994) Comprehensive QA for radiation oncology: report of AAPM radiation therapy committee task group 40. Med Phys 21(4):581–618
37. Laakso J, Kulvik M, Ruokonen I, Vahatalo J, Zilliacus R, Farkkila M, Kallio M (2001) Atomic emission method for total boron in blood during neutron-capture therapy. Clin Chem 47(10):1796–1803
38. Linko S, Revitzer H, Zilliacus R, Kortesniemi M, Kouri M, Savolainen S (2008) Boron detection from blood samples by ICP-AES and ICP-MS during boron neutron capture therapy. Scand J Clin Lab Invest 68(8):696–702
39. Liu HB, Greenberg DD, Capala J, Wheeler FJ (1996) An improved neutron collimator for brain tumor irradiations in clinical boron neutron capture therapy. Med Phys 23: 2051–2060
40. Marek M, Viererbl L, Burian J, Jansky B (2001) Determination of the geometric and spectral characteristics of BNCT beam (neutron and gamma-ray). In: Hawthorne MF, Shelly K, Weirsema RJ (eds) Frontiers in neutron capture therapy. Kluwer Academic/Plenum Publishers, New York, pp 381–399
41. Mijnheer BJ, Battermann JJ, Wambersie A (1987) What degree of accuracy is required and can be achieved in photon and neutron therapy? Radiother Oncol 8:237–252
42. Moro D, Colautti P, Lollo M, Esposito J, Conte V, De Nardo L, Ferretti A, Ceballos C (2009) BNCT dosimetry performed with a mini twin tissue-equivalent proportional counters (TEPC). Appl Radiat Isot 67(7–8 Suppl):S171–S174
43. Morris GM, Coderre JA, Hopewell JW, Micca PL, Rezvani M (1994) Response of rat skin to boron neutron capture therapy with p-boronophenylalanine or borocaptate sodium. Radiother Oncol 32(2):144–153
44. Morris GM, Coderre JA, Bywaters A, Whitehouse E, Hopewell JW (1996) Boron neutron capture therapy irradiation of the rat spinal cord: histopathological evidence of a vascular-mediated pathogenesis. Radiat Res 146:313–320
45. Morris GM, Micca PL, Nawrocky MM, Weissfloch LE, Coderre JA (2002) Long-term infusions of p-boronophenylalanine for boron neutron capture therapy: evaluation using rat brain tumor and spinal cord models. Radiat Res 158(6):743–752
46. Moss RL, Aizawa O, Beynon D, Brugger R, Constantine G, Harling O, Liu HB, Watkins P (1997) The requirements and development of neutron beams for neutron capture therapy of brain cancer. J Neurooncol 33(1–2):27–40
47. Mukai K, Nakagawa Y, Matsumoto K (1995) Prompt gamma ray spectrometry for in vivo measurement of boron-10 concentration in rabbit brain tissue. Neurol Med Chir (Tokyo) 35(12):855–860
48. Munck af Rosenschöld PM, Verbakel WF, Ceberg CP, Stecher-Rasmussen F, Persson BRR (2001) Toward clinical application of prompt gamma spectroscopy for in-vivo monitoring of boron uptake in boron neutron capture therapy. Med Phys 28(5):787–795

49. Munck af Rosenschöld P, Ceberg CP, Giusti V, Andreo P (2002) Photon quality correction factors for ionization chambers in an epithermal neutron beam. Phys Med Biol 47(14):2397–2409
50. Munck af Rosenschöld P, Giusti V, Ceberg CP, Capala J, Sköld K, Persson BR (2003) Reference dosimetry at the neutron capture therapy facility at Studsvik. Med Phys 30(7):1569–1579
51. Munck af Rosenschöld P, Capala J, Ceberg CP, Giusti V, Salford LG, Persson BR (2004) Quality assurance of patient dosimetry in boron neutron capture therapy. Acta Oncol 43(4):404–411
52. Nigg DW (2003) Computational dosimetry and treatment planning considerations for neutron capture therapy. J Neurooncol 62:75–86
53. Nigg DW, Wheeler FJ, Wessol DE, Capala J, Chadha M (1997) Computational dosimetry and treatment planning for boron neutron capture therapy. J Neurooncol 33:93–104
54. Raaijmakers CPJ, Konijnenberg MW, Verhagen VH, Mijnheer BJ (1995) Determination of dose components in an epithermal neutron beam for boron neutron capture therapy. Med Phys 22:321–329
55. Raaijmakers CPJ, Kronijenberg MW, Dewit L, Haritz D, Huiskamp R, Philipp K, Siefert A, Stecher-Rasmussen F, Mijnheer BJ (1995) Monitoring of blood-10B concentration for boron neutron capture therapy using prompt gamma-ray analysis. Acta Oncol 34:517–523
56. Raaijmakers CP, Nottelman EL, Konijnenberg MW, Mijnheer BJ (1996) Dose monitoring for boron neutron capture therapy using a reactor-based epithermal neutron beam. Phys Med Biol 41(12):2789–2797
57. Raaijmakers CP, Konijnenberg MW, Mijnheer BJ (1997) Clinical dosimetry of an epithermal neutron beam for neutron capture therapy: dose distributions under reference conditions. Int J Radiat Oncol Biol Phys 37(4):941–951
58. Raaijmakers CP, Bruinvis IA, Nottelman EL, Mijnheer BJ (1998) A fast and accurate treatment planning method for boron neutron capture therapy. Radiother Oncol 46(3):321–332
59. Raaijmakers CPJ, Nottelman EL, Mijnheer BJ (2000) Phantom materials for boron neutron capture therapy. Phys Med Biol 45(8):2353–2361
60. Rassow J, Stecher-Rasmussen F, Voorbraak W, Moss R, Vroegindeweij C, Hideghéty K, Sauerwien W (2001) Comparison of quality assurance for performance and safety characteristics for boron neutron capture therapy in Petten/NL with medical electron accelerators. Radiat Oncol 59:99–108
61. Riley KJ, Binns PJ, Greenberg DD, Harling OK (2002) A physical dosimetry intercomparison for BNCT. Med Phys 29(5):898–904
62. Riley KJ, Binns PJ, Harling OK (2003) Performance characteristics of the MIT fission converter based epithermal neutron beam. Phys Med Biol 48(7):943–958
63. Rogus RD, Harling OK, Yanch JC (1994) Mixed field dosimetry of epithermal neutron beams for boron neutron capture therapy at the MITR-II research reactor. Med Phys 21:1611–1625
64. Ryynänen PM, Kortesniemi M, Coderre JA, Diaz AZ, Hiismäki P, Savolainen S (2000) Models for estimation of the (10)B concentration of BPA-fructose complex infusion in patients during epithermal neutron irradiation in BNCT. Int J Radiat Oncol Biol Phys 48:1145–1154
65. Seppälä T, Vähätalo V, Auterinen I, Kosunen A, Nigg DW, Wheeler FJ, Savolainen S (1999) Modelling of brain tissue substitutes for phantom materials in neutron capture therapy (NCT) dosimetry. Radiat Phys Chem 55:239–246
66. Seppälä T, Auterinen I, Aschan C, Serén T, Benczik J, Snellman M, Huiskamp R, Ramadan UA, Kankaranta L, Joensuu H, Savolainen S (2002) In-vivo dosimetry of the dog irradiations at the Finnish BNCT facility. Med Phys 29(11):2629–2640
67. Spevacek V, Marek M, Dvorak P, Novotny ml J, Viererbl L, Flibor S (2002) Application of gel dosimeter in three-dimensional dosimetry for boron neutron capture therapy. In: Sauerwein W, Moss R, Wittig A (eds) Research and development in neutron capture therapy. Monduzzi Editore, Bologna, pp 359–365
68. Svantesson E, Capala J, Markides KE, Pettersson J (2002) Determination of boron-containing compounds in urine and blood plasma from boron neutron capture therapy patients. The importance of using coupled techniques. Anal Chem 74(20):5358–5363

69. Uusi-Simola J, Heikkinen S, Kotiluoto P, Serén T, Seppälä T, Auterinen I, Savolainen S (2007) MAGIC polymer gel for dosimetric verification in boron neutron capture therapy. J Appl Clin Med Phys 8(2):114–123
70. Verbakel WFAR (2001) Validation of the scanning -gamma-ray telescope for in vivo dosimetry and boron measurements during BNCT. Phys Med Biol 46(12):3269–3285
71. Voorbraak WP, Järvinen H, Auterinen I, Gonçalves IC, Green S, Kosunen A, Marek M, Mijnheer BJ, Moss RL, Rassow J, Sauerwein W, Savolainen S, Serén T, Stecher Rasmussen F, Uusi-Simola J, Zsolnay EM (2003) Recommendations for the dosimetry of boron neutron capture therapy (BNCT). The JRC, Petten, the Netherlands, 2003
72. Wittig A, Moss RL, Stecher-Rasmussen F, Appelman K, Rassow J, Roca A, Sauerwein W (2005) Neutron activation of patients following boron neutron capture therapy of brain tumors at the high flux reactor (HFR) Petten (EORTC Trials 11961 and 11011). Strahlenther Onkol 181(12):774–782
73. Wojnecki C, Green S (2001) A computational study into the use of polyacrylamide gel and A-150 plastic as brain tissue substitutes for boron neutron capture therapy. Phys Med Biol 46(5):1399–1405
74. Zamenhof RG, Murray BW, Brownell GL, Wellum GR, Tolpin EI (1975) Boron neutron capture therapy for the treatment of cerebral gliomas: I. Theoretical evaluation of the efficacy of various neutron beams. Med Phys 2:47–60

Prescribing, Recording and Reporting of BNCT

15

Jürgen Rassow and Wolfgang A.G. Sauerwein

Contents

J. Rassow
NCTeam, Department of Radiation Oncology,
Former Institute for Medical Radiation Physics,
University Duisburg-Essen,
University Hospital Essen, D-45259, Essen, Germany
e-mail: juergen.rassow@uni-due.de

W.A.G. Sauerwein (✉)
NCTeam, Department of Radiation Oncology,
University Hospital Essen,
University Duisburg-Essen, D-45122, Essen, Germany
e-mail: w.sauerwein@uni-due.de

W.A.G. Sauerwein et al. (eds.), *Neutron Capture Therapy*,
DOI 10.1007/978-3-642-31334-9_15,

15.1 Aim of Prescribing, Recording and Reporting

When a malignant disease of a patient is presented for radiotherapy, three documentation steps are required: before the start, prescribing; during the course of therapy, recording; and after finishing, writing the final report (reporting).

- Prescribing is the first step for the radiation oncologist, where he identifies the patient, describes the disease including the anamnestic data and fixes the aim of the radiotherapy, the method and concept of the treatment and the facility to be used. For BNCT, this includes any details on pretreatment operations, the ^{10}B carrier and the required ^{10}B concentration in blood at the time of radiotherapy. The therapist has to detail the planning target volume and the regions at risk and at least the minimum and maximum absorbed dose in the clinical target volume and the maximum tolerable absorbed dose in the organs at risk. The radiation oncologist prescribes the mode of treatment planning, mostly with dose-volume histograms, based on computer tomography and decides which of the treatment plans is the best and to be chosen. He also decides whether field verification and in vivo dosimetry should be applied and which additional actions, e.g. simulator, or support, e.g. for positioning, is necessary. Information on the (medical) staff present, date of prescription and signature are obligatory.
- Recording is the second step, performed mainly during the radiotherapy itself. As well as the name of the hospital, the therapy facility, identification of the patient, the realised treatment plan and treated clinical target volumes, all details of the treatment are to be recorded, such as dates of each fraction, geometrical and dosimetrical settings of the facility, actual ^{10}B concentrations at the beginning and the end of the treatment, etc. If any deviations from the prescribed plan occur, the reason and the specific action taken are to be described. Information on persons present, dates and signatures are obligatory.
- Reporting is the third step and needs uniformity in definitions and terminology in all therapy centres worldwide in order that information on therapy results can be exchanged. For publications, where patient identification is omitted and where information on persons involved and where signatures are not necessary or only in reduced form, all data must be reported which may be necessary to be able to repeat and recalculate the therapy details. Also, for different facilities, with different neutron energy spectra and filtering, actual knowledge on weighting and correction factors must be supplied. The required data includes
  - A short description of the disease, including histology, grading, tumour extension, stage and earlier or simultaneous therapy actions and diagnostics.
  - The aim and treatment technique, e.g. reactor type and radiation quality, including filtering, neutron energy spectrum, number and chronology of fractions,^{10}B carrier and ^{10}B concentration in blood during treatment of each fraction.
  - A description of clinical target volumes and organs at risk, including any hot spots.
  - The entire total absorbed dose, as well as the total weighted dose together with the absorbed dose of all dose components and the corresponding

weighting factors used in all tissues, as well as the maximum and minimum doses in the clinical target volume and the maximum dose in the organs at risk and any hot spots. Further information on spatial dose distributions and dose-volume histograms are helpful, if available. Reporting of total weighted dose values only is absolutely insufficient. These values can only be of help internally as a guiding principle for the radiotherapist, but cannot be transferred to different treatment facilities with different energy spectra of neutrons in other centres, as the weighted dose values can be calculated only on the basis of values of the dose components with knowledge of the corresponding weighting factors in the different tissues.

- The treatment planning programme used and the calculation data, especially for the dose components, which can only be calculated from mean fluence values of epithermal neutrons.
- The side effects and clinical history of the patient (if available).

15.2 Problem of Dose Specification for BNCT in Comparison to Conventional Photon and Electron Therapy

Absorbed dose is a fundamental quantity used in all therapeutic applications of ionising radiation. Measurement and reporting of the absorbed dose is crucial to the understanding of any radiation effects [1]. Absorbed doses can never be measured in body tissues directly as it is unknown, how much energy is used for warming and how much for chemical reactions in cells. The dose measurement for photon and electron therapy, which both act by energy transfer via electrons, is therefore, based on conversion of the measured value of an ionisation chamber, calibrated in terms of water absorbed dose, in the absorbed dose in body tissues. The necessary correction factors are well known.

The dose evaluation for BNCT is completely different because in contrast to the photon and electron absorbed dose with the same RBE there are in BNCT four dose components acting with different RBE:

D_B: boron dose from the $^{10}B(n,\alpha)^7Li$ reaction with α- and Li particles with mean ranges of 8.9 and 4.8 μm, respectively
D_p: high-LET (proton) dose from the $^{14}N(n,p)^{14}C$ reaction
D_n: neutron dose of mainly fast and epithermal neutrons
D_γ: gamma-ray dose mainly from the capture reaction $^1H(n,\gamma)^2D$

The first two dose components cannot be measured in principle, but only calculated indirectly based on the fluence of epithermal neutrons and the ^{10}B and ^{14}N concentrations in tissue, respectively.

The total absorbed dose D_T is the sum of these four dose components;

$$D_T = D_B + D_p + D_n + D_\gamma . \tag{15.1}$$

In photon and electron therapy, it is possible to relate the biological effect of radiation to only one dose parameter. This is impossible for BNCT even when using specific biological weighting factors for each of the dose components. The four dose components have not only a different effect quantitatively but cause also different biological reactions. Therefore, the assumption of only one acting biologically weighted dose parameter is unreal. Otherwise, a conventional photon or electron therapy with corresponding higher absorbed dose could be applied.

Thus, only as a qualitative first approximation and guiding principle, but not in a quantitative reliable manner, it is possible to take into account the different biological effectiveness of each dose component with a vaguely determined weighting factor to get a total weighted dose D_w.

$$D_w = w_c D_B + w_p D_p + w_n D_n + w_\gamma D_\gamma . \tag{15.2}$$

For the boron dose D_B and the proton dose D_p, the weighting factor includes the probability that a reaction particle of the nuclear reaction of the thermal neutron with ^{10}B and ^{14}N, respectively, occurs. For the former, there is the additional probability that the reaction particle really hits the cell nucleus. Therefore, the weighting factor w_c for D_B is called a compound factor. This factor depends on the ^{10}B carrier used and the tissue, where the nuclear reaction takes place. The uncertainty of the compound factor w_c has been reported to be 16–36 % for the ^{10}B carriers BSH [2] and for BPA, respectively.

15.3 Uncertainties for Evaluation and Biological Weighting of Dose Components

D_B: The spatial ^{10}B distribution on a cellular level in tissue is unknown, especially the probability of the positioning of ^{10}B in the extracellular, the intracellular space or the cell membrane. Even for a nuclear reaction of a thermal neutron with a ^{10}B atom in the intracellular space, only a probability can be calculated that one of the two reaction particles (α- particle or ^{7}Li particle) hits the cell nucleus and has a lethal effect on the cell. The calculation of the boron dose cannot be based on the real ^{10}B distribution at the cellular level, which is unknown, especially in tumour tissues, but only on the assumption of a homogeneous ^{10}B concentration in the different tissues with a fixed relation to the ^{10}B concentration in blood, which is measurable. For a curative tumour therapy, it is necessary to kill tumour cells down to about 10^{-8}. Conversely, it is unknown if each cell in a group of 10^{-8} tumour cells contains enough ^{10}B atoms to make sure that in a statistical Poisson distribution, at least one lethally acting reaction in each cell nucleus occurs. The uncertainty for the calculation of the boron dose component D_B is, therefore, caused by the uncertainty of knowledge of the spatial distribution of ^{10}B atoms, and of the cross-section of the nuclear reaction of thermal neutrons with ^{10}B and the locally changing, and not well known, energy distribution of the neutrons.

D_p: The distribution of N atoms on the cellular level in a given tissue can be assumed to be homogeneous. The same assumption is valid for the distribution of neutrons. Thus, the uncertainty of the proton dose component D_p is caused by the locally changing and not well known energy distribution of the neutrons and their cross-section for the proton generating reaction $^{14}N(n,p)^{14}C$.

D_n: The uncertainty of the determination of the neutron absorbed dose D_n is due to an imprecise knowledge of the locally changing energy spectrum of the fast and epithermal neutrons. One has further to take into account that the diameter of the most commonly used tissue-equivalent (TE) ionisation chambers is large compared to the very steep dose gradient of the neutron dose, so that the measurement of the dose at a specific point is difficult. The weighting factor w_n is normally taken over the whole target volume, although the RBE value is dependent on the locally changing energy spectrum of the neutrons. This causes further uncertainties.

D_γ: The uncertainty of the determination of the gamma-ray absorbed dose component is much larger than in photon and electron therapy, because the measurement must be performed in a high background of neutron radiation, by ionisation chambers which must be as neutron insensitive as possible.

Several parameters have a large influence on the weighting factors used [3]:

- As the dose-effect curves of the four dose components have different shapes, the RBE strongly depends on the absorbed dose. In order to predict the effects along isodose surfaces, real RBE factors, which vary with the absorbed dose of each component, would have to be considered. This is, of course, never done.
- The biological end points of the four dose components are not directly comparable. As the interaction mechanisms of nuclear reaction particles and of photons may differ, a unique factor cannot be used to calculate the biological end points. Different weighting factors are associated with different biological end points. For example, in a healthy tissue tolerance study using dogs and BSH, the compound factor w_c was found to be 0.37 ± 0.06 and 0.65 ± 0.04 for neurological symptoms and MRI-visible changes, respectively [2]. The fundamental question as to the choice of the most suitable end point for a BNCT treatment still begs to be answered.
- The neutron energy spectrum strongly influences the nuclear reactions induced by fast, epithermal and thermal neutrons. As the worldwide BNCT centres have different neutron sources and filter devices, the primary neutron spectra differ essentially from one facility to another. In addition, for a given facility, the neutron energy spectrum varies at depth in the patient due to the moderation of the fast and epithermal neutrons. This effect has never been exactly estimated, but it is obvious that it increases the uncertainty of the weighting factors.
- Two different boron compounds, BPA-f [4–6] and BSH [7] are used in BNCT clinical trials. Their mechanisms for crossing the blood–brain barrier is different, the intracellular uptake differs considerably and consequently the boron biodistributions and the interaction mechanisms vary. This fact can be taken into

account using compound factors derived from radiological investigations. For the BPA-f compound, a boron concentration in the tumour 3.5 times higher than that in blood is commonly assumed [5]. In this case, the compound factor w_c is 3.8 and 1.3 for glioblastoma multiforme tissues and healthy brain tissues, respectively [2]. For the BSH compound, the boron concentration in the tumour and in the brain is supposed to be equal to that in blood [2]. In this case, the compound factor w_c is equal to 0.37 for the brain and to 0.81 for all other organs with or without an organ-blood barrier. It became evident from the human pharmacokinetic and BPA/BSH uptake studies [8, 9] that the interpatient and intrapatient variability is quite high. The assumption of a homogeneous boron concentration at the intra- and extracellular level is straightforward but not really fulfilled. In fact, the real deviation of the ^{10}B concentration to the assumed average one generates further unknown deviations. These local deviations have quantitatively the greatest impact on the used weighting factors and on the calculated boron dose component.

- The type of organs or tissues has an influence on the weighting factors also. For a given radiation quality, the RBE values determined for a given tissue are also applied to other tissues. This assumption results in further uncertainties whose reduction needs further investigations.
- The weighting factors determined by in vitro and animal studies are directly applied to humans and the corresponding uncertainty cannot be quantified. More clinical trials are still mandatory in order to get more information about the limiting doses at the organs at risk.

15.4 Resulting Recommendations on Prescribing, Recording and Reporting

In general, all data should be prescribed, recorded and reported, which are necessary for the identification of the patient and the circumstances of the disease, the methods and details of the therapy and the facilities and parameters used and details of the treatment planning and calculation assumptions. For publications, where patient identification is omitted, all data must be reported, which are necessary to repeat and recalculate the therapy even with different facilities (neutron energy spectra and filtering), as well as more actual knowledge of weighting and correction factors. The dose and volume specifications should be reported in publications in accordance with ICRU-IAEA recommendations [10, 11].

Volumes:

- Gross tumour volume (GTV)
- Clinical target volume (CTV)
- Planning target volume PTV)
- Treated volume
- Irradiated volume
- Organs at risk
- Information on tissues and their volumes

Absorbed dose distribution (at least):

- Dose variation in the planning target volume and representation of spatial dose distribution by
  - Maximum absorbed dose D_{max}
  - Minimum absorbed dose D_{min}
  - Hot spots
  - Representative absorbed dose values in organs at risk
- Dose-volume histograms

and additionally, dose information, such as absorbed dose values for additional critical points or tissues.

For reports on BNCT, it is very important that all dose specifications must be given separately for all four absorbed dose components. Additionally, the values for total absorbed dose D_T and total weighted dose D_w (the latter together with the used weighting factors for each tissue) may be given.

The information on boron absorbed dose must include information on the ^{10}B carrier, the boron concentrations for all treatment fractions, the assumptions for the specification of ^{10}B concentration in the target and the treated volume based on measurements of concentration in blood.

All dose values must have the unit gray (Gy) (never gray-equivalent or RBE-gray, which is in contrast to the rules of SI units and recommendations of ICRU).

It might be worthwhile to remind at this place that a similar discussion is ongoing with respect on reporting of proton-beam therapy. The basic issue is much simpler as compared to the complex situation in BNCT, only the RBE of protons being slightly different from unit. However, due to the fact that for decennia only some few places in the world have offered proton irradiation to patients, it was possible to develop a common practice reporting an 'equivalent' or 'cobalt-equivalent' dose, defined as the product of the absorbed dose and the RBE of the proton beam (that is close to 1.1). In 2007, ICRU Report 78 [12] clearly states, 'the use of the term "equivalent dose" as defined above cannot be recommended for therapeutic applications', the term being reserved for radiation protection purposes. Similar to BNCT papers, it has been common practice in publications on proton therapy to report 'equivalent dose' in units of 'gray-equivalent' or cobalt gray equivalent' using symbols such as CGE or GyE. Referring to the SI (system International d'Unités/International System of Units), ICRU 78 states, 'the use of CGE,GyE or Gy(E) is not recommended'. Similar to the proposals made by IAEA-TECDOC-1223 [10] for BNCT, ICRU 78 suggests to replace in proton therapy 'equivalent dose' by the quantity RBE-weighted absorbed dose D_{RBE}; the special name of the unit of both absorbed dose and RBE-weighted dose is gray (Gy). This brief excursion into another branch of modern radiotherapy was made to underline the importance of a common language for all radiotherapy applications as well as to demonstrate that the problems of reporting innovative beams are not limited to BNCT. The solutions for BNCT as described above are coherent with international standards for other beam quality. Their use therefore is recommended.

Following ICRU 78, we can summarise for BNCT: The concepts of absorbed dose D_T with the four dose components D_B, D_p, D_n, and D_γ and the weighted dose D_w serve different purposes. D_T is a physical quantity deriving from measurement and/

or calculation, whereas D_w is a biologically weighted quantity. As such, D_T will have a primary role in dosimetry protocols and a crucial role in any clinical protocol and final report. The weighted dose D_w might be better suited to a comparison of effects in BNCT obtained under different situations, for the selection of appropriate irradiation time if switching from one neutron beam to another or if changing the delivery mode of the boron compound. Whether the quantities absorbed dose and or weighted dose should be used in clinical practice in the different steps of treatment preparations and planning procedures is a matter of experience and local policy. Quoting again ICRU 78: 'It is, however, important and obligatory that the quantities involved be clearly specified to avoid any risk of confusion'.

References

1. BIPM (2006) Bureau International des Poids et Mesures: the international system of units (SI), 8th edn. BIPM, Sèvres
2. Gabel D, Philipp KHI, Wheeler FJ, Huiskamp R (1998) The compound factor of the $^{10}B(n,\alpha)^{7}Li$ reaction from borocaptate sodium and the relative biological effectiveness of recoil protons for induction of brain damage in Boron Neutron Capture Therapy. Radiat Res 149:378–386
3. Rassow J, Sauerwein W, Wittig A, Bourhis-Martin E, Hideghéty K, Moss R (2004) Advantage and limitations of weighting factors and weighted dose quantities and their units in Boron Neutron Capture Therapy. Med Phys 31:1128–1134
4. Busse PM, Zamenhof RG, Harling OK, Kaplan I, Kaplan J, Chuang CF, Goorley JT, Kiger WS III, Riley KJ, Tang L, Solares GR, Palmer MR (2001) The Harvard-MIT BNCT program – overview of the clinical trials and translational research. In: Hawthorne MF, Shelley K, Wiersema RJ (eds) Frontiers in neutron capture therapy, vol 1. Kluwer Academic/Plenum Press, New York, Boston, Dordrecht, London, Moscow, pp 37–60
5. Diaz AZ, Chanana AD, Capala J, Chadha M, Coderre JA, Elowitz EH, Iwai J, Joel DD, Liu HB, Ma R, Pendzick N, Peress NS, Wielopolski L (2001) Boron Neutron Capture Therapy for glioblastoma multiforme. Results from the initial phase I/II dose escalation studies. In: Frontiers in neutron capture therapy, vol 1. Kluwer Academic/Plenum Publishers, New York, pp 61–72
6. Färkkilä M, Aschan C, Auterinen I, Benczik J, Hüsmäki P, Jääskelainen J, Järviluoma E, Joensuu H, Kallio M, Kankaanranta L, Kortesniemi M, Kosunen A, Kotiluoto P, Kulvik M, Laakso J, Pakkala S, Rasilainen M, Salmenhaara S, Savolainen S, Seppälä T, Serén T, Snellman M, Suominen M, Tenhunen M, Toivonen M, Tähtinen L, Vähätalo J (2001) At the threshold of clinical trials. The status of the Finnish BNCT project. Front Neutron Capture Ther 1:129–131
7. Sauerwein W, Rassow J, Mijnheer BJ (1997) Considerations about specification and reporting of dose in BNCT. In: Larsson B, Crawford J, Weinreich R (eds) Advances in neutron therapy, vol II, Chemistry and biology. Elsevier, Amsterdam, pp 531–534
8. Kiger WS III, Palmer MR, Riley KJ, Zamenhof RG, Busse PM (2002) Pharmacokinetic modeling for boronophenylalanine-fructose mediated neutron capture therapy. ^{10}B concentration predictions and dosimetric consequences. In: Sauerwein W, Moss R, Wittig A (eds) Research and development neutron capture therapy. Monduzi Editore, International Proceedings Division, Bologna, pp 985–992
9. Wittig A, Hideghéty K, Paquis P, Heimans J, Vos M, Goetz C, Haselsberger K, Grochulla F, Moss R, Morrissey J, Bourhis-Martin E, Rassow J, Stecher-Rasmussen F, Turowski B, Wiestler M, de Vries MJ, Fankhauser H, Gabel D, Sauerwein W (2002) Current clinical results of the EORTC-study 11961. In: Sauerwein W, Moss R, Wittig A (eds) Research and development neutron capture therapy. Monduzi Editore, International Proceedings Division, Bologna, pp 1117–1122

10. Wambersie A, Gahbauer RA, Whitmore G, Levin CV (2001) Dose and volume specification for reporting NCT: an ICRU-IAEA initiative. Current status of neutron capture therapy (International Atomic Energy Agency Report No. IAEA-TECDOC-1223, 2001), pp 9–10
11. Gahbauer RA, Gupta N, Blue T, Carpenter D, Sauerwein W, Wambersie A (2001) Reporting a BNCT irradiation. Application of the ICRU recommendations to the specific situation in BNCT. In: Hawthorne MF, Shelley K, Wiersema RJ (eds) Frontiers in neutron capture therapy, vol 1. Kluwer Academic/Plenum Press, New York, Boston, Dordrecht, London, Moscow, pp 561–569
12. International Commission on Radiation Units and Measurements (2007) Prescribing, recording, and reporting proton-beam therapy (ICRU report 78). J ICRU 7(2):27, ISSN 1473-6691

Treatment Planning

16

W.S. Kiger III and Hiroaki Kumada

Contents

W.S. Kiger III (✉)
Department of Radiation Oncology, Beth Israel Deaconess Medical Center,
Harvard Medical School, 330 Brookline Avenue, Shapiro 505, Boston, MA 02215, USA
e-mail: wkiger@bidmc.harvard.edu

H. Kumada
Faculty of Medicine, Proton Medical Research Center, University of Tsukuba, 2-1-1 Amakubo,
Tsukuba, Ibaraki 305-8576, Japan
e-mail: kumada@pmrc.tsukuba.ac.jp

W.A.G. Sauerwein et al. (eds.), *Neutron Capture Therapy*,
DOI 10.1007/978-3-642-31334-9_16,

16.1 Introduction

Treatment planning for neutron capture therapy (NCT) involves computation and analysis of the radiation dose distribution in a patient for determination of the neutron beam orientations and radiation fluence (monitor units) to enable delivery of an optimized radiation dose distribution that will comply with the dose prescription and optimize the dose to the target volume while respecting dose limits for normal tissues and organs at risk. Aspects of NCT treatment planning are discussed in reviews by Nigg et al. [1, 2] and Nievaart et al. [3].

Treatment planning for NCT differs markedly from treatment planning for photons or electrons in conventional radiotherapy and, in some ways, is significantly more complex. Therapeutic advantage in NCT is obtained principally through the tumor selectivity of a neutron capture agent (e.g., ^{10}B) rather than through precise geometric targeting of multiple well-collimated radiation fields onto the target volume. The low-energy neutron beams used in NCT are usually not highly collimated and, if they are, any directionality is rapidly lost with depth in tissue due to neutron scattering and thermalization. In conventional radiotherapy, only a single low-LET dose component must be computed, the dose from primary photons or electrons, both of which are ultimately delivered by electrons. In contrast, with NCT the radiation field is a complex mixture of high- and low-LET dose components with varying biological effectiveness that depends on both the tissue and the chemical form of the neutron capture agent. Five different dose components arising from neutron and photon interactions in tissue must be accounted for in NCT treatment planning calculations. The spatial distribution of each dose component is different and depends on the tissue composition as well as the neutron and photon fluence spectra.

The algorithms generally used for dose calculations in clinical photon radiotherapy are computationally efficient and range from simple empirical algorithms based on dose measurements in a water phantom to complex model-based algorithms (e.g., convolution-superposition). Although generally regarded to be the most accurate algorithms, direct solutions of the Boltzmann transport equation like Monte Carlo simulation or the discrete ordinates method are rarely used in clinical photon radiotherapy because they are computationally expensive. NCT treatment planning systems (TPSs), on the other hand, exclusively rely on Monte Carlo simulation for dose calculations because of the complex, scatter-dominated nature of the radiation transport processes involved.

This chapter will describe both technical and clinical aspects of NCT treatment planning. The technical topics addressed include computational aspects such as approaches for modeling the patient geometry and simulating the neutron beam as well as aspects of dose calculation and calibration of planning systems. The clinical section of the chapter describes the treatment planning process, including patient data acquisition, target volume definition, model construction, beam selection, and finally dose prescription and plan evaluation. Issues related to treatment planning during and after treatment delivery are also discussed. These include patient positioning, boron compound pharmacokinetics, retrospective dosimetry, and dose reporting.

16.2 Computational Aspects of Treatment Planning

NCT treatment planning systems must perform several essential functions:

- Construction of a customized patient model from tomographic images including definition of structures such as target volumes and organs at risk
- Selection of neutron beam orientations relative to the patient model
- Simulation of radiation transport through the patient model and computation of dose using a model of the neutron beam
- Analysis and visualization of dose, for example, using isodose curves and dose-volume histograms, to enable selection of an optimal treatment plan and determination of appropriate beam monitor units (fluence) to be delivered

Technical aspects of these functions such as approaches to patient geometry modeling, neutron beam source definition, dose calculation, planning system calibration, and validation will be considered in this section.

16.2.1 Patient Geometric Modeling Approaches

NCT treatment planning systems employ individualized patient models for radiation transport calculations. Generally, the 3D models are constructed from information in tomographic medical images of a patient, usually CT (computed tomography) or MR (magnetic resonance) images. Several different types of geometric representation are used in planning systems. Unlike in photon and electron radiotherapy planning, the dose grid is often independent from the geometric representation of the patient.

16.2.1.1 Voxel Models

A voxel model is a 3D array of contiguous rectangular prisms, each of which is assumed to be internally uniform in composition. Each element of the array is known as a volumetric element or voxel. Typically, voxels are generally somewhat larger than the pixels of the medical images, usually ~2–10 mm on a side. Construction of a voxel model involves overlaying a 3D rectilinear mesh on the 3D array of a patient's medical images, usually CT images, and determining the frequency distribution of tissue types in each voxel. Usually, only a small number of tissue types are used and the tissues or materials are defined using a combination of Hounsfield unit (CT image intensity value) thresholds applied to the image data and user-contoured structures, as illustrated in Fig. 16.1. In the NCTPlan TPS, for example, the materials are air, soft tissue (e.g., brain), bone, and tumor [4–6]. The composition of each voxel is a mixture of the four principal materials based on the volume fraction of each material identified in the voxel. For computational reasons, however, it is necessary to limit the number of combinations of materials to avoid defining an excessively large number of material mixtures in the transport code. This is often done by rounding the volume fractions of the principal materials to discrete fractions, for example, the nearest 10 % or 20 % increments using rules designed to minimize the effect of rounding on neutron transport [7]. The model construction process is illustrated in Fig. 16.1.

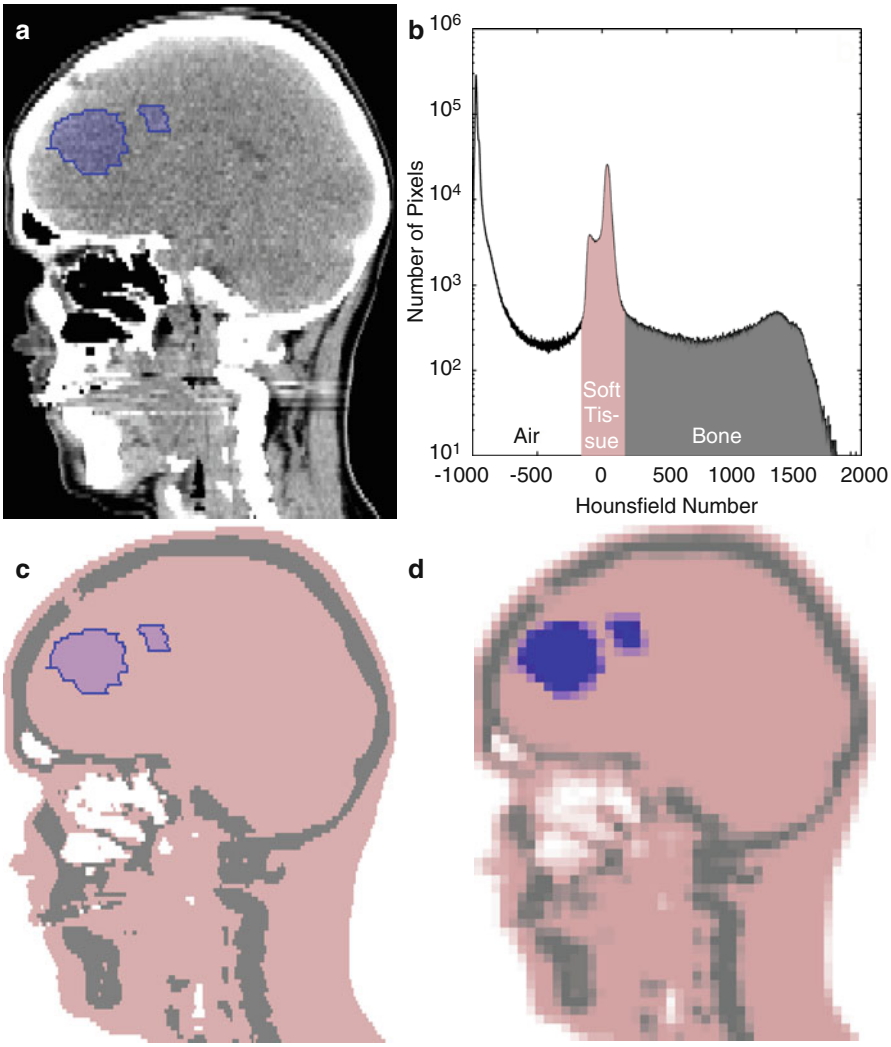

Fig. 16.1 Construction of a voxel model from CT image data in the MiMMC treatment planning system. (**a**) Sagittal CT image slice with contoured target volumes shown in blue. (**b**) Image intensity histogram showing the range of Hounsfield numbers for air, soft tissue, and bone and (**c**) the resulting thresholded sagittal image. (**d**) The corresponding slice through a 4-mm voxel model

Voxel models are used ubiquitously in Monte Carlo-based photon and electron beam planning and are the earliest and most frequently used geometric modeling technique in NCT treatment planning because of their simplicity. Most often the voxel matrix and scoring mesh (for dose calculation) are identical because this is most efficient. A particular advantage of voxel models is that they are very easy and quick to produce. In contrast to some of the other modeling techniques, producing a voxel model usually requires relatively little effort from the planner as a result of

automated material assignment algorithms based on CT image data. Fig. 16.2a shows an axial slice through voxel model of a brain tumor patient, and Fig. 16.2b shows a cutaway 3D view of the same model.

A shortcoming of the voxel modeling technique is that, for large voxel sizes, the contour of the external surface and internal interfaces may not be well preserved. This geometric infidelity may degrade the accuracy of calculated doses, particularly near air-tissue interfaces, although, to a large extent, the use of materials mixing to account for partial volume effects mitigates the impact of large voxel size. The effect of voxel size on dose accuracy has not been well studied quantitatively except on the central axis of some simple phantoms [7, 8]. Reducing voxel size improves the accuracy of calculated doses, but several computational issues arise with small voxels. First, because of the smaller sampling volumes, fewer particle tracks will score in each voxel, increasing the statistical uncertainty of calculated doses. This can of course be offset by simulating more particle histories, but because there are many more surface crossings and scores to compute during the particle tracking process, transport calculations can be slowed dramatically with smaller voxels. Averaging dose over several voxels can improve statistics, but averaging reduces

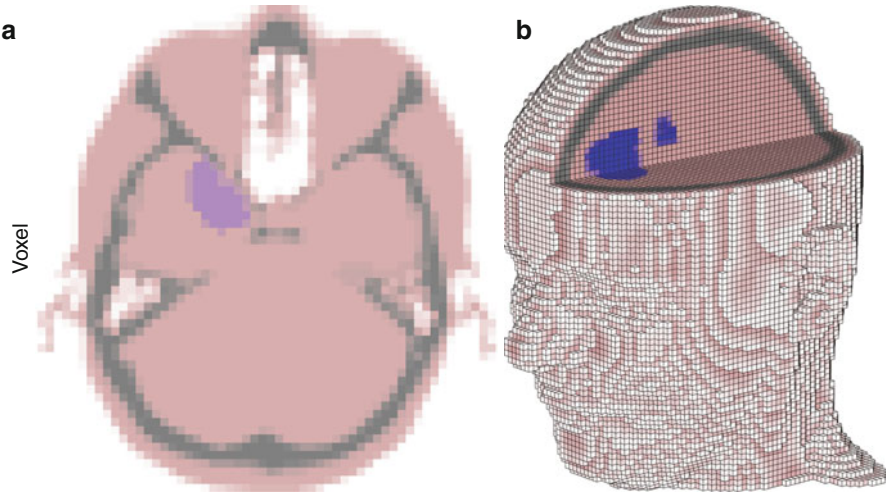

Fig. 16.2 Comparison of geometric modeling techniques used in NCT treatment planning calculations. The *left column* shows a 2D slice through each model around the level of the eyes and the *right column* shows corresponding 3D renderings of each type of model. (**a**) Color encodes mixture density and tumor volume fraction in this 3-mm voxel model, with air shown as white, soft tissue pink, bone gray, and tumor blue. (**b**) A cutaway view of the voxel model showing the target volumes. (**c**) Air, skin, skull, brain, brain stem, eyes, optic chiasm, and sinuses are defined in this univel model of one of the authors. Each univel corresponds to a pixel in the MR images used to derive the model, which have a pixel size of $1 \times 1 \times 2$ mm^3. (**d**) Surface rendering of the univel model. (**e**) Control points indicated by plus signs guide the placement of the spline in the NURBS model, which is overlaid on an MR image. (**f**) Wire-frame rendering of the NURBS model showing the outer boundaries of skin (*cyan*), skull (*white*), brain (*green*), CTV (*yellow*), edema (*blue*), and GTV (*red*). The nose points to the left

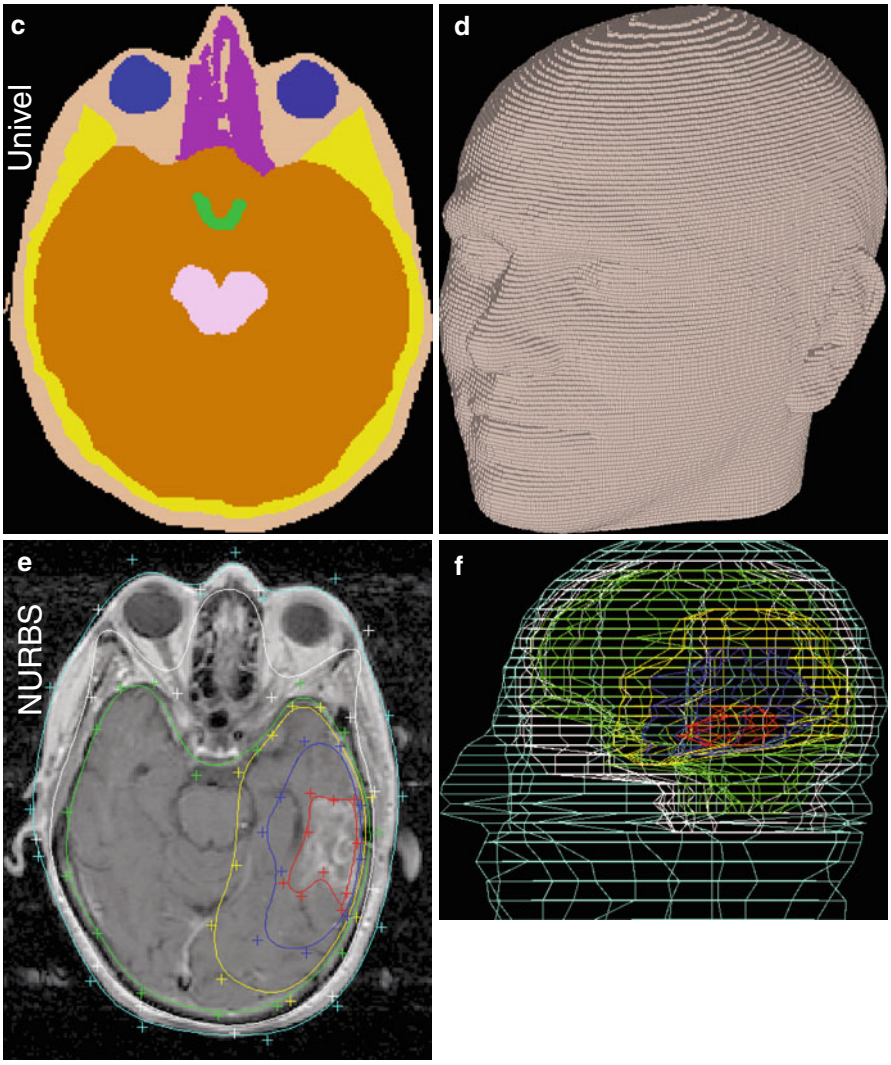

Fig. 16.2 (continued)

spatial resolution, which counteracts decreased voxel size. Very small voxels can pose significant computational issues for some transport codes [9], depending on details of how the calculations are done, but these issues are being addressed with improvements in software [10].

Most planning systems using voxel models employ voxels of a single size for simplicity. However, it can be advantageous to have finer resolution (small voxels) near the beam entrance where the dose gradient is usually steep and lower resolution (larger voxels) distant from the beam entrance where the dose gradient is shallow [11]. This approach, known as the "multi-voxel model" is used in the JCDS

planning system [12, 13]. The multi-voxel model approach works well for single-field treatment plans, where the voxel grid can be aligned with the beam, but has limited applicability to multi-field plans.

16.2.1.2 Univel Models

Uniform volume element, or "univel," models are similar to voxel models in their use of a uniform rectangular grid to describe the patient geometry, but they differ in that each univel represents a single pixel of the medical image stack rather than the average composition for a region encompassing many pixels. Unlike voxel models, univel models do not use material mixing because the univel size is very small. Geometrically, a univel model can be considered as a voxel model in the limit of small voxels. However, the key difference between voxel and univel models is actually not in the geometric representation but rather in the algorithms used to track particles through the geometry. Univel models employ fast tracking algorithms based on integer arithmetic similar to those used for line drawing in bitmap computer graphic images rather than traditional floating point tracking algorithms [14, 15]. The fast integer tracking algorithms involve a small degree of approximation in tracking, but this is reported to be negligible for the generally small univel sizes used [14]. The SERA treatment planning system developed at Idaho National Laboratory (INL) and Montana State University (MSU) implements the univel model in its seraMC transport module [16].

Univel models offer very high geometric fidelity, with the same spatial resolution as the medical images. The effort associated with producing such a high-resolution model can be significant, however, because the composition of each univel/pixel in the stack of medical images must be identified and defined. Generally, this is accomplished by having the planner "paint" each pixel with a color that maps to a particular material composition, using a combination of manual and image processing techniques such as thresholding. This process may be tedious and time-consuming. Thus, geometric accuracy is in principle very good but in some regions may be limited by the effort of the treatment planner in interpreting and drawing the anatomy. Also, it is important to realize that with univel models, although the geometry is specified with a fine mesh (~1 mm elements), generally the independent scoring mesh used for dose calculations is significantly larger, usually 10 mm, which could lead to interpolation error that is larger than one might expect for a high-resolution geometry. A univel model based on MR images of one of the authors is depicted in Fig. 16.2c and d. Further advantages of univel models include the ability to define as many regions as desired (each with a unique material) and the fact that, unlike in NURBS models, the regions do not have to be defined as a hierarchy, with each region completely enclosed by next region in the hierarchy.

16.2.1.3 Nonuniform Rational B-Spline (NURBS) Models

Nonuniform Rational B-Spline (NURBS) models are a very flexible and powerful 3D modeling technique frequently used in computer graphics rendering. NURBS models allow definition of free-form curves and surfaces with varying degrees of continuity (i.e., in position, direction, and curvature). The NURBS modeling

technique is used in the BNCT_Rtpe planning system developed at INL to define the patient geometry [1, 17, 18]. Anatomic structures are contoured by placing control points in the medical images that guide the location of the curve as illustrated in Fig. 16.2e [19]. Control point placement is done either manually or, in some cases, with edge-detection algorithms. Figure 16.2f shows a wireframe rendering of a NURBS model of a brain tumor patient.

This innovative application of NURBS models allows a very compact and efficient representation of complicated objects with good geometric fidelity and with low memory requirements, but particle tracking is somewhat slower than for other geometric representations as a result of the more complicated surface-finding algorithms. A disadvantage of the technique is that the model definition process can be labor-intensive, and it can sometimes be difficult to manage the control points to produce the desired results. Unintentional overlap of the NURBS surfaces defining adjacent bodies results in an ill-defined region of the geometry and will cause particles entering the region of overlap to be "lost." Also, although the external contour of the patient is represented with high fidelity, some internal structures (e.g., sinuses or skull) may lack definition because they are either impractical or too labor-intensive to delineate [20]. While the NURBS approach is well suited to modeling the geometry of a brain tumor patient, it can be difficult to apply this modeling technique to other geometries, for example, complicated phantoms. A scoring mesh with 10-mm cubic elements superimposed on and independent from the NURBS model defining the patient is used for dose calculations in the BNCT_Rtpe planning system.

16.2.2 Neutron Beam Source Definition

Definition of the radiation source for computations is perhaps the most difficult aspect of treatment planning, because it requires producing an adequately accurate computational representation of the 5-dimensional probability distribution describing the spatial, energy, and angular characteristics of a neutron beam. Methods of defining a neutron beam source for NCT treatment planning involve using either binary phase space files (known as surface source files in the MCNP code) or a set of probability distributions to define the radiation source characteristics at or near the neutron beam aperture to avoid repeating the computationally expensive transport of neutrons through the beam line. The various methods of source definition have different advantages and disadvantages [21, 22].

16.2.2.1 Phase Space File

Phase space (surface source) files record the characteristics (position, direction, energy, time, particle type, statistical weight, and history number) of particles simulated at a particular location in a Monte Carlo simulation, usually at the beam aperture plane in treatment planning simulations. When using phase space files, the particle tracks stored in a phase space file from a previous simulation of the beamline are sampled in subsequent simulations of particle transport through the patient geometry. The primary benefit of using a phase space file is that it introduces no

approximations into the source description; the simulated particles originate from a detailed simulation of the neutron beamline, which should lead to improved dose accuracy, unlike source definitions using probability distributions, which may involve significant approximations. Disadvantages of this method include the extremely large size (up to several gigabytes) of the unportable binary files, lower computational efficiency, increased start-up times for parallel computations, and limitations on the number of particles that can be simulated. Because the number of histories (sample size) in a phase space file is not infinite, the precision of doses calculated with the phase space file is limited due to its latent variance [23] which results from statistical fluctuations in the phase space. Phase space files can be recycled (oversampled several times) to improve dose statistics, but this only improves statistics on dose components derived from thermal neutron interactions and may also have undesirable statistical effects.

16.2.2.2 Planar Probability Density Function

In sources defined with a planar probability density functions (PDFs), probability distributions for the source particle variables (energy and components of position and direction) are usually constructed from prior Monte Carlo [24] or discrete ordinates transport calculations [25, 26] of the neutron beam. In the patient calculations, the probability distributions are sampled to determine starting characteristics for each source particle. Source PDFs may be defined in two ways in the patient transport simulation: "in-air" at the plane of the beam aperture or at a plane inside the collimator a short distance upstream of the beam aperture. In the latter method, a portion of the collimator must be explicitly modeled in the patient simulation, which can complicate patient model construction. Sources modeled inside the collimator generally have a lower level of detail compared to sources modeled in-air, because it is thought that transport of the beam through the collimator helps to define spatial distribution of the beam. Defining the source in-air at the beam exit is more efficient because the computational expense of transport through the collimator is avoided in every patient simulation, but a greater level of detail may be required in the source distributions to achieve the desired level of accuracy in calculated doses. An example of in-air source PDFs may be found in Palmer et al. [24].

Advantages of source PDFs include a compact, portable (usually text) representation, and the ability to sample an effectively unlimited number of particle histories, leading to arbitrarily small statistical uncertainty in calculated doses. The main disadvantage of source PDFs is that they may involve significant approximations and loss of information that reduce the accuracy of computed doses. The fact that the probability distributions for the source variables (energy spectrum, spatial distribution, angular distribution) may be inseparable is also problematic to constructing source PDFs. The level of detail in source PDFs needed to achieve accurate dose calculations has not been studied thoroughly, especially for the source-in-collimator method. Recent studies have suggested that, as implemented in several planning systems, source PDFs may not represent neutron beam source characteristics with adequate accuracy, particularly with regard to treatment of the angular distribution [21, 22].

16.2.2.3 Beam Directions

Most planning systems achieve multiple beam orientations by holding the patient geometric model fixed and rotating the beam model around the patient model, because this allows the convenience of a single dose grid, eliminating the need for interpolation between dose grids for multi-field plans. The JAEA planning system JCDS, however, in addition to the standard method, can employ a novel approach wherein the patient model is rotated into the desired alignment with a fixed beam model. This approach is feasible because, most often, single-field treatments are planned with JCDS.

16.2.3 Dose Calculations

This section discusses aspects of dose calculations for NCT treatment planning.

16.2.3.1 Computational Methods

All clinical NCT treatment planning systems employ Monte Carlo simulations for calculation of doses in individualized models of the patient or phantom. Generally, dose (actually kerma to be precise) is calculated by integrating the neutron or photon flux spectrum computed using a track length density estimator of flux against energy-dependent kerma factors. For efficiency, the integration is done on-the-fly so that it is unnecessary to store the flux spectra at each point in the dose grid. In some planning systems, doses are computed on an element-wise basis, while in others doses are calculated using kerma factors precomputed for a particular tissue composition, for example, ICRU brain composition. The latter method is more computationally efficient but less flexible than the former. In either case, boron dose is computed using an independent set of kerma factors (usually for 1 μg/g ^{10}B) so that it can be scaled to match the concentrations in tissues of interest. Collision-based estimators of dose have also been studied and may have some advantages over track length density estimators [27], but they are not used by any clinical planning systems.

For all dose components except the photon dose, the charged particles that ultimately deliver the dose have ranges that are very small compared to the mesh element size of the dose grid so that kerma approximates dose extremely well. Energetic electrons produced by photon interactions in tissue can have a range over 1 cm, similar to or larger than the dose grid element size. Nevertheless, electron transport is not performed because of its high computational expense; coupled neutron-photon-electron transport calculations converge very slowly. In most NCT applications, the kerma approximation is believed to have a very low impact on photon dose accuracy because the induced photon dose component, which dominates the incident photon dose in most beams, is mainly isotropic.

The general-purpose Monte Carlo radiation transport code MCNP [28], developed at Los Alamos National Laboratory, is widely used as a dose calculation engine in BNCT treatment planning systems, because, among other reasons, it is well validated, relatively easy to use, offers flexibility in source definition and

robust variance reduction techniques, and has a large user base. Different computational approaches to the geometric representations of voxel models and the dose scoring (tally) techniques in the MCNP code can have a dramatic influence on computation speed for treatment planning simulations [9]. A modification to MCNP known as the "lattice speed tally patch," initially implemented in version 4B of the code, allowed a dramatic speedup for treatment planning calculations in lattice models [29]. This patch has since been incorporated into the code base [30] and recently (in MCNP5 version 1.50) improved to facilitate calculations with models with very many small voxels. Another recent improvement to MCNP, the mesh tally, offers a dose calculation grid that is independent of the geometric grid with relatively little additional computational cost.

Other methods of dose calculation besides Monte Carlo simulation that have been studied include deterministic transport methods such as the S_n (discrete ordinates) method [18, 31, 32] as well as faster, more approximate algorithms such as the simplified P_3 approximation [33], removal-diffusion theory [34], and empirical methods [35]. However, these methods have not been applied in clinical planning systems for various reasons.

16.2.3.2 Tissue Compositions and Boron Concentrations

Unlike in radiotherapy with photons and electrons, where heterogeneous dose calculations are based only on electron density derived from CT image data, dose calculations for NCT require that the actual tissue composition be modeled. Modeling different tissue types is necessary because elemental composition varies significantly between tissues and because neutron cross sections also vary greatly between nuclides. A computational study evaluating the required complexity of patient models demonstrated significant shifts in position and changes in the value of the dose maximum of up to 9 % when the skull (which has a lower hydrogen density) is replaced by skin in simulation of cranial irradiations [36]. The atomic densities of hydrogen and nitrogen have the greatest influence on neutron transport and dosimetry because of their cross sections and abundance. ICRU reports 44 and 46 provide reference composition data and densities for a wide range of tissues [37, 38]. For some earlier clinical trials of BNCT for intracranial disease and most related radiobiological studies, Brooks brain composition [39] was used, but now ICRU compositions [38] are recommended for consistency across trials. The major difference between the Brooks brain and ICRU brain compositions is a 20 % difference in nitrogen concentration, which leads to a similar difference in thermal neutron dose [8].

Because its large neutron capture cross section results in significant thermal neutron flux depression, it is necessary to explicitly model ^{10}B in the tissue composition used in transport calculations [5, 40]. For prospective planning, boron concentrations should be specified for both normal tissues and tumor using reasonable assumptions for the expected concentrations based on pharmacokinetic studies. As an example of the significance of this effect, a ^{10}B concentration of 30 μg/g ^{10}B in brain tissue reduces the maximum thermal neutron flux in a head phantom by about 10 % and produces a similar reduction in dose components derived from thermal neutrons [8]. For gadolinium NCT, the effect of thermal neutron flux depression is

substantially larger and more important [41] than for boron because of the enormous (255,000 b) neutron capture cross section of ^{157}Gd. For applications like boron neutron capture synovectomy (BNCS), where extremely high ^{10}B concentrations (e.g., >10,000 μg/g) can be achieved [42], thermal neutron flux depression is also quite substantial and must be accounted for.

16.2.3.3 Nuclear Cross Section Data

Two types of representations of nuclear cross section data are used in radiation transport calculations for treatment planning: point-wise continuous energy cross sections and multigroup cross sections. Point-wise continuous energy cross section data achieve a high-fidelity representation of the evaluated nuclear data though linear interpolation between a large number of specified points. Multigroup cross section data have a less accurate but more compact and computationally efficient representation, using a single discrete value for the cross section over a range of particle energies. Some special-purpose radiation transport codes used in treatment planning (e.g., rtt_MC and seraMC) employ multigroup cross section data because of advantages in computational speed. Continuous energy cross section data are more accurate than multigroup data, but for broad spectrum beams, multigroup cross section data generally produce results that are accurate. However, in some cases, where the incident neutron spectrum is peaked around energies where a resonance in the neutron cross section is present, the flattening of the resonance in the multigroup data can produce large deviations. This problem has only been demonstrated for monoenergetic beams used in computational studies [43, 44]. Nevertheless, when using multigroup cross sections, it may be advisable to perform comparative simulations with continuous energy cross sections.

A related factor that has a significant influence on neutron transport calculations is the thermal neutron scattering treatment [8]. At low neutron energies, the thermal motion of nuclei and their chemical binding to other atoms affects the kinematics of neutron scattering, influencing the energy and angle of outgoing neutrons. For neutron scattering with hydrogen, the impact of chemical binding is particularly large and it is important that this effect is properly modeled in transport calculations. For example, using a thermal neutron scattering treatment where the effect of chemical binding is omitted, that is, the free gas scattering law, underestimates calculated boron, thermal neutron, and induced photon doses by 30–37 % [8]. Some transport codes used in NCT treatment planning (i.e., MCNP) allow for a thermal neutron scattering treatment that accounts for binding of hydrogen with only a single element (e.g., oxygen) in each material, while others (rtt_MC and seraMC) permit mixing scattering of hydrogen bound to either oxygen or carbon. The latter method seems more appropriate for human tissue, but calculations indicate that the difference between these two approaches is negligible [22].

16.2.3.4 Kerma Factors and Dose

A few different schemes of accounting for the different dose components have been used in NCT clinical dosimetry. Some of the differences between accounting

schemes amount to differences in nomenclature, while others result in small differences in dosimetry. In the physical dosimetry of NCT, four dose components are measured: boron dose, thermal neutron dose, fast neutron dose, and photon dose [45, 46]. In computational dosimetry of NCT used in treatment planning, the calculated photon dose is usually subdivided into incident and induced photons so that the number of calculated dose components totals five [8]. Across all planning systems in clinical use, the boron dose and photon dose have identical definitions. The thermal neutron and fast neutron dose components, however, are defined and accounted for differently by the various planning systems in use. The dose components are defined as follows:

- Incident photon dose arises from photons produced by neutron interactions in the beamline. Incident photons are started (i.e., born) in the simulation of radiation transport through the patient model. They are not produced by neutron interactions in this simulation; they are sampled from a source distribution or phase space file produced in an earlier simulation of the neutron beam. This component is also known as the source or structural photon dose component.
- Induced photon dose arises from photons produced by neutron interactions in the patient and possibly other surrounding material (e.g., a collimator that is explicitly modeled in the simulation). The principal contributor to the induced photon dose is neutron capture by hydrogen ($^{1}H(n,\gamma)^{2}H$), which produces a 2.2 MeV γ-ray. The distinction between incident and induced photon doses is made to facilitate their independent adjustment to match measurements during the calibration process. The photon dose is sometimes termed total photon dose to emphasize that it is the sum of incident and induced photon dose components.
- Boron dose results from neutron interactions with ^{10}B, primarily through the $^{10}B(n,\alpha)^{7}Li$ neutron capture reaction. Fig. 16.3 shows the energy-dependent kerma factor for ^{10}B at a concentration of 15 μg/g.
- Thermal neutron dose is the dose produced by thermal neutron ($E_n < 0.5$ eV) interactions in tissue excluding that dose from thermal neutron-induced photons (which is tracked separately and included in the induced photon dose) and dose from boron. Most of the thermal neutron dose arises from neutron capture by $^{14}N(n,p)^{14}C$, which releases 626 keV, most of which is carried away from the recoiling ^{14}C nucleus by a proton. For ICRU brain composition [38], which contains 2.2 % nitrogen by mass, about 96 % of the thermal neutron dose comes from the $^{14}N(n,p)^{14}C$ reaction. The remainder (~4 %) of the dose is primarily due to the recoiling deuteron from radiative neutron capture by hydrogen ($^{1}H(n,\gamma)^{2}H$). The energy-dependent neutron kerma factors for ICRU brain composition are shown in Fig. 16.3. Thermal neutron dose depends on the tissue composition, particularly the nitrogen concentration. For example, when irradiated with the same thermal neutron fluence, the dose to skin will be about 1.9 times higher than in brain, mainly because of the higher nitrogen concentration in skin (4.2 % by mass).
- Fast neutron ($E_n > 0.5$ eV) dose is primarily (>90 %) due to elastic neutron collisions with hydrogen, which produce recoil protons. Fast neutron collisions with

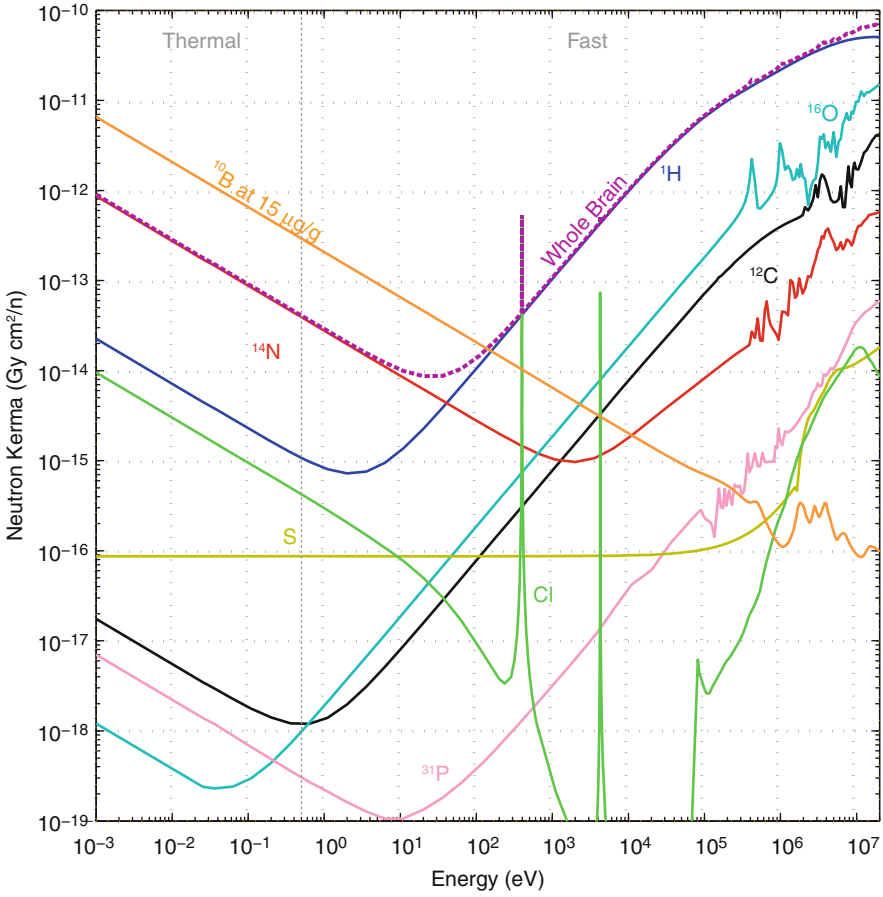

Fig. 16.3 Contributions to energy dependent neutron kerma factors for ICRU brain from different elements. For comparison, the kerma factor for ^{10}B is included, shown for a concentration of 15 µg/g. The *dashed vertical line* at 0.5 eV indicates the boundary between fast and thermal neutrons (Adapted from data in Ref. [8])

other abundant nuclei such as oxygen, carbon, and nitrogen contribute significantly to the fast neutron dose. Around capture resonances at 398 eV and 4.3 keV, the chlorine (n,p) reaction also contributes to the fast neutron dose. The rationale for separating fast neutron dose and thermal neutron dose on the basis of an energy cutoff around 0.5 eV is to mirror the dose measurement process using the activation foils with the cadmium difference technique, where the upper limit on the thermal neutron flux is defined by the cadmium cutoff around 0.5 eV (where the cadmium neutron capture cross section drops from ~10,000 barns to low values). Separating the calculated neutron doses in a manner similar to measurements facilitates comparison of measured and calculated doses for validation and calibration.

A second method of accounting for the fast and thermal neutron doses separates these neutron-derived dose components according to target element:

- Hydrogen dose is the locally deposited dose from neutron interactions with hydrogen. It includes dose from recoil protons liberated by fast neutron collisions with hydrogen but usually omits dose from the recoil deuteron in the $^{1}H(n,\gamma)^{2}H$ reaction. The 2.2 MeV gamma ray produced by hydrogen neutron capture is separately tracked, because it does not deposit its energy locally and is accounted for in the induced photon dose.
- Nitrogen dose is the locally deposited dose resulting from neutron interactions with nitrogen, including the $^{14}N(n,p)^{14}C$ reaction and fast neutron collisions.
- Other dose components: In conjunction with the hydrogen and nitrogen dose, doses for oxygen and carbon are also sometimes calculated since they contribute significantly to dose through fast neutron recoils, especially at higher energies.

In principle, the sum of the thermal and fast neutron dose components should equal the sum of the hydrogen plus nitrogen and other minor elements that contribute mainly at high energies. However, there can be some small differences between the totals for these two approaches.

In addition to the individual dose components, two different sums of the dose components are used:

- Total dose is the sum of all dose components without any weighting, that is, physical absorbed dose. Total dose is used more often in radiobiology experiments than in clinical practice.
- Biologically weighted dose is the weighted sum of all dose components, each multiplied by a weighting factor which is usually an experimentally measured RBE (relative biological effectiveness) or CBE (compound biological effectiveness) factor [47]. Weighted dose expresses the radiation dose in approximately photon-equivalent units to account for the varying biological effectiveness of the different high- and low-LET dose components. Most often, dose prescriptions are expressed in weighted dose. Strictly speaking, the units of weighted dose are gray (Gy) since biological weighting factors are unit-less, but weighted dose is often expressed in units denoted as Gy_w to distinguish it from unweighted physical absorbed dose.

Each planning system has its own set of kerma factors used for dose calculations. The differences between the kerma factors used by the various planning systems for a given dose component are mostly small, but a few differ significantly [22, 48]. Also, those transport codes that use multigroup cross section data also use multigroup kerma factors.

16.2.3.5 Statistical Uncertainty

Due to the stochastic nature of the Monte Carlo simulation process, the calculated dose at each point in the computational grid has an associated statistical uncertainty (standard deviation); that is, the calculated dose is known imprecisely. Shortly after a simulation starts, few particles have been scored and statistical uncertainties are high. As more and more particles are simulated, more particles score at each point in the computational grid, and the relative contribution of each

particle to the mean dose scored (which is the calculated dose) is reduced. Thus, with increasing numbers of simulated histories, the fluctuations in the calculated dose are reduced, and the calculated dose converges on its "true" value. AAPM task group 105 provides an instructive review of statistical issues associated with Monte Carlo-based treatment planning [49].

The standard deviation of calculated doses is affected by several factors. Standard deviation decreases with more histories and is roughly inversely proportional to the square root of the number of histories. The size of individual elements of the scoring mesh also affects statistical uncertainty. With a finer mesh, fewer particles will score in each element; standard deviation is roughly inversely proportional to the square root of the volume of each mesh element. For phase space files, variability of particle weight can also contribute to statistical uncertainties. High weight particles recorded in a phase space file that sometimes result from unfavorable variance reduction techniques in the prior upstream simulation of the beam can introduce high variance to an otherwise acceptable calculation. Typically, with a 1-cm^3 scoring mesh, standard deviations well under 1 % at the dose maximum are easily achievable for most dose components with a few tens of millions of histories, but this depends on the specific details of the beam and source model.

Unfortunately, most planning systems do a poor job of reporting the statistical uncertainty of calculated doses. It is nevertheless important for the treatment planner to keep statistical uncertainty in mind, because until enough histories have been simulated that the calculation is well converged, the calculated doses may deviate significantly from their final, well-converged values. In other words, if not enough histories are simulated to obtain convergence for a treatment plan, the actual delivered doses may differ from planned doses significantly. For example, during a dosimetric renormalization study, it was observed that the maximum weighted dose for a particular patient decreased by 5 % when the number of particle histories was increased from 0.5 to 15 million [22, 50]. Quick simulations with low numbers ($<10^6$) of histories can be useful for scoping calculations, where the planner wants to rapidly assess different beam orientations, but only well-converged calculations with large numbers of histories should be used in the final plan for calculation of the monitor units to be delivered.

16.2.4 Planning System Quality Assurance and Verification

Quality assurance of planning systems is an ongoing process that begins with software developers and continues with the end users of a TPS. A detailed treatment of this expansive topic is beyond the scope of this chapter; AAPM task group 53 provides extensive guidance on quality assurance of clinical radiotherapy treatment planning systems, much of which is directly applicable to NCT treatment planning systems [51]. Complex software like treatment planning systems is difficult to test thoroughly. To assist with dosimetric aspects of the quality assurance process for new TPSs and to aide in evaluating the accuracy of existing NCT TPSs, two suites of reference problems have been developed. The first set of reference problems provides depth-dose data for a range of monoenergetic and

broad spectrum neutron and photon beams calculated on the beam central axis in a head phantom using the well-benchmarked Monte Carlo transport code MCNP [8]. The second set of reference problems extends the first by adding two phantoms, a large rectangular water phantom irradiated with an epithermal neutron beam and a leg phantom that simulates treatment of peripheral melanoma lesions with a thermal neutron beam [22, 52]. More importantly, for the two anatomic phantoms, the second test suite includes the multidimensional dose data commonly used for analysis in clinical treatment planning, that is, isodose curves and dose-volume histograms. In all of the reference calculations, the phantom geometries were modeled using geometric primitives (i.e., combinatorial geometry) thereby avoiding approximations in geometry usually employed by planning systems. For both sets of reference problems, image data of each phantom are provided that can be imported into planning systems to allow development of treatment plans for comparison with the reference data.

16.2.5 Planning System Calibration and Validation

It is sometimes assumed that when Monte Carlo simulation is used for dose calculations, high levels of accuracy are guaranteed. This misconception should be avoided. Prerequisites for accurate dose calculations include, in addition to a good physics model, a simulated radiation source that faithfully represents the actual radiation source. Errors or inaccuracies in software or the radiation source definition can lead to significant errors in calculated dose. Validation, the process of confirming calculations with measurements, is perhaps even more important for NCT planning systems than for external beam photon planning systems because of the uniqueness of each neutron beam and because NCT planning systems have small user bases. Validation is an important opportunity for carefully assessing the accuracy of the TPS and source model and ensuring that they work as expected.

The fundamental quantity of interest in radiotherapy is dose, that is, energy deposited by ionizing radiation per unit mass of medium, and this is the quantity that must be used for calibration and validation of the planning system in appropriate phantoms. Calibrating to other measured quantities such as fluence is not appropriate and in some circumstances may lead to errors [22]. Dose measurements for TPS calibration should be made using instruments with calibrations traceable to national or international standards as described in Chap. 13 and 14. Other types of measurements such as in-air spectral measurements may be helpful if problems in the beam source definition are identified, but recent results [21, 22] suggest that, at least for some beams, the source phase space may be too complex to be well described by spectral measurements at a single point or by integral angular distributions.

Calculations for TPS calibration and validation should attempt to closely match the measurement conditions. For instance, if an A-150 tissue equivalent plastic (TEP) ion chamber is used for dose measurements, kerma factors for A-150 TEP should be used for calculations. Likewise, neutron flux calculations should mimic measurements. For example, at Harvard-MIT, where gold foil activation measurements of

thermal neutron flux are made using the cadmium difference technique, a cadmium-differenced[1] gold cross section is used to weight calculations of the 2,200 m/s (0.0253 eV) thermal neutron flux. Note that, as indicated above, this neutron flux comparison aides in evaluation of the TPS but is not, strictly speaking, used for calibration. An additional consideration is that the planning system itself must be used for calibration rather than a distinct computational model (e.g., an MCNP model), and the same type of geometric representation used for simulating patient irradiations must be used to represent the phantom in calibration simulations. Otherwise, subtle errors may go undetected [22, 50].

A number of different kinds of phantoms have been used in TPS validation and calibration. Water is a frequent choice for phantom material since it mimics the transport characteristics of brain [53] and many other tissues rather well and is readily available in high purity. Large rectangular water phantoms, like those commercially available for conventional radiotherapy, often have motorized drive systems that allow remote repositioning of ion chambers or other detectors to facilitate measurement at multiple positions. The flexibility that these phantoms afford in positioning detectors is particularly advantageous for measuring along multiple axes. The disadvantage of large water phantoms is that, most often, they do not mimic the actual clinical situation well. The very large mass of the phantom in comparison to a much less massive patient or anthropomorphic phantom raises the thermal neutron flux and induced photon dose by 20–30 % or more [54, 55]. The augmented photon and thermal neutron dose further increase the difficulty of fast neutron measurements. Also, patients have irregular, curved external surfaces, and rectangular water phantoms do not test the ability of planning systems or source models to handle such geometries. Furthermore, features of the angular distribution that may be important in anthropomorphic phantoms can be less significant in large rectangular water phantoms [22]. It may be prudent to calibrate in a phantom that has geometric characteristics more similar to the clinical target of interest than a large rectangular water phantom.

Comparing measurements and calculations in two different phantoms, like a large rectangular water phantom and a smaller anthropomorphic phantom, provides a good test for the TPS and source model. Rectangular water phantoms afford freedom of position for dosimeters, while anthropomorphic (or simpler appropriately sized and shaped dosimetry) phantoms offer more clinically relevant and realistic conditions to assess accuracy and calibrate the TPS. A number of different anthropomorphic phantoms have been used in BNCT clinical dosimetry [56]. One well-known example is the MIT ellipsoidal head phantom [57].

Generally, TPS calibration involves adjusting the dose rates calculated with the TPS to match measurements and determining a relationship between beam monitor count rates and dose rate in a reference phantom. Two different approaches can be used to adjust calculations to match measurements for calibration.

[1] The cadmium-differenced gold cross section is the difference between an unattenuated "bare" gold absorption cross section and the gold cross section attenuated by 0.439 g/cm^2 cadmium.

The first approach for adjustment involves applying post facto multiplicative scale factors to each of the five calculated dose components to improve agreement with measurements. Generally, least squares analysis is used to determine the scale factors and residuals should be plotted to assess whether a systematic difference exists between measurements and adjusted calculations. Clearly, this approach to correction is simple, adjusting only the gross magnitude, and these scalar adjustments will not alter the shapes of the dose curves to improve agreement. When using this method, generally one should find that the scale factors for the thermal neutron dose, boron dose, and induced photon dose are very nearly identical because all three are derived from thermal neutrons, either directly or indirectly. Of course, these scale factors should also very closely follow the scale factor determined for the thermal neutron flux. Because of the large uncertainty associated with fast neutron measurements in-phantom, it can be very helpful to also compare measurements and calculations in-air, where the measurement uncertainty is lower due to the elimination of the induced photon dose component. Similarly, for the incident photons, which may be a small fraction of the total photon dose, in-air comparisons of measurements and calculations are valuable.

Independent adjustments of the induced and incident photons are appropriate and usually necessary because the two components arise from different sources. Induced photons are produced in the phantom, mainly by the $^{1}H(n,\gamma)$ reaction, while the incident photons arise in the beam from various reactions, both prompt and delayed. The incident photon component can be difficult to correctly model because delayed gammas can contribute significantly to this component and most codes used for simulating neutron beams are not able to handle delayed gammas well because of their time-dependent nature. This difficulty often leads to scale factors for incident photons that are larger than others, for example, for the MIT fission converter beam, the scale factor for incident photons is ~2.0, while those for other dose components are close to unity [55, 58].

The second, more complicated method of adjusting calculated doses to match measurements involves tuning the source definition in the Monte Carlo model. This is usually limited to altering the (total) source strength for either the neutrons or the incident photons or modifying a portion of the neutron or photon spectra. This method offers greater flexibility but is not preferred because identifying the region of the multidimensional phase space requiring adjustment is seldom straightforward. This method cannot be applied to sources using phase space files without heroic efforts; it is otherwise limited to sources defined using probability distributions. As with the first method, least squares and residual analysis are helpful in assessing agreement.

Validation in a large water phantom should include comparison of measurements and calculations on several axes so that the agreement in three dimensions can be assessed. These comparisons should include depth-dose profiles on the central axis and at off-axis positions, for example, in the penumbra, to assess the penetration of the beam as well as horizontal and vertical profiles (orthogonal to the central axis, e.g., at the depth of the thermal neutron flux maximum) to assess the width of the beam and its symmetry, as illustrated in Fig. 16.4. Furthermore, if the beam source definition and TPS assume rotational symmetry of the beam around its axis, then the validity of this assumption should also be assessed with measurements. Significant

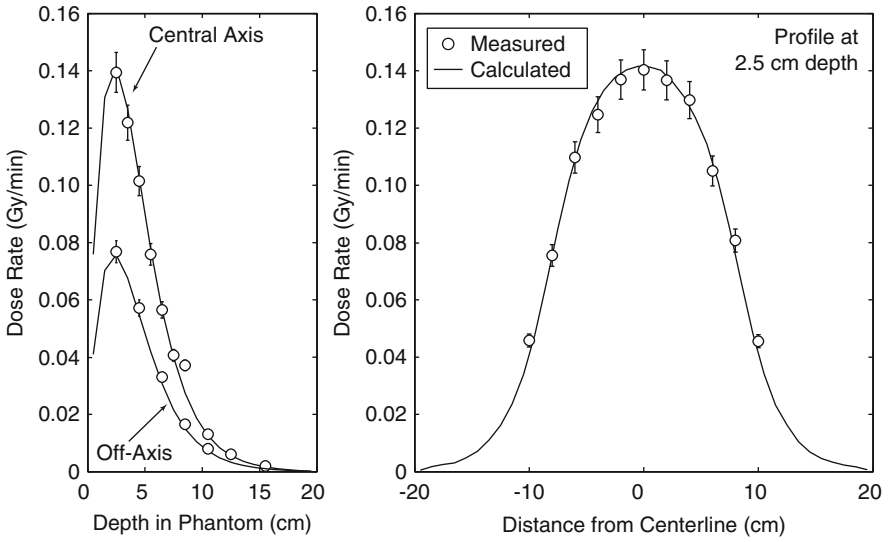

Fig. 16.4 Part of planning system validation, using a comparison of measured and calculated thermal neutron dose rates in a large rectangular water phantom. These data for the MIT fission converter beam are assessed on the central axis of the beam, at off-axis positions at a distance of 8 cm from the central axis, and in a horizontal profile at 2.5-cm depth, near the thermal neutron flux maximum [55]

differences between calculations and measurements that cannot be corrected by simple scaling may indicate a need to reassess the source model. The report of AAPM task group 53 [51] and IAEA report TRS430 [59] provide guidance on acceptable tolerances for deviation between dose measurements and TPS calculations for photon and electron radiotherapy. Although the measurement uncertainties in NCT dosimetry are considerably higher than for photons and electrons, this guidance is nevertheless instructive for NCT practitioners.

A recent interinstitutional comparison of clinical NCT dosimetry identified large differences between computed clinical dosimetry and dose measurements made using a common method [60]. External quality assurance checks on machine calibration are quite common in external beam radiotherapy and are frequently required for participation in interinstitutional clinical trials [61, 62]. With the high level of complexity and lack of standardization of NCT physical and computational dosimetry, external checks on clinical dosimetry can provide a valuable confirmation of the TPS calibration. Such dosimetric comparisons are considered by many to be an important prerequisite to initiating human clinical trials.

Finally, during the calibration process, it may be convenient to define a "beam monitor unit" that packages a large number of beam monitor counts into a more meaningful and intuitive quantity. For example, useful definitions of a monitor unit include beam monitor counts corresponding to 1 min of irradiation at full power or corresponding to delivery of a certain dose in the calibration phantom, for example, 1 cGy_w at d_{max}.

Table 16.1 Characteristics of NCT treatment planning systems used in clinical trials

TPS	BNCT_Rtpe	MacNCTPlan	JCDS	SERA	NCTPlan
Developers	INEEL	Harvard-MIT	JAEA	INEEL/MSU	Harvard-MIT + CNEA
Operating system	HP UX	Macintosh	Windows	Linux & Solaris	Windows
Geometry model	NURBS	Voxel	Voxel/ multi-voxel	Univel	Voxel
Transport	rtt_MC	MCNP4B[a]	MCNP5	seraMC	MCNP4B[a]/5
Cross section data	Multigroup	Continuous energy	Continuous energy	Multigroup	Continuous energy
Source definition	In-collimator PDF	In-air PDF	Phase space file	In-collimator PDF	In-air PDF/ phase space file

[a]A modified version of MCNP4B is used for transport calculations

Table 16.2 Characteristics of NCT treatment planning systems in development

TPS	THORPlan	MCDB	BDTPS	MiMMC	MINERVA
Developers	Tsing Hua University	IAPCM, Beijing	Pisa/JRC Petten	Harvard-MIT	INL/MSU
Platform	Windows	Windows	Windows	MATLAB	Java
Geometry model	Voxel	Voxel	Voxel	Voxel	Univel
Transport	MCNP4C	MCNP4C[a]	MCNPX	MCNP4B[a]/5	JART

All of these TPSs employ continuous energy cross section data
[a]A modified version of the code is used for transport calculations

16.2.6 Treatment Planning Systems

All current NCT treatment planning systems are noncommercial and have been developed by small teams usually with expertise in nuclear engineering. Table 16.1 lists characteristics of the 5 TPSs that have been used in clinical trials of NCT. NCT planning systems in development (not yet used clinically) are listed in Table 16.2.

16.3 Clinical Aspects: The Treatment Planning Process

In this section, process of treatment planning for BNCT is described. The workflow of the treatment planning process for BNCT is similar to other types of radiotherapy such as external beams of photons, electrons, or protons. The major differences with treatment planning of conventional external beam radiation are that (1) dose targeting is obtained through the biochemical selectivity of the boron compound rather than through geometric targeting of highly collimated beams of radiation, (2) distributions of several dose components are generally computed using the Monte Carlo radiation transport methods, and (3) consequently, the time required for planning may be longer than for conventional radiotherapy, depending on what computational resources are available for dose calculations.

16.3.1 Patient Data Acquisition

In the treatment planning process, a 3D computational model of each patient is constructed for dose calculations. Tomographic medical images of the patient are acquired as the fundamental data of the model. A series of axial CT and/or MR images are usually employed. The matrix size of each CT image is usually 512×512 pixels, and the size for MR is usually 256×256. Slice thickness is usually around 2–5 mm, but a few planning systems have particular requirements for slice thickness and image size. When high resolution imaging is needed, a narrow slice thickness, such as 2 mm, is used. However, for most types of computational models, the image resolution is not directly related to calculation accuracy.

Immediately prior to imaging, reference points on the skin of the patient may be selected, marked with ink, and their spatial coordinates measured using a 3D digitizer [63]. Prior to scanning, an adhesive-backed radiographic marker (a Teflon or metallic BB) is applied to each reference point, enabling identification of the points on imaging. The reference points may later be used in the positioning process to aid in localizing the beam entry point or other points of interest.

In recent years, acquisition of PET image data with ^{18}F-BPA, the radiolabeled analog of boronophenylalanine, has been recommended. The ^{18}F-BPA PET data provides information on the BPA concentration ratio between the tumor and normal tissue regions [64, 65]. Prior acquisition of ^{18}F-BPA PET data helps to determine whether BNCT is indicated for a patient as well as to provide information on the ^{10}B distribution for treatment planning [66].

16.3.2 Image Processing

For the format of the images, newer planning systems generally use the DICOM format, which is the standard in the medical imaging field. More familiar image formats such as bitmap and JPEG can also be used in some planning systems. Older planning systems use other formats. For example, SERA and BNCT_Rtpe use the QSH image format, while NCTPlan and MacNCTPlan use the multipage TIFF format. For those planning systems, image data from the CT or MR scanner must be converted into the appropriate format. Prior to loading images, some planning systems that directly rely on the image data to construct voxel models may require that the images be cleaned. That is, the image data may need to be manipulated to eliminate defects such as dental artifacts and to erase patient-supporting devices like head cups and the scanner table to the same grayscale value as air. Using the DICOM image format facilitates the modeling process because important geometric information such as slice thickness, pixel size, and axial position are stored in the header part of DICOM image files. If conventional image formats like bitmap or TIFF are used, this geometric information must be supplied by the user since the conventional image formats lack this important information.

16.3.3 Target Volume Definition

Contouring target volumes and organs at risk on the tomographic images is an early step in the treatment planning process. These volumes are chosen according to the definitions given in ICRU reports 50 and 62 [67, 68]. First, gross tumor volume (GTV) is specified as the gross extent of disease that is palpable, visible, or demonstrable on imaging. For postoperative irradiation of malignant brain tumors, it is difficult to define the GTV precisely because most of the tumor volume is removed in the debulking operation. In this case, the enhancing rim of the excised tissue is defined as the GTV. For an effective therapy, not only must the gross disease be treated, but also the nearby tissue containing subclinical microscopic disease must be treated. For this reason, the clinical target volume (CTV) is defined as tissue that contains GTV and/or subclinical, microscopic disease. In BNCT for malignant brain tumors in Japan, the CTV is usually defined as a 2-cm expansion of the GTV. Some treatment planning systems, like JCDS, can define the CTV region automatically based on the GTV. Other regions such as the planning target volume (PTV), treated volume, and irradiated volume are defined as appropriate. If ^{18}F-BPA PET data can be acquired, the ^{18}F-BPA data may be utilized to help define the target volumes as mentioned above. Edematous regions, which often contain subclinical disease, are defined as the situation demands. Furthermore, several organs at risk should be defined in addition to the target volumes. The organs at risk are normal tissues near the CTV whose radiation sensitivity may significantly influence the treatment plan. Contouring the target volumes and organs at risk allows quantitative evaluation of competing treatment plans by using dose-volume histograms (DVHs) and relevant dose statistics such as maximum dose, mean dose, and minimum dose for the defined volumes.

16.3.4 Model Construction

To perform neutron and photon transport calculations and determine the dose distribution, a 3D computational model of the patient, with appropriate material compositions and densities, must be constructed from the tomographic images. In conventional radiotherapy, treatment planning calculations usually assume the patient's body to have the composition of water, either with a density scaled to match that observed in the patient's CT data (heterogeneous calculations) or with a uniform density of water inside the body, that is, 1.0 g/cm^3 (homogeneous calculations). As discussed in Sect. 16.2.3.2, such a simple approach is not feasible for BNCT treatment planning because neutron cross sections vary dramatically between nuclides and because elemental composition also differs between tissues and may significantly affect neutron transport. Thus, in BNCT treatment planning, detailed elemental compositions and densities must be defined for Monte Carlo radiation transport calculations. The tissue composition data generally employed are those recommended by ICRU report 46 [38] with the addition of the neutron capture agent

(^{10}B or ^{157}Gd) mixed into the tissue at appropriate concentrations so that thermal neutron flux depression is correctly modeled in neutron transport calculations.

To create a computational model, regions of the same composition in the body (and surrounding air) must be identified in each image slice. Neutron behavior in tissue depends largely on hydrogen density. Thus in models for BNCT treatment planning, human tissue and air are separated, and furthermore, the body tissue is differentiated into soft tissue and bone, because the hydrogen density differs greatly between these tissues. As shown in Fig. 16.1, when using CT images, the three regions can be easily distinguished by applying thresholds to the CT image values (Hounsfield numbers) of every pixel since there is a piecewise linear relationship between density and Hounsfield number. When using MRI data, the regions must be separated manually on every slice since such a convenient relationship does not exist as for CT. Depending on the capabilities of the treatment planning system and the requirements of the treatment protocol, structures such as skin, brain, or other organs may be separated in distinction to the soft tissue. The 3D computational model of the patient is constructed using one of the three methods of geometric representation, that is, a voxel, univel, or NURBS model, as described in Sect. 16.2.1.

Alteration of the model beyond what is visible in the image data may also be appropriate, depending on the conditions during treatment. For example, regions of shielding materials made of lithium fluoride (LiF) loaded polyethylene and/or build-up materials such as bolus used during treatment are defined as needed. Also, in intraoperative BNCT with thermal neutron beams, which had been conducted in Japan until the early 2000s, irradiations were performed with the scalp and skull above the tumor reflected. Hence, for treatment planning of intraoperative BNCT, the regions of reflected skin and skull were replaced by air to accurately simulate irradiation during craniotomy.

16.3.5 Beam Selection

Using a 3D computational model constructed as described above, irradiation conditions such as beam orientation, size, and shape are set. Because most facilities are reactor-based and have fixed beams, treatments are not isocentric. In typical treatment plans, the beam orientation is often determined by aligning the central axis of the beam to the center of the CTV or GTV. However, when organs at risk are located inside the irradiation field, near the target volumes, the beam may be offset in order to reduce dose delivered to healthy organs. For single-field irradiations, usually an optimum treatment plan results from setting the beam orientation to minimize the distance between the surface of body and the deepest point of the CTV, where its minimum dose occurs; this approach will maximize the minimum dose to the CTV. In the case of two-field or multi-field irradiations, bilateral or obtuse angle treatment plans are usually applied to suppress the maximum skin and/or normal tissue doses, especially if the radiation fields overlap.

In Japan, both reactor-based BNCT facilities have spectrum shifting systems which can change the neutron spectrum from epithermal to thermal; a few other

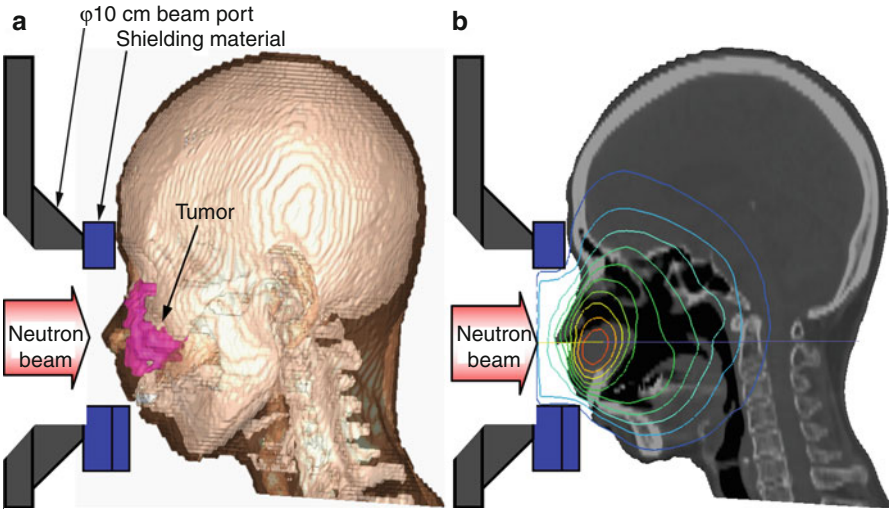

Fig. 16.5 Computational dosimetry for head and neck cancer BNCT using the JCDS planning system showing (**a**) 3D rendering of the patient model and (**b**) the calculated thermal neutron flux distribution. Custom blocking using LiF-loaded plastic is used to shield the eyes and other organs at risk

facilities also have both epithermal and thermal neutron beams available. Nevertheless, epithermal neutron beams are applied in most treatments. However, in BNCT for superficial tumors such as melanoma and meningioma, a less-penetrating thermal or mixed thermal-epithermal neutron beam is employed. Hence, an appropriate neutron spectrum should be chosen depending on the depth of the target and availability of neutron beams.

Neutron beam size and shape in BNCT differ from other external beam radiation modalities, which generally use adjustable collimator jaws and blocking devices such as the multi-leaf collimator to conform a highly collimated radiation field to the target volume. Neutron beam ports for BNCT are typically circular in shape. Usually, a circular beam size at least as large as the target volume is applied to ensure coverage of the target. Generally, open fields are employed in BNCT treatments, but occasionally blocking is used to shield sensitive areas or achieve other dosimetric goals. For example, in Japanese BNCT treatments for head and neck cancer, LiF-loaded thermoplastic shielding is placed over the eyes to block these radiosensitive organs, as shown in Fig. 16.5. During the treatment planning process, the appropriate size and location of the shielding materials must be determined. A different blocking technique often used in Japanese BNCT for malignant brain tumors, the central beam shielding method, is applied to improve dose distribution around target volumes [69]. In this technique, a small disc made of LiF-loaded thermoplastic resin is fixed in the center of the beam aperture, and the resulting annular beam irradiates the patient. This innovative form of intensity modulation serves to flatten the peak of the thermal neutron flux distribution and improve the dose uniformity. The disc must be sized appropriately for the

situation since the beam intensity and dose distribution in the body change with both disc size and beam port size. A related technique, which uses lithium metal filtration applied uniformly over the whole beam, achieves modest improvements in beam penetration by hardening the epithermal neutron spectrum [70].

16.3.6 Plan Evaluation and Optimization

Standard tools for dose visualization and analysis such as isodose contours and DVHs are generally used to evaluate treatment plans in BNCT. The presentation of dose in BNCT treatment planning is, however, somewhat unconventional. Typically, total weighted doses for tumor tissue and for normal tissue(s) are calculated separately, each for the entire dose grid using different boron concentrations and weighting factors (RBEs) assumed for each tissue. This means that when isodose contours are shown, as in Fig. 16.6, the calculated tumor dose is not limited to the extent of the target volume. Conversely, the normal tissue dose is also shown inside the target volume as in Fig. 16.6. The rationale for this approach is that the exact boundary of the tumor is unknown, and microscopic, subclinical disease extends well beyond the enhancing tumor volume detectable on imaging. For the purpose of developing and optimizing the treatment plan, it is not important, and probably not helpful, to see a composite set of tumor and normal tissue isodose contours. Because dose targeting is obtained through the selectivity of the boron, the task of the treatment planner is to deliver adequate thermal neutron fluence to the target volume, and this is more easily optimized using distinct sets of isodose contours for tumor and normal tissue.

Optimizing a treatment plan involves selecting the orientation, size, and, in some cases, spectrum for a beam or set of beams to deliver the radiation dose. Generally, a plan that produces the highest dose in target volumes while complying with the dose prescription and respecting dose limits on normal tissues and organs at risk is optimal. However, other important factors such as irradiation time and patient position during irradiation must also be considered since these affect the implementation of the plan, that is, treatment delivery. For single-field treatment plans, optimization of the plan is usually relatively straightforward; it only involves choosing among several candidate beams and determining the desired dose and the corresponding number of beam monitor units to deliver. For multi-field treatment plans, optimization is substantially more complicated because one must choose a few (usually nonoverlapping) fields from a pool of candidate fields and determine how the fields should be weighted[2] in order to best achieve the dosimetric objectives of the treatment. In most planning systems, it is very time-consuming and tedious to manually search the treatment plan parameter space to determine the optimal set of fields and their weights for any more than a very small number of candidate fields. To solve this problem, a simplex search algorithm to optimize the boron dose to a

[2] Beam weight is most often taken to be proportional to beam monitor units, but other definitions, such as fraction of dose delivered to a point or structure, may also be used.

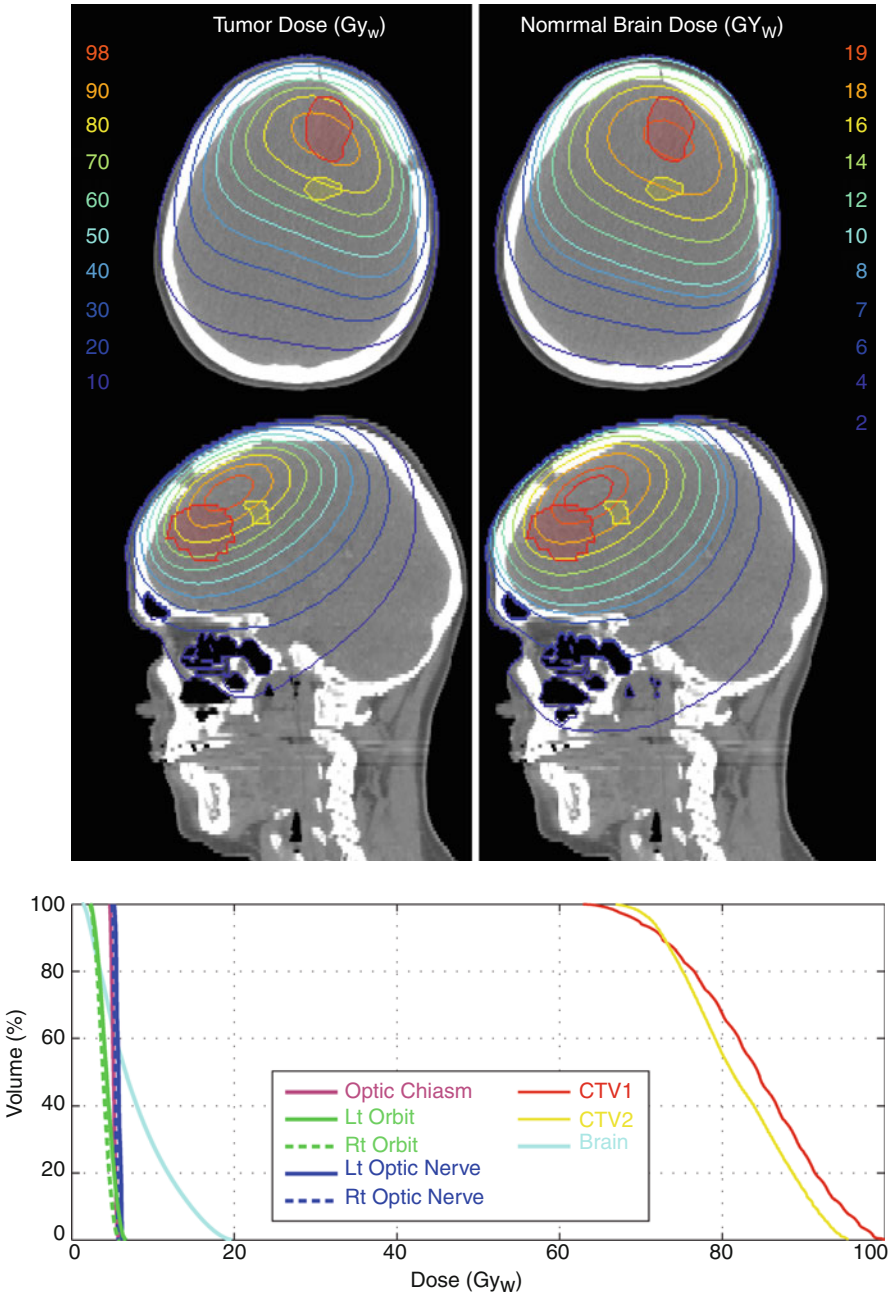

Fig. 16.6 Three-field treatment plan for a brain tumor (GBM) patient calculated using the MiMMC planning system. The prescription is a mean brain dose of 7.7 Gy$_w$. Isodose contours calculated for tumor and normal brain are shown on axial and sagittal slices through the target volumes. The integral dose-volume histograms (DVHs) summarize dosimetry for structures of interest including target volumes and organs at risk

large number of target volumes, subject to constraints on the organs at risk, has been implemented in software external to the treatment planning system [3, 71]. A similar approach, based on optimizing parameters of the weighted dose DVHs for target volumes and organs at risk, has been used to plan treatments for a small number of patients at Harvard-MIT [58].

16.3.7 Dose Prescription

In external beam radiotherapy, radiation dose is usually prescribed to the tumor or target volume or a convenient point nearby. In BNCT, the situation is more complicated as a result of the numerous dose components and other factors not normally encountered in conventional radiotherapy modalities such as the different calculations of dose for normal tissue and tumor tissue. Because many clinical trials have a phase I orientation, where safety and determination of the tolerance dose are principal endpoints, prescriptions are frequently defined by a limit on normal tissue dose rather than by delivery of a desired tumor dose. Another factor supporting the use of normal tissue dose is that the estimates for boron concentrations in tumor tissue are not considered to be particularly reliable.

Several different methods of dose prescription have been used in clinical trials of BNCT. Most use the (total) weighted dose for prescription since it expresses the composite dose in approximately photon-equivalent dose units. Early methods prescribed maximum weighted dose in the patient (wherever it occurred) [24] or in particular organs, for example, brain. Additional limits on the maximum weighted dose to other organs at risk, for example, skin, oral mucosa, and spinal cord, are also frequently applied. Some later protocols employed the mean weighted dose to an organ at risk (i.e., brain) as the prescription point [58] or employed limits on both maximum and mean weighted dose to the volume [72, 73]. In those protocols, the use of the mean brain dose reflects an intent to incorporate dose-volume aspects of the dose response into the prescription. Subsequently, mean brain dose was shown to be more strongly correlated with the incidence of somnolence (which was expected to precede more significant neurological toxicity) than maximum brain dose [50]. Prescriptions based on the minimum weighted dose in the target volume have also been used. This approach is attractive in the phase II setting where the principal endpoint is efficacy, but a disadvantage of this approach is that the dose delivered to the prescription point is particularly sensitive to errors in predicted blood boron concentration. An exception to the use of weighted dose is the clinical trial for glioblastoma at Petten using BSH (EORTC trial 11961), which employed the dose group identification Point (DGIP) concept for dose prescription. In this method, the boron dose component is prescribed at the location of the thermal neutron fluence maximum in the patient, the DGIP [59]. An advantage of this approach is that it avoids the use of weighting factors, which are associated with significant uncertainty and an imprecise dose-response model, but it also makes transfer of clinical experience to other facilities more difficult since the prescription does not account for all dose components.

16.3.8 Treatment Plan Quality Assurance

Before delivery of a treatment plan, the plan must be reviewed by a qualified medical physicist and the responsible physician for quality assurance purposes. The review should include assessing whether the dose prescription is met and whether doses delivered to each structure (organs at risk and target volumes) are reasonable and within acceptable limits. The medical physicist should also check that the beam monitor units or irradiation time are reasonable and correct.

In external beam radiotherapy with photons, the check of monitor units is usually realized as a simple hand calculation of dose, independent from the planning system, using tabulated data based on measurements in a large water phantom. Provided that the calculation point is judiciously chosen, the simple manual dose calculation algorithms available for photons generally work very well, yielding agreement within a few percent of sophisticated model-based algorithms. Unfortunately, similar manual techniques for NCT dose calculations do not exist. For this reason, monitor unit checks for NCT treatment plans are frequently based on comparisons with in-phantom dose measurements. For example, at JAEA an extensive set of measurements using a simple water phantom was prepared to confirm treatment plans. This data set includes measurements of neutron flux and dose components along the central axis of the beam in the phantom, beam profiles at various depths, output measurements, and the effect of phantom size and beam port size on the dose components. The data set includes measurements for each beam port. Treatment plans are checked by comparing the available benchmark data and dosimetry results in the plan. Moreover, comparison with other, similar treatment plans previously delivered may aid review of the plan.

16.4 Treatment Delivery

This section describes aspects of treatment planning relevant to treatment delivery, including patient positioning and immobilization, pharmacokinetic modeling for ^{10}B prediction, and retrospective analysis and dose reporting.

16.4.1 Patient Positioning and Immobilization

Patient positioning and immobilization influence implementation of a treatment plan and consequently also affect therapeutic efficacy. Therefore, precise patient positioning and immobilization are required. In addition, quick positioning work in the irradiation room is often needed because dose to the patient as well as the medical team should be kept as low as is reasonably achievable. Positioning patients for BNCT treatment is more difficult than for other external beam radiation modalities, because neutron beam ports at nuclear reactors are stationary and cannot be rotated around the patient as medical linacs can. Thus, to achieve the desired field orientation, the patient is moved rather than the beam. Positioning and immobilization

must be done in consideration of the patient's posture and comfort, because the patient must maintain a fixed position relative to the beam port during irradiation. Simulating treatment, either in a simulator room or in the actual treatment room, well before radiation delivery is important to ensure that the treatment plan is in fact deliverable and to establish the details of the immobilization technique to be applied. A number of unique approaches for patient positioning have been proposed, and various techniques and devices have been developed at each BNCT facility [56, 63, 74–76]. In this section, typical methods are introduced.

Most BNCT facilities have a simulator that replicates the geometry of the treatment room for the purpose of positioning, immobilizing, and marking the patient in a convenient environment outside the treatment room where the dose rate is low. Simulators have a dummy beam port mounted on the walls and multiple lasers that project along the central beam axis or to other reference points. A patient is positioned with the dummy beam port by using the lasers and supporting devices like cushions, head cups, or, in some cases, a stereotactic frame. Reference marks (ink) which are required for patient positioning in the treatment room are applied to the patient. The simulator enables the medical team to go to behind the dummy beam port and observe irradiation field on the patient from the beam's eye view. The irradiation room has a set of lasers identical to those in the simulator; lasers lines projected from the left and right lateral walls and from the ceiling intersect on the beam central axis. When positioning the patient in the treatment room, by matching the laser lines and marks on the patient or several features such as the nose, ears, and eyes, the patient can quickly and precisely be placed in the irradiation position.

Another technique for positioning patients for treatment employs reference points marked on the patient in combination with a 3D digitizer to determine the beam entry point and a template fitted to the patient's head to determine the proper beam orientation [63]. A coordinate transformation between the CT image data and reference points on the patient determined by a least squares algorithm based on singular value decomposition is used to map the beam entry point from the planning system onto the patient with the 3D digitizer. The beam entry point marked on the patient is aligned with a removable beam's eye view laser to set position and the source to surface distance is checked with a precisely machined wooden block.

For malignant brain tumor treatments, patients are often positioned on a treatment couch supine. In head and neck cancer cases treated in Japan, most patients are immobilized on a chair-style treatment couch in a sitting posture. BNCT in Japan is now usually conducted without general anesthesia. Hence, to maintain position relative to the beam port face and to prevent movement of the patient during irradiation, the head or body, including the target volume, should be immobilized with a face mask and/or bands fixed to the treatment couch. For the sitting posture, the immobilization requires particular attention since the head may easily move. However, strong tightening produces discomfort and consequently induces further patient movement. Hence, immobilization with consideration of comfort is required.

To verify positioning and immobilization of a patient, the distance between several fiducial marks or features on the body and the beam port face are measured just before irradiation. In the measurement, a 3D digitizer may be used to determine coordinates of the marks on the patient relative to the beam port. In BNCT treatments at JAEA, the digitizer measurements are fed back to treatment planning system after irradiation to reconstruct the actual irradiation conditions and conduct a retrospective evaluation. Any patient movements during irradiation are monitored remotely using video cameras installed in the irradiation room. If significant movement of the patient is observed, the patient may be instructed through the audio intercom system to take proper corrective action.

16.4.2 Pharmacokinetic Modeling for ^{10}B Prediction

The concentration of boron in both tissues and blood varies with time after administration of boron drugs. Since the boron dose component is directly proportional to the boron concentration in tissue, this time dependence must be accounted for in clinical dosimetry. Generally, tissue boron concentrations are modeled by using the product of the estimated blood boron concentration and a static tissue to blood boron concentration ratio as a surrogate for the actual tissue boron concentration because measuring in vivo tissue boron concentrations in real time is extremely difficult.[3] For example, in BPA-F-mediated BNCT of glioblastoma multiforme, the tumor to blood concentration ratio is commonly assumed at 3.5:1, while the brain to blood boron concentration ratio is assumed to be 1:1 [78]. Clearly, the boron concentration during irradiation is important for treatment planning because it affects the calculation of the beam monitor units (fluence) to be delivered to the patient in each field. Generally, a preliminary estimate of beam monitor units to be delivered for each field is computed as part of the treatment plan based on an assumed boron concentration. Since the actual boron concentration during treatment generally differs from that assumed in the preliminary calculation, the estimated beam monitor units must be revised accordingly during the course of treatment.

Estimating the correct number of beam monitor counts to deliver for a field requires predicting the mean blood boron concentration during the field. Because interindividual variation in blood boron concentration profiles is significant, up to ~50 % with BPA-F [79], the blood boron concentration profile is usually measured for each patient, starting with the boron compound infusion and continuing until ~24 h after irradiation. Figure 16.7 shows the initial portion of a blood boron concentration profile for an infusion of BPA-F. Various schemes are available for blood boron concentration prediction that range in complexity and accuracy. One of the

[3] It is important to appreciate that the common assumption of static ratios between tissue and blood boron concentrations is only made for convenience of dosimetry and does not reflect the actual pharmacokinetics at all times, generally characterized by the dynamic tissue loading and washout observed in animal models [77] and in PET studies of humans using [^{18}F]BPA-F [64, 65].

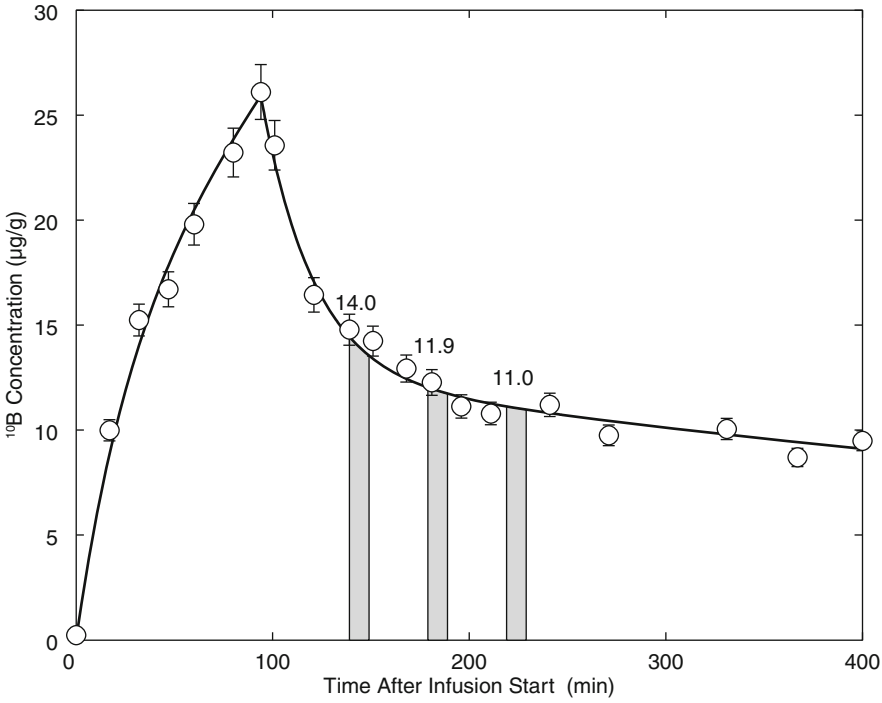

Fig. 16.7 Measured blood ^{10}B concentration profile and fitted pharmacokinetic model for a patient who received a 1.5-h infusion of 350 mg BPA/kg. Using only blood ^{10}B measurements available before the start of each irradiation (indicated by the *three shaded areas*), the pharmacokinetic model must accurately predict the mean ^{10}B concentration during each field so that the correct number of beam monitor units can be delivered. Mean ^{10}B concentrations are shown above each field (Adapted from data in Ref. [79])

simplest approaches involves measuring a blood sample drawn immediately before irradiation and another drawn at the (estimated) midpoint and extrapolating linearly to predict the mean concentration during irradiation [80]. More sophisticated approaches for boron concentration prediction using multi-compartment pharmacokinetic models and exponential washout models are available [81, 82]. These methods make full use of the available data and offer better accuracy. Different strategies for using these models may be appropriate, depending on how many blood boron data points are available at the time of prediction [79, 83]. For short irradiations, where the beam monitor units must be determined in advance, it is essential to be able to predict blood boron concentrations in advance based only on the partial data that are available at the start of irradiation. On the other hand, for long irradiations, accurate prediction of the blood ^{10}B concentration in advance of irradiation is less important because, if frequent blood sampling is done during irradiation, then almost all of the concentration data used to determine the mean concentration during irradiation is available before the end of irradiation and can be used to forecast the mean boron concentration [24].

Multi-fraction courses of treatment afford the opportunity to correct the deviations between planned and delivered doses that result from incomplete knowledge of the boron concentration at the initiation of irradiation. Typically, significant errors in delivered dose result from inaccuracies in the predicted blood boron concentration rather than from errors in the delivered neutron fluence; the prescribed beam monitor counts can be delivered with an accuracy of ~1 %. The boron concentration can be predicted much more accurately during the second or later fractions of a multi-fraction treatment since a complete blood boron profile has already been acquired and the pharmacokinetic model parameters are already well determined. The improved accuracy of prediction allows adjustment of the prescribed fluence to compensate for dose deviations that occurred in earlier fractions. Using this strategy, differences between prescribed and delivered doses can be limited to 1.5 % or less [58]. A final point regarding pharmacokinetics and multi-fraction treatments with multiple fields is that, by reversing the field order between fractions, the mean blood boron concentration of different fields can be equalized. This may be radiobiologically advantageous.

16.5 Retrospective Analysis and Dose Reporting

Because the beam monitor units actually delivered and the actual boron concentration(s) during treatment generally differ from the planned monitor units and boron concentration(s) used in the treatment plan, it is necessary to recompute the treatment plan using these updated quantities to retrospectively calculate delivered doses for reporting in the patient's chart and elsewhere. Generally, the Monte Carlo radiation transport calculations are not rerun because the change in thermal neutron flux depression resulting from a slightly different boron concentration in tissue is usually small. This retrospective analysis generally takes place after blood boron measurements are complete, but for multi-fraction treatments an intermediate analysis may be necessary to adjust planned doses in subsequent fractions to correct for deviations in doses delivered during initial fractions.

The objective of dose reporting is to enable the transfer of clinical experience between institutions. ICRU reports 50 and 62 provide detailed guidance for reporting doses from external beam radiotherapy with photons [67, 68]. Much but not all of these recommendations are directly applicable to BNCT. Because of the complexity of BNCT dosimetry and radiobiology, more information must be reported than for conventional radiotherapy [59]. The doses reported should be the doses delivered, that is, as computed in the retrospective treatment plan. Generally, the following information should be reported:

- A clear definition of the method of dose prescription elaborating how and where the dose is prescribed, leading to the determination of beam monitor units
- Any additional constraints on planned doses
- Prescribed dose and the dose actually delivered to the prescription "point"
- Dose statistics (minimum, maximum, mean, etc.) for target volumes and relevant organs at risk

- Weighting factors used to compute weighted dose
- Blood boron concentrations during treatment and assumptions for tissue to blood boron concentration ratios or tissue measurements if available

A few additional considerations are important. When possible, that is, for doses at a point (e.g., a minimum or maximum for a structure) and for mean doses in a structure, individual absorbed dose components should be reported in addition to the weighted dose. For other kinds of weighted dose DVH statistics, decomposition of the weighted dose into individual dose components may not be possible. Reporting of individual absorbed dose components is important because the weighting factors used are known only imprecisely and, perhaps more importantly, because the use of RBEs and weighted dose represents an incomplete dose-effect model [84]. Individual dose component data are needed if weighted doses are to be reassessed in the future with improved weighting factors or for new weighting factors or other radiobiological models to be derived from analysis of clinical data. To facilitate future reanalysis with more sophisticated dose-effect models, it may be helpful to also report the duration and timing of irradiations so that fractionation and dose rate effects may be taken into account [85]. In reporting doses, distinctions between absorbed dose and weighted dose should be made clear. Moreover, when weighted dose is reported, only the total weighted dose should be reported rather than the sum of a subset of dose components. Reporting so much data, four dose components plus a weighted sum, for each point of interest may seem onerous, but this data is a key result of a clinical trial. Further discussion on dose reporting may be found in Chapter15.

16.6 Future Directions

NCT treatment planning is a complex, multidisciplinary effort requiring close cooperation between medical physicists, physicians, nuclear engineers, and other members of the medical team to achieve the desired goal, a safe and successful treatment. This chapter has attempted to provide a comprehensive overview of the technical and clinical aspects of NCT treatment planning. Now some directions for future work on this topic will be considered.

As is the case for conventional treatment planning systems for photons and electrons, planning systems for NCT require careful calibration and validation to achieve the desired level of accuracy. The significant differences sometimes observed between planned and measured doses [60] should dispel the notion that the Monte Carlo dose calculations are inherently accurate. A greater emphasis on dosimetric validation of the beam models used in treatment planning is needed. The assumptions and approximations employed in the beam models used clinically for planning calculations need to be recognized and studied so that their impact on clinical dosimetry can be more fully understood.

Like NCT physical dosimetry, techniques for treatment planning are not standardized. Although it is not necessary that all planning systems use the same method of calculating dose, all planning systems should calculate the same dose for the same set of conditions, and some basic level of standardization is desirable. Utilizing

a consistent set of kerma factors would be a good starting point. Evaluation of the older planning systems using a set of reference problems has proved to be enlightening [22, 52]. Further intercomparisons of treatment planning systems, particularly the newer ones, are needed.

Nearly all of the planning systems developed before ~2001 have a fixed voxel size or scoring mesh with 1-cm^3 elements. This limitation is a holdover from the early 1990s when the available computing power was barely adequate and Monte Carlo treatment planning simulations took a few days to complete a few million histories. With the dramatic improvements in computing hardware in the intervening years and the capability to parallelize calculations, distributing computational effort over a number of computers, calculation times have been reduced to a few minutes or hours, allowing reductions in voxel size, which are associated with a significant additional computational expense. Although the coarse 1-cm grids do not pose significant dosimetric accuracy issues for the treatment of deep-seated tumors, they can be problematic for calculation of superficial doses, which are important for some disease sites currently of clinical interest such as head and neck cancer and subcutaneous melanoma. For this reason, it is desirable to move away from the 1-cm grids historically used and employ finer grids with the caveat that extremely fine grids will introduce problems with statistical fluctuations and very long computation times. Most of the newer planning systems are able to use finer computational grids.

The number of NCT treatment planning systems available or in development has proliferated from 2 to 3 in the early 1990s to about 10 at present. Planning system development is an intellectually stimulating task for physicists and engineers, but developing new planning systems when others are already available at little or no cost may not necessarily be a wise use of the limited resources available for NCT research. Although the availability of multiple planning systems allows for a healthy "competition" and comparison of the different planning systems, introducing new planning systems is not necessarily beneficial. Associated with each planning system is a dosimetric uncertainty owing to the software bugs and quirks that are present in all planning systems as well as the differences in computational methods. Although the associated dosimetric errors appear to be decreasing as the technology (and developers) matures [22, 52], each new planning system introduces dosimetric uncertainty into the limited pool of clinical data. Fully understanding and quantifying the differences between planning systems require significant time and effort that may not be fully justified. Sharing treatment planning software with other research groups at little or no cost, as the Harvard-MIT and INL BNCT research programs have done, has benefited the NCT community, among other ways, by avoiding the duplication of development efforts. A better model of software development, however, may be the open source model, where the software source code can be examined, critiqued, and improved by users as well as the principal developers.

Acknowledgments The authors would like to thank Drs. C. Wojnecki and J.R. Albritton for helpful discussions, for critically reviewing the manuscript, and for assistance producing Fig. 16.2.

References

1. Nigg DW, Wheeler FJ, Wessol DE, Capala J, Chadha M (1997) Computational dosimetry and treatment planning for boron neutron capture therapy. J Neurooncol 33:93–104
2. Nigg DW (2003) Computational dosimetry and treatment planning considerations for neutron capture therapy. J Neurooncol 62:75–86
3. Nievaart VA, Daquino GG, Moss RL (2007) Monte Carlo based treatment planning systems for boron neutron capture therapy in Petten, the Netherlands. J Phys Conf Ser 74:021012, 10.1088/1742-6596/74/1/021012
4. Zamenhof RG, Clement S, Lin K, Lui C, Ziegelmiller D, Harling OK (1989) Monte Carlo treatment planning and high-resolution alpha-track autoradiography for neutron capture therapy. Strahlenther Onkol 165:186–188
5. Zamenhof RG, Clement SD, Harling OK, Brenner JF, Wazer DE, Madoc-Jones H, Yanch JC (1990) Monte Carlo based dosimetry and treatment planning for neutron capture therapy of brain tumors. In: Harling OK, Zamenhof RG, Bernard JA (eds) Neutron beam design, development and performance for neutron capture therapy. Plenum Publishing Corp, New York
6. Zamenhof R, Redmond E, Solares G, Katz D, Riley K, Kiger S, Harling O (1996) Monte Carlo-based treatment planning for boron neutron capture therapy using custom designed models automatically generated from CT data. Int J Radiat Oncol Biol Phys 35:383–397
7. Gonzalez SJ, Carando DG, Santa Cruz GA, Zamenhof RG (2005) Voxel model in BNCT treatment planning: performance analysis and improvements. Phys Med Biol 50:441–458
8. Goorley JT, Kiger WS III, Zamenhof RG (2002) Reference dosimetry calculations for neutron capture therapy with comparison of analytical and voxel models. Med Phys 29:145–156
9. Kiger III WS, Albritton JR, Hochberg AG, Goorley JT (2004) Performance enhancements of MCNP4B, MCNP5, and MCNPX for Monte Carlo radiotherapy planning calculations in lattice geometries. Los Alamos National Laboratory, LA-UR-04-4751 and LA-UR-04-6972, http://laws.lanl.gov/x5/MCNP/publication/pdf/LA-UR-04-4751.pdf and http://laws.lanl.gov/x5/MCNP/publication/pdf/LA-UR-04-6972.pdf
10. Booth TE, Brown FB, Bull JS, Forster RA, Goorley JT, Hughes HG, Martz RL, Prael RE, Sood A, Sweezy JE, Zukaitis AJ (2008) MCNP5 1.50 Release Notes. Los Alamos National Laboratory, LA-UR-08-2300
11. Wallace SA, Allen BJ, Mathur JN (1996) Monte Carlo neutron photon treatment planning calculations: modeling from CT scans with variable voxel size. In: Mishima Y (ed) Cancer neutron capture therapy. Plenum Press, New York
12. Kumada H, Yamamoto K, Matsumura A, Yamamoto T, Nakagawa Y, Nakai K, Kageji T (2004) Verification of the computational dosimetry system in JAERI (JCDS) for boron neutron capture therapy. Phys Med Biol 49:3353–3365
13. Kumada H, Yamamoto K, Yamamoto T, Nakai K, Nakagawa Y, Kageji T, Matsumura A (2004) Improvement of dose calculation accuracy for BNCT dosimetry by the multi-voxel method in JCDS. Appl Radiat Isot 61:1045–1050
14. Frandsen MW (1998) Rapid geometry interrogation for a uniform volume element-based Monte Carlo particle transport simulation. M.S. thesis, Department of Computer Science, Montana State University, Bozeman
15. Frandsen MW, Wessol DE, Wheeler FJ, Babcock RS, Harkin GJ, Starkey JD (1998) Rapid geometry interrogation for a uniform volume element-based Monte Carlo particle transport simulation. In: Proceedings of the 1998 American Nuclear Society Radiation Protection and Shielding Division topical meeting. American Nuclear Society, La Grange Park, 1998
16. Wheeler FJ, Wessol DE, Wemple CA, Nigg DW, Albright CL, Cohen MT, Frandsen MW, Harkin GJ, Rossmeier MB (2001) SERA – an advanced treatment planning system for neutron therapy. In: Current status of neutron capture therapy. International Atomic Energy Agency, IAEA-TECDOC-1223, Vienna, 2001
17. Wheeler FJ, Nigg DW (1992) Three-dimensional radiation dose distribution analysis for boron neutron capture therapy. Nucl Sci Eng 110:16–31

18. Nigg DW (1994) Methods for radiation dose distribution analysis and treatment planning in boron neutron capture therapy. Int J Radiat Oncol Biol Phys 28:1121–1134
19. Wessol DE, Wheeler FJ (1993) Creating and using a type of free-form geometry in Monte Carlo particle transport. Nucl Sci Eng 113:314–323
20. Verbakel WF, Hideghety K, Morrissey J, Sauerwein W, Stecher-Rasmussen F (2002) Towards in vivo monitoring of neutron distributions for quality control of BNCT. Phys Med Biol 47: 1059–1072
21. Albritton JR, Kiger WS III (2008) Neutron beam source definition techniques for NCT treatment planning. In: Zonta A, Altieri S, Roveda L, Barth R (eds) Proceedings of the 13th international congress on neutron capture therapy: a new option against cancer. ENEA, Rome
22. Albritton JR (2009) Computational aspects of treatment planning for neutron capture therapy. Ph.D. thesis, Nuclear Science and Engineering Department, Massachusetts Institute of Technology, Cambridge
23. Sempau J, Sanchez-Reyes A, Salvat F, ben Tahar HO, Jiang SB, Fernandez-Varea JM (2001) Monte Carlo simulation of electron beams from an accelerator head using PENELOPE. Phys Med Biol 46:1163–1186
24. Palmer MR, Goorley JT, Kiger WS III, Busse PM, Riley KJ, Harling OK, Zamenhof RG (2002) Treatment planning and dosimetry for the Harvard-MIT phase I clinical trial of cranial neutron capture therapy. Int J Radiat Oncol Biol Phys 53:1361–1379
25. Seppälä T, Serén T, Auterinen I (2001) Source characterisation for the rtt_MC treatment planning program at FiR 1. In: Hawthorne FM, Shelley K, Wiersema RJ (eds) Frontiers in neutron capture therapy. Kluwer Academic/Plenum Publishers, New York
26. Seppälä T (2002) FiR 1 epithermal neutron beam model and dose calculation for treatment planning in neutron capture therapy. Ph.D. thesis, Department of Physical Sciences, University of Helsinki, Helsinki
27. van der Marck SC, Hogenbirk A (2002) ORANGE, a Monte Carlo dose engine for BNCT. In: Sauerwein W, Moss RL, Wittig A (eds) Research and development in neutron capture therapy. Monduzzi Editore, Bologna
28. X-5 Monte Carlo Team (2003) MCNP – a general Monte Carlo N-particle transport Code, Version 5. Los Alamos National Laboratory, LA-UR-03-1987
29. Goorley JT, McKinney G, Adams K, Estes G (2001) MCNP enhancements, parallel computing and error analysis for BNCT. In: Hawthorne FM, Shelley K, Wiersema RJ (eds) Frontiers in neutron capture therapy. Kluwer Academic/Plenum Publishers, New York
30. Goorley T (2004) MCNP5 Tally enhancements for lattices (aka Lattice Speed Tally Patch). Los Alamos National Laboratory, LA-UR-04-3400, http://mcnp-green.lanl.gov/publication/pdf/Lattice_Speed_Tally.pdf
31. Moran JM, Nigg DW, Wheeler FJ, Bauer WF (1992) Macroscopic geometric heterogeneity effects in radiation dose distribution analysis for boron neutron capture therapy. Med Phys 19:723–732
32. Ingersoll DT, Slater CO, Redmond EL II, Zamenhof RG (1997) Comparison of TORT and MCNP dose calculations for BNCT treatment planning. In: Larsson B, Crawford J, Weinreich R (eds) Advances in neutron capture therapy. Elsevier, Amsterdam
33. Kotiluoto P, Hiisamaki P, Savolainen S (2001) Application of the new MultiTrans SP3 radiation transport code in BNCT dose planning. Med Phys 28:1905–1910
34. Albertson BJ, Blue TE, Niemkiewicz J (2001) An investigation on the use of removal-diffusion theory for BNCT treatment planning: a method for determining proper removal-diffusion parameters. Med Phys 28:1898–1904
35. Raaijmakers CP, Bruinvis IA, Nottelman EL, Mijnheer BJ (1998) A fast and accurate treatment planning method for boron neutron capture therapy. Radiother Oncol 46:321–332
36. Wojnecki C, Wittig A, Bourhis-Martin E (2002) Patient geometry modeling for treatment planning. In: Sauerwein W, Moss R, Wittig A (eds) Research and development in neutron capture therapy. Monduzzi Editore, Bologna
37. International Commission on Radiation Units and Measurements (1989) Tissue substitutes in radiation dosimetry and measurement. ICRU Report 44

38. International Commission on Radiation Units and Measurements (1992) Photon, electron, proton, and neutron interaction data for body tissues. ICRU Report 46
39. Brooks RA, Di Chiro G, Keller MR (1980) Explanation of cerebral white-gray contrast in computed tomography. J Comput Assist Tomogr 4:489–491
40. Ye SJ (1999) Boron self-shielding effects on dose delivery of neutron capture therapy using epithermal beam and boronophenylalanine. Med Phys 26:2488–2493
41. Goorley JT (2002) A comparison of three gadolinium based approaches to cancer therapy. Ph.D. thesis, Nuclear Engineering Department, Massachusetts Institute of Technology, Cambridge
42. Binello E (1999) Efficacy of boron neutron capture synovectomy in an animal model. Ph.D. thesis, Nuclear Engineering Department, Massachusetts Institute of Technology, Cambridge
43. Albritton JR (2001) Analysis of the SERA treatment planning system and its use in boron neutron capture synovectomy. M.S. thesis, Nuclear Engineering Department, Massachusetts Institute of Technology, Cambridge
44. Wojnecki C, Green S (2002) A preliminary comparative study of two treatment planning systems developed for boron neutron capture therapy: MacNCTPlan and SERA. Med Phys 29:1710–1715
45. Rogus RD, Harling OK, Yanch JC (1994) Mixed field dosimetry of epithermal neutron beams for boron neutron capture therapy at the MITR-II research reactor. Med Phys 21:1611–1625
46. Binns PJ, Riley KJ, Harling OK, Kiger WS III, Munck af Rosenschold PM, Giusti V, Capala J, Skold K, Auterinen I, Seren T, Kotiluoto P, Uusi-Simola J, Marek M, Viererbl L, Spurny F (2005) An international dosimetry exchange for boron neutron capture therapy. Part I: Absorbed dose measurements. Med Phys 32:3729–3736
47. Coderre JA, Morris GM (1999) The radiation biology of boron neutron capture therapy. Radiat Res 151:1–18
48. Goorley T, Capala J, Wheeler F, Kiger WS III, Zamenhof R, Palmer MR, Nigg D (2001) A comparison of two treatment planning programs: MacNCTPlan and BNCT_RTPE. In: Hawthorne FM, Shelley K, Wiersema RJ (eds) Frontiers in neutron capture therapy. Kluwer Academic/Plenum Publishers, New York
49. Chetty IJ, Curran B, Cygler JE, DeMarco JJ, Ezzell G, Faddegon BA, Kawrakow I, Keall PJ, Liu H, Ma CM, Rogers DW, Seuntjens J, Sheikh-Bagheri D, Siebers JV (2007) Report of the AAPM Task Group No. 105: issues associated with clinical implementation of Monte Carlo-based photon and electron external beam treatment planning. Med Phys 34:4818–4853
50. Albritton JR, Binns PJ, Riley KJ, Coderre JA, Harling OK, Kiger WS III (2006) Comparison of doses delivered in clinical trials of neutron capture therapy in the USA. In: Nakagawa Y, Kobayashi T, Fukuda H (eds) Advances in neutron capture therapy. International Society for Neutron Capture Therapy, Takamatsu
51. Fraass B, Doppke K, Hunt M, Kutcher G, Starkschall G, Stern R, Van Dyke J (1998) American Association of Physicists in Medicine Radiation Therapy Committee Task Group 53: quality assurance for clinical radiotherapy treatment planning. Med Phys 25:1773–1829
52. Albritton JR, Kiger WS III (2006) Development of reference problems for neutron capture therapy treatment planning systems. In: Nakagawa Y, Kobayashi T, Fukuda H (eds) Advances in neutron capture therapy. International Society for Neutron Capture Therapy, Takamatsu
53. Wojnecki C, Green S (2001) A computational study into the use of polyacrylamide gel and A-150 plastic as brain tissue substitutes for boron neutron capture therapy. Phys Med Biol 46: 1399–1405
54. Kiger WS III, Santa Cruz GA, González SJ, Hsu F-Y, Riley KJ, Binns PJ, Harling OK, Palmer MR, Busse PM, Zamenhof RG (2002) Verification and validation of the NCTPlan treatment planning program. In: Sauerwein W, Moss RL, Wittig A (eds) Research and development in neutron capture therapy. Monduzzi Editore, Bologna
55. Riley KJ, Binns PJ, Kiger WS III, Harling OK (2002) Clinical dosimetry of the MIT FCB. In: Sauerwein W, Moss RL, Wittig A (eds) Research and development in neutron capture therapy. Monduzzi Editore, Bologna
56. Kortesniemi M (2002) Solutions for clinical implementation of boron neutron capture therapy in Finland. Ph.D. thesis, Department of Physical Sciences, University of Helsinki, Helsinki

57. Harling OK, Roberts KA, Moulin DJ, Rogus RD (1995) Head phantoms for neutron capture therapy. Med Phys 22:579–583
58. Kiger WS III, Lu XQ, Harling OK, Riley KJ, Binns PJ, Kaplan J, Patel H, Zamenhof RG, Shibata Y, Kaplan ID, Busse PM, Palmer MR (2004) Preliminary treatment planning and dosimetry for a clinical trial of neutron capture therapy using a fission converter epithermal neutron beam. Appl Radiat Isot 61:1075–1081
59. International Atomic Energy Agency (2004) Commissioning and quality assurance of computerized planning systems for radiation treatment of cancer. IAEA Technical Report Series No. 430
60. Riley KJ, Binns PJ, Harling OK, Albritton JR, Kiger WS III, Rezaei A, Skold K, Seppälä T, Savolainen S, Auterinen I, Marek M, Viererbl L, Nievaart VA, Moss RL (2008) An international dosimetry exchange for BNCT part II: computational dosimetry normalizations. Med Phys 35:5419–5425
61. Kirby TH, Hanson WF, Gastorf RJ, Chu CH, Shalek RJ (1986) Mailable TLD system for photon and electron therapy beams. Int J Radiat Oncol Biol Phys 12:261–265
62. Izewska J, Andreo P (2000) The IAEA/WHO TLD postal programme for radiotherapy hospitals. Radiother Oncol 54:65–72
63. Kiger WS III, Albritton JR, Lu XQ, Palmer MR (2004) Development and application of an unconstrained technique for patient positioning in fixed radiation beams. Appl Radiat Isot 61:765–769
64. Imahori Y, Ueda S, Ohmori Y, Kusuki T, Ono K, Fujii R, Ido T (1998) Fluorine-18-labeled fluoroboronophenylalanine PET in patients with glioma. J Nucl Med 39:325–333
65. Kabalka GW, Smith GT, Dyke JP, Reid WS, Longford CPD, Roberts TG, Reddy NK, Buonocore E, Hubner KF (1997) Evaluation of fluorine-18-BPA-fructose for boron neutron capture treatment planning. J Nucl Med 38:1762–1767
66. Nichols TL, Kabalka GW, Miller LF, Khan MK, Smith GT (2002) Improved treatment planning for boron neutron capture therapy for glioblastoma multiforme using fluorine-18 labeled boronophenylalanine and positron emission tomography. Med Phys 29:2351–2358
67. International Commission on Radiation Units and Measurements (1993) Prescribing, recording, and reporting photon beam therapy. ICRU Report 50
68. International Commission on Radiation Units and Measurements (1999) Prescribing, recording, and reporting photon beam therapy (Supplement to ICRU Report 50). ICRU Report 62
69. Sakurai Y, Ono K (2007) Improvement of dose distribution by central beam shielding in boron neutron capture therapy. Phys Med Biol 52:7409–7422
70. Binns PJ, Riley KJ, Ostrovsky Y, Gao W, Albritton JR, Kiger WS III, Harling OK (2007) Improved dose targeting for a clinical epithermal neutron capture beam using optional ^{6}Li filtration. Int J Radiat Oncol Biol Phys 67:1484–1491
71. Nievaart S, Moss R, Sauerwein W, Wittig A (2006) Use of linear programming to obtain an optimum, multi-beam treatment plan in NCT. In: Nakagawa Y, Kobayashi T, Fukuda H (eds) Advances in neutron capture therapy. International Society for Neutron Capture Therapy, Takamatsu
72. Joensuu H, Kankaanranta L, Seppälä T, Auterinen I, Kallio M, Kulvik M, Laakso J, Vahatalo J, Kortesniemi M, Kotiluoto P, Seren T, Karila J, Brander A, Jarviluoma E, Ryynanen P, Paetau A, Ruokonen I, Minn H, Tenhunen M, Jaaskelainen J, Farkkila M, Savolainen S (2003) Boron neutron capture therapy of brain tumors: clinical trials at the Finnish facility using boronophenylalanine. J Neurooncol 62:123–134
73. Henriksson R, Capala J, Michanek A, Lindahl SA, Salford LG, Franzen L, Blomquist E, Westlin JE, Bergenheim AT (2008) Boron neutron capture therapy (BNCT) for glioblastoma multiforme: a phase II study evaluating a prolonged high-dose of boronophenylalanine (BPA). Radiother Oncol 88:183–191
74. Kumada H, Yamamoto K, Torii Y, Matsumura A, Yamamoto T, Nakagawa Y (2000) Development of the patient setting system for BNCT at JRR-4. In: Proceedings of the ninth international symposium on neutron capture therapy for cancer, Osaka, 2000
75. Wielopolski L, Capala J, Pendzick NE, Chanana AD (2000) Patient positioning in static beams for boron neutron capture therapy of malignant glioma. Radiat Med 18:381–387

76. Watkins P, Vroegindeweij C, Garbe S, Hideghety K (2001) Patient positioning at the HFR Petten. In: Hawthorne FM, Shelley K, Wiersema RJ (eds) Frontiers in neutron capture therapy. Kluwer Academic/Plenum Publishers, New York
77. Chuang CF (1999) Experimental evaluation and mathematical modeling of the pharmacokinetics of boronophenylalanine-fructose (BPA-f) in murine tumor models. Ph.D. thesis, Nuclear Engineering Department, Massachusetts Institute of Technology, Cambridge
78. Coderre JA, Chanana AD, Joel DD, Elowitz EH, Micca PL, Nawrocky MM, Chadha M, Gebbers JO, Shady M, Peress NS, Slatkin DN (1998) Biodistribution of boronophenylalanine in patients with glioblastoma multiforme: boron concentration correlates with tumor cellularity. Radiat Res 149:163–170
79. Kiger WS III, Palmer MR, Riley KJ, Zamenhof RG, Busse PM (2003) Pharmacokinetic modeling for boronophenylalanine-fructose mediated neutron capture therapy: ^{10}B concentration predictions and dosimetric consequences. J Neurooncol 62:171–186
80. Chanana AD, Capala J, Chadha M, Coderre JA, Diaz AZ, Elowitz EH, Iwai J, Joel DD, Liu HB, Ma R, Pendzick N, Peress NS, Shady MS, Slatkin DN, Tyson GW, Wielopolski L (1999) Boron neutron capture therapy for glioblastoma multiforme: interim results from the phase I/II dose-escalation studies. Neurosurgery 44:1182–1193
81. Kiger WS III, Palmer MR, Riley KJ, Zamenhof RG, Busse PM (2001) A pharmacokinetic model for the concentration of ^{10}B in blood after boronophenylalanine-fructose administration in humans. Radiat Res 155:611–618
82. Shibata Y, Matsumura A, Yamamoto T, Akutsu H, Yasuda S, Nakai K, Nose T, Yamamoto K, Kumada H, Hori N, Ohtake S (2003) Prediction of boron concentrations in blood from patients on boron neutron capture therapy. Anticancer Res 23:5231–5235
83. Kortesniemi M, Seppälä T, Auterinen I, Savolainen S (2004) Enhanced blood boron concentration estimation for BPA-F mediated BNCT. Appl Radiat Isot 61:823–827
84. Rassow J, Sauerwein W, Wittig A, Bourhis-Martin E, Hideghety K, Moss R (2004) Advantage and limitations of weighting factors and weighted dose quantities and their units in boron neutron capture therapy. Med Phys 31:1128–1134
85. Jones B, Townley J, Dale R, Hopewell J, Green S (2004) The use of biological equivalent dose (BED) concept to assess mixed low and high LET radiations with particular reference to BNCT. In: Coderre JA, Rivard MJ, Patel H, Zamenhof RG (eds) Eleventh world congress on neutron capture therapy. International Society for Neutron Capture Therapy, Waltham, 2004

Part V

Biology

Boron Neutron Capture Therapy: Application of Radiobiological Principles

17

John W. Hopewell, Gerard M. Morris, Amanda E. Schwint, and Jeffrey A. Coderre

Contents

J.W. Hopewell (✉)
Particle Therapy Cancer Research Institute and Green Templeton College, University of Oxford, Oxford, UK
e-mail: john.hopewell@gtc.ox.ac.uk

G.M. Morris
Medical Department, Brookhaven National Laboratory, Upton, NY, USA
e-mail: gmamorris@tiscali.co.uk

A.E. Schwint
Department of Radiobiology, Constituyentes Atomic Center, National Atomic Energy Commission, San Martín, Buenos Aires, Argentina
e-mail: schwint@cnea.gov.ar

J.A. Coderre
Ora Inc., 300 Brickstone Square, Andover, MA, USA
e-mail: joderre@oraclinical.com

W.A.G. Sauerwein et al. (eds.), *Neutron Capture Therapy*,
DOI 10.1007/978-3-642-31334-9_17,

17.1 Introduction

The first treatments of patients with glioblastoma, in the early 1950s on the Medical Research Reactor at Brookhaven National Laboratory, were carried out using a thermal neutron beam and borax as the boron carrier [22]. Those treatments were undertaken after extremely limited preclinical animal studies. Published are scant details of experiments outlining the uptake of borax in transplanted, methylcholanthrene induced brain tumors in mice, relative to plasma and normal brain [22]. Comparable data were also published for individual patients [42] along with attempts to compute radiation energies and to estimate effects in normal and neoplastic brain tissue. However, the understanding of the increased biological effectiveness of particle irradiation relative to x- or γ-rays was in its infancy at this time. Although never published, a small study was carried out on dogs (Calvo, personal communication 1996) to assess the safety of the proposed clinical irradiation protocol. Four animals were exposed to thermal neutrons after the administration of borax; they remained fit and well after 48 h, and thus, the treatment was judged to be safe.

While such an approach might appear strange in the present era, it should be recognized that none of the present concepts underlining the radiobiological basis of radiotherapy were established at that time and then even conventional radiotherapy had developed largely on the basis of anecdotal evidence from observations on patients exposed to x-rays. Thus, the early attempts at boron neutron capture therapy (BNCT) were understandably inadequate in terms of the ability to estimate and predict responses from such a complex, mixed field, of irradiation. The use of an inadequate boron compound and a poorly penetrating thermal neutron beam were additional drawbacks of those earlier studies.

A greater understanding of the increased biological effectiveness of particle radiation, relative to x- or γ-rays, has come from studies related to the application of fast neutron radiotherapy [23]. However, yet again, the initial clinical attempts at fast neutron therapy were compromised by a lack of radiobiological knowledge. The early investigators were well aware that fast neutrons were biologically more effective than x-rays and animal experiments were done to determine the relative biological effectiveness (RBE), the ratio of absorbed doses from the novel experimental radiation and x-rays required to produce the same biological effect. However, patients were still seriously overdosed in the initial patient studies [78]. Later, it became evident that this was because the initial neutron experiments were carried out using large single doses and that the RBE values obtained were applied to patients treated with fractionated irradiation doses. It was not recognized at that time that the increase in RBE with decreasing dose per fraction is a relatively large effect [25].

While relevant and extensive preclinical studies are now often the norm and should indeed be mandatory, the problems of the past should serve as a pointer to the future use of BNCT, particularly for new applications. Failure to take full account of the current understanding of radiobiological principles or the application of

inappropriate radiobiological weighting factors to new applications could result in clinical under- or overdosage of patients and significantly delay the full clinical application of this potentially useful radiotherapy modality.

17.2 Basic Radiobiological Considerations

BNCT considered as a mixed field irradiation exposure, the principle components of which include, in addition to the alpha particles and lithium ions resulting from the boron neutron capture reaction:

$$^{10}\mathrm{B} + {}^{1}\mathrm{n} = {}^{7}\mathrm{Li} + {}^{4}\mathrm{He}\,(\alpha) + 2.79\ \mathrm{MeV},$$

γ-rays both incident within the neutron beam and those induced by the neutron hydrogen capture reaction:

$$^{1}\mathrm{H} + {}^{1}\mathrm{n} = {}^{2}\mathrm{H} + \gamma + 2.2\ \mathrm{MeV}$$

plus protons, either as recoil protons from fast neutron interactions, largely with hydrogen, or from neutron capture with tissue nitrogen:

$$^{14}\mathrm{N} + {}^{1}\mathrm{n} = {}^{14}\mathrm{C} + {}^{1}\mathrm{p} + 580\ \mathrm{keV}$$

These various absorbed dose components contributing to the total radiation dose are usually assumed to act independently from each other in treatment planning such that the total photon-equivalent dose (D_w) is given by the equation:

D_w = (absorbed γ-ray dose • DRF) + (absorbed recoil proton dose • RBE_n) + (absorbed nitrogen capture dose • RBE_N) + (absorbed ^{10}B capture dose • CBE)

where DRF is the dose-reduction factor for γ-rays, which varies with dose-rate; RBE_n is the relative RBE of fast neutrons; RBE_N the equivalent value for protons from the nitrogen capture reaction; and CBE the compound biological effectiveness factor which is a compilation of the RBE of alpha particles and ^{7}Li ions and the microdistribution of ^{10}B in a particular tissue. Due to the short range of these particles in tissue, 9 and 5 μm, respectively, the biological effect of energy deposition depends critically on both the gross and microscopic localization of boron in tissues and cells. For example, the energy from the boron neutron capture reactions occurring within the lumen of a blood vessel may be completely dissipated within the blood volume and in a sense "wasted."

For this reason, the radiobiological properties of each dose component need to be examined separately, although consideration should also be given to the possibility that there may be an interaction between high linear energy transfer (LET) components of the total dose and the low-LET, γ-rays.

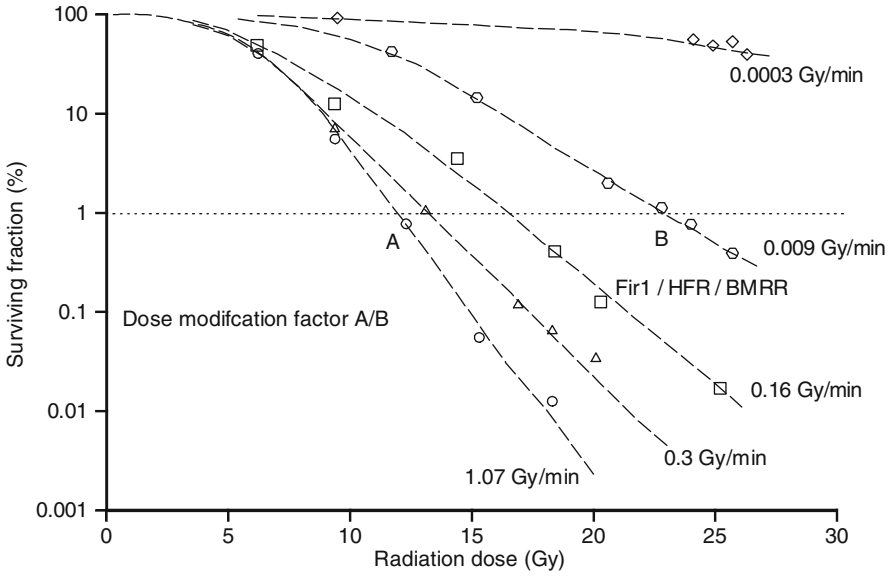

Fig. 17.1 In vitro cell survival curves for Chinese hamster cells after irradiation with ^{60}Co γ-rays at various dose-rates. The dose-reduction factor is the ratio of doses to produce the same effect from different dose-rates, for example, *A*/*B* for a dose rate of 0.009 Gy/min. The dose-rates of γ-rays in typical clinical epithermal beams (e.g., FiR1, HFR, BMRR) are in the range 0.16–0.009 Gy/min (Reproduced from Hopewell et al. [39]; with permission)

17.2.1 Radiobiological Properties of γ-Rays

The radiobiological effects of low-LET x- or γ-rays have been extensively investigated since they are the predominant radiation used in radiation therapy. The radiobiological property of most significance for BNCT, where currently single exposures are widely used, is the variation in the biological effectiveness of γ-rays with dose-rate. This dose-rate effect is due to the repair of sublethal radiation damage to DNA with time. For prolonged exposures to low dose-rate γ-rays, the effectiveness is decreased compared to γ-rays delivered at a dose-rate of 1 Gy/min or more. This can be clearly illustrated by examining the effects of different dose-rates on the clonogenic survival of cells in vitro [4]. For a given absorbed radiation dose, the level of cell survival increases as the dose-rate is reduced (Fig. 17.1). In this example, for a clonogenic cell survival of 1%, the DRF for an equivalent effect would be <0.7 for dose-rates of <0.16 Gy/min (DRF: the ratio of doses at high dose-rate to low dose-rate required to produce the same biological effect). The γ-ray dose-rates for the present generation of clinical epithermal neutron beams are in the range 0.16–0.086 Gy/min, clearly indicating that these γ-rays would be less biologically effective than those delivered at approximately 1 Gy/min, that is, a DRF of <1.0. The relative positions of the dose-rates for γ-rays of

Table 17.1 Variation in the γ-ray characteristics of three different epithermal neutron beams that have been used clinically for BNCT

Beam (location)	FiR1 (Helsinki)	HFR (Petten)	BMRR (Brookhaven)
γ-ray contribution (%)	80.0	66.8	73.0
Dose-rate (Gy/min)	0.076	0.035	0.017
Dose-rate reduction factor	0.6	0.5	0.45
	–	(1.0)[a]	(1.0)[a]

[a]DRF values assumed by the centers involved

three epithermal neutron beams that have been used in clinical trials, Helsinki (FiR1), Petten (HFR), and Brookhaven National Laboratory (BMRR), are indicated in this example, and the detailed γ-ray characteristics are given in Table 17.1.

When BNCT is used for the treatment of glioblastoma, then the dose-limiting normal tissue is the central nervous system (CNS). The radiation response of this tissue, along with many other tissues has been shown to depend on dose-rate and as a consequence the time of exposure. In the case of the spinal cord, a useful model to study for CNS responses, the dose-rate effect is demonstrated by an increase in the dose associated with a 50% incidence of radiation-induced myelopathy (ED_{50}), as the dose-rate is decreased in two species, the rat and the pig (Fig. 17.2). When these ED_{50} values are normalized, relative to the value for irradiation at the highest dose-rate in this instance of 1.8 Gy/min, there is a linear relationship between dose-rate (log scale) and the DRF. For dose-rates <0.1 Gy/min, comparable to existing epithermal neutron beams, the DRF is <0.7 as is illustrated in the examples in Table 17.1. The dose-rate effect for γ-rays was not taken into account in the initial studies in many centers, including Petten and BMRR. The likely implications of this are discussed below.

The effects of dose-rate, based on extensive historical data [21], were considered in recent experimental animal studies to determine weighting factors for normal lung tissue [45], just as they were for studies of CNS toxicity in experiments on dog brain at the FiR1 reactor [6]. When overall exposure times are short (<10 min) as in some biological studies with thermal neutron beams [20, 59, 60], then, and only then, can the effects of repair of sublethal damage be considered sufficiently small to be ignored.

Recently, models have been developed to enable the calculation of equivalent doses based on the kinetics of repair of sublethal irradiation damage for photon irradiation [54]. This allows the calculation of equivalent photon doses for different overall irradiation times, for single exposures, and for fractionated irradiation with incomplete repair intervals. The kinetics of repair of sublethal damage have also been established for CNS tissue following exposure to a wide range of exposure times using irradiation sources of differing dose-rates [75]. This is characterized by a short and a long repair parameter with half-times of 0.19 and 2.16 h, respectively.

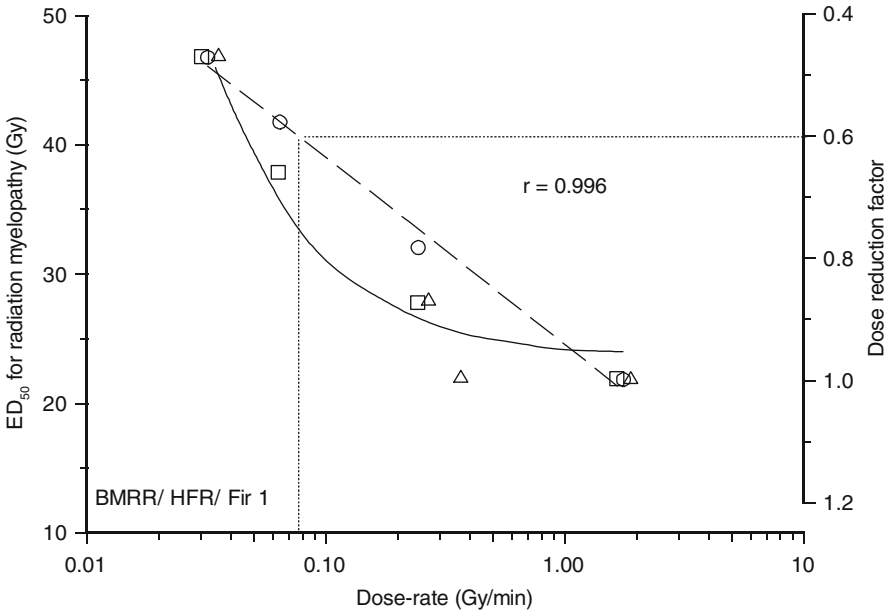

Fig. 17.2 Variation in the ED_{50} for radiation-induced myelopathy in the pig (Δ) and rat (□) as a function of dose-rate. The ED_{50} values for dose rates of <1.0 Gy/min are expressed as a ratio of the highest dose-rate of 1.8 Gy/min (Dose reduction factor – DRF). The DRF (○) was linearly related to the dose-rate, correlation coefficient 0.996 (Reproduced from Hopewell et al. [39]; with permission)

17.2.2 Radiobiological Properties of Fast Neutrons

Studies into the relative biological effectiveness of fast neutrons have been carried out in relation to neutron therapy. Neutron facilities for therapy vary in the energy spectrum of the neutrons produced. The implications of this have been compared using a range of in vitro and in vivo assays. The most extensive set of comparative studies has used the mouse intestinal crypt assay [31]. These studies showed up to a 50% difference in biological effectiveness when other neutron beams were compared to a relatively high average energy reference beam. The higher the mean energy of the neutron beam, the lower the RBE.

In vitro studies, using V79 cells, with relatively monoenergetic neutron sources, have shown a defined relationship between neutron energy and RBE [34]. For this cell line and for damage assessed at the doses required to reduce the surviving fraction to 37% (D_{37}), neutrons with an energy of 0.3–0.4 MeV appeared to be the most biologically effective with an RBE of ~6.0. As the energy of the neutrons was increased, the RBE value decreased, appearing to reach a minimum value of 1.7 for neutron energies in the range 5–15 MeV (Fig. 17.3). For neutron energies lower than 0.3 MeV, the RBE also declined, being less than 4.0 for 0.1 MeV (100 keV) neutrons. In an unrelated study with 24 keV neutrons from a filtered reactor beam, the trend continued for the same endpoint [58]. The recoil protons from these lower energy neutrons would be expected to have the highest LET.

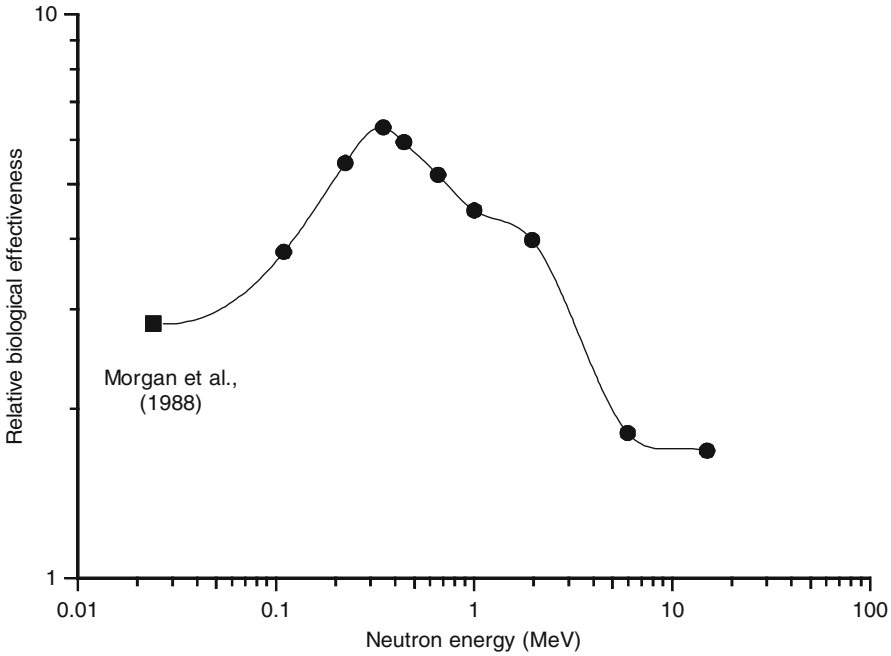

Fig. 17.3 Variation in the RBE, based on a surviving fraction of 37% (D_{37}) of V79 cells, with neutron energy (Data from Hall et al. [34] (●))

These in vitro studies also showed that the RBE depends on the level of effect at which doses are compared. Based on the linear quadratic (LQ) model of cell survival, there will be an upper limit to the RBE for the different energy neutrons and this will be the ratio of the values of α, the initial slope of the cell survival curves [8] such that:

$$\mathrm{RBE}_{\max} = \alpha_{\mathrm{H}} / \alpha_{\mathrm{L}}$$

where α_{H} and α_{L} are the values of alpha for fast neutrons and photons, respectively.

This dependence of the RBE on the level of effect is reflected in the increase in RBE with decreasing dose/fraction in dose fractionation studies [23]. This represents the decreasing level of effect produced by a reduction in the dose/fraction as fraction numbers are increased. RBE values can also be highly dependent on the particular tissue studied by a factor of ~2 [23]. Thus, the use of a single value for the RBE of a particular radiation quality is most unlikely to be applicable to all tissues.

17.2.3 Radiobiological Properties of Protons from the Nitrogen Capture Reaction

The protons produced as a consequence of the thermal neutron/nitrogen capture reaction have a low energy of 580 keV and thus have very high-LET characteristics.

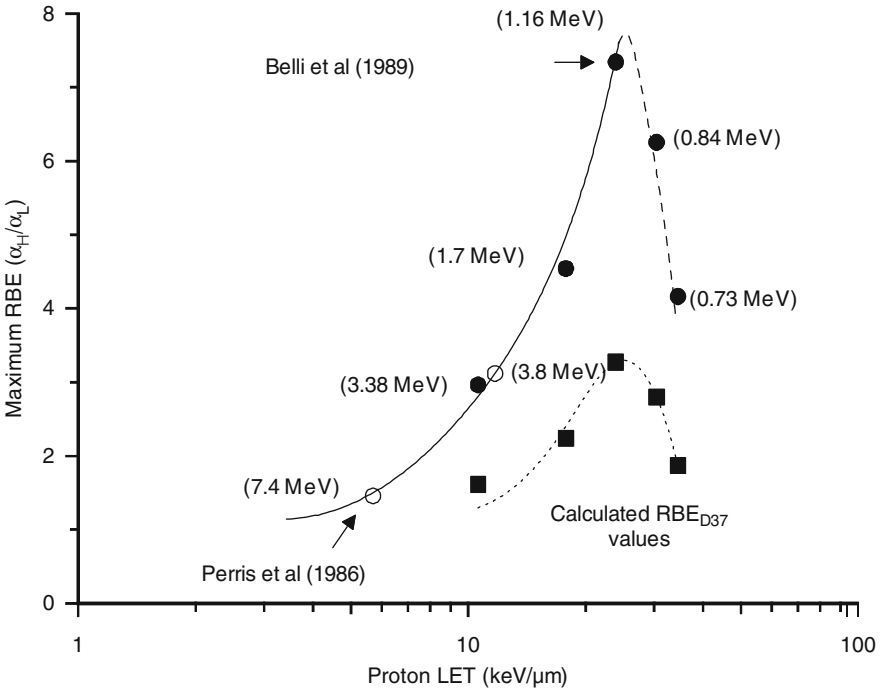

Fig. 17.4 Variation in RBE_{max} for V79 cells with proton energy. RBE values at D_{37} have been calculated for comparison

There are no ways of directly determining the RBE of this energy of protons from a mixed field irradiation involving either thermal or epithermal neutron irradiations, and hence, for practical reasons, the nitrogen capture dose is frequently included with the fast neutron dose, as a combined beam high-LET dose.

Only a limited number of studies have been undertaken using monoenergetic protons at similar energies [5, 72]. Those studies, like those with fast neutrons, were carried out using V79 cells. For protons of decreasing energy (increasing LET) from 7.4 to 1.16 MeV, the RBE_{max} increased from a little over 1.0 up to a maximum value of ~7.0. For lower proton energies of 0.84 and 0.73 MeV, the RBE_{max} declined progressively from the maximum value (Fig. 17.4). In order to be able to compare the RBE values from these studies with those involving different energies of fast neutrons, the D_{37} was calculated from the LQ cell survival curve parameters reported by the authors. This information is plotted on the same figure for comparison. The D_{37} RBE values for V79 cells show the same general pattern of change with increase in LET but are lower than the corresponding RBE_{max} values. These RBE values, based on the D_{37}, appeared to be lower than might have been anticipated from the fast neutron studies (Fig. 17.3). This observation brings into question any assumption that the biological weighting factor used for recoil protons should be the same as that for fast neutrons and for protons from the nitrogen capture reaction, a common assumption in BNCT treatment planning.

17.2.4 Implications for the Weighting of Dose for Epithermal Neutron Beams

For reactor-based epithermal neutron beams, where there is likely to be major differences in the dose-rate of the γ-ray dose component, and also in the fast neutron spectra of the incident beam, there would appear to be a need to compare their biological effectiveness, as was the case for fast neutron therapy facilities [31]. The short-term crypt colony assay, which proved to be so useful in comparing the biological effectiveness of different fast neutron beams, has been used to examine the RBE of a number of thermal/epithermal neutrons beams. In an initial publication, the RBE of the epithermal neutron beam at the Massachusetts Institute of Technology (MIT) was determined at two depths in a phantom, 2.5 and 9.7 cm [32], and was found to decrease with depth, reflecting the reduced contribution of the high-LET component to the total dose at the greater depth. An attempt was made to estimate the RBE of the high-LET component of the total dose at these two depths. However, for that analysis, the authors used a DRF of 1.0 for the γ-ray dose component, despite the fact that the photon dose-rate at the greater depth in particular was low (~0.15 Gy/min) compared to that of the photon irradiation used in the control experiments (0.83 Gy/min). In their paper, the authors did express concern that all radiobiological mechanisms had not been taken into account in the analysis. Although not as extensive as for the dose-rate information for the spinal cord and lung, information does exist for the effects of dose-rate on jejunum crypt survival [26]. Those studies suggest that a DRF of ~0.7 would have been more appropriate to use in the calculations of the high-LET dose component RBE at a depth of 9.7 cm. At a depth 2.5 cm a larger DRF (<1.0) would be applicable. Use of more appropriate weighting factors for the γ-ray dose component would have resulted in a higher estimate of the weighting factor for the high-LET dose component. These details may not be that important because within a given facility, the overall RBE of the beam at a given depth for a specified tissue does not change. The problem arises when these separate weighting factors of an individual beam's dose components are used to estimate the photon-equivalent dose in a different facility where not only the γ-ray dose-rate may be different but also the fast neutron spectra. This view is supported by a more recent publication [33] where the results from the crypt colony assay are compared for 7 BNCT facilities worldwide.

It has already been mentioned that, although a low DRF of 0.45 (relative to a high dose-rate of 1.8 Gy/min) has been estimated to be appropriate for the CNS for use with the epithermal neutron beam at the BMRR and elsewhere, a value of 1.0 was actually used (Table 17.1). In a separate analysis [6], the dose-related incidence of a number of different endpoints, after epithermal neutron irradiation of dog brain on the FiR1 beam, were converted into photon-equivalent doses based on the weighting factors derived from studies on dogs and used clinically for the epithermal neutron beam at BMRR, namely 1.0 for low-LET γ-ray component and 3.2 for the high-LET component of the beam [30]. The use of the above weighting factors, adopted for use with the BMRR beam, for the FiR1 beam consistently produced an overestimate of the equivalent photon dose received when compared with the actual data for dogs irradiated with 6 MV x-rays. This is illustrated for the endpoint of single and multiple

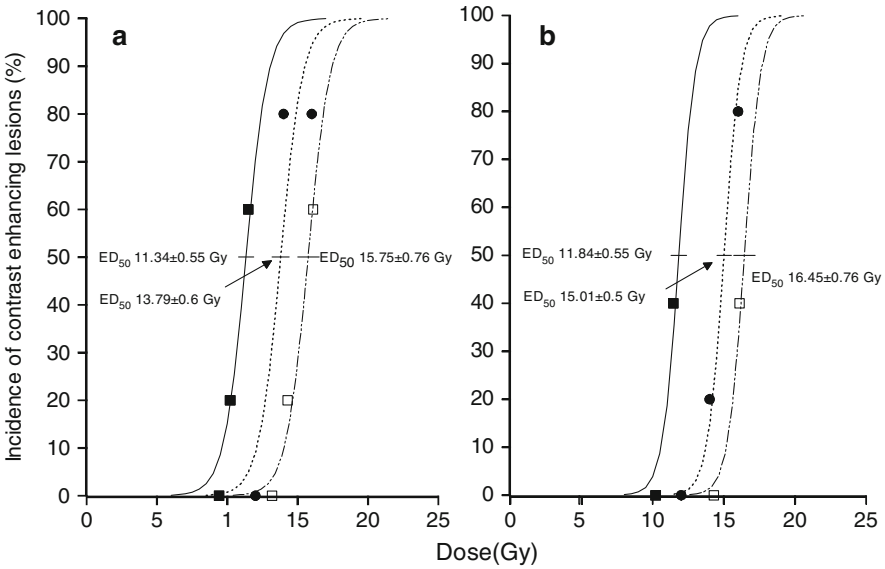

Fig. 17.5 Dose-related incidence of either (**a**) single or (**b**) multiple contrast-enhanced lesions on T1-weighted magnetic resonance images in the brain of dogs after irradiation with either epithermal neutrons (■) from the FiR1 beam or from 6 MeV x-rays (●). The photon-equivalent doses for the different physical epithermal beam doses used in this study were also calculated using the weighting factors developed for the BMRR (□). These weighted doses produced ED_{50} (± SE) values that were significantly higher than the experimentally observed ED_{50} values for photon irradiation (Reproduced from Hopewell et al. [39]; with permission)

permanent contrast-enhancing lesions on MRI in Fig. 17.5. The average overestimate of the photon-equivalent dose using the BMRR weighting factors for the FiR1 beam was 12%. These data illustrate the inherent dangers of applying weighting factors derived in one epithermal neutron beam to another neutron beam, no matter how similar the two beams may appear from the point of view of the absorbed dose components.

This view is strongly supported by recent re-evaluation (Millar, personal communication, 2010), where the kinetics of repair of sublethal damage for CNS tissue have been considered in the calculation of equivalent x-ray doses for the different experiments that were carried out to establish weighting factors for the FiR1 and BMRR epithermal neutron beams. For example, for the endpoint of multiple contrast-enhancing lesions in the brain of dogs, the x-ray ED_{50} for that effect of 15.01 Gy was given in 18.75 min (0.8 Gy/min). The experimentally derived iso-effective dose for the FiR1 beam (~80% photons) would have been delivered in 158 min. The calculated dose, equivalent to 15.01 Gy of x-rays in 18.75 min, delivered in 158 min, is 19.31 Gy based on repair kinetic parameters. This indicates a DRF of 0.78, higher than the value of 0.6 used in an earlier publication [6]. In the original calculation of

the DRF, the actual reference dose-rate of 0.8 Gy/min was not used and, based on the information provided in Fig. 17.2, the dose-rate of the epithermal neutron beam was compared with a reference dose rate of 1.8 Gy/min to give the DRF. Using the revised DRF of 0.78, calculated using the parameters for the kinetics of repair in CNS tissue, where the times for repair of sublethal damage were matched for the beam and x-rays alone, a lower estimate of the RBE of the high-LET component of the FiR1 beam was obtained, 3.3 as compared with the original 3.9 [6].

For the experimental studies on the BMMR, historical data based on the results from CT and not MRI to recognize changes in the brain of Beagle dogs were used [24]. The x-ray doses in this study were given at a higher dose-rate of 3 Gy/min. To calculate weighting factors for the BMRR epithermal beam using the endpoint of lethal necrosis, the ED_{50} for this effect was 14.8 Gy (4.9 min exposure) of x-rays compared with 9.23 Gy (158 min exposure) for the BMMR epithermal beam. There is also a need for caution in accepting these data since only two dogs were irradiated at this epithermal beam dose and also because Labradors and not Beagle dogs were used. Despite the limitations of the BMMR study, calculations, based on the same repair parameter, the x-ray equivalent dose for 14.8 Gy given in 4.9 min was 20.24 Gy in 158 min, DRF 0.73. The associated RBE of the high-LET component of the BMMR epithermal neutron beam (~73% photons) is thus 4.1, higher than that for the FiR1 beam. These weighting factors are closer to the alternative weighting factors of 0.6 and 4.4 for the low- and high-LET components of the BMMR beam, originally proposed by Gavin et al. [30], but never adopted.

The difference in the DRF for the photon components of the dose in the FiR1 and BMMR epithermal neutron beams of 0.78 and 0.73, respectively, is due to the difference in the original exposure times required to give the reference x-ray only doses in the two experiments. Had the reference x-ray dose, in the above example for multiple contrast-enhancing changes on MRI, of 15.01 Gy given in 18.75 min (0.8 Gy/min) been delivered at 3 Gy/min as in the BMMR related study, then the equivalent x-ray dose would have been reduced to 14.15 Gy (given in 4.7 min), and as a result, the DRF would be the same: 0.73. This finding points to the importance of taking into account the significance of the fast component of repair for reference x-ray exposure times of 10–30 min.

An alternative approach for the comparison of the biological effectiveness of the high-LET components of the dose, both within the same beam and between beams, involved the use of a simple in vitro cell survival model. This was initially described in 2001 [48]. Briefly, V79 cells were irradiated in suspension at different depths (20–65 mm) in a water-filled cylindrical phantom.

Over the period of irradiation, the temperature of the water was kept at 4 °C. This prevented the repair of sublethal irradiation damage over the variable exposure times both within the same beam and for different beams. Thus, the need to correct for the variable dose-rates of the γ-ray components to the dose was avoided, DRF 1.0.

The usefulness of this model can best be illustrated by reference to a recent comparison of the biological effectiveness of the moderated accelerator-based epithermal neutron beam at the University of Birmingham, UK, and the reactor-based

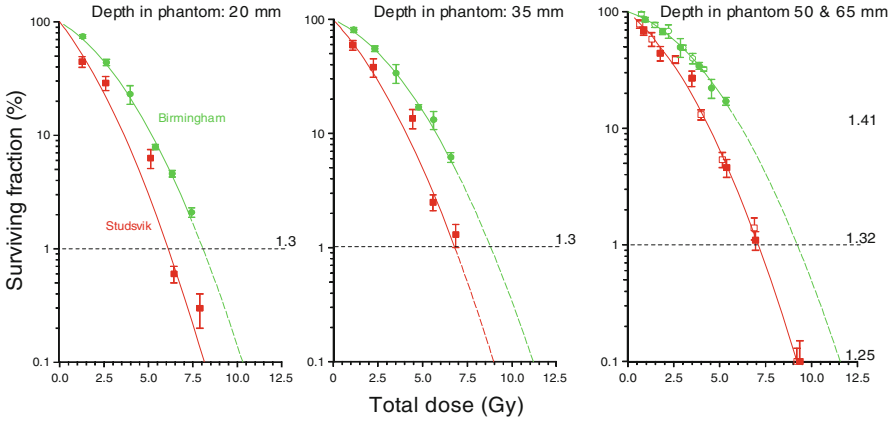

Fig. 17.6 Variation in survival of V79 cells irradiated with epithermal neutrons from either the Studsvik reactor-based beam (■, □) or the Birmingham accelerator-based beam (●,○). The curves are shown for irradiation at (**a**) 20 mm, (**b**) 35 mm, (**c**) 50 mm (■, ●) plus 65 mm (□, ○) depths in the phantom. *Error bars* represent ± SE (Reproduced from Hopewell et al. [39]; with permission)

epithermal neutron beam at Studsvik Medical, Sweden [49]. At all depths in the phantom, the biological effectiveness of the Studsvik beam, for a given total absorbed dose, were always greater than that for the Birmingham beam. For both beams, the survival data obtained for irradiation at 50 and 65 mm depths in the phantom were comparable and have been combined in this analysis. Cell survival curves were not always complete down to a surviving fraction level of 0.1%, especially for the Birmingham beam. This was due to the very low dose-rates (0.58–1.04 Gy/h, depending on depth in the phantom) resulting in very long exposure times, compared with the comparatively higher dose-rates at Studsvik (8.2–16.2 Gy/h). Extrapolation of the cell survival curves was based on the linear and quadratic parameter fits to data points available (Fig. 17.6). The ratio of doses for the same level of cell survival was independent of the depth in the phantom, 1.3, 1.3, and 1.33 for a depth of 20, 35, and 50 plus 65 mm, respectively. However, the dose ratio did depend on the survival level used for the comparison, for example, ranging from 1.41 at 10% survival to 1.25 at 0.1% survival. These differences seem to be related to the differences in the neutron spectra, particularly the fast neutron contribution to the total dose, in the Studsvik beam (Fig. 17.7). The difference in the fast neutron contribution to the total absorbed dose was 51% at 20 mm and 83% at 65 mm depth, while the difference in the total high-LET contribution was 24–26%. Comparable neutron spectra at 50 and 65 mm depth are consistent with the similar cell survival data at these two depths for both beams. Similar differences in the high-LET content of the beam as a function of depth might be a simple explanation as to why the dose ratios for a given level of cell survival were independent of the depth in the phantom. However, more intercomparisons are required before any definitive general conclusions can be drawn.

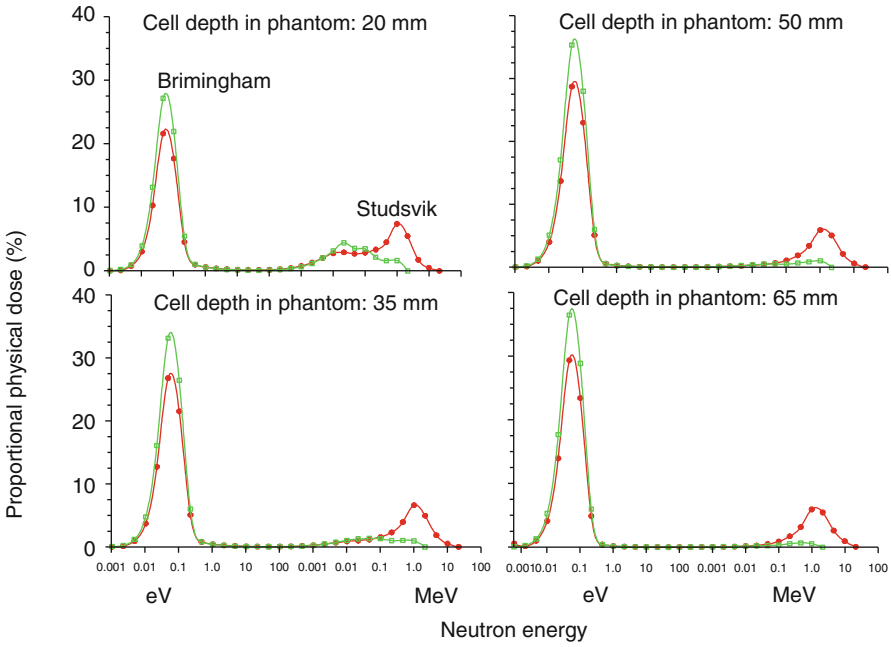

Fig. 17.7 MCNP model calculations for the neutron spectra of the Studsvik reactor- (●--●) and Birmingham accelerator-based (□--□) epithermal neutron beams at depths of 20, 35, 50, and 65 mm in a phantom, the depths used for V79 cell irradiations. Each data point represents the midpoint in an energy bin of finite width (Modified from Mason [49], modified by Mason and Giusti, personal communication 2006)

17.3 Radiobiological Properties of Boron Capture Agents

The poor selectivity for tumor of the boron compounds used in the early BNCT clinical trials was recognized as one of the factors contributing to their unsuccessful outcome. A search for better boron delivery agents was initiated in the 1960s. The amino acid, *p*-boronophenylalanine (BPA) and the sulfhydryl borane ($Na_2B_{12}H_{11}SH$, or BSH) were two of the compounds evaluated in those studies. Compound development continues to be an active area of BNCT research.

However, given the degree of characterization required, in particular, toxicity evaluation and radiobiological studies, it would take several years for any new compound to enter a clinical trial. At this time, BPA and BSH are the only two boron compounds in use for clinical BNCT, hence, much of this section of the chapter will necessarily focus on the radiobiological studies that have been reported for these two agents. The approaches used to characterize these compounds for both normal tissues and tumors should also be applied to newer agents.

The absorbed dose to tissues resulting from ^{10}B capture is a function of the neutron fluence and the ^{10}B concentration in blood and in the parenchymal tissue

surrounding the blood vessels. For the compounds BPA and BSH, the dose contribution from the $^{10}B(n,\alpha)^{7}Li$ reaction for normal tissues is routinely calculated based on the blood ^{10}B concentration over the course of irradiation. No direct account is taken of the ^{10}B content of the parenchyma or of the vascular endothelial cells in any dose calculations. This is because it is not yet possible to measure normal tissue concentrations of ^{10}B during the course of irradiation. Noninvasive imaging techniques are under development to achieve this objective [41, 56]. However, there would be a requirement to measure tissue boron levels if, for example, compounds such as one from a family of porphyrins, copper tetra-phenyl-carboranyl porphyrin (CuTCPH), were developed. These compounds are retained in tumor and normal tissues to variable degrees but are cleared from the blood [57]. The use of blood boron levels, which may be approaching the lower limit of accurate measurement, may then be misleading. However, for BPA and BSH, the physical absorbed dose delivered to normal tissues has historically been described in terms of the absorbed dose delivered to the blood and the CBE factors calculated are defined so as to be the multiplicative factor that transforms the blood dose into the biologically effective normal tissue dose. Thus, if in the future, measurements of boron levels in normal tissues become available, these CBE factors should not be used. If the normal tissue blood ratio is <1.0, then the photon-equivalent dose to the normal tissue, from the $^{10}B(n,\alpha)^{7}Li$ reaction, would be underestimated, while if the ratio was >1.0, then the photon-equivalent dose would be overestimated. The photon-equivalent dose, from the $^{10}B(n,\alpha)^{7}Li$ reaction, has been overestimated in some publications. For example, in a therapeutic study involving the treatment of spontaneous nasal planum squamous cell carcinoma in cats [82], the photon-equivalent doses to the skin and oral mucosa were calculated using the available CBE factors based on blood boron levels. The tissue boron levels and not the blood boron levels were used in this example, and thus, the dose contribution from the $^{10}B(n,\alpha)^{7}Li$ reaction was overestimated because normal tissue blood ratios were >1.0.

Experimentally derived CBE factors must always be used with caution in clinical treatment protocols. The biodistribution profile of a given boron delivery agent needs to be as thoroughly characterized as possible in the relevant animal models and in patients. In particular, the vascular/nonvascular ^{10}B partition ratio in the animal model used to derive the CBE factor must be similar to the ratio in patients at the time of irradiation. It must be emphasized that comparability of ^{10}B biodistributions is a prerequisite to translating an animal model-derived CBE factor to the clinical situation. At the low doses of BPA (250–290 mg BPA/kg body weight) that were used in the BNL clinical trial, the ^{10}B distribution in human brain was similar to that measured during radiobiological studies in the rat and dog from which the clinical CBE factors were estimated [11, 17].

Given the historical focus on the use of BNCT for treatment of brain tumors (primarily glioblastoma multiforme), the evaluation of effects on the important dose-limiting normal tissues, namely skin, central nervous system (CNS), and oral mucosa have assumed central importance.

17.3.1 Normal Tissue Effects

17.3.1.1 Skin

The response of rat skin to BNC irradiation using BPA or BSH has been studied using the thermal beam of the BMRR [59]. The CBE factors for BPA using the early endpoint of moist desquamation and the late endpoint of dermal necrosis were 3.7 ± 0.7 and 0.73 ± 0.42, respectively. The CBE factors for BSH with moist desquamation and dermal necrosis endpoints were 0.55 ± 0.06 and 0.86 ± 0.08, respectively. It is evident from these findings that the microdistribution of these two compounds had a marked effect on the CBE factor obtained. BPA would appear to accumulate in metabolically active basal stem cells within the epidermis, which would account for the very high CBE factor. For the endpoint of dermal necrosis, where the vascular endothelium represents the likely target cell population, the CBE factor values for BPA and BSH were comparable. Observations using neutron activation autoradiography suggest that BPA and BSH have a similar microdistribution in the dermis (Morris, unpublished data, 1999). The clinical implications of these findings are that, per unit boron concentration, BSH mediated BNCT causes less damage to the epidermis than BPA mediated BNCT.

The biological effect of BPA based BNCT on human malignant melanoma using thermal neutrons has produced important information on the effect of this treatment on human skin [27]. Based on boron measurements in blood and skin, these investigators estimated the boron concentration in the skin at the time of BNCT to be between 1.3 and 1.5 times the concurrent level in the blood.

The CBE factor has been derived for the skin in other species. A value of 2.4 has been reported for BPA using acute reactions in hamster skin as the endpoint [37]. The results of dog irradiations with epithermal neutrons at the BMRR indicated a CBE factor for BSH of 0.5 [29].

For the porphyrin CuTCPH, a promising experimental boron delivery agent, the CBE factor was 1.8, for the early endpoint of moist desquamation, calculated in the standard way, using the boron concentration in the blood [66]. In the CuTCPH study, irradiation was carried out when the blood boron level was low (~1.5 μg/g), 72 h after the initiation of a 48 h infusion of the compound. The CBE factor was much lower, 0.1, if the boron concentration in the skin was used in the calculations. This suggests that although there was a significant accumulation of boron in the skin at the time of irradiation, there were relatively low levels of boron in epidermal cells, and that the bulk of the boron was in the dermis.

17.3.1.2 CNS

The development of late changes in the CNS after radiation exposure has traditionally been described in terms of damage to specific target cell populations, the loss of which is responsible for specific functional and histologically identifiable injury. Conflicting theories have considered either the vascular endothelial cell or elements of the CNS parenchyma, or both, to be the critical target cells. More recently, radiation damage to the vasculature during BNCT has been shown to be the probable

cause of necrosis in the rat spinal cord, suggesting that the vascular endothelium is the primary radiation target in the CNS [20, 61].

The spinal cord of rats has been used to study the response of normal CNS to BNCT [60, 63]. The late effects seen in the spinal cord following single BNCT exposures are similar to those seen in the brain [30, 61]. The radiosensitivity of the rat brain and spinal cord to fractionated irradiation are also comparable [83]. The late end point of limb paralysis (myeloparesis) for the evaluation of radiation-induced spinal cord damage is clearly defined while histological and morphometric endpoints that have been used to assess damage to the brain are time consuming.

The CBE factors for BPA and BSH, measured experimentally, do indeed reflect the different biodistributions of these two boron compounds in the sense that BPA crosses the blood brain barrier while BHS does not. In the case of BSH, the CBE factor was calculated to be 0.53 ± 0.10 [60]. This value is approximately three times lower than that for BPA (1.34 ± 0.13) at a comparable blood ^{10}B concentration of ~20 μg ^{10}B/g. The threefold difference in the CBE factors was of the same order as that predicted by Rydin et al. [76] who calculated that the fraction of the dose received by the vessel wall would be one-third to one-fifth that delivered to an infinite pool of blood, depending on the diameter of a vessel, based solely on geometry.

In the derivation of CBE factors for potential use in clinical protocols, it is advisable to use a wide range of blood ^{10}B concentrations. Studies carried out using BSH indicated that the CBE factor estimate remains constant at about 0.5 for blood ^{10}B levels ranging from 20 to 120 μg/g [62]. However, progressive escalation of the blood dose of BPA to deliver blood ^{10}B concentrations in the range 20–90 μg/g resulted in CBE factors that varied from 0.66 to 1.34 [63]. Irradiations of the spinal cord in these studies took place 1 h after the administration of the BPA. At this time point, major differences were found in the relative distribution of ^{10}B in the blood and the CNS parenchyma, such that for the highest blood ^{10}B concentration (90 μg/g), the ratio of the level of ^{10}B in the blood to that in the CNS parenchyma was a factor of 3.5 higher than at the lowest blood ^{10}B concentration (20 μg ^{10}B/g). This major change in the partition ratio of ^{10}B between the blood and parenchyma at the time of irradiation was the reason for the observed variations in the calculated CBE factors for different concentrations of ^{10}B in the blood [63]. In the clinical situation, BPA is administered more slowly (e.g., 2 h i.v. infusion), and as a result, it is unlikely that there would be a pronounced change in the ^{10}B concentration ratio between the blood and the CNS parenchyma at higher BPA doses than those currently used. These experimental data emphasize the importance of thorough preclinical and clinical biodistribution studies in protocols involving escalation of the dosage of a boron compound or an alteration in the infusion schedule. In addition, the dependence of CBE factors on experimental conditions makes it critical that studies intended to provide CBE factors for clinical use must be designed to approximate the clinical situation as closely as possible.

Studies of the response of the brain of dogs to single-dose BNCT were carried out using the epithermal neutron beams at the BMRR and at the high flux reactor at Petten using BPA or BSH, respectively [28, 30, 40]. The attenuation of the

epithermal neutrons, as a function of depth, produced a nonuniform dose across the brain. The BNCT doses used for comparison to the published x-ray data [24] were defined as the average absorbed dose (Gy) in the volume of the dog brain that received between 90 and 100% of the maximum brain dose. This corresponded to a volume of about 30 cm^3, or about 20% of the brain volume. There were differences in the volumes and dose distributions between the 4 MeV x-rays used in the historical studies and the BNCT irradiations; however, the volume that received the prescribed doses were relatively large and potential volume effects on the iso-effect dose (ED_{50} for abnormalities noted on MRI scans and severe neurological deficit requiring euthanasia) could be excluded. The CBE factors, determined by comparing effects on the normal brain to the published data for hemi-brain irradiation with 4 MeV x-rays [24], were 1.1 for BPA and 0.3–0.5 for BSH [28, 30, 40]. These CBE factors are in agreement with the values derived independently for the rat spinal cord [60]. It should be noted that the historical photon results were based on the results of CT scans and not MRI, and although considerable thought was given to the comparability of effects using these two methods, this is the type of comparison that should be avoided if at all possible. As already indicated, historical photon controls were not used for the determination of the RBE of the FiR1 epithermal neutron beam [6]. This enabled the same MRI and histological methods to be used to evaluate dose-related changes in dog brain from both the epithermal neutron beam and the photon irradiation controls.

For CuTCPH, the CBE factors calculated using the same rat spinal cord as in the studies described previously were 4.4 and 3.8, calculated on the basis of the boron concentration in the blood or the parenchyma, respectively [66]. This finding is in accord with measurements of the boron concentration in the parenchyma of the cord, which were higher than in the blood, tissue: blood concentration ratio 1.9:1. These relatively high CBE factors could also indicate a selective accumulation of this boronated porphyrin in the walls of blood vessels in the CNS, damage to which is believed to be responsible for late CNS morbidity [20]. There is general evidence to indicate that porphyrins have a significant affinity for blood vessels (e.g., [7, 68]).

17.3.1.3 Oral Mucosa

Only a limited number of reports have documented the CBE factors (based solely on the ^{10}B concentration in the blood) for the oral mucosa, using ulceration of the ventral surface of the tongue of rats as the end point. For the boron delivery agent BPA, a CBE factor of 4.9 was estimated [19]. This CBE factor is considerably higher than that reported for BSH (CBE factor ~0.3) in the same model [64]. These major differences in the CBE factor indicate variations in the microdistribution of these two boron delivery agents in the mucosal epithelium. Average boron measurements (DCP-AES) of whole tissue samples from the ventral surface of the tongue showed appreciable uptake of ^{10}B (~21 μg/g) at 3 h after administration of BSH at a dose of 55 mg/kg [64]. A similar finding was reported for BPA administered at a ^{10}B concentration similar to that used for BSH, where the level of ^{10}B in the ventral surface of the tongue at 3 h after administration was estimated to be ~23 μg/g [64, 65].

These data, while indicating that the overall concentrations of ^{10}B in the tongue were similar for both boron delivery agents, provide no information with regard to the biodistribution profile in different anatomical regions of the tissue. Ion microscopy studies of ^{10}B in tissues [64, 65] have enabled the microdistribution of this element to be analyzed with considerably greater precision than previously possible. Ion microscopy analysis revealed that the level of ^{10}B in the mucosal epithelium was very low after BSH administration [64]. In contrast, the ^{10}B content of the mucosal epithelium was ~3.5 times higher in rats receiving BPA. In the case of BSH, the majority of ^{10}B was located in the lamina propria and not in the mucosal epithelium. This differs from the findings for BPA where the ^{10}B content of the mucosal epithelium was fairly similar to that in the lamina propria; the boron concentration ratios for mucosal epithelium: lamina propria were 1:6 for BSH and 1:1.5 for BPA. Also, ^{10}B accumulation in the mucosal epithelium was five times higher with BPA than BSH. These data indicated that a major factor contributing to the difference in the CBE factors for BSH and BPA, despite similar gross boron tissue concentrations, was the relatively low uptake of BSH in the mucosal epithelium.

When using CuTCPH as the boron capture agent, gross levels of boron in the oral mucosa of the rat were found to be high, with a mucosa: blood ratio of 49:1 [67]. Irradiation with thermal neutrons in the presence of CuTCPH gave a CBE factor of ~0.04, using ulceration as the endpoint. This value was calculated using measurements of the estimated content of boron in the oral mucosa at the time of irradiation [67]. If the absorbed dose from the $^{10}B(n,\alpha)^{7}Li$ reaction was calculated on the basis of the boron concentration in the blood at the time of irradiation, the CBE factor was appreciably increased to ~1.7 [67]. However, as mentioned previously, the boron levels in blood were very low at the time of irradiation. Indeed, the boron concentrations in the blood were close to the level of detection in this irradiated series of animals. As a consequence, the CBE factor calculated on the basis of blood levels can only be viewed as a rough approximation.

17.3.2 Tumor Response

Experimental therapeutic studies related to BNCT have been carried out in a variety of animal tumor models. BPA mediated BNCT has been shown to inhibit the growth of melanoma, producing high local tumor control rates, in mice, hamsters, and pigs [13, 55]. BPA has also proved to be effective in BNCT studies on hamster derived melanoma, grown as xenografts, in the rabbit eye [71]. The first successful treatment of a brain tumor (rat 9L gliosarcoma) was carried out by Joel et al. in the late 1980s using the dimeric form of BSH as the boron capture agent and the BMRR thermal neutron beam [44]. This was followed, in 1992, by another study involving the first irradiation of the 9L gliosarcoma in the rat with BPA-mediated BNCT [14]. These experiments were repeated in 1994 using an improved BPA delivery system of BPA complexed with fructose (BPA-F) to increase the solubility. This produced long-term tumor-free animal survival rates approaching 100% [16]. Additional studies by Saris et al. [77], with the murine GL 261 glioma, and Matalka et al. [51],

with a human melanoma cell line (MRA 27) implanted in the brain of nude rats, also demonstrated the efficacy of BPA mediated BNCT. More recently, the preferential uptake of BPA and BSH by the rat F98 glioma has been considerably enhanced by the disruption of the blood brain barrier following the intracarotid injection of mannitol [84, 85]. Dramatic further improvements in F98 tumor growth inhibition were subsequently observed in BNCT studies, using a combination of both BPA and BSH [1] using the blood brain barrier disruption approach. Since this earlier work, multiple translational studies have been performed in different tumor models, using different boron compounds, routes of compound administration, and a range of administration strategies [3].

While the CBE factors for the skin, CNS, and oral mucosa are fairly well defined for both BPA and BSH, those for use in estimating the photon-equivalent dose to tumor are much less certain. For BPA, CBE factors of 4.0, 3.8, and 3.6 were obtained for a surviving fraction of 10, 1, and 0.1 %, respectively, for the rat 9L gliosarcoma model, based on the in vivo irradiation of intracranially implanted tumors in situ, with removal immediately after irradiation and the assay of clonogenic cell survival in vitro [15]. CBE factors of 1.3, 1.2, and 1.2 were also derived in the same way for BSH for the 9L gliosarcoma. Again, as would be expected, slightly higher values were obtained for the highest level of cell survival. This later study was based primarily on values for the oxidized dimeric form of BSH (BSSB). The CBE factors for both BSH and BSSB evaluated for cultured cells in vitro were much higher both for BSSB (range 3.6–3.1) and BSH (range 3.2–2.8) [15]. This difference reflects the likely heterogeneous boron distribution in solid tumors relative to cells in culture and warns against the application of any CBE values derived totally from cells in vitro to an in vivo situation. Ideally, CBE factors for boron capture agents such as BPA and BSH should be derived directly using an in vivo assay. This is difficult for the intracranially implanted 9L gliosarcoma because of the high risk of normal tissue complications that would result from the large single dose of x-rays that would be needed to control this tumor. An assessment of local tumor control after x-irradiation is an essential requirement for the calculation of a CBE factor.

An assumed requirement for an effective boron capture agent is that the compound should accumulate in tumor relative to blood and normal tissues. However, the preferential uptake of the boron compounds by tumor tissue does not explain differences in CBE values between tumor tissue and normal tissue. Potentially, differences in the microdistribution determined by features such as tumor cell metabolism and tumor cell geometry (large nuclei, changes in nucleus/cytoplasm ratio, etc.) vs. normal cell metabolism and geometry account for differences in CBE values. Historically, calculations of the physical radiation dose from the $^{10}B(n,\alpha)^{7}Li$ neutron capture reaction have been made based on an estimate of the gross boron concentration in tumor tissue. Since this cannot be routinely measured directly, biodistribution studies need to be carried out in advance of experimental animal or patient studies to determine the tumor: blood or tumor: normal tissue concentration ratios for boron. The tumor: blood boron ratio is then used to estimate tumor boron levels from measurements of blood samples at the time of irradiation, which in the case of the boron compound currently used clinically, occurs within a few hours of compound administration.

This is different from studies in normal tissues where the boron concentration in the blood at the time of irradiation is used directly to calculate an absorbed dose. This is then converted into a weighted dose using the appropriate CBE factor. Examples of published tumor:blood boron concentration ratios include those for the rat 9L gliosarcoma, which are 3.3 ± 0.5 for BPA (oral administration) and 3.2 ± 0.4 for BPA-F. For BSH and its dimeric form, BSSB, the corresponding values were much lower, 0.71 ± 0.2 and 0.76 ± 0.2, respectively [38]. This low ratio, suggesting no selective uptake relative to blood, was not considered to be a drawback because this compound, which does not cross the intact blood brain barrier, had been developed specifically for the treatment of primary gliomas. The tumor:brain boron concentration ratios for these two compounds, BHS and BSSB, were very high, that is, ~8 and ~17, respectively; these boron carriers cross easily through the disrupted blood brain barrier into tumor tissue [38]. These numbers have to be viewed with caution because boron measured in brain, or indeed in other normal tissues, may reflect the amount of boron present in the residual blood in any tissue sample. The concentration ratios reported above in the rat 9L gliosarcoma model are comparable with those obtained for gliomas, based on pharmacokinetic studies in man [18, 79].

More recently, biodistribution studies have been carried out on chemically induced primary squamous cell carcinomas in the hamster cheek pouch. For compounds such as GB-10 ($Na_2{}^{10}B_{10}H_{10}$), which is related to BSH, the distribution of boron in tumor, relative to adjacent normal tissues, is not influenced by a selective blood vessel barrier of the type found in the CNS. The tumor:blood boron concentration ratios ranged from 2.8 to 4.8 for BPA and from 0.8 to 1.0 for GB-10, depending on the dose and administration protocol but not in a clearly defined way [35]. Thus, based on these two tumor models, uptake of the current group of clinically used boron carriers and related compounds by tumor relative to blood does not change significantly with tumor model. However, it must be emphasized that this in itself does not indicate the same biological effectiveness. There is an urgent need to establish CBE factors for different tumor types and to avoid the use of CBE factors derived for the 9L gliosarcoma for other tumor types.

Another boron carrier for which comparative data exist for these two tumor types is CuTCPH. Tumor:blood boron concentration ratios ranged from 80:1 in subcutaneously implanted 9L gliosarcoma to 16:1 in the same tumor implanted intracerebrally [57]. In squamous cell carcinomas of the hamster cheek pouch, even higher values of 99:1 were obtained [47]. These high tumor: blood boron concentration ratios were all measured 3 days after the first administration of a series of i.p. injections of the compound, delivered over periods up to 48 h. They were associated with very low blood boron concentrations, which cannot be reliably used to estimate tumor boron levels in a clinical scenario. These high tumor:blood boron concentration ratios measured in the hamster cheek pouch model do not necessarily correlate with high levels of local tumor control. A combination of high absolute boron concentration values and a favorable compound localization, that is, a high CBE factor are pivotal to obtaining the greatest biological effect. This fact stresses the need for radiobiological studies to evaluate the potential therapeutic efficacy of a particular boron carrier. The therapeutic effect of boron carriers must not be predicted on the basis of tumor:blood boron concentration ratios alone.

The importance of the use of in vivo models to assess the likely effectiveness of BNCT mediated by a boron compound has recently been illustrated by studies with GB-10 on induced squamous cell carcinomas in the hamster cheek pouch [81]. As indicated above, GB-10 does not target these tumors selectively and yet GB-10 mediated BNCT still produced a 70% overall initial tumor response rate with no damage to the normal tissues of the cheek pouch. Analysis using light microscopy has indicated that GB-10 mediated BNCT damages the abnormal tumor blood vessels, but spares blood vessels in precancerous and normal tissue. The stroma of the tumor was characterized by marked hemorrhaging, caused by the rupture of blood vessel walls, congestion, and edema. No damaged or ruptured blood vessels were detected in any of the fields of precancerous or normal tissue examined throughout the follow-up period of 30 days. Blood vessels of tumors are believed to be structurally and functionally abnormal. Tumor blood vessels have been reported to be dilated and altered in the sense that their walls exhibited fenestrations, vesicles, and transcellular holes. There were widened interendothelial cell junctions and a discontinuity or absence of the basement membrane [9]. Regardless of the effectiveness of GB-10 mediated BNCT, the working hypothesis is that GB-10 leaks from the abnormal tumor blood vessels into the extracellular space and accumulates in the vicinity of endothelial cells. In addition, in terms of purely physical geometric considerations, the dose distribution in dilated tumor vessels would be closer to the charged particle equilibrium distribution than in normal (narrower) blood vessels where a boron concentration gradient will exist between blood adjacent to the luminal wall of the blood vessel, the endothelial cell, and the surrounding tissue. With GB-10 located in the blood and in the extracellular space around blood vessels, a selective tumor effect would result from selective blood vessel damage rather than from the selective uptake of the boron compound by the tumor [81]. This proposed mechanism is in contrast to the traditional BNCT paradigm which ascribes selective tumor damage to selective boron uptake by tumors. Furthermore, it illustrates the limitations of gross bio-distribution studies and the need to perform in vivo BNCT studies to evaluate the potential therapeutic efficacy of a boron compound.

As indicated previously, achieving high tumor:normal tissue and tumor:blood mean boron concentration ratios is clearly an asset. However, using this approach alone, BNCT will not be optimized unless at least the majority of all the tumor clonogenic cells are targeted, regardless of their position in the tumor and metabolism and degree of differentiation or proliferation. Given that tumors are very often heterogeneous, targeting of all the appropriate tumor cell populations is an acknowledged challenge in oncology. In the case of BNCT, the tumor cell populations that are poorly loaded with boron will be significantly underdosed. The combined administration of boron compounds with different uptake properties should contribute to a more homogeneous targeting within a heterogeneous tumor and in this way to the therapeutic efficacy of BNCT [2, 35, 36, 70, 80]. Studies with induced squamous cell carcinoma in the hamster cheek pouch model have highlighted the difficulty of achieving complete remissions, within 30 days, in larger tumors (>100 mm^3) treated with BPA-mediated BNCT alone [46]. Conversely, BNCT mediated by GB-10 and BNCT mediated by a combination of GB-10 and BPA induced complete remission in some of these large tumors [81]. Improved tumor

response could be partially ascribed to improved tumor cell targeting by a combined compound administration protocol [36]. The combined administration of GB-10 and BPA achieved a statistically significant 1.8-fold increase in the targeting homogeneity of boron, over GB-10 alone, and a statistically significant 3.3-fold increase in targeting homogeneity of boron over BPA alone [36]. This conclusion was based on a reduced coefficient of variation in the gross measurements in multiple samples in individual animals. Thus, in this case at least, combined administration of two boron compounds with different properties and uptake mechanisms (BPA and GB-10) improved targeting homogeneity. Moreover, GB-10 mediated BNCT, in particular, may contribute, via a selective effect on tumor blood vessels, to the treatment of larger tumors that are more difficult to treat on a "cell by cell" basis. GB-10 and BPA could combine vascular targeting and cellular targeting, respectively, to achieve an improved tumor response in a similar manner to what was recently been reported for dual-mode photodynamic therapy [10].

An additional potential advantage of combined boron compound administration protocols lies in the finding that they can deliver increased absolute amounts of boron to tumor tissue [35]. For similar tumor:normal tissue ratios, high, non-toxic, absolute ^{10}B concentrations are an advantage because they allow for shorter irradiation times and a concomitant reduction in the background dose from the neutron beam [12]. In addition to the multiple variables described above that influence the value of CBE factors for tumors, for a single boron carrier, little is known about the interaction between boron carriers administered concomitantly in different proportions. The improvement in targeting homogeneity described above, for example, would conceivably result in a synergistic therapeutic effect when boron carriers are administered jointly. Within this context, the CBE value of a combination of boron compounds must be determined in vivo and cannot be calculated based on the individual CBE values for each boron compound. The fact that tumor control by BNCT mediated by certain boron compounds might be due to vascular damage rather than direct killing of tumor cells and available evidence that targeting of heterogeneous tumor cell populations plays a pivotal role in the biological effect of BNCT [81] also questions the validity of some CBE values determined using in vivo irradiation/in vitro assays [19] since this excludes the evaluation of any effect on tumor response specifically involving the tumor vasculature.

All of the above considerations stress the need to establish CBE factors under conditions that resemble, as closely as possible, the clinical scenario that the experiments are attempting to characterize.

17.4 Future Research Requirements

17.4.1 Interaction Between High and Low-LET Radiations

In the routine practice of BNCT, it is, as indicated previously, assumed that the different components of the mixed field irradiation act independently of each other. However, only a relatively small increase in the biological effectiveness of γ-rays, when given in combination with a high-LET radiation relative to γ-rays alone, would

significantly reduce the apparent RBE/CBE of the high-LET components of this mixed beam irradiation. While of considerable importance for the understanding of BNCT, the potential interaction between high- and low-LET radiations has not been extensively studied nor directly investigated in relation to BNCT. The only studies that have been undertaken, with relevance to this question, have been the sequential irradiation of V79 cells with fixed doses of either fast neutrons or ^{238}Pu α-particles (140 keV/μm), prior to exposure to high dose-rate x-rays [52, 53].

For high dose-rate x-rays and α-particles given totally separately, the RBE of the α-particles, relative to x-rays, was approximately 6.0, 3.0, and 2.4 for clonogenic cell survival levels of 50, 10, and 1%, respectively (Fig. 17.8a). When a fixed dose of 0.5 Gy of α-particles, which reduced clonogenic cell survival by 50%, was given immediately prior to x-rays, the resulting x-ray cell survival curve was still curvilinear. Normalization of the data back to an initial 100% survival showed the x-ray (with 0.5 Gy of α-particles) cell survival curve to be unchanged relative to x-rays alone (Fig. 17.8b). This was not the case when the initial α-particle dose was increased to a fixed dose of either 2.0 or 2.5 Gy. The RBE of x-rays combined with the higher dose of α-particles was ≥1.15 when compared with x-rays given alone (Fig. 17.8c, d). McNally et al. [53] concluded that "alpha particles cause damage capable of interacting with x-ray damage." However, the relationship is not a simple one; it depends on the relative mix of high- and low-LET radiation. These results raise important questions although results from studies with fixed doses of α-particles or neutrons do not necessarily predict the response of cells and tissues when a fixed percentage of high-LET radiations (recoil protons from fast neutrons, protons from nitrogen capture and α-particles, and lithium ions from the ^{10}B capture) is given concomitantly with γ-rays, sometimes at relatively low dose rates. Carefully designed investigations are needed to address this issue, using a proportion of high-LET radiation to the total absorbed dose, of the same order of magnitude as that present in tissue during BNCT exposures. In a recent study [73] in which V79 cells were concomitantly irradiated with x-rays and alpha particles, no evidence for any interaction was found. However, in this study, the percentage contribution of alpha particles to the total absorbed dose was <19%, and thus, the results obtained are still consistent with the earlier studies of McNally et al. [53]. This as been reaffirmed by a very recent study [50] where evidence for the interaction between gamma-rays and fast neutrons, in a mixed field irradiation with epithermal neutrons , was not only shown to be dependent on the proportion dose of contribution from the high-LET dose component but also suggested that it might also be influenced by the energy spectrum of the fast neutron dose component.

17.4.2 Use of Existing Boron Compounds for New Medical Applications

The determination of CBE factors, which represent the biological effectiveness of the ^{10}B(n,α)^{7}Li reaction products in specific normal tissues at risk as a result of any new application, should be a mandatory part of any development program. Reports

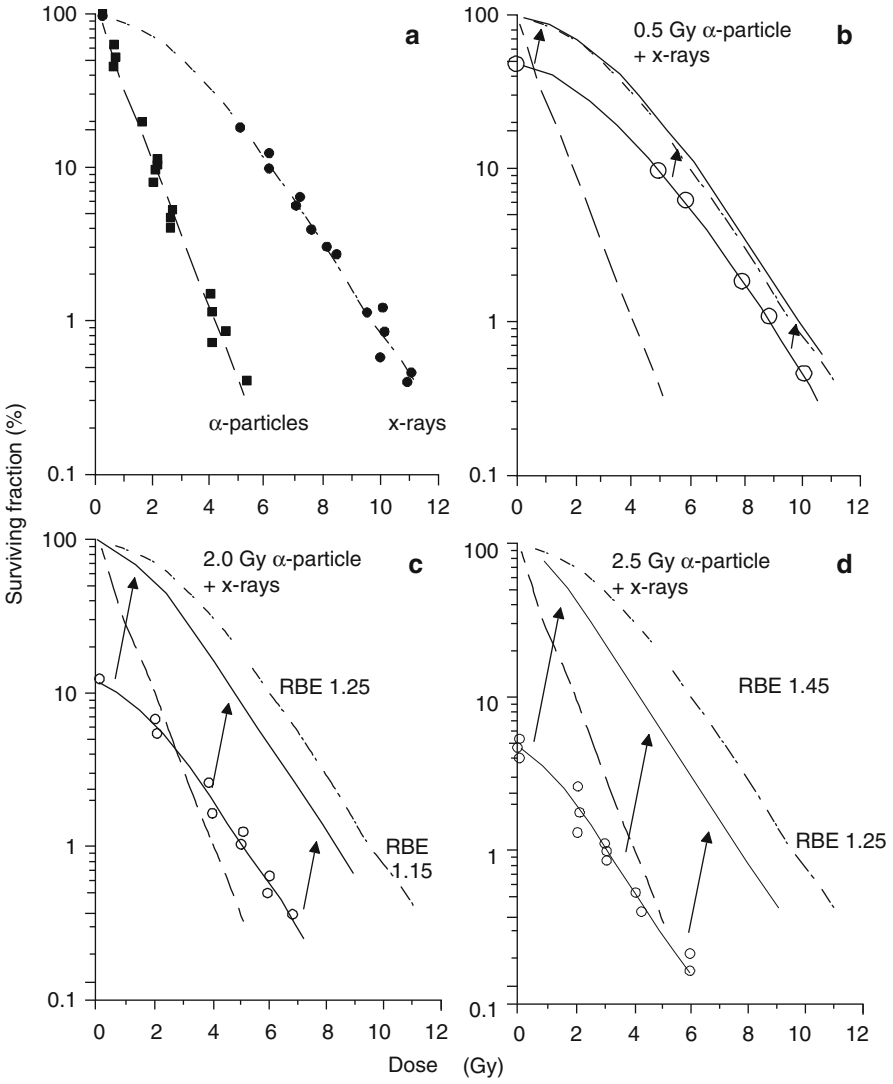

Fig. 17.8 Clonogenic cell survival curves for V79 cells after irradiation with either (**a**) x-rays [3 Gy/min] or α-particles [0.35 Gy/min; 140 keV/μm] alone or with a fixed dose of α-particles, (**b**) 0.5 Gy, (**c**) 2.0 Gy, or (**d**) 2.5 Gy followed by a variable dose of x-rays. For these combined irradiations, the curve for each irradiation type is given as a reference. For these combined irradiations, the actual data (O-O) has been normalized to 100 % cell survival (-). The RBE values result from the comparison of this normalized data with x-irradiation alone (Reproduced from Hopewell et al. [39]; with permission)

of adverse normal tissue reactions with any new radiotherapy modality are a cause for concern and a justifiable reason for the closure of studies, as has proven to be the case for BNCT in the past. CBE factors for a specific normal tissue, using existing boron carriers, cannot safely be applied to other normal tissues.

An example that perhaps demonstrates these concerns was the extrapolation of weighted doses, obtained from the clinical studies at Brookhaven National Laboratory with an epithermal neutron beam, for the safe treatment of patients with glioblastoma with BPA-mediated BNCT, to the extracorporeal treatment of livers in patients with colorectal metastases using the same neutron capture agent [74]. An additional complication in these investigations was that a thermal, and not an epithermal neutron beam, was used. This was judged to be acceptable, and it was suggested to be a conservative choice because the RBE of 14.3 MeV D-T generated fast neutrons for liver tissue was more than 30% greater in comparison with that of thermal neutrons for brain tissue. The end point selected for the liver was the clonogenic survival of hepatocytes in vitro [43], which has no proven link with the development of late radiation damage to liver and where the RBE will depend on the level of cell survival at which damage was assessed. The brain endpoint was based on the ED_{50} for radiation myelopathy in rats [59, 60]. This endpoint is associated with an approximately fixed level of cell survival in endothelial cells, and not parenchyma cells [20], making this a very poor comparison. Although it was recognized that a limiting tolerance dose was needed to be established for the liver using appropriate animal experiments [69], the same assumptions were still used in subsequent dose modeling studies. In the absence of appropriate data, there is always the tendency for early proposals to be perpetuated. In such situations where there is considerable uncertainty in the radiobiological parameters, it is much more appropriate to quote total absorbed doses, including the breakdown of that total absorbed dose into its different components. Otherwise, important information for potential future use will be lost.

17.4.3 Use of Novel Boron Compounds and Alternative Neutron Sources

Experience from fast neutron therapy has shown that even small changes in the neutron spectra can result in a change in the relative RBE of a particular beam [31]. With the currently available beams for BNCT, there is at present insufficient information to be able to predict the likely biological effectiveness of any new neutron source. More studies of the type that used V79 cells to compare the biological effectiveness of the fast neutron component of epithermal beams at Studsvik and Birmingham are required. This would avoid the difficulties in interpretation brought about by other confounding variables, such as the variations in effects resulting from the dose-rate of the γ-ray dose component. Simple short-term studies, such as those proposed by Gueulette et al [32], would also provide a guide to the relative effectiveness of different beams.

For new compounds, the key issue is the determination of the CBE factor for the specific normal tissues at risk of developing adverse effects and depends on the tumor site treated for which a particular boron compound is proposed. These studies do not need to be undertaken on an epithermal beam, which for most tissues may require the use of a large animal model. The use of a well characterized thermal beam would be suitable, preferably one where exposure times are short so the confounding effects of a low dose-rate from the γ-ray dose component can be avoided.

BNCT may be one of the most complicated therapeutic modalities ever to reach the stage of human clinical trials. As the application of BNCT continues to expand into new tumor sites, the radiobiological principles discussed in this chapter assume central importance. It is essential that all available radiobiological information from prior BNCT experience, as well as from other modalities such as fast neutrons, be evaluated and integrated into the plans for future BNCT development.

Those who cannot remember the past are condemned to repeat it.
George Santayana

References

1. Barth RF, Yang WL, Rotaru JH et al (1997) Neutron-capture therapy of brain-tumours – enhanced survival following intracarotid injection of either sodium borocaptate or boronophenylalanine with or without blood–brain-barrier disruption. Cancer Res 57:1129–1136
2. Barth RF, Yang W, Coderre JA (2003) Rat brain tumor models to assess the efficacy of boron neutron capture therapy: a critical evaluation. J Neurooncol 62:61–74
3. Barth RF, Coderre JA, Vicente MG et al (2005) Boron neutron capture therapy of cancer: current status and future prospects. Clin Cancer Res 11:3987–4002
4. Bedford JS, Mitchell JB (1973) Dose-rate effects in synchronous mammalian cells in culture. Radiat Res 54:316–327
5. Belli M, Cherubini R, Finotto S et al (1989) RBE-LET relationship for the survival of V79 cells irradiated with low energy protons. Int J Radiat Biol 55:93–104
6. Benczik J, Seppälä T, Snellman M et al (2003) Evaluation of the relative biological effectiveness of a clinical epithermal neutron beam using dog brain. Radiat Res 159:199–209
7. Berenbaum MC, Hall GW, Hoyes AD (1986) Cerebral photosensitisation by haematoporphyrin derivative. Evidence for an endothelial site of action. Br J Cancer 53:81–89
8. Cárabe-Fernández A, Dale RG, Jones B (2007) The incorporation of the concept of minimum RBE (RBE_{min}) into the linear-quadratic model and the potential for improved radiobiological analysis of high-LET treatments. Int J Radiat Biol 83:27–39
9. Carmeliet P, Jain RK (2000) Angiogenesis in cancer and other diseases. Nature 407:249–264
10. Chen B, Pogue BW, Hoopes PJ et al (2005) Combining vascular and cellular targeting regimens enhances the efficacy of photodynamic therapy. Int J Radiat Oncol Biol Phys 61:1216–1226
11. Coderre JA (1992) A phase 1 biodistribution study of p-boronophenylalanine. In: Moss R, Gabel D (eds) Boron neutron capture therapy: towards clinical trials of glioma with BNCT. Plenum Press, New York, pp 111–121
12. Coderre JA, Morris GM (1999) The radiation biology of boron neutron capture therapy. Radiat Res 151:1–18
13. Coderre JA, Slatkin DN, Micca PL et al (1991) Boron neutron capture therapy of a murine melanoma with para-boronophenylalanine – dose response analysis using a morbidity index. Radiat Res 128:177–185
14. Coderre JA, Joel DD, Micca PL et al (1992) Control of intracerebral gliosarcomas in rats by boron neutron capture therapy with p-boronophenylalanine. Radiat Res 129:290–296
15. Coderre JA, Makar MS, Micca PL et al (1993) Derivations of relative biological effectiveness for the high-LET radiations produced during boron neutron capture irradiations of the 9L rat gliosarcoma in vitro and in vivo. Int J Radiat Oncol Biol Phys 27:1121–1129
16. Coderre JA, Button TM, Micca PL et al (1994) Neutron capture therapy of the 9L rat gliosarcoma using the p-boronophenylalanine-fructose complex. Int J Radiat Oncol Biol Phys 30:643–652

17. Coderre JA, Elowitz EE, Chadha M et al (1997) Boron neutron capture therapy of glioblastoma multiforme using the p-boronophenylalanine-fructose complex and epithermal neutrons: trial design and early clinical results. J Neurooncol 33:141–152
18. Coderre JA, Chanana AD, Joel DD et al (1998) Biodistribution of boronophenylalanine in patients with glioblastoma multiforme: boron concentration correlates with tumor cellularity. Radiat Res 149:163–170
19. Coderre JA, Morris GM, Micca PL et al (1999) The effects of boron neutron capture irradiation on oral mucosa: evaluation using a rat tongue model. Radiat Res 152:113–118
20. Coderre JA, Morris GM, Micca PL et al (2006) Late effects of radiation on the central nervous system: role of vascular endothelial damage and glial stem cell survival. Radiat Res 166:495–503
21. Down JD, Easton DF, Steel GG (1986) Repair in the mouse lung during low dose-rate irradiation. Radiother Oncol 6:29–42
22. Farr LE, Sweet WH, Robertson JS et al (1954) Neutron capture therapy with boron in the treatment of glioblastoma multiforme. Am J Roentgenol Radium Ther Nucl Med 71:279–293
23. Field SB (1976) An historical survey of radiobiology and radiotherapy with fast neutrons. Curr Top Radiat Res Q 11:1–86
24. Fike JR, Cann CE, Davis RL et al (1984) Computed tomography analysis of the canine brain: effects of hemi-brain x irradiation. Radiat Res 99:294–310
25. Fowler JF (1982) Workshop summary. Int J Radiat Oncol Biol Phys 8:2207–2210
26. Fu KK (1991) Influence of dose rate on normal tissue tolerance. In: Gutin PH, Leibel SA, Sheline GE (eds) Radiation injury to the nervous system. Raven, New York, pp 69–90
27. Fukuda H, Hiratsuka J, Honda C et al (1994) Boron neutron capture therapy of malignant melanoma using ^{10}B-paraboronophenylalanine with special reference to evaluation of radiation dose and damage to the skin. Radiat Res 138:435–442
28. Gabel D, Philipp KH, Wheeler FJ et al (1998) The compound factor of the 10B(n, α)7Li reaction from borocaptate sodium and the relative biological effectiveness of recoil protons for induction of brain damage in boron neutron capture therapy. Radiat Res 149:378–386
29. Gavin PR, Wheeler FJ, Huiskamp R et al (1992) Large animal studies of normal tissue tolerance using an epithermal neutron beam and borocaptate sodium. In: Moss R, Gabel D (eds) Boron neutron capture therapy: towards clinical trials of glioma. Plenum Press, New York, pp 197–209
30. Gavin P, Kraft S, Huiskamp R, Coderre J (1997) A review: CNS effects and normal tissue tolerance in dogs. J Neurooncol 33:71–80
31. Gueulette J, Beauduin M, Grégoire V et al (1996) RBE variation between fast neutron beams as a function of energy. Intercomparison involving 7 neutron therapy facilities. Bull Cancer Radiother 83(Suppl):55s–63s
32. Gueulette J, Binns PJ, De Coster BM et al (2005) RBE of the MIT epithermal neutron beam for crypt cell regeneration in mice. Radiat Res 164:805–809
33. Gueulette J, Liu H-M, Jiang S-H et al (2006) Radiobiological characterization of the epithermal neutron beam produced at the Tsing Hua open-pool reactor (THOR) for BNCT: comparison with other BNCT facilities. Ther Radiol Oncol 13:135–146
34. Hall EJ, Novak JK, Kellerer AM et al (1975) RBE as a function of neutron energy. I. Experimental observations. Radiat Res 64:245–255
35. Heber E, Trivillin VA, Nigg D et al (2004) Biodistribution of GB-10 ($Na_2{}^{10}B_{10}H_{10}$) compound for boron neutron capture therapy (BNCT) in an experimental model of oral cancer in the hamster cheek pouch. Arch Oral Biol 49:313–324
36. Heber EM, Trivillin VA, Nigg DW et al (2006) Homogeneous boron targeting of heterogeneous tumors for boron neutron capture therapy (BNCT): chemical analyses in the hamster cheek pouch oral cancer model. Arch Oral Biol 51:922–929
37. Hiratsuka J, Fukuda H, Kobayashi T et al (1991) The relative biological effectiveness of B-10-neutron capture therapy for early skin reaction in the hamster. Radiat Res 128:186–191

38. Hopewell JW, Morris GM, Coderre JA (1994) Determination of radiobiological parameters for the safe clinical application of BNCT. In: Auterinen I, Kallio M (eds) Proceedings of the CLINCT BNC T Workshop. Helsinki University of Technology Report TKK-F-A718, pp 86–93
39. Hopewell JW, Benczik J, Mason A (2009) Radiobiology program requirements for boron neutron capture therapy at a nuclear research reactor. In: Sauerwein WAG, Moss RL (eds) Requirements for boron neutron capture therapy (BNCT) at a nuclear research reactor. European Commission Joint Research Centre, Institute for Energy, Petten, The Netherlands pp 50–61
40. Huiskamp R, Gavin PR, Coderre JA et al (1996) Brain tolerance in dogs to boron neutron capture therapy with borocaptate sodium (BSH) or boronophenylalanine (BPA). In: Mishima Y (ed) Cancer neutron capture therapy. Plenum Press, New York, pp 591–596
41. Imahori Y, Ueda S, Ohmori Y et al (1998) Fluorine-18-labeled fluoroborono-phenylalanine PET in patients with glioma. J Nucl Med 39:325–333
42. Javid M, Brownell GL, Sweet WH (1952) The possible use of neutron-capturing isotopes such as boron 10 in the treatment of neoplasms. II. Computation of the radiation energies and estimates of effects in normal and neoplastic brain. J Clin Invest 31:604–610
43. Jirtle RL, DeLuca PM, Hinshaw WM et al (1984) Survival of parenchymal hepatocytes irradiated with 14.3 MeV neutrons. Int J Radiat Oncol Biol Phys 10:895–899
44. Joel DD, Fairchild RG, Laissue JA et al (1990) Boron neutron capture therapy of intracerebral rat gliosarcomas. Proc Natl Acad Sci USA 87:9808–9812
45. Kiger JL, Kiger WS 3rd, Riley KJ et al (2008) Functional and histological changes in rat lung after boron neutron capture therapy. Radiat Res 170:60–69
46. Kreimann EL, Itoiz ME, Longhino L et al (2001) Boron neutron capture therapy for the treatment of oral cancer in the hamster cheek pouch model. Cancer Res (Advances in Brief) 61:8638–8642
47. Kreimann EL, Miura M, Itoiz ME et al (2003) Biodistribution of a carborane-containing porphyrin as a targeting agent for boron neutron capture therapy of oral cancer in the hamster cheek pouch. Arch Oral Biol 48:223–232
48. Mansfield C, Hopewell JW, Beynon TD et al (2001) A biological comparison of neutron beams used for BNCT research. In: Hawthorne F et al (eds) Frontiers in neutron capture therapy. Kluwer Academic/Plenum Publishers, New York, pp 407–411
49. Mason AJ (2005) A comparison of epithermal neutron beams for BNCT. Ph.D. thesis, University of Birmingham, Birmingham
50. Mason AJ, Giusti V, Green S et al (2011) Interaction between the biological effects of high- and low-LET radiation dose components in a mixed field exposure. Int J Radiat Biol 87:1162–1172
51. Matalka KZ, Bailey MQ, Barth RF et al (1993) Boron neutron capture therapy of intracerebral melanoma using boronophenylalanine as a capture agent. Cancer Res 53:3308–3313
52. McNally NJ, de Ronde J, Hinchliffe M (1984) The effect of sequential irradiation with X-rays and fast neutrons on the survival of V79 Chinese hamster cells. Int J Radiat Biol Relat Stud Phys Chem Med 45:301–310
53. McNally NJ, de Ronde J, Folkard M (1988) Interaction between X-ray and α-particle damage in V79 cells. Int J Radiat Biol Relat Stud Phys Chem Med 53:917–920
54. Millar WT, Hopewell JW (2007) Effects of very low dose-rate $^{90}Sr/^{90}Y$ exposure on the acute moist desquamation response of pigskin: comparison based on predictions from dose fractionation studies at high dose rate with incomplete repair. Radiother Oncol 83:187–195
55. Mishima Y, Ichihashi M, Nakanishi T et al (1983) Cure of malignant melanoma by single thermal neutron capture treatment using melanoma seeking compounds: 10B/melanogenesis interaction to in vitro/in vivo radiobiological analysis to preclinical studies. In: Fairchild RG, Brownell G (eds) Proceedings of the first international symposium on neutron capture therapy. Brookhaven National Laboratory, Upton, pp 355–364
56. Mishima Y, Imahori Y, Honda C et al (1997) In vivo diagnosis of human melanoma with positron emission tomography using specific melanoma-seeking ^{18}F-DOPA analogue. J Neurooncol 33:163–169

57. Miura M, Joel DD, Smilowitz HM et al (2001) Biodistribution of copper carboranyltetraphenylporphyrins in rodents bearing an isogeneic or human neoplasm. J Neurooncol 52:111–117
58. Morgan GR, Mill AJ, Roberts CJ et al (1988) The radiobiology of 24 keV neutrons. Measurement of the relative biological effect free-in-air, survival and cytogenetic analysis of the biological effect at various depths in a polyethylene phantom and modification of the depth-dose profile by boron 10 for V79 Chinese hamster and HeLa cells. Br J Radiol 61:1127–1135
59. Morris GM, Coderre JA, Hopewell JW et al (1994) Response of rat skin to boron neutron capture therapy with p-boronophenylalanine or borocaptate sodium. Radiother Oncol 32:144–153
60. Morris GM, Coderre JA, Hopewell JW et al (1994) Response of the central nervous system to boron neutron capture irradiation: evaluation using rat spinal cord model. Radiother Oncol 32:249–255
61. Morris GM, Coderre JA, Bywaters A et al (1996) Boron neutron-capture irradiation of the rat spinal-cord – histopathological evidence of a vascular-mediated pathogenesis. Radiat Res 146:313–320
62. Morris GM, Coderre JA, Hopewell JW et al (1996) Boron neutron capture irradiation of the rat spinal cord: effects of variable doses of borocaptate sodium. Radiother Oncol 39:253–259
63. Morris GM, Coderre JA, Micca PL et al (1997) Central nervous system tolerance to boron neutron capture therapy with p-boronophenylalanine. Br J Cancer 76:1623–1629
64. Morris GM, Smith DW, Patel H et al (2000) Boron microlocalisation in oral mucosal tissue: implications for boron neutron capture therapy. Br J Cancer 82:1764–1771
65. Morris GM, Coderre JA, Smith DR (2001) A rat model of oral mucosal response to boron neutron capture therapy. In: Hawthorne F et al (eds) Frontiers in neutron capture therapy. Kluwer Academic/Plenum Publishers, New York, pp 1273–1277
66. Morris GM, Coderre JA, Hopewell JW et al (2003) Porphyrin-mediated boron neutron capture therapy: evaluation of the reactions of skin and central nervous system. Int J Radiat Biol 79:149–158
67. Morris GM, Coderre JA, Micca PL et al (2005) Porphyrin-mediated boron neutron capture therapy: a preclinical evaluation of the response of the oral mucosa. Radiat Res 163: 72–78
68. Nelson JS, Liaw LH, Orenstein A et al (1988) Mechanism of tumor destruction following photodynamic therapy with hematoporphyrin derivative, chlorin, and phthalocyanine. J Natl Cancer Inst 80:1599–1605
69. Nievaart VA, Moss RL, Kloosterman JL et al (2006) Design of a rotating facility for extracorporal treatment of an explanted liver with disseminated metastases by boron neutron capture therapy with an epithermal neutron beam. Radiat Res 6:81–88
70. Ono K, Masunaga S, Suzuki M et al (1999) The combined effect of borono phenylalanine and borocaptate in boron neutron capture therapy for SCCVII tumors in mice. Int J Radiat Oncol Biol Phys 43:431–436
71. Packer S, Coderre JA, Saraf S et al (1992) Boron neutron capture therapy of anterior chamber melanoma with p-boronophenylalanine. Invest Ophthalmol Vis Sci 33:395–403
72. Perris A, Pialoglou P, Katsanos AA et al (1986) Biological effectiveness of low energy protons. I. Survival of Chinese hamster cells. Int J Radiat Biol Relat Stud Phys Chem Med 50:1093–1101
73. Phoenix B, Green S, Hill MA et al (2009) Do the various radiations present in BNCT act synergistically? Cell survival experiments in mixed alpha-particle and gamma-ray fields. Appl Radiat Isot 67:S318–S320
74. Pinelli J, Altieri S, Fossati F et al (2001) Operational modalities and effects of BNCT on liver metastases of colon adenocarcinoma. In: Hawthorne F et al (eds) Frontiers in neutron capture therapy. Kluwer Academic/Plenum Publishers, New York, pp 1427–1440
75. Pop LA, Millar WT, van der Plas M et al (2000) Radiation tolerance of rat spinal cord to pulsed dose rate (PDR-) brachytherapy: the impact of differences in temporal dose distribution. Radiother Oncol 55:301–315

76. Rydin RA, Deutsch OL, Murray BW (1976) The effect of geometry on capillary wall dose for boron neutron capture therapy. Phys Med Biol 21:134–138
77. Saris SC, Solares GR, Wazer DE et al (1992) Boron neutron capture therapy for murine malignant gliomas. Cancer Res 52:4672–4677
78. Stone RS (1948) Neutron therapy and specific ionization. Am J Roentgenol Radium Ther 59:771–785
79. Stragliotto G, Fankhauser H, Gutin PH et al (1995) Biodistribution of boron sulfhydryl for boron neutron capture therapy in patients with intracranial tumors. Neurosurgery 36:285–293
80. Trivillin VA, Heber EM, Itoiz ME et al (2004) Radiobiology of BNCT mediated by GB-10 and GB-10 + BPA in experimental oral cancer. Appl Radiat Isot 61:939–945
81. Trivillin VA, Heber EM, Nigg DW et al (2006) Therapeutic success of boron neutron capture therapy (BNCT) mediated by a chemically non-selective boron agent in an experimental model of oral cancer: a new paradigm in BNCT radiobiology. Radiat Res 166:387–396
82. Trivillin VA, Heber EM, Rao M et al (2008) Boron neutron capture therapy (BNCT) for the treatment of spontaneous nasal planum squamous cell carcinoma in felines. Radiat Environ Biophys 47:147–155
83. van der Kogel AJ (1991) Central nervous system radiation injury in small animal models. In: Gutin PH, Leibel SA, Sheline GE (eds) Radiationinjury to the nervous system. Raven, New York, pp 91–111
84. Yang W, Barth RF, Carpenter DE et al (1996) Enhanced delivery of boronophenylalanine for neutron capture therapy by means of intracarotid injection and blood–brain barrier disruption. Neurosurgery 38:985–992
85. Yang W, Barth RF, Rotaru JH et al (1997) Boron neutron capture therapy of brain tumours: enhanced survival following intracarotid injection of sodium borocaptate with or without blood–brain barrier disruption. Int J Radiat Oncol Biol Phys 37:663–672

Tolerance of Healthy Tissues and Ideal Radiation Dose on BNCT

18

Yoshinobu Nakagawa and Teruyoshi Kageji

Contents

18.1 Introduction

Glioblastoma, a poorly differentiated glioma, is considered to be the most malignant and intractable type of brain tumor. It usually grows in the white matter of the cerebrum, and then, it rapidly invades normal brain tissue. Most patients with such an invasive glioma (including anaplastic astrocytoma and low-grade astrocytoma in addition to glioblastoma) are beyond the point of a curative surgical removal of the tumor because of the risk of damage to the surrounding normal brain tissue. Despite aggressive treatment with combined surgery and chemotherapy or high-dose radiation therapy, the median survival of glioblastoma patients is typically 9–10 months, and fewer than 5 % survive for 5 years. It is difficult to control the infiltrating tumor cells, even with ultrahigh-energy radiotherapy, such as proton-beam therapy or heavy-ion radiotherapy because of its characteristic brag peak. Trials of dose escalation using stereotaxic linac radiation, Gamma Knife radiation, or proton-beam

Y. Nakagawa (✉)
Department of Neurosurgery, Kagawa National Children's Hospital,
Kagawa 765-0051, Japan
e-mail: ynakagawa0517@yahoo.co.jp

T. Kageji, M.D.
Department of Neurosurgery, School of Medicine, The University of Tokushima,
Kuramoto-cho 3-18-15, Tokushima 770-8503, Japan
e-mail: kageji@clin.med.tokushima-u.ac.jp

W.A.G. Sauerwein et al. (eds.), *Neutron Capture Therapy*,
DOI 10.1007/978-3-642-31334-9_18, © Springer-Verlag Berlin Heidelberg 2012

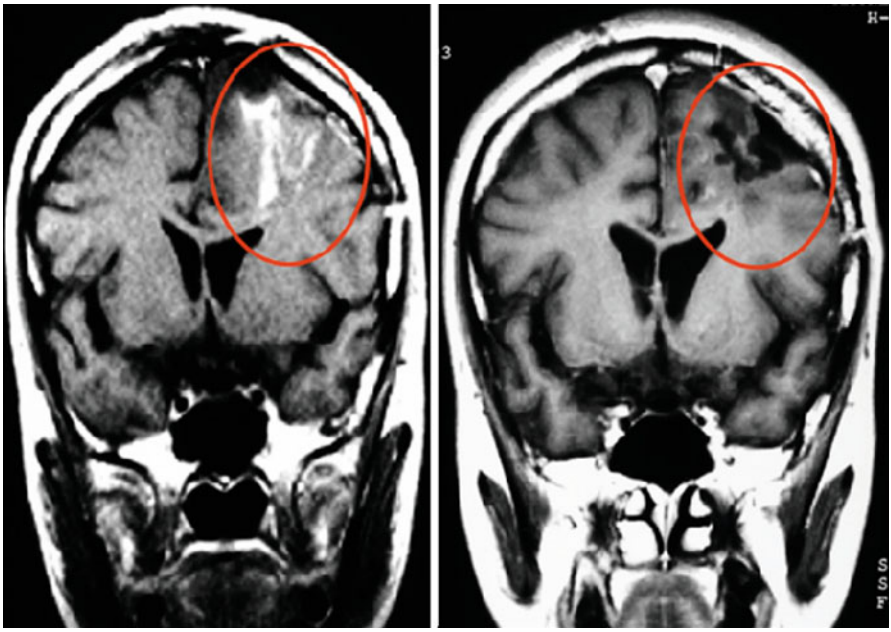

Fig. 18.1 MRI (Gd+) before BNCT (*left*) and 2 years after BNCT (*right*). A 41-year-old female suffered from headache, epileptic seizures, and right hemiparesis. A magnetic resonance image (MRI) showed an enhanced mass in the left parietal lobe. She underwent craniotomy and partial resection of the tumor. The histological diagnosis was glioblastoma. BNCT was performed at KUR in August 1992. The enhanced area (*circle*) demonstrated that the tumor that was present prior to BNCT had completely disappeared after BNCT. There was little damage in the brain parenchyma around the lesion after BNCT

therapy have been conducted in efforts to escalate the tumor volume radiation dose. However, no effective trials have yet been reported. Proton-beam therapy, Gamma Knife therapy, and conventional radiotherapy all employ gamma- or X-ray irradiation. Such radiation beams with low LET are not tumor specific; therefore, high-dose irradiation with low-LET radiation beams produces extensive damage to surrounding normal brain tissue. It is well known that radiation therapy using X-ray or gamma-ray irradiation improves clinical outcome in patients with malignant tumors but also increases the risk of a poor quality of life with chronic neurocognitive effects and functional deficits (Fig. 18.1) [1]. To control invasive and radioresistant tumors such as glioblastomas and anaplastic astrocytomas without severe damage to the normal brain tissue, therapy targeted at the cell level is necessary.

18.2 Clinical Experience – Antitumor Effect

Clinical trials of BNCT were initiated in 1951 at Brookhaven National Laboratory by Sweet and Javid, Javid et al., and Farr et al. [2]. However, the trials were discontinued after 1961 due to discouraging clinical results. The researchers reported that

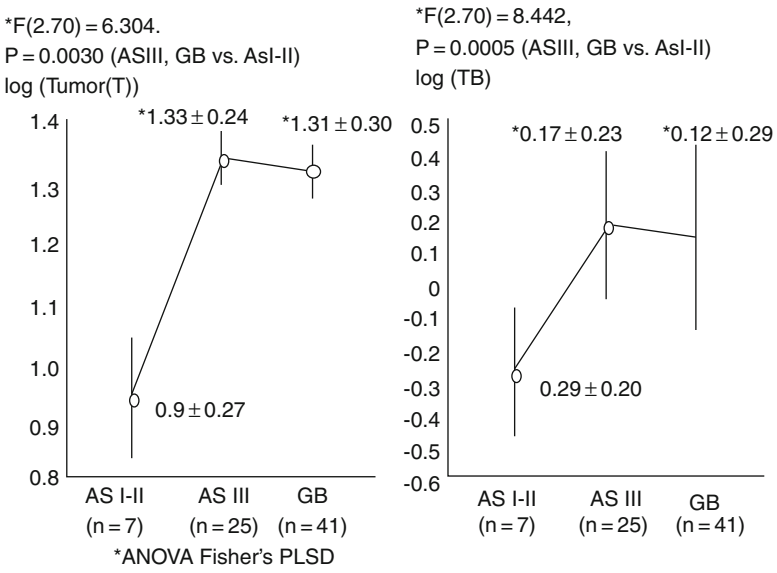

Fig. 18.2 Comparison of the boron uptake in low-grade astrocytoma (*AS I-II*), anaplastic astrocytoma (*AS III*), and glioblastoma (*GB*). There were significant differences between AS III, GB, and AS I-II. Pathologically, the density of the tumor cells of ASIII and GB was much higher than in ASI-II. The findings demonstrated the selective accumulation of BSH in the tumor cells

important factors in their initial failure may have been the contamination of the neutron source, first neutron, and gamma ray as well as the inadequate selectivity of the boron compounds. H. Hatanaka, a member of the original Boston team, identified a new boron compound, sodium-mercaptoundecahydrododecaborate ($Na_2B_{12}H_{11}SH$:BSH). The toxicity, distribution, and the metabolism of BSH were studied by Soloway et al. In 1968, Hatanaka modified the BNCT studied in the United States and resumed BNCT in Japan using BSH [3]. Kageji et al. demonstrated its selective accumulation in tumor tissue using clinical data (Fig. 18.2) [4].

Since 1968, various clinical trials of BNCT were conducted not only in Japan but also in the United States and Europe. Most of the trials (with the exception of our study) focused on how to escalate the radiation dose, including gamma rays. Our concept of BNCT provides for selective destruction of tumor cells using heavy-charged particles yielded up by $^{10}B(n,\alpha)7Li$ reactions. To improve the clinical results, our efforts have therefore concentrated on escalating the dose of alpha particles and recoiling lithium-7(^7Li) in the clinical target volume. The physical dose of the two heavy particles is determined by the neutron fluence at the target point and the boron concentration in the tumor tissue. According to our analysis, the ratio of boron concentration (BSH) in tumor tissue and blood is nearly stable at around 1.2–1.69. The escalation of the radiation dose can be achieved by improving the penetration of the thermal neutron beam. We designed several trials that involved the use of heavy water, whole brain irradiation, and multidirectional radiation with

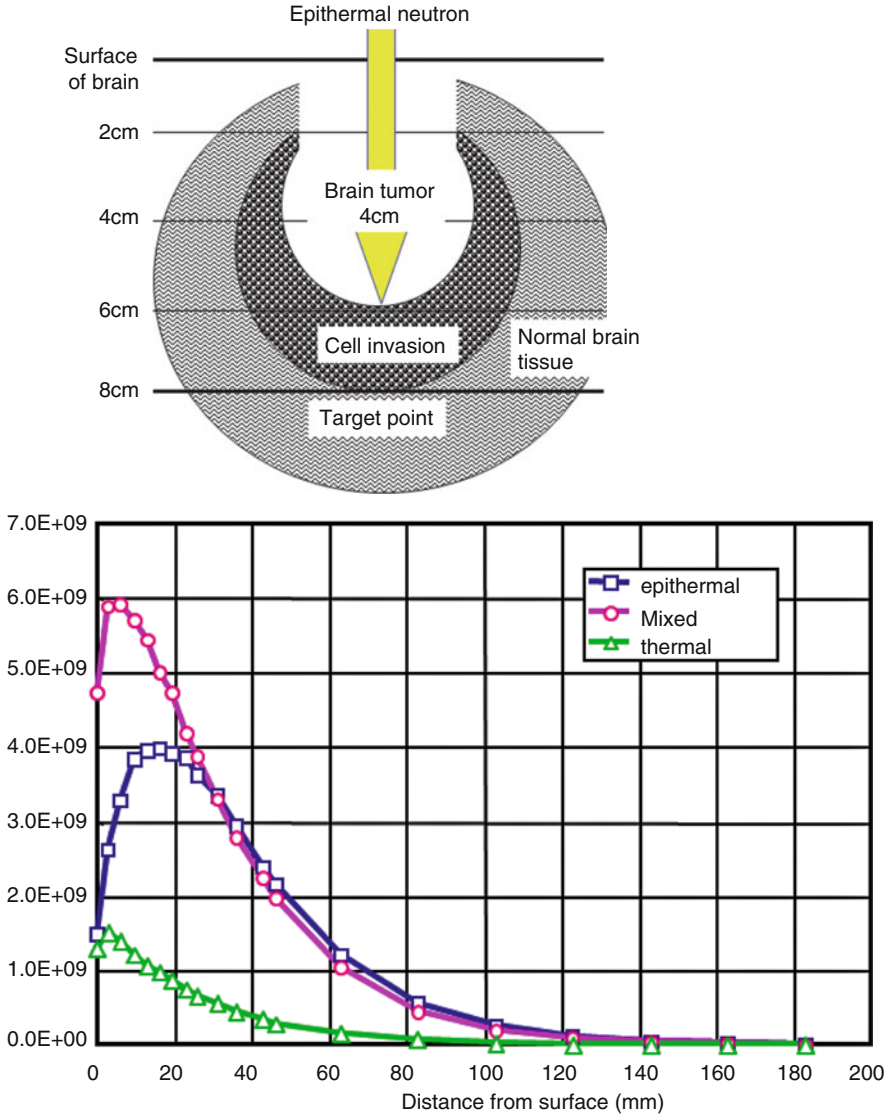

Fig. 18.3 Penetration of neutron beams and the efficacy of debulking surgery. If a brain tumor is grossly debulked and the cavity is filled with air, then epithermal neutrons can reach the base of the cavity without any marked attenuation. The peak of the thermal neutron is located at a depth of from 1–2 cm from the surface of the cavity, which is the target point. The clinical target volume, which includes the zone of cell-level infiltration, can be efficiently radiated

thermal neutrons. We found that creating an air-filled cavity in the cortex by the surgical debulking of the tumor tissue to be the most effective method, and it significantly improved neutron penetration (Fig. 18.3) [5–7]. After a gross total resection of the tumor, we recommend that the clinical target volume is isolated at

Table 18.1 Radiation necrosis and related factors

	Necrosis (+) ($n=19$)	Necrosis (–) ($n=164$)
Age	38.5 ± 19.0	41.8 ± 18.6
Radiation time	254 ± 99	218 ± 108 (min)
B-10 in blood	28.9 ± 9	22 ± 10 (ppm)
Neutron fluences	2.1E ± 0.6	1.7E ± 0.8 (13 n/cm^2)
Maximum vascular dose	21.8 ±8.1	9.4 ± 5.1 (Gy)

2 cm outside the debulking cavity. If the plan is to fill the whole cavity with air and to irradiate it with epithermal neutron beams, the peak of the flux is at a 1–2 cm depth from the surface of the cavity. This layer represents the clinical target volume per se and signifies that the maximum radiation dose will be selectively delivered to the infiltrated tumor cells, thereby providing the most effective and efficient radiation. An alternative strategy is the introduction of epithermal neutrons [8]. As reactors at the Research Reactor Institute of Kyoto University (KUR) and the Japan Atomic Energy Research Institute (JRR-4) came on line, epithermal neutrons became available for medical use. The combination of surgery and irradiation using epithermal neutrons was included in the design of trials aimed at developing new treatment strategies for patients with malignant brain cancer.

18.3 Clinical Experience – Effects on Normal Tissue

The other theme of the clinical trials was the protection of normal brain tissue [9]. We studied all patients in whom radiation necrosis was demonstrated after BNCT. Radiation necrosis was primarily diagnosed by CT and/or MRI. Necrotic findings were determined by low-intensity areas on MRI T1-weighted images with contrast enhancement and high-intensity areas on T2-weighted images. Low-density areas with contrast enhancement on CE-CT also indicated necrosis. The abnormal findings should be newly evident beside the primary tumor. Radiation necrosis was found in 19 patients (19/183 10.4 %). Fourteen of those 19 patients displayed radiographic changes as well as clinical symptoms such as motor weakness and speech disturbance. Five out of those 14 patients had an epileptic seizure within 1 week after BNCT. The remaining five patients displayed only radiographic change without neurological deterioration. Radiation necrosis demonstrated by CT or MRI was observed at 2 months to 2 years after BNCT. Only one glioblastoma patient who underwent two-dimensional radiation showed acute brain swelling 2 weeks after BNCT. There were no significant differences between the two groups (between the patients with necrosis and those without necrosis) in age, radiation time, boron concentration, and maximum neutron fluence. However, the vascular radiation dose, as calculated according to the report of Kitao and Rydin, showed marked differences. The vascular radiation dose of the patients with radiation necrosis was 21 ± 8.1 Gy, while the vascular dose of the patients without radiation necrosis was 9.4 ± 5.1 Gy. After this study, in order to reduce the incidence of radiation necrosis, we decided the maximum vascular dose should be less than 15 Gy in our protocols (Table 18.1).

Table 18.2 Comparison of clinical outcome and tumor volume radiation dose ($n=105$, between 1977 and 1997)

Patient survival	Radiation dose (Gy)	Radiation time (min)
More than 10 years ($n=6$)	18.2 ± 3.3	240 ± 66
More than 5 years ($n=11$)	12.4 ± 3.5	210 ± 76
More than 3 years ($n=12$)	9.8 ± 5.0	252 ± 61
Less than 3 years($n=76$)	9.9 ± 6.0	231 ± 84

The radiation dose is demonstrated by the physical dose of boron n-alpha reaction

Since 1968 in our series in Japan, significant differences between patients with good and poor outcomes were observed with respect to the physical radiation dose and maximum neutron fluence. Six patients out of 105 lived more than 10 years after BNCT. The estimated tumor volume radiation dose in this group was 18.2 ± 3.3 Gy. It was 12.4 ± 3.5 Gy in 11 patients who lived more than 5 years. There were no significant differences between the 12 patients who lived more than 3 years and the 76 patients who lived less than 3 years. There was also no remarkable difference in the radiation time between the groups. We consequently recommended that the ideal radiation dose (physical dose of boron n-alpha reaction) to control glioblastoma should thus be more than 15 Gy (Table 18.2).

We previously reported that gamma rays do not play an important role in BNCT. While gamma and X-rays represent sparsely ionizing radiation with low LET values (gamma rays, LET = 0.3 keV/μm; 250 kV X-rays, LET = 0.3 keV/μm), the two heavy-charged particles have high LET values (α particle, 1.47 MeV, range = 7.5 μm, average LET = 196 keV/μm; Li^+ ion, 0.84 MeV, range = 5.2 μm, average LET = 162 keV/μm), thus suggesting that the biological effectiveness of the heavy-charged particles is significantly different from that of low-LET radiation. For successful BNCT, a sufficient amount of ^{10}B must accumulate in the tumor cells, and a sufficient dose of thermal neutrons must be radiated on the tumor cells and absorbed by ^{10}B. The RBE was highest when LET was around 100 keV/μm. It is still undetermined whether the efficacy of the heavy-charged particles is attributable to double-strand breakage of DNA after ionizing radiation. For the correct evaluation of the delivered dose in BNCT, it is therefore necessary to differentiate between the physical dose of the heavy particles and gamma rays.

18.4 Future Strategy

To correctly evaluate the delivered dose in BNCT, it is necessary to differentiate between the physical dose of the heavy particles and gamma rays. To assess the efficacy of BNCT and to facilitate effective radiation planning, it is also necessary to estimate and compare the physical dose of charged particles in the gross tumor, clinical target volume, and planned target volume. We expect that, in the future, additional advances in treatment strategies that take advantage of the combination of irradiation with epithermal neutron beams and neurosurgery will allow the radiation dose to be fine-tuned, thereby optimizing the outcomes of patients with

malignant brain tumors. The recent BNCT trend was therefore a return to the older strategy, which escalates gross tumor radiation volume (including gamma rays). This strategy may be a traditional method.

References

1. Mulhern KR et al (2004) Late neurocognitive sequelae in survivors of brain tumors in childhood. Lancet Oncol 5:399–408
2. Sweet HW, Javid M (1952) The possible use of neutron-capturing isotopes such as boron-10 in the treatment of neoplasm. I. Intracranial tumor. J Neurosurg 9:200–209
3. Hatanaka H, Nakagawa Y (1994) Clinical results of long-surviving brain tumor patients who underwent boron neutron capture therapy. Int J Radiat Oncol Biol Phys 28:1061–1066
4. Kegeji T et al (2001) Optimal timing of neutron irradiation for boron neutron capture therapy after intravenous infusion of sodium borocaptate in patients with glioblastoma. Int J Radiat Oncol Biol Phys 51:120–130
5. Nakagawa Y (1994) Boron neutron capture therapy: the past to the present. Int J Radiat Oncol Biol Phys 28:1217
6. Nakagawa Y, Hatanaka H (1997) Boron neutron capture therapy-clinical brain tumor study. J Neurooncol 33:105–115
7. Nakagawa Y et al (2003) Clinical review of Japanese experience with boron neutron capture therapy and a proposed strategy using epithermal neutron beams. J Neurooncol 62:87–99
8. Kageji T et al (2006) Boron neutron capture therapy using mixed epithermal and thermal neutron beams in patients with malignant glioma – correlation between radiation dose and radiation injury and clinical outcome. Int J Radiat Oncol Biol Phys 65:1446–1455
9. Kageji T et al (2006) Correlation between BNCT radiation dose and histopathological findings in BSH-based intra-operative BNCT for malignant glioma. Adv Neutron Capture Ther 2006:35–36

Part VI

Clinical Applications

Clinical Trials in BNCT: A Challenging Task

19

Andrea Wittig and Wolfgang A.G. Sauerwein

Contents

19.1 Introduction

In oncology, scientists are constantly searching to develop innovative, more effective, and less toxic treatments to improve local tumor control, survival of patients, and quality of life. Among many others, Boron Neutron Capture Therapy (BNCT) is one innovative approach to reach this goal.

A. Wittig (✉)
Department of Radiotherapy and Radiation Oncology,
Philipps-University Marburg, Marburg, Germany
e-mail: andrea.wittig@med.uni-marburg.de

W.A.G. Sauerwein
NCTeam, Department of Radiation Oncology, University Hospital Essen,
University Duisburg-Essen, D-45122, Essen, Germany

W.A.G. Sauerwein et al. (eds.), *Neutron Capture Therapy*,
DOI 10.1007/978-3-642-31334-9_19, © Springer-Verlag Berlin Heidelberg 2012

Following positive preclinical investigations, clinical trials are essential in the developmental process of innovative approaches, to prove a new treatment safe and efficient. To ensure protection of research subjects, the conduction of clinical trials is strictly regulated by national laws based on international guidelines. These complex rules were primarily developed for investigating new drugs but have been extended to medicinal products and therapeutic procedures for humans in a general way including "advanced therapies." The trial strategy to develop a new treatment has been well established for drugs. However, a clear design for clinical trials to test and implement binary treatment modalities such as BNCT is missing [1].

The main distinctions between conventional therapies and BNCT are the following:

1. The treatment concept of BNCT varies fundamentally from conventional therapies. Current radiooncological techniques optimize the dose distribution by applying the radiation of the beam as conformal as possible to the tumor (selective damage to the tumor by ballistic precision). On the contrary, BNCT can irradiate an extended area where microscopic disease is expected. The selective damage to the tumor cells is not achieved by the direct action of the primary beam but is obtained by the neutron capture reactions releasing high-LET particles where ^{10}B atoms are present. The therapeutic effect occurs only when the ^{10}B atoms, delivered to the tumor by a dedicated compound, are irradiated with thermal neutrons [1, 2].
2. The binary nature of the BNCT treatment principle requires investigation of a compound susceptible of targeting tumor cells however without an own therapeutic effect. Such boron carrier must go through standard clinical testing like all other investigational drugs; however, conventional methods to test such compound are not strictly applicable [1].
3. Standards for prescribing and reporting the irradiation dose are missing as are standards reporting on the concentration and distribution of boron and/or boron compounds. Very different methods with certainly different end points exist to measure the boron concentration and boron distribution. All such methods deliver valuable but often fundamentally differing information and cannot be easily compared. Also, not all of these methods are valuable for clinical decisions, e.g., as they are too demanding, and it takes days to weeks until results are available.
4. BNCT uses an irradiation beam that is not established for clinical practice and that produces a complex dose distribution with high- and low-LET components.
5. To date, an epithermal neutron beam with a fluence, which is necessary for BNCT, can only be produced by a nuclear reactor. This involves the use of technical equipment that is not aimed for clinical applications and which may thus need special licensing.
6. Most irradiation facilities are not hospital-based and not located in a medical environment but located at research sites, e.g., at a research reactor.
7. Radiation facilities and beams used for BNCT to date differ considerably not only from facilities and beams used for conventional radiotherapy, but beams used for BNCT also differ among themselves. These differences complicate the

conduction of multicenter trials, which will be necessary at a certain point in the developmental process of BNCT.

8. In spite of a large number of preclinical investigations, data often lack consistency and comparability. Early preclinical and clinical investigations were not conducted according to today's standards (e.g., GMP); therefore, results of such investigations must be interpreted with care, especially when used as basis for developing trial concepts.
9. To date, commercial companies show modest interest in drug development and technological developments related to BNCT as the method is still quite far from being judged for superiority against current standard treatments. Drug development, however, usually conducted by the pharmaceutical industry needs specialized facilities and financial resources.
10. Beneath the special characteristics of the therapeutic principle, the design of clinical trials in BNCT is challenged by the highly complex and interdisciplinary nature of BNCT, which requires expertise in many fields such as neutron physics, (boron) chemistry, radiobiology, radiooncology, specialized analytical methods, and pharmacology. Such knowledge is usually available at selected academic institutions only. BNCT also needs expertise of specialists (e.g., nuclear physicists) who are not used to work in the medical field or even in clinical trials.
11. As BNCT can be offered at selected institutions only, patients often travel long distances to be treated, which complicates the issue of timely, qualified, and well-documented recruitment but also follow-up of patients. Cooperation across state borders could be established in some clinical projects, which however require respecting national laws of all countries involved and also sometimes lead to linguistic barriers especially for patients.

These aspects make clinical trials in BNCT a challenging task for the scientists as well as for the regulatory authorities. Innovative clinical trial designs are necessary in conjunction with innovative organizational and administrative concepts and a strict quality assurance to meet these challenges. Additionally, in-depth training of all staff involved is required. Multidisciplinary and international cooperation is highly desirable and economic.

In the last years, efforts were already made to develop clinical trial strategies aiming to mature BNCT to a treatment modality. The following chapters describe ideas and possible solutions to cope with the described challenges.

19.2 Design of Clinical Trials

Cancer clinical trials include research in different phases. After successful preclinical studies, a new treatment is evaluated through a series of clinical trials, methodologically built, to test safety and efficacy. Clinical trials involving new drugs are commonly classified into four constitutive phases [3]. The development process usually proceeds through all four phases, and if it passes successfully through phases 0–III, a drug will be approved by the National Regulatory Authority for use in the general population. Due to the binary nature of BNCT,

Table 19.1 Phases of clinical research in BNCT with a newly developed ^{10}B compound

Phase	Main end points
Phase 0_{DRUG} ("translational research")	Selective accumulation of ^{10}B as delivered by the compound in the tumor (surrogate end point) as a first in human proof of principle in subtherapeutic dosing, pharmacokinetics, pharmacodynamics
Phase I_{DRUG}	Tolerability and safety of the drug in (near-)therapeutic doses, selective accumulation of ^{10}B as delivered by the compound in the tumor and in normal tissues, pharmacokinetics, pharmacodynamics
Phase I_{BNCT}	Tolerability and safety of a combination of the compound with neutron irradiation (BNCT), dose finding first with subtherapeutic but ascending doses (dose escalation of the compound dose and/or the irradiation dose)
Phase II_{BNCT}	Efficacy of BNCT at therapeutic doses of the drug and of the irradiation dose, determination of the optimal dosing (drug and irradiation), antitumor effect
Phase III_{BNCT}	Therapeutic effect of BNCT as compared the standard treatment

we propose to adapt these testing phases as specified in Table 19.1 to closely follow established standards but to additionally consider the specific needs for BNCT.

19.2.1 Preclinical Studies

The design and conduction of clinical trials must rely on preclinical data. Therefore, the preclinical phase is decisive for the success of a new treatment option.

Before any new treatment is made available for investigations in patients, it must be tested on cell cultures and on animals. Drug development encompasses the entire process of compound discovery and all steps necessary to take a selected chemical through all required preclinical tests (phase 0: compound synthesis, characterization, analysis; phase 1: short-term toxicity studies, first pharmaceutical studies in animals, complete chemical evaluation, preformulation studies, in vitro and in vivo tests to determine toxic and pharmacological effects, genotoxicity, drug absorption, metabolism and toxicity of metabolites, speed of excretion of the drug and metabolites; phase 2: start of human testing) before it is allowed to be investigated in humans. The set of preclinical tests necessary is highly standardized and regulated by law and is usually conducted by the pharmaceutical industry. Only when these studies suggest that the treatment is safe, it is then tested in clinical trials with patients.

The compounds sodium mercaptoundecahydro-*closo*-dodecaborate (BSH, $Na_2{}^{10}B_{12}H_{11}SH$) [4] and L-*para*-boronophenylalanine (BPA, $C_9H_{12}{}^{10}BNO_4$) [5] have been developed and tested long before these strict regulations came into place. Therefore, results of early preclinical and clinical investigations concerning both compounds must be interpreted with care, and some essential information is still missing, e.g., concerning the metabolism of both compounds. Despite these facts,

today, both compounds are usually allowed to be used as experimental drugs in clinical trials as quite some information in humans already exists (see Chap. 8).

If however new compounds are designed and tested for BNCT in an academic environment, it is highly recommended that tests at a very early stage of development are conducted according to the established rules for preclinical testing, as further investigation of a promising compound would otherwise be severely delayed.

19.3 Clinical Studies

19.3.1 Phase 0

A phase 0 clinical trial usually investigates pharmacodynamics and pharmacokinetics of a new drug in very small, subtherapeutic doses.

For BNCT, the compound should additionally be tested for selective uptake in the selected tumor entity in the sense of a proof of principle. The surrogate end point (^{10}B concentration) facilitates the testing process enormously. However, it does not eliminate the need for a standard phase I trial evaluating the toxicity of the combination of drug and irradiation in BNCT. This is especially true as the combined biological effects of a heterogeneous ^{10}B distribution and an irradiation containing low- and high-LET components can solely be investigated in trials involving irradiation [1].

The trial design streamlines testing such characteristics early in the development, thus preventing therapeutic failures during costly BNCT trials, which involve irradiation of patients [2]. One example for such trial design is the EORTC trial 11001, which is a prospective translational research/phase 1 clinical trial. The trial aims to identify tumor entities that may be treated with BNCT by demonstrating a selective uptake of the compounds sodium mercaptoundecahydro-closo-dodecaborate (BSH) or para-boronophenylalanine (BPA) or both compounds [2, 6]. The amount of the drugs infused in such trial must be below the dose at which toxic events are expected. The evaluation of toxicity is however a decisive part of such trial. In an early clinical trial without therapeutic intent, the number of patients must be kept to a minimum. The low number of patients allows descriptive statistics only, which is also common to phase I clinical trials.

Trials including translational research are sometimes termed as phase V.

19.3.2 Phase I

Phase I trials are designed to investigate pharmacovigilance and dose ranging in often subtherapeutic doses in a higher number of patients (20–100).

In BNCT, first, a phase I_{DRUG} trial should be conducted to test the tolerability and safety of the drug alone in (near-)therapeutic doses and should deepen knowledge on selective accumulation of ^{10}B as delivered by the compound in the tumor but also in normal tissues as this is decisive for side effects. Further end points would be pharmacokinetics (necessary especially for timing of drug application and irradiation) and pharmacodynamics of the new drug.

In a subsequent phase I_{BNCT} trial, tolerability and safety of a combination of the new compound with neutron irradiation (BNCT) are first evaluated. Such trial aims also at a dose finding first with subtherapeutic but ascending doses, while dose escalation of the drug and/or of the irradiation dose are possible and should be decided on considering the characteristics of the drug.

19.3.3 Phase II

A phase II trial investigates whether a new drug has any efficacy at the therapeutic dose. Efficacy is usually tested in 50–300 patients.

A phase II trial of BNCT would therefore determine the efficacy a BNCT treatment at therapeutic doses of the drug and at a therapeutic irradiation dose concerning the antitumor effect. Optimal dosing (concerning drug and irradiation) and timing are still to be established in specifically designed parts of the study in this phase. In BNCT clinical research, trials in this phase would often be designed as case series to test safety and activity of BNCT with the respective drug in a selected group of patients.

19.3.4 Phase III

Phase III is often randomized controlled multicenter trials to definitely determine the therapeutic effect of the new treatment in comparison to the current treatment standard in a large group of patients (200–3,000 or more).

A phase III trial would therefore investigate the therapeutic effect of BNCT comparing such treatment with the current "golden standard" anticancer treatment. Currently, investigations related to BNCT worldwide have not yet reached this phase. Due to patient numbers, long duration, and difficulties concerning the treatment facilities, such trial would be most expensive and time-consuming to run. Questions concerning an international standard for describing the ^{10}B concentration and ^{10}B distribution as well as prescribing and reporting the irradiation dose would need to be solved before a multicenter trial is possible. Differences in radiation beams would still exist and should be considered when results of different centers are compared. In the current situation with only very few facilities, running conduction of a phase III trial is hardly possible; therefore, the development of new hospital- and accelerator-based facilities are a decisive step toward a clinical development of the method. For reference of trial methodology the following websites may be consulted: www.wikipedia.org/wiki/clinical_trial and www.who.int/ictrp/en and www.eortc.be

19.4 Laws and Regulations

All clinical trials must comply with international guidelines such as the guidelines of International Conference on Harmonisation of Technical Requirements for Registration of Pharmaceuticals for Human Use (ICH) [7], e.g., the rules for good clinical practice (guideline E6(R1)), and all applicable directives and national laws,

e.g., The Rules Governing Medicinal Products in the European Union [8] (equally regulatory guidance of the US Food and Drug Administration) [9]. Clinical trials are closely supervised by appropriate regulatory authorities.

According to our experience, it is very useful to include regulatory authorities already in the discussion of the trial concept and continuously during the process of writing the trial protocol and conducting the trial, especially if transnational scientific cooperation is aimed to be established. The time period needed until regulatory and administrative rules are set must not be underestimated and can be shortened through continuous cooperation with regulatory authorities.

It is highly recommended to register trials at ClinicalTrials.gov, which is the largest clinical trials registry and searchable database of clinical trials run by the United States National Library of Medicine at the National Institutes of Health.

19.5 Ethical Conduct

Each clinical trial must follow ethical rules (e.g., Declaration of Helsinki) and must be approved by an ethics committee before permission is granted to run the trial. To be ethic, detailed informed consent is necessary from each patient before he/she is included in the trial.

Often, subjects included in BNCT clinical trials are in exceptional circumstances (life-threatening disease, sometimes terminal phase of life, patients participating for altruistic reasons), which can lead to ethical questions that have been answered quite differently by research groups/ethics committees in the past. Such questions can arise especially as BNCT is still an experimental treatment option, as BNCT in some concepts contains procedure that can cause severe side effects, e.g., special surgical procedures, liver transplantation, re-irradiation, and heavily pretreated patients.

There are also ethical concerns associated with conducting very early-phase clinical trials, including the risk-benefit ratio and the lack of treatment intent. The risk for patients can be reduced by very limited drug exposure, which is below the no observable adverse effect level (NOAEL = Highest Dose Administered Without any Toxicity), whereas the critical proof of principle and data on pharmacokinetics and distribution can still be gained. Such data help the design of more elaborated trials, which are based on early clinical data rather than on animal models [2].

It is the responsibility of each clinical research group and each individual investigator in cooperation with the local ethics committee to plan and conduct such trials following international standards and in the best possible and most responsible way to ensure that the rights and safety of trial subjects are protected. This also includes careful documentation of all procedures, careful follow-up of patients even if they live at distance, and timely publication of results.

19.6 Safety and Quality Assurance

Some of the above mentioned challenges can be faced by implementing a strict quality assurance system, which is however essential in all clinical trials.

The clinical trial protocol plays a central role in the process of planning, conducting, evaluating, and publishing clinical trials. The protocol is used to gain confirmation of the trial design and adherence by all study investigators, even if conducted in various centers or countries. The protocol covers the trial design and the informed consent and defines the statistical power. The format and content of clinical trial protocols in the United States, European Union, Japan, Canada, and Australia have been standardized to follow Good Clinical Practice guidance (guideline E6(R1)) issued by the International Conference on Harmonisation of Technical Requirements for Registration of Pharmaceuticals for Human Use (ICH) [7].

As most irradiation facilities are not hospital-based and not located in a medical environment, but on research sites, such facilities must be equipped with all medical equipment needed for patient treatments to handle medical emergencies. Further, medical and nonmedical staff must be trained accordingly to manage regular and emergency treatments. Excellent cooperation with an academic hospital located close to the research site as well as agreements concerning patient transportation is mandatory.

Training of staff is also of utmost importance to understand the specific terminology and needs of all disciplines involved, e.g., medical staff, medical physicist, nuclear physicists, reactor operators, and in some cases security guards.

The installation of research-oriented coordinating and support structures might facilitate the conduction of trials across national borders. As the scientific community experienced in BNCT is rather small and as the regulatory requirements are increasing, cooperation between scientists becomes tremendously important if BNCT is to be further developed. Of utmost importance is also systematic training and continuing education of all scientists involved – not only of the clinical investigators but also of scientists of other disciplines. Such training ensures scientifically sound and safe patient treatments as well as reliable follow-up investigations.

References

1. Wittig A, Collette L, Moss R, Sauerwein WA (2009) Early clinical trial concept for boron neutron capture therapy: a critical assessment of the EORTC trial 11001. Appl Radiat Isot 67(7–8 Suppl):S59–S62
2. Wittig A, Collette L, Appelman K, Buhrmann S, Jackel MC, Jockel KH et al (2009) EORTC trial 11001: distribution of two 10B-compounds in patients with squamous cell carcinoma of head and neck, a translational research/phase 1 trial. J Cell Mol Med 13(8B):1653–1665
3. Sauerwein W, Zurlo A (2002) The EORTC Boron Neutron Capture Therapy Group: achievements and future perspectives. Eur J Cancer 38 Suppl 4 S31–34
4. Soloway AH, Hatanaka H, Davis MA (1967) Penetration of brain and brain tumor. VII. Tumor binding sulfhydryl boron compounds. J Med Chem 10:714–717
5. Snyder HR, Reedy AJ, Lennarj WJ (1958) Synthesis of aromatic boronic acids. Aldehyde boronic acids and a boronic acid analog of tyrosine. J Am Chem Soc 80:835–838
6. Wittig A, Malago M, Collette L, Huiskamp R, Buhrmann S, Nievaart V et al (2008) Uptake of two ^{10}B-compounds in liver metastases of colorectal adenocarcinoma for extracorporeal irradiation with boron neutron capture therapy (EORTC Trial 11001). Int J Cancer 122(5):1164–1171
7. ICH. http://ec.europa.eu/enterprise/pharmaceuticals/eudralex/eudralex_en.htm. Accessed on 2012
8. European Commission. The rules governing medicinal products in the European Union. http://ec.europa.eu/enterprise/pharmaceuticals/eudralex/eudralex_en.htm. Accessed on 2012
9. U.S. Food and Drug Administration, regulatory guidance. Research List of Guidance Documents. http://www.fda.gov/Drugs/GuidanceComplianceRegulatoryInformation/Guidances/ucm310704.htm. Accessed on 2012

External Beam BNCT for Glioblastoma Multiforme

20

Tetsuya Yamamoto and Akira Matsumura

Contents

20.1 Introduction

The clinical data show that the external beam BNCT appeared to be effective for the adjuvant treatment of newly diagnosed GBM after tumor resection. The optimization of dosage and of boron delivery agents, the combined use of different boron agents, and the combination of BNCT with other therapeutic modalities have been studied for the purpose of improving BNCT. The need for better evidence-based data, either through randomized trials or by using the prospective case control methodology, is clear from reviewing these clinical reports.

T. Yamamoto, M.D., Ph.D. (✉)
Department of Neurosurgery and Radiation Oncology,
Faculty of Medicine, University of Tsukuba,
1-1-1 Tennohdai, 305-8575, Tsukuba, Ibaraki, Japan
e-mail: yamamoto.neurosurg@gmail.com

A. Matsumura, M.D., Ph.D.
Department of Neurosurgery, Faculty of Medicine, University of Tsukuba,
1-1-1 Tennohdai, 305-8575, Tsukuba, Ibaraki, Japan

W.A.G. Sauerwein et al. (eds.), *Neutron Capture Therapy*,
DOI 10.1007/978-3-642-31334-9_20,

20.2 Multimodal Treatment for Newly Diagnosed GBM

GBM, a common type of incurable malignant brain tumor in adults, shows rapid tumor growth and wide-spreading invasion to the surrounding normal brain tissue. Despite the recent improvements in multimodal therapies that include surgery, radiotherapy, and chemotherapy, GBM easily recurs and continues to have a median overall survival time (OS) of less than 1.5 years.

Several emerging therapeutic modalities for selected patients have achieved rather small survival benefits for patients with GBM, for which the overall survival (OS) is still less than 2 years. Image-guided surgery utilizing fluorescence with 5-aminolevulinic acid, neuronavigation, and intraoperative magnetic resonance imaging (MRI) have enabled more complete resections of the contrast-enhancing part of the tumor, resulting in prolongation of the postoperative survival time [1, 2]. Concomitant and adjuvant use of temozolomide with standard photon radiotherapy has demonstrated a significant survival advantage compared to radiotherapy alone with minimal additional toxicity. The median OS was 14.6 months with temozolomide plus radiotherapy and 12.1 months with radiotherapy alone [3]. Approximately 25 % of the patients who received temozolomide plus radiotherapy survived 24 months. Bevacizumab, humanized immunoglobulin G1 monoclonal antibody to vascular endothelial growth factor, has been shown to have activity in malignant gliomas when combined with irinotecan. Some recent studies have shown that the combination of bevacizumab and irinotecan is an effective treatment for recurrent GBM and has moderate toxicity [4–6].

20.3 Rationale for BNCT

Randomized trials of postoperative fractionated photon radiation at a total dose of 45–60 Gy have demonstrated a significant improvement in survival time [7–12]. However, failure pattern analyses have revealed an 80–90 % incidence of local recurrence due to the presence of microscopic invading cells at distances of 2–3 cm [13, 14]. Favorable results were seen in some dose-escalation studies, which involved dose escalation for the main tumor mass rather than the infiltration area using additional stereotactic radiosurgery, fractionated proton beam radiation, or other conformal radiotherapy techniques [15–19]. Fitzek et al. reported that a dose of 90 Gy in accelerated fractionation with photon and proton irradiation could provide a very high rate of tumor control in the central lesion, extending the median survival time (MST) of GBM patients treated by this modality to 20 months. However, recurrence often occurred in the 70–80 Gy volume, and radiation necrosis also frequently occurred [19].

There is no doubt that the external beam photon radiation fails to address the microscopic invading GBM cells [20]. Extensive therapy sufficient to cover microscopic invasion into the healthy brain tissue such as surgical resection or high-dose radiations inevitably leads to some degree of posttherapeutic neurological deterioration [21].

There is an urgent need for a method that can deliver tumor-cell-selective high-dose radiotherapy to an extended target area encompassing the microscopic invasion while avoiding radiation damage to the surrounding normal brain tissue in this incurable disease.

20.4 Technical Aspects

1. Boron Compound
   Two boron delivery agents are available and have been used in recent clinical BNCT trials of newly diagnosed GBM, BPA, and BSH. BPA has been used in all recent external beam clinical BNCT trials for GBM except in EORTC phase I trial 11961, in which BSH was administered prior to 4 fractions of BNCT on 4 consecutive days [22, 23]. An average blood boron dose of 30 μg/g during neutron irradiation was used in BSH-mediated BNCT, while 10–30 μg/g was used in BPA-mediated BNCT (Table 20.1).

   BPA is actively transported through the tumor cell membrane due to the elevated rate of amino acid transport in proliferating cells [34, 35]. Although the uptake of BPA highly depends on individual tumors, high tumor-to-normal-BPA-uptake ratios (2.1–7.1) were demonstrated in the ^{18}F-BPA-PET study of newly diagnosed GBMs [32]. Crystallization in the urine, oliguria, renal failure, and fever are possible adverse effect of BPA injection.

   BSH biodistribution studies have suggested that the primary mode of BSH distribution is passive diffusion from blood to tumor tissue via the disrupted blood–brain barrier. Tumor-to-blood boron concentration ratios of 0.5–1.0 have been reported in human patients treated with BSH-mediated BNCT [22, 36]. Vascular irritation, fever, skin reaction (erythema), and peripheral vasoconstriction have been reported as probable adverse effects of BSH injection [22, 33].
2. Epithermal Neutrons
   An epithermal (high-energy) neutron beam is essential for external beam, closed-cranium BNCT and was first applied at the BNL. The epithermal neutrons are moderated in scalp and cranial tissue to become thermal (low-energy) neutrons that can be captured more efficiently by ^{10}B nuclei. The epithermal neutron beam has been used for clinical trials for GBM at the FiR1 clinical reactor of the Finnish BNCT center, MITR-II of MIT in the USA, the High Flux Reactor (HFR) Petten in the Netherlands, the Studsvik facility in Sweden, the LVR-15 reactor at the Nuclear Research Institute in Rez, Czech Republic, and JRR-4 of the JAEA and the Kyoto University Reactor (KUR) in Japan [37].
3. Longer Perfusion of BPA
   Preclinical data suggest that a longer infusion time may improve the homogeneity of boron accumulation in tumors in BPA-mediated BNCT [35, 38, 39]. The long-term infusion method was applied in a Swedish clinical trial (900 mg/kg for 6 h), where the average boron concentration in blood was 24.7 μg/g [30].

Table 20.1 Summary of external beam BNCT clinical trials for newly diagnosed GBM currently or recently completed

Trial (references)	Number of evaluated patients (year), median age of patients	Boron drug: dose, infusion time	Average blood ^{10}B level (μg/g)	Normal brain dose[a] peak/ave. (Gy)	Minimum tumor dose in GTV[a] (Gy)	Median survival (months)	Neutron irradiation (photon radiation)	Reactor
BNL, phase I/II [24, 25]	53 (1994–1999), (56.5 years for 1 field)	BPA: 250–330 mg/kg, 2 h	12–16	8.4–14.8/1.8–8.5	18–55 (data from 38 of 53 subjects)	13 (1 field: 14.8, 2 fields: 12.1, 3 fields: 11.9)	Single fraction (no)	BMRR, BNL, USA
Harvard/MIT, phase I [26, 27]	20 (1997–1999)[b], 56 years	BPA: 250–350 mg/kg, 1–2 h	10–12	8.7–16.4/2.7–7.4	7.3–24.8	12	1 or 2 fractions (no)	MITR-II, M-67, MIT, USA
EORTC 11961, phase I [23]	26 (1997–2002), 58 years	BSH: 100 mg/kg/min	30[c]	8.6–11.4 Gy (physical boron dose) /ND	ND	13.2 for 10.4 Gy cohort[d]	4 fractions (no)	HFR, Petten, the Netherlands
University of Helsinki and VTT, phase I/II [28, 29]	30 (1999–2005), 55.5 years for 18pts	BPA: 290–500 mg/kg, 2 h	ND	8.1–13.5/3–6 Gy	ND	21.9 for 450 mg/kg cohort	Single fraction (no)	Fir1, Helsinki, Finland
Studsvik, phase II [30]	29 (2001–2003), 53 years	BPA: 900 mg/kg, 6 h	24.7	7.0–15.5/3.3–6.1 Gy	15.5–54.3	14.2[e]	Single fraction (no)	Studsvik AB Sweden
NRI Rez, phase I [31]	5 (2001–)	BSH:100 mg/kg, 1 h	~20–30	14.2 >/ 2 Gy	ND	ND	Single fraction (no)	LVR-15, NRI Rez, Czech Republic

Osaka Medical College, phase II [32]	10 (Protocol 1: 2002–2004), 59 years 11 (Protocol 2: 2004–2006), 47.5 years	BPA:250 mg/kg, 1 h BSH:100 mg/kg, 1 h BPA:700 mg/kg, 6 h BSH:100 mg/kg, 1 h	61 for BPA and BSH	Prescribed peak dose 13 Gy > Prescribed peak dose 15 Gy >	16.3–63.0 26.9–65.4	14.1 M 23.5	Single fraction (no) Single fraction (20–30 Gy/10–20 fraction)	KUR, KURRI and JRR-4, JAEA, Japan,
University of Tsukuba and JAEA, phase I/II [33]	8 (1998–2007), 65 years	BPA:250 mg/kg, 1 h BSH:5 g/body,1 h	34.6 for BSH, 17.4 for BPA	8.4–14.1/2.5–3.4	15.5–42.5	27.1/11.9	Single fraction (30 Gy/15 fraction or 30.6 Gy/17 fraction)	JRR-4, JAEA, Japan,

[a]Weighted dose D_w
[b]Includes two melanomas. Patients underwent BNCT at MITR-II, FCB is not included
[c]Four fractions in consecutive days, 100 mg/kg the first day, enough to keep the average blood concentration at 30 μg/g during treatment day 2–4
[d]Mean survival time for the third dose group
[e]Survival time calculated from BNCT treatment. The median interval from histological diagnosis to BNCT was 40 days

The longer perfusion method was also employed in a trial at Osaka Medical College (700 mg/kg for 6 h) [32].

4. Fractionation
   Experimental studies using a rat spinal cord model and a dog brain model revealed that fractionation of BNCT leads to a minor sparing effect of the central nervous system (CNS) [40, 41]. BNCT was performed in a single fraction at BMRR, FiR1, and the Studsvik facility using BPA, a single fraction at LVR-15 using BSH, and in JRR-4 and KUR using BSH and BPA. The fractionation can be used to improve the homogeneous distribution of boron and to split the relatively long irradiation time. In the EORTC 11961 trial in Petten, neutron irradiation was performed using 4 fractions with BSH administration prior each fraction on 4 consecutive days. Two fractions with BPA administration in each fraction on consecutive days were used in the Harvard-MIT trial [37].
5. Combination
   The combination of BPA and BSH was first applied to clinical BNCT for GBM by Miyatake with the intention that these different compounds would accumulate in different subpopulations of tumor cells [42]. The combined use of boron compounds was based on experimental data, which showed different uptake characteristics of the cell-cycle dependency of tumor cells [34, 35]. In an early attempt to use the combination of BPA and BSH, the majority of the estimated boron dose component was derived from BPA. Intravenous injection of BSH (100 mg/kg) followed by injection of BPA (250–700 mg/kg) has caused no severe drug-related toxicity. Further optimization of this method and comparative studies between the combination and single use of boron drugs are needed.
6. Additional Photon Irradiation
   Experimental data suggest that the combination of BNCT and photon radiation leads to significant gains in survival [43]. The additional fractionated photon irradiation at a dose of 20–30 Gy was performed after BSH/BPA-mediated BNCT with a prescribed normal brain peak dose of 13–15 Gy in the clinical situation [32, 33]. Two different protocols for small numbers of patients were well tolerated without any severe acute or subacute adverse events. Although it is not certain whether the additional photon irradiation could play a role in the clinical response to BNCT, the survival of two small cohorts in two different protocols seemed to be favorable (median OS: 23.5 and 27.1 months). Further optimized studies are warranted.
7. Air-Filled Space Method
   An air-filled balloon was used in the early trials to facilitate the transport of thermal neutrons to the deep margins of the tumor bed at MIT [44, 45]. This idea was widely adopted in Japanese intraoperative BNCT. Using this idea, the air-filled space method was attempted in external beam BNCT in which cerebrospinal fluid was replaced by air via an Ommaya reservoir [32].
8. BPA-PET
   In the dose planning of BNCT, the determination of the ^{10}B concentration in the tumor is needed. ^{18}F-labeled positron emission tomography (PET) can be used to calculate the lesion-to-normal (L/N) ratio of BPA for estimating the tumor dose

and to determine whether a patient might be a suitable candidate for BNCT [46]. An apparent linear correlation in tumor uptake has been found between ^{18}F-BPA-PET and ^{11}C-MET-PET, which has been more extensively studied for cancer diagnosis, including GBM [47]. Using the PET data, more precise dosimetry to correlate the clinical responses and radiation dose to the tumor and normal brain may be possible in the near future.

20.5 Clinical Applications

External beam BNCT was initiated in 1994, using BPA-F and epithermal neutrons at the BMRR. In this clinical phase I/II trial, 53 GBMs were irradiated using 1, 2, or 3 irradiation fields to evaluate the safety and effectiveness of external beam BNCT [24, 25]. No severe adverse event was found in relation to a 2-h intravenous injection of BPA-F at a dose of 250–330 mg/kg BPA. BPA precipitates in the urine, which show a potential risk of renal dysfunction, were found in patients receiving 330 mg/kg BPA, suggesting the limitation of the amount of BPA-F that can be given. One of the 17 subjects treated using 2 fields and 4 of the 10 subjects treated using 3 fields had grade 3 radiation toxicity (somnolence with or without motor weakness, expressive aphasia, ototoxicity) based on the Cooperative Group Common Toxicity Criteria and Radiation Therapy Oncology Group (RTOG)/EORTC early and late radiation-related morbidity criteria [25]. An average brain dose of 8 Gy or a larger volume of the brain receiving a dose in excess of 10 Gy seems to be a determining factor of acute and subacute central nervous system toxicity [24, 48]. The best median survival time of 14.8 months was found in the one-field BNCT cohort. Although the survival time of 13 months for all 53 subjects was similar to that obtained by conventional treatment using fractionated photon radiation and temozolomide [3], the first applications of the single-fraction BPA-mediated BNCT were well tolerated by patients with GBM.

A BPA-mediated BNCT clinical trial for GBM was carried out at Harvard/MIT in the period between 1996 and 1999 using 1 fraction or 2 fractions on consecutive days and 1–3 fields depending on the size and location of the tumor [26]. The fractionation was intended to improve the ^{10}B distribution to be more homogeneous, to help sparing normal brain tissue to some extent by fractionating the photon component, and to split the relatively long irradiation time at MITR-II. No adverse event was found in relation to the intravenous injection of 250 mg/kg BPA over 1 h, 300 mg/kg over 1.5 h, and 350 mg/kg over 1.5 h. The tumors with volumes >60 cm^3 were associated with a 67 % incidence of developing National Cancer Institute (NCI) CommonToxicity Criteria (version 2) grade 3 or higher symptoms, suggesting a relation to increased intracranial pressure, while volumes <60 cm^3 had a 19 % incidence. The median survival in this primary phase I trial was 12 months.

A BSH-mediated BNCT phase I trial was started in 1997 (EORTC trial 11961) at the Petten Irradiation Facility, Netherlands. Irradiation was performed using 4 fractions on 4 consecutive days. The BSH was applied four times with a dose to reach 30 ppm ^{10}B in blood over the total irradiation time. At the first day, all patients

received 100 mg BSH/kg bodyweight. Four patient cohorts were irradiated with increasing irradiation doses. In this phase I trial, the dose was prescribed to the thermal neutron flux maximum and increased by 10 % for the next cohort after an observation period from at least 6 months. The starting dose was set at $D_B = 8.6$ Gy, $D_p \leq 0.6$ Gy, $D_n \leq 0.9$ Gy, and $D_\gamma \leq 5.8$ Gy. The last cohort received $D_B = 11.4$ Gy, $D_p \leq 0.9$ Gy, $D_n \leq 1.2$ Gy, and $D_\gamma \leq 7.7$ Gy. No dose-related side effects could be observed, and the limiting radiation dose was not reached. The mean survival was 10.4 months for the first dose group, 11.3 months for the second dose group, 13.2 months for the third dose group, and 11.3 months for the fourth dose group [23, 49]. The study showed the feasibility and safety of a fractionated BNCT application using BSH at a dose of 100 mg/kg infused with a dose rate of 1 mg/kg/min.

Researchers at the NRI in Rez started a BSH -mediated BNCT phase I trial in 2001 (infusion of 100 mg BSH/kg). BNCT was well tolerated with only modest toxicity. Although a final report has not been made, the median time to progression and overall survival were shorter than expected with conventional treatment [31, 50].

In the phase II study at the Studsvik BNCT facility, 29 patients suffering from GBM received 900 mg/kg BPA-F in a 6-h infusion [30, 51]. Neutron irradiation was performed using two fields. Peak and average weighted absorbed doses D_w to the brain were in the ranges of 7.0–15.5 Gy and 3.3–6.1 Gy, respectively. The minimum dose to the tumor volume and the target volume (defined as tumor plus edema plus a 2-cm margin) ranged from 15.4 to 54.3 Gy and 8.8–30.5 Gy, respectively. Four patients developed WHO grade 3–4 toxic events including epileptic seizures, hematuria, thrombosis, and erythema. The median time from BNCT treatment to tumor progression was 5.8 months, and the median survival time after BNCT was 14.2 months.

In the trial conducted by Osaka Medical College [32], the first ten patients suffering from GBM were administered 100 mg/kg of BSH and 250 mg/kg of BPA in a 1-h infusion (protocol 1), and the latter 11 patients were administered 100 mg/kg of BSH and 700 mg/kg of BPA in a 6-h injection (protocol 2). A daily fraction 2 Gy XRT was applied in protocol 2 for a total dose of 20–30 Gy. For treatment planning, the neutron irradiation time was determined to limit the peak brain dose to 13 and 15 Gy in protocols 1 and 2, respectively. No serious acute toxicity has been reported other than alopecia, which was found in all of the patients. The MST for protocols 1 and 2 together was 15.6 months, and for protocol 2, the MST was 23.5 months.

In the Finnish phase I/II trial conducted by Helsinki University Central Hospital and the VTT (Technical Research Centre of Finland), 290 mg/kg of BPA were infused over 2 h in the first 12 patients suffering from GBM using two fields [28, 29]. The BPA dose to subsequent patients was escalated from 330 mg/kg ($n = 1$) to 360 mg/kg ($n = 3$), 400 mg/kg ($n = 3$) and 450 mg/kg ($n = 3$), and 500 mg/kg ($n = 8$). The maximum tolerated dose was reached at the BPA-F dose level of 500 mg/kg, where grade 3 ($n = 2$) and grade 4 ($n = 1$) CNS toxicity was found. The median OS values for the dose groups of 290, 330/360, 400, 450, and 500 mg BPA/kg were 13.4, 11.0, 16.9, 21.9 and 14.7 months, respectively. Consequently, the dose level of 450 mg/kg was found to be the optimal BPA dose for further BNCT studies of newly diagnosed GBM.

In the trial at the University of Tsukuba and Tokushima University at JRR-4 of JAEA, 250 mg/kg of BPA were infused over 1 h, and 5 g BSH/kg were infused over 1 h in eight patients with a single irradiation field [33]. All patients received additional photon radiation defining the signal abnormality in the T2-weighted MRI after completion of BNCT. The combination of BPA-F infusion and BSH infusion was well tolerated, and no serious (grade 3 or 4) BNCT-related acute toxicity was observed. The median OS and the time to progression were 27.1 and 11.9 months, respectively. The 1- and 2-year survival rates were 87.5 and 62.5 %, respectively. The clinical experience is summarized in Table 20.1.

20.6 Comparison with Other Treatments

The clinical trials of external beam BNCT have revealed that the median time to progression varies from 6 to 12 months and the median survival time varies from 12 to 27 months. All the clinical data over a decade were obtained using nonrandomized series. The clinical data show that the external beam BNCT appeared to be effective for the treatment of newly diagnosed GBM after surgical tumor resection. The optimization of dosage and delivery boron agents, the combined use of different boron agents, and the combination of BNCT with other therapeutic modalities have been studied for the purpose of improving BNCT. Although the difference in survival time between early external beam BNCT and "standard" conventional radiotherapy with temozolomide [3] is only modest, the best survival data of the recent external beam BNCT appear to be comparable to the best results of recent studies of high-dose radiotherapies, which show median survival times of 19–26 months [15–17, 19, 52, 53].

Though over 15 years have passed since the initiation of external beam BNCT trials at BNL, the survival benefits in GBM remain controversial. No prospective randomized trial nor any study categorized as a level A study according to the UK National Health Service system has been reported. Eight prospective level B studies have been performed. Four of eight studies, even in subgroups of the patient population, suggest that external beam BNCT may improve survival in newly diagnosed GBM. Of these eight studies, four primarily phase I trials failed to demonstrate survival prolongation but did demonstrate only modest toxicity. The need for better data, either through randomized trials or using the prospective case control methodology, is evident from reviewing these clinical reports.

References

1. Stummer W, Pichlmeier U, Meinel T et al (2006) Fluorescence-guided surgery with 5-aminolevulinic acid for resection of malignant glioma: a randomized controlled multicentre phase III trial. Lancet Oncol 7:392–401
2. Nimsky C, Ganslandt O, von Keller B, Fahlbusch R (2006) Intraoperative visualization for resection of gliomas: the role of functional neuronavigation and intraoperative 1.5 T MRI. Neurol Res 28:482–487

3. Stupp R, Mason WP, van den Bent MJ et al (2005) Radiotherapy plus concomitant and adjuvant temozolomide for glioblastoma. N Engl J Med 352:987–996
4. Vinjamuri M, Adumala RR, Altaha R et al (2009) Comparative analysis of temozolomide (TMZ) versus 1,3-bis (2-chloroethyl)-1 nitrosourea (BCNU) in newly diagnosed glioblastoma multiforme (GBM) patients. J Neurooncol 91:221–225
5. Ali SA, McHayleh WM, Ahmad A et al (2008) Bevacizumab and irinotecan therapy in glioblastoma multiforme: a series of 13 cases. J Neurosurg 109:268–272
6. Vredenburgh JJ, Desjardins A, Herndon JE 2nd et al (2007) Bevacizumab plus irinotecan in recurrent glioblastoma multiforme. J Clin Oncol 25:4722–4729
7. Walker MD, Alexander E Jr, Hunt WE et al (1978) Evaluation of BCNU and/or radiotherapy in the treatment of anaplastic gliomas: cooperative clinical trial. J Neurosurg 49:333–343
8. Walker MD, Green SB, Byar DP et al (1980) Randomized comparisons of radiotherapy and nitrosoureas for the treatment of malignant glioma after surgery. N Engl J Med 303: 1323–1329
9. Kristiansen K, Hagen S, Kollevold T et al (1981) Combined modality therapy of operated astrocytomas grade III and IV: confirmation of the value of postoperative irradiation and lack of potentiation of bleomycin on survival time: a prospective multicenter trial of the Scandinavian Glioblastoma Study Group. Cancer 47:649–652
10. Sandberg-Wollheim M, Malmstrom P, Stromblad LG et al (1991) A randomized study of chemotherapy with procarbazine, vincristine, and the lomustine with and without radiation therapy for astrocytoma grade 3 and/or 4. Cancer 68:22–29
11. Anderson AP (1978) Postoperative irradiation of glioblastomas. Results in a randomized series. Acta Radiol Oncol Radiat Phys Biol 17:475–484
12. Bleehen NM, Stennning SP (1991) A Medical Research Council trial of two radiotherapy doses in the treatment of grades 3 and 4 astrocytoma. Br J Cancer 64:769–774
13. Gasper LE, Fisher BJ, Macdonald DR et al (1992) Supratentorial malignant glioma: patterns of recurrence and implications for external beam local treatment. Int J Radiat Oncol Biol Phys 24:55–57
14. Oppitz U, Maessen D, Zunterer H et al (1999) 3D-recurrence-patterns of glioblastomas after CT-planned postoperative irradiation. Radiother Oncol 53:53–57
15. Tanaka M, Ino Y, Nakagawa K et al (2005) High-dose conformal radiotherapy for supratentorial malignant glioma: a historical comparison. Lancet Oncol 6:953–960
16. Nwokedi EC, DiBase SJ, Jabbour S, Herman J, Amin P, Chin LS et al (2002) Gamma knife stereotactic radiosurgery for patients with glioblastoma multiforme. Neurosurgery 50:41–47
17. Baumert BG, Lutterbach J, Bernays R et al (2003) Fractionated stereotactic radiotherapy boost after post-operative radiotherapy in patients with high-grade gliomas. Radiother Oncol 67: 183–190
18. Souhami L, Seiferheld W, Brachman D et al (2004) Randomized comparison of stereotactic radiosurgery followed by conventional radiotherapy with carmustine to conventional radiotherapy with carmustine for patients with glioblastoma multiforme: report of Radiation Therapy Oncology Group 93–05 protocol. Int J Radiat Oncol Biol Phys 60:853–860
19. Fitzek MM, Thornton AF, Rabinov JD et al (1990) Accelerated fractionated proton/photon irradiation to 90 cobalt gray equivalent for glioblastoma multiforme: results of a phase II prospective trial. J Neurosurg 91:251–260
20. Halperin EC, Burger PC, Bullard DE (1988) The fallacy of the localized supratentorial malignant glioma. Int J Radiat Oncol Biol Phys 15:505–509
21. Sullivani FJ, Herscher LL, Cook JA et al (1994) National Cancer Institute (phase II) study of high-grade glioma treated with accelerated hyperfractionated radiation and iododeoxyuridine: results in anaplastic astrocytomas. Int J Radiat Oncol Biol Phys 30:583–590
22. Hideghety K, Sauerwein W, Wittig A et al (2003) Tissue uptake of BSH in patients with glioblastoma in the EORTC 11961 phase I BNCT trial. J Neurooncol 62:145–156
23. Wittig A, Hideghety K, Paquis P et al (2002) Current clinical results of the EORTC-study 11961. In: Sauerwein W, Moss R, Wittig A (eds) Research and development in neutron capture therapy. Monduzzi Editore, Bologna, pp 1117–1122

24. Diaz AZ (2003) Assessment of the results from the phase I/II boron neutron capture therapy trials at the Brookhaven National Laboratory from a clinician's point of view. J Neurooncol 62: 101–109
25. Chanana AD, Capala J, Chadha M et al (1999) Boron neutron capture therapy for glioblastoma multiforme: interim results from the phase I/II dose-escalation studies. Neurosurgery 44: 1182–1193
26. Busse PM, Harling OK, Palmer MR et al (2003) A critical examination of the results from the Harvard-MIT NCT program phase I clinical trial of neutron capture therapy for intracranial disease. J Neurooncol 62:111–121
27. Palmer MR, Goorley JT, Kiger WS III et al (2002) Treatment planning and dosimetry for the Harvard-MIT phase I clinical trial of cranial neutron capture therapy. Int J Radiat Oncol Biol Phys 53:1361–1379
28. Joensuu H, Kankaanranta L, Seppälä T et al (2003) Boron neutron capture therapy of brain tumors: clinical trials at the Finnish facility using boronophenylalanine. J Neurooncol 62:123–134
29. Kankaanranta L, Koivunoro H, Kortesniemi M et al (2008) BPA-based BNCT in the treatment of glioblastoma multiforme: a dose escalation study. In: Zonta A, Altieri S, Roveda L, Barth R (eds) Proceedings of the 13th International Congress on Neutron Capture Therapy "A new option against cancer". ENEA, Italian National Agency for New Technologies, Energy and the Environment. ISBN: 88-8286-167-8, Florenz, pp. 30–32
30. Henriksson R, Capala J, Michanek A et al (2008) Boron neutron capture therapy (BNCT) for glioblastoma multiforme: a phase II study evaluating a prolonged high-dose of boronophenylalanine (BPA). Radiother Oncol 88:183–191
31. Burian J, Marek M, Rataj J et al (2002) Report on the first patient group of the phase I BNCT trial at the LVR-15 reactor. In: Sauerwein W, Moss R, Wittig A (eds) Research and development in neutron capture therapy. Monduzzi Editore, Bologna, pp 1107–1112
32. Kawabata S, Miyatake S, Kuroiwa T et al (2008) Boron neutron capture therapy for newly diagnosed glioblastoma. J Radiat Res (Tokyo) 50:51–60
33. Yamamoto T, Nakai K, Kageji T et al (2009) Boron neutron capture therapy for newly diagnosed glioblastoma. Radiother Oncol 91:80–84
34. Ono K, Masunaga SI, Suzuki M et al (1999) The combined effect of boronophenylalanine and borocaptate in boron neutron capture therapy for SCCVII tumors in mice. Int J Radiat Oncol Biol Phys 43:431–436
35. Yoshida F, Matsumura A, Shibata Y et al (2002) Cell cycle dependence of boron uptake from two boron compounds used for clinical neutron capture therapy. Cancer Lett 87:135–141
36. Soloway AH, Hatanaka H, Davis MA (1967) Penetration of brain and brain tumor. VII. Tumor-binding sulfhydryl boron compounds. J Med Chem 10:714–747
37. Coderre JA, Turcotte JC, Riley KJ et al (2003) Boron neutron capture therapy: cellular targeting of high linear energy transfer radiation. Technol Cancer Res Treat 2:1–21
38. Joel DD, Coderre JA, Micca PL, Nawrocky MM (1999) Effect of dose and infusion time on the delivery of p-boronophenylalanine for neutron capture therapy. J Neurooncol 41:213–221
39. Smith D, Chandra S, Barth R et al (2001) Quantitative imaging and microlocalization of boron-10 in brain tumors and infiltrating tumor cells by SIMS ion microscopy: relevance to neutron capture therapy. Cancer Res 61:8179–8187
40. Morris GM, Coderre JA, Hopewell JW et al (1997) Response of the central nervous system to fractionated boron neutron capture irradiation: studies with borocaptate sodium. Int J Radiat Biol 71:185–192
41. Coderre JA, Morris GM, Micca PL et al (1995) Comparative assessment of single-dose and fractionated boron neutron capture therapy. Radiat Res 144:310–317
42. Miyatake S, Kajimoto Y, Kawabata S et al (2005) Modified boron neutron capture therapy for malignant gliomas performed using epithermal neutron and two boron compounds with different accumulation mechanisms: an efficacy study based on findings on neuroimages. J Neurosurg 103:1000–1009
43. Barth RF, Grecula JC, Yang W et al (2004) Combination of boron neutron capture therapy and external beam radiotherapy for brain tumors. Int J Radiat Oncol Biol Phys 58:267–277

44. Sweet WH, Soloway AH, Brownell GL (1963) Boron-slow neutron capture therapy of gliomas. Acta Radiol 1:114–121
45. Yamamoto T, Matsumura A, Yamamoto K et al (2002) In-phantom two-dimensional thermal neutron distribution for intraoperative boron neutron capture therapy of brain tumours. Phys Med Biol 47:2387–2396
46. Imahori Y, Ueda S, Ohmori Y et al (1998) Positron emission tomography-based boron neutron capture therapy using boronophenylalanine for high-grade gliomas: part II. Clin Cancer Res 4:1833–1841
47. Nariai T, Ishiwata K, Kimura Y et al (2008) PET pharmacokinetic analysis to estimate boron concentration in tumor and brain as a guide to plan BNCT for malignant cerebral glioma. In: Zonta A, Altieri S, Roveda L, Barth R (eds) Proceedings of the 13th international congress of neutron capture therapy. A new opinion against cancer. ENEA, Roma, pp 244–247
48. Coderre JA, Hopewell JW, Turcottea JC et al (2004) Tolerance of normal human brain to boron neutron capture therapy. Appl Radiat Isot 61:1083–1087
49. Vos MJ, Turowski B, Zanella FE et al (2005) Radiologic findings in patients treated with boron neutron capture therapy for glioblastoma multiforme within EORTC trial 11961. Int J Radiat Oncol Biol Phys 61:392–399
50. Honová H, Safanda M, Petruzelka L et al (2004) Neutron capture therapy in the treatment of glioblastoma multiforme. Initial experience in the Czech Republic. Cas Lec Cesk 143:44–47
51. Capala J, Stenstam BH, Sköld K et al (2003) Boron neutron capture therapy for glioblastoma multiforme: clinical studies in Sweden. J Neurooncol 62:135–144
52. Shrieve DC, Eben A, Black PM et al (1999) Treatment of patients with primary glioblastoma multiforme with standard postoperative radiotherapy and radiosurgical boost: prognostic factors and long-term outcome. J Neurosurg 90:72–77
53. Gannett D, Stea B, Lulu B et al (1995) Stereotactic radiosurgery as an adjunct to surgery and external beam radiotherapy in the treatment of patients with malignant gliomas. Int J Radiat Oncol Biol Phys 33:461–468

Clinical Results of Sodium Borocaptate (BSH)-Based Intraoperative Boron Neutron Capture Therapy (IO-BNCT)

21

Teruyoshi Kageji, Yoshinobu Nakagawa,
and Hiroaki Kumada

Contents

T. Kageji, M.D. (✉)
Department of Neurosurgery, School of Medicine, The University of Tokushima,
Kuramoto-cho 3-18-15, Tokushima 770, Japan
e-mail: kageji@clin.med.tokushima-u.ac.jp

Y. Nakagawa, M.D.
Department of Neurosurgery, National Kagawa Children's Hospital,
Kagawa, Japan
e-mail: ynakagawa0517@yahoo.co.jp

H. Kumada, M.D.
Division of Biomedical, Faculty of Medicine, University of Tsukuba,
Tokai, Japan
email: kumada.hiroaki@jaea.go.jp

W.A.G. Sauerwein et al. (eds.), *Neutron Capture Therapy*,
DOI 10.1007/978-3-642-31334-9_21, © Springer-Verlag Berlin Heidelberg 2012

21.1 Introduction

The first clinical trials of BNCT were conducted at the Brookhaven Graphic Reactor and the Brookhaven Medical Research Reactor during 1951 and 1952 and at the Massachusetts Institute of Technology Reactor from 1959 to 1962 [3]. The boron compounds used were boric acid and borate as the boron carrier. The clinical results were discouraging: none of the patients survived for 1 year. Serious complications such as acute brain swelling and delayed cerebral necrosis resulted from the high boron content in the blood and normal brain tissue [3]. In 1968, Hatanaka introduced BSH as a boron carrier in Japan, and between 1968 and 1998 more than 170 patients with malignant intracranial tumors, especially GBM, were treated with BNCT in combination with BSH and pure thermal neutron beam [4, 5, 12, 13]. For BNCT to become a useful treatment modality, it is crucial that boron compounds be evaluated biologically and clinically. The clinical outcomes were favorable in patients whose GBM were located within a 4-cm depth from the brain surface [4, 5]. However, they were unsatisfactory in patients whose tumors were situated in deeper regions because neutron fluence delivery into deep regions was inadequate. Therefore, the epithermal neutron beam was developed at several international institutions to improve neutron delivery. At the Japan Atomic Energy Research Institute (JAERI) and the Kyoto University Research Reactor Institute (KUR) in Japan, mixed epithermal and thermal neutron beams were introduced for BNCT in 1998, before the independent introduction of epithermal neutron beam. Use of the mixed neutron beam can improve thermal neutron distribution in deeper sites, which in turn increases the therapeutic efficacy of BNCT. We have performed BSH-based intraoperative BNCT using mixed epithermal and thermal neutron beams since 1998. During neutron irradiation, inserted gold wires are used to measure neutron flux around and into the tumor tissue. Using neutron flux data obtained from individual points such as the brain surface, the center of the tumor bulk, and the area of invasion, we can analyze the actual radiation dose at each point. With these accurate radiation-dose data, we can then study the clinical course of each BNCT-treated patient.

While gold-wire measurements can evaluate the actual radiation dose, they yield no information on the dose delivered at other sites; therefore, this method fails to provide information concerning the real maximal and minimal radiation dose at other sites of interest. Therefore, a new dose-evaluation system for BNCT, the Japan Atomic Energy Research Institute (JAERI) Computational Dosimetry System (JCDS) was developed; it allows evaluation of the BNCT radiation dose on computed tomography (CT)- and magnetic resonance imaging (MRI) scans [8, 9]. In addition, it facilitates achieving the appropriate head position and angle with respect to the neutron beam port during irradiation. The JCDS for BNCT dose evaluation has been introduced clinically since 2001.

21.2 Actual State-of-the-Art Treatment

Glioblastoma multiforme (GBM) tumor cells infiltrate deeply into surrounding brain tissue and may even reach the contralateral hemisphere. After a decade of intensive research, these cells remain extremely resistant to all current forms of

therapy including surgery, chemo-, radio-, immuno-, and gene therapy. Despite aggressive treatments using combinations of therapeutic modalities, the median survival and 5-year survival rate were 9–10 months and less than 5 %, respectively [2, 11]; the new anticancer drug temozolomide (TMZ) improved clinical outcomes. Randomized clinical trials of TMZ and radiotherapy (RT) vs. RT alone showed that the median survival was 14.6 months with combined therapy and 12.1 months in GBM patients receiving radiotherapy alone [1, 15]. The 2-year survival rate was 26.5 % with radiotherapy plus TMZ and 20.4 % with radiotherapy alone [15].

21.3 Rationale for BNCT

Boron neutron capture therapy (BNCT) uses heavy charged particles yielded up by boron-10 (^{10}B) (n, α) reactions [10]. It is a promising modality for the selective irradiation of tumor tissue. BNCT involves the nuclear reaction of the ^{10}B nucleus with thermal neutrons (n_{th}). In this reaction, the boron nucleus disintegrates into α-helium (^{4}He) and lithium (^{7}Li) particles according to the equation: $^{10}B + n_{th} \rightarrow [^{11}B] \rightarrow {}^{4}He + {}^{7}Li + 2.31$ MeV. The densely ionizing particles have enough biologic effectiveness and a short length that, at 4–9 μm, is almost equal to the size of the tumor cells. If the boron compound selectively accumulates in tumor cells, selective targeting of the reaction on tumor cells may constitute highly effective treatment. As BNCT offers the possibility of selective tumor-cell killing without damage to adjacent normal brain tissue, it may be an optimal treatment for glioblastoma, which is highly invasive to healthy normal tissue [3, 4, 13].

21.4 Technical Aspect

21.4.1 Dose Planning

Based on the radiation dose of BNCT, we applied a new concept of BNCT to the physical radiation dose of the boron n-alpha reaction. To compare the radiation effect of the 2 heavy charged particles and to evaluate the efficacy of BNCT, we determined the physical dose of the boron n-alpha reaction. To identify the correct target point, it is necessary that all patients be diagnosed and followed by MRI. Gross tumor volume (GTV) dose is defined as the physical dose at the center of the tumor bulk, which coincides with the enhanced area on gadolinium (Gd)-enhanced MRI. Clinical target volume (CTV) dose is defined as the physical dose at a site about 2–3 cm from the bottom of the tumor cavity, which coincides with the deepest margin of the high-intensity area on T2-weighted MRI. Vascular volume (VV) dose is defined as the physical dose absorbed by endothelial cells of the vasculature in the normal cortex near the brain surface.

The BNCT radiation dose was analyzed with physical boron dose (gold wire, Gy), physical boron dose (JCDS, Gy), weighted boron dose (JCDS, Gy(w)), and weighted total dose (JCDS, Gy(w)).

21.4.2 Patients and Protocols

To be enrolled in this study, the patients had to satisfy all of the following criteria: their age was below 70 years, their gliomas were of grades III–IV, they had no serious systemic diseases, and their general condition was good according to the Karnofsky Performance Scale (KPS > 70).

The radiation dose (i.e., the physical dose of the boron n-alpha reaction) in the protocol used between 1968 and 1998 (P1998) prescribed a maximum GTV dose of 15 Gy. In 2001, a new dose-escalated protocol was introduced (P2001, $n = 11$); it prescribed a minimum GTV and CTV dose of 15 and 18 Gy, respectively. In both protocols, the maximum VV dose was restricted to below 15 Gy. We have also introduced a new dose-planning method, the JAERI Computational Dosimetry System (JCDS) in P2001.

21.4.3 Procedure of BSH-Based Intraoperative BNCT (IO-BNCT)

To improve neutron penetration into the brain tissue and to deliver a large enough dose of thermal neutron beam to the target point, we remove as much as possible of the tumor bulk and prepare a cavity 2–3 weeks prior to BNCT. BSH is diluted in 500 ml saline, the osmolarity is adjusted to 370, and the solution (80–100 mg BSH/kg body weight) is administered in the course of 1 h by rapid intravenous infusion at 12–15 h before neutron irradiation. The patient is taken to the reactor on the day of BNCT. With the patient under general anesthesia, the skin flap is reopened and the bone flap is removed. A thin silastic rubber balloon filled with air is placed into the previously prepared tumor cavity, thus maintaining the size of the cavity during neutron irradiation and improving neutron distribution. We insert several gold wires into and/or around the tumor tissue to measure neutron flux. After the entire head is covered with sterile plastic drapes to prevent infection, the patient is moved into the irradiation chamber. Simultaneous neutron beam monitoring devices are attached to the brain surface. With the patient under remote-controlled general anesthesia, the head is fixed toward the neutron port. Just before the start of neutron irradiation, tumor tissue and blood samples are obtained to measure the boron concentration; we use prompt gamma-ray spectrometry for analysis during irradiation. To monitor the exact neutron flux at each point of interest, the previously inserted gold wires are pulled out at 15–30 min intervals after switching the reactor to full power [7, 13, 14].

21.5 Results

21.5.1 Thermal Neutron and BSH-Based IO-BNCT (1977–1997)

Our retrospective analysis of the appropriate radiation dose of n-alpha reaction included 105 patients with glial tumors treated in Japan between 1978 and 1997

Table 21.1 Relationship between GTV dose and survival in 105 glial tumor patients treated with thermal neutron and BSH-based IO-BNCT between 1978 and 1997

Survival period	GTV dose (Gy)	Radiation time (min)
>10 years ($n=6$)	18.2±3.3*	240±66
>5 years ($n=11$)	12.4±3.5**	210±76
>3 years ($n=12$)	9.8±5.0	252±61
<3 years ($n=76$)	9.9±6.0	231±84

GTV dose: physical dose of boron n-alpha reaction measured with gold wires
*$p<0.01$; **$p<0.05$

Table 21.2 Relationship between GTV dose, glioma grade, and survival in 105 patients treated with thermal neutron and BSH-based IO-BNCT between 1978 and 1997

Glioma grade	Survival > 3 years ($n=29$)	Survival < 3 years($n=76$)
Grade II	11.4±4.6 Gy ($n=10$)	7.1±3.0 Gy ($n=5$)
Grade III	15.3±7.4 Gy* ($n=13$)	10.5±8.5 Gy ($n=11$)
Grade IV	15.6±3.1 Gy** ($n=6$)	9.5±5.9 Gy ($n=60$)

Radiation dose: physical dose of boron n-alpha reaction calculated as the minimum GTV dose at the deepest point of the tumor as demonstrated on CT and MRI
*$p<0.01$; **$p<0.01$

with thermal neutron and BSH-based IO-BNCT. Among them, 6 (5.7 %) survived for more than 10 years and 11 (10.5 %) for more than 5 years. The estimated GTV dose was significantly higher in the 10-year survivors. On the other hand, the dose was not significantly different between patients who lived more than 3 years and those who survived less than 3 years [13, 14] (Table 21.1).

When 105 patients were divided according to whether they survived for more (group 1; $n=29$) or less than 3 years (group 2; $n=76$), we noted that those with longer survival had received a significantly higher GTV radiation dose. In patients with grade II glioma, it was 11.4±4.6 Gy (group 1) versus 7.1±3.0 Gy (group 2), in those with grade III, it was 15.3±7.4 Gy (group 1) versus 10.5±8.5 Gy (group 2), and in patients with glioblastoma (grade IV), it was 15.6±3.1 Gy (group 1) versus 9.5±5.9 Gy (group 2). In grade III and IV, there were significant statistical differences in GTV radiation dose between group 1 and group 2. Similarly, irrespective of the glioma grade, patients exposed to the higher tumor volume radiation dose experienced longer survival [13, 14] (Table 21.2).

21.5.2 Epithermal Neutron and BSH-Based IO-BNCT (1998–2004)

Nineteen glial tumor patients were treated with epithermal neutron beam and BSH-based IO-BNCT between 1998 and 2004. Radiation doses were analyzed with JCDS measurement. Eight and eleven patients were treated under protocol 1998 and 2001, respectively. We retrospectively estimated the maximal vascular volume (VV) dose at the brain surface, minimum radiation dose delivered to the tumors (GTV), and

Table 21.3 BNCT radiation dose of gold wire and JCDS measurement in 19 patients with epithermal neutron and BSH-based IO-BNCT

(a) Maximal VV (vascular volume) dose at the brain surface		
	P1998	P2001
Physical boron dose (gold wire, Gy)	11.38 ± 4.20	14.40 ± 3.45
Physical boron dose (JCDS, Gy)	11.60 ± 4.29	14.71 ± 3.67
Weighted boron dose (JCDS, Gy(w))	29.01 ± 10.72	36.78 ± 9.16
Weighted total dose (JCDS, Gy(w))	34.76 ± 13.49	43.61 ± 10.27
(b) Minimum gross tumor volume (GTV) dose		
	P1998	P2001
Physical boron dose (gold wire, Gy)	18.00 ± 2.45	20.52 ± 5.31
Physical boron dose (JCDS, Gy)	16.92 ± 2.30	19.31 ± 6.62
Weighted boron dose (JCDS, Gy(w))	42.29 ± 5.75	48.27 ± 16.54
Weighted total dose (JCDS, Gy(w))	48.05 ± 6.06	55.10 ± 17.67
(c) Minimum clinical target volume (CTV) dose		
	P1998	P2001
Physical boron dose (gold wire, Gy)	13.26 ± 2.93	11.62 ± 2.93
Physical boron dose (JCDS, Gy)	13.00 ± 6.99	10.84 ± 6.99
Weighted boron dose (JCDS, Gy(w))	32.49 ± 7.05	27.11 ± 17.47
Weighted total dose (JCDS, Gy(w))	38.25 ± 7.07	33.94 ± 18.49

Table 21.4 Radiation injury and vascular volume at brain surface in 19 patients with epithermal neutron and BSH-based IO-BNCT

(a) Frequency of radiation injury with each protocol		
Protocol	P1998	P2001
Acute injury	0 (0 %)	3 (27 %)
Delayed injury	1 (13 %)	6 (55 %)
(b) Vascular volume (VV) dose at the brain surface and radiation injury		
	Radiation injury (+)	Radiation injury (−)	*p* value
Acute injury	15.8 ± 1.4 Gy	12.6 ± 4.3 Gy	0.1925
Delayed injury	13.8 ± 3.8 Gy	13.2 ± 4.8 Gy	0.9079

Table 21.5 Radiation dose in long survivors and non-long survivors in patients with GBM

	Long survivors ($n = 4$)	Non-long survivors ($n = 12$)	*p* value
Gross tumor volume (GTV) dose (physical dose of gold wire; Gy)			
Maximum	30.0 ± 10.9	22.4 ± 4.6	0.1146
Minimum	23.1 ± 7.3	18.1 ± 3.2	0.1456
Mean	26.4 ± 8.8	20.4 ± 3.9	0.0152
Clinical target volume (CTV) dose (physical dose of gold wire; Gy)			
Maximum	20.2 ± 5.2	14.7 ± 3.8	0.0966
Minimum	12.7 ± 2.1	12.2 ± 3.2	0.8846
Mean	16.5 ± 2.8	13.6 ± 3.0	0.1293

target points (CTV) under P1998 and P2001. Although the minimum GTV and CTV values for P2001 were approximately 1.1–1.4 times higher than for P1998, the differences were not statistically significant (Table 21.3).

Acute radiation injury resulting in generalized convulsions within one week of BNCT occurred in three patients in early period of P2001. This was attributable to the delivery of an excessive dose to the brain surface. At 15.8 ± 1.4 Gy, the maximum VV dose was about 1.3 times higher in patients with than those without acute radiation injury (12.6 ± 4.3 Gy); however, the difference was not statistically significant ($p = 0.1925$, Table 21.4). In later period of P2001, we reduced the VV dose, and none of the six patients in this period manifested acute radiation injury. Delayed radiation injury, recognized by neurological deterioration, appeared 3–6 months after BNCT; it occurred in 1 of 8 (13 %) P1998 patients and 6 of 11 (55 %) P2001 patients. The maximum VV dose was 13.2 ± 4.8 Gy in patients with, and 13.2 ± 4.8 Gy in those without delayed radiation injury ($p = 0.9079$, Table 21.4) [7].

The mean postdiagnosis follow-up period for all 19 patients was 26 months (range 5–90 months). At the time of the latest analysis (October 1, 2008), 16 of the 19 patients had died. The cause of death was CSF dissemination in 4, tumor invasion to the brain stem (central nervous system (CNS) dissemination) in 1, both CSF and CNS dissemination in 1, and local recurrence and CSF dissemination in 1 patient; 4 patients died of suspected local recurrence or radiation necrosis (no histopathological verification), 2 of wound infection, 2 of distinct metastasis, and 1 died of unknown causes. CSF and/or CNS dissemination without local recurrence at the primary site was the cause of death in 6 (38 %) of 16 patients.

Of the five autopsied patients, none demonstrated local tumor regrowth in the primary site, and two manifested only radiation necrosis but no tumor cells. The other three harbored residual tumor cells. In two there was CSF dissemination, and tumor cells were recognized throughout the subarachnoid space, and in the other patient, tumor cells had massively invaded the ipsilateral and contralateral hemisphere and brain stem from the bottom of the tumor cavity via the corpus callosum and cerebral peduncle [6].

As shown in Table 21.5, the maximum, minimum, and mean GTV value in patients who survived more than 2 years was significantly higher than in those who did not. The mean GTV dose for long survivors and non-long survivors were 26.4 ± 8.8 and 20.4 ± 3.9 Gy, respectively. The difference was statistically significant ($p = 0.0152$). There were, however, no significant statistical differences in maximum GTV dose ($p = 0.1146$) and minimum GTV dose ($p = 0.1456$). To determine the radiation dose to the area of invasion in these patients, we compared their CTV values. We found that the maximum, minimum, and mean CTV doses were higher in patients who survived for more than 2 years than in those who did not; however, the differences were not statistically significant (maximum CTV dose; $p = 0.0096$, minimum CTV dose; $p = 0.8846$, mean CTV dose; $p = 0.1293$) [7].

The estimated median survival time (MST) after diagnosis was 17.4 months in our 17 GBM patients. In 6 GBM patients treated under P1998, estimated MST after diagnosis was 15.5 months; their 1-year survival rate was 66.7 %, and none survived for 2 years. In contrast, all 11 GBM patients treated under P2001 had an estimated postdiagnosis MST of 19.5 months; their 1-, 2-, and 3-year survival rate was 63.6, 32.7 and 32.7 %, respectively. Three GBM patients survived more than 3 years after diagnosis (Fig. 21.1).

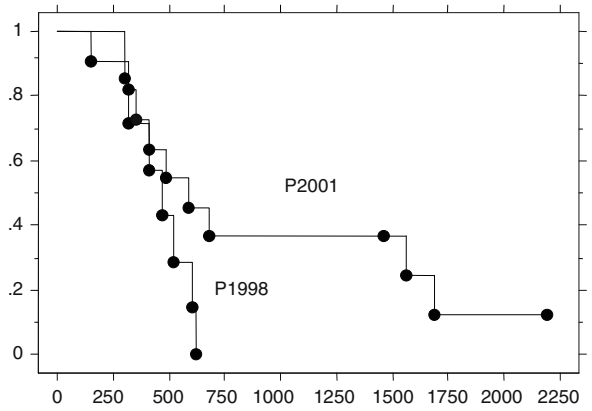

Protocol	Pts.	MST (month)	1-ys (%)	2-ys (%)	3-ys (%)
P1998	6	15.5	66.7	0	0
P2001	11	19.5	63.6	32.7	32.7

Fig. 21.1 Median survival time (MST) after diagnosis in patients with glioblatoma treated with epithermal neutron and BSH-based IO-BNCT

21.6 Level of Evidence

Our clinical study of BNCT is equivalent to "level B" of the UK National Health Service.

21.7 Further Development

We have shifted to the nonoperative BNCT in combination the two different boron compound as BSH and BPA. We believe these clinical data such as radiation dose of BSH-based IO-BNCT can contribute to the nonoperative BNCT.

References

1. Athanassiou H, Synodinou M, Maragoudakis M et al (2005) Randomized phase II study of temozolomide and radiotherapy compared with radiotherapy alone in newly diagnosed glioblastoma multiforme. J Clin Oncol 23:2372–2377
2. Davis FG, Freels S, Grutsch J et al (1998) Survival rates in patients with primary malignant brain tumors stratified by patient age and tumor histological type: an analysis based on surveillance, epidemiology, and end results (SEER) data. J Neurosurg 88:1973–1991
3. Hatanaka H (1986) Introduction. In: Hatanaka H (ed) Boron neutron capture therapy for tumors. Nishimura, Niigata, pp 1–28

4. Hatanaka H, Kamano S, Amano K et al (1986) Clinical experience of boron-neutron capture therapy for gliomas. A comparison with conventional chemo-immuno-radiotherapy. In: Hatanaka H (ed) Boron neutron capture therapy for tumors. Nishimura, Niigata, pp 349–379
5. Hatanaka H, Nakagawa Y (1994) Clinical results of long-surviving brain tumor patients who underwent boron neutron capture therapy. Int J Radiat Oncol Biol Phys 28:1061–1066
6. Kageji T, Nagahiro S, Uyama S et al (2004) Histopathological findings in autopsied glioblastoma patients treated by mixed neutron beam BNCT. J Neurooncol 68:25–32
7. Kageji T, Nagahiro S, Matsuzaki K et al (2006) Boron neutron capture therapy using mixed epithermal and thermal neutron beams in patients with malignant glioma – correlation between radiation dose and radiation injury and clinical outcome. Int J Radiat Oncol Biol Phys 65: 1446–1455
8. Kumada H, Yamamoto K, Matsumura A et al (2004) Verification of the computational dosimetry system in JAERI (JCDS) for boron neutron capture therapy. Phys Med Biol 49:3353–3365
9. Kumada H, Yamamoto K, Nakai K et al (2004) Improvement of dose calculation accuracy for BNCT dosimetry by the multi-voxel method in JCDS. Appl Radiat Isot 61:1045–1050
10. Locher GL (1936) Biological effects and therapeutic possibilities of neutron. Am J Roentgenol 36:1–13
11. Mehta MP, Masciopinto J, Rozental J et al (1994) Stereotactic radiosurgery for glioblastoma multiforme: report of a postoperative study evaluating prognostic factors and analyzing long-term survival advantage. Int J Radiat Oncol Biol Phys 30:541–549
12. Nakagawa Y (1994) Boron neutron capture therapy: the past to the present. Int J Radiat Oncol Biol Phys 28:1217
13. Nakagawa Y, Hatanaka H (1997) Boron neutron capture therapy – clinical brain tumor study. J Neurooncol 33:105–115
14. Nakagawa Y, Pooh K, Kobayshi T et al (2003) Clinical review of Japanese experience with boron neutron capture therapy and a proposed strategy using epithermal neutron beams. J Neurooncol 62:87–99
15. Stupp R, Mason WP, van den Bent MJ et al (2005) Radiotherapy plus concomitant and adjuvant temozolomide for glioblastoma. N Eng J Med 352:987–996

Boron Neutron Capture Therapy for Malignant Meningiomas

22

Shinji Kawabata and Shin-Ichi Miyatake

Contents

22.1 Introduction

The management of malignant meningioma (MM) is very difficult. In a large series of patients with this tumor, the MM recurrence rate was reported to be 78–84 % within 5 years [4, 12], and the median survival of patients 6.89 years. Late mortality due to recurrence was to be 69 % after the initial surgery [12]. Although some treatments for recurrent MM have been reported, a standard treatment has not yet been developed.

We propose here a novel radiation modality, boron neutron capture therapy (BNCT), for the treatment of MMs. The rationale for BNCT for MMs was that a relatively high accumulation of boronophenylalanine (BPA) was observed in MM in the preliminary study by positron emission tomography (PET) [16]. The first case of MM treated by BNCT showed a drastic shrinkage of the mass immediately after BNCT with prolonged survival [16]. Therefore, we applied this novel treatment for a series of MM patients, and their radiographic improvements were reported elsewhere [9].

S. Kawabata • S.-I. Miyatake (✉)
Department of Neurosurgery, Osaka Medical College,
2-7 Daigaku-machi, Takatsuki City, Osaka 569-8686, Japan
e-mail: neu070@poh.osaka-med.ac.jp

W.A.G. Sauerwein et al. (eds.), *Neutron Capture Therapy*,
DOI 10.1007/978-3-642-31334-9_22, © Springer-Verlag Berlin Heidelberg 2012

In this chapter, we describe our clinical experiences with treating MM by BNCT and the patients' typical responses, clinical courses, and problems after the treatment.

22.2 Patients and Methods

Fourteen cases of MM were treated by 22 rounds of BNCT from 2005 to 2008. Repetitive BNCTs were applied in several cases intentionally. These 14 cases were histologically diagnosed with anaplastic meningioma in 9 cases, papillary meningioma in 2, rhabdoid meningioma in 1, sarcoma in 1, and atypical meningioma in 1. All cases except one were recurrent cases that had been treated with repetitive surgery and conventional X-ray radiotherapy (XRT) with and without stereotactic radiosurgery (SRS).

The patients received ^{18}F-BPA-PET to assess the distribution of BPA and to estimate the boron concentration in tumors before neutron irradiation. Here, BPA is one of the boron compounds for the treatment, as described above. The tumor/normal brain (*T*:*N*) ratio of BPA uptake can be estimated from this study, and dose planning was made according to this *T*:*N* ratio, as described previously [8]. Fourteen, seven and one rounds of BNCT were applied for these patients in the Kyoto University Research Reactor (KUR), Japan Atomic Energy Agency Research Reactor-4 (JRR-4), and Finnish Research Reactor (FiR1), respectively. In all three atomic reactors, an epithermal beam was used for the neutron source. Eleven rounds of BNCT were performed with 5 g of BSH and 500 mg/kg body weight of BPA. Seven rounds of BNCT were performed with 5 g of BSH and 700 mg/kg body weight of BPA. Four rounds of BNCT were performed with 500 or 700 mg/kg body weight of BPA alone. BSH was administrated intravenously 12 h prior to neutron irradiation, and BPA was administrated for 2–3 h just prior to and during neutron irradiation.

The neutron irradiation time was determined so as not to exceed 15 Gy-Eq to the normal brain or 12 Gy-Eq to the scalp. Here, Gy-Eq (Gy:Gray) means a biologically equivalent X-ray dose that can give equivalent effects to total BNCT radiations. Neutron irradiation was performed without craniotomy and without anesthesia. After the treatment, the doses given were precisely re-estimated. The follow-up MRI or CT scans with contrast enhancements were applied for assessments every 2–3 months after the treatments.

22.3 Results

22.3.1 Parameters of BNCT in Each Patient

Thirteen of 14 patients received a BPA-PET study prior to neutron irradiation. The *T*:*N* ratios of ^{18}F-BPA in this series determined by the PET study were 2.0–5.0. The mean value of the *T*:*N* ratio in this series was 3.9, and the standard deviation (SD) was 0.9. The maximum tumor dose for gross tumor volume (GTV) was 76.6±24.9 as mean±SD Gy-Eq. The minimum tumor dose for GTV was 24.0±12.2 Gy-Eq. The maximum (peak) brain dose was 11.0±2.0 Gy-Eq. All cases showed shrinkage of the

enhanced volume immediately after the treatments. The median survival time of these 14 cases after the first BNCT was 13.8 ± 6.4 months, and five patients are still alive.

22.3.2 Representative Cases

Case presentation (case numbers were assigned to MM patients sequentially as BNCT was applied):

Case 2

A 48-year-old female had been operated on five times in the past 2 years with the histological diagnosis of anaplastic meningioma, and received with 60 Gy XRT and one SRS. In each operation, no residual tumor was recognized on neuro-images just after the surgery. She was introduced to our clinic because of uncontrollable lesions in the right parietal and occipital area, as shown in Fig. 22.1. We applied the first BNCT to the apparent right parietal and occipital lesions. After the first BNCT, the original parietal and occipital lesions kept shrinking during the observation period. She was treated with additional BNCT (second and third), 4 months after the first BNCT for new lesions that appeared in the cerebellum and just beneath the skin flap. These BNCTs showed a marked decrease in GTV, as shown in Fig. 22.1. Unfortunately,

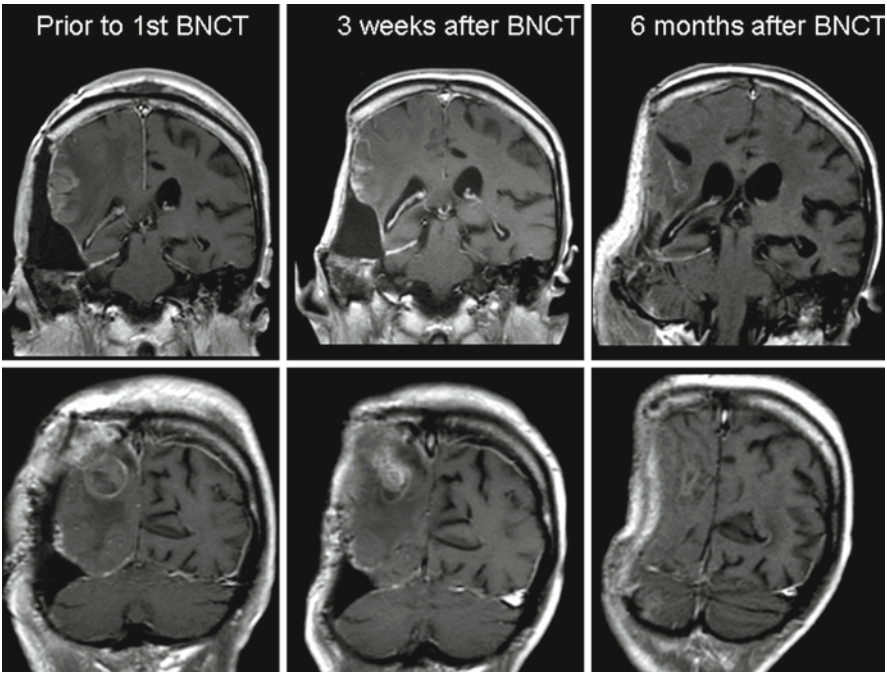

Fig. 22.1 Sequential change of Gd-enhanced T1-weighted image in case 2. *Left*, *middle*, and *right* column show the MRI taken prior to, 3 weeks after, and 6 months after the first BNCT, respectively

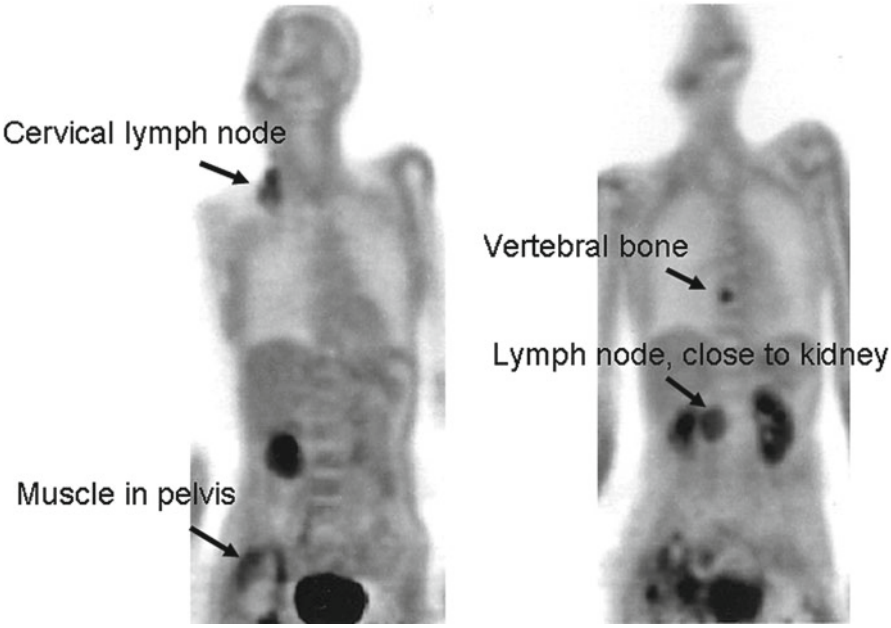

Fig. 22.2 Systemic F-BPA-PET taken 10 months after the first BNCT. This PET image shows tracer accumulation in lymph nodes at the cervical area, close to the kidney, vertebral bone, and muscle in the pelvis showing systemic metastases of the original tumor. However, the original intracranial lesions show only faint accumulation

we lost this patient to the systemic metastasis of the original meningioma. These metastases were shown in the follow-up systemic F-BPA-PET, as shown in Fig. 22.2. These PET images showed the metastasis in the cervical lymph nodes and thoracic paravertebral, right para-kidney, and the huge mass in the pelvis.

Case 10

A 62-year-old male had been operated on three times with 50 Gy XRT in the past 2 years with the histological diagnosis of anaplastic meningioma. In this case, BNCT did not show a prominent reduction of mass size just after treatment, but showed decreased enhancement of the tumor mass 6 weeks after BNCT (Fig. 22.3). However, the mass became voluminous 2.5 months after BNCT, and spontaneously decreased again in size and in enhancement of the core of the mass with decreased peri-lesional edema 6 months after the treatment (Fig. 22.3). In this case, BNCT could control the mass well locally; however we lost this patient to uncontrollable, shunt-ineffective hydrocephalus due to CSF dissemination, as shown in Fig. 22.4.

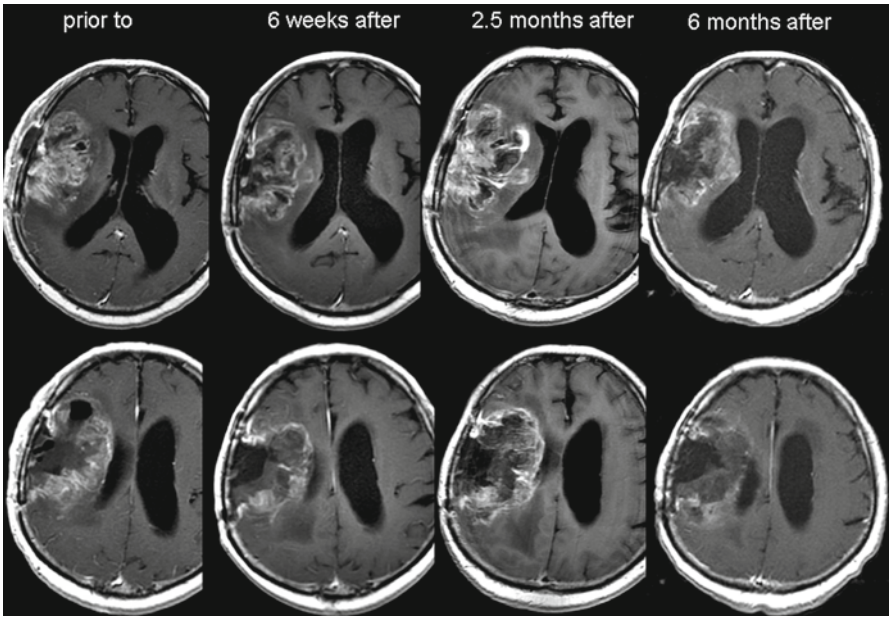

Fig. 22.3 Sequential change of Gd-enhanced T1-weighted image in case 10. From *left* to *right*, four columns show the MRI taken prior to, 6 weeks after, 2.5 months after, and 6 months after BNCT, respectively

22.4 Discussion

The clinical features of malignant meningioma are invasive behavior and a high tendency toward recurrence, as described above. Only radical resection constitutes an effective landmark for good prognosis for malignant meningiomas [12]. In general, meningiomas themselves are known to be radio-insensitive [14], and the effects of radiotherapy on malignant meningiomas are controversial [6]. Even with SRS, the 5-year survival and progression-free survival of malignant meningiomas are only 40 and 26 %, respectively [11]. In addition, once the tumor has recurred, local tumor control is difficult [13]. In fact, most patients in our series received repetitive surgical resections during the short clinical course, even though there might be the bias that uncontrollable cases were introduced to our institute.

There has been only one report concerning BPA-PET study for malignant meningiomas [5]. The above report showed that the *T*:*N* ratio of BPA in the malignant meningiomas is 2.5–3.5. As we reported previously [8], in our series of patients undergoing BNCT for malignant gliomas in recurrent cases, the *T*:*N* ratio determined by BPA-PET study was almost the same as the current one for recurrent malignant meningioma. Even in the recurrent gliomas, all cases showed radiographic improvement after BNCT [8, 10], so malignant meningioma might be a good candidate also from this point of view.

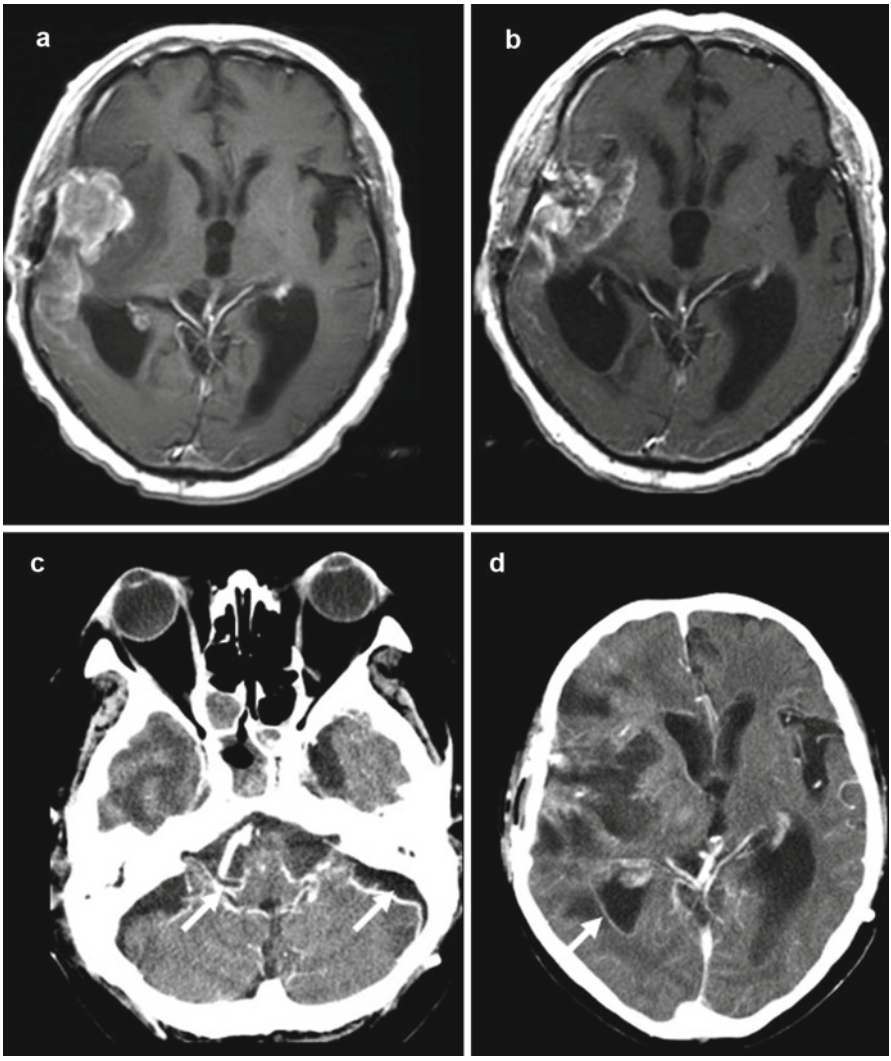

Fig. 22.4 Hydrocephalus due to CSF dissemination of MM in case 10. (**a**, **b**) Gd-enhanced MRI taken prior to and 6 months after BNCT. In (**b**), tumor shrinkage and ventricular dilatation were observed. (**c**, **d**) Contrast-enhanced CT images taken 9 months after BNCT. *White arrows* show the enhancement of leptomeninges and ventricular wall demonstrating CSF dissemination of the original tumor

There has been only one report published in the literature [15] aside from our publications [9, 16]. Stenstam et al. reported two cases of MM treated by BNCT with good response of the lesions [15]. Not only their case report, but also our current case series showed a good response of MMs to BNCT, although our current series should be judged as level C according to the "Oxford Centre for Evidence-based Medicine Levels of Evidence and Grades of Recommendation."

We introduced two representative cases in Sect. 22.3 (cases 2 and 10). In both cases, BNCT could control the local tumor very well; however, we lost the patient in case 2 to systemic metastasis and the case 10 patient to CSF dissemination. Of our current 14 cases, 5 patients are still alive. We lost three patients to systemic metastases and three to CSF dissemination. We lost one patient to another cause of death (concomitant gastric cancer), one to local tumor progression, and another to radiation injury. Almost all cases of MM introduced to BNCT were recurrent. Therefore, radiation injury should be kept in our mind. Bevacizumab might be effective for this inevitable pathology, as reported by Gonzalez et al. [3]. Finally, let us stress that even in MMs, "pseudoprogression" commonly occurs just after BNCT, as we reported for case 10 [7]. Pseudoprogression has been recognized and widely accepted in the treatment for malignant gliomas as a transient increase in the volume of the enhanced area just after chemo-radiotherapy, especially when using temozolomide [2]. Also in the literature, pseudoprogression often occurs after intensive treatments [1]. Therefore, pseudoprogression observed in BNCT proves the intensity of this unique particle radiation. We also need to keep this pathophysiology in mind and should not misdiagnose this as local tumor progression. These issues are important for the further development of BNCT for MMs.

References

1. Brandsma D, Stalpers L, Taal W et al (2008) Clinical features, mechanisms, and management of pseudoprogression in malignant gliomas. Lancet Oncol 9:453–461
2. Chamberlain MC, Glantz MJ, Chalmers L et al (2007) Early necrosis following concurrent Temodar and radiotherapy in patients with glioblastoma. J Neurooncol 82:81–83
3. Gonzalez J, Kumar AJ, Conrad CA et al (2007) Effect of bevacizumab on radiation necrosis of the brain. Int J Radiat Oncol Biol Phys 67:323–326
4. Jaaskelainen J, Haltia M, Servo A (1986) Atypical and anaplastic meningiomas: radiology, surgery, radiotherapy, and outcome. Surg Neurol 25:233–242
5. Joensuu H, Kankaanranta L, Seppala T et al (2003) Boron neutron capture therapy of brain tumors: clinical trials at the Finnish facility using boronophenylalanine. J Neurooncol 62: 123–134
6. Mahmood A, Caccamo DV, Tomecek FJ et al (1993) Atypical and malignant meningiomas: a clinicopathological review. Neurosurgery 33:955–963
7. Miyatake SI, Kawabata S, Nonoguchi N et al (2009) Pseudoprogression in boron neutron capture therapy for malignant gliomas and meningiomas. Neuro Onocol 11(4):430–436
8. Miyatake S, Kawabata S, Kajimoto Y et al (2005) Modified boron neutron capture therapy for malignant gliomas performed using epithermal neutron and two boron compounds with different accumulation mechanisms: an efficacy study based on findings on neuroimages. J Neurosurg 103:1000–1009
9. Miyatake S, Tamura Y, Kawabata S et al (2007) Boron neutron capture therapy for malignant tumors related to meningiomas. Neurosurgery 61:82–90, discussion – 1
10. Miyatake S, Kawabata S, Yokoyama K et al (2009) Survival benefit of Boron neutron capture therapy for recurrent malignant gliomas. J Neurooncol 91:199–206
11. Ojemann SG, Sneed PK, Larson DA et al (2000) Radiosurgery for malignant meningioma: results in 22 patients. J Neurosurg 93(Suppl 3):62–67
12. Palma L, Celli P, Franco C et al (1997) Long-term prognosis for atypical and malignant meningiomas: a study of 71 surgical cases. J Neurosurg 86:793–800

13. Salazar OM (1988) Ensuring local control in meningiomas. Int J Radiat Oncol Biol Phys 15:501–504
14. Simpson D (1957) The recurrence of intracranial meningiomas after surgical treatment. J Neurol Neurosurg Psychiatry 20:22–39
15. Stenstam BH, Pellettieri L, Sorteberg W et al (2007) BNCT for recurrent intracranial meningeal tumours – case reports. Acta Neurol Scand 115:243–247
16. Tamura Y, Miyatake S, Nonoguchi N et al (2006) Boron neutron capture therapy for recurrent malignant meningioma. Case report. J Neurosurg 105:898–903

Feasibility for Intramedullary Spinal Glioma

23

Kei Nakai and Akira Matsumura

Contents

23.1 Introduction

Spinal cord tumors are lesions that occur within or adjacent to the spinal cord. They are considered to be intra-axial in location and can be either primary or metastatic. Spinal cord tumors are relatively rare and account for 2 % of all central nervous system tumors. Tumors arising within the spinal cord itself are called intramedullary tumors, one-third of which are located in the intramedullary compartment [1, 2]. The spinal cord has the characteristic of integrated neuronal axons existing within a small diameter. Since spinal cord pathways are interrupted, neurologic dysfunction may be produced distally. Major complaints of the patients are unremitting pain, sensory dysesthesia, and muscular weakness.

K. Nakai (✉) • A. Matsumura
Department of Neurosurgery, Faculty of Medicine, University of Tsukuba,
1-1-1 Tennodai, Tsukuba, Ibaraki 305-8575, Japan
e-mail: knakai@md.tsukuba.ac.jp

W.A.G. Sauerwein et al. (eds.), *Neutron Capture Therapy*,
DOI 10.1007/978-3-642-31334-9_23,

The majority of intramedullary tumors are gliomas, either ependymomas or astrocytomas. Spinal ependymomas are associated with a significantly better prognosis than both supratentorial and infratentorial tumors, particularly when complete resection is possible. According to McGuire et al., the 5-year survival was reported as 86.6 % of the 55 spinal ependymoma cases [3]. Postoperative radiotherapy may be useful when complete resection cannot be achieved, but both early and delayed relapses can occur. Spinal astrocytomas are similar to intracranial astrocytomas; the clinical course of these astrocytic lesions can be predicted by their pathologic features: long-term survival is related to tumor grade. A recent report showed that the median overall survival of the patients with spinal anaplastic astrocytomas was 72 months, the 5-year survival was 59 %, and the median overall survival of glioblastoma patients was 9 months [4]. There is a lack of randomized data supporting the use of fractionated radiotherapy for patients with low-grade tumors that are incompletely resected, but all high-grade tumor patients should receive postoperative radiation.

BNCT has been evaluated for various malignant diseases, but no report has described its application to spinal tumors. The objective of this simulation was to clarify the feasibility of single-fraction or fractioned BNCT for patients with spinal malignant tumors.

23.2 Actual State-of-the-Art Treatment

MRI scan and neurological examination are necessary for preoperative diagnosis and treatment planning. The initial management of a spinal tumor is surgical removal.

In the case of ependymomas, value of postoperative radiotherapy is controversial and not supported by randomized trials. Several case series were reported; one paper showed that the postoperative radiotherapy did not appear to confer any protection against local recurrence or disease progression in spinal ependymoma [5]. The other reported that the addition of postoperative radiotherapy may achieve long-term tumor control in over one-half of the patients with residual spinal ependymomas [6]. A common way of radiation therapy for the patients with ependymomas of the spinal cord after subtotal resection or biopsy alone, including the cases of anaplastic ependymoma, is 50 Gy in 25 fractions [7].

With regard to astrocytomas, low-grade astrocytomas show nonaggressive clinical behavior, while anaplastic astrocytomas or glioblastomas show poor survival rates. Regardless of management, survival with glioblastoma is generally less than one year [4]. Malignant astrocytic tumors do poorly, despite aggressive resection, and thus biopsy is recommended prior to definitive surgery. In spite of the lack of randomized data supporting the use of fractionated radiotherapy for malignant spinal cord astrocytomas, low-grade tumors that are incompletely resected and all high-grade tumors should receive postoperative radiation.

Radiation toxicity of the nervous system has three phases: acute (during the course of radiation), early delay (weeks to 3 months after radiation), and delayed

reaction (more than 3 months). Most prominent radiation injury of spinal cord irradiation is a self-limited transient myelopathy and the more serious chronic progressive myelopathy. Acute spinal cord toxicity is rare. However, a transient myelopathy may develop within delayed phase. Evidence derived from large groups of patients suggests that the incidence of myelopathy is less than 0.5 % after 50 Gy of conventional fractionated irradiation [8, 9]. The best estimate of the dose expected to cause a 5 % risk of myelopathy within 5 years is approximately 60 Gy in 2.0 Gy daily fractions [10, 11]. The 1991 National Cancer Institute task force report concluded a cord length dependent 5 % risk of exceeding the tolerance dose at 5 years (TD 5/5) of 50 Gy (5 and 10 cm) and 47 Gy (20 cm) [12]. The use of stereotactic radiotherapy technique for the treatment of spinal lesions has been limited because the targeting of the tumor required that the spine be fixed with a large frame and clamps applied to the spinous processes. Recently, image-guided frameless stereotactic radiosurgery system (CyberKnife) allowed the treatment of spinal lesions, but there is no large experience to date with spinal radiosurgery that has previously developed optimal doses [13, 14].

23.3 Rationale for BNCT

Conventional external beam radiotherapy lacks the precision to allow delivery of large doses of radiation near the spinal cord. Achieving tumor targeting high dose irradiation by BNCT promises the possibility to treat serial organs such as the spinal cord more effectively and safely.

23.4 Technical Aspects and Results

23.4.1 Anteroposterior and Posteroanterior Irradiation

First, we generated treatment plans for three different situations of spinal cord tumors using the JAEA Computational Dosimetry System (JCDS). JCDS is a BNCT simulation system which was developed and has been improved by Japan Atomic Energy Agency [15, 16]. A three-dimensional model was created using medical CT and MRI images. We defined the postulated spinal tumor as impinging on the cervical cord. The JCDS requires user-defined parameters, namely, boron concentrations, relative biologic effectiveness (RBE) values, and compound biologic effectiveness (CBE) factors of the chosen boron compound. This study made use of boronophenylalanine (BPA). An epithermal mode beam, 3.5 MW of JRR-4, a 12-cm collimator, and a shielding module made of lithium fluoride were used together for the calculation. First, we defined the beam directions as (1) anteroposterior (*AP*) and (2) posteroanterior (*PA*). The values used in the simulation are summarized in Table 23.1, and the three-dimensional model is shown in Fig. 23.1. The normal tissue dose limit was set to below 9.0 Gy for each session (fraction). After the MCNP calculation of the beam and target model, the JCDS output was visualized and analyzed.

Table 23.1 RBE and CBE, boron concentration used for this simulation

Boron compound		BPA
Tumor/normal tissue ratio		3.5
	Boron concentration	RBE,CBE
Tumor	42	3.8
Normal tissue	12	1.35
Spinal cord	12	1.35
Mucosa	12	4.9
bone	0	

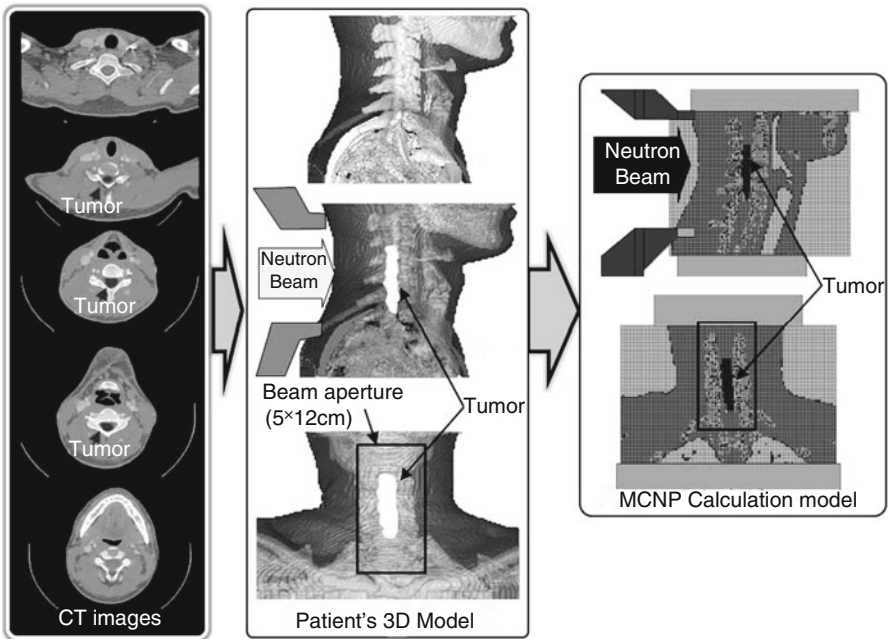

Fig. 23.1 The schema of the spinal cord tumor model. *Left*: serial CT image and postulated tumor, *middle*: three-dimensional reconstruction of the model, *right*: voxel model for MCNP calculation

Table 23.2 summarizes the tumor dose and normal tissue dose of opposing portal irradiations. The first irradiation was anteroposterior (*AP*), and the second irradiation was posteroanterior (*PA*). *AP*+*PA* implied that *AP* and *PA* irradiations were performed as a 2-fraction irradiation. Simple opposed two-field irradiation achieved 28.0 Gy as a minimum tumor dose, 7.3 Gy as a maximum normal spinal dose, and 7.4 Gy as a maximum skin dose. The thermal neutron flux was 1.98×10^9 and 1.73×10^9 at the *AP* and *PA* irradiation, respectively. Irradiation time was 30 and 38 min at the *AP* and *PA* irradiation, respectively; these were tolerable periods without general anesthesia. The dose distribution and dose profile of *AP*+*PA* irradiation on the beam's central axis are shown in Fig. 23.2.

The results showed the feasibility of BNCT for malignant spinal cord tumors. Coderre et al. reported dose-related changes in the incidence of developing myelopathy in rats; the authors determined the ED_{50} as 13.8 Gy using intraperitoneal

Table 23.2 Summary of the simulated dose

		AP+PA	AP	PA	RL	LR	L45	R45	L45+R45+PA
Irradiation time (min)		30+38	30	38	40.3	35.7	37.1	36.9	27+28.4+28.6
Tumor dose (Gy)	Max.	34.7	22.4	20.5	16.9	15.5	20.1	22.2	38.7
	Ave.	32.0	16.1	15.9	10.7	8.8	13.7	14.3	36.0
	Mini.	28.0	11.3	11.3	6.5	4.3	9.4	9.8	31.0
Normal tissue (Gy)	Max.	10.0	9.0	9.0	10.0	10.0	10.0	10.0	10.0
Spinal cord (Gy)	Max.	7.3	4.6	4.2	3.5	3.2	4.0	4.4	8.1
Skin (Gy)	Max.	7.4	7.0	7.4	8.5	8.0	7.9	8.0	6.4
Thermal neutron flux, $\times 10^9$ ($n/cm^2/s$)	Max.		1.98	1.73	1.98	2.26	1.97	1.99	
Thermal neutron fluence, $\times 10^{12}$ (n/cm^2)	Max.	4.24	4.01	4.09	4.80	4.84	4.40	4.40	3.97

AP anteroposterior irradiation, *PA* posteroanterior irradiation, *RL* right to left, *LR* left to right, *L45* left anterior oblique 45°, *R45* right anterior oblique 45°

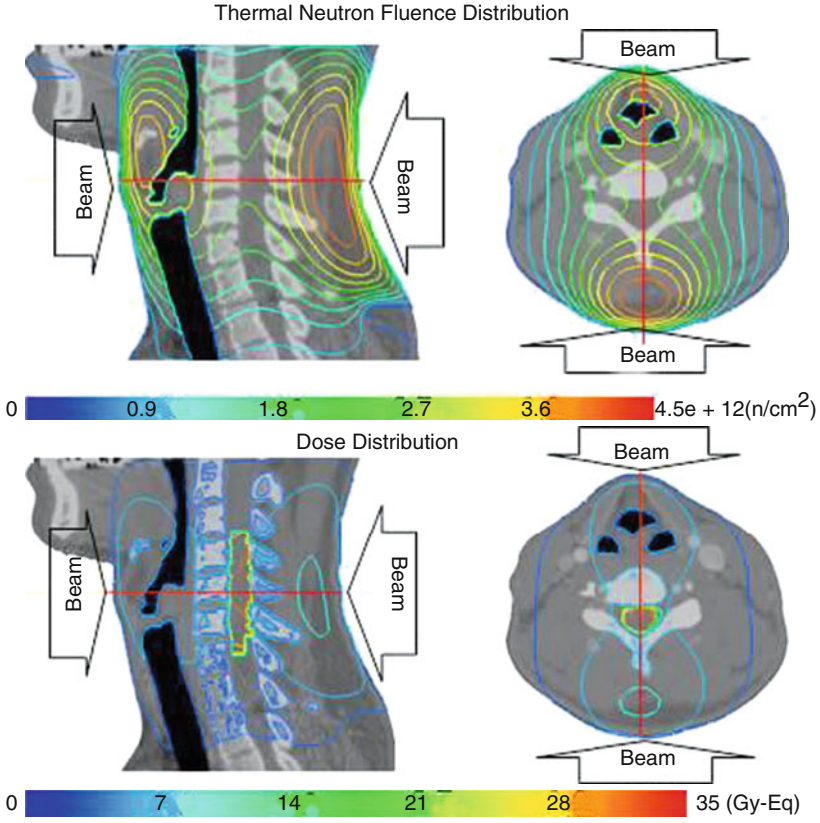

Fig. 23.2 Simulated results of AP+PA irradiation. Schematic view of thermal neutron fluence distribution (*left upper*) and dose distribution (*right upper*), dose profile on beam central axis (*left lower*) and dose volume histogram (*right lower*)

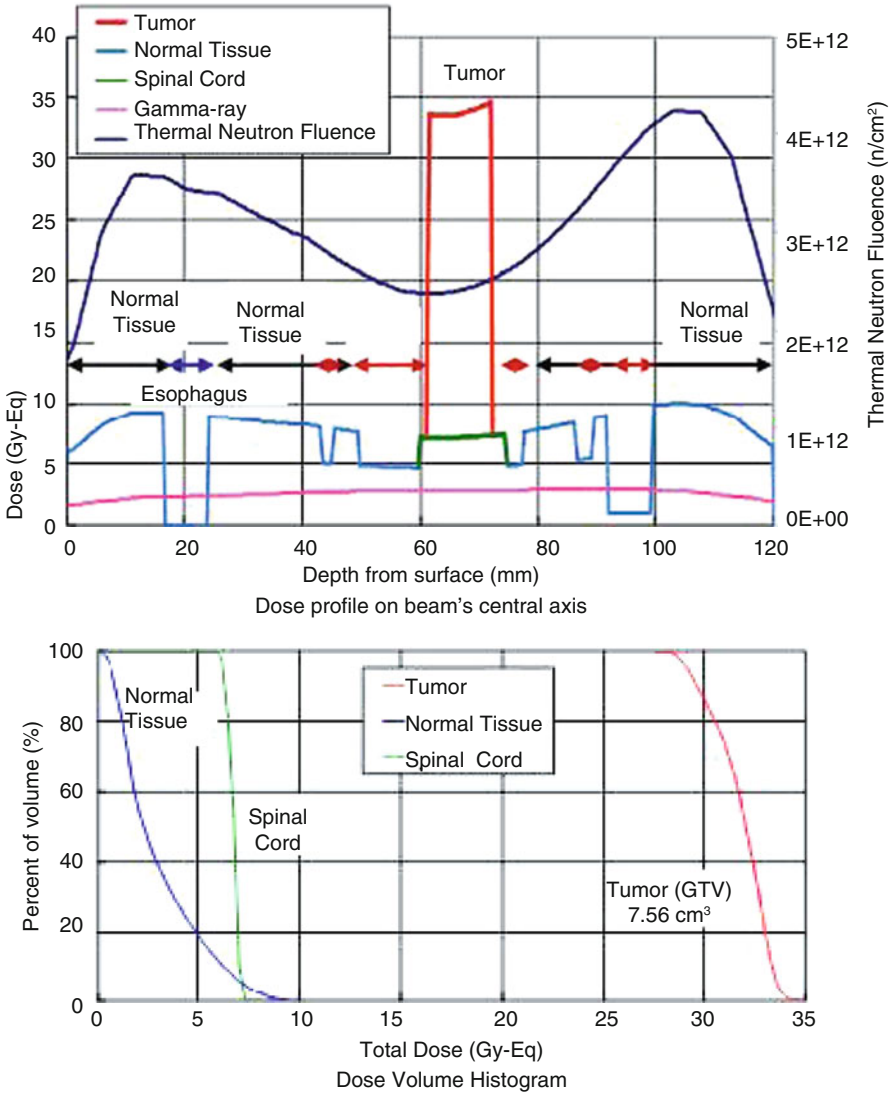

Fig. 23.2 (continued)

BPA administration and found no spinal damage below 11 Gy [17]. Morris et al. reported the dose response of the rat spinal cord and radiation damage [18]. The authors used i.v. BPA. According to this data, the ED_{50} for myeloparesis was 12.9 Gy in rats irradiated after i.v. administration of BPA. With a 10–20 % safety margin, we set 9 Gy as the upper limit for normal tissue exposure in a single session and 10 Gy for the total normal tissue dose. Under this limitation, the simulation achieved a minimum tumor dose of 28.0 Gy.

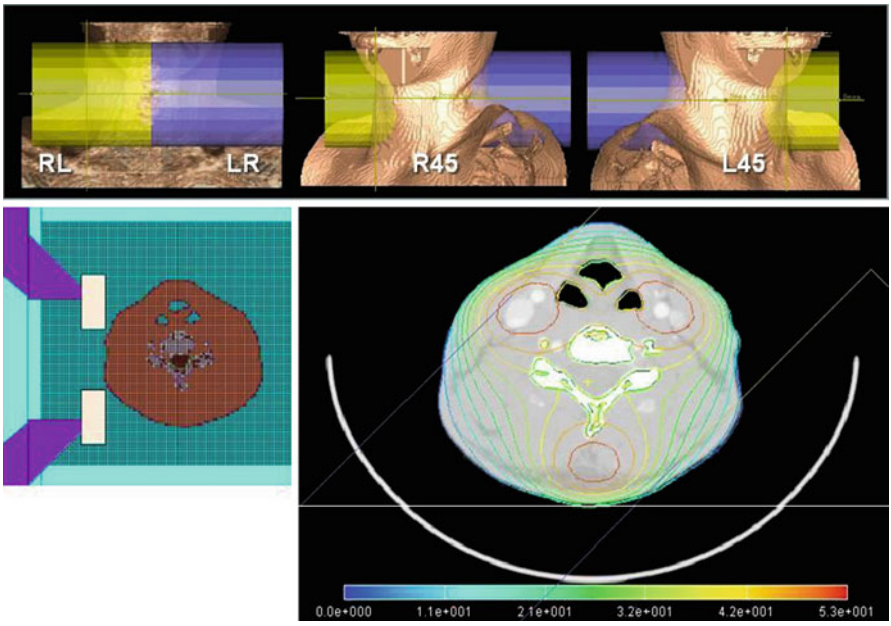

Fig. 23.3 Simulated results of lateral and oblique irradiation. Schematic view of lateral irradiation and oblique irradiation (*upper*), axial view of the beam port (*left lower*) and dose distribution of the three-beam irradiation

Fractionated irradiation is suitable for BNCT of spinal cord tumors because it reduces the normal tissue damage and concentrates the tumor dose. Compared with single-fraction irradiation, 2-fraction opposing portal irradiation increased the normal tissue dose only by 10 % while the minimum tumor dose more than doubled.

23.4.2 Lateral and Oblique Irradiation

To reduce mucosal dose of nasal, oral, pharyngeal cavity, we designed two opposite lateral irradiation directions (*RL* and *LR*, right to left and left to right) and three-beam irradiation, oblique and *PA* projection (Fig. 23.3). Table 23.2 shows the simulated results of the *RL*, *LR*, *R45*, and *L45* (right anterior oblique 45° and left anterior oblique 45°) beam directions. Three-beam irradiation was simulated using *PA*, *R45*, and *L45* directions. Lateral irradiation was limited because of the interference between the beam port and the patient's shoulder, requiring the use of the extensive collimator at JRR4 and resulting in the lower neutron fluence and longer irradiation time. The three-beam irradiation achieved 36.0 Gy as a minimum tumor dose, 8.1 Gy as a maximum normal spinal dose, and 6.4 Gy as a maximum skin dose. The beam direction avoided the naso-oral and pharyngeal cavity. But the carotid artery and veins were included in the irradiation fields (Fig. 23.3). Irradiation time was 27, 28, and 28 min at the *PA*, *L45*, and *R45* irradiation directions,

respectively. The dose distribution of the three-beam irradiation at the axial slice is shown in Fig. 23.3. Treatment with multiple beam direction requires to repeat BPA administration and neutron irradiation. As a result, the BNCT maneuver becomes more complicated, but the dose profile shows the feasibility of BNCT for patients with spinal tumors.

One limitation of this study concerns the boron distribution. We postulated that the tumor boron concentration is 42 ppm and the normal tissue concentration is 12 ppm. However, the spinal cord vasculature or tissue perfusion circumstances are not the same as those of brain tissue, and the pharmacokinetics of the boron compounds may differ. It is important to determine the BPA pharmacokinetics by an F^{18} BPA-PET study and experimentally determine the values that we use here presumptively.

23.5 Level of Evidence

Preclinical evaluation. Categories labeled D: expert opinion without explicit critical appraisal, or based on physiology, bench research or first principles. Defined by the UK National Health Service.

23.6 Further Development

We need to define the distribution of boron in spinal tumors and plan to study BPA-PET scan of spinal tumor patients. As the spine is a common metastatic site for many tumor types, the simulation for extamedullary spinal tumors should be done. To avoid mucosal reaction in the radiated field, the experience of head and neck tumors should be used in the further preclinical simulation design.

References

1. Kim MS et al (2001) Intramedullary spinal cord astrocytoma in adults: postoperative outcome. J Neurooncol 52(1):85–94
2. Reimer R, Onofrio BM (1985) Astrocytomas of the spinal cord in children and adolescents. J Neurosurg 63(5):669–675
3. McGuire CS, Sainani KL, Fisher PG (2009) Both location and age predict survival in ependymoma: a SEER study. Pediatr Blood Cancer 52(1):65–69
4. McGirt MJ et al (2008) Extent of surgical resection of malignant astrocytomas of the spinal cord: outcome analysis of 35 patients. Neurosurgery 63(1):55–60; discussion 60–61
5. Sgouros S, Malluci CL, Jackowski A (1996) Spinal ependymomas–the value of postoperative radiotherapy for residual disease control. Br J Neurosurg 10(6):559–566
6. Whitaker SJ et al (1991) Postoperative radiotherapy in the management of spinal cord ependymoma. J Neurosurg 74(5):720–728
7. Shaw EG et al (1986) Radiotherapeutic management of adult intraspinal ependymomas. Int J Radiat Oncol Biol Phys 12(3):323–327
8. Marcus RB Jr, Million RR (1990) The incidence of myelitis after irradiation of the cervical spinal cord. Int J Radiat Oncol Biol Phys 19(1):3–8

9. McCunniff AJ, Liang MJ (1989) Radiation tolerance of the cervical spinal cord. Int J Radiat Oncol Biol Phys 16(3):675–678
10. Jeremic B, Djuric L, Mijatovic L (1991) Incidence of radiation myelitis of the cervical spinal cord at doses of 5500 cGy or greater. Cancer 68(10):2138–2141
11. Fowler JF et al (2000) Clinical radiation doses for spinal cord: the 1998 international questionnaire. Radiother Oncol 55(3):295–300
12. Emami B et al (1991) Tolerance of normal tissue to therapeutic irradiation. Int J Radiat Oncol Biol Phys 21(1):109–122
13. Nelson JW et al (2008) Stereotactic body radiotherapy for lesions of the spine and paraspinal regions. Int J Radiat Oncol Biol Phys 73(5):1369–1375
14. Gerszten PC, Welch WC (2004) Cyberknife radiosurgery for metastatic spine tumors. Neurosurg Clin N Am 15(4):491–501
15. Kumada H et al (2004) Verification of the computational dosimetry system in JAERI (JCDS) for boron neutron capture therapy. Phys Med Biol 49(15):3353–3365
16. Kumada H et al (2004) Improvement of dose calculation accuracy for BNCT dosimetry by the multi-voxel method in JCDS. Appl Radiat Isot 61(5):1045–1050
17. Coderre JA et al (1995) Comparative assessment of single-dose and fractionated boron neutron capture therapy. Radiat Res 144(3):310–317
18. Morris GM et al (2002) Long-term infusions of p-boronophenylalanine for boron neutron capture therapy: evaluation using rat brain tumor and spinal cord models. Radiat Res 158(6):743–752

BNCT for Advanced or Recurrent Head and Neck Cancer

24

Teruhito Aihara and Norimasa Morita

Contents

T. Aihara (✉) • N. Morita
Department of Otolaryngology, Head and Neck Surgery,
Kawasaki Medical School, Okayama, Japan
e-mail: aiteru@med.email.ne.jp; nori.morita@gmail.com

W.A.G. Sauerwein et al. (eds.), *Neutron Capture Therapy*,
DOI 10.1007/978-3-642-31334-9_24, © Springer-Verlag Berlin Heidelberg 2012

24.1 Introduction

Head and neck cancers (HNCs) account for approximately 10 % of all cancers, and about 90 % of them are squamous cell carcinoma (SCC). Surgery represents the mainstay of treatment for resectable primary site. However, the main drawback of surgery, especially for advanced T-stage cancer, is deterioration of patients' QOL because the head and neck have many important physiological and cosmetic functions. On the other hand, the patients with unresectable cancer are candidates for radiation therapy or chemoradiotherapy. Although these therapies are effective for SCC, it is difficult to perform reradiation therapy for SCCs that recur after these therapies, because of intolerable of surrounding normal tissue against reradiation therapy. In addition, these SCCs might show radioresistance. T3-4 advanced non-SCCs, such as adenocarcinoma, mucoepidermoid carcinoma, and adenoid cystic carcinoma, also show radio- and chemoresistance. BNCT is high linear energy transfer (LET) radiation and tumor-selective radiation without serious damage of surrounding normal tissue. BNCT might be effective and safe in the patients with inoperable, locally advanced head and neck cancers even if that recur at previously irradiated sites.

24.2 Actual State-of-the-Art Treatment

24.2.1 Locally Advanced and Recurrent SCC

The reported tumor effective rate and the median survival of 69 patients with advanced/recurrent HNSCC who received palliative chemotherapy and/or radiation therapy were approximately 30 % and 6–10 months, respectively [1]. The 2-year locoregional progression-free survival and overall survival rates in 105 patients with recurrent HNC who underwent re-RT were 42 and 37 %, respectively [2].

24.2.2 Non-SCC in the Head and Neck Without Malignant Melanoma

The postoperative radiation therapy improved local control from 75 to 83 % among 100 patients with non-SCC, such as mucoepidermoid, adenoid cystic, acinic cell, and adenocarcinoma, of the major salivary glands [3]. Operation with postoperative radiotherapy improved the 10-year estimates of locoregional control to 63 % in 70 patients with resectable T3-4 non-SCC of the major salivary glands [4].

24.3 Rationale for BNCT

There are several advantages in applying BNCT to head and neck cancers. First, the head and neck have many important physiological and cosmetic functions. Surgery can be a great influence on his/her QOL in the patients with advanced or

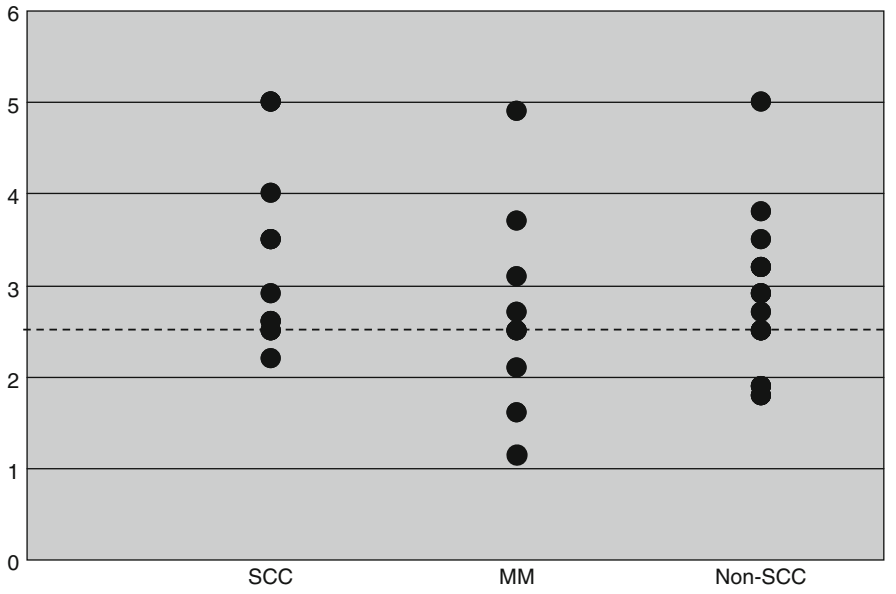

Fig. 24.1 Kawasaki Medical School (KMS) group data of ^{18}F-BPA-PET. Eleven patients with recurrent SCC and eight patients with non-SCC were registered in ^{18}F-BPA-PET study from October 2003 to September 2007. There was no difference in the *T*/*N* ratio between SCC and non-SCC group. Ten of 11 patients with SCC and 10 of 13 patients with non-SCC showed *T*/*N* ratio of 2.5 and over and underwent BNCT

recurrent HNCs. Therefore, organ preservation is one of the most important things. Second, there are many patients with SCC that recur after intensive treatment, including surgery and chemoradiotherapy, and locally advanced non-SCC that cannot be controlled by conventional cancer therapy. Third, as head and neck cancers exist superficially and are not very far from the skin surface, it is possible to administer curative doses to the target by using an epithermal neutron beam.

24.3.1 ^{18}F-BPA-PET Study

The accumulations of BPA (*para*-boronophenylalanine) in the tumor and surrounding normal tissue were imaged and quantified by an ^{18}F-BPA-PET (fluorine-18-labeled BPA positron emission tomography) study before BNCT in all patients [5].

The tumor/blood, normal tissue/blood, and tumor/normal tissue (*T*/*N*) ratios of ^{18}F-BPA intensity were estimated 40 min after ^{18}F-BPA i.v. administration. *T*/*N* ratios of SCC and non-SCC patients are shown in Fig. 24.1.

24.4 Technical Aspects and Clinical Applications

24.4.1 Indications for BNCT

1. A newly diagnosed T3/T4 advanced and recurrent HNC.
2. The maximum depth of tumor is within 5 cm in depth from the skin surface to achieve a curative dose of the target by using an epithermal neutron beam.
3. *T*/*N* ratio is more than 2.5. *T*/*N* ratio is calculated by the results of ^{18}F-BPA-PET.
4. Consent to perform BNCT is obtained from the patient and their family.
5. Approval for BNCT is given by our Medical Ethics Committee.

24.4.2 Treatment Procedures

The patient undergoes CT scan for treatment planning just prior to BNCT using a computer work stations equipped with the Japan Atomic Energy Research Institute Computational Dosimetry System (JCDS) [6] dose planning software.

The total dose of BPA (L-enantiomer, >95 % ^{10}B enriched) is 500 mg/kg body weight (BW). Two hours before neutron irradiation, intravenous administration of 200 mg/kg BW/h of BPA is started. To monitor the boron concentration in the blood, venous blood samples were obtained every 1 h from starting BPA administration to finishing neutron irradiation. The boron concentrations in the blood are measured by prompt γ-ray analysis and/or inductively coupled plasma-atomic emission spectrometry (ICP-AES). The blood boron concentration curves are plotted against time. The tumor and normal tissue boron concentrations are estimated by the results of ^{18}F-BPA-PET.

Patients are positioned on the treatment table in the irradiation room of the reactor and attached the collimator to shield normal tissue, and then tumor site is irradiated with epithermal neutron with the BPA flow rate of 100 mg/kg BW/h [7]. All patients are placed in a sitting or supine position during irradiation. After final setting of the patients, thermoluminescence dosimeters (TLDs) are attached to the skin surface involved in the irradiation field, and gold wires are placed in the collimator for dosimetry. We placed a gelatin sheet, 5 mm thickness, on the skin of the radiation field to enhance the irradiation dose at the tumor surface. Neutron flux (n/cm^2/s) is measured using gold wires 15 min after the start of irradiation. The neutron irradiation time is decided using the JCDS based on the neutron flux measured at 15 min after the start of irradiation and the estimated blood boron concentration curves.

24.4.3 Radiation Doses by BNCT

BNCT for the HNC is performed using epithermal neutron beam of the reactor with single fraction in our group (two fractions in Finland group [8]). The control dose

to the tumor is planned to be more than 20 Gy (weighted dose), and the maximum dose to tumor surrounding normal tissue is set not to exceed 15 Gy. These values were calculated by JCDS on the basis of the mean blood boron level during neutron irradiation and directly measuring the neutron flux at the tumor site using gold wires. These treatment doses are achieved by the indications of BNCT (2) and (3).

24.5 Results

24.5.1 Observations from Kawasaki Medical School

Ten patients with recurrent SCC, 7 patients with recurrent non-SCC (adenoid cystic carcinoma, 2 cases; adenocarcinoma, 1; papillary adenocarcinoma, 2; mucoepidermoid carcinoma, 1; and undifferentiated cancer, 1), and 3 with newly diagnosed T4 advanced non-SCC (adenoid cystic carcinoma, 2 cases and acinic cell carcinoma, 1) underwent BNCT between October 2003 and September 2007. The median follow-up time was 15.9 months (range, 3-56 months). Local response of these 20 patients after BNCT was as follows: 11 showed complete remission (CR) clinically. Figure 24.2 represents the images of CT and ^{18}F-BPA-PET before, and that of CT 5 months after treatment in recurrent SCC case which showed CR with BNCT. Seven patients showed partial remission (PR), and 2 did no change. The effective rate [(CR + PR)/total cases] was 90 % [9]. No severe acute or chronic normal tissue reactions (more than grade II of the RTOG/EORTC score) were experienced in any patients. Ten patients died 3–20 months (median 11.6 months) after BNCT, and the main cause of death was distant metastasis.

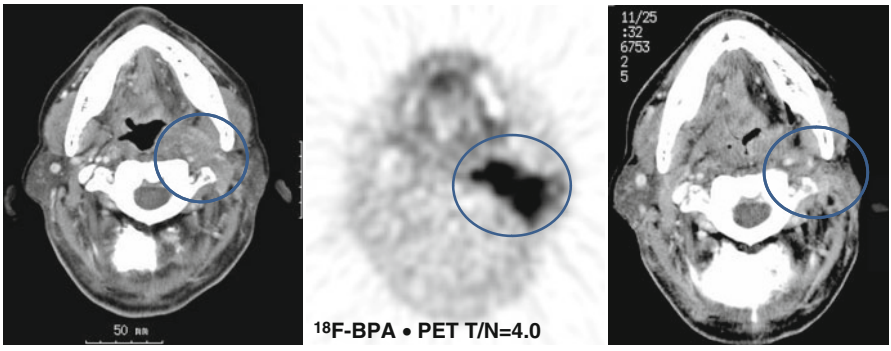

Fig. 24.2 Recurrent primary unknown SCC. The tumor recurred after full-dose conventional radiotherapy combined with chemotherapy. (**a**) CT shows the recurrent tumor at left parapharyngeal space as indicated by the circle. (**b**) ^{18}F-BPA-PET study reveals that *T*/*N* ratio is 4.0. (**c**) The tumor completely disappeared five months after BNCT. Unfortunately, this patient died of distant metastasis 2 years after BNCT. However, local recurrence was not observed

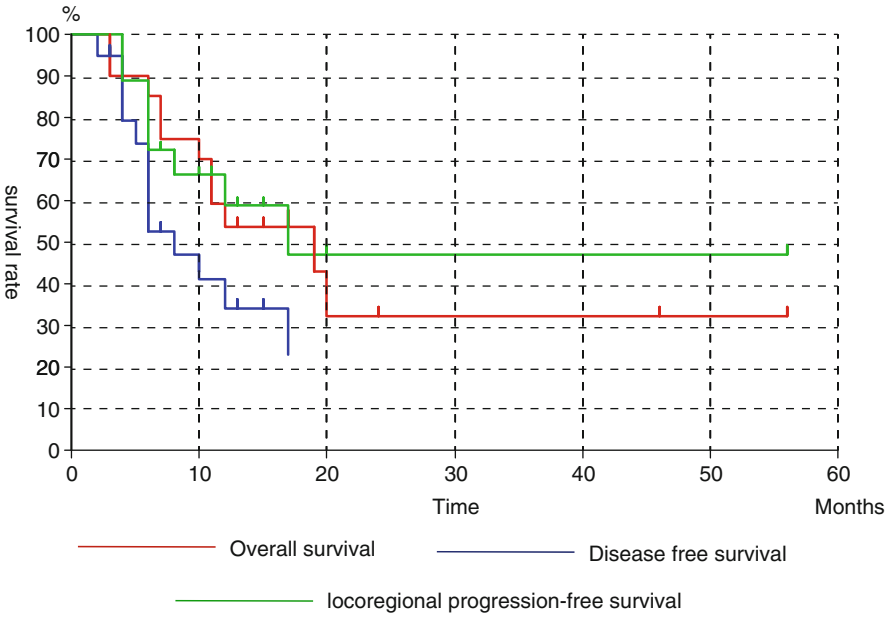

Fig. 24.3 Kaplan-Meier survival curve. Two-year locoregional progression-free survival and overall survival rates are 47.7 and 32.3 %, respectively

In all patients, 1- and 2-year overall survival rates were 53.8 and 32.3 %, respectively, and the 1- and 2-year disease free survival rates were 34.2 and 0 %. However, the 1- and 2-year locoregional progression-free survival rates were 58.8 and 47.7 %, respectively (Fig. 24.3). All three patients with newly diagnosed T4 advanced non-SCC showed complete response of the primary site within 3 months after BNCT. The 1-year locoregional progression-free survival rate was 100 %, and overall survival rate was 100 % at 18 months in these three patients.

24.5.2 Results obtained at Osaka University

Six patients with recurrent HNCs were registered (squamous cell carcinoma, 3 cases; sarcoma, 1; and mucoepidermoid carcinoma of the parotid gland, 1). Local response of the 6 patients after BNCT was as follows: 1 showed clinically CR, 4 PR, and 1 progressive disease. The effective rate was 80 %. Four patients died 2–10 months after BNCT (median 6.7 months) [10].

24.5.3 Results from Helsinki

Twelve patients received BNCT between December 2003 and December 2005. Local response of the 12 patients after BNCT was as follows: 7 showed clinically

CR, 3 PR, and 2 stable disease. The effective rate was 83 %. The median duration of disease progression was 9.8 months, and the median overall survival time was 13.5 months. Five (41 %) patients were alive without recurrence with a median follow-up of 14.0 months (range, 12.8–19.2 months) [8].

Conclusion

BNCT for recurrent SCC and locally advanced non-SCC in the head and neck is a promising modality that might be indicated in the following situations:

1. The maximum depth of tumor is within 5 cm in depth from the skin surface.
2. *T*/*N* ratio is more than 2.5 which is calculated by the results of ^{18}F-BPA-PET.

BNCT increases the chance for local control in these patients. However, main cause of death in the patients is distant metastasis, and overall survival rate is not significantly improved by BNCT compared to conventional cancer treatments. A combination of BNCT with chemotherapies should be considered in high-risk patients to improve overall survival.

24.6 Level of Evidence

Levels of evidence (LOE): Level III

The UK National Health Service: Level D

24.7 Further Development

In Japan, BNCT for head and neck cancer will be performed using a neutron accelerator from end of 2012.

References

1. Worden FP, Moon J, Samlowski W, Clark JI, Dakhil SR, Williamson S, Urba SG, Ensley J, Hussain MH (2006) A phase II evaluation of a 3-hour infusion of paclitaxel, cisplatin, and 5-fluorouracil in patients with advanced or recurrent squamous cell carcinoma of the head and neck. Cancer 107:319–327
2. Lee N, Chan K, Bekelman J, Zhung J, Narayana A, Wolden S, Shah J, Kraus D, Pfister D, Zelefsky M (2007) Salvage re-irradiation for recurrent head and neck cancer. Int J Radiat Oncol Biol Phys 68:731–740
3. Fu KK, Leibel SA, Levine ML, Friedlander LM, Boles R, Phillips TL (1977) Carcinoma of the major and minor salivary glands. Cancer 40:2882–2890
4. Chen AM, Granchi PJ, Garcia J, Bucci MK, Fu KK, Eisele DW (2007) Local-regional recurrence after surgery without postoperative irradiation for carcinomas of the major salivary glands. Int J Radiat Oncol Biol Phys 67:982–987
5. Imahori Y, Ueda S, Ohmori Y, Sakae K, Kusuki T, Kobayashi T, Takagaki M, Ono K, Ido T, Fujii R (1998) Positron emission tomography-based boron neutron capture therapy using boronophenylalanine for high-grade gliomas: part II. Clin Cancer Res 4:1833–1841

6. Kumada H, Yamamoto K, Torii Y (2001) Development of computational dosimetry system and measurement of dose distribution in water head phantom for BNCT in JAERI. In: Proceeding of the 2000 workshop on utilization of research reactors. JAERI-Conference 2001, Taejon, 2001, pp 357–362
7. Ono K, Masunaga S, Kinashi Y, Nagata K, Suzuki M, Sakurai Y, Maruhashi A, Kato I, Nakazawa M, Ariyoshi Y, Kimura Y (2006) Neutron irradiation under continuous BPA injection for solving the problem of heterogenous distribution of BPA. In: Nakagawa Y, Kobayashi T, Fukuda H (eds) Advances in neutron capture therapy. International Society for Neutron Capture Therapy, Kagawa, pp 27–30. ISBN 4-9903242-0-X
8. Kankaanranta L, Seppälä T, Koivunoro H, Saarilahti K, Atula T, Collan J, Salli E, Kortesniemi M, Uusi-Simola J, Mäkitie A (2007) Boron neutron capture therapy in the treatment of locally recurred head and neck cancer. Int J Radiat Oncol Biol Phys 69:475–482
9. Aihara T, Hiratuka J, Nishiike S, Morita N, Uno M, Sakurai Y, Maruhashi A, Ono K, Harada T (2006) Using BPA alone for boron neutron capture therapy of recurrent head and neck malignancies. In: Nakagawa Y, Kobayashi T, Fukuda H (eds) Advances in neutron capture therapy. International Society for Neutron Capture Therapy, Kagawa, pp 5–6. ISBN 4-9903242-0-X
10. Kato I, Ono K, Sakurai Y, Ohmae M, Maruhashi A, Imahori Y, Kirihata M, Nakazawa M, Yura Y (2004) Effectiveness of BNCT for recurrent head and neck malignancies. Appl Radiat Isot 61:1069–1073

Studies on the Possible Application of BNCT to Thyroid Cancer

25

Mario A. Pisarev, Maria A. Dagrosa,
and Guillermo J. Juvenal

Contents

M.A. Pisarev (✉)
Department of Radiobiology,
National Atomic Energy Commission, Av Libertador 8250 (1429),
Buenos Aires, Argentina

Department of Human Biochemistry, University of Buenos Aires,
School of Medicine, Buenos Aires, Argentina
e-mail: pisarev@cnea.gov.ar

M.A. Dagrosa • G.J. Juvenal
Department of Radiobiology,
National Atomic Energy Commission, Av Libertador 8250 (1429),
Buenos Aires, Argentina

National Research Council of Argentina,
Rivadavia 1917 (1033), Buenos Aires, Argentina
e-mail: dagrosa@cnea.gov.ar; juvenal@cnea.gov.ar

W.A.G. Sauerwein et al. (eds.), *Neutron Capture Therapy*,
DOI 10.1007/978-3-642-31334-9_25,

25.1 Introduction

Thyroid cancer may occur as a differentiated or an undifferentiated or anaplastic form. The differentiated forms, such as papillary or follicular carcinomas, are in general of a relatively benign prognosis. Most if not all still have a normal uptake of iodine, and therefore surgical thyroidectomy is completed with a therapeutic dose of ^{131}I. In many cases, these forms are well controlled and complete remission of the tumor is obtained. In other instances, the prognosis is not so good. The undifferentiated (UTC) form or the recurrence of some differentiated forms of this pathology has lost their capability to concentrate radioiodine, and therefore the therapeutic dose of this halogen is useless. These last forms are very aggressive and have a fatal outcome in rather a short time after their diagnosis. As a consequence, new treatments are being explored in order to offer these patients a better future. Thanks to the advances in the knowledge of their molecular biology, new chemotherapeutic compounds have been developed and are currently being studied in several clinical trials. Besides, we have started some years ago the study of the possibility of the application of BNCT to the treatment of these pathologies [1, 2].

25.2 Experimental "In Vitro" Studies

We started by analyzing the uptake of a boronated compound, p-borophenylalanine (BPA), by cultured thyroid cells. The results demonstrated that a cell line of undifferentiated cancer had a higher uptake than cells obtained from human thyroid follicular adenoma or from normal glands. When we compared proliferating with quiescent cells of anaplastic cancer, the BPA uptake was the same. This data is quite interesting since it makes a difference with the usual response of tumors to radiotherapy in which only proliferating cells are responsive [3].

25.3 Experimental "In Vivo" Studies

The next step was to develop an animal model. Nude NIH mice were transplanted with the same cell line. This tumor had a very active growth, and in some animals lung metastasis was demonstrated resembling the human UTC behavior. When the biodistribution of BPA was examined by the ICP-AES method, we could again observe a significant greater uptake by the tumor than the normal tissues such as the original thyroid, skin distal to the implant, and other organs. However, the skin around the transplant, which is invaded by cancer cells, had a higher concentration of BPA than the other normal tissues. Only the kidney, where BPA is excreted, had values of boron greater than other tissues. Time-course studies showed that the peak of BPA concentration in the tumor cells was dependent on the amount of compound injected. When a dose of 350 mg/kg body weight was administered, the peak occurred after 60 min, while it took place after 90 min of the i.p. injection with a dose of 600 mg/kg body weight. The tumor/normal tissues boron ratios were calcu-

lated for both doses, and the results again demonstrated a selective uptake by the tumor with a ratio larger than 3. Total boron was between 18 and 24 ppm [3, 4]. The large uptake by the tumor could be reflecting a more active metabolism. Mishima et al. [5] showed, with the use of ^{18}F labeled BPA, a net incorporation rate in the tumor four times higher than that in normal tissues. The mechanism of transport of BPA was analyzed in the glioblastoma cell line GS-9L and in the fibroblast cell line V79. The results supported the hypothesis that BPA is transported by the L amino acid transport system [6].

The complete BNCT treatment was performed in our mice. They were transplanted as before. After 14 days, they were transported to the Bariloche Atomic Center, 1,500 km south from Buenos Aires. After a 24-h recovery, they were injected with BPA, anesthetized, and submitted to an appropriate neutron beam. Only the tumor area was exposed, while the rest of the body was shielded. The growth of the tumor was measured in order to determine the response to the complete treatment. The following groups of mice served as controls: (a) nontreated, BPA injected; (b) irradiated, no BPA; (c) no treatment or injections at all; and (d) BPA + irradiation. All animals survived without toxic effects. The results showed that the nonirradiated mice had a progressive growth of the tumor. Those irradiated without BPA showed an initial slowdown of growth, which reassumed to the slope curve of the other controls after a few days. Those treated by BNCT had two types of response. Animals with a rather larger initial tumor size had a significant stop in tumor growth, but without a complete disappearance, while those with a smaller initial size were histopathologically cured and the transplanted area was replaced by fibrotic tissue in 50 % of the mice. These studies were confirmed by additional experiments. The tumor response was proportional, with a positive significant correlation, to the degree of DNA damage determined by the comet assay and to the total physical absorbed dose [7]. It is known that the DNA damage induced by radiation and the capacity of repair by the cells depend on the quality of radiation. High LET radiations (alpha particle and heavy ions) are biologically more effective than those of low LET (gamma or X-rays) because it causes DNA lesions more complex and difficult to repair [8].

In order to further optimize our encouraging results, we started studies by combining BPA with another boron compound, boronated porphyrin (BOPP). Studies performed in animals bearing a glioma cell line demonstrated that the injection of BOPP caused a significant boron uptake. BOPP,4-bis-(α,β-didihidroxyethyl)-deutero-porphyrin IX is a boronated porphyrin that was synthesized by Kahl in 1989, and it has 40 atoms of boron-10 by molecule against one atom alone in the BPA molecule [9]. Mice transplanted with the UTC cells were injected with BOPP (kindly provided by Prof. SB Kahl, University of California at San Francisco, USA), administered via i.p. or i.v. However, in our model, we failed to observe a selective boron uptake compared to normal tissues after 1 day of administration. Therefore, another protocol was assayed. BOPP was injected via i.p. from 1 to 7 days before BPA, and the boron uptake was measured 60 min after BPA administration. We observed that with the combination of 5 days after BOPP and 60 min after BPA, the boron uptake was 45 ppm, doubling the results obtained with BPA alone [10]. Next,

these animals were irradiated as in the previous studies with the neutron beam of Bariloche Nuclear Reactor (RA6). The animals were followed during 3 months, and a complete stop in tumor progression and a complete disappearance of the tumor cells were observed histologically in 100 % of the mice. The subcellular studies demonstrated that 10B is concentrated in the mitochondria [11].

In our laboratory, in other group of studies, we demonstrated that nicotinamide (NA) injection caused a significant increase in the radiosensitivity to ^{131}I treatment in normal and goitrous rats. This effect was related to the increase in thyroid blood flow. NA causes at the same time an increase in the expression of eNOS synthase and in the generation of peroxides, which are responsible for tissue damage [12]. The possible action of NA on boron uptake was studied demonstrating that it does not affect the uptake by the tumor, NA has been utilized in patients with head and neck tumors submitted to conventional external radiotherapy, with encouraging results [13]. When NA was administered during 3 days prior to BPA + irradiation, a tendency to slightly improve the outcome of the treatment was observed. The determination of apoptosis in tumor samples by measurements of the caspase-3 activity showed an increase significance in the BNCT (BPA + NA) group at 24 h and after the first week post irradiation in the three BNCT groups (BPA alone and combine with NA or BOPP). TUNEL analysis confirmed these results. We could conclude that although nicotinamide combined with BPA produces an increase of apoptosis at early times, only the group irradiated after the combined administration of BPA and BOPP significantly improves the therapeutic response [11].

These encouraging results led us to study larger animals. Dogs can present spontaneous UTC, which behaves similarly to the human tumor, causing dyspnea due to compression of the trachea, and to produce metastasis in the rest of the body. We studied the uptake of BPA in 8 dogs that had an indication of surgery at the School of Veterinary Sciences, University of Buenos Aires, with previous signed informed consent from the owners. The animals were anesthetized and infused during 60 min with a solution of BPA-fructose and then transported to the operating room. Blood samples were obtained every 15 min, and during surgery, samples of normal thyroid and of areas of the tumor were taken to measure boron concentration and for histopathology. The boron concentration in the tumor was greater than that in blood or in normal thyroid but with scattered values. When the histopathology was taken into consideration, the different areas from each tumors were classified as homogeneous or heterogeneous, the latter with areas of dead tumor cells and with fibrosis and adipose tissue. A clear correlation was demonstrated between the quality of cellularity, amount of live cells, and the boron uptake. We may then conclude that BNCT may be effective for the treatment of UTC in dogs [14].

25.4 Radiobiological Studies

In order to apply BNCT to a tumor, it is necessary to consider a number of factors. They include not only the size and shape of the tumor, the boron compound to be used and its uptake and time of persistence in the tumor area, as well as the radiobiological characteristics of the tumor. The relative biological effectiveness factor

(RBE) of the neutron beam and the compound biological effectiveness factor (CBE), which combines the beam and the boron compound, are used in order to obtain the total physical absorbed dose. These radiobiological factors permit the comparison with the conventional treatment or with other neutron beams. In collaboration with the group of the Massachusetts Institute of Technology (Cambridge, MA, USA) a series of studies were performed with the ARO cells. The cells were incubated with BPA alone or with the mixture of BPA + BOPP and irradiated with increasing doses of either neutrons or X-rays. The biological endpoint (generation of new cells) was evaluated by the colony formation assay and values of 3.9 and 2.6 for the CBE of BPA and BPA + BOPP, respectively, were obtained. The value obtained for the combination was consistent with being additive. For the neutron beam, the RBE gave a value of 1.2 [15].

We also evaluated in vitro the mechanisms of damage induced by BNCT by cytokines block micronuclei assay (CBMN) and by the cell fraction survival using a colorimetric assay of viability (MTT). We also calculated the relative biological effectiveness factor (RBE) of the neutron beam and the compound biological effectiveness (CBE) values for BPA and BOPP. The frequency of micronucleated binucleated UTC cells and the number of MN per micronucleated binucleated cells showed a dependent dose relationship until around 2 Gy. The response to gamma rays was significantly less than the other treatments. The irradiation with neutrons alone and neutrons + BOPP showed curves that did not differ significantly and showed less DNA damage than neutrons + BPA. A decrease in the survival fraction as a function of the physical dose was observed for all the treatments. We also observed that neutrons and neutrons + BOPP did not differ significantly and that BPA is the more effective compound. The RBE and CBE factors calculated from CBMN and MTT assays, respectively, gave the following values: beam RBE, 4.4 ± 1.1 and 2.4 ± 0.6; CBE for BOPP, 8.0 ± 2.2 and 2.0 ± 1; and CBE for BPA, 19.6 ± 3.7 and 3.6 + 1.3. These values represent the first experimental values obtained for the RA-3 (nuclear reactor of Ezeiza) in a biological model and will be useful for future dosimetric experimental studies of the application of BNCT to UTC [16].

25.5 Clinical Studies

A protocol for biodistribution studies in humans was established and approved by the research and ethics committees of seven hospitals in Buenos Aires, followed by the approval of the Ministry of Public Health of Argentina. In each case, the signed informed consent of the patients was also obtained. These studies are underway and so far three patients have been analyzed, but further studies are required in order to arrive at a conclusion.

A similar study was carried on in Germany. Wittig et al. [17] have analyzed the boron uptake in patients suffering from recurrence of differentiated thyroid cancer and one with UTC. In those infused with 50 mg/kg bw BSH within 60 min prior to surgery, the tumor/blood ratio was around 0.9 while the tumor/muscle ratio was 1.9. When BPA was infused (100 mg/kg bw), the tumor/blood ratio was around 1.7 while the tumor/normal tissues ratio was around 0.9. These authors concluded that

BNCT might not be useful for recurrent differentiated thyroid cancer [17]. Meanwhile, one patient with a relapsed papillary thyroid cancer was treated by BNCT in Japan in September 2003. No adverse effects were observed and the patient survived up to 18 months [18].

25.6 Recent Advances

Besides the UTC sometimes the relapse of human differentiated thyroid cancer occurs with a more aggressive form which lacks iodine uptake.

The aim of these studies was to evaluate the possibility of treating differentiated thyroid cancer by BNCT. These carcinomas are well controlled with surgery followed by therapy with 131I; however, some patients do not respond to this treatment. BPA uptake was analyzed both in vitro and in nude mice implanted with cell lines of differentiated thyroid carcinoma. The boron intracellular concentration in the different cell lines and the bio-distribution studies showed the selectivity of the BPA uptake by this kind of tumor [19].

In other studies we have evaluated the mechanisms of cellular response to DNA damage induced by BNCT. Thyroid carcinoma cells were incubated with 10BPA or 10BOPP and irradiated with thermal neutrons. The surviving fraction, the cell cycle distribution and the expression of p53 and Ku70 were analyzed. Different cellular responses were observed for each irradiated group. The decrease of Ku70 in the neutrons +BOPP group could play a role in the increase of sensitization to radiation [20].

Acknowledgments The original studies from our laboratory were supported by grants from the National Research Council (CONICET), the National Agency for Science and Technology (FONCyT), the University of Buenos Aires, and the Atomic Energy Commission. All authors are established researchers from CONICET.

References

1. Ain KB (1998) Anaplastic thyroid carcinoma: behavior, biology, and therapeutic approaches. Thyroid 8:715–726
2. Chandrakanth A, Ashok RS et al (2006) Anaplastic thyroid carcinoma: biology, pathogenesis, prognostic factors and treatment approaches. Ann Surg Oncol 13:1–12
3. Dagrosa MA, Viaggi M, Kreimann E, Garavaglia R, Farías S, Agote M, Cabrini RL, Juvenal G, Pisarev MA (2002) Selective biodistribution of p-borophenylalanine by undifferentiated thyroid carcinoma for boron neutron capture therapy (BNCT). Thyroid 12(1):7–12
4. Viaggi M, Dagrosa MA, Gangitano D, Belli C, Larripa I, Cabrini R, Pisarev M, Juvenal G (2003) A new animal model for human undifferentiated thyroid carcinoma. Thyroid 13:529–536
5. Mishima Y, Imahori Y, Honda C, Hiratsuka J, Ueda S, Ido T (1997) In vivo diagnosis of human melanoma with positron emission tomography using specific melanoma-seeking ^{18}F-DOPA analogue. J Neurooncol 33:163–169
6. Wittig A, Sauerwein WA, Coderre JA (2000) Mechanisms of transport of p-borono-phenylalanine through the cell membrane in vitro. Radiat Res 153:173–180

7. Dagrosa MA, Viaggi M, Longhino J, Calzetta O, Cabrini R, Edreira M, Juvenal G, Pisarev M (2003) Experimental application of boron neutron capture therapy (BNCT) to undifferentiated thyroid carcinoma (UTC). Int J Radiat Oncol Biol Phys 57(4):1084–1092
8. Rydberg B (1996) Clusters of DNA damage induced by ionizing radiation: formation of short DNA fragments. II. Experimental detection. Radiat Res 145:200–209
9. Kahl SB, Koo MS (1992) Synthesis and properties of tetrakiscarborane-carboxylate esters of 2, 4-bis (–dihydroxyethyl) deuteroporphyrin IX. In: Allen BJ, Moore DE, Harrington BV (eds) Progress in neutron capture therapy for cancer. Plenum Press, New York, pp 223–226
10. Dagrosa MA, Viaggi M, Jiménez Rebagliati R, Batistoni D, Kahl SB, Juvenal G, Pisarev M (2005) Biodistribution of boron compounds in an animal model of undifferentiated thyroid cancer for boron neutron capture therapy. Mol Pharm 2(2):152–156
11. Dagrosa MA, Thomasz L, Longhino J, Perona M, Calzetta O, Blaumann H, Jiménez Rebagliati R, Cabrini RL, Kahl SB, Juvenal GJ, Pisarev MA (2007) Optimization of the application of boron neutron capture therapy (BNCT) to the treatment of undifferentiated thyroid cancer (UTC). Int J Radiat Oncol Biol Phys 69(4):1059–1066
12. Agote M, Viaggi M, Kreimann E, Krawiec L, Dagrosa MA, Juvenal GJ, Pisarev MA (2001) Influence of nicotinamide on the radiosensitivity of normal and goitrous thyroid in the rat. Thyroid 11:1005–1009
13. Horsman MR, Siemann DW, Chaplin DJ et al (1997) Nicotinamide as a radiosensitizer in tumor and normal tissues: the importance of drug dose and timing. Radiother Oncol 45:167–174
14. Dagrosa MA, Viaggi M, Jimenez Rebagliati R, Castillo VA, Batistoni D, Cabrini RL, Castiglia S, Juvenal GJ, Pisarev MA (2004) Biodistribution of p-borophenylalanine (BPA) in dogs with spontaneous undifferentiated thyroid carcinoma (UTC). Appl Radiat Isot 61(5):911–915
15. Dagrosa MA, Chung Y, Riley K, Binns P, Kahl S, Pisarev M, Coderre J (2006) Compound biological effectiveness (CBE) factors in human undifferentiated thyroid cancer (UTC). Advances in Neutron Capture Therapy. Proceedings of ICNCT 12, Takamatsu, Kagawa, 2006, pp 157–160
16. Dagrosa M, Crivello M, Thorp S, Perona M, Pozzi E, Casal M, Cabrini R, Kahl S, Juvenal G, Pisarev M (2008) Radiobiological studies in a human cell line of undifferentiated thyroid cancer. Proceedings of 13 ICNCT, Florence, 2008, pp 337–340
17. Wittig A, Sheu Y, Kaiser GM, Lang S, Jöckel H, Moss R, Stecher-Rasmussen F, Rassow J, Colette L, Sauerwein W (2008) New indications for BNCT? Results from the EORTC trial 11001. Proceedings of 13 ICNCT, Florence, 2008, pp 39–42
18. Hiratsuka J, Morita N, Aihara T, Imajo Y, Maruhashi A, Ono K (2006) First clinical trial of boron neutron capture therapy for thyroid cancer. Advances in Neutron Capture Therapy. Proceedings of ICNCT 12, Takamatsu, Kagawa, 2006, pp 7–9
19. Dagrosa MA, Carpano M, Perona M, Thomasz L, Nievas S, Cabrini R, Juvenal G, Pisarev M (2011) Studies for the application of boron neutron therapy to the treatment of differentiated thyroid cancer. Appl Radiat Isot 69:1752–1755
20. Perona M, Pontigia O, Carpano M, Thomasz L, Thorp S, Pozzi E, Simian M, Kahl SB, Juvenal G, Pisarev N, Dagrosa A (2011) Un Vitro studies of cellular response to DNA damage induced by boron neutron capture therapy. Appl Radiat Isot 69:1732–1738

Malignant Melanoma

26

Junichi Hiratsuka and Hiroshi Fukuda

Contents

J. Hiratsuka (✉)
Department of Radiation Oncology, Kawasaki Medical School,
Okayama, 701-0192, Japan
e-mail: hiratuka@med.kawasaki-m.ac.jp

H. Fukuda
Department of Nuclear Medicine and Radiology, Institute of Development,
Aging and Cancer, Tohoku University, Sendai, 980-8575, Japan
email: hiro@idac.tohoku.ac.jp

W.A.G. Sauerwein et al. (eds.), *Neutron Capture Therapy*,
DOI 10.1007/978-3-642-31334-9_26,

26.1 Introduction

In 1972, an experimental study on boron neutron capture therapy (BNCT) for malignant melanoma was initiated by Mishima and his colleagues (Kobe University group). They first proposed employing BNCT for malignant melanomas utilizing the specific melanin synthesis activity of melanoma cells. For that purpose, ^{10}B-paraboronophenylalanine (BPA) was reevaluated by his group. After 15 years of basic research, this team started the first clinical trial of cutaneous melanoma BNCT using BPA in 1987 [1–12]. Thanks to improvement in boron delivery agents and low-energy neutron beam technology, several BNCT clinical trials for melanoma were started in the world: at the Massachusetts Institute of Technology in 1994 for cutaneous melanoma and in 1996 for intracerebral melanoma (Harvard/MIT group) [13–15], at the high flux reactor in Petten in 2002 for brain metastases of melanoma (Petten/Essen group) [16, 17], at RA-6 reactor in Argentina in 2003 for cutaneous melanoma (Argentina group) [18, 19], and at KUR and JRR-4 in Japan in 2003 for mucosal melanomas of the head and neck (Kawasaki group) [20]. The number of melanoma patients treated with BNCT is much smaller than that of glioglastoma because surgical excision has been considered to be the most effective and curative therapy in the treatment of melanoma. There are few reports about the local response and survival of patients with cutaneous and mucosal malignant melanomas treated by BNCT. Each group has its protocol and primary end point. The following chapter summarizes the current clinical results.

26.2 Actual State-of-the-Art Treatment

According to treatment guidelines of the National Cancer Institute (NCI), clinical and histological factors as well as the anatomic location of the lesion have impact on the prognosis of malignant melanoma. Surgical excision continues to be the mainstay in the treatment of primary cutaneous melanoma, aiming to completely remove the lesion at the primary site using adequate resection margins in order to provide durable local disease control. The risk of lymph node and/or systemic metastasis increases with increasing thickness of the primary lesion. Therefore, in patients suffering from melanoma with Breslow thickness of 2 mm, complete lymph node dissection should be considered if the sentinel lymph node(s) is microscopically or macroscopically positive. Patients with melanomas that have a Breslow thickness more than 4 mm should be considered for adjuvant therapy with high-dose interferon, which has shown to increase relapse-free survival and overall survival (OS) when compared to observation [21]. However, melanoma that has spread to distant sites is rarely curable with standard therapy. Treatment of mucosal melanoma of the head and neck has not been standardized. Surgery is usually chosen as the first therapy if the primary lesion is resectable. Radiotherapy is a valuable option for selected groups of patients especially as a palliative treatment option in patients suffering from metastatic melanomas, medically inoperable patients, patients with large facial lesions which may involve wide surgical resections with extensive facial

reconstruction causing serious functional and cosmetic problems, or patients who have refused surgery [22]. Because of the very limited indication of radiotherapy for melanomas, there have been few reports on the efficacy for primary mucosal melanomas [23]. Adjuvant radiotherapy may be indicated to control local disease, especially for patients with questionable surgical margins.

Several institutes have reported clinical results using Cf-252 neutron brachytherapy [24] or proton radiotherapy [25], by which high radiation doses can be delivered to the target volume. Because of the high rate of treatment failure in stage II melanoma or higher, clinical trials exploring adjuvant chemotherapy and/or biologic therapy, or immunotherapy, are appropriate choices when possible for newly diagnosed patients. Options evaluated are, for example, dacarbazine (DTIC), temozolomide, and cancer vaccines.

26.3 Rationale for BNCT

The first BNCT applications on melanomas of the skin have to be considered as "proof of principle" of the modality. There is a different situation in advanced or recurrent mucosal melanomas of the head and neck after the standard therapies, where no efficient treatment exists. BNCT has several advantages as salvage therapy to the head and neck mucosal melanomas. First, the head and neck have many important physiological and cosmetic functions. Therefore, the quality of life after treatment has a great influence on the quality of life of patients with a head and neck tumor. When ^{10}B is selectively accumulated in tumor cells, these cells can be destroyed by thermal neutron irradiation without serious damage to the surrounding normal tissue. Theoretically, BNCT can be considered to be an ideal local treatment because the structure and function of the irradiated normal tissues are preserved, whereas surgical procedures have a negative impact on postsurgical life due to functional and aesthetic problems. Second, as tumors located in the head and neck region are located close to the skin surface, it might be possible to administer curative radiation doses to the target by utilizing an epithermal neutron beam. The advantage of an epithermal neutron beam over thermal beams is that it penetrates a few centimeters into human tissue before forming a thermal peak. Consequently, with an epithermal neutron beam it may be possible to treat deeper seated tumors. Third, there are many patients with melanoma located in the head and neck region which cannot be controlled by conventional cancer therapy. Fourth, ^{18}F-BPA-PET studies allow to identify patients who may be treated with BNCT due to selective uptake of ^{18}F-BPA [20].

26.4 Melanoma and BPA

Originally, BPA was developed with the reasoning that since the biosynthesis of melanin requires tyrosine as a precursor, the boronated form of this amino acid might be selectively taken up by melanoma cells [6]. It has been proven that p-BPA

accumulates selectively in melanoma cells, and several in vivo and in vitro studies support the hypothesis that this compound is taken up by melanoma cells in a similar manner to tyrosine. Mishima et al. used this compound as a capture agent for BNCT of melanoma in experimental animals and clinically in patients [7–9]. Using ^{11}B-NMR studies, their group found that melanin monomers, intermediates for melanin polymer formation, and BPA can form a chemical complex in the solution system [2]. The authors concluded that the complex formation between BPA and melanin monomers plays an important role in the selective accumulation of BPA within melanoma cells.

However, Coderre et al. [26] reported that this compound was also selectively taken up in vivo by nonpigmented tumors including murine mammary tumors and rat gliosarcomas. They suggested that there are other mechanisms of p-BPA uptake which are independent of melanin synthesis and that accumulation of p-BPA in rapidly growing animal tumors could be due to the metabolic demand for the amino acids needed for protein synthesis. It has been proven that p-BPA is transported not only as a tyrosine analogue for melanin synthesis but also as an amino acid analogue [27, 28].

Recently, this compound has also been utilized for BNCT of brain tumors [29] and head and neck malignancies [30, 31].

26.5 Technical Aspects

1. BPA is very hard to be dissolved in saline, and it can be solubilized at neutral pH by complexation with fructose [3]. Intravenous administration of BPA-fructose complex for 2–3 h and blood sampling.
2. Construction of a neutron collimator to shield normal tissues using ^{6}Li containing thermoplastic with 10 mm in thickness (Fig. 26.1).
3. Final setting and fixation of the patient to the irradiation beam port (Fig. 26.2).
4. Attachment of thermoluminescence detectors (TLD) and gold wires to the skin of the irradiation field for dosimetry. Neutron flux measurement using gold wire 15 min after the start of irradiation. LiF sheets (10 mm thick) were chosen as the collimator material to shield normal tissues from neutron exposure. The radiation field was defined with a 1–2 cm safety margin from the clinical target volume.
5. Prescribing of dose. All doses are expressed in weighted (Gy (w)) units using RBE and CBE factors [32]. To express the total BNCT dose in a common, photon-equivalent unit, enabling comparison with conventional photon irradiation, for tumor and for each of the normal tissues at risk, each of the high-LET dose components (physical dose in Gy) is multiplied by an experimentally determined biological effectiveness factors (RBE and CBE). The total photon-equivalent BNCT dose can then be expressed as the sum of the biological-effectiveness-corrected physical-absorbed dose components. The biological effectiveness factors used in the trial of intracranial melanoma BNCT at Harvard/MIT group were 3.2 for both fast and thermal neutrons, 1.3 for ^{10}B (n, α)^{7}Li reaction, and 1.0 for

Fig. 26.1 A neutron collimation to shield normal tissues using ^{6}Li containing thermoplastic (10 mm thickness) in BNCT for melanoma of the nasal cavity (case no. 3)

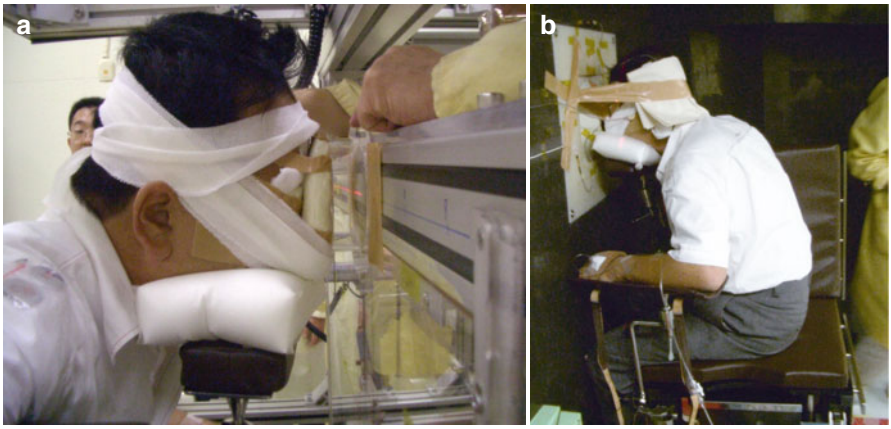

Fig. 26.2 Simulation (**a**) and final setting (**b**) of the patient to the irradiation beam port (case no. 3)

Table 26.1 Biological effectiveness factors used in calculating photon equivalent doses during BNCT at the KUR and JRR-4

Dose component	Biological effectiveness factor (CBE* or RBE**)
$^{10}B(n, \alpha)^{7}Li$ reaction [BPA]	CBE for tumor (melanoma) = 3.8
	CBE for normal skin = 2.5
	CBE for normal mucosa = 4.9
	CBE for central nerve system = 1.35
Thermal neutron	RBE = 3.0
Fast neutron	RBE = 3.0
γ-ray	RBE = 1.0

*CBE** compound biological effectiveness, *RBE*** relative biological effectiveness

gamma rays. In the case of cutaneous melanoma of the extremities, these values were 4.0 for the fast neutron, the thermal neutron and the ^{10}B (n, α)^{7}Li reaction, and 0.5 for gamma rays. Table 26.1 lists the biological effectiveness factors [RBE of the fast neutron and thermal neutron, CBE for the $^{10}B(n, \alpha)^{7}Li$ reaction] that have been chosen for use in the clinical BNCT trial in Japan. The time for neutron irradiation ranged from 20 to 60 min, depending on the blood boron levels, the tumor depth, and the limiting dose to the nearest critical organ. All groups always irradiate the tumor at the maximum tolerable dose for surrounding normal tissues regardless of the ^{10}B concentration in the tumor.

6. Fractionation. BNCT has generally been delivered in a single fraction. Some groups described the benefit of a fractionated course of BNCT. Both of Harvard/MIT group and Petten/Essen group applied the schedule of two fractions on consecutive days. This required a second BPA infusion for the second dose. Their rationale for the two-fraction approach was that the second BPA administration could lead to a redistribution of boron into tumor cells missed on the first fraction, that is, an attempt to improve the uniformity of tumor cell kill [33]. Each field was given on each treatment day. An under- or overdose to a given field which might be caused by differing ^{10}B concentrations on the first day could be corrected on the second day of irradiation [17].

26.6 Clinical Applications

In general, the following criteria were used to determine patient eligibility for BNCT:

- Patients with malignant melanoma pathologically confirmed
- Patients with melanomas that have relapsed after conventional cancer therapies
- Patients with normal renal and hepatic functions
- Patients without severe concomitant disease
- Hematological data within normal range
- Patients with an anticipated general life expectancy of ≥1 year and PS ≥ 2
- Patients who have given a written informed consent to perform BNCT

EORTC protocol 11011 for metastatic melanoma BNCT includes some criteria other than those above mentioned [17]:

1. The lesion proposed for irradiation must be brain metastases or soft tissue metastases of head and neck or the extremities.
2. The lesion must be measurable with MRI scan.
3. No prior radiation therapy to the site intended to be irradiated with BNCT.
4. Patient must have recovered from toxic effects of previous anticancer therapy.

Japanese protocol eligibility criteria includes a *T*/*N* uptake ratio of ^{18}F-BPA ≥ 2.5.

26.7 Results

26.7.1 Cutaneous Melanoma

26.7.1.1 Kobe University Group

Twenty-four patients were treated with BNCT between July 1987 and April 2005. In Kobe series, the patients were administered 170–210 mg/kg·BW of BPA for 3–5 h and irradiated with thermal beam. Details of their BNCT procedures have been reported elsewhere [12]. Briefly, this group always irradiated 18 Gy (w), which is a maximum tolerable dose to the normal skin, to the tumor surrounding skin regardless of ^{10}B-concentration in the tumor. A neutron fluence yielding 18 Gy (w) to the skin is optimized by using a measured ^{10}B-concentration in the blood (ppm) and mean skin-to-blood ^{10}B-concentraion ratio (factor of 1.3).

The 24 patients, 10 males and 14 females, ranged in age from 48 to 85 years , with an average age of 67 years . The patient characteristics are shown in Table 26.2. The target areas were 20 primary lesions and 4 metastatic lesions. The melanoma types were acral lentiginous melanoma (ALM) in 13 patients, nodular melanoma (NM) in 6 patients, and lentigo maligna melanoma (LMM) in 5 patients. As for the tumor site, 14 were on the sole of foot, 6 on the face, 2 on the leg, and 2 on the finger. Local responses are shown in Table 26.2. The absorbed doses to the tumor

Table 26.2 Tumor characteristics and tumor response rate

	Patient number	CR (%)	Non-CR
Primary/meta			
Primary	20	15 (75)	5
Meta	4	2(50)	2
Type			
NM	6	2 (33)	4
ALM and LMM	18	15 (83)	3
Tumor site			
Sole	14	10 (71)	4
Face	6	5 (83)	1
Leg	2	1 (50)	1
Finger	2	1 (50)	1

NM nodular melanoma, *ALM* acral lentigious melanoma, *LMM* lentigo maligna melanoma, *CR* complete regression

ranged from 18.6 to 68.5 Gy (w). The complete regression (CR) rates were 75 % (15/20) and 50 % (2/4) for the primary and metastatic lesions, respectively. Among the primary lesions, the CR rates according to melanoma type were 33 % (2/6) for NM and 83 % (15/18) for non-NM (ALM + LMM). None of the 17 lesions with CR showed local recurrences in the radiation field during follow-up ranging (follow-up period: 4–15 years). The percentage of CR in non-NM was excellent, whereas that in NM was poor. There are a number of possible reasons for the poor response cases in NM. The most likely explanation is a lower boron concentration in the melanoma than the assumption. Because it is not possible to directly measure ^{10}B concentration in the tumor during neutron irradiation, the predetermined tumor-to-blood ^{10}B concentration ratio of 3.0 was used [12]. That value was based on the measured data in operated patients, but the variation in the ratio was very large (3.40 ± 0.83), and the lowest measured ratio was 1.3. The second reason for poor responses may be the difference in radiosensitivity between NM and non-NM. Johanson et al. [34] noted that NM was completely different from LMM both in biological terms and in terms of response to radiotherapy. Another explanation is lower radiation doses than estimated at the deepest point of the nodular melanoma. Gold wires and gold foil were placed on the surface of the melanoma to determine precisely the neutron flux irradiated to the tumor in each patient. However, it was difficult to obtain an accurate and approximate neutron flux at the deepest point of thick melanomas, especially in nodular types. At the time when the Kobe University group treated patients with NM, computational dosimetry systems such as JCDS and SERA, ^{18}F-BPA-PET studies, and the epithermal beam were not available in Japan. At present, since these modalities can be applied to BNCT against NM, the responses may improve drastically. The 5-year cause-specific survival rates were 60 % for all cases and 75 % for primary melanoma cases. All of the four metastatic cases died from systemic metastasis within 3 years after BNCT. Absorbed doses to the skin ranged from 12.0 to 37.1 Gy (w). According to CTCAE v.3.0, 2, 16, 3, and 3 patients had side effects of grades 1, 2, 3, and 4, respectively. Eighteen of the 24 cases had tolerable skin damage (less than Grade 2). In particular, five cases of facial melanomas were cured without any cosmetic or functional problems of the facial skin. Although six cases exceeded the tolerable skin damage level, three (skin absorbed doses: 15.7 Gy (w), 24.0 Gy (w), 37.1 Gy (w)) of them were cured with medication against radiation dermatitis. The remaining three cases (skin absorbed doses: 22.3 Gy (w), 23.4 Gy (w), 29.2 Gy (w)) developed severe skin damage resulting in skin grafts.

26.7.1.2 Harvard/MIT Group

At the Massachusetts Institute of Technology (MIT), melanoma BNCT clinical trials have been started in 1994 for cutaneous melanoma and in 1996 for intracerebral melanoma. Between September 1994 and May 1996, they performed cutaneous melanoma BNCT clinical trials with an epithermal beam of MITR. Four patients suffering from cutaneous melanoma of the extremities were treated using BPA as part of a phase I trial designed to study the normal tissue reaction following BNCT. BPA was administered as a 400-mg/kg oral preparation. At the reactor, a blood sample was drawn just prior the neutron irradiation. Biopsies of tumor and normal

tissue were carried out for determination of intracellular boron-10 concentration. Based on the results of ^{10}B assay of the blood, tumor, and normal tissues samples, the required epithermal neutron fluence was calculated to deliver 2.5 Gy (w) per fraction to normal tissue. Each patient received four daily fractions of a prescribed dose of 2.5 Gy (w) per fraction for a nominal total of 10 Gy (w) maximum dose to normal tissue. This trial was designed to escalate the total dose from 10 Gy (w) to 12.5 Gy (w). The biological effectiveness factors (RBE and CBE) used in the trial were 4.0 for the fast neutron, the thermal neutron, and the ^{10}B (n, α)^{7}Li reaction and 0.5 for gamma rays. There was no observed boron compound toxicity and, thus far, no radiation-induced normal tissue reactions or any other untoward events related to the high oral doses of the boron compound or to the neutron irradiations.

Although technically not part of a phase I trial, the local response of the tumors to BNCT was investigated, and it was gratifying that all evaluable patients experienced at least a partial response even at the lowest dose level. Three patients experienced regrowth of the disease within the irradiation field. The single patient who achieved a complete pathological response remains free of disease at this site [13, 14].

26.7.1.3 Petten/Essen Group

Petten and Essen group started the EORTC phase I trial 11011 on melanoma in 2002 at the high flux reactor (HFR) in Petten. The first aim of the trial was to assess the therapeutic activity, the efficacy, and the safety of BNCT using BPA in patients with metastases of malignant melanoma. BNCT is applied in 2 fractions with the epithermal beam. Each patient received prior to each fraction of irradiation a dose of 350-mg BPA/kg BW in form of a BPA-fructose complex. The infusion was applied intravenously via central venous catheter over 90 min. The irradiation was started after the end of infusion.

The second aim was to measure the boron concentration as delivered with BPA in tissues and inside individual cells. Sample of tumor and surrounding healthy tissues was collected during a planned surgical intervention, which took place prior to the BNCT irradiation. The trial contains an optional biodistribution sub-study, which is done if operable metastases are removed prior BNCT. If the patient participated in the sub-study, 350-mg BPA/kg BW was administered within 90 min prior to surgery. The infusion was given via central venous catheter and started 120 min prior to tissue sampling. Surgery was done to remove an operable metastasis. Inoperable metastases were treated with BNCT. The microscopic distribution of ^{10}B was evaluated with Laser-SNMS, TOF-SIMS, and EELS. The concept of the study had been developed in close collaboration with the Harvard/MIT group. In case of diffuse brain metastases, the whole brain was irradiated homogeneously using 5 irradiation beams from different directions. The dose was prescribed as the weighted dose D_w applied as an average dose to the whole brain of 7 Gy but not exceeding a dose to the skin $D_{w(skin)}$ of 22 Gy and a dose to the optic chiasm of 8 Gy. For the purpose of calculating the neural tissue dose, the tumor was assumed to be part of the normal brain tissue, and no specific factor for tumor tissue was used for this specific purpose. The prescribed dose was given in two fractions preferably on 2 consecutive days, but the application of the two fractions within 3 days is also

acceptable. Each field was given on each treatment day. An under- or overdose to a given field which might be caused by differing ^{10}B concentrations on the first day could be corrected on the second day of irradiation.

Four patients suffering from multiple brain metastases have been included. All patients completed protocol treatments. Two patients underwent the biodistribution study. The boron concentrations were 55.2–72.3 ppm (tumor-blood ratio: 3.4–4.3). This group reported that the pharmacokinetics of the BPA could be predicted very precisely using a two-compartment model.

In all patients, the whole brain was irradiated homogenously using five irradiation beams from different directions in two consecutive fractions. As the preliminary results, one patient suffered from arrhythmia absoluta after the BPA infusion for the first fraction. Some patients experienced seizures several days after the BNCT.

In all cases, they observed a partial response or no change of the metastases in the irradiated volume; however, none of the patients survived more than 3 months [16, 17].

26.7.1.4 Argentina Group

A phase I/II protocol of a planned cohort of thirty patients for treating cutaneous melanomas with BNCT was initiated in Argentina in 2003. The protocol was designed to evaluate the efficacy and toxicity of BNCT for cutaneous skin melanomas located at the extremities. BPA-fructose was infused intravenously over 90 min. at a dose of 14 g/m^2. The skin was considered the organ at risk for acute and late toxicity. The maximum tolerable dose for skin was adopted as the prescription dose, regardless of the boron concentration in the tumor. For a pre-planning dosimetry, a biodisribution of boron was performed. Blood samples were taken every 10 or 15 min for about 300 min. Punch biopsies of normal skin and tumor were performed 1 h after the end of BPA administration.

Three patients (six irradiations) with multiple subcutaneous skin metastases, which progressed to chemotherapy, were treated. There were no metastases in other organs. Patients were infused with BPA-fructose and irradiated in the hyperthermal (a mixed thermal and epithermal) neutron beam of the RA-6 facility. The skin doses were scaled 16.5–24 Gy (w) in the six irradiations. The dose is prescribed as weighted dose. The tumor dose was calculated considering the tumor-to-blood boron concentration ratio = 3.5. With a minimum follow-up of 10 months, objective tumor response was observed in most of the melanomas treated. CR was noticed in all nodules of one out of three patients who received higher tumor doses (43–57 Gy(w)). There was a Grade 1 RTOG/EORTC skin acute reaction in two patients and a Grade 3 skin acute reaction in one patient with complete response. No late toxicity was observed [18, 19].

26.7.2 Mucosal Melanoma (Kawasaki Group)

Based on several treatment regimens of cutaneous melanomas, since 2003, the Kawasaki Medical School group (Kawasaki group) has started a clinical trial on patients with mucosal melanomas of the head and neck using an epithermal beam.

Table 26.3 Patient characteristics

Patient	Age/gender	Tumor site	Stage	Previous treatment	Boron *T/N* ratio
1	55/male	Nasal cavity	rT1	Surgery + chemotherapy	3
2	74/female	Nasal cavity	rT1	Surgery + chemotherapy	3
3	73/male	N cavity	T1	Chemotherapy	3
4	66/male	Cervical LN	N2b	Surgery (primary)	3
5	71/female	Nasal cavity	rT4	Surgery + chemotherapy	3.1
6	64/male	Maxillary sinus	rT2	Surgery + chemotherapy	2.7
7	69/male	Maxillary sinus	T4	Chemotherapy	3.7
8	74/female	Nasal cavity	rT1	Surgery + chemotherapy	3
9	69/male	Nasal cavity	rT1	Surgery + chemotherapy + RT	2.5
10	72/male	Cervical LN	N2a	Surgery + chemotherapy	2.5
11	73/female	Labia minora	T2	Chemotherapy	3

T/N ratio tumor/normal tissue ratio, *RT* radiotherapy

This group has added ^{18}F-BPA-PET findings to their protocol. The eligibility of patients for BNCT and the dose calculation were based on ^{18}F-BPA-PET findings [20]. Since 2006, BPA is injected at a dose of 500 mg/kg and at a speed of 200 mg/kg/h for the initial 2 h, and the speed decreased to 100 mg/kg/h for the remaining 1 h, and neutron irradiation is done during the final 1 h. The ^{10}B concentration in blood at the completion of neutron irradiation remains on average at 96 % of the ^{10}B-concentration at the start of irradiation [35]. Optimization of the absorbed dose was based on the measured blood boron concentration and neutron flux. Normal tissue and melanoma absorbed doses were calculated by the mean blood boron level and the neutron flux at the tumor site using gold wires, based on the ratios obtained by ^{18}F-BPA-PET study. If the tumor/normal tissue (*T/N*) ratio could not be obtained by ^{18}F-BPA-PET study because of thinness of the tumor or small tumor size, the value reported by Fukuda et al. [12] was used instead, for which the *T/N* ratio was approximately 3.0. This value was based on data of patients suffering from cutaneous melanoma. The *T/N* ratio in mucosal melanoma is assumed to be almost the same as the *T/N* ratio in cutaneous melanoma. The total eye absorbed dose of 11 Gy (w) was used as the dose-limiting factor for five patients whose eyes were included in the irradiation field. The key point of their treatment policy is that we always irradiate the tumor at the maximum tolerable dose for surrounding normal skin (18 Gy (w)) regardless of the ^{10}B concentration in the tumor. The maximum doses for the normal skin, mucosa, and eyes were planned not to exceed 18, 18, and 11 Gy (w), respectively. Dose calculations and treatment plan evaluations were made with the JCDS (JAERI Computational Dosimetry System) at the JRR-4 of Japan Atomic Energy Research Institute (JAERI) and with SERA at the KUR of the Kyoto University Research Reactor Institute (KURRI).

Eleven patients with mucosal melanomas were treated by BNCT between August 2005 and November 2007. Tables 26.3 and 26.4 summarize patient description, tumor characteristics, and clinical outcome.

The 11 patients, 7 males and 4 females, ranged in age from 55 to 74 years old, with an average age of 69 years old. The target areas were nine primary lesions and

Table 26.4 Treatment administered and outcome

Patient (case no.)	Tumor dose (Gy) average/ minimum	Normal tissue dose (Gy)	Tumor response	Complications (CTCAE v.3.0)	Locoregional control (months)	Outcome
1	18.9/16.1	9.6 (eye)	CR	Grade 2	40+	40/alive
2	35.9/29.6	10.3 (eye)	PR	Grade 1	23	32/alive
3	40.2/24.0	10.0 (eye)	CR	Grade 1	18	32/alive
4	33.8/23.0	8.2 (skin)	PR	Grade 2	18+	18/DOC (liver meta)
5	41.2/19.0	10.1 (eye)	CR	Grade 1	10+	10/DOC (brain meta)
6	24.0/21.1	15.1 (oral mucosa)	PR	Grade 1	9+	9/DOC (spinal meta)
7	54.6/23.3	16.6 (oral mucosa)	NC	Grade 1	12	22/alive
8	35.9/29.6	10.3 (eye)	PR	Grade 1	10	22/alive
9	38.3/27.2	16.4 (oral mucosa)	CR	Grade 1	3	7/DOC (lung meta)
10	74.0/23.4	19.0 (skin)	PR	Grade 1	2	6/DOC (brain meta)
11	32.0/25.6	14.0 (mucosa)	CR	Grade 2	13+	13/DOC (lung meta)

CR complete regression, *PR* partial regression, *NC* no response, *DOC* death of cancer

two metastatic lesions. As for the tumor site of the nine primary melanomas, six were in the nasal cavity, two were in the maxillary sinus, and one was in the labia minora. Two patients with cervical lymph node metastases had already undergone resection of the primary melanoma, and the cervical lymph node was the only lesion, so they were enrolled into this trial. All patients received BNCT as a salvage therapy for recurrent mucosal melanoma.

26.7.2.1 Local Control

Almost all patients responded to BNCT. Five patients achieved complete response (CR), five partial response (PR), and one no response.

No local recurrence has been observed in three out of the five CR patients. No regrowth has been observed in two out of the five PR patients.

In six patients with local relapse, these local relapses occurred within 2 years after BNCT, even though some of these patients had good initial responses.

26.7.2.2 Complications

The most frequent acute side effects were radiation mucositis and radiation dermatitis. No patients suffered from severe acute reaction (more than Grade 3), and all the patients became symptom-free within a few months after BNCT.

At the time of analysis, none of the five survivors suffered from a late reaction (follow-up period: 22–40 months). Acute and late toxicity with this method was acceptable.

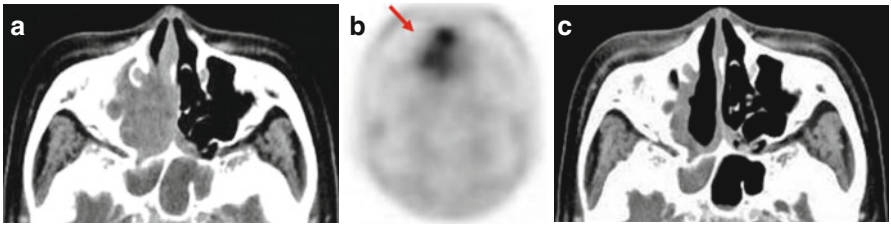

Fig. 26.3 Mucosal malignant melanoma case. 71 years old. Relapse occurred in the right nasal cavity 6 months after resection and chemotherapy. She rejected re-operation. (**a**) Shows CT findings just before BNCT. The tumor occupied the right nasal cavity. (**b**) The *T*/*N* ratio was 3.1. BNCT was carried out in August 2006. (**c**) Shows CT findings 4 months after BNCT. In spite of CR of the target lesion, she died from brain metastasis 10 months after BNCT without the local failure

26.7.2.3 Survival

Six of the 11 patients died with distant metastasis 6–18 months after BNCT, and four are alive with local relapse. Only one of the five patients who showed CR is presently alive with no evidence of local or distant failure.

As far as the local control is concerned, this result indicates that viable cancer cells are left in the target area, even though the tumor response shows radiological or endoscopic CR, and that it is hard to cure mucosal melanomas completely by a single BNCT alone. It may be necessary to add another treatment to achieve pathologically complete cure. Theoretically, there are three strategies for overcoming this problem.

First is to perform a second BNCT 3–6 months after first BNCT, even though tumor regrowth findings are not found. This treatment schedule is similar to that of the Finland BNCT group for locally recurred head and neck cancer [36]. They have carried out two BNCT treatments 3–5 weeks apart. Second is to add BSH to BPA. This combination was proposed by Ono [37] and may be able to compensate each others' weakness. This protocol has been carried out by a glioma BNCT group [29]. Third is to add 3D conformal radiotherapy, proton beam irradiation, or concurrent chemotherapy. Further long-term follow-up is required to assess the most effective way to achieve pathologically complete local cure.

Figure 26.3 shows the clinical results of case 5 treated at JRR-4 in their protocol. This case was a patient with a recurrent melanoma of the right nasal cavity following surgery and chemotherapy. In spite of CR of the target lesion, the patient died from brain metastasis 10 months after BNCT. Local failure at the site treated with BNCT was not observed.

26.8 Level of Evidence

The level of evidence for treating melanoma with BNCT chapter is Level C according to the UK National Health Service. The clinical results in this chapter were not the outcome from randomized controlled clinical trials, a retrospective cohort study or a case–control study.

26.9 Further Development

Although BNCT, as a local cancer therapy, makes it possible to cure recurrent or residual melanomas after conventional therapy in some patients, the actual effect of BNCT cannot be evaluated on newly diagnosed lesions as a first line therapy. On the basis of experience with BNCT of melanoma, a new protocol is under consideration.

This protocol is for BNCT of melanoma as neoadjuvant therapy followed by surgery. If the lesion shows CR after BNCT, the patient will be followed carefully without surgery. If CR is not observed, surgery will be carried out as scheduled.

The pathological response of BNCT can be estimated by surgery, and the pathological findings will bring very important information about where and how viable cancer cells exist.

References

1. Mishima Y (1973) Neutron capture treatment of malignant melanoma using ^{10}B-chlorpromazine compound. In: McGovern VJ, Russell P (eds) Pigment Cell, vol 1, Mechanisms in Pigmentation. S. Karger, Basel, pp 215–221
2. Fukuda H, Kobayashi T, Matsuzawa T et al (1987) RBE of a thermal neutron beam and the 10B(n, α)7Li reaction on cultured B-16 melanoma cells. Int J Radiat Biol 51:167–175
3. Yoshino K, Suzuki K, Mori Y et al (1989) Improvement of solubility of p-boronophenylalanine by complex formation with monosaccarides. Strahlenther Onkol 165:127–129
4. Hiratsuka J, Kono M, Mishima Y (1989) RBEs of thermal neutron capture therapy and 10B(n, α)7Li reaction on melanoma-bearing hamsters. Pigment Cell Res 2:352–355
5. Mishima Y, Ichihashi M, Hatta S et al (1989) New thermal neutron capture therapy for malignant melanoma: melanogenesis-seeking ^{10}B molecule-melanoma cell interaction from in vitro to first clinical trial. Pigment Cell Res 2:226–234
6. Mishima Y, Honda C, Ichihashi M et al (1989) Treatment of malignant melanoma by single neutron capture treatment with melanoma-seeking ^{10}B-compound. Lancet II:388–389
7. Hiratsuka J, Fukuda H, Kobayashi T et al (1991) The relative biological effectiveness of ^{10}B-neutron capture therapy for early skin reaction in the hamster. Radiat Res 128:186–191
8. Fukuda H, Hiratsuka J, Honda C et al (1994) Boron neutron capture therapy of malignant melanoma using ^{10}B-paraboronophenylalanine with special reference to evaluation of radiation dose and damage to the normal skin. Radiat Res 138:435–442
9. Mishima Y (1996) Selective thermal neutron capture therapy of cancer cells using their specific metabolic activities—Melanoma as prototype Cancer. In: Mishima Y (ed) Neutron Capture Therapy. Plenum Press, New York, pp 1–26
10. Yoshino K, Mishima Y, Kimura M et al (1997) Capture of p-boronophenylalanine in malignant melanoma cells by complex formation with melanin monomers, DOPA, DHI and DHICA. BPA trapping mechanism. In: Larsson B, Crawford J, Weinreich R (eds) Advances in Neutron Capture Therapy. Elsevier Science, Amsterdam, pp 234–238
11. Fukuda H, Honda C, Wadabayashi N et al (1999) Pharmacokinetics of ^{10}B-p-boronophenyla lanine in tumors, skin and blood of melanoma patients: a study of boron neutron capture therapy for malignant melanoma. Melanoma Res 9:75–83
12. Fukuda H, Hiratsuka J, Kobayashi T et al (2003) Boron neutron capture therapy (BNCT) for malignant melanoma with special reference to absorbed doses to the normal skin and tumor. Australas Phys Eng Sci Med 26:78–84

13. Madoc-Jones H, Zamenhof R, Solares G et al (1996) A phase-Idose escalation trial of boron neutron capture therapy for subjects with metastatic subcutaneous melanoma of the extremities. In: Mishima Y (ed) Cancer Neutron Capture Therapy. Plenum Press, New York, pp 707–716
14. Busse PM, Zamenhof R, Madoc-Jones H et al (1997) Clinical follow-up of patients with melanoma of the extremity treated in a phase I boron neutron capture therapy protocol. In: Larson B, Crawford J, Weinreich R (editors) Advances in Neutron Capture Therapy, Volume I: 60–64
15. Palmer MR, Goorley JT, Kiger WS III et al (2002) Treatment planning and dosimetry for the Harvard-MIT PhaseIIclinical trial of cranial neutron capture therapy. Int J Radiat Oncol Biol Phys 53:1361–1379
16. Sauerwein W, Zurlo A (2002) The EORTC boron neutron capture therapy (BNCT) group: achievements and future projects. Eur J Cancer 38:S31–S34
17. Wittig A, Sauerwein W, Moss R, et al. Early phaseIstudy o BNCT in metastatic malignant melanoma using the boron carrier BPA (EORTC protocol 11011). In advances in Neutron Capture Therapy 2006 (Y. Nakagawa, T Kobayashi and H Fukuda Ed.) 284–287. (Proceedings of ICNCT-12), 2006
18. Gonzales SJ, Bonomi MR, Santacruz GA et al (2004) First BNCT treatment of a skin melanoma in Argentina: dosimetric analysis and clinical outcome. Appl Radiat Isot 61:1101–1105
19. Roth BM, Bonomi MR, Gonzalez SJ, et al (2006) BNCT clinical trials of skin melanoma patients in Argentina. Proceedings of ICNCT-12. Edited by Nakagawa Y, Kobayashi T and Fukuda H: 14–17
20. Morita N, Hiratsuka J, Kuwabara C, et al. (2006) Successful BNCT for patients with cutaneous and mucosal melanomas: Report of 4 cases. Proceedings of ICNCT-12. Edited by Nakagawa Y, Kobayashi T and Fukuda H: 18–20
21. Kirkwood JM, Strawderman MH, Ernstoff MS et al (1996) Interferon alfa-2b adjuvant therapy of high-risk resected cutaneous melanoma: the Eastern Cooperative Oncology Group Trial EST 1684. J Clin Oncol 14(1):7–17
22. Geara FB, Ang KK (1996) Radiation therapy for malignant melanoma. Surg Clin North Am 76(6):1383–1398
23. Harwood AR, Cummings BJ (1982) Radiotherapy for mucosal melanomas. Int J Radiat Oncol Biol Phys 8:1121
24. Vtyurin BM, MedvedevVS AnikinVA et al (1994) Neutron branchytherapy in the treatment of melanoma. Int J Radiat Oncol Biol Phys 28:703–709
25. Umebayashi S, Uyeno K, Tsujii H et al (1995) Proton radiotherapy for malignant melanoma of the skin. Dermatology 190:210–213
26. Coderre JA, Glass JD, Fairchild RG et al (1990) Selective delivery of boron by the melanin precursor analogue p-boronophenylalanine to tumors other than melanoma. Cancer Res 50: 138–141
27. Papaspyrou M, Feinendegen LE, Müller-Gärtner H-W (1994) Preloading with L-tyrosine increases the uptake of boronophenylalanine in mouse melanoma cells. Cancer Res 54(24):6311–6314
28. Wittig A, Sauerwein WA, Coderre JA (2000) Mechanisms of transport of *p*-Borono-phenylalanine through the cell membrane *in vitro*. Radiat Res 153(2):173–180
29. Miyatake S, Kawabata S, Kajimoto Y et al (2005) Modified boron neutron capture therapy for malignant gliomas performed using epithermal neutron and two boron compounds with different accumulation mechanisms: an efficacy study based on findings on neuroimages. J Neurosurg 103:1000–1009
30. Kato I, Ono K, Sakurai Y et al (2004) Effectiveness of BNCT for recurrent head and neck malignancies. Appl Radiat Isot 61:1069–1073
31. Aihara T, Hiratsuka J, Morita N et al (2006) First clinical case of boron neutron capture therapy for head and neck malignancy. Head Neck 28:850–855
32. Coderre JA, Morris GM (1999) Review; The radiation biology of boron neutron capture therapy. Radiat Res 151:1–18

33. Coderre JA, Hopewell JW, Turcotte JC et al (2004) Tolerance of normal human brain to boron neutron capture therapy. Appl Radiat Isot 61:1083–1087
34. Johanson CR, Harwood AR, Cummings BJ et al (1983) 0-7-21 Radiotherapy in nodular melanoma. Cancer 51:226–232
35. Ono K, Masunaga S, Kinashi Y, et al. (2006) Neutron irradiation under continuous BPA injection for solving the problem of heterogenous distribution of BPA. Proceedings of ICNCT-12. Edited by Nakagawa Y, Kobayashi T and Fukuda H: 27–30
36. Kankaanranta L, Seppala T, Koivunoro H et al (2007) Boron neutron capture therapy in the treatment of locally recurred head and neck cancer. Int J Radiat Oncol Biol Phys 69:475–482
37. Ono K, Masunaga S, Suzuki M et al (1999) The combined effect of boronophenylalanine and borocaptate in boron neutron capture therapy for SCCVII tumors in mice. Int J Radiat Oncol Biol Phys 43:431–436

Application of Neutron Capture Therapy for Locally Recurrent Breast Cancer

27

Hironobu Yanagie

Contents

27.1 Introduction

The incidence of breast cancer is increasing, so it is also increasingly important to plan treatment protocols for recurring cases [1, 2]. Breast cancer may recur after primary resection both locally (thoracic wall: 23 %, local lymph nodes: 19 %) and at distant sites (bone: 23 %, lung: 18 %, and liver: 4 %). The treatment of local

H. Yanagie
Department of Nuclear Engineering and Management, Graduate School of Engineering, The University of Tokyo, 7-3-1 Hongo, Bunkyo-ku, Tokyo 113-8655, Japan

Cooperative Unit of Medicine and Engineering, The University of Tokyo Hospital, Tokyo, Japan

Department of Surgery and Gastroenterology, Kyorindo Clinic, Kanagawa, Japan
e-mail: yanagie@n.t.u-tokyo.ac.jp

W.A.G. Sauerwein et al. (eds.), *Neutron Capture Therapy*,
DOI 10.1007/978-3-642-31334-9_27, © Springer-Verlag Berlin Heidelberg 2012

recurrences can be curative or palliative to avoid the occurrence of bleeding, ulcer formation, and unpleasant odors.

The cytotoxic effect of boron neutron capture therapy (BNCT) is due to a nuclear reaction between ^{10}B and thermal neutrons ($^{10}B + {}^{1}n \rightarrow {}^{7}Li + {}^{4}He$ (α) + 2.31 MeV (93.7 %)/2.79 MeV (6.3 %)). The resulting lithium ions and α particles are high linear energy transfer (LET) particles, which produce large biological effects. Their short range in tissue (5–9 μm) restricts radiation damage to those cells in which the boron atoms are located at the time of neutron irradiation.

27.2 Actual State-of-the-Art Treatment

Combined chemo- and radiotherapies are established in breast cancer treatment. Sequencing chemotherapy and radiotherapy in locoregional advanced breast cancer patients after mastectomy are recommended. Massimo et al. reported that the first trial evaluated 5-fluorouracil, doxorubicin (Adriamycin), and cyclophosphamide (FAC) therapy administered as induction chemotherapy, followed by radiotherapy and further adjuvant chemotherapy with either FAC or cyclophosphamide, methotrexate, and 5-fluorouracil (CMF), and the second trial used the same regimen of induction chemotherapy, followed by mastectomy, adjuvant FAC, and radiotherapy. Cameron et al. reported that targeting the human epidermal growth factor receptor type 2 (HER2) in breast cancer patients whose tumors overexpress HER2 was clearly demonstrated to be effective in clinical trials with the monoclonal antibody trastuzumab [3]. Geyer et al. reported that the addition of lapatinib to capecitabine may extend the time to disease progression and progression-free survival in patients with metastatic disease refractory to trastuzumab-, anthracycline-, and taxane-containing regimens [4].

Radiation therapy is commonly used to local control of locoregional breast cancer [5–8]. Skin ulcers and bone necrosis may appear after irradiation because of the lower tolerance of the thoracic wall after mastectomy. Therefore, a dose of about 40–50 Gy is recommended for recurrences. The treatment of locoregional recurrence after breast cancer is based on the achievement of locoregional control by radical surgery and adjuvant postoperative radiotherapy. The efficacy of post-mastectomy radiation therapy (PMRT) in improving local control and long-term survival has been demonstrated. The purpose of PMRT is to prevent the recurrent tumors of the thoracic wall and also to prevent distant metastasis, and then PMRT will be useful to elongate the survival disease free periods. Chung reported that the intra-mammary recurrence rate is 2–10 % with reserved operation + PMRT, and 15–40 % with reserved operation only. The survival advantage of PMRT has been established in patients with a 10 % risk of locoregional recurrence. When PMRT is used, careful treatment planning, particularly with regard to the cardiac dose, is critical to minimize serious late effects of treatment [9]. Recent prospective trials of PMRT in combination with systemic chemotherapy clearly demonstrated the benefit of this combined adjuvant therapy for both locoregional recurrence and survival outcomes. PMRT is recognized as a standard adjuvant treatment for patients with more than

four positive axillary nodes according to the guidelines and recommendations. Hiraoka et al. reported that escalation of the postmastectomy radiation dose to 66 Gy appeared to benefit patients with disease that responds poorly to chemotherapy; those with positive, close, or unknown margin status; and those <45 years of age [10]. In cooperation with the FRM I, the Department of Radiation Therapy of the Technische Universität München has been managing a fast-neutron irradiation facility used for tumor therapy for several years. Very promising results have been achieved for various types of near-surfaces tumors, especially in the region of the head and neck and for certain breast tumors, in case of tumors with high resistance to X-ray-treatment, such as malignant melanomas; neutrons often show spectacular success. Until now, more than 700 patients have been treated with fast neutrons at the FRM I. The new beam of the Munich Fission Neutron Therapy Facility at FRM II is in use for the treatment of slow-growing and/or well-differentiated tumors, such as adenoid cystic carcinoma and hypoxic tumors. Generally, all shallow tumor lesions, such as ear, nose and throat tumors, lymph node metastases, or skin metastases from various cancer diseases, and chest wall metastases of breast cancer, are considered suitable for neutron irradiation [11].

27.3 Rationale for BNCT and Clinical Applications

In the recurrent breast cancer, several patients after the reserved mammary gland operation showed a simila progression as in inflammatory cancer. Walshe et al. reported that inflammatory breast cancer (IBC) is the most aggressive manifestation of primary breast cancer, and IBC presents with unique clinical characteristics (erythema, warming, peau d'orange, breast enlargement, and diffuse induration of the breast on palpation), rapid progression, and poor survival compared to non-IBC breast cancers [12].

The higher risk of disease recurrence immediately after diagnosis and the distinctive pattern of soft-tissue relapse strongly support Massimo's hypothesis that these patients have already developed micrometastatic disease at the time of clinical diagnosis [13]. The purpose of treatments for locally recurrent breast cancer are (1) to cure the disease with suppression of recurrence tumor, which is very difficult (rare case) and (2) to locally control ulcer formations of the thoracic wall, bleeding, and unpleasant odors, etc. It is important to recover the quality of life and prolong the survival period with systemic chemotherapy and hormonal therapy. BNCT may have major importance for large local recurrences after radiotherapy (with or without mastectomy). The benefits of the application of BNCT to recurrent and advanced breast cancer (including inflammatory breast cancer-like type) are that BNCT is a selective therapy on the cell level, and if the boron atoms accumulate in the cancer cells, then the inflammatory breast cancer is easily invaded, and they spread to the neighboring tissue in a cell unit. BNCT is considered the ideal therapy for locally recurrent breast cancer that is tolerant to the conventional multiple therapies (including radiation therapy). Kato et al. began BNCT using BSH and BPA for recurrent parotid gland carcinoma for the first time, and Aihara and Hiratsuka et al. performed

BNCT using BPA for recurrent head and neck cancer [14, 15]. They reported excellent preliminary results with improvement of quality of life after treatment.

27.4 Technical Aspects

1. The patient with recurrent breast cancer has a ^{18}F-BPA-PET study performed for dose estimation before neutron irradiation, and the tumor/normal-tissue boron concentration ratio (*T*/*N* ratio) is obtained for dose evaluation on BNCT. A *T*/*N* ratio of more than 2.5 is recommended according to the results of BNCT for adenocarcinoma of head and neck cancer.
2. The patient with recurrent breast cancer arrives at the JRR4 or KUR 1 day before BNCT. The patient has the simulation performeed using JCDS or SERA dosimetry systems, respectively. Also the irradiation position and the beam directions are determined.
3. Para-boronophenylalanine (^{10}BPA) is administered to the patient in a fructose solution by drop intravenous injection before BNCT(500 mg/kg body weight/6 h).
4. BNCT is performed using an epithermal beam at JRR4 (3.5 MW) or KUR (5.0 MW). The tumor dose at the deepest part and the dose of both normal skin and fat tissue are planned as more than 20 Gy and less than 10 Gy at the simulation, respectively.
5. The patient is transferred to the nearest cooperative hospital after BNCT for resting for 1 or 2 days.
6. The patient returns to the home hospital for continuous follow-up.

27.5 Results

We performed the BNCT simulation with MRI images using JCDS for a recurrent breast cancer patient for whom partial resection reserving the mammary gland was performed, and we evaluated neutron flux dosimetry in the horizontal irradiation position using a phantom model of a mammary gland at Kyoto University Research Reactor, and also evaluated neutron flux dosimetry at Japan Atomic Energy Research Institute.

27.5.1 Phantom Model Estimation for BNCT for Breast Cancer

Preparation of Phantom Model: We used a phantom-shaped mammary gland (height: 4 cm, width : 12 cm) because irradiation therapy after mastectomy is commonly performed from the horizontal direction to avoid toxicity to the lung and heart as pulmonitis and cardiac dysfunction are possible in case of direct neutron irradiation from the thoracic wall. Gold wires and TLDs were attached in a 2-cm range from the front side of the phantom (Fig. 27.1).

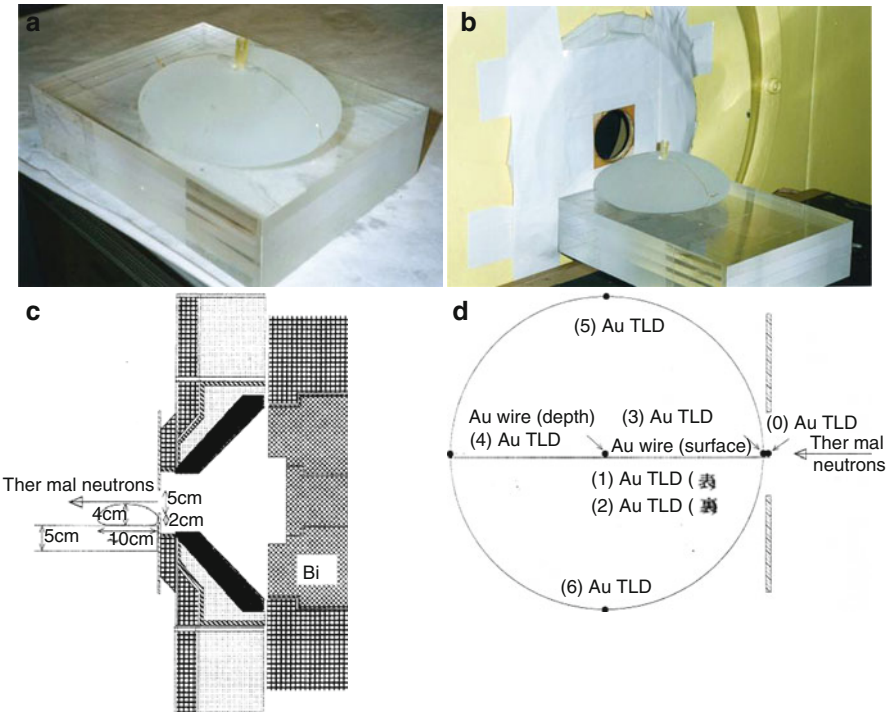

Fig. 27.1 Estimation with phantom model of mammary gland for BNCT. (**a**) Phantom shaped mammary gland, (**b**) phantom model was irradiated at thermal neutron beam port of KURR, (**c**) experiment setting of phantom model of mammary gland at KURR, (**d**) position of gold wire and TLD on phantom model

Neutron Irradiation: We used the thermal neutron mode (OO-0011) for dosimetry of the phantom model [16, 17]. Irradiation was performed at the Neutron Irradiation Facility of the Kyoto Research Reactor (KKR). Irradiation was performed with LiF collimation (5 cm ϕ). The thermal neutron flux was measured by gold wire, and the gamma dose rate was measured by TLD. The measured values of neutron gradation depend on the distance from the surface of the phantom.

Estimation for BNCT Using a Phantom of the Mammary Gland: The preclinical BNCT trial is performed at Kyoto University Research Reactor (KUR) in Kumatori, Osaka. The thermal neutron irradiation mode (OO-0011) was used.

It is estimated as follows: the position of the tumor is estimated as the upper lateral position of the mammary gland; thermal neutron flux is 5.16 E+08 n/cm^2/s at the surface of the phantom (Fig. 27.2). In this evaluation, the concentration of ^{10}B is estimated 30 ppm, the tumor/blood ratio of the boron concentration is 3, the skin/blood ratio of the boron concentration is 1.2, the tumor RBE is 3.8, and the skin RBE is 2.5. The tumor RBE dose and skin RBE dose became 47 Gy and 12.4 Gy at 1 h thermal neutron irradiation with the 30 ppm ^{10}B blood concentration at KUR, respectively. Thermal neutron irradiation with Void and LiF collimation

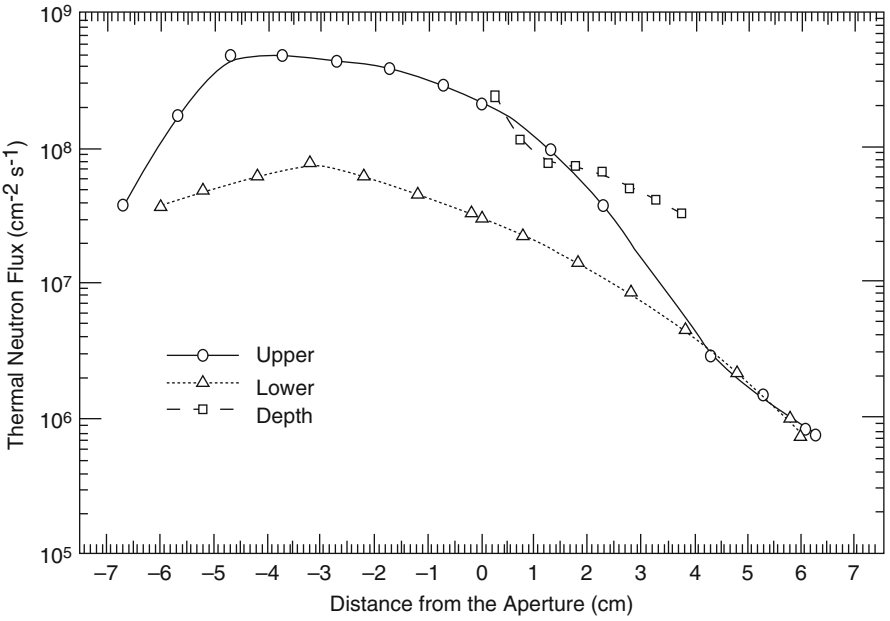

Fig. 27.2 Thermal neutron fluxes of the phantom model of the mammary gland at KURR

can be focused to the target field selectively, minimizing the irradiation dose to adjacent organs.

27.5.2 JCDS Model Estimation for BNCT of Breast Cancer

Neutron dosimetry with JAERI Computational Dosimetry System (JCDS) for a breast cancer patient: BNCT was simulated in a patient with an invasive recurrent tumor on the residual left mammary gland. LiF collimation was used to selectively irradiate the tumor while sparing the adjacent normal organs (lung, heart). The Neutron Beam Facility at JRR4 enables carrying out boron neutron capture therapy with epithermal neutron beams. The JAERI Computational Dosimetry System (JCDS), which can estimate distributions of radiation doses in a patient's head by simulation in order to support the treatment planning for epithermal neutron beam BNCT, was developed. We applied this JCDS for evaluation of the neutron dosimetry for this case. Kumada et al. reported that JCDS is a software that creates a three-dimensional head model of a patient by using a CT scan and MRI images, and that it generates an input data file by automatically calculating the neutron flux and gamma-ray dose distributions in the brain with the Monte Carlo code MCNP. It displays these dose distributions on the head model for dosimetry by using the MCNP calculation results [18]. The JCDS has the following advantages: (1) a detailed 3D model of the patient's head can be easily obtained from the CT and MRI

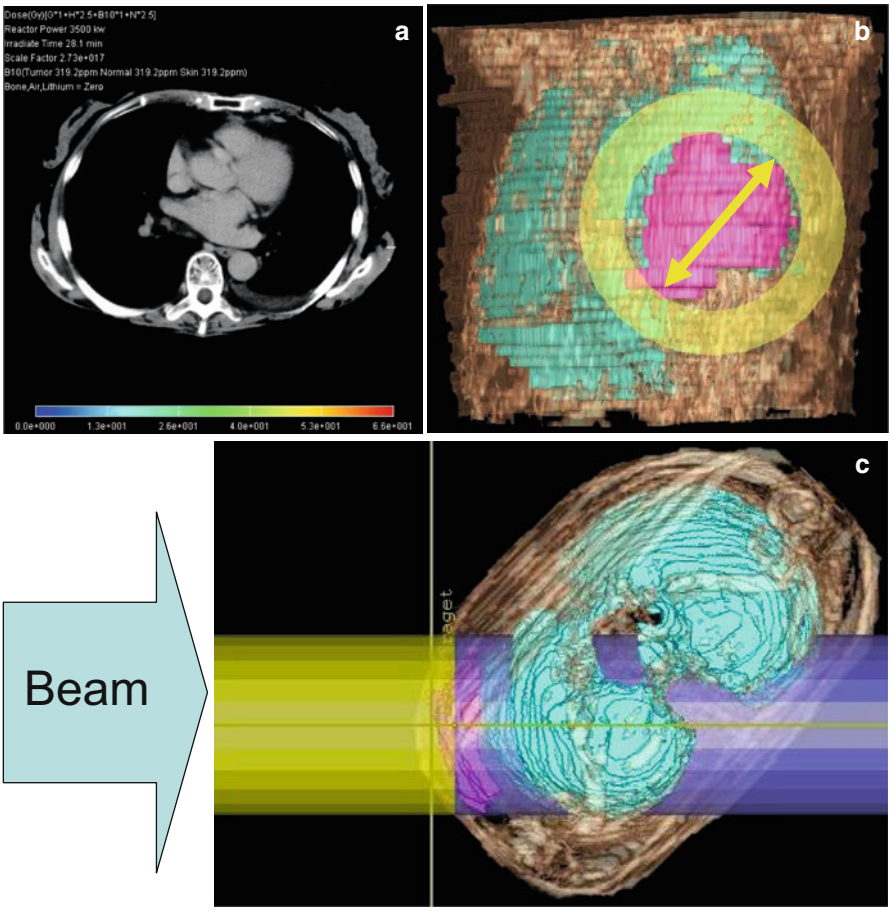

Fig. 27.3 JCDS simulation for a patient with left recurrent breast cancer. (**a**) CT scan of recurrent tumor on residual left mammary gland, (**b**) 3D model of patient, frontal view, condition: collimation was performed 12 cm from the beam port of JRR4, (**c**) irradiation setting on sagittal view

data, (2) the 3D head image is editable to simulate the state of a head after surgery, and (3) the JCDS can provide information for the Patient Setting System, which can facilitate positioning the patient for irradiation swiftly and accurately.

We performed the dosimetry with the JCDS in the condition of BNCT using epithermal neutron beams (Fig. 27.3). To decrease the skin side effects, the skin RBE dose was limited to 10 Gy. The tumor RBE dose was estimated to be 3.5, and the blood BPA concentration to be 24 ppm. The minimum tumor RBE dose is 16.6 Gy, the mean tumor RBE dose is 46.5 Gy, and the maximum tumor RBE dose is 64.3 Gy. The two-dimensional distributions of neutron beams revealed that the peak of the beam was fitted to the tumor site (Figs. 27.4 and 27.5). In the case of a round-type mammary gland, the distribution of neutron beams has the tendency to shift a little to neighboring tissues from the tumor site. For calibration of the beam

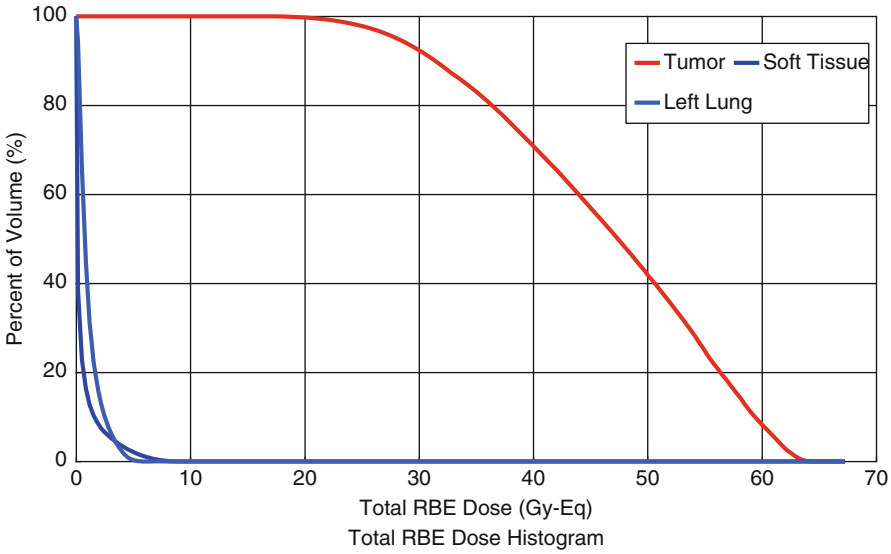

Fig. 27.4 Total RBE dose histogram in a case of recurrent left breast cancer

peaks to the tumor, it is necessary to perform a few changes of the size of beam port and the beam direction, and to add some voiding of the neighbor sites of tumors.

We applied the JCDS to the dosimetry of epithermal neutrons, direction of neutron beams, and patient positioning for BNCT [19, 20]. We also evaluated the epithermal neutron dose to decrease the skin side effects. High-resolution whole-body dosimetry systems, such as JCDS and SERA, will be very useful for evaluating thermal/epithermal neutron dosimetry and the application of BNCT to recurrent or advanced breast cancer.

27.6 Level of Evidence

BNCT is not performed on patients with recurrent breast cancer, so the rank of evidence is Level D according to the UK National Health Service categories.

27.7 Future Development

We hope to start BNCT applications for recurrent and advanced breast cancer patients.

We performed the estimation of dosimetry of neutron fluence on recurrent tumors using the patient databases. The irradiation directions are determined using JCDS or SERA simulations with restriction of the normal tissue RBE dose. If the recurrent tumor is localized to the thoracic wall, BNCT is usually performed from the frontal

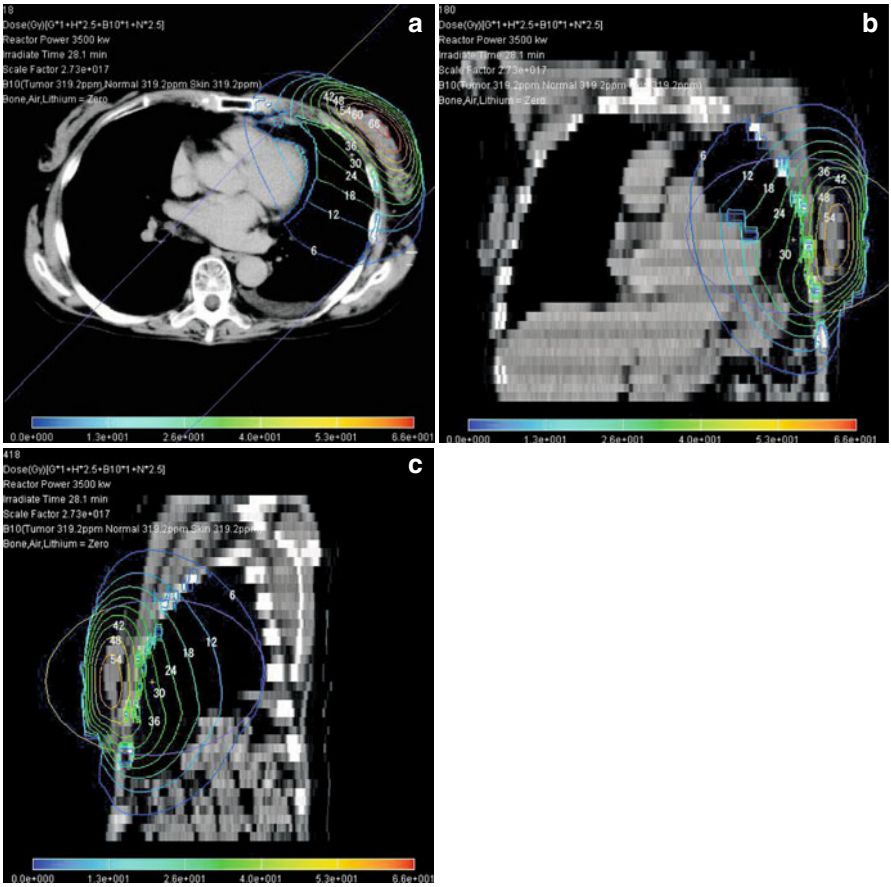

Fig. 27.5 Two-dimensional distributions of epithermal neutron beams at JRR4 using JCDS evaluation. (**a**) Tumor RBE dose dosimetry on CT scan, (**b**) frontal view, (**c**) lateral view

direction with restriction of the normal tissue RBE dose (for example, lung, heart, skin, and fat tissue). We also hope to measure the accumulation of BPA in breast cancer with ^{18}F-^{10}BPA-PET according to Imahori's method [21].

Multidisciplinary management is necessary for recurrent breast cancer (including the inflammatory breast cancer type), but drug-resistant situations have developed in some patients. Recently, Rich et al. reported that cancer stem cells, or tumor-initiating cells, displayed resistance to radiation because of increased activation of the DNA damage checkpoint. Hypoxia and stem cell maintenance pathways may provide therapeutic targets to improve cancer patient treatments [22]. The benefits of the application of BNCT to recurrent and advanced breast cancer (including inflammatory breast cancer) are that it is a selective therapy on the cell level, and if the boron atoms accumulate in the cancer cells, then the inflammatory breast cancer easily invades and spreads to the neighboring tissue in a cell unit.BNCT is considered the ideal

therapy for locally recurrent breast cancer that is tolerant to the conventional multiple therapies (including radiation therapy). A goal is the development of a boron delivery system for selective accumulation in the breast cancer cells [23–27].

References

1. Nielsen HM, Overgaard M, Grau C, Jensen AR, Overgaard J (2006) Loco-regional recurrence after mastectomy in high-risk breast cancer–risk and prognosis. An analysis of patients from the DBCG 82 b&c randomization trials. Radiother Oncol 79(2):147–155
2. Bristol IJ, Woodward WA, Strom EA, Cristofanilli M, Domain D, Singletary SE, Perkins GH, Oh JL, Yu TK, Terrefe W, Sahin AA, Hunt KK, Hortobagyi GN, Buchholz TA (2008) Locoregional treatment outcomes after multimodality management of inflammatory breast cancer. Int J Radiat Oncol Biol Phys 72(2):474–484
3. Cameron DA, Stein S (2008) Drug insight: intracellular inhibitors of HER2 – clinical development of lapatinib in breast cancer. Nat Clin Pract Oncol 5(9):512–520
4. Geyer CE, Forster J, Lindquist D, Chan S, Romieu CG, Pienkowski T, Jagiello-Gruszfeld A, Crown J, Chan A, Kaufman B, Skarlos D, Campone M, Davidson N, Berger M, Oliva C, Rubin SD, Stein S, Cameron D (2006) Lapatinib plus capecitabine for HER2-positive advanced breast cancer. N Engl J Med 355(26):2733–2743
5. Ballo MT, Strom EA, Prost H, Singletary SE, Theriault RL, Buchholz TA, McNeese MD (1999) Local-regional control of recurrent breast carcinoma after mastectomy: does hyperfractionated accelerated radiotherapy improve local control? Int J Radiat Oncol Biol Phys 44(1):105–112
6. Liao Z, Strom EA, Buzdar AU, Singletary SE, Hunt K, Allen PK, McNeese MD (2000) Locoregional irradiation for inflammatory breast cancer: effectiveness of dose escalation in decreasing recurrence. Int J Radiat Oncol Biol Phys 47(5):1191–1200
7. Touboul E, Buffat L, Belkacémi Y, Lefranc JP, Uzan S, Lhuillier P, Faivre C, Huart J, Lotz JP, Antoine M, Pène F, Blondon J, Izrael V, Laugier A, Schlienger M, Housset M (1999) Local recurrences and distant metastases after breast-conserving surgery and radiation therapy for early breast cancer. Int J Radiat Oncol Biol Phys 43(1):25–38
8. Willner J, Kiricuta IC, Kölbl O (1997) Locoregional recurrence of breast cancer following mastectomy: always a fatal event? Results of univariate and multivariate analysis. Int J Radiat Oncol Biol Phys 37(4):853–863
9. Chung CS, Harris JR (2007) Post-mastectomy radiation therapy: translating local benefits into improved survival. Breast 16(Suppl 2):S78–S83
10. Hiraoka M, Mitsumori M, Shibuya K (2002) Adjuvant radiation therapy following mastectomy for breast cancer. Breast Cancer 9(3):190–195
11. Wagner FM, Kneschaurek P, Kastenmüller A, Loeper-Kabasakal B, Kampfer S, Breitkreutz H, Waschkowski W, Molls M, Petry W (2008) The munich fission neutron therapy facility MEDAPP at the research reactor FRM II. Strahlenther Onkol 184(12):643–646
12. Walshe JM, Swain SM (2005–2006) Clinical aspects of inflammatory breast cancer. Breast Dis 22:35–44
13. Cristofanilli M, Valero V, Buzdar AU, Kau SW, Broglio KR, Gonzalez-Angulo AM, Sneige N, Islam R, Ueno NT, Buchholz TA, Singletary SE, Hortobagyi GN (2007) Inflammatory breast cancer (IBC) and patterns of recurrence, understanding the biology of a unique disease. Cancer 110(7):1436–1444
14. Kato I, Ono K, Sakurai Y, Ohmae M, Maruhashi A, Imahori Y, Kirihata M, Nakazawa M, Yura Y (2004) Effectiveness of BNCT for recurrent head and neck malignancies. Appl Radiat Isot 61(5):1069–1073
15. Aihara T, Hiratsuka J, Morita N, Uno M, Sakurai Y, Maruhashi A, Ono K, Harada T (2006) First clinical case of boron neutron capture therapy for head and neck malignancies using 18 F-BPA PET. Head Neck 28(9):850–855

16. Sakurai Y, Kobayashi T (2000) Characteristics of the KUR heavy water neutron irradiation facility as a neutron irradiation field with variable energy spectra. Nucl Instrum Meth A 453:569–596
17. Sakurai Y, Kobayashi T, Ono K et al (2002) Study on accelerator-base neutron irradiation field aiming for wider application in BNCT – spectrum shift and regional filtering. In: Sauerwein W (ed) Research and development in neutron capture therapy. Monduzzi Editore, Bologna, pp 259–263
18. Yanagie H, Sakurai Y, Ogura K, Kobayashi T, Furuya Y, Sugiyama H, Kobayashi H, Ono K, Nakagawa K, Takahashi H, Eriguchi M (2007) Evaluation of neutron dosimetry on pancreatic cancer phantom model for application of intraoperative boron neutron-capture therapy. Biomed Pharmacother 61(9):505–514
19. Kumada H (2001) The development of a computational dosimetry system for BNCT at JRR-4. In: Hawthorne MF (ed) Frontiers in neutron capture therapy. Kluwer, New York, pp 611–614
20. Yanagie H, Kumada H, Sakurai Y, Nakamura T, Furuya Y, Sugiyama H, Ono K, Takamoto, S, Eriguchi M, Takahashi H (2009) Dosimetric evaluation of neutron capture therapy for local recurrenced breast cancer. Appl Radiact Isot 67(7-8 Supp):S63–66
21. Imahori Y, Ueda S, Ohmori Y, Sakae K, Kusuki T, Kobayashi T, Takagaki M, Ono K, Ido T, Fujii R (1998) Positron emission tomography-based boron neutron capture therapy using boronophenylalanine for high-grade gliomas: part I. Clin Cancer Res 4:1825–1832
22. Rich JN (2007) Cancer stem cells in radiation resistance. Cancer Res 67(19):8980–8984
23. Yanagie H, Ogata A, Sugiyama H, Eriguchi M, Takamoto S, Takahashi H (2008) Application of drug delivery system to boron neutron capture therapy for cancer. Expert Opin Drug Deliv 5(4):427–443
24. Yanagie H, Tomita T, Kobayashi H, Fujii Y, Takahashi T, Hasumi K, Nariuchi H, Sekiguchi M (1991) Application of boronated anti-CEA immunoliposome to tumour cell growth inhibition in in vitro boron neutron capture therapy model. Br J Cancer 63(4):522–526
25. Yanagie H, Tomita T, Kobayashi H, Fujii Y, Nonaka Y, Saegusa Y, Hasumi K, Eriguchi M, Kobayashi T, Ono K (1997) Inhibition of human pancreatic cancer growth in nude mice by boron neutron capture therapy. Br J Cancer 75(5):660–665
26. Wei Q, Kullberg EB, Gedda L (2003) Trastuzumab-conjugated boron-containing liposomes for tumor-cell targeting; development and cellular studies. Int J Oncol 23(4):1159–1165
27. Yanagie H, Kobayashi H, Takeda Y, Yoshizaki I, Nonaka Y, Naka S, Nojiri A, Shinnkawa H, Furuya Y, Niwa H, Ariki K, Yasuhara H, Eriguchi M (2002) Inhibition of growth of human breast cancer cells in culture by neutron capture using ^{10}B-containing liposomes. Biomed Pharmacother 56:93–99

Liver Metastases

28

A. Zonta, L. Roveda, and S. Altieri

Contents

A. Zonta
Department of Surgery, IRCCS S. Matteo Hospital, Pavia, Italy
e-mail: zontaris@libero.it

L. Roveda
Unit of Oncologic Surgery, Cancer Center of Excellence
Fond. "T. Campanella", Catanzaro, Italy
e-mail: roveda.l@libero.it

S. Altieri (✉)
Department of Physics, University of Pavia, Pavia, Italy

National Institute of Nuclear Physics (INFN), Section of Pavia, Pavia, Italy
e-mail: saverio.altieri@pv.infn.it

W.A.G. Sauerwein et al. (eds.), *Neutron Capture Therapy*,
DOI 10.1007/978-3-642-31334-9_28, © Springer-Verlag Berlin Heidelberg 2012

28.1 Introduction

28.1.1 General Remarks About BNCT

BNCT is a new therapeutic option for treating cancer that was conceived several decades ago, around the halfway into the twentieth century, but has not found its "ideal" indication yet. It has some positive features: actually it is not a highly complex procedure nor is it particularly expensive, when compared to the benefit of a success gained over a tumor. On the negative side, BNCT requires a multidisciplinary approach to the delicate problems that are involved in clinical cases. It is based on the use of thermal or epithermal neutrons, which are currently only produced by nuclear reactors, and thus are not available everywhere. Strict cooperation between surgeons and radiotherapists is mandatory, especially in treating some neoplastic localizations.

However, the balance between these positive and negative features of BNCT does not completely justify the difficulties BNCT encounters in the exact definition of its therapeutic role. In our opinion, it is more about the clinical situations in which it has been usually employed. For BNCT, as for any other entirely new therapeutic proposal, the most attractive field of application is the treatment of diseases that have no curative alternatives and in cases where the favourable peculiarities of the procedures can be best exploited.

A new therapeutic tool against cancer should be evaluated according to three main criteria: efficacy, selectivity, and specificity. A therapy is considered effective when it is able to kill all clusters of neoplastic cells; it is selective when it is possible to limit its action to the diseased part of the organism; finally, a therapy is specific if in the delimited field of action it is able to kill only the tumor cells. For example, surgery is distinguished by high efficiency, good selectivity, and poor specificity; chemotherapy of solid tumors has no selectivity, fair specificity, and reasonable efficacy; traditional radiotherapy is affected by no specificity, moderate selectivity, and variable efficacy. From this point of view, BNCT ideally has full specificity – if the boron uptake is limited to tumor cells – and is also, theoretically again, highly selective and effective when applied according to proper indications that exploit its tumor-searching capacity.

The clinical condition that offers the best indication for BNCT is then given by a tumor composed of cells with an elevated uptake capacity for a non-toxic boron

compound and is limited to an organ with the following characteristics: its normal cells are not able to concentrate the same compound, and the diseased organ can be entirely exposed to a homogeneous neutron flux. This way, not only a portion but also the whole volume of the diseased organ can be treated with the same absorbed dose in both known and unknown tumor nodules, merely depending on the boron concentration reached in their cells.

28.2 Liver Metastases as a Therapeutic Target

28.2.1 The Reasons for a Choice

Hepatic metastases, when diffused to all lobes of the liver, are a major problem in oncology for at least two reasons: their frequency and their resistance to the usual anti-neoplastic approaches.

28.2.2 Incidence

In Europe and USA, metastatic cancer comprises the largest group of malignant tumors in the liver.

This organ can be considered as a filter through which all splanchnic blood passes and is purified of its abnormal content, both biochemical and corpuscular in nature. Cells detached from primary tumors of the abdominal area are forced to penetrate the narrow liver sinusoid channels, where stopping them is easier and longer lasting. For these reasons, hepatic metastases are more common in patients suffering from gallbladder, pancreas, colon and stomach tumors. In these areas, the percentage of cases with liver involvement can vary from 50 to almost 80 %. However, other localizations of primary tumors reach a similar incidence. Among them, the most significant kinds of tumors are bronchopulmonary, breast and ovary carcinomas and melanoma. In effect, tumor cell shedding is a precocious and continuous phenomenon in most malignant tumors. It is also noteworthy that in a significant number of cases, even in *post-mortem* examinations, metastases of unknown primary tumors are found in the liver. This group of cases accounts for an incidence not less than that of colorectal tumors [1].

For other tumors, the incidence of hepatic metastases is lower, indicating that liver colonization is not merely caused by a mechanical hindrance between cell sizes and vascular spaces. A chemical affinity between sinusoid endothelium receptors and components of neoplastic cell membranes is well known, and its importance has been adequately demonstrated and stressed [2]. It can account for the large variability of frequency in liver metastases observed in some non-splanchnic tumors. A particularly low incidence is observed in thyroid tumors.

Liver involvement in the natural history of a tumor is a relatively late phenomenon that coincides with severe worsening in the clinical evolution of the disease. It is customary to distinguish between synchronous metastases, when liver colonization

is evident at the diagnosis of the primary tumor, and metachronous metastases, when they appear later. These two populations of patients have a different prognosis because in the synchronous lesions, even if treated, the neoplastic disease is more aggressive and survival is shorter.

28.2.3 Intra-Hepatic Localizations

A larger incidence of liver metastases is usually observed in the right lobe. This is explained by its higher, more direct blood inflow because the right portal branch has almost the same direction as the portal trunk, whereas the detachment of the left branch is at an angle.

With regard to the number of metastases, it is useful to distinguish between solitary, multiple unilateral, and multiple bilateral (or diffuse) nodules.

In each hepatic lobe, the situation of nodules can be central (and even para-hilar), peripheral, or sub-capsular (and even protrusive): the surgical problems that are posed by their resection are of course different, but, no doubt, especially in the case of diffuse nodules, other microscopic foci exist, beyond the recognizable lesions.

28.2.4 Liver versus Lymph Node Metastases

For some yet unknown reasons, in most splanchnic tumors the formation of hematogenous metastases in the liver and by lymphatic drainage into lymph nodes does not proceed in parallel. Patients with a large neoplastic involvement of the liver may show an only minor local diffusion to lymphatic stations close to the primary tumor; on the contrary, other patients with an important metastatic disease to first-order and regional lymph nodes never experience liver metastases, at least clinically. These discrepancies are more often observed during the early phases of the clinical evolution, because in the advanced stages, the corresponding pathological patterns tend to overlap. Therefore, in some patients with splanchnic tumors, and in particular in colorectal cancer, we can expect an early "liver-only" metastatic disease that may occur especially when the local lymph node involvement is minor. In these cases, an aggressive therapeutic approach to diseased liver is highly justified, of course when the primary tumor has been radically excised with an accurate local and regional lymph node care.

28.2.5 Actual State of Liver Metastases Treatment

Treatment of metastatic cancer of the liver is far from being uniform, and the best choice of therapy for attending this disease is a source of controversy. In trying to distinguish what is accepted by universal consent from what is debatable, a clear distinction should be made between patients in whom a surgical approach is feasible and all the others. Resection is the only therapeutic option with curative effect on malignant liver tumors, but in over 70 % of cases, it is not applicable.

Liver resection for metastatic colon and rectum carcinoma is associated with 20–51 % 5 year patient survival [3]. Many factors are responsible for this large variability of data. Undoubtedly patients with more advanced disease, as revealed by multiplicity of lesions, wide liver involvement, and signs of liver dysfunction, have a poorer prognosis [4]. In order to quantify the likely clinical outcome, an index based on liver volume after resection ("future liver remnant" = FLR) has been elaborated and proved effective. In patients with normal liver, the minimum FLR required is 25 %; in patients who have received intensive chemotherapy or are affected by diabetes, fatty liver or liver fibrosis, it is 40 %; in patients with cirrhosis, 50–60 %. Therefore, the quality of the patient population has a direct influence on the type of allowed resections and on the results of the surgical approach. However, the latter must be judged considering that the natural history of untreated liver metastases is always discouraging, with the median survival for such patients being less than 2 years, with 5-year survival being exceptional. Another widely recognized factor is experience of the surgeon and of the structure employed for treatment [5]. An aggressive attitude towards the neoplastic disease no doubt appears rewarding [6]. Extrahepatic disease does not contraindicate liver resection as long as radical surgery is feasible. Moreover, repeated liver resections are possible with results comparable to the ones gained by initial liver resection. However, many institutions will not surgically treat patients with five or more bilateral liver metastases [7].

For small metastases, the type of resection, whether anatomic lobectomy or wedge resection, apparently does not influence survival. However, for large solitary metastases or for multiple unilateral nodules, lobectomy is more effective.

Given the priority of resection in the treatment of liver metastases, the interest in the other therapeutic options is mainly focused on the ones that are useful for patients with unresectable metastases or that are able to assure additional benefits after surgery. The main other approaches in the treatment of liver metastases are the following, in decreasing order with respect to efficacy, width of indications and frequency of use: chemotherapy, made by systemic administration or by hepatic arterial infusion (HAI), and the various local ablation techniques.

Systemic chemotherapy. In spite of its extensive use in the treatment of patients with hepatic metastases from abdominal cancers, systemic regimens of chemotherapy have produced low response rates and only minor benefits on survival. The drug involved in most trials is 5-fluorouracil (5-FU) or its active metabolite, 5-fluorodeoxyuridine (5-FUDR). The median survival offered by this product, possibly associated with other more recent drugs, is in the order of 10–17 months [8, 9]. The objective response rate reported in the literature is in the 20 % range. An increment of this rate is attainable with Lederfolin (Europe) and/or Levamisol (USA). Further increments can derive from the addition of a monoclonal antibody to vascular endothelial growth factor, when receptors are present [10]. However, during treatment apparently resistant clones of cells are selected, so in later phases of chemotherapy an uncontrolled spreading of neoplastic nodules frequently occurs even outside the liver, in the peritoneal cavity, adrenal glands and lungs.

Systemic chemotherapy has also been used in neoadjuvant regimens, i.e., before surgical treatment of liver metastases, in patients with severe liver dysfunction in order to improve their clinical condition for later surgical aggression.

HAI chemotherapy. In this variant of the traditional pharmacological approach to liver metastasis treatment, a regional infusion of drugs is provided through the hepatic artery. This can be done surgically, by inserting a small catheter into the gastroduodenal artery at laparotomy and advancing it up to the common hepatic artery. The gastroduodenal artery is tied distally, as are all branches afferent to pylorus and duodenal bulb. Cholecystectomy is also recommended to avoid chemical cholecystitis. More recently, a port-catheter system has been placed radiologically by percutaneous femoral artery puncture at the groin, making use of the Seldinger technique, and pushing the distal end of catheter in the hepatic artery or in a sub-branch. The proximal end is connected to a port located subcutaneously and easily accessible by skin puncture. The infusion flow rate is controlled by an external hepatic artery infusion pump. The rational for this chemotherapy modality is that liver metastases have been shown to receive most of their blood supply from hepatic arterial circulation. In effect, intra-arterial chemotherapy is associated with an increased response rate (62 %) in comparison with systemic infusion. The role of HAI in prolonging patient survival is controversial, with affirmative [11, 12] and negative answers [13, 14] found in the literature. A particular use of this chemotherapeutic approach as an adjuvant to a complete surgical resection has been adopted, with demonstration of a statistically significant survival benefit [15]. Another important advantage of hepatic infusion performed by high total body clearance drugs (such as 5-FUDR and also 5-FU) is that patients feel better because of the lack of systemic chemotherapy side effects. On the contrary, local and regional toxicity in HAI is not negligible: gastritis/duodenitis up to ulcers (21 %), biliary sclerosis (21 %), and above all chemical hepatitis (71 %) are due to a combined effect of ischemic and inflammatory responses to drugs by bile ducts and interstitial tissue. These figures can be improved by modulating doses and flow rate regimens [16].

Local ablation. This term is used to indicate a series of methods intended to realize a tumor destruction in situ by physical means (heat, cold) or chemical substance (ethanol, formalin). High levels of energy are delivered inside the liver into tumor target by electrodes or thin trocar-type probes, percutaneously inserted and externally guided by means of ultrasound (US) or computed tomography (CT) scans. The degree of ablation is normally monitored by US. The most widely used procedures are radiofrequency-, cryo-, laser- or microwave ablation, ethanol injection, and high-intensity focused ultrasound application. For all these techniques, the limit is the difficulty treating large numbers and special sites or sizes of nodules. Tumors close to major hepatic vessels may not reach temperatures low or high enough because of the thermal sink effect of blood. Also a location near the external surface of the liver or close to important biliary ducts may cause concern. In these cases, the intraoperative use of the procedure proved to be more effective and safer. Nodules of large size may not be treated with uniform effectiveness; therefore, a high likelihood of recurrence exists. Placement of probes into the tumor may result in spillage of cells into the peritoneal cavity upon withdrawal of the probe at the end of the procedure.

Despite good local control of single treated metastases, a survival benefit is difficult to demonstrate. Local tumor progression, intra-hepatic and extra-hepatic

tumor recurrences are common. The 3-year survival rates are in the range of 37–58 %, and 5-year survival, when reported, varies from 7 to 30 % [17]. An objective comparative evaluation of the results obtained with local tumor ablation procedures is difficult, if not impossible, because they are largely dependent on the previous morbid history of each patient, selection criteria, ability and experience of the performer, techniques applied, overlapping of different therapies, and so on. Among all these factors, the selections bias appears the most important. However, several studies have described prolonged survival for such patients [18], so local ablation remains an alternative for patients with unresectable liver metastases.

28.2.6 The Real Outcome of a Patient with Liver Metastases: A Factual Appraisal of Current Therapies Based on Personal Experience

When considering all therapeutic possibilities for liver metastases, we have at our disposal a great number of excellent clinical reviews. Many of them, however, are focused on how to obtain the best results from the application of single treatment options. This obviously excludes patients who are less likely to have a positive outcome (such as the elderly, those with more advanced disease stages, etc.). Therefore, the target of maximum outcome brings the risk of denying some minor benefits, such as a limited survival time, to patients who have no other hope. If we have in mind to do everything possible for each single patient, then we are forced to take into account the realistic impact of all therapeutic approaches in large series of homogeneously treated patients, "leaving no stones unturned." To reach this target, we reexamined all cases of liver metastases observed at our institution during a period of almost 15 years (from January 1989 to March 2003). The survey we now propose complies with the following criteria:

- The series of patients is continuous (no preliminary selection is accepted).
- All patients submitted to surgery are operated on by the same surgeon (AZ).
- The surgical approach is always highly aggressive.
- Radical surgery is performed whenever possible.
- Hepatic resections are performed also with palliative purposes (debulking).
- Surgery is always the first choice (a preoperative chemotherapy protocol is never followed).
- Intra-arterial and/or systemic chemotherapy is always used in the postoperative course or as an alternative to surgery as long as the maximum planned dose is reached.
- Poor general conditions are less important than local prohibitive situations in planning the pharmacological vs. surgical approaches.
- A minor peritoneal carcinosis is not considered an absolute contraindication to surgery.

The comprehensive results of this retrospective survey can be summarized as follows.

Table 28.1 Malignant tumors metastatic to the liver treated at our hospital division

Tumor	Primary tumors		Patients enrolled	
	n	%	*N*	%
Colon-rectum	303	58	257	61.5
Stomach	76	14	55	13.1
Pancreas	70	13	48	11.5
Biliary system	26	5	22	5.3
Unknown primary	17	3	10	2.4
Kidney and urinary bladder	10	2	7	1.7
Breast	9	2	9	2.1
Ovary	7	1.4	6	1.4
Neuroendocrine	4	0,8	2	0.5
Bronchogenic	4	0,8	2	0.5
Total	526	100	418	100

Table 28.2 Synchronous vs. metachronous metastases

Tumor	Synchronous metastases		Metachronous metastases		Total
	n	%	*n*	%	*n*
Colon-rectum	198	65.3	105	34.7	303
Stomach	68	89.5	8	10.5	76
Pancreas	66	94.3	4	5.7	70
Biliary system	24	92.3	2	7.7	26
Unknown primary	8	47.1	9	52.9	17
Kidney and urinary bladder	1	10	9	90	10
Breast	–	–	9	100	9
Ovary	3	42.9	4	57.1	7
Neuroendocrine	4	100	0	0	4
Bronchogenic	1	25	3	75	4
Total	373		153		526
%		71		29	

The total number of patients with liver metastases was 526; of them, 303 were from colorectal cancer. The distribution of clinical cases according to primary tumors is shown in Table 28.1. On average, 20 % of patients were lost to the survey for several reasons.

The metastases were predominantly synchronous in the most represented kinds of tumors (Table 28.2).

As far as the classification of liver metastases is concerned, we used the tumor grading and the inherent staging of disease proposed by Gennari and colleagues [19, 20]. This system is based on the results of imaging studies, such as US, CT, or magnetic resonance (RM) imaging, which are able to identify the neoplastic nodules, to document their size and site, and to estimate the percent of liver volume involved in the disease. It is usually easy to obtain reliable knowledge of these data, possibly confirmed by surgical exploration. From a simple combination of them, a staging

Table 28.3 Gennari classification of tumor grade and stage of disease in liver metastases (slightly modified)

H1	Hepatic involvement ≤ 25 %	
H2	25 % ≤ hepatic involvement ≤ 50 %	
H3	Hepatic involvement ≥50 %	
s	Solitary metastasis	
m	Multiple metastases localized at only one lobe	
b	Bilateral metastases	
Stage		
I	H1 s	
II	H1 m, b	H2 s
III	H2 m, b	H3 s, m, b
IV	(a) Minimal intra-abdominal extrahepatic disease (laparotomic inspection) (b) Extrahepatic disease	

Table 28.4 Treatment of liver metastases (526 patients)

Group A: intended curative operations	Major hepatic resections (hemihepatectomies, lobectomies, tri-segmentectomies)	10 %	Total surgical resective approach = 60 %
	Minor hepatic anatomic resections (bi-segmentectomies, segmentectomies)	19 %	
	Wedge resections – nodulectomies	18 %	
Group B: palliative operations (debulking)	Non-anatomic resections	13 %	
Group C: non-resective approach	Surgical port-a-cath implantation (for intra-arterial chemotherapy, sometimes in addition to surgical liver resections)	24.7 %	
	Intraoperative RF-ablation	2 %	Total non-surgical approach = 40 %
Group D	Resections of primary tumor without invasive treatment of liver metastases	38 %	

system is derived that has proved useful for assessing prognosis and planning therapy (Table 28.3).

The therapeutic procedures we performed on the patients are provided in Table 28.4.

Considering now separately the large chapter of colorectal metastatic disease into the liver and in particular the intrahepatic distribution of nodules, we observed a minor frequency of patients with a solitary large nodule and a much higher incidence of multiple bilateral metastases (Table 28.5).

By employing the Gennari classification to the liver metastases of colorectal carcinoma, we noted a maximum incidence of Stage III and IV, i.e., patients in the most advanced phases of disease with a higher than 25 % involvement of the liver, multiple localizations and/or extra-hepatic infiltrating diffusion of metastases (Table 28.6).

Table 28.5 Liver metastases from colorectal cancer. Number/patient and intra-hepatic distribution (303 patients)

Nodules number	Unilateral %	Bilateral %
1	17	1
2	5	4
3	2	4
Multiple	5	62

Table 28.6 Tumor grade grouping and staging of patients with colorectal metastases to the liver according to Gennari classification (257 patients)

Hepatic metastasis (H)	%	Stage	%
H1 s	16.2	I	12.1
H1 m	9.4	II	15.2
H1 b	8.2		
H2 s	1.6		
H2 m	3.2	III	44.5
H2 b	38.1		
H3 b	23.3		
		IV a	15.2
		IV b	13
		Total IV	28.2

Table 28.7 Treatment of liver metastases from colorectal cancer (257 patients)

Group of treatment	*n*	%
Group A: intended curative liver resections	98	38
Group B: palliative liver resections	36	14
Group C: intra-arterial port-a-cath	49	19
Group D: no invasive treatment of metastases	74	29

Table 28.8 Median survival (months) of patients with liver metastases from colorectal cancer

All patients	11.7	Patients of group A of treatment	16.0
Patients with synchronous metastases	10.33	Patients with synchronous metastases	12.0
Patients with metachronous metastases	14.26	Patients with metachronous metastases	17.0

In order to have series of patients as comparable and homogeneous as possible, we grouped them according to the type of treatment (four groups from A to D). Aiming at always giving them the highest curative option allowed by their local or general conditions, the choice of treatment automatically selected the starting status of the patients. Therefore, the obtained results are dependent on both the different therapeutic efficacies of the adopted procedure and on the various severities of the disease, but inside each group, the variability of this last condition is minimized. The numerical distribution among the four groups of treatments is reported in Table 28.7. Median survival of all patients and of the ones affected by synchronous or metachronous metastases, and the corresponding data for the patients of group A of treatment are provided in Table 28.8.

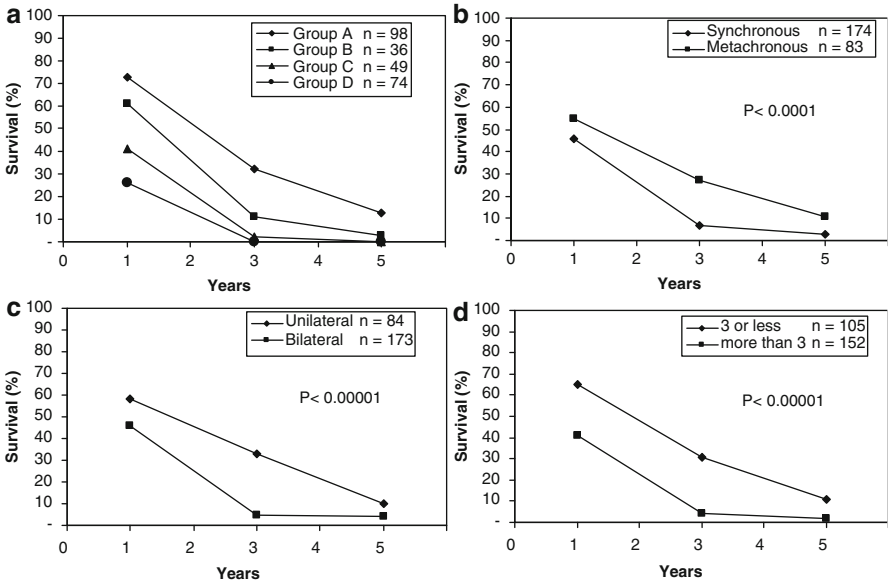

Fig. 28.1 Liver metastases from colorectal cancer. Survival graphs of patients: (**a**) by treatment group (see text); (**b**) depending on the type of metastases (synchronous vs. metachronous); (**c**) in relation to intrahepatic diffusion of metastases (unilateral vs. bilateral) and (**d**) according to the number of metastases (three or less vs. more than three)

The survival graphs for patients in each of the treatment groups are in Fig. 28.1a, but the differences in this grouping of data are not statistically significant when adopting the log-rank test. On the contrary, there are highly significant differences in time of survival when we compare synchronous vs. metachronous (Fig. 28.1b) or bilateral vs. unilateral metastases (Fig. 28.1c), or the number of liver metastases (>3 vs. ≤=3) (Fig. 28.1d).

Also the differences in survival between patients with or without peritoneal carcinosis (Fig. 28.2a) or in patients subjected to an intended radical liver resection, in which the edges of the surgical specimen proved to be free-of-tumor or infiltrated at the pathological examination (Fig. 28.2b), resulted in high significance.

By making use of the Gennari classification system, we again obtained highly significant differences in the survival of patients with H1 vs. H2+H3 liver tumor patterns (Fig. 28.2c) and in I+II vs. III+IV stages of disease (Fig. 28.2d).

Briefly considering the liver metastases from stomach carcinoma, the characteristics of this patient cohort are summarized in Table 28.9. Liver metastases were treated in less than half of the patients, and only a third of them could undergo a resection (Table 28.10). Because of the highly aggressive nature of this disease, the median survival of patients was definitely inferior to metastases from colorectal tumors (Table 28.11). Only in clinical cases in group A did we observe one patient who survived 5 years after the operation.

The discouraging results we observed in the subgroup of patients with pancreatic tumors are summarized in Table 28.12.

Nine women were suffering from liver metastases from breast carcinoma, and they were all recruited for the survey. Table 28.13 refers to the features of this subgroup, to the therapeutic procedures we adopted, and to results obtained in terms of patients' median survival.

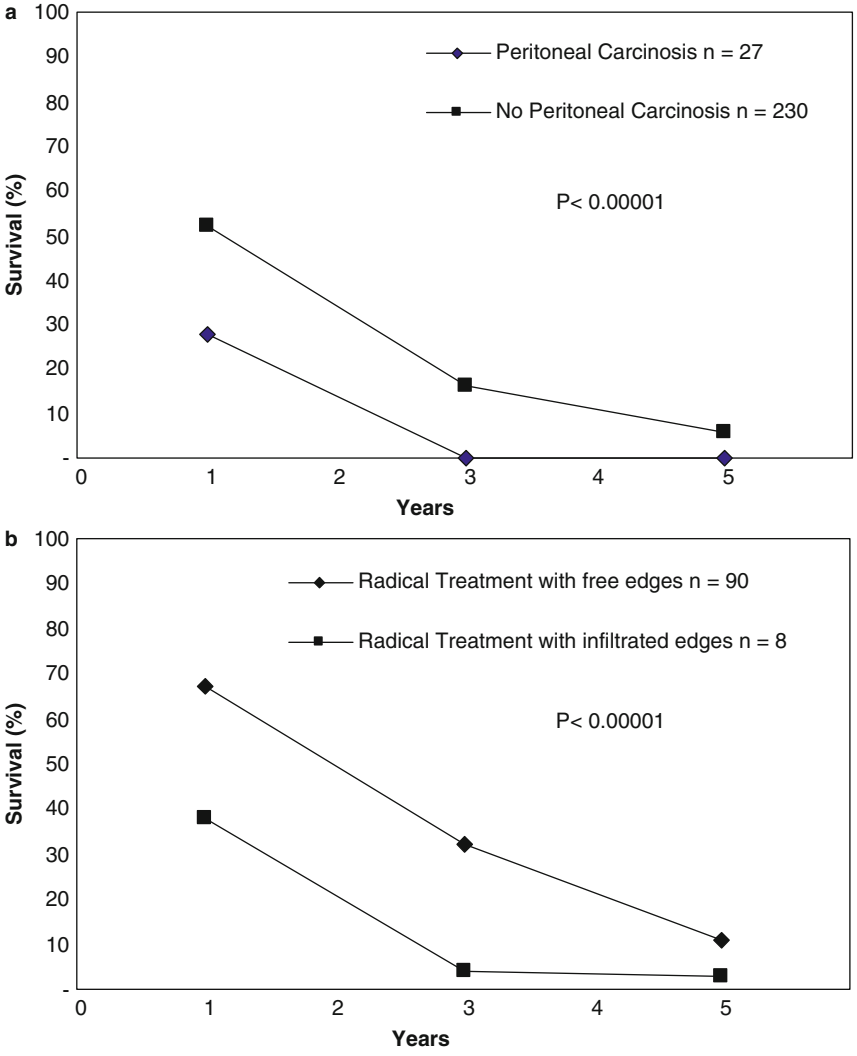

Fig. 28.2 Liver metastases from colorectal cancer. Survival of patients: (**a**) with or without peritoneal carcinosis; (**b**) in relation to the presence or absence of neoplasia in the edges of resection specimen; (**c**) when grouping patients according to liver tumor grade or (**d**) to stage of disease (Gennari classification system)

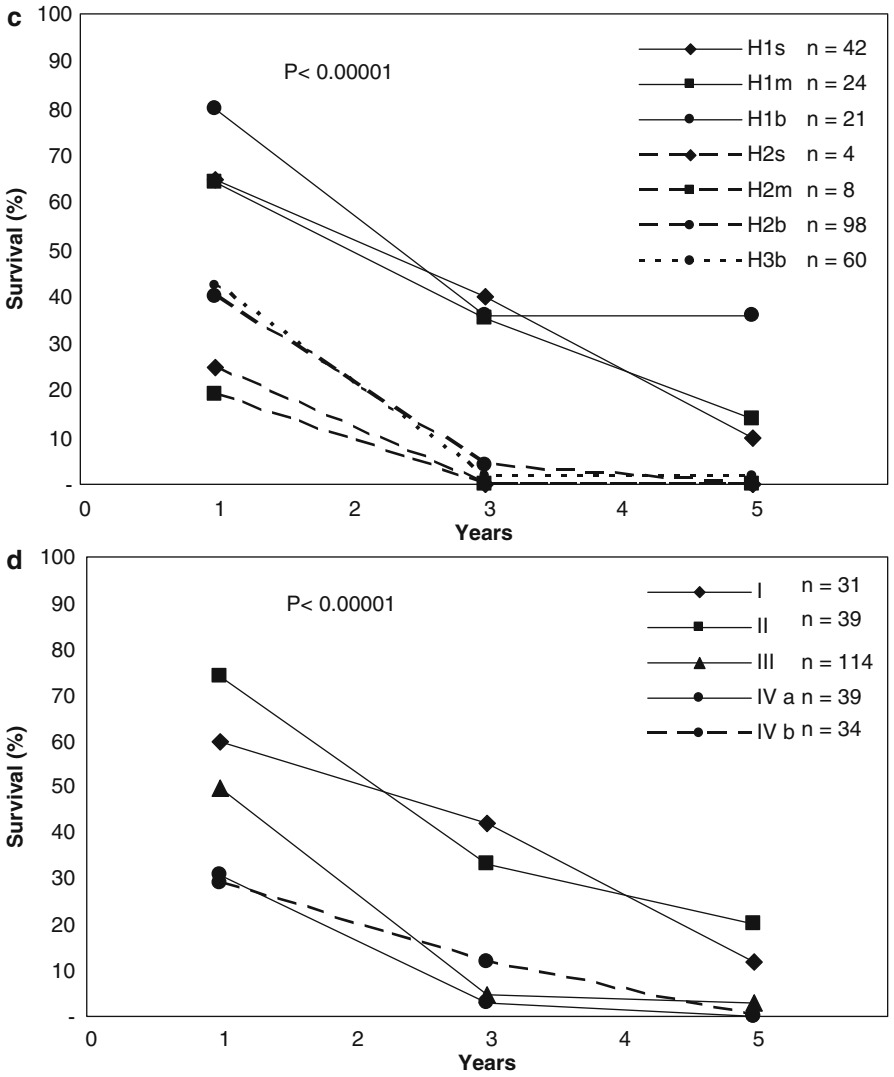

Fig. 28.2 (continued)

Table 28.9 Liver metastases from stomach cancer

Number of patients	76	Number of enrolled patients	55
Type of metastases	Synchronous 87 %	Unilateral	25 %
	Metachronous 13 %	Bilateral	75 %
Prevailing patterns according to Gennari classification		Tumor grade: H2 b	50 %
		Stage of disease:	III 46 %
			IV a 34 %

Table 28.10 Treatment of liver metastases from stomach cancer (55 patients)

Group of treatment	*n*	%
Group A: intended curative liver resections	6	11
Group B: palliative liver resections	12	22
Group C: intra-arterial port-a-cath	7	13
Group D: no invasive treatment of metastases	30	54

Table 28.11 Median survival (months) of patients with liver metastases from stomach cancer

All patients	7.16
Patients with synchronous metastases	6.56
Patients with metachronous metastases	11.28

Table 28.12 Liver metastases from pancreas cancer

Number of patients	70	Enrolled patients	48 (69 %)	Group A	6 (12 %)
Type of metastases	Synchronous: 44 (92 %) Metachronous: 4 (8 %)	Median survival (months)	All patients: 3.46 Group A: 5.67		

Table 28.13 Liver metastases from breast cancer

Number of patients	9	Mean age	57.6 years
Type of metastases	Metachronous[a]: 9 (100 %)	Type of treatment:	Group A: 67 % Group B[b]: 33 %
Number of metastases	3 or less: 4 (44 %) More than 3: 5 (56 %)	Median survival (months)	All patients: 31 Group A: 36 Group B: 7.9

[a]Average free-of-disease time after primary tumor operation: 35.75 months
[b]In all these cases, liver hilus lymph nodes were found positive

28.2.7 Conclusive Remarks

This survey was aimed to give a factual outline of the real therapeutic possibilities we can offer to patients with liver metastases from various primary tumors. It refers to a situation existing until some years ago, but we don't think recent changes have been significant. The difficulties we meet when approaching a controversial matter like this arise essentially because both the clinical population and therapeutic proposals are very heterogeneous. In order to overcome these obstacles at least partially, we tried to collect a great number of patients without any preventive selection and to apply a rigorous operative protocol. Given that the best chance of cure is generally assured by surgery, operations were performed whenever possible, with radical or palliative purposes. Debulking was considered a real therapeutic option when supplemented with intra-arterial and/or systemic chemotherapy.

The results we obtained depended essentially on the type of primary tumor, on presentation modalities and the diffusion pattern inside the liver with metastatic disease, and on general conditions. Primary tumors of the pancreas and biliary tract, and synchronous, bilateral, multiple metastases with involvement of more than

25 % of the liver volume, when at most a palliative resection can be performed, have the poorest prognosis and shortest survival time. In regard to the clinical picture, the appearance of ascites and/or icterus is the most ominous sign. On the contrary, colorectal tumors with limited local growth and only a few metachronous liver metastases confined to one lobe, in patients in a good state of health, when resection is possible and is really radical with free-of-disease edges of the specimen, have a much more favorable course, even if it is not exceptional.

However, we must not forget that besides these two opposing situations, a subgroup of patients does exist: it is numerically significant and comprises some people of young age, in excellent states of health, already radically operated on for a primary tumor, perhaps a colorectal cancer, but with multiple scattered liver metastases, which proved to be chemotherapy-resistant. These patients are condemned to die without any reliable therapy because surgery is excluded owing to the type of intrahepatic diffusion of the disease; RF ablation accomplishes only temporary palliation, and chemotherapy has already been proven ineffective. They represent a dramatic challenge to any oncology therapist and urgently require a new solution to their problems.

28.3 Technical Aspects of a BNCT Application to Liver Tumors: Scientific and Clinical Issues

Always keeping in mind that BNCT efficacy can be obtained only if its excellent characteristics of specificity and selectivity are preserved, we worked out a theoretical project addressed to the treatment of hepatic diffuse neoplastic disease based on the boron enrichment of the liver metastases followed by irradiation of the explanted organ in the thermal neutron field obtained in a proper facility of a nuclear reactor. After the treatment, the organ is re-implanted in the patient, thus preserving the whole body from any radiation side effects and ensuring the treatment of all the nodules and the isolated tumoral cells present inside the liver.

The four stages of the procedure are:

- Pre-loading of cancer cells with a ^{10}B compound so as to reach a minimal ^{10}B content in tumor cells of 40 ppm and a concentration ratio between tumor and normal cells of at least 3.
- Surgical isolation of the liver and its washing after ^{10}B loading with a chilled B-free perfusion solution in order to protect the organ from normothermic ischemia and to clear it of blood content, thus avoiding the risk of an unspecific radiation damage to vascular structures.
- Extracorporeal liver irradiation with thermal neutrons by immersion of the isolated organ in a proper neutron field rather than in a beam.
- Reconnection of the irradiated liver to the donor organism.

In order to turn this project into a therapeutic proposal, it was necessary to solve several problems and to clarify some questionable aspects. The methods we used in this preliminary work will be exposed hereafter in separate areas according to the prevailing nature of the required competence.

28.3.1 Area of Physical Interest

The main topics related to physics that were faced in order to irradiate the explanted liver inside a neutron field are the following:

1. Design, realization, and characterization of the neutron field.
2. Calculation of the treatment plan.
3. Set-up of a system for the measurement of the boron concentration in biological samples and for the imaging of its spatial distribution.

28.3.2 Irradiation Facility and Treatment Plan

An ideal treatment plan, able to exploit BNCT capability in the treatment of diffuse malignancies, must deliver a lethal dose to the tumor, regardless of its spatial distribution inside the organ. At the same time, the treatment plan must keep the dose absorbed by the normal cells as low as possible, and, in any case, below their tolerance level. This goal can be reached by creating a thermal neutron field as uniform as possible inside the organ. According to the dimensions and the characteristics of the organ to be irradiated, neutron sources with different energies and geometries can be used [21, 22]. In Pavia, the disseminated hepatic metastases were treated using a neutron field obtained inside the thermal column of the research nuclear reactor Triga Mark II, operating at 250 kW. The design of the facility was obtained by Monte Carlo studies, in particular, by calculations performed with the transport code MCNP [23]. A scheme of the liver irradiation facility built inside the reactor is shown in Fig. 28.3 [24, 25]. In this position, the liver is sunk in a field of thermal neutrons irradiating the organ from all directions.

The γ background coming from the reactor core was lowered with two bismuth screens whose overall thickness is 20 cm. In the irradiation channel, the neutron flux was measured with the activation method (Au, Cu, Al, Ni … foils and wires); the γ dose was measured by BeO Thermo-Luminescent Dosimeters (TLD). The results of in-air measurements in the liver irradiation position are listed in Table 28.14.

In order to study the dose distribution inside the organ, a Teflon phantom modeling the explanted liver was constructed. It consists of a spherical segment 6 cm high, with a circular base of radius of 15 cm, filled with a hepato-equivalent solution [24]. The phantom base, corresponding to the inferior surface of the in situ organ is placed downward and in a horizontal setting, so as to mimic the loading plane of an isolated liver. The phantom was equipped with thin copper wires along the *X*, *Y* and *Z* axes, as shown in Fig. 28.4, and was irradiated in the liver position. After irradiation, the copper wires were cut into pieces 0.5 cm long, and a Ge detector was employed to measure the ^{64}Cu activity by γ spectrometry. The measured activity was then used to evaluate the thermal neutron flux using the Westcott formalism [25, 26]. The same model was reproduced in an MCNP input. The organ volume was divided into cubic voxels of $1 \times 1 \times 1$ cm^3, creating five meshes of voxels at $Z = 1, 2, 3, 4, 5$ cm starting from the base of the liver along the vertical axis (*Z*-axis) (Fig. 28.4).

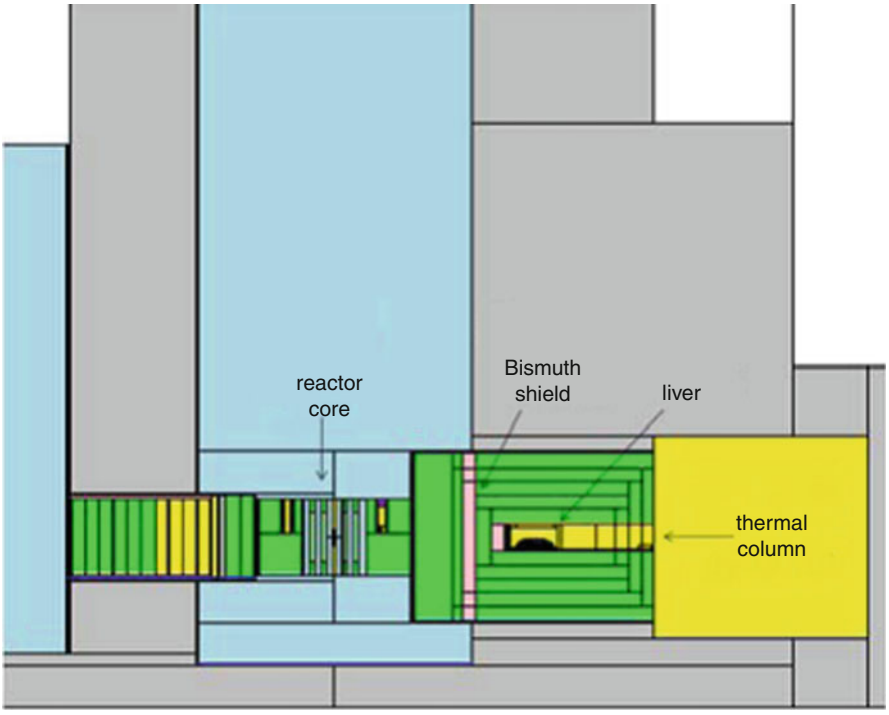

Fig. 28.3 Vertical section of a part of the Triga Mark II reactor: the core, the liver model in the irradiation position obtained in the thermal column, and the bismuth screens inserted to lower the γ radiation from the core are visible

Table 28.14 Neutron flux and γ dose in air at the liver irradiation position

$\Phi_{th}(cm^{-2}\ s^{-1})$	<0.2 eV	1.4×10^{10}
Φ_{epi}	0.2 eV ÷ 0.5 MeV	3.3×10^{07}
Φ_{fast}	>3.5 MeV	2.0×10^{06}
Φ_{fast}	>8.2 MeV	9.4×10^{04}
D_{γ} (Gy·cm²)	1.6×10^{-13}	

The experimental flux values obtained in the Teflon phantom were then compared with the results of the flux calculation in the voxels corresponding to the copper wires analyzed. The thermal neutron flux distributions along *X*-axis, both experimental and calculated, are reported in Fig. 28.5a.

The agreement between the Monte Carlo calculations and the experimental measurements is good, but the neutron flux distribution is far from uniform because the "hepatic solution" drastically changes its behavior, mainly along the longitudinal *X*-axis. The ratio between maximum and minimum thermal neutron flux values is $\Phi_{max}/\Phi_{min} = r \approx 4$. To make the flux distribution more uniform, the organ is rotated by 180° halfway throughout the irradiation time. The effect of this rotation is shown in Fig. 28.5b where the thermal neutron flux distribution is reported along the *X*-axis,

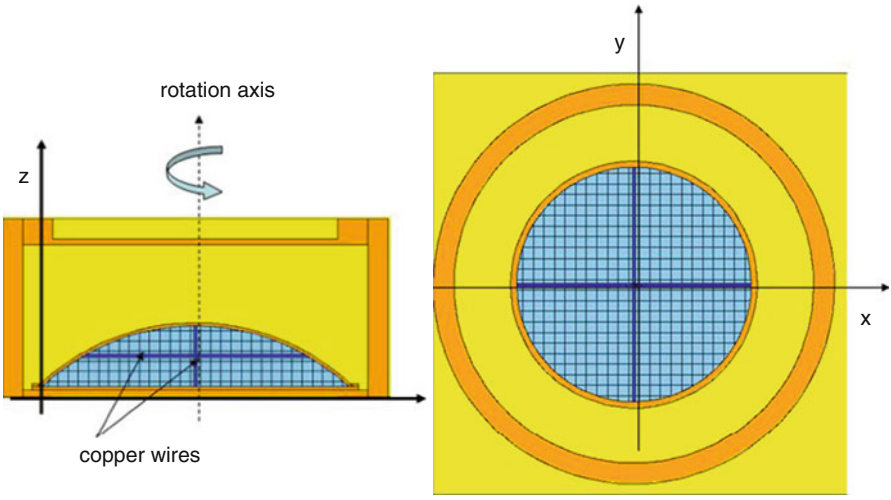

Fig. 28.4 MCNP geometry of the liver phantom inside the Teflon holder, vertical (*left*) and horizontal sections (*right*). The 1-cm^3 voxels and the copper wires for thermal neutron measurement are visible

for each mesh, from 1 to 5 cm from the base. The ratio between maximum and minimum flux values was thus lowered to $r = 2.31$.

To give an idea of how the thermal neutron flux uniformity would affect the dose distribution inside the liver, the dose volume histograms (DVH) were calculated in the liver model described above.

Using the thermal neutron flux in each voxel of the phantom, the contributions to the absorbed dose from reactions on nitrogen ($^{14}N(n, p)^{14}C$) and on boron ($^{10}B(n, \alpha)^7Li$) were calculated. The epithermal neutron flux component ($E_n > 0.2$ eV) was two orders of magnitude lower than the thermal one, so the epithermal and fast neutron contributions coming from the elastic scattering on hydrogen were neglected. For the calculations, the following conditions were assumed:

1. a ^{10}B concentration $CH = 8$ ppm in the healthy liver;
2. a ^{10}B concentration $CT = 50$ ppm in the tumor;
3. an irradiation time T_{irrad} suitable to deliver a minimum thermal neutron fluence $\Psi = 4 \times 10^{12}$ cm^{-2} independently at its position inside the organ.

To evaluate the irradiation time, the tumor was assumed to be located in a voxel where the thermal flux was minimum (Φ_{min}); thus, $T_{irrad} = 4 \cdot 10^{12} / \Phi_{min}$. The dose D_{vox-i} was then calculated for each voxel using the equation $D_{vox-i} = (D_N + D_B \cdot CH) \cdot \Phi_i \cdot T_{irrad}$ where D_N and D_B are doses from nitrogen (3 % in weight) and from boron (1 ppm), respectively. Finally, the dose histograms were built weighting the dose contributions in each voxel with the factor: $w_i = Vol_{vox-i} / Vol_{liver}$. The cumulative function of this histogram represents the DVH. The results of these calculations are reported in Fig. 28.6a(a1). The dose delivered to the tumor varies from 15 to 35 Gy, while the normal tissues absorb a dose in the range of 3–7 Gy. The fraction of healthy organ that absorbs the different dose values can be inferred from the DVH

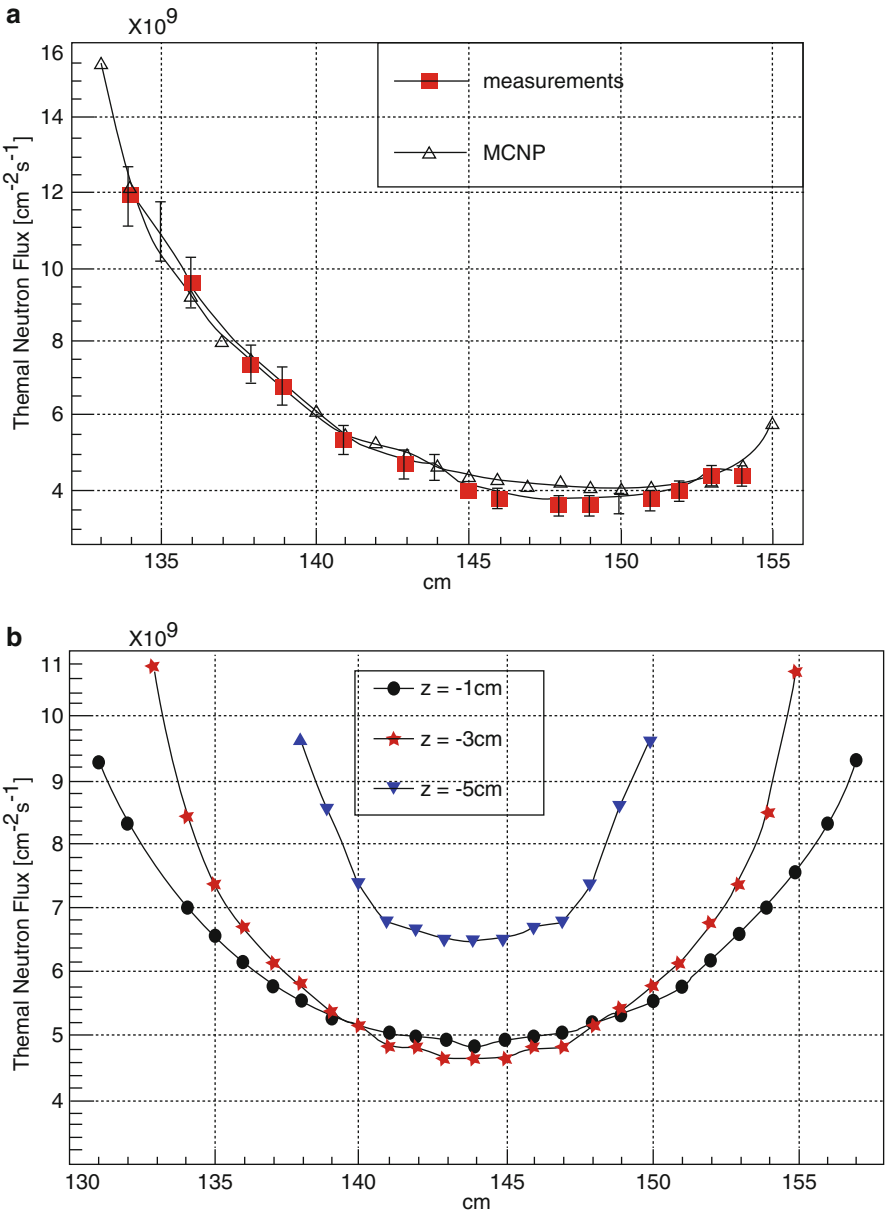

Fig. 28.5 Thermal neutron flux distribution along the longitudinal *X*-axis in the phantom, filled with the hepatic solution. (**a**) Comparisons between MCNP calculations and experimental measurements at $Z=3$ cm; (**b**) calculated flux distribution after rotation of 180° halfway through the irradiation time

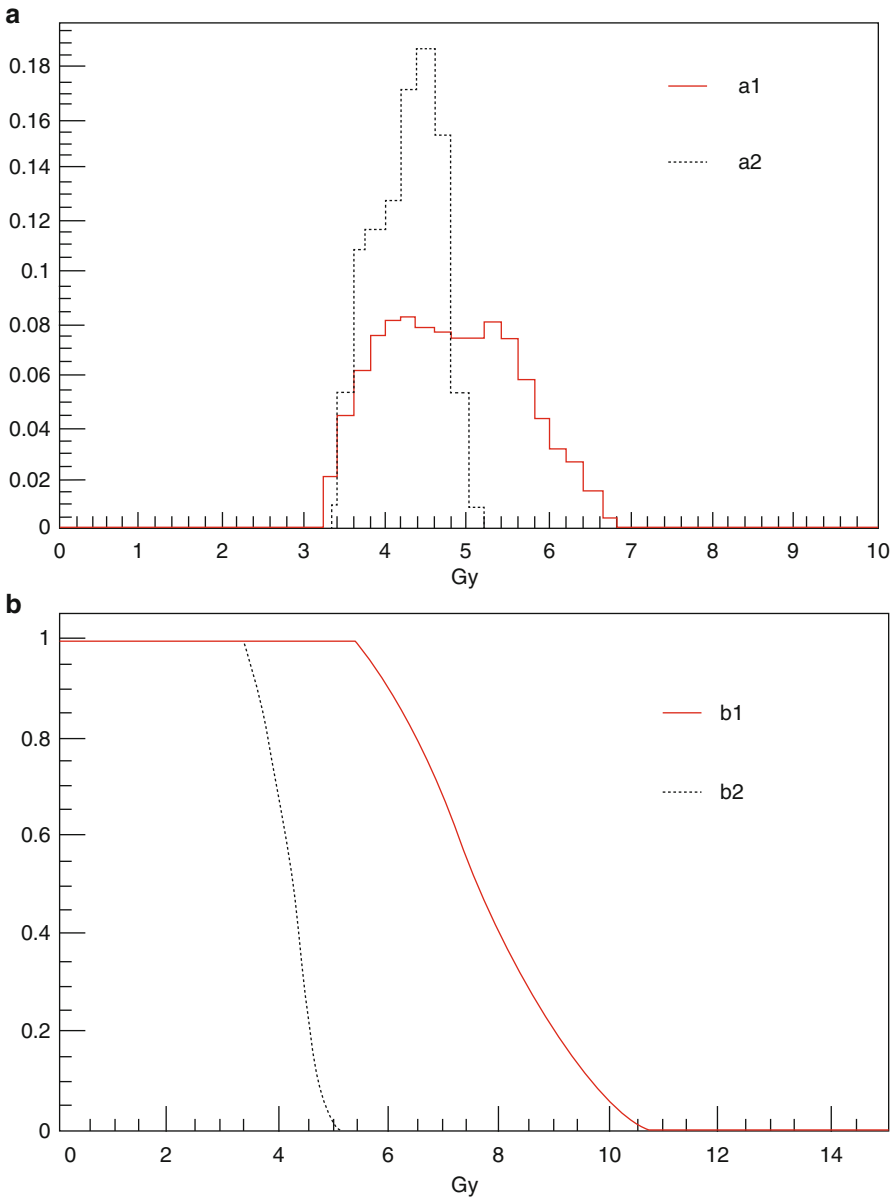

Fig. 28.6 Histograms of the absorbed dose (**a**) and DVH (**b**). The *red curves* (a1 and b1) refer to the facility used for the patient treatment, reported in Fig. 28.1. The *black curves* (a2 and b2) refer to a different thermal column configuration that would allow a more uniform thermal neutron flux distribution in the organ model [27]

in Fig. 28.6b(b1). The black curves (a2 and b2) refer to a different thermal column configuration, which would allow a more uniform thermal neutron flux distribution inside the liver model, as described in [27].

Table 28.15 Values of the boron concentration and of the absorbed dose at the reference point produced by a neutron fluence $\Psi_n = 4 \times 10^{12}$ cm^{-2} in the normal liver and in the tumor of the two treated patients

Boron concentration(ppm)			Absorbed dose (Gy)	
	First patient	Second patient	First patient	Second patient
Tumor	47 ± 2	45 ± 5	18 ± 1	18 ± 1
Liver	8 ± 1	8 ± 1	6 ± 0.3	6 ± 0.3
Tumor/liver	5.9	5.6	3	3

In the treatment of the two patients, the liver was positioned into two sterile Teflon bags with a chilled UW solution, and then in a rigid Teflon transport case. The thickness of the rigid holder was chosen in order to protect the organ from mechanical shocks and to ensure proper thermal isolation. The holder was previously cooled at 4 °C and then kept at the same temperature, placing a layer of dry ice on its cover. The quantity of dry ice was experimentally determined to keep the liver at a constant temperature of around 4 °C for at least 1 h. For both treated patients, the time elapsed between the surgical operation for the explantation and the return of the liver to the hospital for the reimplantation was about 45 min. During this time, the organ temperature was monitored with two thermocouples placed in contact with the Teflon bag (one on the top and one on the bottom) containing the liver.

For each patient, a proper treatment plan was assessed. Starting from the CT scan data, a geometrical model was designed taking into account the organ dimensions, and the neutron flux distribution was computed inside it. The irradiation time was fixed to deliver a neutron fluence of $\Psi = 4 \times 10^{12}$ cm^{-2} in a reference point in the organ model. For both patients, the irradiation time was about 10 min. The absorbed dose in the reference point was calculated by the relation $D_{H,T}$ (Gy) = 3.6 + 0.32 $C_{H,T}$ (ppm), where $C_{H,T}$ represents the boron concentration in the healthy and in the tumoral tissues, respectively. The boron concentration was measured by the α spectroscopy method [28] in two couples of tumoral and healthy samples taken from the liver after 1 and 2 h from the beginning of the boronophenylalanine (BPA)-fructose solution infusion. In the previous relation used for the dose calculation, the term equal to 3.6 represents the dose absorbed by the healthy tissue and/or by the tumor when the liver without boron is exposed to the neutron irradiation field at a fluence of $\Psi = 4 \times 10^{12}$ cm^{-2}; for more than 70 %, this is due to the γ radiation (three components: 0.64 Gy of γ background in the irradiation position without liver, 1.948 Gy and 0.144 Gy produced, respectively, by the reactions $^{1}H(n,\gamma)^{2}H$ and $^{35}Cl(n,\gamma)^{36}Cl$ on hydrogen and on chlorine present in the liver). The remaining 30 % is due to the reaction $^{14}N(n, p)^{14}C$ on nitrogen. The value of the γ dose was overestimated because it was evaluated assuming electronic equilibrium conditions in each point of the liver.

Table 28.15 reports the boron concentration values in the samples taken before the treatment, the doses absorbed by the tumor and the healthy tissues in the reference point, and for a fluence of $\Psi = 4 \times 10^{12}$ cm^{-2}; the dose delivered to the healthy tissue in the rest of the organ should have a distribution analogous to the one shown in Fig. 28.6(a1, b1).

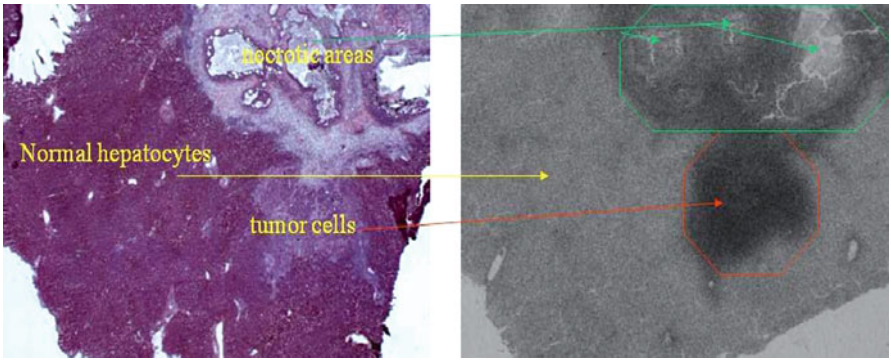

Fig. 28.7 Image (*left*) of a thin slice of a sample of a human liver metastatic nodule (standard hematoxylin & eosin staining) and (*right*) corresponding neutron autoradiography image. Within a distance of a few millimeters, normal hepatocytes, necrotic areas and tumor cells are simultaneously present. Neutron autoradiography image shows boron concentration in the tumor is higher than in the normal hepatocytes

28.3.3 Measurement of the Boron Concentration

The measurement of the boron concentration in biological samples is based on the spectrometry of the charged particles emitted in the capture reaction on boron. The tissue samples taken from the organ are frozen in liquid nitrogen, cut into 70-μm-thick slices using a cryostat, and deposited on Mylar disks. For the measurement, each disk is placed in front of a solid state silicon detector and exposed to a thermal neutron flux. The concentration is calculated selecting an area of the spectrum formed only by the α particles coming from the reaction $^{10}B(n, \alpha)^{7}Li$.

Since the tumor is disseminated, a sample of healthy tissue could contain tumoral nodules, and a tumoral sample could contain a part of healthy or necrotic tissue (Fig. 28.7).

In order to correctly evaluate the ratio $T = C_T/C_H$ between the concentrations in tumor and in normal cells, it is mandatory to know the histological composition of the analyzed sample. For this purpose, for each measurement, three thin slices from both healthy and tumor samples are obtained. The first one is used to measure boron concentration as described, the second one for histopathological analysis, and the last one for boron imaging by neutron autoradiography [27]. In this way, it is possible to collect information about the morphology of the tissues, the spatial distribution of boron, and the quantitative concentration. Using this method, the boron concentrations in human samples (Table 28.15) and in animal samples obtained from a rat model were measured.

28.3.4 Area of Biological Interest

Several issues and methods of study will be mentioned here: all of them are of interest when planning experiments addressed to defining the theoretical bases of a new

BNCT application, optimizing the liver's extra-corporeal irradiation, and extending its indications.

Choice of the clinical target. For the above-discussed reasons, we dealt with the BNCT treatment of liver metastases from colorectal cancers. This choice was favored by the circumstance that both a strand of syngeneic rats (BD-IX) and a cell line named DHD/K12/TRb (DHD), which was established from a colon adenocarcinoma chemically induced in BD-IX rats by 1,2-dimethylhydrazine oral administration [29], are available on the market. We think however that also some types of primary liver tumors could benefit from BNCT treatment.

Cancer cell cultures for in vitro *^{10}B selective uptake studies.* All our data were obtained using the DHD cell line that grows as a monolayer in a medium composed by a mixture of HAM'S F10 and DMEM (1:1 v/v) supplemented with 10 % fetal bovine serum and gentamicin (40 μg/ml). The medium is enriched with the ^{10}B carrier at various concentrations when cells are in the exponentially growing phase [30]. The time of contact is a noteworthy variable.

At the end of the incubation period, as we want to mimic the condition of an isolated organ that will be washed to clean all its blood and boron contents away. The ^{10}B-enriched medium is removed, and cells are recovered and washed in ^{10}B-free medium. A fraction of cells is then deep-frozen in liquid nitrogen for intracellular ^{10}B evaluation. In all our experiments, we used ^{10}BPA as the boron carrier at concentrations ranging from 10 to 160 ppm (or μg/ml). The effects of two different incubation times (4 and 18 h) were studied. The cellular ^{10}B content was determined by the mass spectroscopy method ICP-MS or by α-spectrometry [31].

In vitro *evaluation of two opposite phenomena in cells: ^{10}B content storage and loss.* The accumulation of ^{10}B into cells appears mediated by an active transport mechanism because the intracellular ^{10}B content is higher than that of the culture medium at any tested concentrations. There is also a mild increase of the intracellular ^{10}B concentration with increasing time of contact (Fig. 28.8a,b).

The study of ^{10}B uptake by tumors is complicated by the fact that ^{10}B in cells is present in two forms, i.e., tightly and loosely bound: this last one can actually be lost by exposing cells to a ^{10}B-deprived medium. The release of the ^{10}B loosely bound fraction is important because, if it occurs after and as consequence of liver washing, it could lower the efficacy of neutron irradiation on the tumor and make the calculation of the doses incorrect.

Therefore, the total ^{10}B concentration in cells is the sum of two fractions: the released and the retained one. The first is determined by the total of the ^{10}B content in the three subsequent cell washings performed after incubation to remove the ^{10}B of treatment from the culture medium; the second is evaluated by analyses of ^{10}B content of the cell pellet obtained after the washings.

The release of the loosely bound fraction (or washout) was studied after incubation [32], maintaining ^{10}B-enriched cell cultures at two temperatures (37 and 4 °C) and in two modalities of cell cultures, i.e., adherent to the substrate or resuspended in the culture medium. The washout phenomenon is more pronounced in cell suspensions and is greatly reduced at 4 °C (Fig. 28.9a,b).

In vitro *appreciation of radiation damage to cells.* In order to investigate this topic, by means of DNA flow cytometric analyses we evaluated the cell cycle

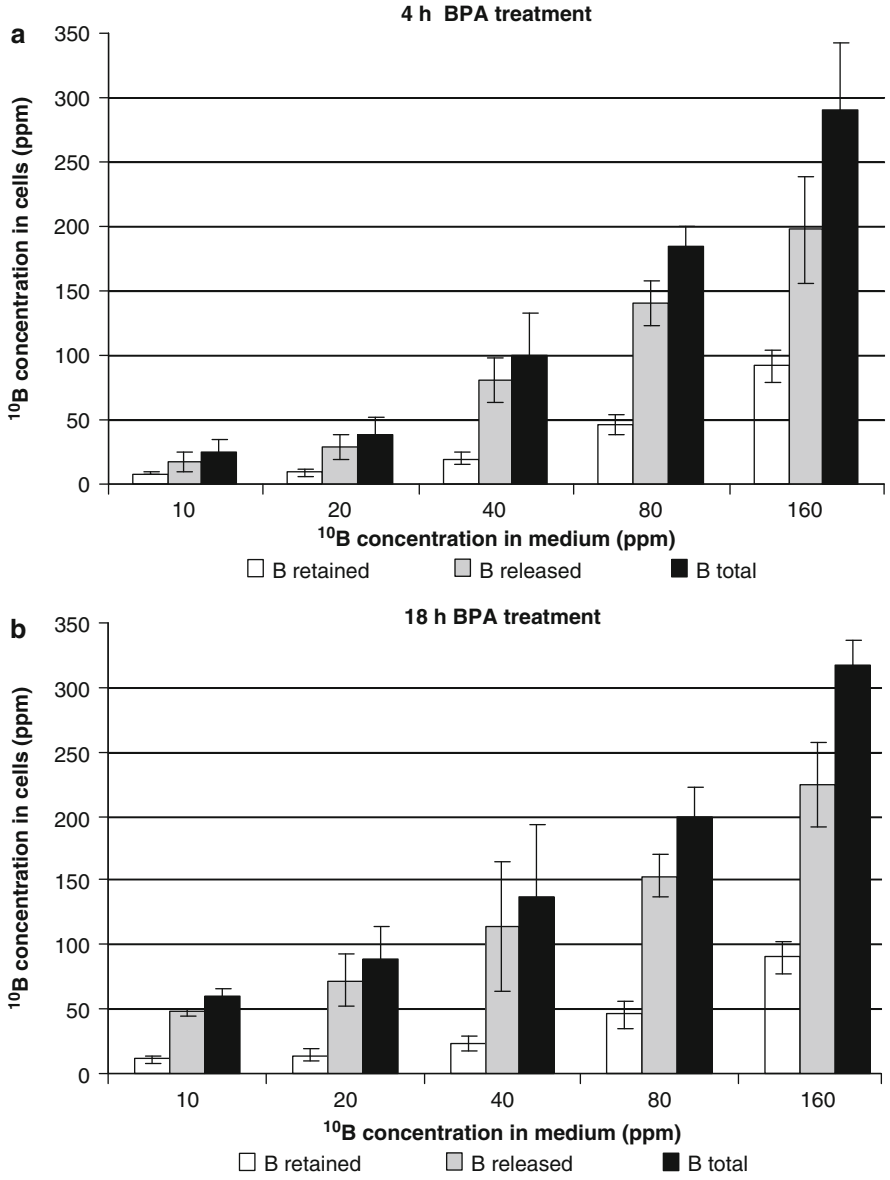

Fig. 28.8 Intracellular ^{10}B concentrations as a function of ^{10}BPA concentration in the culture medium. Total ^{10}B, retained and released ^{10}B contents are indicated: (**a**) after 4 h and (**b**) after 18 h of cell contact with boronated medium

modifications and the DNA damages following the BNCT treatment [33]. Flow cytometry is a technique of flowing cell analysis able to measure physical or chemical characteristics that can be detected by a fluorescence probe. One of its main applications is cell DNA content analysis, whose result is a histogram that

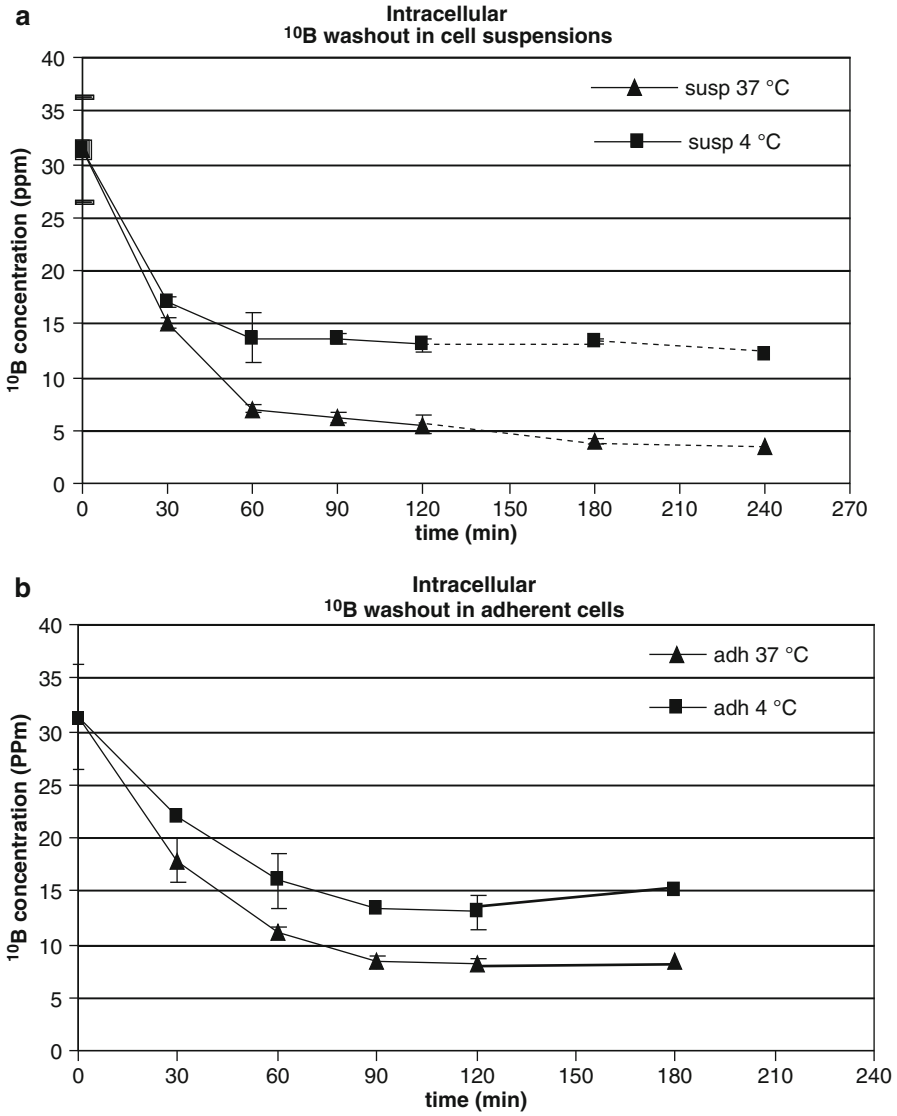

Fig. 28.9 Washout of intracellular ^{10}B contents by exposing ^{10}B-loaded cells to ^{10}B-deprived medium at 4 and 37 °C: (**a**) DHD cells when floating in suspension; (**b**) same type of cells when adherent to a substrate

gives information on both the cell cycle and ploidy status of the studied population (Fig. 28.10).

Moreover, cell proliferative capacity was evaluated by testing cell plating efficiency.

Liver metastases induction in rats. ^{10}B loading and distribution in metastases and normal tissue. Multiple and sometimes confluent hepatic metastases can be

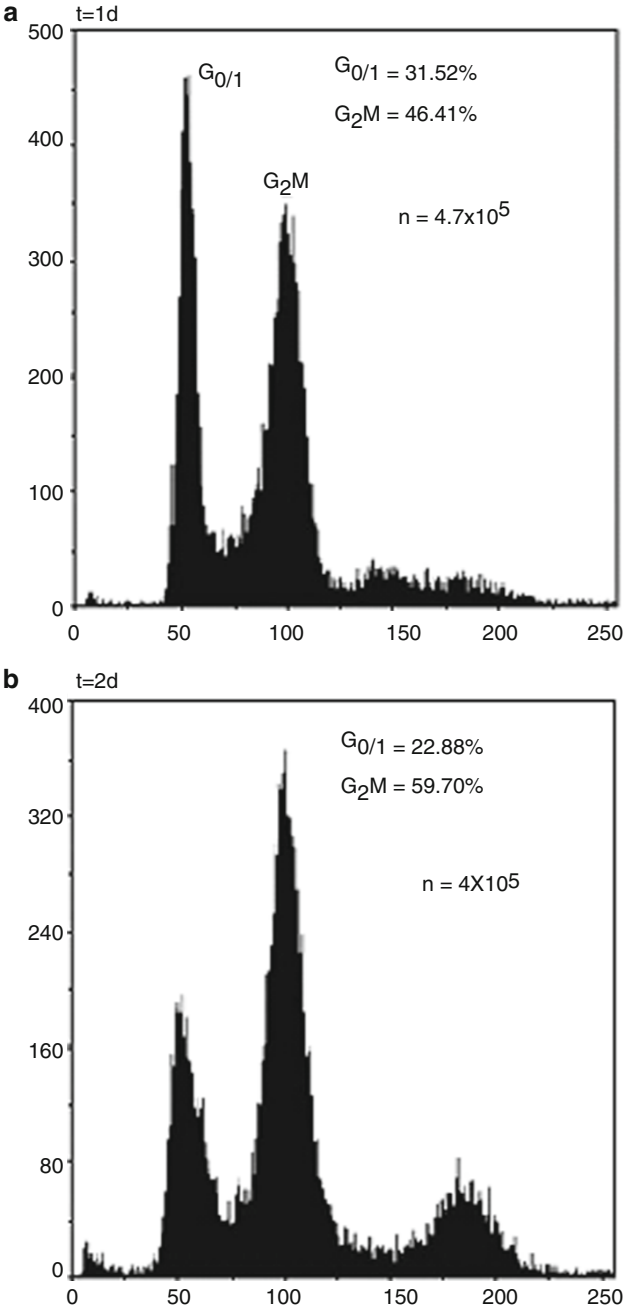

Fig. 28.10 Flow cytometric DNA histograms of in vitro cultures of a DHD cell line at different times after a BNCT treatment (1, 2, 7, and 12 days-box a, b, c and d respectively). $G_{0/1}$ indicates the cell fraction, corresponding to resting or presynthetic cells, in relation to the all of the cells in the culture; G_2M is the dividing diploid cell fraction. At 1 day the analysis gives an almost normal result. The histograms on the following days show increasingly severe damage of cell DNA with aneuploidy, excess of cell debris, and a fall in *n* values (number of recollected cells from each flask) (From Zonta et al. [33])

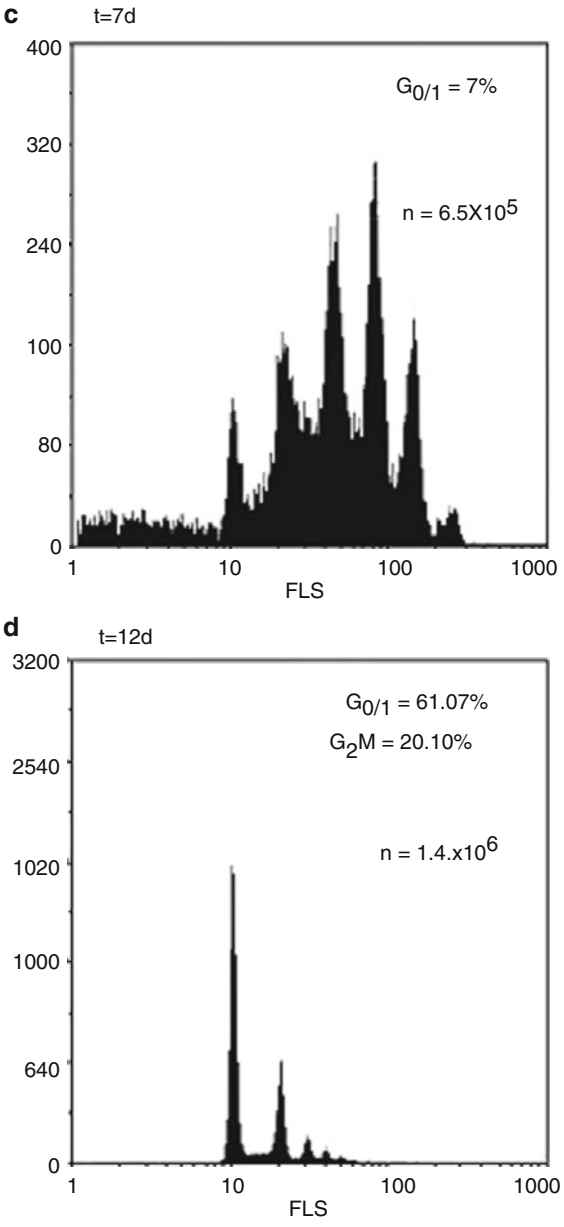

Fig. 28.10 (continued)

induced in BD-IX male rats by intrasplenic injection under general anesthesia of 2×10^7 cells obtained from the syngenic DHD line. During the injection, the left branch of the portal vein is clamped: in this way each animal gives samples of both tumoral (from the right lobe) and healthy liver tissue (from the left lobe). At the end of the operation, the rat is splenectomized.

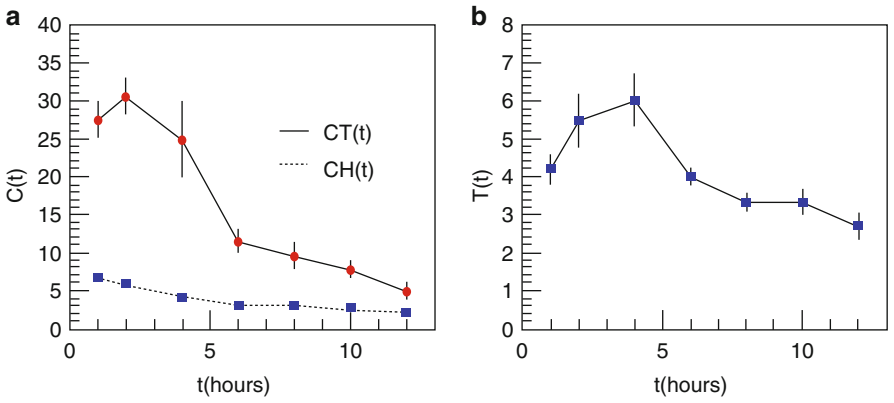

Fig. 28.11 Boron concentration measurement results in the animal model. A population of 100 rats was analyzed. (**a**) Boron concentration as a function of time interval between the BPA infusion and the anima sacrifice, in tumor and in healthy liver. (**b**) Boron concentration ratio in tumor and healthy liver

Fifteen days later, the same animals are re-anesthetized, and a dose of 300 mg ^{10}BPA/kg body weight is slowly (5 min) injected through the dorsal penis vein, using the fructose complex of ^{10}BPA-HCl, supplied by BBI, Raleigh, NC, USA, with ^{10}B enrichment of more than 95 % (100 mg BPA is combined with 2 ml 0.3 M fructose solution; pH is adjusted to 7.4–7.5 with 2 N NaOH solution) (BPA-F).

At given times (usually 1, 2, 4, 6, 8, and 12 h after ^{10}B solution injection), the rats are killed under general anesthesia; the liver is extracted with a small portion of the portal vein and correspondent aorta, washed with 5 % glucose solution through these last vessels, and frozen. Thin slices of tumoral and normal liver tissue are cut and processed for histological analysis in order to evaluate the tumor percentage in each sample [34]. Results of the ^{10}B concentration measured by the α-spectrometry method in tumor and healthy liver are reported in Fig. 28.11a; the ratio of boron concentration in tumour and healthy liver are shown in Fig. 28.11b; in the time interval between 1 and 5 h, this ratio is higher than 4; it reaches a value of about 6 between 2 and 4 h.

BNCT of experimentally induced liver metastases in rats. Liver metastases are induced in BD-IX strain rats, and a BPA-F solution is injected as the above described. After 2–4 h, the animal is killed, and the liver, after being washed and refrigerated at 4 °C, is irradiated in the reactor thermal column until a neutron fluence of 7×10^{12} cm^{-2} is reached (12 min). In the meantime, a hepatectomy is performed on a syngenic or allogenic (Lewis or Wistar Furth) recipient rat under general anesthesia (these last strains of rats are more resistant to surgical stress). The isolated irradiated liver is then transplanted orthotopically in the recipient rat under general anesthesia. The liver transplantation was always performed according to a modification of the Kamada method [35]. We are indebted to Miss Ferguson of the Mayo Clinic, Rochester, MN, USA, for her valuable advice and personal performance of some liver transplantations in rats.

Table 28.16 BNCT of isolated liver in rats. Distribution of animals in the experimental groups

	0	1	2	
Treatment	Liver transplant	^{10}BPA infusion + liver transplant	^{10}BPA inf. + neutron irr. + liver transplant	Total
A Healthy rats	11	3	2	16
B Rats with liver metastases	2	7	35	44
Total	13	10	37	60

In this part of the program, we had to overcome several technical difficulties. Just to give an example, 60 experiments were planned in such a way that each important stage of the procedure could have its own control. All donor animals were BD-IX strain rats. Two experimental groups of animals were predetermined: group A consisted of 16 healthy rats; group B was composed of 44 rats with liver metastases. In each group the animals were stratified according to the type of treatment: liver transplant only; or ^{10}BPA i.v. infusion + liver transplant; or ^{10}BPA infusion + neutron irradiation + liver transplant (Table 28.16). Of the treated rats, some were discarded because of intraoperative death or too short survival times (<3 h after the end of the surgical procedure). The remaining rats were evaluated in one of two ways: they were either killed at preset times for morphological studies (not later than 6 days in case of an allogenic recipient to avoid the interfering effects of a rejection reaction) or followed until death (only syngenic recipients), taking note of their survival times (Table 28.17). Samples of normal and tumor tissues were analyzed by light and electronic microscopy, and confirmed the highly specificity and efficacy of BNCT [34, 36–38].

28.3.5 Area of Surgical Interest

As already mentioned, the procedure of extra-corporeal liver BNCT consists basically, from the surgical point of view, of a liver auto-transplantation with a prolonged liver-less phase because of the need for moving the isolated organ to the nuclear reactor after being washed and chilled. The targets to reach in the preparatory phase of the project were essentially the following ones.

Experimental approach to liver auto-transplantation. The whole procedure of liver auto-transplantation was performed on 58 Landrance and Large-White pigs, of both sexes, weighting 35 ± 4 kg, under general anesthesia and asepsis. Several variations in surgical technique were tested in order to optimize the outcome of the operation, which basically encompasses three sequential phases:

- Isolation of the liver by dissecting all connections with the surrounding structures but preserving the vascular (portal vein, hepatic artery, infra-hepatic vena cava, supra-hepatic vena cava) and biliary (choledocus) connections;

Table 28.17 BNCT of isolated liver in rats. Survival results after different treatments and BNCT (see Table 28.16)

Treatment	0	1	2 (BNCT)
A			
Total	11	3	2
Discarded			
Intraop. death	2	1	1
Survival < 3 h	–	–	–
Evaluated			
Killed	4 (2d-3d-6d-53d)	1 (3d)	1 (1d)
(at days)	5	1	–
Surviving (for days)	(1d-2d-2d-64d-68d)	(2d)	
B			
Total	2	7	35
Discarded	1	1	17
Intraop. death	0	0	9
Survival <3 h	1	1	8
Evaluated	1	6	18
Killed	0	0	6 (3d-3d-4d-4d-5d-6d)
(at days)	1	6	12
Surviving (for days or hours)	(6d)	(8h-1d-2d-2d-14d-59d[a])	(4h-4h-4h-4h-4h-8h-8h-1d-1d-1d-2d-4d)

[a]The cause of death is spreading of tumor

- Removal of the liver by dividing the mentioned connections. The liver was perfused with chilled University of Wisconsin (UW) solution and then preserved in a refrigerated (4 °C) box for 2–3 h. In the meantime, the animal was maintained on active extracorporeal circulation by a centrifugal pump (Biomedicus Inc.), shunting the blood at a high flow rate from the inferior vena cava, just caudal to the liver, and from the trunk of vena porta to the superior vena cava cannulated at the level of the thoracic aditus through a cervicotomy;
- Liver transplant into the same "donor" animal with anastomoses of the four previously mentioned vessels and choledocus.

Training on pigs was of invaluable importance for refining our surgical technique. Moreover, it proved that in these conditions, a vena-vena extracorporeal circulation can last 8 h and even longer, without needing i.v. heparin.

Survival of liver-less pigs. Special interest was paid to determiming the maximum time a pig can survive without its own liver. To this end, we carried out hepatectomies on 20 Large White pigs. Throughout the operation time and until the death of the animal, the arterial pressure and acid-base balance were monitored, while a slow infusion of electrolyte balanced solution was maintained. Acidic unbalance was corrected when necessary by supplementing various volumes of $NaHCO_3$ isosmotic solution. At the end of the hepatectomy, a short internal cava-caval and

Table 28.18 Liver autotransplantation pre-BNCT

Diagnosis	Type of autotransplantation	Survival (since the autotransplantation)	Cause of death
HCC (fibrolamellar hepatocellular carcinoma)[a]	*Ex situ*	18 years	Still alive
Metastases from colon carcinoma	In situ	3 years 1 month	Recurrence
HCC (trabecular variant)	In situ	1 year 8 months	Recurrence
Metastases from colon carcinoma	In situ	12 days	Liver failure
Metastases from colon carcinoma	In situ	2 years 5 months	Recurrence
Focal nodular hyperplasia	In situ	9 years	Still alive
Cavernous hemangioma	In situ	8 years 8 months	Still alive
Metastases from colon carcinoma	In situ	1 years 6 months	Recurrence

[a]A pancreatic duodenectomy (Whipple operation) was performed simultaneously for acute hemorragic pancreatitis

porta-caval bypass was set up by anastomosing the stumps of the infra-hepatic inferior vena cava, portal vein, and supra-hepatic inferior vena cava to the ends of an upturned Dacron en-Y vascular prosthesis. Since the start of the liver-less phase, the narcosis was easily maintained with small amounts of inhalation agents (Fluothane).

These experiments allowed us to learn how to manage anesthesia and to define the "mean survival time" in liver-less conditions. This was 8 ± 3 h, but in two animals a "maximum survival time" of 24 h was obtained [36].

Liver autotransplantation on patients without BNCT. Before starting the clinical application of the extracorporeal BNCT project, the liver auto-transplant method was also applied to eight patients affected by severe malignant or benign neoplastic diseases of the liver. In all these cases, the conventional technique of hepatic resection could not be carried out because of the volume, number, or localization of the tumor masses. Radical surgery, with possible reconstruction of vital intra-hepatic structures, could instead be easily accomplished on a hypothermic and bloodless liver (bench surgery) by adopting a liver autotransplantation procedure.

This technique can be performed in accordance with two modalities. One of these is called the "ex situ autotransplant," in which the liver is completely isolated and removed from the patient. In the other variant of the surgical technique, the "in situ autotransplant," the liver is isolated, but only the supra-hepatic vena cava is interrupted, whereas the portal vein, hepatic artery, choledocus, and infra-hepatic vena cava are all clamped, but not dissected, except for a small hole in the portal vein to introduce a washing catheter.

The clinical experience with the eight patients was highly promising. We had no operative mortality and only one perioperative death due to hepatic insufficiency (the healthy portion of liver we could save at the end of resection was too small to support all hepatic functions). The first patient is still alive and free-of-disease after more than 18 years. Nevertheless, three out of five patients with liver malignancies had recurrences. Some details of the clinical cases are listed in Table 28.18.

28.4 Clinical Applications

28.4.1 The Preliminaries

Having completed the experimental phase of our project, we decided to test the clinical impact of the proposed procedure. According to Italian rules and regulations for innovative therapeutic protocols, three organizations had to approve the application of the project on patients. They are in order: the Ethics Committee of our hospital, its medical and scientific management, and the Italian Ministry of Health.

First of all, we drew up a very detailed protocol of our previous experimental work in reference to neutron irradiation of ^{10}B-loaded neoplastic tissues and in vitro cultures of neoplastic cells, and to its effects on normal and tumor cells. The protocol also contained an accurate description of the aseptic method that would be followed by the Pharmacology Department of San Matteo Hospital of Pavia in the preparation of a germ-free pyrogen-free p-^{10}BPA-F solution for intravenous infusion. There was also a list of all needed surgical instruments and apparatus, a timed description of the operative phases and fields, and a minute enumeration of the steps and persons in charge of them during the transfer of the isolated organ from the hospital to the nuclear reactor and the return. The streets the ambulance would drive through would be closed to traffic by the police.

According to our previous experimental work, the indications for the treatment were restricted to patients suffering from diffuse unresectable liver metastases from a colorectal carcinoma already radically excised, and in case chemotherapy had proven to be ineffective. The candidate should be young (<55 year), with liver-only metastases and without impairment of vital organs and functions. In particular, patients with any previous hepatitis, ascites, or icterus in progress would not be accepted. The galactose elimination capacity (GEC), elected as liver function test, should be reasonably good (>40 %; normal value >70 %). Two other exclusion criteria were phenylketonuria because of the chemical nature of the ^{10}B carrier BPA and previous radiotherapy of the abdomen.

The approval of the Ethics Committee was very difficult to obtain. It took some 2 years with many heated disputes, while in the meantime the candidates died. At last consent was granted for a single patient as a compassionate therapeutic act. The approvals of the other organizations soon followed.

For the second patient, the same procedure was applied, but this time it was a little quicker.

28.4.2 The Operations

In December 2001, we started the program of extracorporeal application of BNCT on isolated human livers. The procedure basically consists of three phases.

In the *early surgical phase*, a wide subcostal laparotomy is performed with cranial extension in the midline. We soon thoroughly explore the site of the previous colectomy,

the local and remote lymph node stations, all peritoneal organs, and accessible portions of the extraperitoneal viscera. Any suspected lesion is excised, and the pathological outcome is awaited before resuming the operation. An intraoperative UV scan with microgaseous contrast medium allows constructing an accurate map of neoplastic localizations in the liver. After cholecystectomy, the dorsal liver ligaments are severed. The inferior vena cava is dissected at a level both caudal and cranial to liver and encircled with two tapes. A straight portion of a colic vein is isolated in the mesocolon; the peripheral end is tied, and a thin cannula is inserted in the vein towards the liver. At this point, the infusion of the ^{10}B carrier BPA can start at a dose of 300 mg/kg body weight. For example, for a man weighting 70 kg, 720 ml of a 0.14 M solution of ^{10}BPA-F would be injected during a 2-h period through a delivery pump. The pump speed would therefore be set at a rate of 360 ml/h.

One hour after the start of perfusion and at the end of it, we collect samples of tumor and normal liver tissue for ^{10}B measurements and to evaluate the prevalence of neoplastic cells on normal hepatocytes in the same histological specimen. When a satisfactory ratio of concentrations has been reached, we proceed to the next surgical steps by isolating the left femoral vein at the groin and the inferior mesenteric vein just caudal to the pancreas tail, and connecting them to an extracorporeal circuit equipped with a Biopump. Thus, the blood collected from the sub-diaphragmatic sections of the body can be re-infused into the cranial ones through the previously isolated and cannulated left axillary vein. Now all connections of the liver with surrounding structures are dissected except for the vascular and biliary ones. The porta-cava-caval extracorporeal circulation is started, and the last connections are clamped and transected. Hepatectomy can be completed in this way.

Radiotherapeutic phase: On the bench, the isolated liver is washed with several liters of chilled UW solution, and put into two sterile Teflon bags and in a rigid Teflon transport case fitted with temperature probes. The liver is then carried from the hospital to the adjacent Triga Mark II nuclear reactor. During the neutron irradiation, liver temperature and neutron fluence are continuously monitored. The duration of irradiation is foreseen to be about 10 min. During the irradiation, the liver is arranged in a Teflon box where dry ice blocks provide good temperature control (it must never exceed 10 °C). At the end of neutron treatment, the liver, still wrapped in its bags, is taken back to the operating theatre, and carefully and aseptically extracted and washed again with chilled UW solution.

Late surgical phase: The liver is reconnected to the vascular and biliary stumps of the patient. The first anastomosis is performed at the level of the inferior suprahepatic vena cava; the second one is between the ends of the infrahepatic vena cava. If the latter are separated by too great a distance, interposing a segment of Dacron tube prosthesis is recommended. Afterwards, the portal ends are reconnected, the extracorporeal circulation is stopped, and normal circulation is restored.

The arterial anastomosis is performed with microsurgical technique with nylon 7/0 interrupted stiches; the reconstruction of biliary continuity is achieved with an end-to-end common duct anastomosis by previous introduction of a Kehr-type drain. The operation is completed with a new intraoperative US scan to verify the absence of emboli or thrombosis in all major vessels.

The first patient was a 48-year-old man, affected by 14 synchronous bilateral metastases from a pT3 G2 N1 M1 sigmoid adenocarcinoma (liver), according to the UICC-TNM classification of tumors, resected 7 months before. At the end of a complete course of standard chemotherapy, the hepatic situation and clinical state appeared worsened. GEC was 63 %. The operation lasted 21 h on the whole. ^{10}B concentrations in tumor and normal hepatic tissue were 47 ± 2 and 8 ± 1 ppm, respectively. During perfusion with BPA, ^{10}B concentrations in systemic and in portal blood were 7.1 ± 0.1 and 10.3 ± 1, respectively. The duration of neutron irradiation was 11 min. The liver-less time was 5 h 30 min; during this period, bleeding from the surgical field was a major problem. The total transfusion support was: 59 units of packed red blood cells, with 20 being used during the operation (d.o.) and 39 in the following 2 days (p.o.); 35 units of fresh frozen plasma, 8 d.o. and 27 p.o.; 15 units of plasma from apheresis, 11 d.o. and 4 p.o.; 4,560 ml of blood recovered from operative field with a Cell Saver apparatus (Haemonetics) and reinfused to the patient as autologous packed red blood cells.

The second patient was also a man, 39 year old, and was subjected to extracorporeal liver BNCT in July 2003, with 11 small and large synchronous metastases from a pT3 G2 N1 M1 (liver) rectal adenocarcinoma, who had been radically operated on 10 months before. In his clinical picture, three negative aspects were noteworthy: the liver function was poor (GEC 58 %), the right hepatic artery arose from the superior mesenteric artery as a vascular anomaly, and the cardiac function was deficient because of a dilated cardiomyopathy with a stroke volume of 40 %. For this last reason, the chemotherapeutic regimen had been stopped. In comparison with the first patient, the duration of the procedure was shorter (18 h 40 min), in spite of the difficulties raised by the surgical correction of the vascular anomaly, whereas the liver-less time was longer (6 h 10 min). ^{10}B concentrations in tumor and normal tissue were as good as in the first case. In both patients we used a segment of Dacron prosthesis to obtain an easy reconnection of the vena cava.

28.4.3 Perioperative Follow-Up

Immediately after the operation, a set of symptoms appeared, which we are tempted to consider as an expression of a *post-neutron irradiation syndrome*. Their description is of course incomplete because they presented while the patients were under general anesthesia with controlled ventilation. They were both clinical and hematochemical in nature, characterized by hepatic and renal insufficiency with jaundice up to 25 mg% and transitory anuria (during the first 2 weeks), mental confusion, huge facial edema and diffuse subcutaneous imbibition, rhabdomyolysis and profound asthenia. Some hematochemical data are shown in Fig. 28.12. The mentioned aberrations, which were present in both patients, showed the same concatenation in time and evolved towards the complete recovery [33].

A common denominator in the pathogenesis of this complex derangement seems to be a serious alteration of endothelial barrier permeability, as was seen in some experiments after administration of cytokines such as tumor necrosis factor to volunteers [39]. This syndrome could then be due to the abrupt release of large amounts

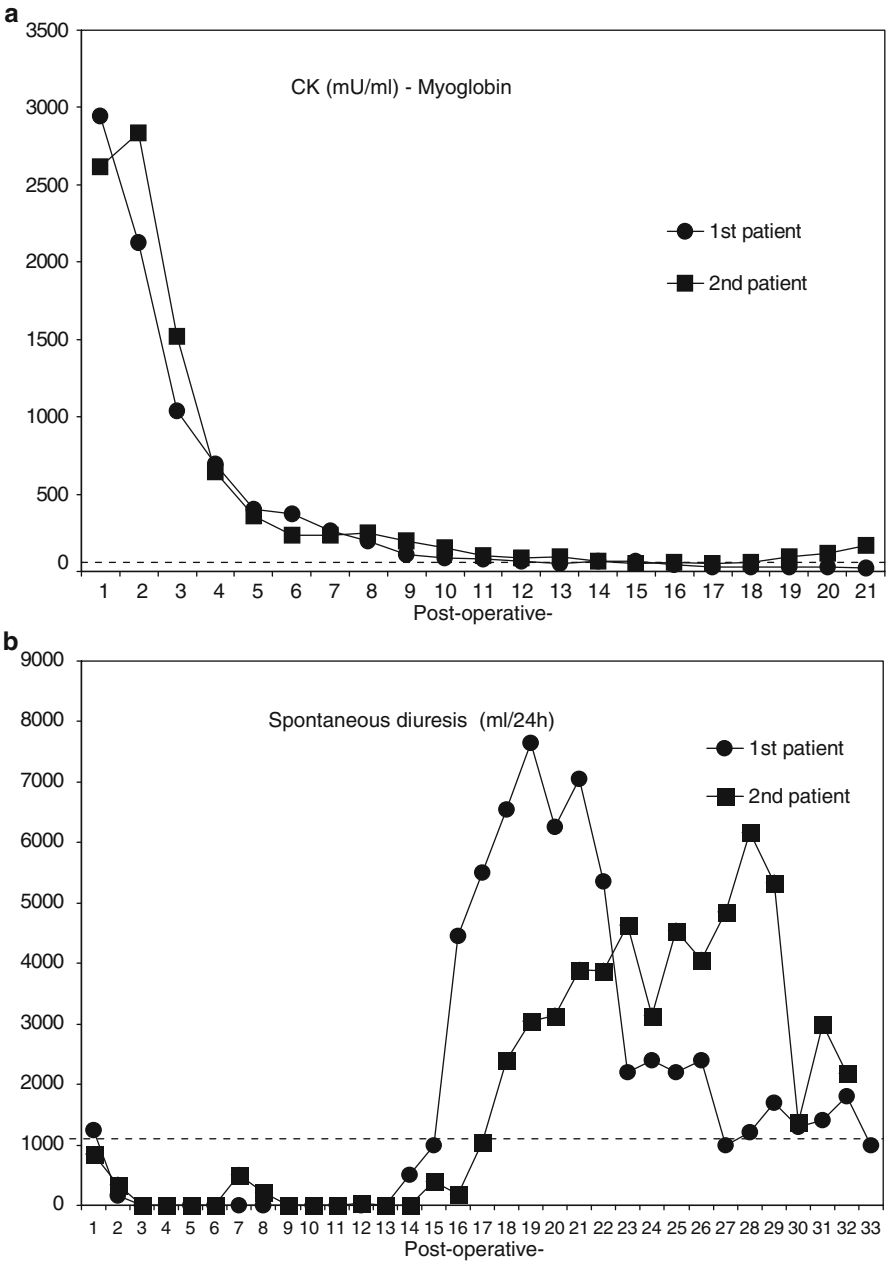

Fig. 28.12 Behavior of some hematochemical tests and of renal function in the two patients treated with liver extracorporeal BNCT during the early postoperative course (first 3 weeks after the operation). *Broken lines* indicate reference values. (**a**) Concentration in serum of creatine kinase (*CK*) (reference values: 55–170 mU/ml) and of myoglobin (only in the second patient; ng/ml normally absent in blood); (**b**) volume of spontaneous diuresis (normal value: 1,200 ml/24 h); (**c**) concentration in serum of the microsomal enzymes aspartate aminotransferase (*AST*) (reference values: 7–40 mU/ml) and (**d**) of alanine aminotransferase (*ALT*) (reference values: 7–40 mU/ml) (From Zonta et al. [33])

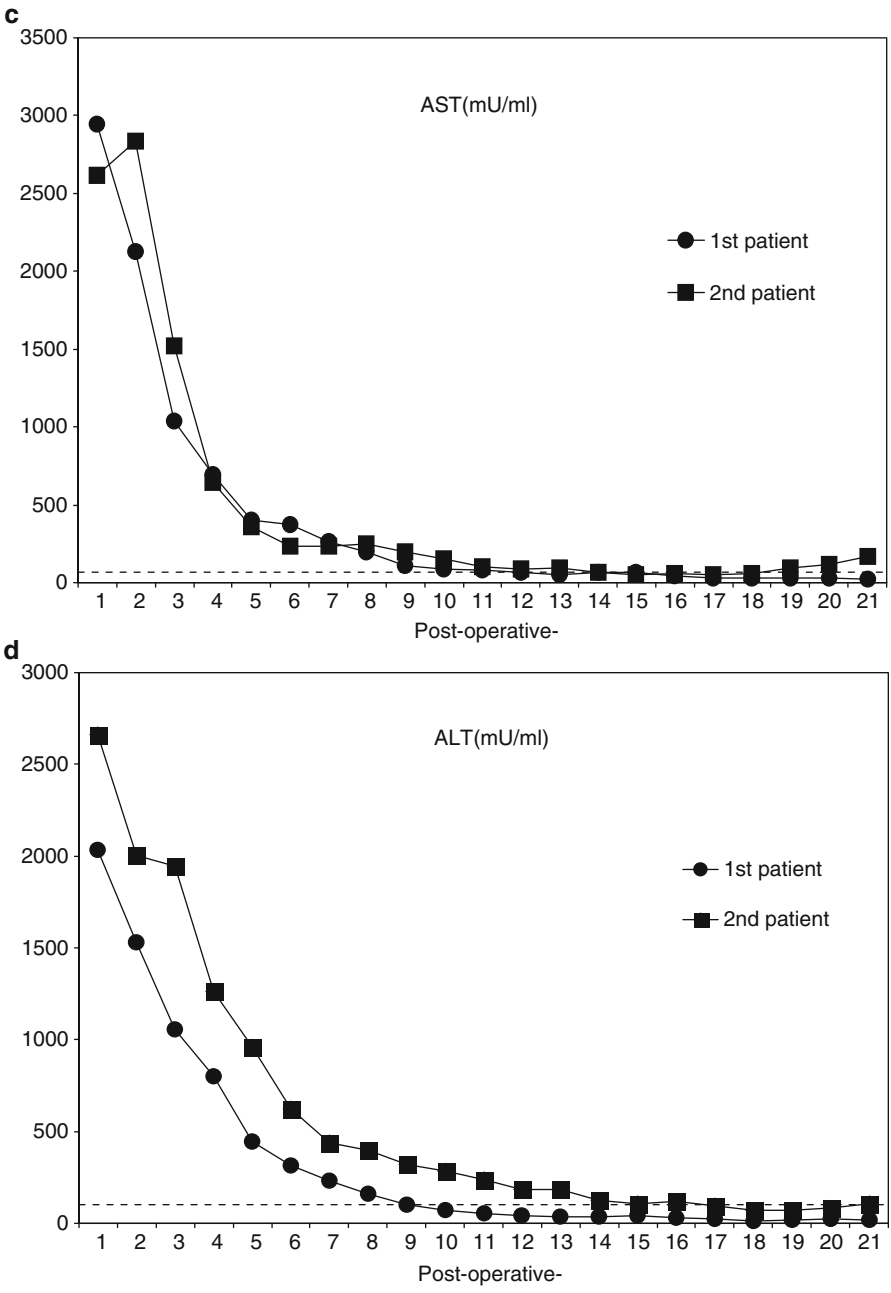

Fig. 28.12 (continued)

of cytokines especially from tumor cells as a result of surgical manipulation and neutron irradiation of metastases. This view is also supported by the results of in-blood evaluation of some cytokines of clinical interest only in the second patient (Fig. 28.13).

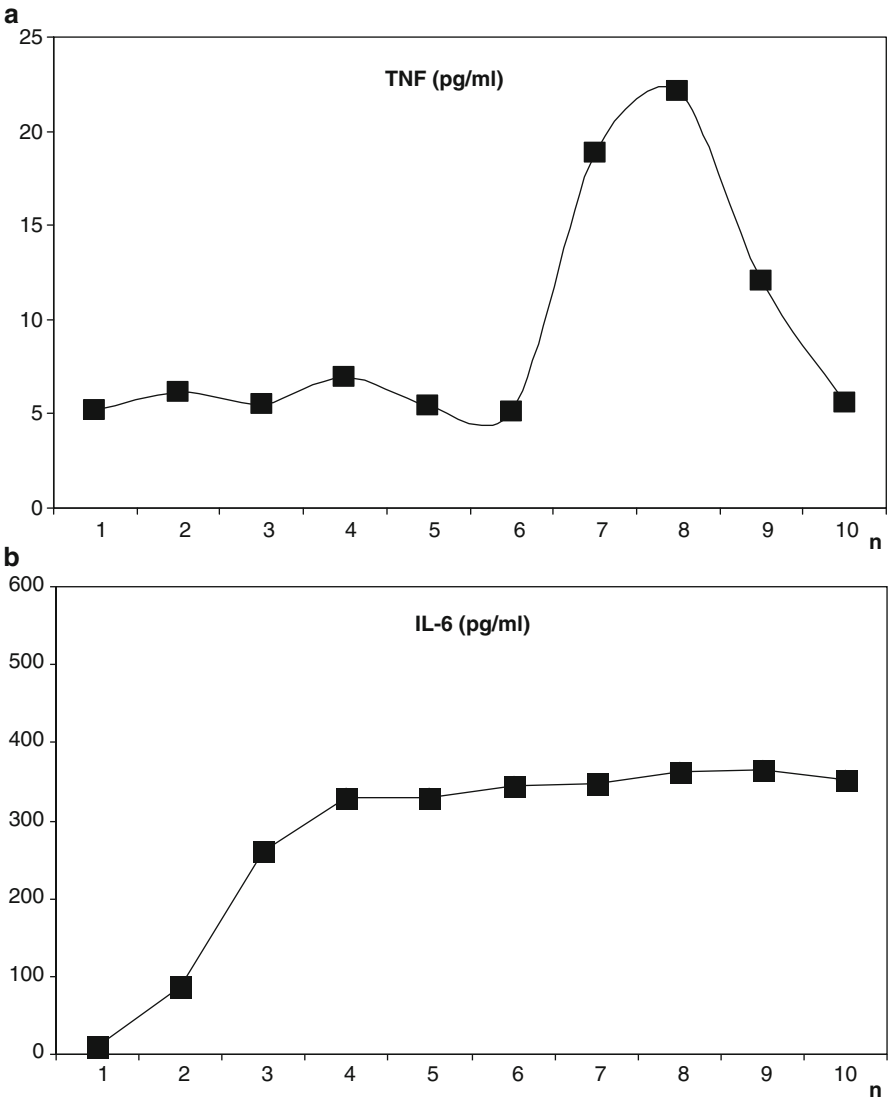

Fig. 28.13 Values of some cytokines of clinical interest, which were analyzed only in the second patient sequentially during the first 48 h after BNCT: *n*1 is preoperative value; *n*2 refers to the end of ^{10}BPA perfusion, *n*3 and 4 are in the anhepatic phase; *n*5–9 are the samples corresponding to 0, 2, 4, 6, and 8 h after the liver reconnection; *n*10 is related to the second postoperative day. (**a**) Tumor necrosis factor (*TNF*), (**b**) interleukin 6 (*IL-6*); (**c**) vascular endothelial growth factor (*VEGF*); (**d**) hepatocyte growth factor (*HGF*)

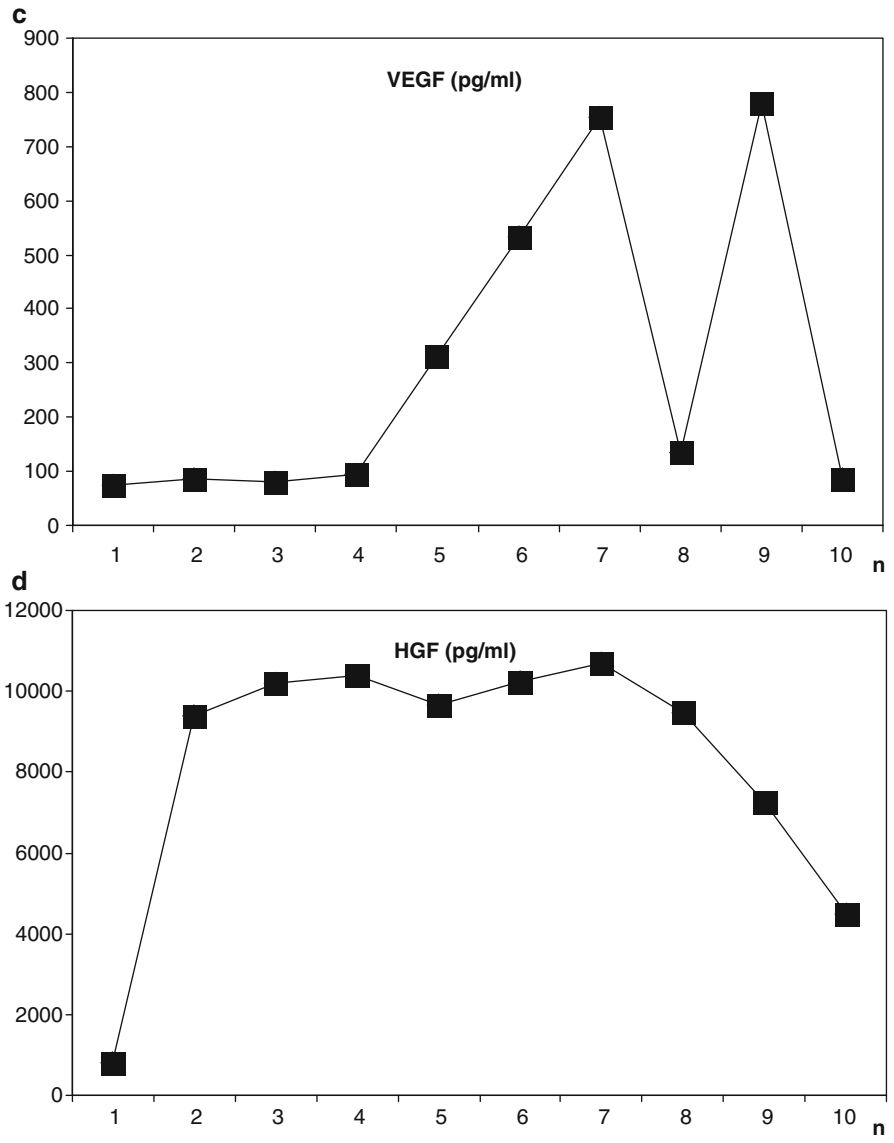

Fig. 28.13 (continued)

28.5 Results

The early oncological effects of BNCT on an isolated liver can be best appreciated in the second patient, and the late results in the first one. Indeed both patients had a similar postoperative course in the first 3 weeks after the treatment, with radiological evidence of large necrosis at the site of previous metastases and also where there was no

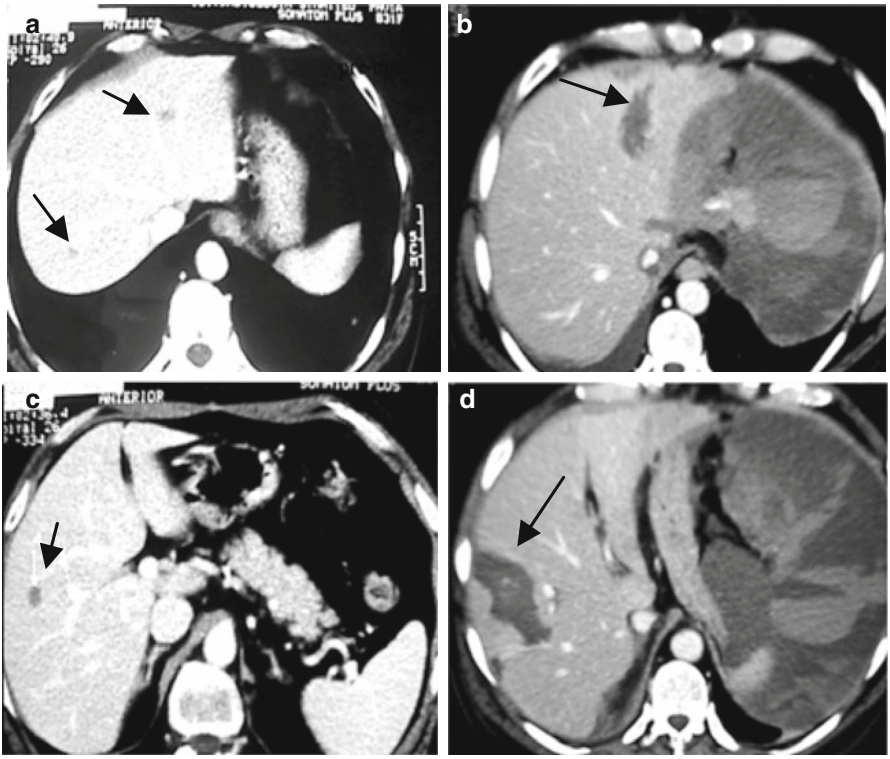

Fig. 28.14 Early effects of extracorporeal BNCT in liver CT images of the first patient. (**a**, **c**) Preoperative CT: liver metastases (*arrows*). (**b**, **d**) Evolution of metastases towards necrosis (*arrows*) in almost corresponding CT scans 7 days after treatment (From Zonta et al. [33], modified)

preoperative evidence of tumor accumulation. We think for this reason that also occult, microscopic spreading of tumor cells was treated with efficacy (Figs. 28.14 and 28.15). Around the end of the first month and in coincidence with the phase of recovery from the *post-irradiation syndrome*, the second patient, who had cardiopathy, showed signs of thrombosis of the hepatic artery, and later on cardiac congestive failure caused his death on the 33rd postoperative day. At autopsy, we had the macro- and microscopic proof of massive necrosis of coagulative type of all liver metastases. In the histological specimens, three other aspects were noteworthy [33]. An intense and widespread hyperplasia of Kupffer cells with clear signs of phagocytic activation of leucocytes and also of hepatocytes was well documented. On the periphery of several metastatic nodules, the presence of vital neoplastic cells with slight proliferative activity requires an explanation. We think that these cells are the morphological expression of the *self-extinction process*, which is responsible, together with necrosis and apoptosis, for the long-lasting cell damage induced by irradiation. A tumor cell population is selected; because of sub-lethal damage to the nuclear structure, it loses most of its proliferative potential and then gradually disappears. The third aspect of histomorphological interest is the collagen deposition that was evident at both light and electronic microscopy

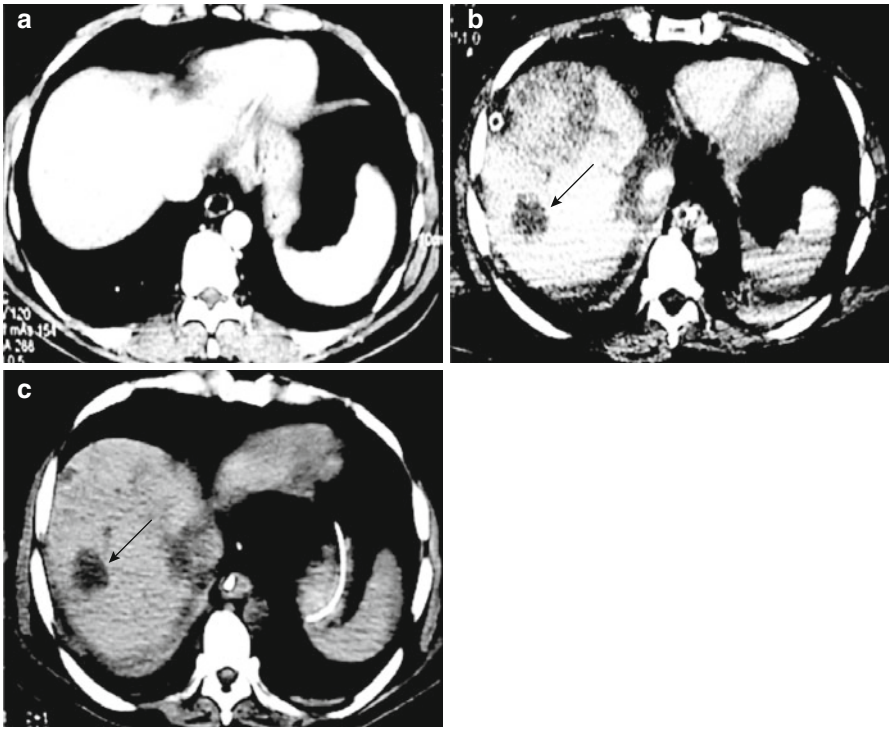

Fig. 28.15 Comparison of images from the liver CT of the second patient. (**a**) Preoperative scan, in which no metastasis is recognizable. (**b**) At 10 days and (**c**) at 21 days after BNCT. A focal area of necrotic damage (*arrows*) is a likely witness of an effectively treated "occult" neoplastic infiltration (From Zonta et al. [33])

studies, and was an early phenomenon. This could explain the hepatic fibrosis documented in both patients without functional impairment or evolution to cirrhosis.

The first patient, on the contrary, had an uneventful postoperative course for a whole year and a half, with gradual disappearance of radiological signs of necrosis in the liver and its replacement by normal hepatic tissue. GEC was improved (73 %). Quality of life (QoL) was excellent, so he got married, too. Twenty months after BNCT, a recurrence of his neoplasia appeared adjacently, but external to the liver left lobe. It was resected, and the patient recovered completely. Thirty-three months after BNCT, other recurrences appeared; they were treated with chemotherapy and a further debulking operation 5 months later. The patient died of abdominal carcinosis 44 months after BNCT. Except for the last few months, his QoL had been very good – a hopeful and reactive patient.

28.5.1 Further Developments and Conclusive Remarks

The clinical application of extracorporeal BNCT on isolated liver demonstrated the feasibility of the procedure, its high efficacy, specificity, and selectivity. It is

therefore a new therapeutic proposal for the treatment of secondary hepatic tumors. There is no possibility to compare it with other curative approaches, because the clinical situation of diffuse chemotherapy-resistant liver metastases does not have any radical alternatives.

Obviously, in the current phase of the project, the described procedure is very challanging in terms of the patient's endurance, physicians' organizing capacity, and clinicians' work devotion.

The procedure can be improved and must be optimized. In our opinion, the issues absolutely needing further study are the following:

- Demonstrating the real nature of *post-irradiation syndrome* and the best way to control it;
- Understanding the etiology of post-BNCT recurrences in depth and reducing them to a minimum;
- Making the most demanding surgical stages of the procedure easier and faster.

We have been working experimentally in this directions for a fair amount of time, and some concepts and proposals have already been elaborated [30, 32, 40]. Finding a solution to all these questions could take time and requires effort, but it is a prerequisite to turning our experimental project into a reliable and widely used therapeutic tool [41]. Of course, important acceleration in our path towards this target could derive from results such as the discovery of new, more specific ^{10}B carriers or the creation of bed-side accelerators for neutron production in view of their medical use.

References

1. Edmondson HA, Peters RL (1982) Neoplasms of the liver. In: Schiff L, Schiff ER (eds) Diseases of the liver, 5th edn. JB Lippincott Company, Philadelphia, pp 1101–1157
2. Quigley JP, Sullivan LM, DeMarinis CM et al (1988) Functional role of specific secreted and cell surface molecules in tumour cell invasion and metastasis. In: Bock G, Whelan J (eds) Metastasis. Ciba foundation symposium 141. Wiley, Chichester, pp 22–47
3. Rodgers MS, McCall JL (2000) Surgery for colorectal liver metastases with hepatic lymph-node involvement: a systematic review. Br J Surg 87:1142–1155
4. Rosen ChB, Donohue JH, Nagorney DM (1995) Liver resection for metastatic colonic and rectal carcinoma. In: Cohen AM, Winawer SJ (eds) Cancer of the colon, rectum and anus. McGraw-Hill Inc, New York, pp 805–821
5. Grundmann RT, Hermanek P, Merkel S et al (2008) Arbeitsgruppe workflow diagnostik und therapie von lebermetastasen kolorektaler karzinome. Zentralbl Chir 133:267–284
6. Heslin MJ, Medina-Franco H, Parker M et al (2001) Colorectal hepatic metastases: resection, local ablation, and hepatic artery infusion pump are associated with prolonged survival. Arch Surg 136:318–323
7. Yan TD, Padang R, Morris DL (2006) Longterm results and prognostic indicators after cryotherapy and hepatic arterial chemotherapy with or without resection for colorectal liver metastases in 224 patients: longterm survival can be achieved in patients with multiple bilateral liver metastases. J Am Coll Surg 202:100–111
8. Saltz LB, Cox JV, Blanke C et al (2000) Irinotecan plus fluorouracil and leucovorin for metastatic colorectal cancer. Irinotecan Study Group. N Engl J Med 343:905–914
9. Douillard JY, Cunningham D, Roth AD et al (2000) Irinotecan combined with fluorouracil compared with fluorouracil alone as first-line treatment for metastatic colorectal cancer: a multicentre randomised trial. Lancet 355:1041–1047

10. Hurwitz H, Fehrenbacher L, Novotny W et al (2004) Bevacizumab plus irinotecan, fluorouracil, and leucovorin for metastatic colorectal cancer. N Engl J Med 350:2335–2342
11. Balch CM, Urist MM, Soong SJ et al (1983) A prospective phase II clinical trial of continuous FUDR regional chemotherapy for colorectal metastases to the liver using a totally implantable drug infusion pump. Ann Surg 198:567–573
12. Harmantas A, Rotstein LE, Langer B (1996) Regional versus systemic chemotherapy in the treatment of colorectal carcinoma metastatic to the liver: is there a survival difference? Meta-analysis of the published literature. Cancer 78:1639–1645
13. Chang AE, Schneider PD, Sugarbaker PH et al (1987) A prospective randomized trial of regional versus systemic continuous 5-fluorodeoxyuridine chemotherapy in the treatment of colorectal liver metastases. Ann Surg 206:685–693
14. Rougier P, Laplanche A, Huguier M et al (1992) Hepatic arterial infusion of floxuridine in patients with liver metastases from colorectal carcinoma: long-term results of a prospective randomized trial. J Clin Oncol 10:1112–1118
15. Kemeny N, Huang Y, Cohen AM et al (1999) Hepatic artery infusion of chemotherapy after resection of hepatic metastases from colorectal cancer. N Engl J Med 341:2039–2048
16. Kemeny NE, Seiter K (1995) Hepatic arterial chemotherapy. In: Cohen AM, Winawer SJ (eds) Cancer of the colon, rectum and anus. McGraw-Hill Inc, New York, pp 831–843
17. McKay A, Dixon E, Taylor M (2006) Current role of radiofrequency ablation for the treatment of colorectal metastases. Br J Surg 93:1192–1201
18. Navarra G, Ayav A, Weber JC et al (2005) Short- and long-term results of intraoperative radiofrequency ablation of liver metastases. Int J Colorectal Dis 20:521–528
19. Gennari L, Doci R, Bozzetti F et al (1985) Proposal for staging liver metastases. In: Hellman K, Eccles SA (eds) Treatment of metastases. Problems and prospects. Taylor & Francis, London, pp 37–40
20. Gennari L, Doci R, Bozzetti F et al (1986) Proposal for staging liver metastases. Recent Results Cancer Res 100:80–84
21. Nievaart VA, Moss RL, Kloosterman JL et al (2006) Design of a rotating facility for extracorporal treatment of an explanted liver with disseminated metastases by boron neutron capture therapy with an epithermal neutron beam. Radiat Res 166:81–88
22. Miller M, Quintana J, Ojeda J et al (2008) New irradiation facility for biomedical applications at the RA-3 reactor thermal column. Appl Radiat Isot. doi:10.1016/j.apradiso.2009.03.107
23. Briesmeister JF (ed) (2000) MCNP – a general Monte Carlo n-particle transport code. Version 4c LA-13709-M Los Alamos National Laboratory
24. Bortolussi S, Altieri S (2007) Thermal neutron irradiation field design for boron neutron capture therapy of human explanted liver. Med Phys 34:4700–4705
25. Westcott CH, Walker WH, Alexander TK et al. (1958) Effective cross section and cadmium ratios for the neutron spectra of thermal reactors. In: Proceedings international conference on the peaceful uses of atomic energy, Geneva, P/202 70 (1959 New York)
26. Westcott CH (1960) Effective cross section of well moderated thermal reactor spectra. Report AECL No. 1101
27. Altieri S, Bortolussi S, Bruschi P et al (2008) Neutron autoradiography imaging of selective boron uptake in human metastatic tumours. Appl Radiat Isot 66:1850–1855
28. Wittig A, Michel J, Moss RL et al (2008) Boron analysis and boron imaging in biological materials for boron neutron capture therapy (BNCT). Crit Rev Oncol Hematol 68:66–90
29. Martin MS, Bastien H, Martin F et al (1973) Transplantation of intestinal carcinoma in inbred rats. Biomedicine 12:555–558
30. Ferrari C, Clerici AM, Mazzini G et al. (2006) The BNCT resistant fraction of cancer cells: an in vitro morphologic and cytofluorimetric study on a rat coloncarcinoma cell line. In: Nakagawa Y, Kobayashi T, Fukuda H (eds) Advances in neutron capture therapy 2006. In: Proceedings 12th international congress on neutron capture therapy, Takamatsu, 2006, p 98–101
31. Pinelli T, Zonta A, Altieri S et al. (2002) Taormina: from the first idea to the application to the human liver. In: Sawerwein W, Moss R, Wittig A (eds) Research and development in neutron capture therapy. Proceedings 10th international congress on neutron capture therapy, Essen, 2002, p 1065–1072

32. Ferrari C, Clerici AM, Zonta C et al. (2008) Boron neutron capture therapy of liver and lung coloncarcinoma metastases: an *in vitro* survival study. In: Zonta A, Altieri S, Roveda L et al. (eds) A new option against cancer. Proceedings 13th international congress on neutron capture therapy, Florence, 2008, p 331–336
33. Zonta A, Prati U, Roveda L et al (2006) Clinical lessons from the first applications of BNCT on unresectable liver metastases. J Phys Conf Ser 41:484–495
34. Roveda L, Prati U, Bakeine J et al (2004) How to study boron distribution in liver metastases from colorectal cancer. J Chemiother 16(Suppl 5):15–18
35. Steffen R, Ferguson DM, Krom RAF (1989) A new method for orthotopic liver transplantation with arterial cuff anastomosis to the recipient common hepatic artery. Transplantation 47: 166–168
36. Pinelli T, Altieri S, Fossati F et al. (2001) Operative modalities and effects of BNCT on liver metastases of colon adenocarcinoma. A microscopical and ultrastructural study in the rat. In: Hawthorne MF et al. (eds) Frontiers in neutron capture therapy. Proceedings 8th international congress on neutron capture therapy, Los Angeles, 2001, p 1427–1440
37. Nano R, Barni S, Gerzeli G et al (1997) Histiocytic activation following neutron irradiation of boron-enriched rat liver metastases. Ann N Y Acad Sci 832:274–278
38. Nano R, Barni S, Chiari P et al (2004) Efficacy of boron neutron capture therapy on liver metastases of colon adenocarcinoma. Optical and ultrastructural study in the rat. Oncol Rep 11:149–153
39. Michie HR, Manogue KR, Spriggs DR et al (1988) Detection of circulating tumor necrosis factor after endotoxin administration. N Engl J Med 318:1481–1486
40. Roveda L, Zonta A, Staffieri F et al (2009) Experimental modified orthotopic piggy-back liver autotransplantation. Appl Radiat Isot. doi:10.1016/j.apradiso.2009.03
41. Zonta A, Pinelli T, Prati U et al (2009) Extra-corporeal liver BNCT for the treatment of diffuse metastases: what was learned and what is still to be learned. Appl Radiat Isot. doi:10.1016/j.apradiso.2009.03.087

Boron Neutron Capture Therapy for Children with Malignant Brain Tumors

29

Yoshinobu Nakagawa and Teruyoshi Kageji

Contents

29.1 Introduction

The ideal treatment for children with a malignant brain tumor should be a treatment that causes as little damage as possible to the developing central nervous system. However, children surviving treatment often have problems associated with tumor invasion of the brain parenchyma, increased intracranial pressure, injury from surgical resection, neurotoxicity induced by chemotherapy, and late effects of radiation therapy. Radiation therapy especially improves clinical outcomes, but also increases the risk of a poor quality of life with chronic neurocognitive effects and functional deficits. The late effects of radiotherapy have been followed and characterized by CT or MRI

Y. Nakagawa (✉)
Department of Neurosurgery, Kagawa National Children's Hospital,
Kagawa 765-8501, Japan
e-mail: ynakagawa0517@yahoo.co.jp

T. Kageji
Department of Neurosurgery, School of Medicine, The University of Tokushima,
Kuramoto-cho 3-18-15, Tokushima 770-8503, Japan
e-mail: kageji@clin.med.tokushima-u.ac.jp

W.A.G. Sauerwein et al. (eds.), *Neutron Capture Therapy*,
DOI 10.1007/978-3-642-31334-9_29,

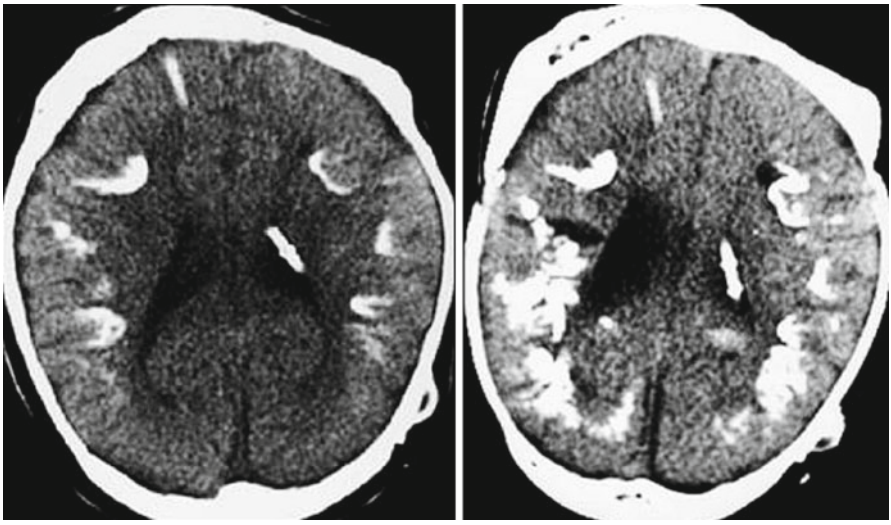

Fig. 29.1 A 2-year-old girl with a brain tumor in the basal ganglia underwent conventional radiotherapy (54 Gy). Follow-up CT demonstrated marked calcification in the parenchyma 6 years (*left*) and 10 years (*right*) after conventional radiotherapy. The patient has marked mental retardation

(Fig. 29.1). However, technical advances in radiotherapy now offer hope for lowering the frequency of neurocognitive sequelae and thus allowing more attention to be focused on the late effects of cancer treatment. Boron neutron capture therapy (BNCT) is a promising modality for the selective irradiation of tumor tissue. The thermal neutron is captured by the 10B-nucleus, which disintegrates into two heavy particles, alpha particles (^{4}He) and recoiling lithium-7 (^{7}Li). These densely ionizing particles have high biological effectiveness and a short path length that is almost equal to the size of tumor cells. If the boron compound selectively accumulates in tumor cells, the particles produced by the nuclear reaction can then selectively kill the tumor cells without causing severe damage to the normal brain tissue. BNCT is therefore considered to be an optimal treatment for malignant brain tumors, which are suspected to invade healthy normal brain tissue in young patients who are still in childhood.

29.2 Treatment with a Thermal Neutron Beam

A total of 183 patients with malignant brain tumors underwent BSH-based intraoperative BNCT from 1968 to 2005. BSH ($Na_2B_{12}H_{11}SH$) is used as a boron carrier. BSH is administered for 1 h by rapid intravenous infusion at 12–15 h before neutron radiation. On the day of BNCT, the patient is taken to the reactor (KUR or JRR4). A craniotomy is then performed with the patient under general anesthesia, and the skin flap and bone flap are reopened. Gold wires previously inserted around tumor tissue are then pulled out 15–20 min after full-power operation of the reactor to measure the exact neutron flux at each point of interest. The neutron

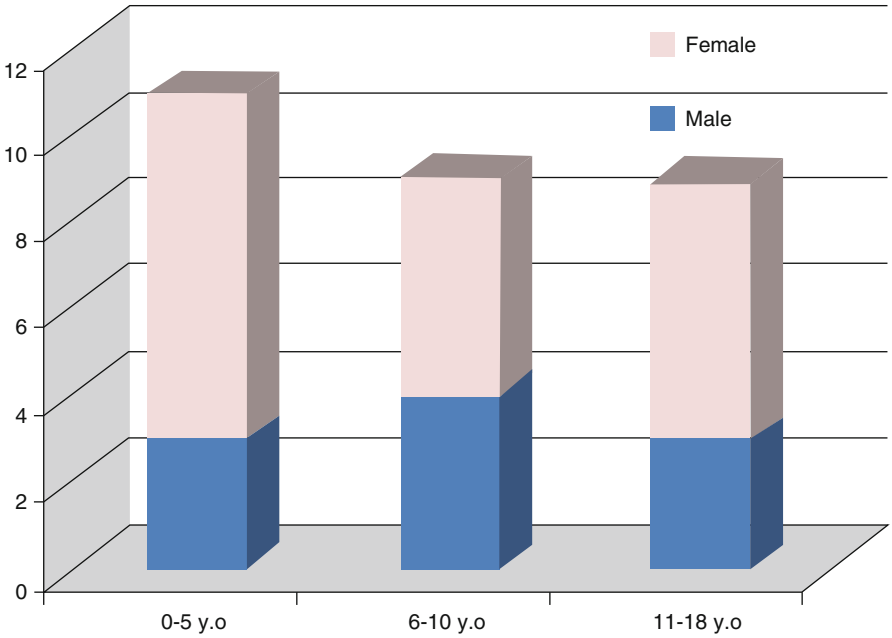

Fig. 29.2 Age and sex distribution of the children treated by BNCT

beam then directly irradiates the lesion. A mixed epithermal and thermal neutron beam replaced the thermal neutron beam in 1998 to improve the neutron beam delivery in deep lesions (BSH-based intraoperative BNCT using a mixed neutron beam). The JAERI Computational Dosimetry System (JCDS) was developed and applied to analyze the BNCT radiation dose in 2002. The physical radiation dose of the boron n-alpha reaction was estimated retrospectively at each point of the gold wire using the neutron fluence, irradiation time, and boron concentration in the tumor. The gross tumor volume (GTV) was defined as the enhanced area on Gd-MRI, and the clinical target volume (CTV) was defined as the high intensity area on T2-MRI. The BNCT radiation dose was compared in patients with or without residual tumor cells.

This important clinical trial showed significant improvements over previously reported outcomes and documented the long-term recurrence-free survival of selected patients with malignant brain tumors. There were 29 patients under 18 years old, including 11 patients under 5 years old (Fig. 29.2). There were four glioblastomas (GBM), nine anaplastic astrocytomas, which included oligoastrocytomas and ependymoma, seven primitive neuroectodermal tumors (PNET), six pontine gliomas, and one anaplastic ependymoma (Fig. 29.3). The most important factor related to the clinical outcome was the physical radiation dose of the boron n-alpha reactions. The total amount of radiation dose and gamma ray was also computed to avoid radiation necrosis [4,5]. The high LET particles generated in brain tissue consist of heavy-charged particles from ^{10}B (n, $\alpha\gamma$)^{7}Li, ^{14}N(n, p)^{14}C, and ^{17}O (n, α)^{14}C, and the recoil deuteron from ^{1}H(n, $\alpha^{2}D$).

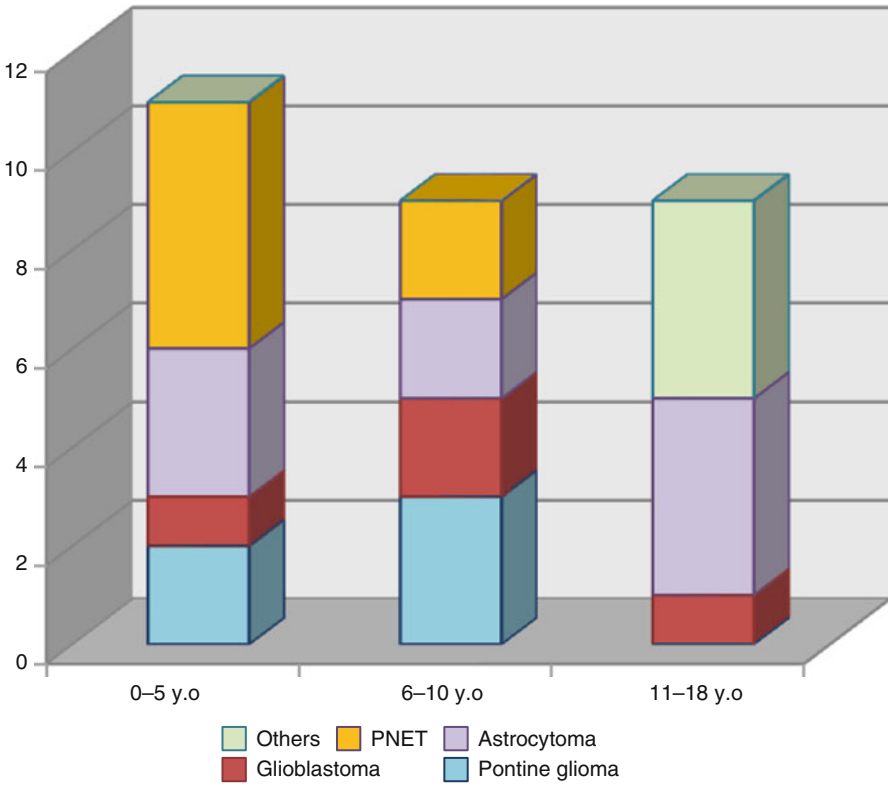

Fig. 29.3 Histology and age distribution

The absorbed dose, however, mainly consists of the two reactions: $^{10}B(n, \alpha)^{7}Li$ and $^{14}N(n, p)^{14}C$. The physical radiation dose was estimated by the equation:

$$D = (6.78E-14\times \mathrm{N} + 7.43E-14\times \mathrm{B})\times \Phi,$$

where
D: physical dose (Gy)
Φ: neutron fluence (n/cm^2)
N: nitrogen concentration %, (N = 2 %), and
B: boron concentration (ppm)

29.3 Illustrative Cases and Results

29.3.1 Case 1: A 14-Month-Old Female with Astrocytoma (Grade 3) in the Cerebellum

The patient's mother noticed a gait disturbance with cerebellar ataxia. MRI demonstrated a large ring-like tumor in the posterior fossa (Fig. 29.4a). The patient underwent

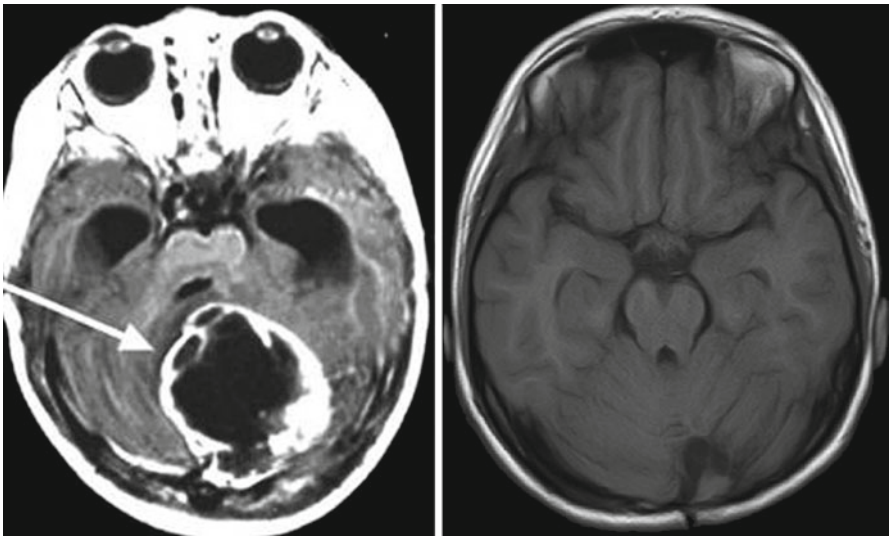

Fig. 29.4 MRI before BNCT (**a**) and at 15 years after BNCT (**b**). The *arrow* indicates a ring-like tumor

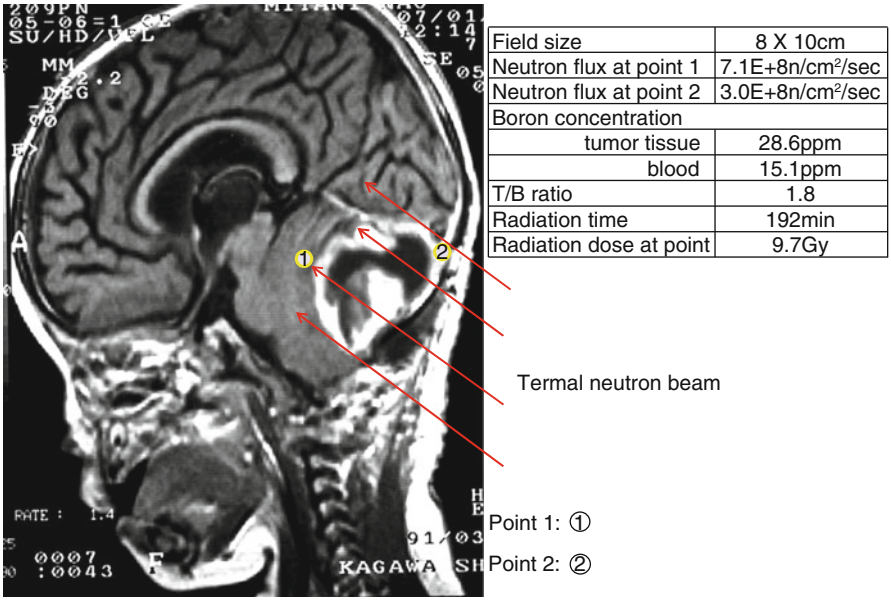

Field size	8 X 10cm
Neutron flux at point 1	7.1E+8n/cm²/sec
Neutron flux at point 2	3.0E+8n/cm²/sec
Boron concentration	
tumor tissue	28.6ppm
blood	15.1ppm
T/B ratio	1.8
Radiation time	192min
Radiation dose at point	9.7Gy

Fig. 29.5 Radiation planning and detailed date

surgical removal of the tumor. The pathological diagnosis was a grade 3 astrocytoma. Follow-up MRI demonstrated an enhanced residual tumor. Thereafter, BNCT was discussed as an additional treatment. BNCT was performed at KUR according to the protocol established in 1992 (Fig. 29.5). The patient was the youngest patient to

Table 29.1 Clinical outcome of seven patients who lived more than 10 years after BNCT

Case no.	Age at BNCT	Histology	Education	Years after BNCT	Outcome
1	1	Astrocytoma (G3)	Student in college	17	Good, ND
2	1	Anaplastic ependymoma	Student in primary school	10	Good, epilepsy
3	5	Astrocytoma (G3)	Student in junior high school	14	Handicapped, motor weakness
4	7	Astrocytoma (G3)	Graduated from senior high school	16	Good
5	8	Astrocytoma (G3)	Graduated from college	18	Good
6	11	Oligo-astrocytoma	Graduated from college	28	Good
7	17	Astrocytoma (G3)	Graduated from senior high school	15	Good

undergo BNCT at that time. Since BNCT, she has so far experienced neither any neurocognitive sequelae nor functional deficits from the neutron beam radiation (Fig. 29.4b). She is currently in college studying veterinary science (Table 29.1).

29.3.2 Case 2: A 1-Year-Old Female with Anaplastic Ependymoma

The patient presented with a severe headache and vomiting. An enhanced MRI demonstrated a huge mass in the right frontal lobe (Fig. 29.6). BSH-based intra-operative BNCT was administered after a partial resection under general anesthesia according to the protocol established 1997. The pathological diagnosis was anaplastic ependymoma.

A total dose of 136.4 mg/kg BSH was given to the patient intravenously. The irradiation time in was 162.0 min. The blood and tumor boron concentrations were 23.0 ppm and 28.0 ppm, respectively. The maximum vascular dose at the brain surface was 17.60 Gy(w). The gamma dose was 5.30 Gy(w). The minimum boron physical and weighted total (boron and gamma) doses in GTV (gross tumor volume) were 19.83 Gy and 54.88 Gy(w), respectively. The minimum boron physical and weighted total (boron and gamma) doses in the CTV (clinical target volume) were 14.11 Gy and 40.58 Gy(w), respectively.

A transient left hemiparesis was noticed 1 year after BNCT. MRA and angiography demonstrated a moyamoya phenomenon on the right middle cerebral artery. The transient attack was controlled after indirect bypass surgery. MRI demonstrated no tumor recurrence or brain atrophy at 9 years after BNCT.

29.4 Clinical Outcome

Seven out of 29 patients have lived more than 10 years after BNCT (Table 29.1). Radiation necrosis was observed in only one patient, who suffered from hemiparesis and neurocognitive sequelae. The Moyamoya disease observed on a follow-up

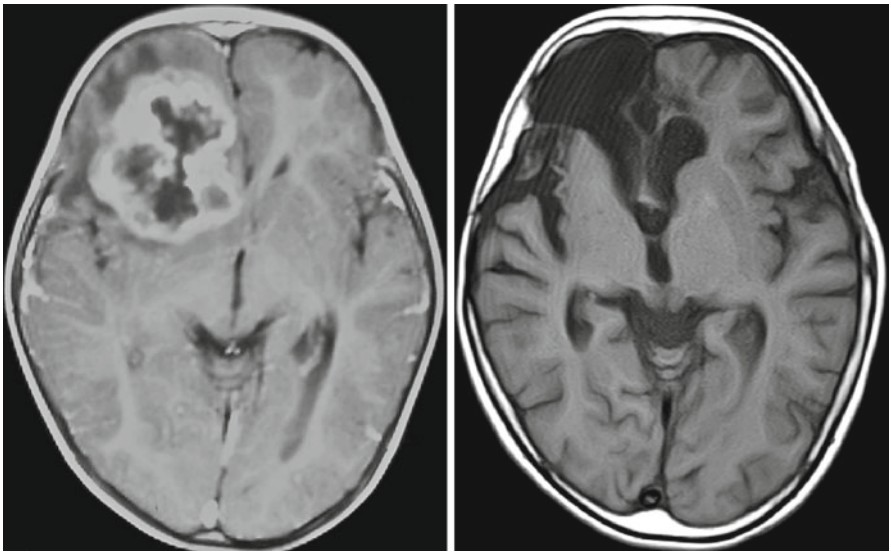

Fig. 29.6 Pre BNCT (*left*), 1 year after BNCT (*right*)

MRA in another patient may have been caused by BNCT. The other five patients had little damage caused by BNCT. One is currently in college, and two other patients graduated from college. BNCT can be applied to malignant brain tumors in children, especially those under 3 or 5 years of age, instead of conventional radiation therapy. Although BNCT was shown to achieve local control at the primary site, it is still difficult to prevent CSF dissemination in patients with glioblastoma and PNET.

References

1. Mulhern KR et al (2004) Late neurocognitive sequelae in survivors of brain tumors in childhood. Lancet Oncol 15:399–408
2. Hatanaka H, Nakagawa Y (1994) Clinical results of long-surviving brain tumor patients who underwent boron neutron capture therapy. Int J Radiat Oncol Biol Phys 28:1061–1066
3. Nakagawa Y (1994) Boron neutron capture therapy: the past to the present. Int J Radiat Oncol Biol Phys 28:1217
4. Nakagawa Y, Hatanaka H (1997) Boron neutron capture therapy-clinical brain tumor study. J Neurooncol 33:105–115
5. Nakagawa Y et al (2003) Clinical review of Japanese experience with boron neutron capture therapy and a proposed strategy using epithermal neutron beams. J Neurooncol 62:87–99
6. Kageji T et al (2006) Boron neutron capture therapy using mixed epithermal and thermal neutron beams in patients with malignant glioma – correlation between radiation dose and radiation injury and clinical outcome-. Int J Radiat Oncol Biol Phys 65:1446–1455
7. Kageji T et al (2006) Correlation between BNCT radiation dose and histopathological findings in BSH-based intra-operative BNCT for malignant glioma. Advances in Neutron Capture Therapy 2006:35–36

Prevention of Vascular Restenosis After Vascular Angioplasty

30

Wataro Tsuruta, Tetsuya Yamamoto,
and Akira Matsumura

Contents

30.1 Introduction

Acute myocardial and cerebral infarction as a result of arteriosclerotic occlusion are major causes of human death. In the case of ischemic heart disease, the indication for surgical revascularization has substantially decreased due to the successful evolution of percutaneous coronary intervention. And while the widely used methods of percutaneous transluminal angioplasty (PTA) and stenting are much less invasive

W. Tsuruta • A. Matsumura
Department of Neurosurgery, Institute of Clinical Medicine,
Graduate School of Comprehensive Human Science, University of Tsukuba,
1-1-1 Tennohdai, Tsukuba, Ibaraki, 305-8575, Japan
e-mail: wataro@cf6.so-net.ne.jp; a-matsumur@md.tsukuba.ac.jp

T. Yamamoto (✉)
Department of Neurosurgery and Radiation Oncology, Institute of Clinical Medicine,
Graduate School of Comprehensive Human Science, University of Tsukuba,
Tsukuba, Japan
e-mail: tetsuya@md.tsukuba.ac.jp

W.A.G. Sauerwein et al. (eds.), *Neutron Capture Therapy*,
DOI 10.1007/978-3-642-31334-9_30,

than surgery for the treatment of coronary artery stenosis, restenosis occurs in 30–60 % of cases [5]. As for treatment of carotid artery stenosis, carotid endarterectomy (CEA) has been the gold standard based on randomized control trials [13, 22]. Recently, carotid artery stenting (CAS) has proven beneficial in patients who are at high risk for CEA [28] and is expected to be widely used in the near future. However, restenosis still occurs after CAS in no less than 5 % of cases [11, 12, 17] and in 10–40 % of intracranial artery stenosis cases [1, 8, 19]. The mechanism of restenosis seems to involve intimal hyperplasia [6, 7], which in turn results from the migration and proliferation of vascular smooth muscle cells (VSMCs) and from the migration and myofibroblastic transformation of adventitia cells. Inhibition of intimal hyperplasia is thus important for the prevention of restenosis. Though several modalities, such as drug-eluting stents or brachytherapy, have been introduced and proven to have efficacy for the inhibition of intimal hyperplasia, restenosis continues to represent a major clinical problem of vascular angioplasty.

30.2 Modalities for the Prevention of Restenosis

Radiation therapy is one method for the prevention of restenosis after coronary PTA/stenting, and brachytherapy with beta or gamma beams has been approved for this purpose by the US Food and Drug Administration [15, 21, 26, 27]. Though difficulties regarding irradiation of normal structures and unstable doses due to limited path length have been improved by the development of various devices and techniques, there is a possibility of late total coronary occlusion without the prolonged use of antiplatelet therapy [9]. In addition, catheterization laboratories that utilize gamma sources of radiation must be reconfigured. Recently, drug-eluting stents have shown a great deal of promise for the prevention of restenosis after coronary PTA/stenting, with reported restenosis rates of less than 10 %. The drug-eluting stents are coated with antiproliferative agents that are released gradually into the vascular tissue for several months. Although favorable outcomes have been reported in some clinical trials [3, 4], there are still long-term safety issues when using drug-eluting stents. There have been reports warning of late thrombosis,chronic thrombosed occlusion due to a lack of in-stent neointimal formation [23]. Since intimal formation inside the stent is disturbed by coated agents and exposed stent is a source of thrombosis, long-term use of antiplatelet drugs is required in patients using these devices. Experimentally, it has been reported that photodynamic therapy with light-sensitive compounds such as porphyrin may prevent restenosis [2, 14]. Despite these modalities for the prevention of restenosis, however, restenosis remains a major, unresolved issue of vascular angioplasty. In regard to radiation therapy, greater attention should be paid to irradiation of normal structures and unstable doses. There is also a potential method for the prevention of restenosis; this method, BNCT (boron neutron capture therapy), is the focus of the present study. Given that boron compounds are incorporated into arterial tissues and more in the impaired intima than the normal one, BNCT might be effective for the prevention of restenosis (Fig. 30.1). Because high-LET particles have limited path lengths in tissue

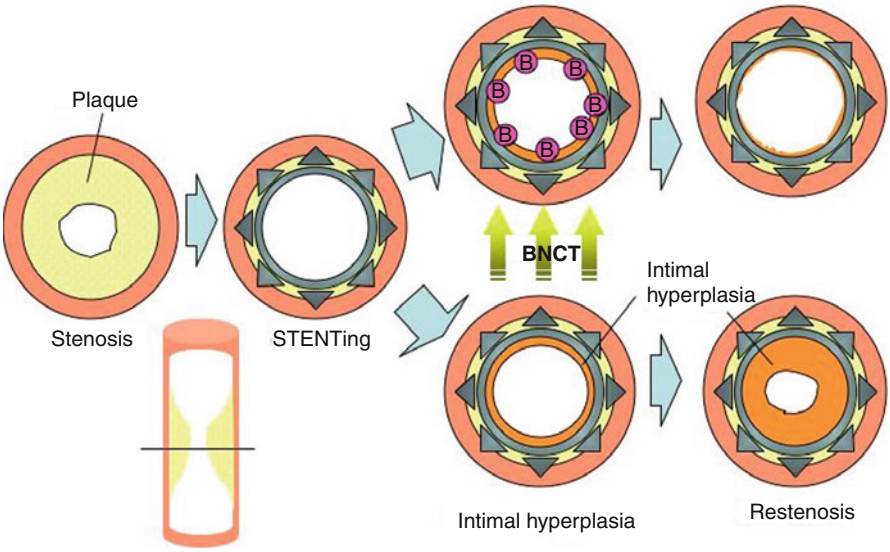

Fig. 30.1 Potential application of BNCT to prevent restenosis. This schema illustrates our hypothesis. If we can identify the kind of boron compounds that are incorporated into arterial tissue and especially into impaired intima, BNCT might have a preventive effect against intimal hyperplasia

(5–9 μm), the destructive effects of boron particles are limited to boron-containing cells. BNCT might thus be superior to beta or gamma-beam brachytherapy from the standpoint of injury of normal structures.

30.3 Application of BNCT for the Prevention of Restenosis

30.3.1 Boron Concentration in Vascular Tissue

We measured the boron concentration in rat arterial tissue, venous tissue, and other normal structures after intravenous administration of boron compounds, i.e., BSH 100 mg/kg, or BPA-fructose complex 250 mgBPA/kg. The boron concentrations of BSH in arterial tissue at 2 (28.6 ppm) and 3 (32.0 ppm) h were higher than in other normal tissues except in kidney (Fig. 30.2). The BSH artery:blood ratio in arterial tissue was higher than the BSH vein:blood ratio. The boron concentrations of BPA in venous tissue at 2 (23.7 ppm) and 3 h (12.3 ppm) were much higher than in other normal tissues (Fig. 30.3). The BPA vein:blood ratio in venous tissue was higher than the BPA artery:blood ratio in arterial tissue. These results suggested BSH was more suitable for targeting of impaired arterial tissue than BPA. We measured the boron concentration in impaired vessels of a rat carotid artery angioplasty model. Just after balloon angioplasty of the right carotid artery, intravenous administration of BSH 100 mg/kg was performed. The bilateral carotid arteries were collected for

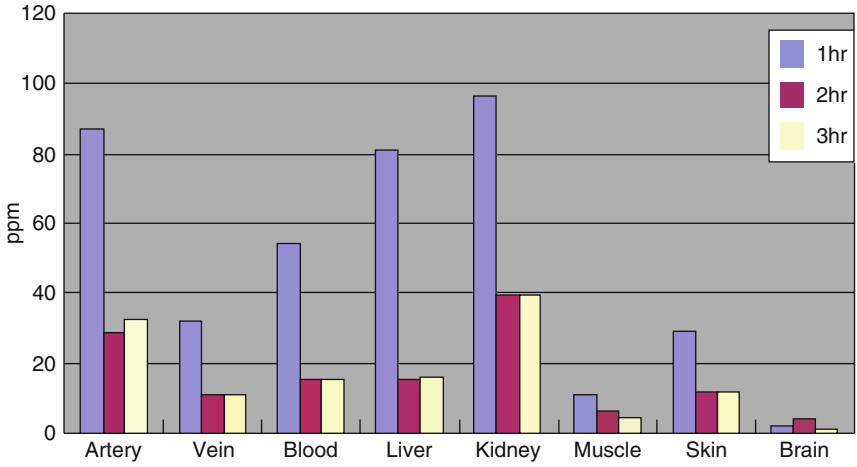

Fig. 30.2 Boron concentrations of BSH in vascular and normal tissue. At 1, 2, and 3 h after BSH administration, the boron concentrations in normal arterial tissue were 86.8, 28.6, and 32.0 ppm, respectively. In normal venous tissue, the concentrations were 31.7, 10.6, and 11.2 ppm. The artery:blood ratios were 1.63, 1.86, and 2.12. The vein:blood ratios were 0.61, 0.74, and 0.74. The boron concentrations of BSH in arterial tissue at 2 and 3 h were higher than in other normal tissues

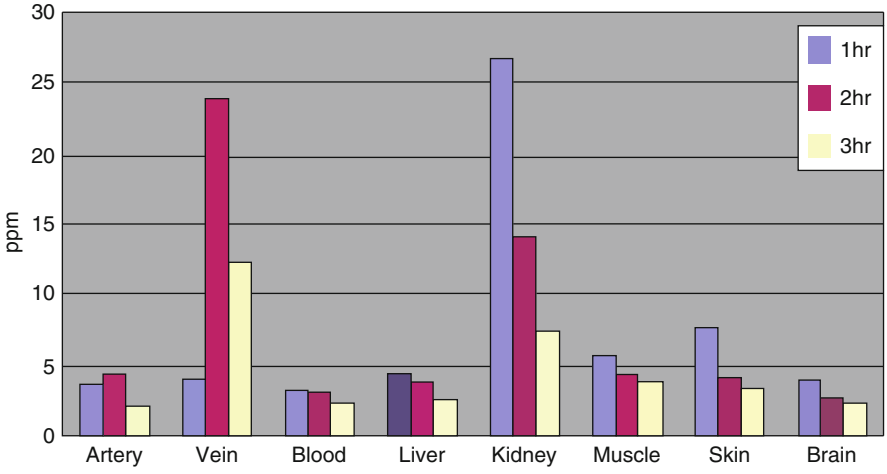

Fig. 30.3 Boron concentrations of BPA in vascular and normal tissue. At 1, 2, and 3 h after BPA administration, the boron concentrations in normal arterial tissue were 3.7, 4.4, and 2.1 ppm, respectively. In normal venous tissue, the concentrations were 4.0, 23.7, and 12.3 ppm. The artery:blood ratios were 1.15, 1.36, and 0.92. The vein:blood ratios were 1.24, 7.96, and 5.12. The boron concentrations of BPA in venous tissue at 2 and 3 h were much higher than in other normal tissues

measuring the boron concentration with the ICP method at either 1, 2, or 3 h. The boron concentration after BSH administration was higher in impaired arterial tissue than in normal arterial tissue at 1 (Fig. 30.4).

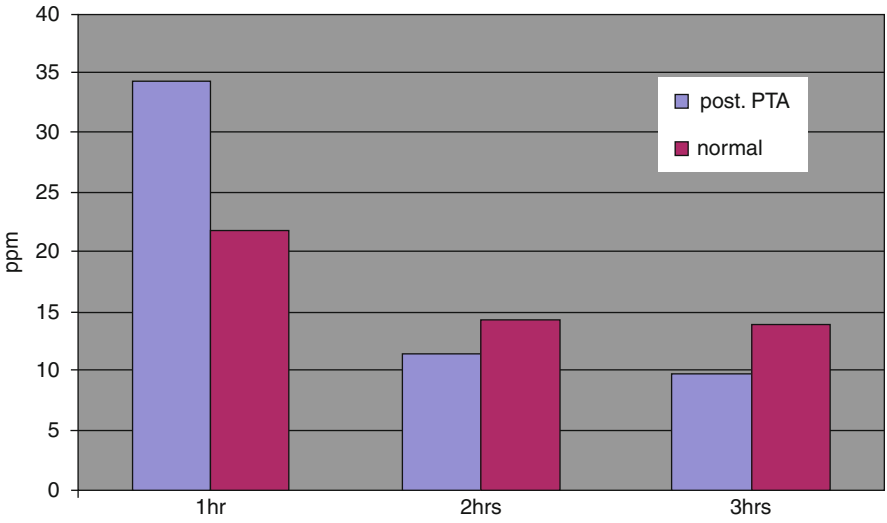

Fig. 30.4 Boron concentration in carotid arteries of the post-angioplasty model. The boron concentration of BSH was 34 ppm in impaired arterial tissue at 1 h, which was higher than the value of 22 ppm in normal tissue at the same time point. There was no significant difference between the concentrations at 2 and 3 h

30.3.2 Efficacy for Prevention of Restenosis

To evaluate whether BNCT with BSH inhibits stenosis in the rat carotid artery post-angioplasty model [24], rats were assigned to two groups ($n=2$ animals per group): one group was administered BSH and the other was administered saline as a control. BSH (100 mg/kg) or saline was administered intravenously 1 h before neutron irradiation. The boron concentration of BSH in the impaired artery was 34 ppm at 1 h in this study. The dosage of BSH used in the present study, 100 mg/kg, was the same as the dosage of BNCT used for glioblastoma. Balloon angioplasty was performed 48 h before neutron irradiation. This is because the transformation of VSMCs into the proliferative phenotype [10], the main cause of intimal hyperplasia, usually occurs 2–3 days after balloon angioplasty, with the accumulation of inflammatory cells in the rat PTA model [24]. Further investigations into the planning of this treatment will be needed to improve its efficacy.

Thirty minutes of neutron irradiation was performed using thermal neutron beam mode I (mixed epithermal-thermal beam) under 2 MW operation at JRR-4 of JAEA. High-LET components physical dose (DB + DN) was 9.01 Gy. Gamma-ray dose was 1.98 Gy. At 14 days after treatment, intimal hyperplasia was significantly diminished in the BSH group (Figs. 30.5 and 30.6). Previous reports have indicated that irradiation with gamma rays using single fraction exposures of more than 5–15 Gy to the rat carotid artery is needed to inhibit intimal hyperplasia [16, 18]. In our investigation with gamma irradiation, more than 5 Gy irradiation was needed. As the gamma-ray dose 1.98 Gy in this experiment was less than 2 Gy as

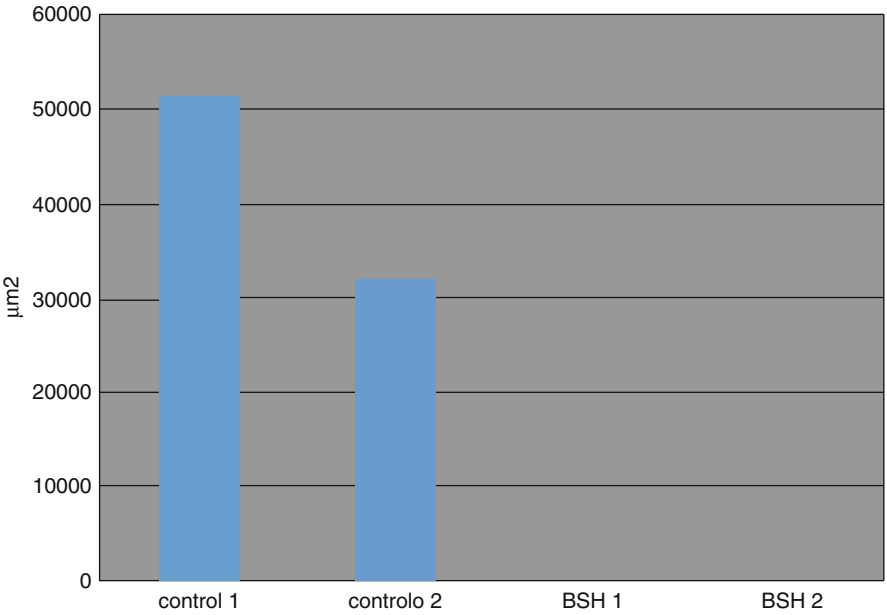

Fig. 30.5 Efficacy of BNCT for prevention of intimal hyperplasia. The intimal hyperplasia area inside of the internal elastic lamina in the injured artery was measured at three points (3, 4, and 5 mm from the bifurcation) using the volumetric soft in Keyence Biozero. An average of three data points was used for evaluation. At 14 days after treatment, the intimal hyperplasia was significantly diminished in the BSH group

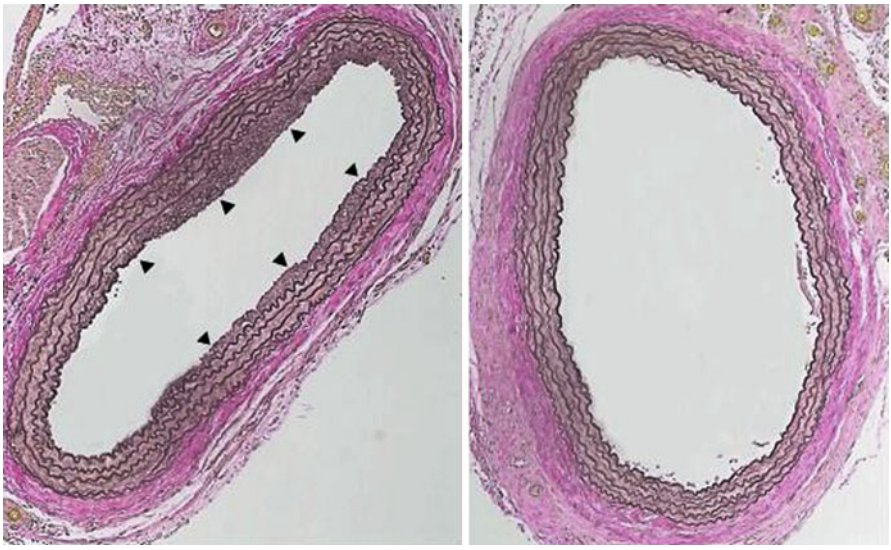

Fig. 30.6 Histological specimen of a rat carotid artery in the post-angioplasty model at 14 days after neutron irradiation (elastica van Gieson staining). *Left*: control group. Intimal hyperplasia was observed in the inner lumen (*arrowheads*). *Right*: BSH group. Intimal hyperplasia was significantly diminished

measured by TLD on the neck skin of irradiated rats in this study, the efficacy of the alpha beams could be evaluated. Intimal hyperplasia was diminished, and adverse effects were not apparent at 14 days. Further investigations should be focused on the minimum dosage for prevention of intimal hyperplasia and tolerance dose of surrounding normal structure because adverse effects caused by irradiation must be avoided especially in the treatment of "nonmalignant" lesion such as restenosis after vascular angioplasty. Moreover, long-term efficacy and safety also should be investigated.

30.4 Perspectives

Turning now to other compounds, the porphyrin used for photodynamic therapy is known to be incorporated into smooth muscle cells, generating intimal hyperplasia [2, 14]. In regard to boronated porphyrin (BOPP), there are no previous reports on the distribution of BOPP in arterial tissue, although Stephen et al. reported that the boron concentration after BOPP administration in venous tissue was around 30 ppm [20]. The BOPP distribution in arterial tissue should also be investigated. Regarding incorporation of boron, targeting with a drug delivery system (DDS) has potential. We previously reported on the prevention of restenosis with active targeting chemotherapy using doxorubicin liposome. This system is controlled via the affinity between E-selectin proteins expressed in intima and sugar chains on the surface of liposomes [25]. DDS with boronated liposome might make it possible to deliver boron preferentially to intima injured by angioplasty.

Conclusion

Restenosis remains the main limitation of vascular angioplasty, though the introduction of drug-eluting stents and brachytherapy has improved the restenosis rate. Late thrombosis of drug-eluting stents and irradiation of normal structures and unstable doses of brachytherapy have been unresolved issues. Our preliminary study with a rat carotid artery model showed the possible application of BNCT for preventing restenosis after angioplasty based on selective irradiation of injured intima. Further investigation of the boron distribution in vascular and normal structures, development of appropriate boron compounds, and evaluation of the tolerability of BNCT for prevention of restenosis will be needed before BNCT can be applied clinically to prevent restenosis after stenting.

References

1. Albuquerque FC et al (2003) A reappraisal of angioplasty and stenting for the treatment of vertebral origin stenosis. Neurosurgery 53:607–14
2. Arakawa K et al (2002) Sonodynamic therapy decreased neointimal hyperplasia after stenting in the rabbit iliac artery. Circulation 105:149–151

3. Babapulle MN, Eisenberg MJ (2002) Coated stents for the prevention of restenosis: part 1. Circulation 106:2734–2740
4. Babapulle MN, Eisenberg MJ (2002) Coated stents for the prevention of restenosis: part 2. Circulation 106:2859–2866
5. Bauters C et al (1996) Mechanism and prevention of restenosis: from experimental models to clinical practice. Cardiovasc Res 31:835–846
6. Bruneval P et al (1986) Coronary artery restenosis following transluminal coronary angioplasty. Arch Pathol Lab Med 110:1186–1187
7. Carson SN et al (1981) Experimental carotid stenosis due to fibrous intimal hyperplasia. Surg Gynecol Obstet 153:883–888
8. Chastain HD II et al (1999) Extracranial vertebral artery stent placement: in-hospital and follow up results. J Neurosurg 91:547–552
9. Costa M et al (1999) Late coronary occlusion after intracoronary brachytherapy. Circulation 100:789–792
10. Fortunato JE et al (1998) Irradiation for the treatment of intimal hyperplasia. Ann Vasc Surg 12:495–503
11. Koebbe CJ et al (2005) The role of carotid angioplasty and stenting in carotid revascularization. Neurol Res 27(Suppl 1):53–58
12. Levy EI et al (2005) Frequency and management of recurrent stenosis after carotid artery stent implantation. J Neurosurg 102:29–37
13. North American Symptomatic Carotid Endarterectomy Trial Collaborators (1991) Beneficial effect of carotid endarterectomy in symptomatic patients with high-grade carotid stenosis. N Engl J Med 325(7):445–453
14. Nyamekye I et al (1995) Photodynamic therapy of normal and balloon-injured rat carotid arteries using 5-amino-levulinic acid. Circulation 91:463–468
15. Raizner AE et al (2000) Inhibition of restenosis with β-emitting radiotherapy: report of the Proliferation Reduction with Vascular Energy Trial (PREVENT). Circulation 102:951–958
16. Sarac TP et al (1995) The effects of low-dose radiation on neointimal hyperplasia. J Vasc Surg 22:17–24
17. Setacci C et al (2003) Determinants of in-stent restenosis after carotid angioplasty: a case-control study. J Endovasc Ther 10:1031–1038
18. Shimotakahara S et al (1994) Gamma irradiation inhibits neointimal hyperplasia in rats after arterial injury. Stroke 25:424–428
19. SSYLVIA Study Investigators (2004) Stenting of symptomatic atherosclerotic lesions in the vertebral or intracranial arteries (SSYLVIA): study results. Stroke 35:1388–1392
20. Stephen BK et al (1996) Cancer neutron capture therapy. Plenum Press, New York
21. Teirstein PS et al (2000) Three-year clinical and angiographic follow-up after intracoronary radiation. Result of a randomized clinical trial. Circulation 101:360–365
22. The Asymptomatic Carotid Atherosclerosis Study Group (1989) Study design for randomized prospective trial of carotid endarterectomy for asymptomatic atherosclerosis. Stroke 20:844–849
23. The BASKET-LATE-Study (2006) Basel stent cost-effectiveness trial – late thrombotic events trial. Herz 31:259
24. Tsuruta W et al (2007) Simple new method for making a rat carotid artery post-angioplasty stenosis model. Neurol Med Chir (Tokyo) 47:525–529
25. Tsuruta W et al (2009) Application of liposomes incorporating doxorubicin with sialyl Lewis X to prevent stenosis after rat carotid artery injury. Biomaterials 30:118–125
26. Waksman R et al (2000) Intracoronary β-radiation therapy inhibits recurrence of in-stent restenosis. Circulation 101:1895–1898
27. Waksman R et al (2000) Intracoronary γ-radiation therapy after angioplasty inhibits recurrence in patients with in-stent restenosis. Circulation 101:2165–2171
28. Yadav JS et al (2004) Protected carotid-artery stenting versus endarterectomy in high-risk patients. N Engl J Med 351(15):1493–1501

Boron Neutron Capture Synovectomy

31

Jacquelyn C. Yanch

Contents

31.1 Introduction

Rheumatoid arthritis (RA) is a chronic, autoimmune disease affecting roughly 1–2 % of the adult population [1]. Although it is a systemic disease with the potential to affect many organs, the prevailing feature is a progressive, deforming arthritis characterized by an inflammatory reaction in the synovium. The synovial membrane is the inner layer of the joint capsule and lines the joint everywhere except over the articular cartilages which cover the ends of the bones. In a patient with RA, the synovium becomes grossly edematous and inflamed resulting in considerable

J.C. Yanch
Departments of Nuclear Science and Engineering and Biological Engineering,
Massachusetts Institute of Technology,
Cambridge, MA, USA
e-mail: jcyanch@mit.edu

W.A.G. Sauerwein et al. (eds.), *Neutron Capture Therapy*,
DOI 10.1007/978-3-642-31334-9_31,

pain and reduced range of motion. If left untreated, the inflammation usually results in progressive joint destruction and deformity leading ultimately to varying degrees of incapacitation [1].

Treatment for RA involves various drugs administered to reduce synovial inflammation, and, for the majority of patients, this approach is effective in providing relief of symptoms. For a significant number of patients, however, one or more joints remain unresponsive, and other means of addressing the inflamed synovium are sought. Surgical removal of the synovium ("synovectomy") is performed via open surgery or arthroscopically via multiple small entries. Both procedures result in removal of up to 80 % of the synovial membrane and alleviation of symptoms in 70–80 % of cases [2–4]. While the synovial membrane will regrow within 6 months of surgery, benefits persist for approximately 5 years. Inflammation, however, eventually returns.

Alternatively, beta-emitting radionuclides can be injected into the fluid space adjacent to the synovium ("radiation synovectomy"). Various radionuclides have been utilized in the clinic with good to excellent results in 60–70 % of patients with duration of palliation similar to that observed following surgical synovectomy [5–7]. Radionuclide activities found to be clinically effective in alleviating symptoms deliver synovial doses of approximately 60–100 Gy [6, 8] in a single administration. This dose is substantially larger than target doses in single-fraction radiotherapy of tumors but is necessary since the goal of radiation synovectomy is *functional* cell death in the synovial membrane, rather than reproductive cell death. (Reproductive cell death, involving only the loss of clonogenicity, is the goal of radiotherapy of tumors and occurs at substantially lower doses [9].)

A significant concern associated with radiation synovectomy is the potential for irradiation of healthy tissues resulting from leakage of the radioactive material out of the joint. Increased levels of chromosomal aberrations in patients undergoing radiation synovectomy with ^{198}Au or ^{90}Y have been reported by several investigators [10, 11]. While the introduction of new preparations of ^{90}Y and use of radionuclides with shorter half-lives and large particulate carriers have reduced the extent of leakage from the joint, concerns persist about the long-term sequela in this patient population caused by radiation synovectomy using beta emitters.

31.2 Boron Neutron Capture Synovectomy (BNCS)

BNCS has been proposed as a means of performing radiation synovectomy without injection of a radioactive material [12]. This is a two-part procedure (Fig. 31.1) involving the local injection of a boron-labeled substance directly into the joint space followed by joint irradiation using a beam of low-energy neutrons.

Local delivery of the ^{10}B compound provides clear advantages over systemic administration for BNCS. First, direct intra-articular injection of a boron-loaded pharmaceutical leads to high levels of boron in the synovial tissue, orders of magnitude greater than concentrations encountered in BNCT. Large boron levels result in high radiation doses upon neutron irradiation of the joint and indicate that the target dose of 100 Gy can be readily achieved. Second, since a greater fraction of

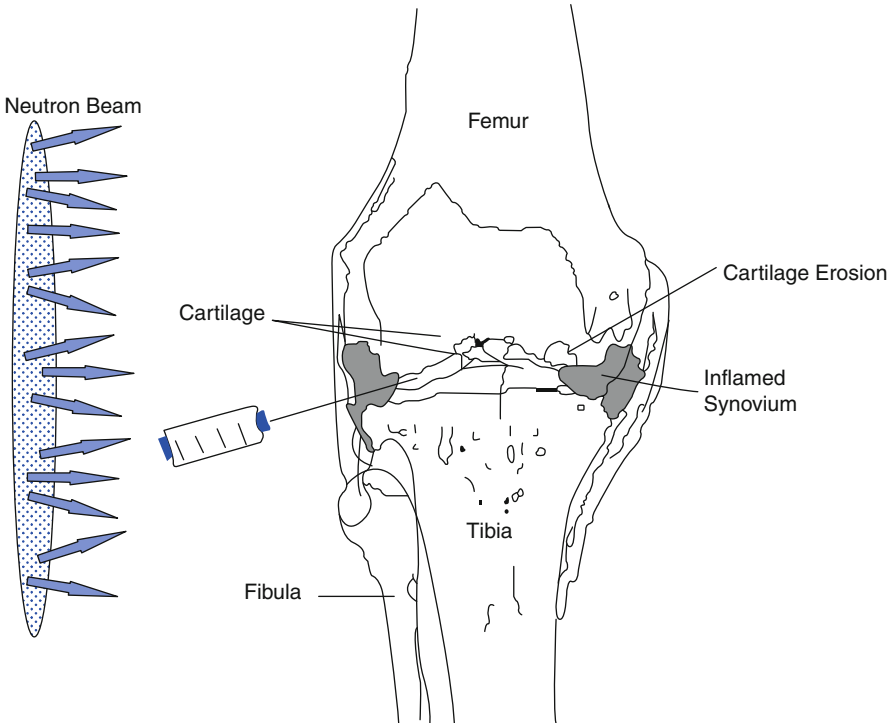

Fig. 31.1 This schematic illustration of boron neutron capture synovectomy shows a coronal view of a rheumatoid human knee joint, the largest articulating joint in the body. In a rheumatoid knee, the joint space is enlarged resulting from increased synovial fluid and thickened inflamed synovial tissue which, in this example, has begun to erode adjoining articular cartilage. For BNCS, a boron-labeled compound will be injected directly into the joint space using a standard lateral approach. The joint will then be irradiated by a low-energy neutron beam

the neutrons in the incident beam undergo capture reactions in boron, the requirements for neutron beam purity can be relaxed since the total healthy tissue dose from fast neutrons or photons in the beam will be low. And third, avoiding systemic administration of the boron-labeled compound reduces the potential for neutron capture dose in the rest of the patient that might result from neutrons streaming through patient shielding or from neutrons scattering within the joint tissues themselves.

31.3 Development of BNCS

31.3.1 Preliminary Compound Investigation

A small number of boron-labeled compounds have been evaluated as candidates for BNCS. Initial studies evaluated uptake of boron in various formulations in *ex vivo* samples

of human arthritic synovium [13, 14]. Compounds were co-incubated with synovium obtained at the time of surgery from knee joints of patients with RA undergoing surgical synovectomy or joint replacement. After incubation, samples were rinsed, incubated in fresh medium for varying periods of time, and then evaluated for bulk boron content using prompt gamma neutron activation analysis (PGNAA). The most promising compound evaluated with this approach was potassium dodecahydrododecaborate ($K_2B_{12}H_{12}$), the salt form of a polyhedral closo boronate ion. Incubation of human rheumatoid synovium in medium containing this compound led to measured synovial boron levels roughly 40–60 % of the concentration in the medium. Subsequent incubation in boron-free medium for varying periods of time demonstrated that significant washout of the compound (~75 %) occurs within the first 30 min. Thereafter, further incubation resulted in no further loss of compound from the synovial tissue [15].

The *in vivo* situation, however, offers other routes of compound egress from the tissue not available in the *ex vivo* washout study, such as the abundant blood vessels in the inflamed synovium. *In vivo* uptake studies were therefore performed using an animal model of arthritis [15]. The antigen-induced arthritis (AIA) model in New Zealand rabbits bears a close resemblance to rheumatoid arthritis in humans and has been used extensively in the evaluation of agents for beta-particle radiation synovectomy. Once synovitis had begun in the rabbits, an injection of $K_2B_{12}H_{12}$ in saline (containing either 5,000 or 150,000 ppm ^{10}B) was injected into the stifle joint. At various times following injection the animals were killed, the synovium and other tissues were dissected, rinsed in saline, and evaluated for boron uptake via PGNAA [15].

Results indicated that, for the expected duration of neutron irradiation, synovial boron levels are extremely high, with an average concentration of 19,000 ppm (based on 150,000-ppm initial local injection) for the time period between 5- and 25-min postinjection. It was also observed that $K_2B_{12}H_{12}$ does not remain in the joint as no boron was measurable after 1–4 h [15]. However, synovial boron levels were very high for sufficiently long for this compound to be used in an evaluation of the efficacy of the BNCS procedure, as described below.

31.3.2 Neutron Beam Design

Neutron beam design for BNCS differs from that for BNCT as a result of a number of features of the disease and of the optimum route of boron administration. First, the synovial membrane of articular joints lies very close to the skin surface, typically within a few mm to 1.5 cm, but extends around the entire joint. Second, most joints considered for treatment lie at some distance from radiosensitive organs in the body. Dose-limiting tissues are therefore likely to be those associated with the irradiated joint, in particular the local skin and the bone surface (since compound leakage is not a significant concern). Third, as discussed above, the ability to inject the boronated compound directly into the joint space leads to high boron levels in the target tissue at the time of irradiation. This means that a greater fraction of the incident neutron fluence results in boron neutron capture events. A more effective use of the neutron flux means that a therapeutic dose can be delivered very quickly. Consequently, the requirements for neutron

beam purity can be relaxed since the total healthy tissue dose from fast neutrons and photons in the beam (which simply scales with irradiation time) will be low.

Extensive beam design, construction, and testing have been performed in conjunction with various neutron sources around the world [12, 16–22]. Design is based on models of human joints, typically the finger or knee, and radiation transport calculations are performed to evaluate the dosimetric effect of different neutron spectra on the joint assuming varying synovial boron concentrations. Beams based on accelerator-generated neutron reactions [12, 16–18], nuclear reactors [19, 20], and isotope sources (both ^{252}Cf [21] and PuBe [22]) have been designed and, in some cases, experimentally validated in phantom or animal studies. Moderator and reflector materials employed in beam design for BNCS do not differ from those proposed for BNCT beam shaping although configurations and dimensions are somewhat different. Combinations of graphite or lead with light water, heavy water, polyethylene, aluminum, and fluental have been shown to produce neutron beams with advantageous treatment parameters.

There is one significant aspect of beam design for BNCS that differs considerably from that for BNCT and this stems from the location of the target tissue. In BNCS, the inflamed synovial membrane is not found in only one location of the joint but is instead located at roughly similar depth, circling the ends of the bony surfaces around the entire joint. Therefore, neutron beams must be designed such that a therapeutic dose is delivered to a shallow depth but around the entire joint. This can be accomplished by placing scattering material behind and to the sides of the joint [17, 18, 20]. Neutrons leaving the joint have the opportunity to scatter back into the tissue, providing an additional opportunity for capture in the boron in the synovium circling the joint. Neutron scattering in low-Z materials is more isotropic, and this will enhance the probability of scattering back into the joint. Graphite, beryllium, D_2O, and polyethylene have been evaluated and give roughly similar improvements in therapeutic parameters over the case of no side or back reflector: a factor of 2–3 reduction in treatment time and factors of roughly two reduction in dose to overlying skin and the bone surfaces [17, 18, 20]. Higher-Z materials, such as lead, give inferior results.

31.3.3 Whole Body Patient Dose in BNCS

Even though no radioactive materials are used in BNCS, patients will experience whole body radiation dose as a result of neutron irradiation of the affected joints. A number of shielding configurations for BNCS of the knee have been evaluated in anthropomorphic phantoms both experimentally and by Monte Carlo simulation [17]. The most effective configuration involves embedding the moderator/reflector assembly in a shielding wall made of boronated polyethylene and adding shielding material around the patient's legs. For synovial boron levels of 19,000 ppm, the effective dose for a shielded patient receiving 100 Gy to the synovium (assuming radiation weighting factors of 4.0, 3.8, and 1.0 for ^{10}B reaction products, neutrons, and photons, respectively) ranged from 1.3 mSv (for a "soft" beam based on the 4-MeV ^{9}Be(p,n) reaction) to 7.2 mSv (for a "hard" beam based on the 2.6-MeV ^{9}Be(d,n) reaction). Simulations indicated that most of the whole body dose resulted

from neutrons entering the joint and then scattering through the rest of the body [17]; it is difficult to reduce this dose component without degrading neutron delivery to the targeted area. [For comparison, the average worldwide dose from 1 year of natural background radiation is roughly 2.4 mSv.] Experimental confirmation for the whole body estimates was performed with a combination of thermoluminescent dosimetry and bubble detectors and using two water-filled tanks representing the torso and one leg. In general, the measured effective dose equivalent doses for both shielded and unshielded configurations agreed with predictions within a factor of 2 [17, 23].

31.3.4 Potential of Gadolinium Neutron Capture Synovectomy

The feasibility of ^{157}Gd as an alternative to boron as a neutron capture agent for synovectomy has been examined by Monte Carlo simulation studies [24]. ^{157}Gd initially appears to be an attractive alternative to boron given its large capture cross section, its large Q value relative to ^{10}B (7.9 MeV compared with 2.8 MeV), and the ready availability of ^{157}Gd-enriched compounds. Thermal neutron capture reactions in ^{157}Gd lead to ^{158}Gd* which deexcites by internal transition and internal conversion leading to emission of gamma rays and conversion electrons with energies as high as several MeV.

Using a moderated neutron beam based on the ^{9}Be(p,n) reaction, Gierga et al. compared Gd-NCS and B-NCS in terms of therapy time, therapeutic ratios, and shielded whole body dose [24]. Results of the investigation demonstrated that use of ^{10}B as a neutron capture agent for synovectomy is markedly superior to use of ^{157}Gd. Therapy times are roughly 27 times longer when using ^{157}Gd with the moderated ^{9}Be(p,n) beam. This is a result of two features of the neutron capture reaction in gadolinium compared with that in boron. First, while the ^{157}Gd capture cross section at thermal energies is 60 times higher than that of ^{10}B, this ratio diminishes quickly with energy and is, for example, only a factor of 2 at 10 keV. Second, although the Q value for the ^{157}Gd capture reaction is more than three times greater than that in ^{10}B, the reaction products, their range in tissue, and their LET substantially differ. Most of the photons generated in the ^{157}Gd reaction leave the target tissue without generating local dose but generating significant healthy tissue dose to the patient. It was found that the total increase in capture cross section over the energy range of the incident beam is not sufficient to overcome the loss of reaction energy from the local area that results from the long mean free path of the photons. Thus, therapy time for Gd-NCS is substantially longer than that required for BNCS using the moderated ^{9}Be(p,n) beam. Longer therapy times lead to substantially higher doses to the rest of the patient, a result primarily of ^{1}H(n,γ)^{2}H reactions from neutrons interacting in the body [24].

31.3.5 Efficacy of BNCS in an Animal Model

The efficacy of the boron neutron capture reaction in ablating the inflamed synovium has been examined in an animal model of arthritis [25]. A 0.25-ml solution of ^{10}B-enriched (100 %) potassium dodecahydrododecaborate ($K_2B_{12}H_{12}$) in

saline containing 150,000 ppm ^{10}B was injected into the stifle joint of New Zealand white rabbits exhibiting synovitis resulting from the AIA procedure. Neutron irradiation was performed with the tandem electrostatic accelerator at the MIT Laboratory for Accelerator Beam Applications using the 1.5 MeV $^{9}Be(d,n)$ neutron-producing reaction [25]. The accelerator target was located within a heavy water moderator which was surrounded by graphite for both neutron reflection and further moderation. The stifle joint was positioned between two graphite side reflectors.

The investigation was performed as a dose escalation study with target doses between 8.0 and 810 Gy. [Radiation weighting factors were applied as described above. Note that no radiobiological data relevant to synovial ablation or other endpoints associated with BNCS are available to estimate radiation weighting factors values for the different radiation types encountered in BNCS. Therefore, weighting factors values used in BNCT were used in the calculations of target dose for the dose escalation study. Clearly, use of BNCT weighting factors for BNCS represents only a crude approximation.] Given the rapid egress of $K_2B_{12}H_{12}$ from the joint (as described in Sect. 31.3.1), irradiation time for each dose cohort was kept constant (25 min) and the accelerator current was varied to achieve the targeted doses. The effects of BNCS were evaluated at 72 h or at 14 days. Whole knees were dissected, fixed, sectioned, and stained with hematoxylin and eosin for histological analysis. In a blinded fashion, slides were examined and scored for evidence of synovial tissue inflammation and necrosis and for effects on the cartilage and other structures in the joint.

Evaluation of the histological results in the synovium showed a clear and significant correlation ($p < 0.001$) of synovial tissue necrosis (Fig. 31.2) with increasing dose delivered [25]. *Thus, it can be concluded that BNCS is, in fact, an effective means of ablating the inflamed synovium.* No adverse effects in overlying skin or in extracapsular tissues were observed. There was, however, indication of cartilage damage (acellularity) in animals receiving the highest dose. Since the AIA model itself will result in eventual cartilage destruction, a subsequent study was performed to specifically evaluate the effects of BNCS on the articular cartilage in the stifle joints of normal rabbits [25]. Nonarthritic animals were irradiated for 25 min to either 40 or 80 Gy. Histological evaluation at the 72 h timepoint showed chondrocyte necrosis in all samples suggesting that the boron compound diffused through the cartilage matrix. The compound used in these proof-of-principle studies is a low molecular weight solute and can diffuse through the joint tissues quite rapidly. It therefore quickly enters the synovium and leaves the joint after a short residence time, as was observed in both the *ex vivo* washout and the *in vivo* uptake studies described above (Sect. 31.3.1). This attribute has clear advantages; however, it also results in the passage of the molecule into the cartilage matrix. At 72 h following neutron irradiation, the death of the chondroctyes was observed throughout the cartilage [25]. Thus, while use of $K_2B_{12}H_{12}$ for BNCS is clearly effective in synovial ablation and was of significant value in the performance of the proof-of-principle studies, this compound is unlikely to be a candidate for clinical use.

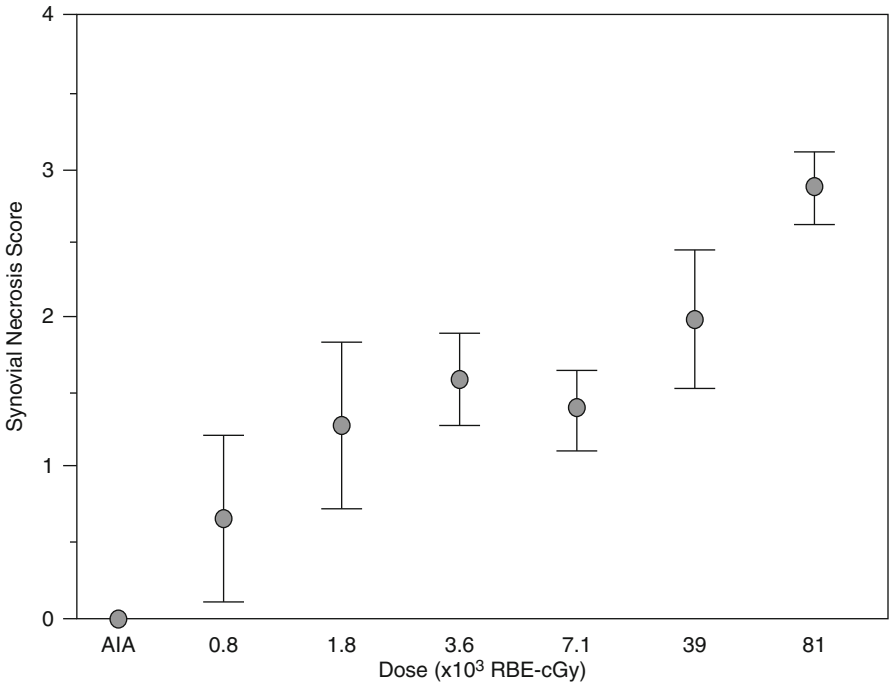

Fig. 31.2 Synovial necrosis scores from synovium samples dissected from AIA stifle joints in New Zealand rabbits treated via BNCS to varying total radiation doses. Necrosis was assessed on a scale of 0–4: 0 (no necrosis), 1 (up to 25 % of tissue is acellular or contains pyknotic cells and debris), 2 (50 % of tissue is necrotic), 3 (75 % of tissue is necrotic), and 4 (complete necrosis of sample). The correlation between dose and necrosis of the BNCS-irradiated tissue as shown above is statistically significant ($p<0.001$) (Figure from reference [25])

31.4 Further Development of BNCS

BNCS has been shown to be an effective means of addressing the synovitis associated with the pain and disability of rheumatoid arthritis. A variety of neutron beams with characteristics suitable for clinical treatments of human joints have been developed at various centers around the world. Like BNCT, however, useful deployment of this experimental approach to the clinic requires further development and testing of suitable boron compounds. Boron-containing liposomes [26] and carborane derivatives [27, 28] are under development as possible candidates. For BNCS, it is possible that useful compounds will be those that are excluded from the cartilage matrix based on size. Since the effective pore size of the cartilage is 1.5–3 nm, a high molecular weight compound or small particles with diameters somewhat larger than this size may be a successful strategy.

References

1. Tehlirian CV, Bathon JM (2008) Rheumatoid arthritis A. Clinical and laboratory manifestations. In: Klippel JH, Stone JH, Crofford LJ, While PH (eds) Primer on the rheumatic diseases, 13th edn. Springer, New York
2. Ishikawa H, Osamu O, Hirohata K (1986) Long–term results of synovectomy in rheumatoid patients. J Bone Joint Surg 68A:198–205
3. Matsui N, Taneda Y, Ohta H, Itoh T, Tsuboguchi S (1989) Arthroscopic versus open synovectomy in the rheumatoid knee. Int Orthop 13:17–20
4. Klug S, Wittmann G, Weseloh G (2000) Arthroscopic synovectomy of the knee joint in early cases of rheumatoid arthritis: follow-up results of a multicenter study. Arthroscopy 16:262–7
5. Kresnik E, Mikosch P, Gallowitsch HJ, Jesenko R, Just H, Kogler D, Gasser J, Heinisch M, Unterweger O, Kumnig G, Gomez I, Lind P (2002) Clinical outcome of radiosynoviorthesis: a meta-analysis including 2190 treated joints. Nucl Med Commun. 23(7):683–8
6. Deutsch E, Brodack JW, Deutch KR (1993) Radiation synovectomy revisited. Eur J Nucl Med 20:1113–1127
7. Delbarre F, Menkes CJ (1974) Non-surgical synovectomy in rheumatoid arthritis. Results obtained by radio-synoviorthesis. Adv Clin Pharmacol 6:134–9
8. Nemec HW, Fridrich R (1977) Retention and dosage in radiation synovectomy with yttrium-90-silicate colloid. Nuklearmedizin 16:113–8
9. Hall EJ (1994) Radiobiology for the radiologist, 4th edn. J.B. Lippincott Company, Philadelphia, p 30
10. de la Chapelle A, Oka M, Rekonen A, Ruotsi A (1972) Chromosome damage after intra-articular injections of radioactive yttrium. Ann Rheum Dis 1:508–12
11. Lloyd DC, Reeder EJ (1978) Chromosome aberrations and intra-articular yttrium-90. Lancet 1:617
12. Yanch JC, Shortkroff S, Shefer RE, Johnson S, Binello E, Gierga D, Jones AG, Young G, Vivieros C, Davison A and Sledge C (1999) Boron Neutron Capture Synovectomy: Treatment of Rheumatoid Arthritis Based on the $^{10}B(n,\alpha)^{7}Li$ Nuclear Reaction. Medical Physics, (26)3:364–375
13. Johnson LS, Yanch JC, Shortkroff S, Sledge C (1996) Temporal and spatial distribution of boron uptake in excised human synovium. In: Mishima Y (ed) Cancer neutron capture therapy. Plenum Press, New York, pp 183–188
14. Binello E, Yanch JC, Shortkroff S, Vivieros C, Yound G, Jones AG, Sledge CB, Davidson A (1997) In vitro analysis of 10B uptake for boron neutron capture synovectomy. In: Advances in neutron capture therapy, vol II. Elsevier, Amsterdam, pp 609–613
15. Yanch JC, Shortkroff S, Shefer RE, Binello E, Gierga D, Jones AG, Young G, Vivieros C, Blackburn B (2001) Progress in the development of boron neutron capture synovectomy for the treatment of rheumatoid arthritis. In: Hawthorne MF, Shelly K, Wiersema RJ (eds) Frontiers in neutron capture therapy. Kluwer Academic, New York, pp 1389–1397
16. Binello E, Ly A, Yanch JC and Shortkroff S (1996) Monte Carlo Investigation of Optimal Neutron Beam Energy for Boron Neutron Capture Synovectomy. Radiation Protection and Shielding (American Nuclear Society, La Grange Park, IL) Vol. 2, 659–664
17. Gierga DP, Yanch JC and Shefer RE (2000) Development and construction of a neutron beam line for accelerator-based boron neutron capture synovectomy. Medical Physics, 27(1): 203–214
18. Verbeke JM, Chen AS, Vujic JS, Leung K (2001) Optimization of Beam-Shaping Assemblies for BNCS Using the High-Energy Neutron Sources D-D and D-T, Nuclear Technology 134(3), 278–293
19. Berlizov AM, Razbudey VF, Shevchenko YB, Tryshyn VV (2006) Prospects of Neutron Capture Synovectomy at Thermal Nuclear Reactors. Nuclear Physics and Atomic Energy, 1, p 67–72

20. Wu J, Chang SJ, Chuang KS, Hsueh YW, Yeh KC, Wang JN, Tsai WP (2007) Dose evaluation of boron neutron capture synovectomy using the THOR epithermal neutron beam: a feasibility study. Phys Med Biol. 52(6):1747–1756
21. Abdalla K, Naqvi AA, Maalej N, Elshahat B (2010) Dose calculation from a D-D-reaction-based BSA for boron neutron capture synovectomy. Appl Radiat Isot. Apr–May;68(4–5): 751–754
22. Vega-Carrillo HR and Manzanares-Acuña E (2003) Neutron Source for Boron Neutron Capture Synovectomy. Alasbimn Journal 5(21)
23. Gierga, DP (2001) Neutron Delivery for Boron Neutron Capture Synovectomy. Ph.D. dissertation, Massachusetts Institute of Technology
24. Gierga DP, Yanch JC and Shefer RE (2000) An investigation of the feasibility of gadolinium for neutron capture synovectomy. Medical Physics, 27(7):1685–1692
25. Shortkroff S, Binello E, Zhu X, Gierga D, Thornhill TS, Shefer R, Jones AG and Yanch JC (2004) Dose Response of the AIA Rabbit Stifle Joint to Boron Neutron Capture Synovectomy. Nucl. Med. Biol. 31(5):663–670
26. Watson-Clark RA, Banquerigo ML, Shelly K, Hawthorne MF, and Brahn E (1998) Model studies directed toward the application of boron neutron capture therapy to rheumatoid arthritis: Boron delivery by liposomes in rat collagen-induced arthritis. PNAS 95(5)2531–2534
27. Valliant JF, Schaffer P (2001) A new approach for the synthesis of isonitrile carborane derivatives. Ligands for metal based boron neutron capture therapy (BNCT) and boron neutron capture synovectomy (BNCS) agents. J Inorg Biochem. 85(1):43–51
28. Valliant, JA, Schaffer P, Britten JF, Davison A, Jones AG and Yanch JC (2000) The synthesis of corticosteroid-carborane esters for the treatment of rheumatoid arthritis via boron neutron capture synovectomy. Tetrahedron Letters, 41:1355–1358

Part VII

Organizational Aspects and Management

Managerial Aspects of BNCT at a Nuclear Research Reactor

32

Wolfgang A.G. Sauerwein and Ray Moss

Contents

W.A.G. Sauerwein (✉)
NCTeam, Department of Radiation Oncology, University Hospital Essen
University Duisburg-Essen, D-45122 Essen, Germany
e-mail: w.sauerwein@uni-due.de

R. Moss
Institute for Energy and Transport, Joint Research Centre, European Commission,
westerduinweg 3, 1755 LE, Petten, The Netherlands
e-mail: raymond.moss@ec.europa.eu

W.A.G. Sauerwein et al. (eds.), *Neutron Capture Therapy*,
DOI 10.1007/978-3-642-31334-9_32, © Springer-Verlag Berlin Heidelberg 2012

32.1 Introduction

Currently worldwide, BNCT when applied to patients still has to be seen as clinical research and hence has to fulfil and follow all legal and institutional requirements for this purpose, which may be different from one country to another. The principles, however, are internationally agreed, and when selecting partners for BNCT, it must be assured that everybody complies with the regulatory requirements. Furthermore, it has to be underlined that in BNCT the use of a non-conventional radiation beam will add a supplementary challenge for the regulatory authorities. The time needed to have a trial protocol accepted cannot be underestimated. It is strongly recommended to start these procedures already during the early discussions when a BNCT facility might be built. A close collaboration with the regulatory authorities is mandatory from the beginning.

This chapter describes aspects of the organisational structure, tasks involved to perform treatment, licensing procedures and quality management, all of which must be considered by groups who are developing a BNCT programme.

32.2 Interdisciplinary Collaboration at a BNCT Facility

From a principle point of view and no matter worldwide, the application of BNCT in human patients needs a multi-institutional and multidisciplinary collaboration, which should be initiated as soon as a group of researchers, which is often associated directly with a research reactor, decides to investigate the possibility to perform patient treatment. By treating patients, a high responsibility and a risk associated with the resulting liability will be on each individual participant and institution. Such a situation can only be handled through contractual agreements, which must define unambiguously the responsibilities and tasks of all the partners.

32.3 The Nuclear Part

The owner of the reactor has in addition to his “normal” tasks and duties, specific responsibilities and liabilities towards the patient. The owner has to realise that when a patient is treated at the reactor, the reactor becomes a medical instrument, which adds a different dimension to the owner’s normal nuclear activities. The owner of the reactor provides the infrastructure for all coworkers to allow them to perform their tasks. It will be mandatory to install communication structures that guarantee regular exchange of information on all aspects of the cooperation but especially about all changes that may influence the treatment.

The reactor owner is responsible for the reactor, the delivery of neutrons, the BNCT facility and the working environment around the facility, that is, security, radioprotection and safety. The reactor owner ensures that these facilities function correctly and that the associated working conditions conform to recognised standards and ensure that the quality assurance of the facility, measurements and presentation of data, for example, checkouts, prompt gamma- ray analysis, dosimetry, etc., conforms to acceptable standards.

Furthermore, the owner of the reactor is responsible for the maintenance and upkeep of the facility and defines the schedule of the reactor and informs all BNCT staff on interruptions in reactor operation. With respect to the radiation beam itself, the owner of the reactor is responsible for the condition and operation of the filtered neutron beam facility, including the safety instrumentation, the interlocking systems, the filter system and the different shutters (if applicable).

If equipment is available to measure the boron concentration in blood during the treatment, for example, a prompt gamma-ray facility or ICP-OES, then the maintenance of this facility must be organised and its correct functioning needs to be controlled and documented.

32.4 The Medical Part

Patient treatment may only be performed together with a hospital and competent medical staff. It is recommended that the hospital must have an academic background with experience and a well-established reputation in oncology.

32.4.1 Radiotherapy

BNCT is one of the most complex forms of radiotherapy. Therefore, when starting a BNCT project, the participation of a radiation-oncology department is mandatory. It is a great advantage, if the radiotherapist involved already has some experience in treating patients with (fast) neutrons, although not mandatory. It must also be taken into consideration that BNCT is not in the mainstream of current research in radiotherapy. In fact, the high complexity of BNCT requires tremendous effort and longer lead times regarding preparation and gaining sufficient knowledge prior to a clinician being able to safely apply BNCT to a patient. The situation is more difficult because no real clinical training on BNCT can be offered easily to a radiation oncologist willing to start in BNCT.

The main tasks of the radiation oncologist, who is in charge of BNCT, are to organise a medical (management) structure, which will allow patient irradiation in a non-medical environment, probably distant from a hospital, and will include training of staff members. It will be necessary for the medical responsible to obtain the legal and ethical permits and licences to implement BNCT at a research reactor. Other tasks will include defining the structure and organisation of the clinical study and patient treatment, specifying and providing the medical equipment, organising the supply of the necessary medical consumables and drugs, coordinating the treatment performed according to the approved protocol, providing the proper and appropriate information about the treatment to the patients and obtaining the signed informed consent form.

For patient treatment, the medical responsible will prepare all relevant clinical data for treatment planning, as well as approving the final treatment plan; decide on the timing and the amount of boron compound to be administered to the patient; take the blood samples from the patients, for example, for boron concentration measurements using prompt gamma analysis or ICP-OES; be responsible for the positioning of the patient for the irradiation; accept responsibility for the starting time

and duration period of the irradiation of the patient; start the irradiation and take the overall responsibility for the welfare of the patient whilst at the reactor site (including concomitant disease and arising acute symptoms).

32.4.2 Medical Physics

The role of the medical physicist is to assure quality and safety of the medical use of ionizing radiation. The medical physicist supports the physician in his/her task to treat patients by providing all necessary physical and technical data to perform a safe and precise treatment and to control all technical equipment involved in the patient treatment. Some aspects of the work are described in the EU Directive 97/43/EURATOM (30 June 1997). Collaboration between the medical physicist and reactor physicists is a precondition to treat a patient with BNCT. The reactor physicists will normally not fulfil the legal requirements to take over the responsibility for patient treatment.

The major tasks of the medical physicist are to define and describe step by step the dosimetry needed to fulfil the requirements of the treatment protocol; to define and describe the quality assurance for all medical physics aspects of the treatment; to be present at all treatments of patients; to be responsible for treatment planning calculations; to perform the quality control calculations with the treatment planning system; to calculate the actual dose given to the patient on the basis of the boron concentration in blood taken before and after the irradiation and to document all actions and data obtained from the measurements and calculations, which have to be archived by the participating hospital.

32.4.3 Pharmacy

The available boronated compounds for BNCT are experimental drugs and cannot be used without special permission of the national agency responsible for new drugs in medicine. To handle such issues, the participation of an experienced pharmacist and of a well-equipped pharmacy at the participating hospital is mandatory. The pharmacy organises the drug supply. Supplying companies must produce the compound according to good manufacturing practice (GMP), which will include a drug master file and written procedures for preparation and quality control of the final product and its intermediates. All actions have to be documented following the legal requirements.

32.4.4 Other Medical Disciplines

The performance of BNCT requires not only the above-mentioned specialists but also surgeons, who select, operate, prepare and provide the follow-up of the patients; anaesthetists, pathologists and diagnostic radiologists familiar with the procedure; nurses to take care of the patient and ambulance drivers to take the patient to and from the reactor.

32.5 Radiation Protection

The treatment of a patient and the potential exposure of personnel to ionising radiation require by the national Nuclear Energy Law that the licence holder (of the reactor) must ensure that radiation protection and monitoring of all personnel, including external staff, is provided and that the correct radiation protection measures are taken and followed.

During BNCT, both the patient and the supporting treatment tools, such as mask and therapy table, become radioactive. As such, measurements of the patient and surrounds should be taken at regular intervals after treatment, checked and written down on an appropriate form. To improve radiological protection of the patient and staff, the radiation beam should be regularly and fully characterised (using activation foils, ionisation chambers, TLDs).

Radiation protection includes the issuing of personal dosimeters (type: universal dosimeter) to all staff, finger or ring dosimeters to the radiotherapists and pen dosimeters to participants classified as visitors, for example, nurse(s) and relatives of the patient. Furthermore, it is necessary to measure and record all material in and out of the reactor and perform activation measurements on all material used in patient treatment. The patient is an exceptional case and, it is not required that a personal dosimeter is issued to the patient. However, following treatment, the patient should be monitored for radioactivity. It is advisable to form a local radiation protection committee for BNCT. The committee has the prime task to review and advise regularly on the radiation protection methods used for BNCT.

32.6 Regulatory Affairs and Licensing for a BNCT Facility

To perform BNCT at a nuclear research reactor, approval must be obtained from the national Ministry of Health or equivalent. As there are usually no regulations or guidelines to perform BNCT, it is necessary to obtain a complete, multifunctional portfolio of approvals, documentation and infrastructural needs in order to have a sound case to be permitted to have a special licence to perform BNCT. The issues which usually have to be resolved are listed briefly below:

- Reactor related: licensing of the reactor as a facility for patient treatment; licensing of the facility, which is not part of a hospital to irradiate patients and gaining local approval on safety aspects, both nuclear and conventional, at the reactor site.
- Protocol related: reconciling the different points of view of different ethics committees in different countries (if applicable); gaining approval of the study protocol by different review boards and handling a non-registered drug to be used in the study protocol following the relevant ICH guidelines [1], as published by the European Medicines Agency (EMEA) [2].
- Patient related: obtaining insurance for patients and building up the local infrastructure for patient care, travel and nursing, including all anticipated emergencies.

- Personnel and institutional related: licensing of (foreign) physicians to treat patients; describing the tasks of all participants and creating the appropriate agreements and contracts to define such structures and applying the appropriate rules for radiation protection of the patients and the staff and concluding contracts (if applicable) with all involved parties.

32.7 Insurances

Special care has to be paid to establish insurance cover for, at least, the following aspects: nuclear incidents; insurance for patients in clinical trials; liability for reactor staff interacting with patients/being involved in patient treatment; liability for staff members from the hospital working at the reactor; liability for further specialists needed, who are not staff from the hospital or the reactor; accident cover for hospital staff during travel to the reactor and work at the reactor and accident cover for patients between hospital and reactor.

32.8 Quality Assurance for BNCT

All BNCT facilities worldwide, performing clinical trials, are presently located at a nuclear research reactor. They are nevertheless, to all intents and purposes, radiotherapy units. In Europe, they must conform to the EU Council Directive on Health Protection 97/43/EURATOM which stipulates that radiotherapy quality assurance programmes are required for performance and safety of radiation units, including testing of performance characteristics on a regular basis (quality control). Consequently, as part of the licensing procedure, QA procedures, or at least well-documented procedures, are needed wherein the testing of certain performance characteristics, including all dosimetric aspects, as well as treatment planning, is written down as standard operating procedures or similarly accepted procedures. In addition, BNCT needs boronated drugs, which up to now are not commercially available as medicine. This introduces additional regulatory and quality requirements related to drugs. Furthermore, BNCT is, to all intent and purposes, still an experimental treatment, a fact that requires dedicated quality management procedures to be followed in clinical trials. This aspect needs to be stressed.

32.9 International Standards for Quality Assurance in Radiotherapy

The performance of BNCT requires the application of national and international rules of safety and quality assurance for nuclear research reactors, for radiation protection and for radiotherapy. The nuclear reactor part is well defined and understood as well as aspects of radiation protection, although specific requirements of reactor safety impose design and safety considerations beyond the con-

ditions of, for example, accelerator-based facilities. The application of established standards and rules for radiotherapy to BNCT, however, is challenging, and few publications have been dedicated to this subject [3–5]. There are no international standards dedicated to BNCT; it is therefore a highly important task to transfer – as far as possible – analogous rules from conventional radiotherapy to BNCT. This work should be carried out in very close collaboration with the national regulatory authorities and supervising bodies [6].

It is recommended to establish quality assurance of safety provisions and functional performance characteristics that conform to the most recent concepts and regulations of the International Electrochemical Commission (IEC) publications or applicable national standards [7–10]. The following IEC standards and technical reports will help for guidance:

For Safety

IEC 60601-2-1 Ed.2:1998 Medical electrical equipment – Part 2–1: Particular requirements for the safety of electron accelerators in the range 1 MeV to 50 MeV [11]. This international standard establishes requirements to be complied with by manufacturers in the design and construction of electron accelerators for use in radiotherapy and defines type tests and site tests.

For Performance

Acceptance tests: IEC 60976: 2007 *Medical electrical equipment – Medical electron accelerators – Functional performance characteristics*. IEC 60976 [12] applies to medical electron accelerators when used, for therapy purposes, in human medical practice. It describes measurements and test procedures to be performed by the manufacturer at the design and construction stage of a medical electron accelerator but does not specify acceptance tests to be performed after installation at the purchaser's site. An important aspect has been introduced by IEC 60976, which recognised that inaccuracies in the test methods must be allowed for when assessing performance. It is assumed in this standard that the irradiation facility has an isocentric gantry, which is not the case in BNCT. It is, however, explicitly mentioned that where the equipment is non-isocentric, the description of performance and test methods may need to be suitably adapted.

Consistency tests: IEC/TR 60977 Ed. 2.0:2008. Medical electrical equipment – Medical electron accelerators – Guidelines for functional performance characteristics [13]. IEC/TR 60977 applies to medical electron accelerators when used, for therapy purposes, in human medical practice. It includes the addition of performance guidelines relating to several relatively new technologies introduced within the last few years, including dynamic beam delivery techniques, such as moving beam radiotherapy, intensity-modulated radiation therapy, image-guided radiotherapy and programmable wedge fields, as well as stereotactic radiotherapy/stereotactic radiosurgery and the use of certain electronic imaging devices but of course does not mention BNCT.

Data Transfer and Data Handling, Coordinates and Scales

IEC 61217 Consol. Ed. 1.2:2008 Radiotherapy equipment – Coordinates, movements and scales. IEC 61217 [14] applies to equipment and data related to the process of tele-radiotherapy, including patient image data used in relation with radiotherapy treatment planning systems, radiotherapy simulators, isocentric gamma beam therapy equipment, isocentric medical electron accelerators and non-isocentric equipment when relevant. The problems raised by this international standard are of high importance for BNCT, especially when hospital-based systems (CT, MRI, treatment simulators) are used to prepare a patient for BNCT at the reactor.

Radiotherapy Treatment Planning Systems **(RTPS)**

(*RTPS*): *IEC 62083 Ed. 1.0: 2000. Medical electrical equipment – Requirements for the safety of radiotherapy treatment planning systems* [15]. An RTPS is principally a software application, and the object of this standard is to establish the requirements for features, associated documentation and testing of the software. This standard applies to the design, manufacture and some installation aspects of an RTPS.

Treatment Room

IEC/TR 61859 Ed. 1.0:1997. Guidelines for radiotherapy treatment rooms design [16]. This technical report applies only to those aspects of the installation ensuring the safety of the patient, the operator and other persons during the radiotherapy equipment use. The installations considered are those in which are located radiotherapy equipment delivering ionizing radiation used for therapeutic purpose; it should be considered when designing the radiation room for BNCT.

Quality control programs, especially for medical electron accelerators, are adopted internationally, such as the IEC publications quoted above. BNCT must follow the same or similar procedures. Furthermore, in following such procedures, this will increase the confidence and reassurance of radiation measurements at the BNCT facility and hence the accuracy of the dose given to the patient.

With respect to quality control procedures related to the beam calibration and patient dosimetry (functional performance characteristics), it can be stated that despite the relatively more complex dosimetry of BNCT, many performance and safety characteristics associated with medical electron accelerators show dependencies on irradiation and operational parameters that are not relevant for BNCT facilities. In fact, quality control for BNCT facilities covers less parameters than that for accelerators [3]. It is therefore or should be somewhat more trivial to set up a BNCT quality control procedure than for a medical electron accelerator. Rassow [3] showed in detail the comparison between the performance and safety characteristics of medical electron accelerators and a BNCT facility and in particular for dose delivery, as well as against stray radiation. For a nuclear research reactor, there should not be, as in the case of a medical electron accelerator, initial measurements that are

performed once and only once during the acceptance test. Due to the beam characteristics being influenced by changes in the configuration of the reactor core, for example, fuel loading and experimental set-up, a more pragmatic approach is needed, that is, regular measurements prior to and after each patient treatment must be performed.

32.9.1 Standard Operating Procedures

It is highly recommended if not mandatory that standard operation procedures (SOP), that describe step by step all relevant procedures concerning the performance of BNCT and the execution of the clinical trial, must be written. They will follow the guidelines of good clinical practice [2, 17]. All SOPs should be collected in one dossier that has to be available at any time for each staff member.

Conclusion

BNCT is thwart with danger and has the potential, if incorrectly applied, to be damaging to the patient. BNCT trials take place at a nuclear research reactor, which apart from being conducted in a non-hospital environment, is known to convey fear to some people. Both aspects cause possible additional safety-related issues. It is therefore of the utmost importance that, as well as designing an optimal physical facility, special attention must be given to a managerial structure that provides safety, beyond normal rules. This involves strict quality management (QM) procedures that offer guaranteed reliable and safe functioning of the treatment [7–10, 18]. QM is therefore a mandatory task. In order to obtain comparable procedures, it is recommended to follow an international standard when designing the QM structure for a BNCT facility. The most convenient way to reach an international standard and to have the possibility to become a licensed quality management system is offered by EN ISO 9001 (2008). This latter aspect will become an important issue when multicenter clinical trials are performed.

References

1. International conference on harmonisation of technical requirements for registration of pharmaceuticals for human use (ICH). http://www.ich.org/
2. European Medicines Agency (EMEA) (2002) Guideline for good clinical practice, ICH harmonised tripartite guideline (CPMP/ICH/135/95). http://www.ema.europa.eu/ema/index.jsp?curl=pages/regulation/general/general_content_000429.jsp&mid=WC0b01ac0580029590
3. Rassow J, Stecher-Rasmussen F, Voorbraak W, Moss R, Vroegindeweij C, Hideghéty K, Sauerwein W (2001) Comparison of quality assurance for performance and safety characteristics of the facility for boron neutron capture therapy in Petten/NL with medical electron accelerators. Radiother Oncol 59:99–108

4. IAEA-TECDOC-1223 (2001) Current status of neutron capture therapy. International Atomic Energy Agency, Vienna, May 2001
5. Daquino GD, and Voorbraak, WP, (2008) A Review of the Recommendations for the Physical Dosimetry of Boron Neutron Capture Therapy (BNCT), EUR 23632 EN, ISBN 978-92-79-10868-6, European Communities
6. Sauerwein W, (2009) Regulatory affairs and licensing for a BNCT facility, in: W. Sauerwein and R Moss (Eds.), Requirements for Boron Neutron Capture Therapy (BNCT) at a Nuclear Research Reactor, EUR 2383 EN, ISBN 978-92-79-12431-0, European Communities, 15–18
7. Sauerwein W, Hideghéty K, Rassow J Moss RL, Stecher-Rasmussen F, Heimans J, Gabel D, De Vries MJ, Paquis P, Touw DJ and the EORTC BNCT Study Group (2001) Boron neutron capture therapy: An interdisciplinary co-operation, in: IAEA-TECDOC-1223 "Current status of neutron capture therapy", International Atomic Energy Agency, Vienna, 96–107
8. Sauerwein W., Moss R.L., Hideghéty K., Stecher-Rasmussen F., De Vries M.J., Paquis P., Vandertop W.P., Van Loenen A.C., Zurlo A., Rassow J. and the EORTC BNCT Study Group (2001) Quality management for BNCT at the High Flux Reactor HFR Petten, in: Gabriele P., Corno S.E., Scielzo G (Eds.), BNCT Radiotherapia per cattura neutronica del boro: stato dell'arte. Edizioni MAF Servizi, Torino, 27–31
9. Sauerwein W., Rassow J., Stecher-Rasmussen F. (2009) Quality assurance for BNCT, in: W. Sauerwein and R. Moss (Eds.), Requirements for Boron Neutron Capture Therapy (BNCT) at a Nuclear Research Reactor, EUR 2383 EN, ISBN 978-92-79-12431-0, European Communities
10. Sauerwein W, Moss R, Rassow J, Stecher-Rasmussen F, Hideghéty K, Wolbers JG, Sack H (1999) Organisation and management of the first clinical trial of BNCT in Europe (EORTC Protocol 11961). Strahlenther. Onkol. 175:108–111
11. Moss RL, Watkins P, Vroegindeweij C, Stecher-Rasmussen F, Huiskamp R, Ravensberg K, Appelman K, Sauerwein W, Hideghéty K, Gabel D. (2001) The BNCT facility at the HFR Petten: Quality assurance for reactor facilities in clinical trials, in: IAEA-TECDOC-1223 "Current status of neutron capture therapy", International Atomic Energy Agency, Vienna, 268–274
12. IEC 60601-2-1 International Standard (1998) Safety of medical electrical equipment, Part 2-1: Particular requirements for electron accelerators in the range 1MeV to 50MeV, International Electrotechnical Commission, Geneva. Ed.2: 1998-06, 1-131, International Electrotechnical Commission, Central Office Geneva http://www.iec.ch
13. IEC 60976 International Standard (2007) Medical electrical equipment - Medical electron accelerators - Functional performance characteristics. International Electrotechnical Commission, Central Office Geneva http://www.iec.ch
14. IEC/TR 60977 Ed. 2.0 Technical Report (2008) Medical electrical equipment - Medical electron accelerators - Guidelines for functional performance characteristics. International Electrotechnical Commission, Central Office Geneva http://www.iec.ch
15. IEC 61217 Consol. Ed. 1.2 International Standard (2008) Radiotherapy equipment - Coordinates, movements and scales. International Electrotechnical Commission, Central Office Geneva http://www.iec.ch
16. IEC 62083 Ed. 1.0 International Standard (2000) Medical electrical equipment - Requirements for the safety of radiotherapy treatment planning systems. International Electrotechnical Commission, Central Office Geneva http://www.iec.ch
17. IEC/TR 61859 Ed. 1.0 Technical Report (1997) Guidelines for radiotherapy treatment rooms design. International Electrotechnical Commission, Central Office Geneva http://www.iec.ch
18. Bohaychuk W, Ball G, (1994) Good Clinical Research Practices, An indexed reference to international guidelines and regulations, with practical interpretation. Hampshire, UK: GCRP Publications

Index

W.A.G. Sauerwein et al. (eds.), *Neutron Capture Therapy*,
DOI 10.1007/978-3-642-31334-9, © Springer-Verlag Berlin Heidelberg 2012